Remote Sensing of Land Cover and Land Use Changes in South and Southeast Asia, Volume 2

Impacts on the Environment

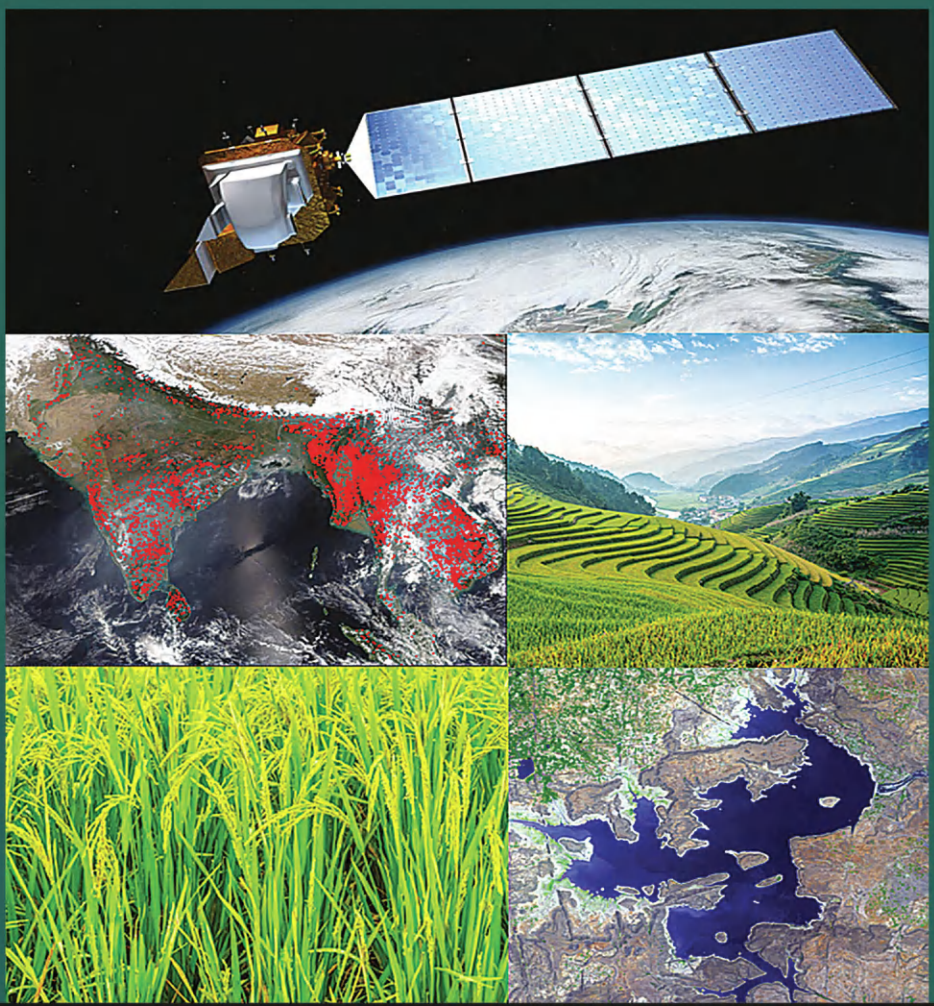

Edited by
Krishna Prasad Vadrevu,
Christopher Justice,
and **Garik Gutman**

CRC Press
Taylor & Francis Group

Remote Sensing of Land Cover and Land Use Changes in South and Southeast Asia, Volume 2

South and Southeast Asian countries are experiencing rapid land cover and land use changes (LCLUC) driven by urbanization, agricultural expansion, deforestation, and infrastructure development. These transformations have significant impacts on biodiversity, water resources, food security, and climate regulation. There is an urgent need to quantify LCLUC impacts to design effective management strategies that help understand, mitigate, and adapt to these changes. Remote sensing data plays a crucial role in providing diverse information essential for assessing land use patterns, quantifying changes, and evaluating both environmental and societal impacts.

Volume 2 explores the complex and dynamic interactions between land use and the environment in the region. It brings together expertise from U.S. contributors of the NASA-funded Southeast Asia Research Initiative (SARI) and collaborators from South and Southeast Asian countries.

Key Features:

- Presents case studies on LCLUC impacts related to food security, heat stress, urbanization, agricultural intensification, water scarcity, forest transitions, and ecosystem health.
- Demonstrates the use of novel machine learning and deep learning algorithms for quantifying LCLUC impacts.
- Explores how satellite remote sensing can reveal hidden patterns, track environmental degradation, and support resource management.
- Highlights the integration of very high-resolution data with mid-resolution satellite data for effective LCLUC impact mapping and monitoring.
- Adopts a multidisciplinary approach, emphasizing the integration of biophysical and socio-economic data to address LCLUC impacts.

This book highlights the transformative power of remote sensing and geospatial technologies while calling researchers, policymakers, and practitioners to action. It offers valuable insights for scientists, geographers, ecologists, remote sensing specialists, and anyone interested in the intersection of land use, development, and environmental sustainability.

Remote Sensing of Land Cover and Land Use Changes in South and Southeast Asia, Volume 2

Impacts on the Environment

Edited by
Krishna Prasad Vadrevu, Christopher Justice,
and Garik Gutman

CRC Press
Taylor & Francis Group
Boca Raton London New York

CRC Press is an imprint of the
Taylor & Francis Group, an **informa** business

Designed cover image: Top image: Satellite imagery plays by far the biggest role in the provision of raw material from which GEOINT is derived. Pictured: Landsat 8 satellite. Credit: USGS. First row left: Vegetation fires from satellite generated by the editors. First row right: iStock. Second row left: Close-up of a rice field, taken by the editors. Second row right: © NASA.

First edition published 2026
by CRC Press
2385 NW Executive Center Drive, Suite 320, Boca Raton FL 33431

and by CRC Press
4 Park Square, Milton Park, Abingdon, Oxon, OX14 4RN

CRC Press is an imprint of Taylor & Francis Group, LLC

ISBN: 978-1-032-49966-6 (hbk)
ISBN: 978-1-032-49967-3 (pbk)
ISBN: 978-1-003-39626-0 (ebk)

DOI: 10.1201/9781003396260

Typeset in Times
by Newgen Publishing UK

Contents

Preface

South and Southeast Asia are regions undergoing rapid land cover and land use changes (LCLUC) driven by urbanization, agricultural expansion, deforestation, infrastructure development, and other factors. These changes have profound implications for biodiversity, water resources, food security, and climate regulation, underscoring the need for effective monitoring and management strategies. Remote sensing data is crucial in mapping and monitoring LCLUC and its impacts. Satellite time-series data provide high-resolution information essential for assessing land use patterns, quantifying the extent of changes, and evaluating their environmental and societal effects. Additionally, remote sensing derived maps can be used to study the drivers behind LCLUC, such as population growth, economic activities, and policy changes, enabling the development of evidence-based solutions. By integrating remote sensing with field data and advanced analytical techniques, researchers can better understand the complex interactions between human and natural systems, ultimately supporting sustainable land management and regional development.

The two-volume book series—*Remote Sensing of Land Cover and Land Use Changes in South and Southeast Asia, Volume 1: Mapping and Monitoring* and *Remote Sensing of Land Cover and Land Use Changes in South and Southeast Asia, Volume 2: Impacts on the Environment*—is a collection of papers from experts who participated in various South/Southeast Asia Research Initiative (SARI, sari.umd.edu) workshops and meetings held in Asia since 2015. SARI is a research activity funded by NASA's Land Cover/Land Use Change (LCLUC) Program (lcluc.umd.edu). SARI aims to develop an innovative regional research, education, and capacity-building program that leverages state-of-the-art remote sensing, natural sciences, and social sciences to advance LCLUC science in South/Southeast Asia. To address LCLUC challenges, SARI employs a systems approach, examining both biophysical and socioeconomic aspects of land systems, including interactions between land use and climate and the interrelationships among policy, governance, and land use. Over recent decades, LCLUC in South/Southeast Asia has attracted significant international attention due to its extensive biophysical and environmental impacts, including transboundary pollution, which has adversely affected air quality and human health. Through SARI meetings, critical drivers and effects of LCLUC have been identified at local, regional, and global scales, highlighting urgent issues requiring immediate attention.

This two-volume book series was conceptualized to meet the research and application needs of the LCLUC community. All three editors of these volumes are renowned experts who have published extensively on LCLUC studies using satellite remote sensing data.

We are pleased to present Volume 2 of this comprehensive work, which brings together a diverse array of studies that highlight the transformative role of satellite remote sensing in LCLUC and its impacts on the environment.

This book delves into the dynamic interactions between land cover, land use, and human–environment systems across South and Southeast Asia, providing insights

into critical issues such as food security, agriculture, urbanization, and environmental sustainability. It offers vital insights into the ecological, socio-economic, and health challenges that define the region today. By integrating remote sensing technologies, satellite data, and socio-economic surveys, each chapter uncovers patterns and trends that shape the landscapes and livelihoods in South/Southeast Asian countries, illustrating environmental changes' complex and interdependent nature.

In Chapter 1, Mittra et al. investigate the factors influencing food insecurity in India's underdeveloped regions, highlighting the role of socio-economic indicators alongside satellite-derived land use data. Their analysis shows how asset ownership and off-farm returns are key drivers of food insecurity, while land cover and land use changes play a lesser role. This sets the stage for the broader environmental impacts discussed in subsequent chapters, where land use changes influence food security and wider socio-economic and environmental outcomes. Di et al. shift the focus to the Ganges Basin in Chapter 2, where urban expansion and agricultural intensification have driven significant land cover changes over the past two decades. Through the lens of remote sensing, they explore the consequences of these changes, including the loss of farmland and the growth of urban areas, linking urbanization's impact on food production to the broader environmental themes in Chapter 1. The study also contributes a new fishpond mapping methodology, showcasing the versatility of remote sensing in tracking complex agricultural landscapes, thus furthering our understanding of how land use and land management practices can optimize food production and environmental health.

In Chapter 3, Bhattarai et al. continue the environmental narrative by examining evapotranspiration (ET) to potential evapotranspiration (PET) ratios across India's agricultural lands. This work extends the discussion on land and water management by focusing on water stress in different regions and the growing need for fine-scale monitoring. It directly connects to the findings in Chapter 2, where urban and agricultural land use changes increase water demand, highlighting the growing challenges of balancing land use and water resources amidst climate change.

Chapters 4 and 5 focus on the forests of India. DeFries et al., in Chapter 4, explore the socio-economic drivers of forest transitions in Central India's dry tropical forests, further connecting the dots between land use changes and environmental degradation. Their study links improving living standards to decreased forest degradation. This important finding echoes Chapter 1's insights into how socio-economic factors, such as asset ownership and livelihoods, impact environmental outcomes. This emphasizes the interconnectedness of socio-economic development, land use changes, and ecological conservation. In Chapter 5, Fleischman et al. discuss how remote sensing can deepen understanding of human–environment interactions in South Asia. They highlight the limitations of current technology and its focus on forest cover, which often overlooks other values in nature. The authors argue for better research and policy-making, emphasizing transparency, understanding technological limitations, and integrating remote sensing with other research techniques to improve human well-being and nature conservation.

Chapters 6 through 9 take the reader into urbanization and its environmental consequences. In Chapter 6, Dasgupta and Kumar's study of thermal and ecological comfort in urban areas links directly to the earlier discussions on land use changes.

Their findings on the relationship between land surface temperatures and urban development underscore how urban sprawl exacerbates environmental stress, particularly in heat-sensitive areas. This directly connects to Chapter 7, where McAvoy et al. uses nighttime satellite data to track urban sprawl's impact on forests, revealing how development encroaches into once-natural landscapes, contributing to environmental degradation and increased human–environment conflict. Chapter 8, by Aithal et al., deepens the urban narrative by focusing on Bengaluru's increasing heat stress, further elaborating on the consequences of land use changes for human health. The authors emphasize the need for urban planning strategies that mitigate the effects of heat stress, particularly in areas with high urban density. Chapter 9, by Joseph et al., is unique and focuses on the Indian Flying Fox bat and its roosting habitats. The study demonstrates how land use changes, particularly highway development and habitat degradation, directly impact wildlife and public health, emphasizing the interconnection between human development, environmental health, and zoonotic disease risks. This study highlights the need for conservation strategies to mitigate environmental damage and public health threats, tying the earlier discussions on land cover changes to a broader understanding of human–wildlife–environment interactions.

Chapter 10 by Kotrike et al. explores the impact of aerosols on cloud lifetime and solar radiation reflectance in Southern India, where industrialization and urbanization have increased aerosol formation. The study analyzes the effects of aerosol optical depth (AOD) on cloud fraction (CF) and precipitation during the southwest monsoon from 2005 to 2019, finding a positive relationship between AOD and CF. Atmospheric stability significantly affects cloud formation in some thunderstorm states but not in more intense storms. Land cover changes, including increased cropland and urban areas, are linked to decreased precipitation, partly due to reduced evapotranspiration from urbanization.

Chapters 11 through 16 focus on Southeast Asia, where LCLUC changes continue to pose significant challenges to the environment and human health. In Chapter 11, Hoffman-Hall explores the relationship between land use change and malaria transmission in Myanmar, showing how deforestation and human activity influence disease spread.

Chapter 12, by Potapohn et al., introduces Thailand's Actionable Intelligence Policy (AIP) platform, which integrates remote sensing data with ground-level information to inform public decision-making. This chapter demonstrates how remote sensing can be used to track environmental changes and facilitate more effective policy interventions, offering a concrete example of how technology can be applied to solve real-world environmental problems.

Chapters 13 and 14 by Brown et al. and Kaewplang et al. use remote sensing to inform agricultural land use planning and crop yield forecasting in Vietnam and Thailand. Their work emphasizes how satellite data can be used to predict and manage agricultural changes, directly contributing to more sustainable agricultural practices and more efficient resource use. Thus, it connects back to the overarching theme of balancing land use, food production, and environmental sustainability.

Chapters 15 and 16 focus on biomass burning. Sentian et al. (Chapter 15) established a biomass-burning emission inventory for the ASEAN region from 2013

to 2021 using remote sensing data to track emissions from burning activities, providing valuable data for mitigating biomass burning's environmental impact. In Chapter 16, Shi et al. develop a high-resolution emission inventory for open biomass burning (OBB) in South and Southeast Asia from 2020 to 2022, revealing significant carbon emissions, primarily from forests and woodlands, along with seasonal variations in burning patterns. Their findings contribute to more accurate air quality models and regional emissions reduction strategies.

Together, these chapters provide a comprehensive view of the impacts of LCLUC, including the dynamic interactions between land use changes, environmental health, socio-economic factors, and technological advancements. The studies demonstrate how remote sensing can be used to understand these impacts and complex interactions, offering insights that inform policy and practical interventions for sustainable development. The book presents a framework for addressing the region's pressing environmental challenges through these interconnected chapters, emphasizing the need for integrated approaches that balance development, conservation, and public health.

This volume will be valuable to anyone interested in remote sensing-based approaches for quantifying LCLUC's environmental impacts. It will be especially useful for environmental scientists, geographers, ecologists, atmospheric scientists, and environmental professionals seeking to deepen their understanding of these impacts.

As editors, we sincerely thank the contributing authors for their exceptional research and dedication. We are also deeply grateful to the reviewers for their invaluable feedback, which has significantly enhanced the quality of this volume. Finally, we sincerely appreciate the guidance and support of Irma Britton and Chelsea Reeves at CRC Press throughout the publication process.

We hope this book becomes a key resource for advancing research and fostering collaboration in remote sensing and land use studies. It is an honor to present this work, and we wish all readers an informative and thought-provoking experience.

Krishna Vadrevu, *Huntsville, Alabama, USA*
Christopher Justice, *College Park, Maryland, USA*
Garik Gutman, *Washington DC, USA*

About the Editors

Krishna Prasad Vadrevu is a remote sensing scientist at NASA's Marshall Space Flight Center in Huntsville, Alabama, USA. His research focuses on land cover and land use change (LCLUC), fire dynamics, and biomass burning emissions. With 25 years of experience in satellite remote sensing, he has an extensive publication record. He currently serves as the Deputy Program Manager for NASA's LCLUC Program (lcluc.umd.edu) and leads the South/Southeast Asia Research Initiative (www.sari.umd.edu).

Christopher Justice, a Distinguished University Professor at the University of Maryland, received his Ph.D. from the University of Reading, UK. He served as Chair of the Department of Geographical Sciences from 2010 to 2021. He is the Project Scientist for NASA's Land Cover Land Use Change (LCLUC) Program, Chief Scientist for HARVEST, and the Land Discipline Co-Lead for NASA's MODIS and Suomi-NPP VIIRS Science Teams. Additionally, he chairs the international GOFC/GOLD Program and co-chairs the GEOGLAM Initiative on global agricultural monitoring.

Garik Gutman is a Program Manager for NASA's Land Cover/Land Use Change (LCLUC) Program in Washington, DC, USA. He has 45 years of research experience in satellite remote sensing, LCLUC, and analyzing the impacts of these changes on climate, the environment, and society. Prior to joining NASA in 1999 as a Program Manager, he was a scientist at the National Oceanic and Atmospheric Administration (NOAA). Dr. Gutman has been a co-editor on several books. He has made significant contributions to advancing LCLUC science globally by establishing and strengthening multiple regional initiatives.

Contributors

Meghna Agarwala
Department of Environmental Studies
Ashoka University
Sonipat, Haryana, India

Bharath H Aithal
Energy and Urban Research Group
Ranbir and Chitra Gupta School of Infrastructure Design and Management
Indian Institute of Technology Kharagpur
West Bengal, India

M V Anusree
Department of Zoology
Kannur University
Mananthavady, Wayanad, Kerala, India

Sandra Baquie
World Bank
Washington, DC, USA

Nishan Bhattarai
Department of Geography and Environmental Sustainability
University of Oklahoma
Norman, Oklahoma, USA

Jarrod Brown
Department of Philosophy
Berea College
Kentucky, USA

Akkarapon Chaiyana
Department of Civil Engineering
Faculty of Engineering
Maha Sarakham University
Maha Sarakham, Thailand

Pooja Choksi
Department of Forest Resources
College of Food, Agriculture and Natural Resources Sciences
University of Minnesota
Minnesota, USA

Anindita Dasgupta
Spatial Computing Laboratory
Department of Data Science and Artificial Intelligence
International Institute of Information Technology
Bangalore, India

Ruth DeFries
Ecology Evolution and Environmental Biology
and
Climate School
Columbia University
New York, New York, USA

Liping Di
George Mason University
Fairfax, Virginia, USA

Aditya Eaturu
University of Alabama Huntsville
Alabama, USA

Joseph J Erinjery
Department of Zoology
Kannur University
Wayanad, Kerala, India

Justin Fain
iSciences, LLC, USA

Forrest Fleischman
Department of Forest Resources
College of Food, Agriculture and Natural Resources Sciences
University of Minnesota
Minnesota, USA

Anita Gautam
Energy and Urban Research Group
Ranbir and Chitra Gupta School of Infrastructure Design and Management
Indian Institute of Technology Kharagpur
West Bengal, India

T Christina Grace
Department of Zoology
Kannur University
Mananthavady, Wayanad, Kerala, India

Zhe Guo
International Food Policy Research Institute
Washington, DC, USA

Garik Gutman
NASA Headquarters
Washington, DC, USA

Bui Thi Minh Ha
University of Social Sciences and Humanities – Vietnam National University
Ho-Chi-Minh City, Vietnam

Ratchawatch Hanchoowong
Department of Civil Engineering
School of Engineering and Industrial Technology
Mahanakorn University of Technology
Bangkok, Thailand

Franky Herman
Climate Change Research Laboratory, Universiti Malaysia Sabah, Malaysia

Amanda Hoffman-Hall
Eckerd College, St. Petersburg, Florida, USA

Rattana Hormwichian
Department of Civil Engineering
Faculty of Engineering
Maha Sarakham University
Maha Sarakham, Thailand

Alfredo Huete
School of Life Sciences
University of Technology Sydney
Sydney, Australia

Chin Jia Hui
Climate Change Research Laboratory, Universiti Malaysia Sabah, Malaysia

Takuya Iwamura
Department F.-A. Forel for Environmental and Aquatic Sciences
University of Geneva
Geneva, Switzerland

Meha Jain
School for Environment and Sustainability
University of Michigan
Ann Arbor, Michigan, USA

Yadvendradev Jhala
Wildlife Institute of India
Dehradun, Uttarakhand, India

Amal Joseph
Department of Zoology
Kannur University,
Mananthavady, Wayanad, Kerala, India

Christopher Justice
University of Maryland College Park
College Park, Maryland, USA

Siwa Kaewplang
Department of Civil Engineering, Faculty of Engineering, Maha Sarakham University, Kantharawichai District, Maha Sarakham, Thailand

Anongrit Kangrang
Department of Civil Engineering
Faculty of Engineering
Maha Sarakham University
Maha Sarakham, Thailand

Venkata Reddy Keesara
Department of Civil Engineering
National Institute of Technology
Warangal, India

Sarika Khanwilkar
Independent scientist
Nagpur, India

Sangwoo Kim
Department of Biological Systems Engineering
Virginia Polytechnic Institute and State University
Blacksburg, Virginia, USA

Werapong Koedsin
Faculty of Technology and Environment
Phuket Campus
Prince of Songkla University
Phuket, Thailand

Tharani Kotrike
Department of Civil Engineering
National Institute of Technology
Warangal, India

Uttam Kumar
Spatial Computing Laboratory
Department of Data Science and Artificial Intelligence
International Institute of Information Technology
Bangalore, India

Man Li
International Food Policy Research Institute
Washington, DC, USA

Yang Liu
Aerospace Information Research Institute
Chinese Academy of Sciences
Beijing, China

Griffin McAvoy
University of Alabama, Huntsville
Alabama, USA

Jessica McCarty
NASA Ames Research Center
USA

M R Midhunlal
Department of Zoology
Kannur University
Mananthavady, Wayanad, Kerala, India

Sarika Mittra
Department of Forest and Wildlife Ecology
University of Wisconsin-Madison
Madison, Wisconsin, USA

Pinki Mondal
Department of Geography and Spatial Sciences
University of Delaware
Newark, Delaware, USA

Harini Nagendra
School of Climate Change and Sustainability
Azim Premji University
Sarjapura, Bengaluru, Karnataka, India

P Neethu
Department of Zoology
Kannur University
Mananthavady, Wayanad, Kerala, India

Ditchaphong Phoomikiattisak
Geo-Informatics and Space Technology Development Agency (GISTDA)
Thailand

Manoj Potapohn
Chiang Mai University
Faculty of Economics
Thailand

Peter Potapov
University of Maryland
College Park, Maryland, USA

P K Prasadan
Department of Zoology
and
Western Ghats Study Centre
Kannur University
Mananthavady, Wayanad, Kerala, India

Haris Prasanchum
Faculty of Engineering
Rajamangala University of Technology Isan
Khon Kaen Campus
Khon Kaen, Thailand

Vijay Ramprasad
Center for Environmental Studies, Williams College, Massachusetts, USA

A Rathinakumar
VAAVAL – Centre for Indian Bat Research on Ecosystem Sustainability
Coimbatore, Tamil Nadu, India

Devireddy Girish Kumar Reddy
Energy and Urban Research Group
Ranbir and Chitra Gupta School of Infrastructure Design and Management
Indian Institute of Technology Kharagpur
West Bengal, India

Teo Yu Rou
Climate Change Research Laboratory, Universiti Malaysia Sabah, Malaysia

V V Saritha
Department of Zoology
Kannur University
Mananthavady, Wayanad, Kerala, India

Justin Sentian
Climate Change Research Laboratory, Universiti Malaysia Sabah, Malaysia and Climate Carbon Neutral Initiative, Sabah, Malaysia

Afshin Shayeghi
Department of Geography and Environmental Sustainability
University of Oklahoma
Norman, Oklahoma, USA

Yusheng Shi
Aerospace Information Research Institute
Chinese Academy of Sciences
Beijing, China

Aditya Singh
Department of Agricultural and Biological Engineering
University of Florida
Gainesville, Florida, USA

David L. Skole
Department of Forestry, Michigan State University, Michigan, USA

M K Smija
Department of Zoology
Kannur University
Mananthavady, Wayanad, Kerala, India

Venkataramana Sridhar
Department of Biological Systems Engineering
Virginia Polytechnic Institute and State University
Blacksburg, Virginia, USA

Neti Srihanu
Faculty of Engineering
Northeastern University
Khon Kaen, Thailand

G Sreenivasa
Department of Zoology
Davangere University
Davangere, Karnataka, India

C C Stefina
Department of Zoology
Kannur University
Mananthavady, Wayanad, Kerala, India

Phadungpon Supinit
Chiang Mai University, Faculty of Economics, Thailand

Junmei Tang
George Mason University
Fairfax, Virginia, USA

Stanley Toops
Miami University
USA

Peou Touch
Independent Researcher, USA

Philip A. Townsend
Department of Forest and Wildlife Ecology
University of Wisconsin-Madison
Madison, Wisconsin, USA

Greg Treiman
SAS, Inc., USA

Svetlana Turubanova
University of Maryland
College Park, Maryland, USA

Johannes Urpelainen
School of Advanced International Studies
Johns Hopkins University
Washington, DC, USA

Krishna Prasad Vadrevu
NASA Marshall Space Flight Center
Huntsville, Alabama, USA

Yajun Wang
Aerospace Information Research Institute
Chinese Academy of Sciences
Beijing, China

Eugene Yu
George Mason University
Fairfax, Virginia, USA

Zhiqi Yu
George Mason University
Fairfax, Virginia, USA

Maryam Zamanialaei
University of California
Berkeley, California, USA

Wei Zhang
International Food Policy Research Institute
Washington, DC, USA

1 Factors Affecting Food Insecurity Across Under-Developed Regions of India, Contrasting Indicators of Household-Scale Socioeconomics and Land Cover Change

Sarika Mittra, Philip A. Townsend, and Aditya Singh

1.1 BACKGROUND

The State of Food Security and Nutrition in the World report (FAO et al., 2020) estimates that the proportion of India's population experiencing moderate to severe food insecurity increased from 27.8% in 2014–2016 to 31.6% in 2017–2018, according to the Prevalence of Moderate and Severe Food Insecurity (PMSFI) measure. Despite a decade-long reduction in the number of undernourished people—from 21.7% in 2004–2006 to 14% in 2017–2019—India still harbors the highest number of undernourished individuals globally, at 189.2 million persons (2017–2019). Although India is a net exporter of food, local food availability varies significantly across regions due to institutional factors, demographics, land use, and environmental degradation. Population growth and urbanization have exerted increasing pressure on land use patterns, with the area under non-agricultural use rising from 9.36 million hectares in 1950 to 26.51 million hectares in 2011 (MOSPI, 2025). The Indian Council of Agricultural Research (ICAR) reports that approximately 36.6% of India's total area is degraded due to factors such as water and wind erosion, chemical degradation (e.g., salinization, acidification), physical degradation (e.g., waterlogging), and other causes like mining (Trivedi et al., 2010). Climate change is expected to exacerbate these trends by increasing stresses on food production. For instance, extreme weather events in 2015 affected 18.33 million hectares, compared to 0.35 million hectares in 2013 and 5.5 million hectares in 2014, resulting in crop losses worth USD

DOI: 10.1201/9781003396260-1

3 billion (Bhushan et al., 2015). Addressing these challenges requires geographically differentiated strategies, but the current efforts are significantly hindered by a lack of spatially explicit information on food security and agriculture. Such information is vital for early trend detection and disentangling the complex relationships between food security and land use.

1.2 INTRODUCTION

The United Nations Committee on World Food Security (1996) defines food security as a state in which all people, at all times, have physical, social, and economic access to sufficient, safe, and nutritious food that aligns with their dietary needs and preferences for an active and healthy life. This widely accepted definition encompasses the dimensions of food availability, access, utilization, and stability of these factors. Food availability, the most directly quantified aspect, pertains to the sufficiency of food supply. National-level food balance data sheets have been utilized to calculate food availability since long before food security emerged in the early 1970s (Jones et al., 2014). Amartya Sen (1981) introduced the concept of "entitlement" to highlight access, emphasizing that food insecurity can exist even with an adequate food supply. Food access includes physical and economic access and ensures equitable distribution at all levels. Utilization involves allocating and absorbing nutritious food, recognizing that availability and access are often evaluated merely in terms of calorie count or production. The final dimension, stability, concerns the other dimensions' sociopolitical and environmental steadiness, ensuring short- and long-term resilience.

At national and regional levels, food availability frequently serves as the primary focus of food security assessments. National-level food security metrics typically depend on food balance sheets, which, as stated, primarily measure food availability and, to a lesser extent, food access. Access is generally evaluated through consumption and expenditure metrics, whereas utilization is often assessed using anthropometry or dietary intake by food groups. Production, calorie consumption, and intake quantities are directly measurable, even at the household level. In India, grain security has traditionally been equated with food security. Although food grain production surged by 400% from 1950–1951 to 2015–2016, the net availability of food grains per person per year only modestly increased from 144.1 kg in 1950–1951 to 169.8 kg in 2015 (GOI, 2016). In comparison, China's average daily per capita caloric supply from agricultural production rose significantly from 1859 kcal/person in 1970 to 3108 kcal/person in 2013. In contrast, in India, the increase during the same period was from 2111 kcal/person to 2459 kcal/person. Food consumption expenditure in India declined by 20% from 1972–1973 to 2011–2012, with a more pronounced decline in rural areas (Deshmukh & Vyavahare, 2018). Food utilization metrics have performed poorly, with 39% of children under five classified as undernourished or stunted in 2014 (Sahu et al., 2015). Additionally, maternal mortality rates have remained persistently high (Saxena, 2018).

At regional scales, spatial variations in food security indicators may reflect differences in basic food supply (Abbade & Dewes, 2015), adequacy of physical infrastructure (Memon & El Bilali, 2019), and availability of institutional support

(Vervisch et al., 2013). Although food security issues in India have been extensively studied (Hertel, 2015; Jain et al., 2013; Mondal et al., 2021; Singh et al., 2002), comprehensive and regional assessments of factors influencing food security are often hindered by the lack of data on key socioeconomic and infrastructure indicators at sufficiently detailed scales, especially those measured consistently across regions. Indicators of poverty, food security, and general "backwardness" are typically formulated using weighted combinations of factors such as the proportion of the population in "backward" castes, infant mortality rates, female workforce participation ratios, and income (Ghosh, 2011; Rathor & Premi, 1986). While these measures are valuable indicators of human development, their combination through simple weighting schemes does not reveal the underlying causal factors leading to the spatial clustering of distressed areas within regions. Regarding food utilization, spatial variations in physical accessibility, such as proximity to transport hubs or markets, can significantly influence household-level land use decisions. There is a critical need for a methodology that integrates food security measures within a geospatial context and combines them into holistic synthetic indicators that explain each causal factor comprehensively. Depending on the local landscape context, factors influencing food security may differ among forested, agrarian, or peri-urban regions and may drive decisions that result in land use changes through sale, conversion, or abandonment.

1.3 METHODS

1.3.1 Study Areas

This study focuses on four distinct sites across India, each with distinct climates and socioeconomic features yet facing shared challenges related to subsistence agriculture and food security The districts selected for this study—Panna, Satna, Tehri Garhwal, and Udaipur—span different climatic zones and are among the 250 most underperforming districts in India according to the Ministry of Panchayati Raj (Figure 1.1). These regions are predominantly rural, marked by hilly terrain, dense forests (except Udaipur), and subsistence farming as the primary livelihood. Agriculture in these districts relies heavily on rain-fed methods with minimal mechanization and faces challenges such as low soil nutrient levels and inefficient water use.

Data collection for this study was conducted through household surveys across the four districts between August 2018 and April 2019. The study aimed to capture a comprehensive range of variables related to food insecurity, including demographic profiles, agricultural production, food availability, livelihoods, and nutrition. A modified version of the Rapid Household Multiple Indicator Survey (RHoMIS) tool was utilized for data collection, facilitated by the Open Data Kit (ODK) software on Android platforms. Surveys were conducted in Hindi, employing locally chosen enumerators to ensure cultural and linguistic alignment. To ensure data quality, rigorous data processing steps were undertaken. Raw data underwent thorough checks for errors, such as unrealistic values and inconsistencies, with local units standardized to international metrics where necessary. Economic data, initially in Indian Rupees, were converted to US Dollars using a mean exchange rate for the study period. To adhere to established ethical standards, we obtained approval from UW-Madison's

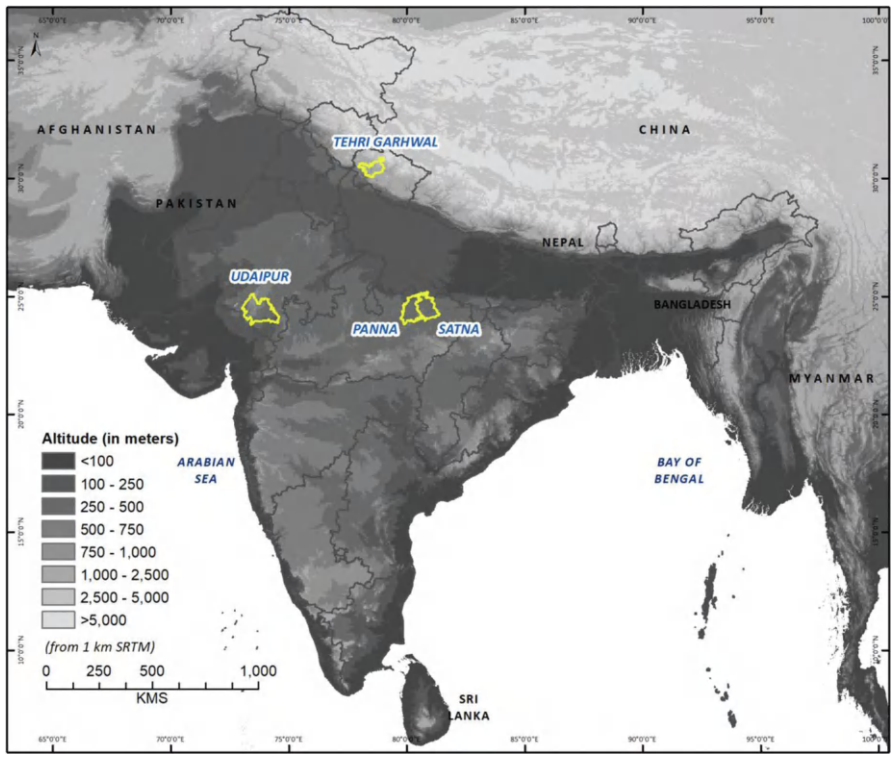

FIGURE 1.1 Study areas in the districts of Panna and Satna (Madhya Pradesh), Tehri Garhwal (Uttarakhand), and Udaipur (Rajasthan).

Education and Social Behavioral Science Institutional Review Boards (IRB). All data were securely stored on a restricted-access Google cloud server, ensuring compliance with data privacy and protection regulations.

The survey aimed to achieve a representative sample by targeting 5% of villages within each district, following the Census of India, 2011. Within selected villages, a further 0.5% of households were surveyed. This sampling strategy aimed to capture diverse socioeconomic and geographic contexts prevalent among smallholder farmers in the study districts. Village and household selection followed a wholly randomized method based on the Census of India. Villages with fewer than 50 households were excluded to ensure an adequate sample size for statistical reliability. This randomized approach minimized bias and ensured that findings could be generalized to each district's broader population of smallholder farmers. The survey was conducted exclusively in Hindi across all four districts, reflecting the primary language spoken by the local communities. Enumerators were selected locally to leverage their knowledge of the area, including dialects and local customs. This local expertise enhanced communication and facilitated accurate data collection, especially concerning nuanced aspects like units of measurement and cultural sensitivities. Before full-scale implementation, a pilot phase was conducted in two villages per district. This trial allowed

researchers to refine survey instruments, including question phrasing and response options. Adjustments were made based on feedback received during the pilot phase to ensure clarity and relevance of questions across different cultural and socioeconomic contexts.

1.4 METHODS AND DATA

1.4.1 Socioeconomic Indicators

All key indicators were standardized for comparative analysis. The Adult Male Equivalent (AME) concept (Weisell & Dop, 2012) was applied to standardize household sizes, enabling caloric consumption comparisons across households. Livestock ownership was quantified using Tropical Livestock Units (TLUs, the equivalent of a 250 kg live-weight animal), facilitating standardized comparisons across sites despite variations in animal sizes and types (Jahnke et al., 1988). The Socio-economic Status (SES) Index following Hong et al. (2006) was derived using factor analysis, incorporating variables such as ownership of agricultural and non-agricultural goods to assess household wealth. The Household Dietary Diversity Score (HDDS) was computed based on the frequency of consumption of 10 food groups (Hammond et al., 2017) during good and bad seasons, adjusted to local dietary patterns and seasonal variations. Potential Food Availability (PFA, in kcal/person/day) was estimated to gauge food availability, considering both on-farm production and income from agricultural and off-farm activities. Market orientation, another critical indicator, measures the proportion of farm products sold versus consumed within households, indicating the degree of market engagement (USDA, 2019). Additional variables included land ownership, economic distress from unpaid debts, stability of food supply, income diversity from on-farm and off-farm sources, and the physical accessibility of villages to nearby markets. All household-level data were aggregated to the village level for analysis, incorporating a spatial indicator—distance to the nearest town—to assess market accessibility. This comprehensive approach allowed for a nuanced exploration of food security dynamics across diverse agricultural settings, highlighting the interplay of environmental, socioeconomic, and geographical factors. The findings from this study contribute valuable insights into localized food security challenges and underscore the importance of tailored interventions to enhance resilience among smallholder farming communities in India.

Food insecurity was directly measured using the self-assessed Household Food Insecurity Access Scale (HFIAS) (Coates et al., 2007), which is based on nine questions that gauge the severity of food insecurity depending on the frequency of occurrence. Respondents were asked to identify the "worst" month in the past 12 months and to assess the frequency of the nine conditions during that month. The responses were then aggregated into a score ranging from 0 to 27, with higher scores indicating greater food insecurity (Figure 1.2). While the indicators effectively measured the latent variables of interest, additional environmental indicators were computed from secondary geospatial sources to supplement the data missing from household surveys. These additional indicators included land cover and land use change (LCLUC), surface soil moisture, and connectivity (roads) cost at the village

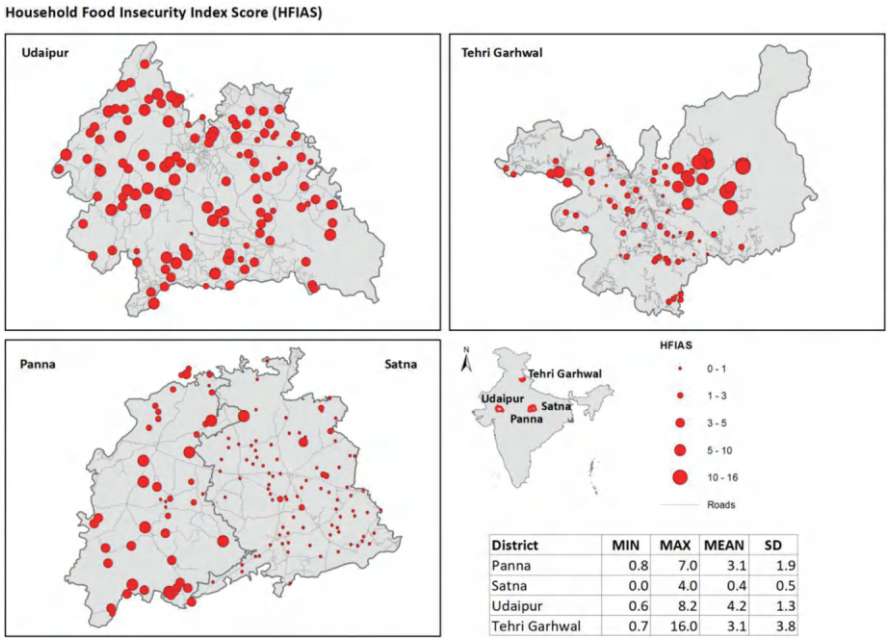

District	MIN	MAX	MEAN	SD
Panna	0.8	7.0	3.1	1.9
Satna	0.0	4.0	0.4	0.5
Udaipur	0.6	8.2	4.2	1.3
Tehri Garhwal	0.7	16.0	3.1	3.8

FIGURE 1.2 Household Food Insecurity Access Scale (HFIAS) measures the level of food insecurity experienced by a household. The score ranges from 0 to 27 with higher scores indicating more food insecurity. Each circle represents a village.

level. The outcome variable encompassed the Household Food Insecurity Access Scale (HFIAS) and the number of months a household experienced food shortages within a year.

1.4.2 Land Cover Change

Land cover and land use change (LCLUC) data for 2001, 2011, and 2018 were derived from a dataset that utilized all available Landsat TM, Landsat ETM+, and Landsat OLI Surface Reflectance data at 30-meter resolution for these years. The analysis employed the Continuous Change Detection and Classification (CCDC) algorithm (Zhu & Woodcock, 2014), a pixel-based method executed after masking out all clouds, cloud shadows, and snow pixels, using all image bands. The CCDC algorithm first detects changes—seasonal, gradual, or abrupt—using harmonic regression for each pixel and assigns a change class based on the type of change. A change is designated when the difference between the predicted and actual pixel value exceeds the root mean squared error (RMSE) multiple consecutive times. The land cover classification is then performed using a Random Forest classifier, utilizing variables estimated from the time-series model that inform the trend, intra-annual (seasonal) and inter-annual differences, and the RMSE from all spectral bands.

The accuracy assessment demonstrated an overall accuracy exceeding 90% for all districts. The training data for this assessment consisted of approximately 9000 ground truth locations collected at randomly generated 30-meter boxes overlaid on Google Earth Imagery at all four sites. The classification scheme for land cover and land use change (LCLUC) was based on a decadal dataset for India that comprised 19 classes (Roy et al., 2016). However, a few classes, such as wetlands and salt pans, were absent in the study sites. To reduce complexity, the remaining courses were aggregated into eight broader categories: forest, crop and fallow land, built-up land, shrubland, barren and wasteland, water bodies, grassland, and permanent snow and ice. Since snow and ice were only present in high-elevation, uninhabited areas of Tehri Garhwal, they were excluded from further analysis. Barren and wasteland were combined due to their similar non-productive and uncultivable nature. Built-up land was excluded because spatial expansion was limited to the district headquarters, which were not included in the sampling sites. Village roads were also inaccurately classified at this pixel resolution, so they were omitted. The aggregation of classes was necessary to satisfy sample size vis-a-vis parameter requirements of the SEM. The land cover class change was estimated as the proportion change in each class. For any given year, class-wise proportional land cover change was estimated as the per-class land cover change per village aggregated up to the district over the 18-year timespan of the analysis. (Figure 1.3).

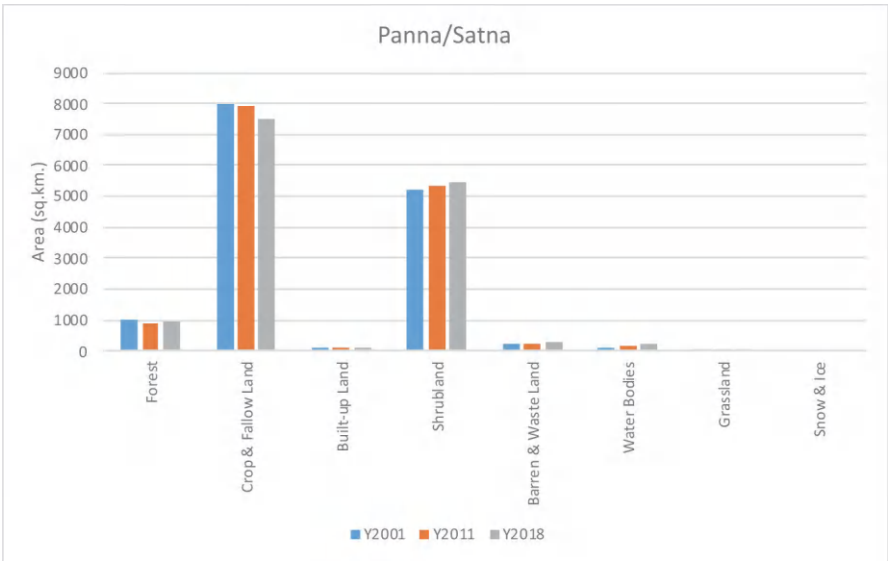

FIGURE 1.3 Area (in sq.km.) covered by land cover land use classes for Districts Panna and Satna for 2001, 2011, 2018.

1.4.3 Other Eco-Geographic Factors

The model included other indicators, such as connectivity cost and proximity to towns, to characterize the effects of physical access. LCLUC maps for the districts across all periods were reclassified into broad classes to satisfy the structural equation modeling (SEM) requirements. Forest types were reclassified into a single forest category, while croplands and fallow lands were combined into cropland due to the seasonal nature of fallow lands in these areas. Sparsely vegetated and unsuitable for cultivation, Wastelands were reclassified as barren land. The built-up land, shrubland, grassland, water bodies, and snow and ice classes remained unchanged (Figure 1.4).

Surface soil moisture was used as a proxy for fine-resolution and current irrigation data (Abolafia-Rosenzweig et al., 2019; Ambrosone et al., 2020; Das et al., 2019; Zappa et al., 2021; Zaussinger et al., 2019). Smallholder farmers in India rely heavily on traditional irrigation methods, except during the monsoon season. Surface soil moisture, indicating water availability in the upper 10 cm of soil, is a key indicator of water stress conditions. Data were extracted from the NASA-USDA Enhanced SMAP Global soil moisture dataset through Google Earth Engine, available from April 1, 2015, to the present (https://earth.gsfc.nasa.gov/hydro/data/nasa-usda-global-soil-moisture-data). The data, at a 10 km × 10 km spatial resolution and in 3-day composites, were averaged over 12 months from June 2018 to May 2019 to coincide with the two main cropping seasons during the survey period (Figure 1.5).

Physical connectivity is crucial for development, as road connectivity in rural areas enhances access to markets, employment, education, and health services, thereby improving agricultural production and livelihoods. The connectivity cost variable was calculated using the least-cost path analysis, commonly used in transportation geography, to determine the most cost-effective route between points (Gowen & de Smet, 2020). The potential markets included all villages with more than 50 households within a 30 km buffer of the study village. This distance was chosen as it approximates a round-trip within a day. Friction was aggregated from slope and road type, with slope data derived from the CGIAR-CSI SRTM dataset Version 4 (Jarvis et al., 2008) and road network data classified into primary, secondary, and tertiary types (ISGCM/Survey of India, 2016). The connectivity cost for each village was calculated based on both friction layers using the Least Cost Path Plugin for QGIS (Gong, 2018/2020) and aggregated using the mean, with lower cost values indicating better connectivity. Spatial autocorrelation of all model variables was checked using Moran's I, and any positive spatial correlation with $p<0.05$ was considered significant. To address this dependency, k-nearest neighbor weights were calculated, and the row-standardized weight matrix was applied to create spatially lagged variables representing each variable's weighted average of neighboring values (Figure 1.6).

1.5 THE CAUSAL MODELING STRATEGY

This study aims to evaluate the interrelationships between the drivers of land cover change and the indicators of food security dimensions through a structural equation model (SEM). SEMs, a set of statistical methods, estimate networks of causal relationships (Lamb et al., 2014). These structural relationships are constructed as

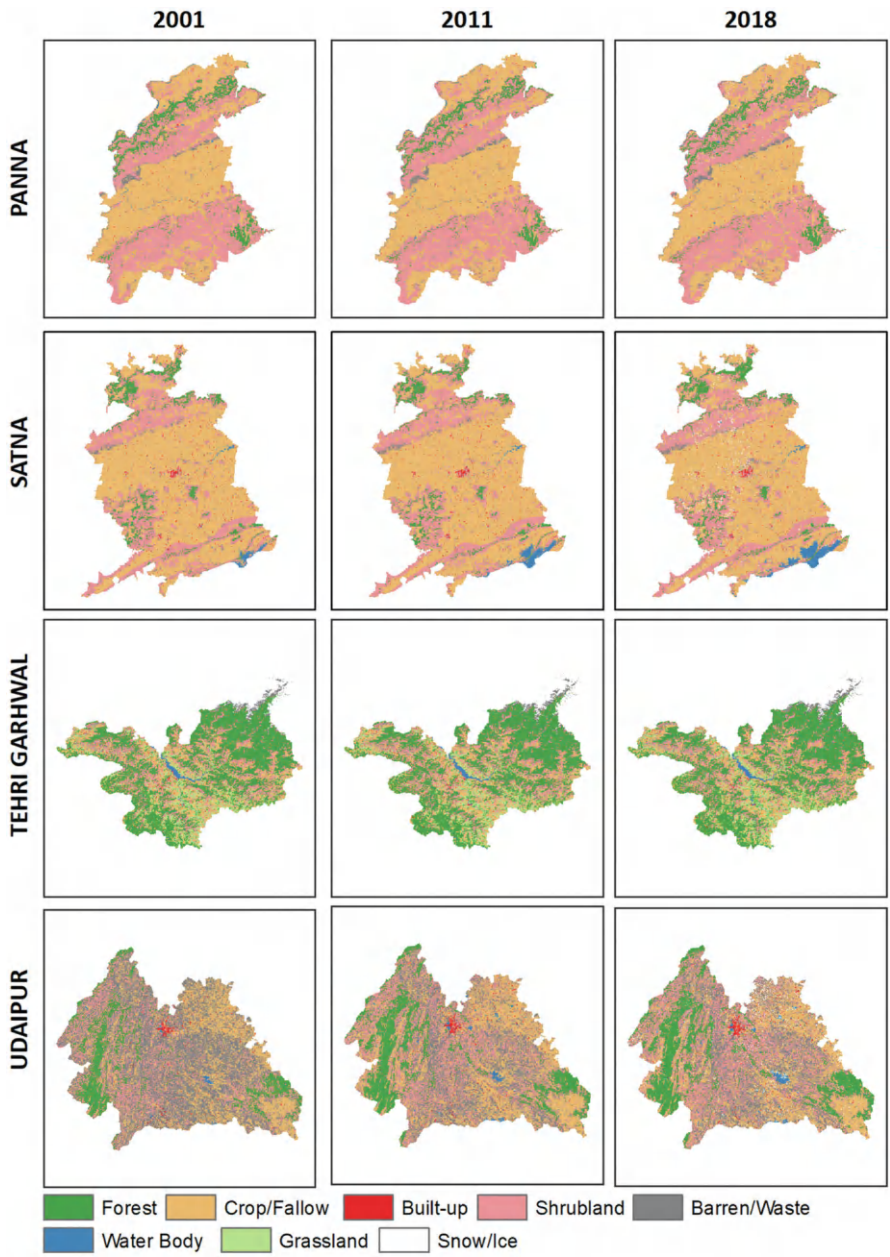

FIGURE 1.4 Land cover land use maps for Panna, Satna, Tehri Garhwal and Udaipur for 2001, 2011, and 2018.

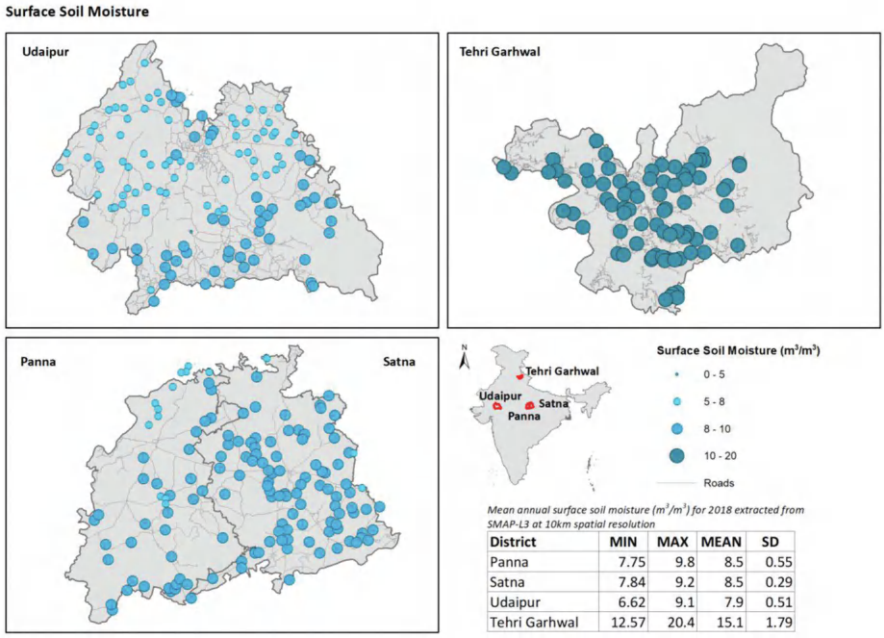

Mean annual surface soil moisture (m^3/m^3) for 2018 extracted from SMAP-L3 at 10km spatial resolution

District	MIN	MAX	MEAN	SD
Panna	7.75	9.8	8.5	0.55
Satna	7.84	9.2	8.5	0.29
Udaipur	6.62	9.1	7.9	0.51
Tehri Garhwal	12.57	20.4	15.1	1.79

FIGURE 1.5 Surface soil moisture (SSM) derived from the NASA-USDA enhanced SMAP global soil moisture data. Data is for the 12-month average for June 2018 to May 2019. Each circle represents a village.

recursive linkages between unmeasured latent concepts, each measured through observable indicators like field or statistically estimated data. Typically, an SEM is visualized as a path diagram illustrating direct and indirect links between endogenous variables (dependent and influenced by other variables), exogenous variables (independent and not influenced by other variables), and the observed and latent variables. The SEM approach estimates size effects (beta coefficients of the arrows and their *p*-values) within an iterative least-squares framework. By estimating all size effects concurrently, the latent variables can be estimated and mapped across the study region using associated beta coefficients.

This study aims to understand the complexity of a system using a causality concept among latent constructs (latent variables, LVs) while describing each LV by measured observations, formally termed manifest variables (MVs), i.e., data in land-derived geospatial variables. The partial least squares (PLS) approach to SEMs, also known as path modeling (PLS-PM), combines path analysis (Alwin & Hauser, 1975; Holland, 1988; Sanchez, 2013) and confirmatory factor analysis (Brown & Moore, 2012). The PLS-PM technique iteratively solves for blocks of the measurement model in the first step (the relation of LVs to MVs). Then, the structural model (the interrelationships between LVs) is estimated in the second step. These steps iterate until the aggregated residual error is minimized (Dijkstra, 2010). The PLS-PM approach relaxes strict distributional and sample size requirements of data and, unlike

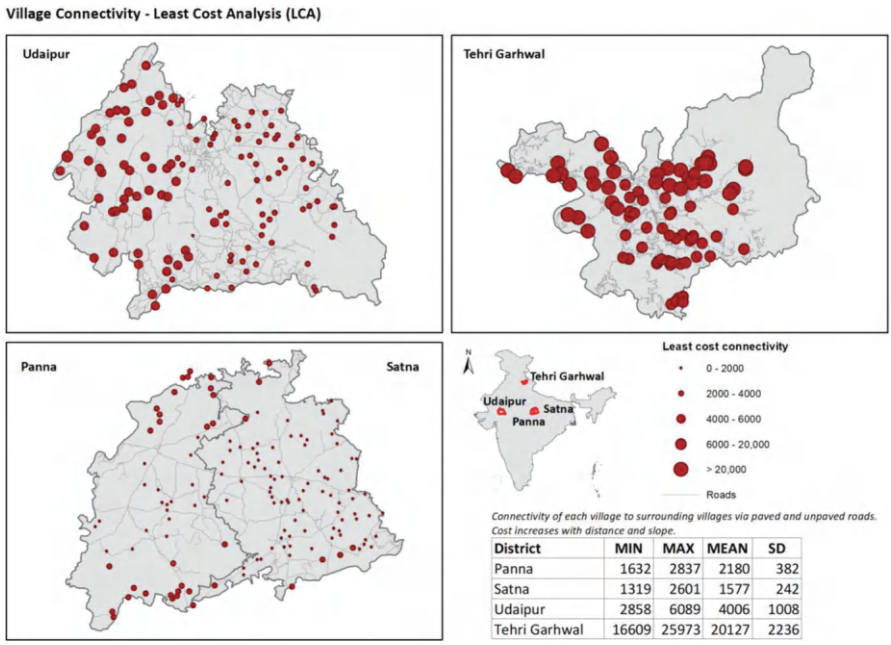

District	MIN	MAX	MEAN	SD
Panna	1632	2837	2180	382
Satna	1319	2601	1577	242
Udaipur	2858	6089	4006	1008
Tehri Garhwal	16609	25973	20127	2236

FIGURE 1.6 Connectivity cost estimated for each village to find how connected or remote they are from their neighboring villages. Smaller circles indicate a low cost of connectivity, meaning they are more connected. Larger circles denote a higher cost of connectivity, meaning they have poor physical connectivity. Each circle represents a village.

covariance-based SEMs (CBSEMs) (Dijkstra, 2010; Reinartz et al., 2009), allows situations where the manifest variables cause changes in latent variables, as opposed to strictly being reflective indicators in CBSEMs. Confidence intervals for parameter estimates are obtained empirically through bootstrapping techniques.

The latent constructs hypothesized in this SEM model revolve around three primary domains: (1) On-farm resources: This construct encompasses variables related to agricultural production and resources derived directly from farming activities. It includes factors such as crop yields and livestock production and how these contribute to household food security. (2) Off-farm resources: This construct captures the contribution of income and resources from non-farm activities to food security. Variables such as income diversity, market orientation (selling surplus produce), and off-farm employment opportunities fall under this category. (3) Socioeconomic well-being: This construct reflects the broader socioeconomic context of households, incorporating factors like wealth accumulation, asset ownership (physical and non-physical), health status, and overall economic stability. Variables such as the SES Index, health indicators, and unpaid debts are integral to this construct.

The EFA phase of the SEM involved exploring the underlying structure of the data to identify the latent variables (LVs) that best represent these constructs. EFA is an empirical technique based on factor analysis that identifies patterns and relationships

among observed variables without specifying *a priori* hypotheses about the structure of latent variables. All collected variables related to food security, socioeconomic status, agricultural production, and livelihoods were initially subjected to EFA. This allowed us to uncover underlying factors (latent constructs) that best explain the covariance among observed variables. The EFA allowed us to group survey variables into the four larger constructs forming the "on-farm resources," "off-farm resources," "socioeconomic status," and "health and nutrition" LVs. We formalize the structure of the PLS Path model as proxies defining semi-subsistence agricultural activity, livelihoods, and exogenous assets, with change in land cover and land use comprising an additional latent variable. The initial model was fitted with the full data for all districts. Subsequently, the median factor scores of food insecurity, the outcome variable, were used to divide the villages into "less food secure" and "more food secure" groups and then compared using the same structural model. Finally, each district (considered a group) was compared with a second group comprising all other districts.

1.6 RESULTS

1.6.1 Socioeconomics

Household food insecurity (HFIAS, Figure 1.2) exhibits the lowest values in Satna, followed by Panna. Tehri Garhwal displays the highest range and the maximum score found among the four districts. The most severe food insecurity occurs in remote high-altitude areas, aligning with other positively correlated food security indicators, such as low market orientation. Udaipur demonstrates the most homogeneous spatial distribution of food-insecure villages. Surface soil moisture (Figure 1.5) is lowest in Udaipur, a semi-arid district located in the west, and highest in Tehri Garhwal, which experiences year-long precipitation and has a dense network of rivers and streams. Despite this, Tehri Garhwal has the least connected villages due to its high altitude, poor network of motorable roads, and sparsely situated villages. This results in the village suffering from the highest connectivity costs—more than twice the maximum cost in all other districts (Figure 1.6). In contrast, villages in Panna, Satna, and Udaipur are better connected, with shorter distances to travel as terrain slope is not a significant issue. However, exceptions include villages around hilly or forested areas in Panna and Satna's northern and southern parts and the western part of Udaipur, where roads are less dense and of poor quality.

1.6.2 Land Use Land Cover Change

Land cover and land use changes in this study are comparable to those in a similar study by Meiyappan et al. (2017) for India, which used the same definitions for change classes but differed in the years of change detection (1985–1995 and 1995–2005). In Panna and Satna, croplands remained stable, while Udaipur experienced a conversion of cropland to shrubland. The LCLUC maps for all districts (Figure 1.3) from 2001, 2011, and 2018 indicate that Panna and Satna are predominantly characterized by crop/fallow land. In contrast, Tehri Garhwal is primarily forested, particularly in the high-altitude regions in the northeastern part of the district. Udaipur is mainly

TABLE 1.1
Percent Land Cover Class within Each District for 2001 and 2018

	Panna 2001	Panna 2018	Satna 2001	Satna 2018	Tehri 2001	Tehri 2018	Udaipur 2001	Udaipur 2018
Forest	7.2	6.5	6.2	6.4	44.7	45.1	11.8	17.9
Crop & Fallow Land	47.6	45.2	61.1	57.9	15.3	14.9	24.9	27.9
Built-up Land	0.3	0.3	1.1	0.8	0.5	0.4	0.8	0.9
Shrubland	42.4	44.9	29.2	30.6	23.5	22.6	20.4	29.4
Barren & Wasteland	1.9	2.4	1.4	1.7	2.9	2.9	41.7	22.7
Water Bodies	0.6	0.7	0.9	2.6	0.2	0.9	0.4	1.2
Grassland	0	0.1	0	0.1	10.6	11	0	0

covered by shrubland and barren/wasteland, with forest patches in some clusters and crop/fallow land interspersed among the dominant classes, except in the northeast and southeast. Completing the Tehri dam in Tehri Garhwal and the Bansagar dam in Satna district accounts for the distinct increase in water area (dam reservoirs) in both districts. The overall land cover changes in each district (Table 1.1) reveal some loss of forests and crop/fallow land, with gains in shrubland and barren/wasteland in Panna, Satna, and Tehri Garhwal. Udaipur saw an increase in all land cover classes except barren/wasteland. Built-up areas remained nearly constant across all districts. The transition probability matrix (Table 1.2) indicates that forests and crop/fallow land were most likely converted to shrubland in Panna, Satna, and Tehri Garhwal. In Udaipur, barren/wasteland had the highest probability of conversion to shrubland.

1.7 THE PATH MODEL

Results from the factor analysis of the household survey formed the foundation for establishing the model structure to identify causal linkages between food security indicators. Five latent variables (LVs) were identified: assets, land cover land use change (LCLUC), availability (of food and on-farm resources), Lack of off-farm returns, and food insecurity. The PLS-PM model achieved an overall goodness-of-fit of 0.50. Moran's *I* test indicated no significant spatial autocorrelation in the LVs and their residuals, $p>0.05$ for all LVs. Measures of unidimensionality (Table 1.3A) showed that most LVs approached the accepted value of Cronbach's alpha (>=0.7), except for assets, and exceeded the accepted value (>=0.7) for Dillon-Goldstein's rho. The estimated coefficients and their bootstrapped mean, standard deviation, and 95% confidence interval, are presented in Table 1.4. Significant effects were observed for all paths except for LCLUC to availability, LCLUC to low off-farm returns, LCLUC to food insecurity, and availability to food insecurity.

The path model, including LVs and coefficients, is illustrated in Figure 1.7. Food insecurity increases with a lack of assets and low returns from off-farm sources but

TABLE 1.2
Transition Probability Matrix Derived from Land Cover Changes from 2001 (Rows) to 2018 (Columns), an 18-year Period

		2018						
	PANNA	**Forest**	**Crop & Fallow Land**	**Built-up Land**	**Shrub-land**	**Barren & Waste Land**	**Water Bodies**	**Grass-land**
2001	Forest	0.985	0.001	0.000	0.012	0.000	0.001	0.000
	Crop & Fallow Land	0.008	0.846	0.002	0.067	0.058	0.018	0.000
	Built-up Land	0.010	0.051	0.761	0.117	0.051	0.010	0.000
	Shrubland	0.234	0.027	0.001	0.722	0.012	0.003	0.000
	Barren & Waste Land	0.026	0.156	0.006	0.302	0.504	0.006	0.000
	Water Bodies	0.003	0.018	0.001	0.004	0.001	0.973	0.000
	Grassland	0.000	0.000	0.000	0.000	0.000	0.000	1.000
	SATNA	**Forest**	**Crop & Fallow Land**	**Built-up Land**	**Shrub-land**	**Barren & Waste Land**	**Water Bodies**	**Grass-land**
	Forest	0.000	0.009	0.000	0.144	0.000	0.002	0.000
	Crop & Fallow Land	0.000	0.918	0.000	0.048	0.011	0.022	0.001
	Built-up Land	0.001	0.102	0.723	0.162	0.005	0.007	0.001
	Shrubland	0.036	0.052	0.000	0.890	0.009	0.012	0.000
	Barren & Waste Land	0.000	0.152	0.001	0.315	0.501	0.029	0.002
	Water Bodies	0.003	0.062	0.000	0.021	0.003	0.909	0.001
	Grassland	0.003	0.214	0.000	0.31	0.035	0.044	0.395
	TEHRI	**Forest**	**Crop & Fallow Land**	**Built-up Land**	**Shrub-land**	**Barren & Waste Land**	**Water Bodies**	**Grass-land**
	Forest	0.98	0.001	0.000	0.011	0.000	0.002	0.006
	Crop & Fallow Land	0.004	0.956	0.002	0.012	0.001	0.01	0.016
	Built-up Land	0.001	0.027	0.715	0.054	0.004	0.161	0.038
	Shrubland	0.032	0.005	0.001	0.915	0.004	0.005	0.039
	Barren & Waste Land	0.000	0.002	0.000	0.013	0.959	0.006	0.015
	Water Bodies	0.002	0.006	0.006	0.023	0.014	0.932	0.016
	Grassland	0.036	0.008	0.001	0.029	0.004	0.023	0.899
	Snow & Ice	0.000	0.000	0.000	0.001	0.004	0.001	0.000
	UDAIPUR	**Forest**	**Crop & Fallow Land**	**Built-up Land**	**Shrub-land**	**Barren & Waste Land**	**Water Bodies**	**Grass-land**
	Forest	0.985	0.001	0.000	0.012	0.000	0.001	0.000
	Crop & Fallow Land	0.008	0.846	0.002	0.067	0.058	0.018	0.000
	Built-up Land	0.01	0.051	0.761	0.117	0.051	0.01	0.000
	Shrubland	0.234	0.027	0.001	0.722	0.012	0.003	0.000
	Barren & Waste Land	0.026	0.156	0.006	0.302	0.504	0.006	0.000
	Water Bodies	0.003	0.018	0.001	0.004	0.001	0.973	0.000
	Grassland	0.000	0.000	0.000	0.000	0.000	0.000	1.000

TABLE 1.3
Measures of Unidimensionality of the PLS-PM Analysis. All Indicators are Reflective (Mode-A) Meaning Manifest Variables are Caused by Their Latent Variable. MVs Indicate the Number of Manifest Variables Measuring Each Latent Variable

A. FULL MODEL	Mode	MVs	C.alpha	DG.rho	eig.1st	eig.2nd
Assets	A	6	0.390	0.612	3.18	1.647
LCLUC	A	5	0.626	0.769	2.10	1.405
Availability	A	6	0.661	0.782	3.04	1.411
Low Off-Farm Returns	A	3	0.675	0.822	1.82	0.672
Food Insecurity	A	2	0.883	0.945	1.79	0.209
B. LESS FS	**Mode**	**MVs**	**C.alpha**	**DG.rho**	**eig.1st**	**eig.2nd**
Assets	A	6	0.138	0.559	3.20	1.198
LCLUC	A	5	0.593	0.753	2.04	1.427
Availability	A	6	0.306	0.516	1.71	1.287
Low Off-Farm Returns	A	3	0.746	0.858	2.02	0.735
Food Insecurity	A	2	0.621	0.841	1.45	0.549
C. MORE FS	**Mode**	**MVs**	**C.alpha**	**DG.rho**	**eig.1st**	**eig.2nd**
Assets	A	6	0.000	0.0448	3.82	1.047
LCLUC	A	5	0.412	0.6594	1.69	1.242
Availability	A	6	0.564	0.8567	4.29	0.822
Low Off-Farm Returns	A	3	0.375	0.6739	1.47	1.129
Food Insecurity	A	2	0.472	0.7913	1.31	0.691

decreases slightly with increased food availability. Changes in land cover and land use negatively impact farming while positively correlating with food insecurity. The model considered land cover and land use change as detrimental to food security, associating it with the loss of forests, cropland, and water bodies and the gain of scrubland and barren/wasteland. The outer model with weights and loadings of each manifest variable to their LV is detailed in Table 1.5. Wealth (or its absence) explained the maximum variability of assets, and increases in barren land explained the maximum variability of LCLUC. The manifest variables of the other LVs had comparatively evenly distributed loadings. Indicators related to expenditure, income, and non-farm activities had greater explanatory power than farming ones. Satna had the lowest incidence of food-insecure villages, while Udaipur had the highest.

Villages were divided into two groups based on the median factor scores for the food insecurity LV: more FS (below median=more food secure) and less FS (above median=less food safe). The goodness-of-fit was 0.38 for both groups (Table 1.6), and measures of unidimensionality (Table 1.3B, 1.3C) showed acceptable values for Dillon-Goldstein's rho, except for the assets LV. Path coefficients derived from bootstrapping showed opposite directions between most LVs but were significant only for the effect of availability on both food insecurity and no off-farm returns. Among the

TABLE 1.4
Path Coefficients for the PLS-PM Model with Bootstrapped Mean Obtained after 500 Iterations

From	To	Original	Mean	SD	2.5 Percentile	97.5 Percentile
*Assets	LCLUC	0.67	0.67	0.05	0.56	0.75
*Assets	Availability	–0.79	–0.79	0.03	–0.85	–0.74
*Assets	Low Off-Farm Returns	0.74	0.74	0.05	0.63	0.81
*Assets	Food Insecurity	0.76	0.75	0.02	0.72	0.80
LCLUC	Availability	–0.05	–0.07	0.07	–0.24	0.04
LCLUC	Low Off-Farm Returns	0.04	0.06	0.07	–0.06	0.23
LCLUC	Food Insecurity	0.03	0.04	0.05	–0.07	0.13
*Availability	Low Off-Farm Returns	–0.55	–0.55	0.07	–0.68	–0.40
Availability	Food Insecurity	–0.22	–0.23	0.16	–0.53	0.05
*Low Off-Farm Returns	Food Insecurity	0.24	0.25	0.07	0.11	0.39

* Indicates paths with significant effects.

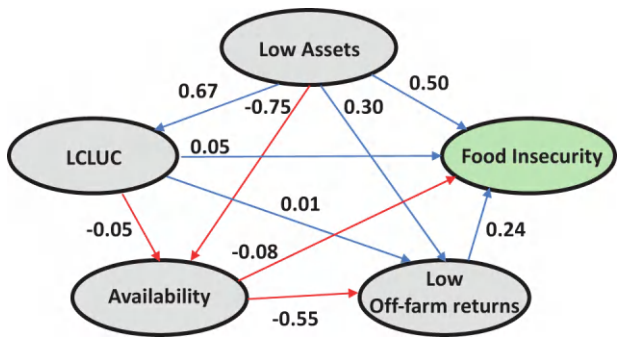

FIGURE 1.7 Path diagram of the PLS-PM outer model showing coefficients and their direction. Inverse relations are shown in red lines.

group models, the comparison of Panna with other districts had the best goodness-of-fit for both groups (Table 1.6). Path coefficients had the same directionality for most LVs in the Panna and Satna groups (Table 1.7). The effect of LCLUC on other LVs was insignificant for any district, while availability had a significant but small effect.

1.8 DISCUSSION

The primary goal of this study was to examine the causal relationships between socioeconomic factors and land cover/land use changes (LCLUC) on food security at the village level in India. The districts selected for this study are predominantly

TABLE 1.5
Manifest Variables Reflected by Respective LVs for the PLS-PM. Loadings are Correlations Between LVs and its Indicators (>0.7 Acceptable), Communality Explains the Amount of Variability Explained by a LV. Communality is Squared Loading and Higher is Better

	Weight	Loading	Communality	Redundancy
Assets				
Land holding	0.09	0.27	0.07	0
Livestock ownership (TLU)	0.41	0.82	0.67	0
Low wealth (SES Index)	0.61	0.92	0.84	0
Low education (Literacy)	0.17	0.41	0.17	0
Aridity (SSM)	-0.01	0.08	0.01	0
Low connectivity (Connectivity cost)	0.12	0.09	0.01	0
LCLUC				
2001.2018_forest	0.44	0.67	0.45	0.20
2001.2018_crop	0.14	0.42	0.18	0.08
2001.2018_scrub	0.29	0.66	0.44	0.19
2001.2018_barren	0.48	0.95	0.90	0.40
2001.2018_water	-0.02	0.08	0.01	0.00
Availability				
Low crop diversity (#crops grown)	-0.01	0.26	0.07	0.04
Pot. food availability (PFA)	0.24	0.57	0.33	0.21
Dietary diversity (HDDS)	0.40	0.36	0.13	0.08
Food sourced from own farm	0.17	0.54	0.29	0.18
Low food expenditure (of total income)	0.40	0.81	0.66	0.41
Seeds bought from market	0.39	0.78	0.61	0.38
Low Off-Farm Returns				
Low market orientation	0.49	0.81	0.65	0.43
Proximity to town (in kms)	0.30	0.73	0.54	0.36
Low proportion of HH income from on-farm	0.49	0.78	0.61	0.41
Food Insecurity				
# Month food shortage	0.54	0.95	0.90	0.55
HFIAS	0.51	0.94	0.89	0.54

TABLE 1.6
Goodness-of-Fit of Models Comparing Two Groups. Group Model 1 was Grouped Based on the Median of Food Insecurity Coefficients Computed in the Full Model

Group Model 1	less FS	0.38	more FS	0.38
Group Model 2	Panna	0.58	Others	0.53
Group Model 3	Satna	0.30	Others	0.51
Group Model 4	Tehri	0.48	Others	0.64
Group Model 5	Udaipur	0.38	Others	0.57

TABLE 1.7
Path Coefficient Results from the District Group Models After Bootstrapping. For Each Pair of LVs, + Indicates the Same Directionality for Both Groups and – Indicates Reverse Directions. Assets Should be Read as Lack of Assets. * Indicates Significant Relations

Relationship	Udaipur-Others	Tehri-Others	Panna-Others	Satna-Others
Assets -> LCLUC	+	+	–	-*
Assets -> Availability	–	+	+	+*
Assets -> Low Off-Farm Returns	–*	+*	+	+
Assets -> Food Insecurity	–	–	–	–
LCLUC -> Availability	–	–	–	–
LCLUC -> Low Off-Farm Returns	+	–	–	–
LCLUC -> Food Insecurity	+	–	-*	–
Availability -> Low Off-Farm Returns	+	-*	–	+
Availability -> Food Insecurity	–*	-*	+	+
Low Off-Farm Returns -> Food Insecurity	+*	–	–*	–*

agricultural, with a high proportion of smallholder farmers. Despite differences in environmental and socioeconomic conditions, these districts perform similarly on human development indices like the Sustainable Development Goal 2 (SDG2) related to hunger, which has remained low and unchanged over time (NITI Aayog, 2021). While these indices typically drive policy decisions at regional and national scales, our study highlights significant local variability in the effects of food security drivers on smallholder farmers.

The Household Food Insecurity Access Scale (HFIAS) is an experience-based survey that captures food availability, accessibility, and adequacy at the household level (Piaskoski et al., 2020). It is a globally accepted indicator that allows for cross-time and space comparisons and can identify the most vulnerable sub-populations and the different dimensions of food security. This is crucial for capturing local variability, as food security experiences may differ significantly even when broad drivers exist. Food security issues can arise in rural households even when food is available on farms due to factors like high costs, lack of market access, and non-nutritious food availability. In our study, Satna was the most food-secure district on average, while Udaipur was the least. Tehri Garhwal had households with the highest food insecurity scores, particularly in remote, high-altitude areas, comparable to similar high scores in the Lumle region of Nepal (Pandey & Bardsley, 2019). As a comparison, Udaipur's district-level mean HFIAS of 4.2 is similar to scores in urban Ouagadougou, Burkina Faso (Becquey et al., 2010; Jacob et al., 2018).

On-farm resources, including land ownership and food from farms, had minimal effects on food security compared to asset ownership and off-farm returns. This finding aligns with other studies that highlight the vulnerability of subsistence

farmers to food insecurity (Allee et al., 2021; Arnalte-Mur et al., 2020; Marchetti & Secondi, 2017; Mondal et al., 2021). The variability introduced by external factors like climate change and labor shortages can further amplify food availability issues (Davis et al., 2021). Thus, food availability has a small but significant effect on food security, particularly for households near the threshold of food insecurity. Off-farm resources, including market-oriented agricultural production and diverse sources of off-farm income, have a more substantial and significant effect on food security. These resources provide necessary purchasing power for other household needs like education and healthcare and ensure food availability, as smallholder farmers typically do not produce enough food year-round (Hammond et al., 2017). However, high dietary diversity without adequate off-farm returns does not guarantee food security, challenging the notion that crop diversity leads to better food security (Singh et al., 2020; Zsögön et al., 2022). Seasonal fluctuations in crop production and dietary diversity often prevent year-round food security (Mondal et al., 2021).

Asset ownership had the most potent effect on food security and other factors. The SES Index (wealth) had a strong positive correlation with nutrition and food security (Hong et al., 2006; Lopez-Ridaura et al., 2018; Mutisya et al., 2015). Unlike off-farm returns, assets provide a buffer during economic distress, supporting food security across all districts. Landholding, while necessary for agricultural production, had a lower impact on food security in this study, which measured the size of owned land rather than access and tenure rights (Goli et al., 2021; Holden, 2020; Mutea et al., 2019). High crop diversity, although a sustainable practice, indicated low food security and small landholdings in the study districts. Overexploitation due to intensive farming can reduce on-farm income, suggesting the need for land aggregation and incentives for conserving agrobiodiversity (James et al., 2001).

LCLUC had a modest effect on food security in our model, reflecting the limited change captured from Landsat imagery in the study areas. Changes from cropland to scrub and wasteland were associated with food security loss, while stable cropland was linked to gains (Agidew & Singh, 2017; Galeana-Pizaña et al., 2021). Socioeconomic factors also drive LCLUC, affecting food security through environmental impacts like soil degradation and biodiversity loss (Mora et al., 2020; Smith et al., 2016; Tubiello et al., 2015). Our study's findings highlight the complex pathways of food insecurity and the need for localized analyses. Wealth consistently correlates with food security, and households with off-farm income are more food secure. On-farm resources had less obvious linkages to food security, emphasizing the importance of market orientation and physical market access. Literacy, typically associated with better food security, had a weaker effect in our study, likely due to geographical constraints in regions like Tehri Garhwal. Future studies should include additional indicators like land tenure and social caste to improve model predictions. Understanding the effects of policies and external factors like food prices and agricultural labor availability is also crucial. Despite its limitations, our model demonstrated the feasibility of simultaneously assessing household food insecurity drivers using multiple socioeconomic and environmental indicators.

1.9 CONCLUSION

Food security is a complex issue influenced by many interacting indicators across various scales, posing challenges in identifying comprehensive causal linkages. Regional and local studies often focus on specific facets of food security to inform targeted policy interventions, potentially overlooking local variability to maximize broader impacts. This study addresses these complexities by modeling key food security indicators for smallholder farmers, incorporating spatial factors within a structural equation model to unravel causal relationships. Using a partial least squares path modeling (PLS-PM) approach, this study estimated the magnitude and direction of factors influencing food security. The findings underscored wealth and livelihood diversity as pivotal factors distinguishing food-secure households from food-insecure ones. While on-farm resources play a significant role for subsistence farmers regarding food and other essential resources, their contribution alone is insufficient to improve food security levels substantially.

The study highlights the importance of off-farm income and asset ownership in bolstering food security among smallholder farmers, aligning with broader trends observed in similar contexts globally. It emphasizes the need for policies and interventions that enhance market access, diversify income sources, and build asset ownership among rural households to foster sustainable food security outcomes. Furthermore, including spatial indicators in the modeling framework enriches our understanding of how geographical factors influence food security dynamics locally. This nuanced approach acknowledges the diverse contexts within which food security operates, ensuring that interventions are tailored to local realities rather than adopting one-size-fits-all approaches.

In conclusion, while on-farm resources remain crucial for subsistence farming communities, addressing food security comprehensively requires leveraging broader socioeconomic factors, such as wealth accumulation and livelihood diversification. Future research and policy efforts should continue to refine these insights, considering local variations and incorporating spatial dynamics to mitigate food insecurity among smallholder farmers effectively.

REFERENCES

Abbade, E. B., & Dewes, H. (2015). Food insecurity worldwide derived from food supply patterns. *Food Security*, *7*(1), 109–120. https://doi.org/10.1007/s12571-014-0405-x

Abolafia-Rosenzweig, R., Livneh, B., Small, E. E., & Kumar, S. V. (2019). Soil moisture data assimilation to estimate irrigation water use. *Journal of Advances in Modeling Earth Systems*, *11*(11), 3670–3690. https://doi.org/10.1029/2019MS001797

Agidew, A. A., & Singh, K. N. (2017). The implications of land use and land cover changes for rural household food insecurity in the Northeastern highlands of Ethiopia: The case of the Teleyayen sub-watershed. *Agriculture & Food Security*, *6*(1), 56. https://doi.org/10.1186/s40066-017-0134-4

Allee, A., Lynd, L. R., & Vaze, V. (2021). Cross-national analysis of food security drivers: Comparing results based on the Food Insecurity Experience Scale and Global Food Security Index. *Food Security*, *13*(5), 1245–1261. https://doi.org/10.1007/s12571-021-01156-w

Alwin, D. F., & Hauser, R. M. (1975). The decomposition of effects in path analysis. *American Sociological Review*, *40*(1), 37. https://doi.org/10.2307/2094445

Ambrosone, M., Matese, A., Di Gennaro, S. F., Gioli, B., Tudoroiu, M., Genesio, L., Miglietta, F., Baronti, S., Maienza, A., Ungaro, F., & Toscano, P. (2020). Retrieving soil moisture

in rainfed and irrigated fields using Sentinel-2 observations and a modified OPTRAM approach. *International Journal of Applied Earth Observation and Geoinformation*, *89*, 102113. https://doi.org/10.1016/j.jag.2020.102113

Arnalte-Mur, L., Ortiz-Miranda, D., Cerrada-Serra, P., Martinez-Gómez, V., Moreno-Pérez, O., Barbu, R., Bjorkhaug, H., Czekaj, M., Duckett, D., Galli, F., Goussios, G., Grivins, M., Hernández, P. A., Prosperi, P., & Šūmane, S. (2020). The drivers of change for the contribution of small farms to regional food security in Europe. *Global Food Security*, *26*, 100395. https://doi.org/10.1016/j.gfs.2020.100395

Becquey, E., Martin-Prevel, Y., Traissac, P., Dembélé, B., Bambara, A., & Delpeuch, F. (2010). The household food insecurity access scale and an index-member dietary diversity score contribute valid and complementary information on household food insecurity in an Urban West-African setting. *Journal of Nutrition*, *140*(12), 2233–2240. https://doi.org/10.3945/jn.110.125716

Bhushan C., Srinidhi A., Kumar V., Singh G. (2015). *Lived Anomaly: How to enable farmers in India cope with extreme weather events*. Centre for Science and Environment, New Delhi, India. pp. 1–72.

Brown, T. A., & Moore, M. T. (2012). Confirmatory factor analysis. In R. H. Hoyle (Ed.), *Handbook of Structural Equation Modeling* (pp. 361–379). The Guilford Press, New York, USA.

Coates, J., Swindale, A., & Bilinsky, P. (2007). *Household Food Insecurity Access Scale (HFIAS) for Measurement of Food Access: Indicator Guide: Version 3: (576842013-001)* [Data set]. American Psychological Association. https://doi.org/10.1037/e576842013-001

Das, N. N., Entekhabi, D., Dunbar, R. S., Chaubell, M. J., Colliander, A., Yueh, S., Jagdhuber, T., Chen, F., Crow, W., O'Neill, P. E., Walker, J. P., Berg, A., Bosch, D. D., Caldwell, T., Cosh, M. H., Collins, C. H., Lopez-Baeza, E., & Thibeault, M. (2019). The SMAP and Copernicus Sentinel 1A/B microwave active-passive high resolution surface soil moisture product. *Remote Sensing of Environment*, *233*, 111380. https://doi.org/10.1016/j.rse.2019.111380

Davis, K. F., Downs, S., & Gephart, J. A. (2021). Towards food supply chain resilience to environmental shocks. *Nature Food*, 2(1), 54–65. https://doi.org/10.1038/s43016-020-00196-3

Deshmukh, M. S., & Vyavahare, S. S. (2018). An analysis of consumption expenditure in India. *European Academic Research*, *5*(10), 5270–5285. www.academia.edu/36668718/An_Analysis_of_Consumption_Expenditure_in_India

Dijkstra, T. K. (2010). Latent variables and indices: Herman Wold's basic design and partial least squares. In V. Esposito Vinzi, W. W. Chin, J. Henseler, & H. Wang (Eds.), *Handbook of Partial Least Squares: Concepts, Methods and Applications* (pp. 23–46). Springer. https://doi.org/10.1007/978-3-540-32827-8_2

FAO, IFAD, UNICEF, WFP, & WHO. (2020). *The State of Food Security and Nutrition in the World 2020*. FAO, IFAD, UNICEF, WFP and WHO. https://doi.org/10.4060/ca9692en

Galeana-Pizaña, J. M., Couturier, S., Figueroa, D., & Jiménez, A. D. (2021). Is rural food security primarily associated with smallholder agriculture or with commercial agriculture?: An approach to the case of Mexico using structural equation modeling. *Agricultural Systems*, *190*, 103091. https://doi.org/10.1016/j.agsy.2021.103091

Ghosh, P. P. (2011). Interstate disparity in India and development strategies for backward states. In S. Hirashima, H. Oda, & Y. Tsujita (Eds.), *Inclusiveness in India: A Strategy for Growth and Equality* (pp. 270–295). Palgrave Macmillan UK. https://doi.org/10.1057/9780230304956_10

GOI. (2016). Agricultural Statistics at a Glance 2016. GOI. https://eands.dacnet.nic.in/PDF/Glance-2016.pdf

Goli, S., Rammohan, A., & Reddy, S. P. (2021). The interaction of household agricultural landholding and Caste on food security in rural Uttar Pradesh, India. *Food Security*, *13*(1), 219–237. https://doi.org/10.1007/s12571-020-01109-9

Gong, X. (2020). *Gooong/LeastCostPath* [Python]. https://github.com/Gooong/LeastCostPath (Original work published 2018).

Gowen, K. M., & de Smet, T. S. (2020). Testing least cost path (LCP) models for travel time and kilocalorie expenditure: Implications for landscape genomics. *PLOS ONE*, *15*(9), e0239387. https://doi.org/10.1371/journal.pone.0239387

Hammond, J., Fraval, S., van Etten, J., Suchini, J. G., Mercado, L., Pagella, T., Frelat, R., Lannerstad, M., Douxchamps, S., Teufel, N., Valbuena, D., & van Wijk, M. T. (2017). The Rural Household Multi-Indicator Survey (RHoMIS) for rapid characterisation of households to inform climate smart agriculture interventions: Description and applications in East Africa and Central America. *Agricultural Systems*, *151*, 225–233. https://doi.org/10.1016/j.agsy.2016.05.003

Hertel, T. W. (2015). The challenges of sustainably feeding a growing planet. *Food Security*, *7*(2), 185–198. https://doi.org/10.1007/s12571-015-0440-2

Holden, S. T. (2020). Policies for improved food security: The roles of land tenure policies and land markets. In S. Gomez y Paloma, L. Riesgo, & K. Louhichi (Eds.), *The Role of Smallholder Farms in Food and Nutrition Security* (pp. 153–169). Springer International Publishing. https://doi.org/10.1007/978-3-030-42148-9_8

Holland, P. W. (1988). Causal inference, path analysis, and recursive structural equations models. *Sociological Methodology*, *18*, 449–484. https://doi.org/10.2307/271055

Hong, R., Banta, J. E., & Betancourt, J. A. (2006). Relationship between household wealth inequality and chronic childhood under-nutrition in Bangladesh. *International Journal for Equity in Health*, *5*(1), 15. https://doi.org/10.1186/1475-9276-5-15

ISGCM/Survey of India. (2016). Roads, Global Map of India. Stanford Digital Repository. https://purl.stanford.edu/qf525mn4696

Jacob, A. M., Rajaram, D., Manjunath, B., & Kunnavil, R. (2018). Assessment of food insecurity and its correlates in a rural community of Karnataka: A case study. *International Journal Of Community Medicine And Public Health*, *5*(11), 4896–4900. https://doi.org/10.18203/2394-6040.ijcmph20184591

Jahnke, H. E., Tacher, G., Kiel, P., & Rojat, D. (1988). Livestock production in tropical Africa, with special reference to the tsetse-affected zone. Proceedings of a *M*eeting *H*eld in Nairobi, 23-27 November 1987. ILCA/International Laboratory for Research on Animal Diseases (ILRAD).

Jain, M., Mondal, P., DeFries, R. S., Small, C., & Galford, G. L. (2013). Mapping cropping intensity of smallholder farms: A comparison of methods using multiple sensors. *Remote Sensing of Environment*, *134*, 210–223. https://doi.org/10.1016/j.rse.2013.02.029

James, A., Gaston, K. J., & Balmford, A. (2001). Can we afford to conserve biodiversity? *BioScience*, *51*(1), 43–52. https://doi.org/10.1641/0006-3568(2001)051[0043:CWATCB]2.0.CO;2

Jarvis, A., Reuter, H., Nelson, A., & Guevara, E. (2008). *Hole-filled seamless SRTM data V4. Tech. Rep., International Centre for Tropical Agriculture (CIAT). Available from* http://srtm.csi.cgiar.org. http://srtm.csi.cgiar.org

Jones, A. D., Shrinivas, A., & Bezner-Kerr, R. (2014). Farm production diversity is associated with greater household dietary diversity in Malawi: Findings from nationally representative data. *Food Policy*, *46*, 1–12. https://doi.org/10.1016/j.foodpol.2014.02.001

Lamb, E. G., Mengersen, K. L., Stewart, K. J., Attanayake, U., & Siciliano, S. D. (2014). Spatially explicit structural equation modeling. *Ecology*, *95*(9), 2434–2442. https://doi.org/10.1890/13-1997.1

Lopez-Ridaura, S., Frelat, R., van Wijk, M. T., Valbuena, D., Krupnik, T. J., & Jat, M. L. (2018). Climate smart agriculture, farm household typologies and food security. *Agricultural Systems*, *159*, 57–68. https://doi.org/10.1016/j.agsy.2017.09.007

Marchetti, S., & Secondi, L. (2017). Estimates of household consumption expenditure at provincial level in Italy by using small area estimation methods: "Real" comparisons using purchasing power parities. *Social Indicators Research*, *131*(1), 215–234. https://doi.org/10.1007/s11205-016-1230-8

Meiyappan, P., Roy, P. S., Sharma, Y., Ramachandran, R. M., Joshi, P. K., DeFries, R. S., & Jain, A. K. (2017). Dynamics and determinants of land change in India: Integrating satellite data with village socioeconomics. *Regional Environmental Change*, *17*(3), 753–766. https://doi.org/10.1007/s10113-016-1068-2

Memon, J. A., & El Bilali, H. (2019). Rural infrastructure and food security. In W. Leal Filho, A. M. Azul, L. Brandli, P. G. Özuyar, & T. Wall (Eds.), *Zero Hunger* (pp. 1–10). Springer International Publishing. https://doi.org/10.1007/978-3-319-69626-3_44-1

Mondal, P., DeFries, R., Clark, J., Flowerhill, N., Arif, Md., Harou, A., Downs, S., & Fanzo, J. (2021). Multiple cropping alone does not improve year-round food security among smallholders in rural India. *Environmental Research Letters*, *16*(6), 065017. https://doi.org/10.1088/1748-9326/ac05ee

Mora, O., Le Mouël, C., de Lattre-Gasquet, M., Donnars, C., Dumas, P., Réchauchère, O., Brunelle, T., Manceron, S., Marajo-Petitzon, E., Moreau, C., Barzman, M., Forslund, A., & Marty, P. (2020). Exploring the future of land use and food security: A new set of global scenarios. *PLOS ONE*, *15*(7), e0235597. https://doi.org/10.1371/journal.pone.0235597

MOSPI. (2025). https://mospi.gov.in/statistical-year-book-india/2013/171

Mutea, E., Bottazzi, P., Jacobi, J., Kiteme, B., Speranza, C. I., & Rist, S. (2019). Livelihoods and Food Security Among Rural Households in the North-Western Mount Kenya Region. *Frontiers in Sustainable Food Systems*, *3*, 98. https://doi.org/10.3389/fsufs.2019.00098

Mutisya, M., Kandala, N., Ngware, M. W., & Kabiru, C. W. (2015). Household food (in)-security and nutritional status of urban poor children aged 6 to 23 months in Kenya. *BMC Public Health*, *15*(1), 1052. https://doi.org/10.1186/s12889-015-2403-0

NITI Aayog. (2021). *SDG India Index and Dashboard 2020-21*. NITI Aayog, Govt. of India. https://sdgindiaindex.niti.gov.in/assets/Files/SDG3.0_Final_04.03.2021_Web_Spreads.pdf

Pandey, R., & Bardsley, D. K. (2019). An application of the Household Food Insecurity Access Scale to assess food security in rural communities of Nepal. *Asia & the Pacific Policy Studies*, *6*(2), 130–150. https://doi.org/10.1002/app5.270

Piaskoski, A., Reilly, K., & Gilliland, J. (2020). A conceptual model of rural household food insecurity: A qualitative systematic review and content analysis. *Family & Community Health*, *43*(4), 296–312. https://doi.org/10.1097/FCH.0000000000000273

Rathor, I. S., & Premi, M. K. (1986). Poverty, development and patterns of rural male outmigration in Uttar Pradesh. *Population Geography: A Journal of the Association of Population Geographers of India*, *8*(1–2), 27–37.

Reinartz, W., Haenlein, M., & Henseler, J. (2009). An empirical comparison of the efficacy of covariance-based and variance-based SEM. *International Journal of Research in Marketing*, *26*(4), 332–344. https://doi.org/10.1016/j.ijresmar.2009.08.001

Roy, P. S., Meiyappan, P., Joshi, P. K., Kale, M. P., Srivastav, V. K., Srivasatava, S. K., Behera, M. D., Roy, A., Sharma, Y., Ramachandran, R. M., Bhavani, P., Jain, A. K., & Krishnamurthy, Y. V. N. (2016). Decadal land use and land cover classifications across India, 1985, 1995, 2005. *ORNL DAAC*. https://doi.org/10.3334/ORNLDAAC/1336

Sahu, S. K., Kumar, S. G., Bhat, B. V., Premarajan, K. C., Sarkar, S., Roy, G., & Joseph, N. (2015). Malnutrition among under-five children in India and strategies for control. *Journal of Natural Science, Biology, and Medicine*, *6*(1), 18–23. https://doi.org/10.4103/0976-9668.149072

Sanchez, G. (2013). *PLS_Path_Modeling_with_R*. https://www.gastonsanchez.com/PLS_Path_Modeling_with_R.pdf

Saxena, N. C. (2018). Hunger, under-nutrition and food security in India. In A. K. Mehta, S. Bhide, A. Kumar, & A. Shah (Eds.), *Poverty, Chronic Poverty and Poverty Dynamics: Policy Imperatives* (pp. 55–92). Springer. https://doi.org/10.1007/978-981-13-0677-8_4

Sen, A., 1981. Ingredients of famine analysis: availability and entitlements. *Quarterly Journal of Economics*, *96*(3), 433–464.

Singh, R. B., Kumar, P., & Woodhead, T. (2002). *Smallholder Farmers in India: Food Security and Agricultural Policy* (RAP Publication: 2002/03; p. 63). FAO Regional Office for Asia and the Pacific. www.fao.org/3/ac484e/ac484e00.htm#Contents

Singh, S., Jones, A. D., DeFries, R. S., & Jain, M. (2020). The association between crop and income diversity and farmer intra-household dietary diversity in India. *Food Security*, *12*(2), 369–390. https://doi.org/10.1007/s12571-020-01012-3

Smith, P., House, J. I., Bustamante, M., Sobocká, J., Harper, R., Pan, G., West, P. C., Clark, J. M., Adhya, T., Rumpel, C., Paustian, K., Kuikman, P., Cotrufo, M. F., Elliott, J. A., McDowell, R., Griffiths, R. I., Asakawa, S., Bondeau, A., Jain, A. K., … & Pugh, T. A. M. (2016). Global change pressures on soils from land use and management. *Global Change Biology*, *22*(3), 1008–1028. https://doi.org/10.1111/gcb.13068

Trivedi, T. P., Sharma, R. P., Bharti, V. K., & Sastri, A. (2010). *Degraded Wastelands of India: Status and Spatial Distribution*. Indian Council of Agricultural Research, National Academy of Agricultural Studies. https://icar.org.in/files/Degraded-and-Wastelands.pdf

Tubiello, F. N., Salvatore, M., Ferrara, A. F., House, J., Federici, S., Rossi, S., Biancalani, R., Condor Golec, R. D., Jacobs, H., Flammini, A., Prosperi, P., Cardenas-Galindo, P., Schmidhuber, J., Sanz Sanchez, M. J., Srivastava, N., & Smith, P. (2015). The contribution of agriculture, forestry and other land use activities to global warming, 1990–2012. *Global Change Biology*, *21*(7), 2655–2660. https://doi.org/10.1111/gcb.12865

USDA. (2019). *Food Data Central*. U.S. Department of Agriculture, Agricultural Research Service. fdc.nal.usda.gov.

Vervisch, T. G. A., Vlassenroot, K., & Braeckman, J. (2013). Livelihoods, power, and food insecurity: Adaptation of social capital portfolios in protracted crises—case study Burundi. *Disasters*, *37*(2), 267–292. https://doi.org/10.1111/j.1467-7717.2012.01301.x

Weisell, R., & Dop, M. C. (2012). The adult male equivalent concept and its application to household consumption and expenditures surveys (HCES). *Food and Nutrition Bulletin*, *33*(3_suppl2), S157–S162. https://doi.org/10.1177/15648265120333S203

Zappa, L., Schlaffer, S., Bauer-Marschallinger, B., Nendel, C., Zimmerman, B., & Dorigo, W. (2021). Detection and quantification of irrigation water amounts at 500 m using Sentinel-1 surface soil moisture. *Remote Sensing*, *13*(9), 1727. https://doi.org/10.3390/rs13091727

Zaussinger, F., Dorigo, W., Gruber, A., Tarpanelli, A., Filippucci, P., & Brocca, L. (2019). Estimating irrigation water use over the contiguous United States by combining satellite

and reanalysis soil moisture data. *Hydrology and Earth System Sciences*, *23*(2), 897–923. https://doi.org/10.5194/hess-23-897-2019

Zhu, Z., & Woodcock, C. E. (2014). Continuous change detection and classification of land cover using all available Landsat data. *Remote Sensing of Environment*, *144*, 152–171. https://doi.org/10.1016/j.rse.2014.01.011

Zsögön, A., Peres, L. E. P., Xiao, Y., Yan, J., & Fernie, A. R. (2022). Enhancing crop diversity for food security in the face of climate uncertainty. *The Plant Journal: For Cell and Molecular Biology*, *109*(2), 402–414. https://doi.org/10.1111/tpj.15626.

2 Understanding Changes in Agricultural Land Use and Land Cover in the Breadbasket Area of the Ganges Basin 2000–2015

A Socioeconomic-Ecological Analysis

Liping Di, Eugene Yu, Junmei Tang, Zhiqi Yu, Wei Zhang, Zhe Guo, and Man Li

2.1 INTRODUCTION

South Asia's agriculture sector is challenged by the need to feed a population expected to increase by 43.8% by 2050 (Goswami 2013) despite limited arable land. This challenge is compounded by rapid urbanization and economic development, which compete with agriculture for land and threaten forests and wetlands. The Ganges Basin, South Asia's breadbasket, is densely populated and experiencing rapid urban expansion (Tsarouchi et al. 2014), putting further pressure on land use. Understanding the drivers and impacts of these changes is crucial for informing sustainable development policies, mainly as South Asia plays a key role in global efforts like the United Nations Sustainable Development Goals.

This research aimed to assess land cover and land use changes (LCLUC) in the Ganges Basin, South Asia's "breadbasket," and understand the drivers and impacts of these changes. The study focused on (1) identifying and assessing LCLUC from 2000–2015, (2) quantifying socioeconomic drivers of LCLUC, (3) developing future LCLUC scenarios until 2030, (4) evaluating impacts of LCLUC on key indicators like food security and income, and (5) disseminating results to inform sustainable development strategies. LCLUC was defined in this project to include changes in agricultural land use, cropping systems, and agricultural intensity. The project used remote sensing and GIS techniques with an integrated modeling framework to address questions about dominant LCLUCs, major socioeconomic drivers, factors driving crop choices in Bangladesh, and potentials for improving the economic-environmental

 DOI: 10.1201/9781003396260-2

performance of crop production. The project contributed to NASA's LCLUC program by developing remote-sensing techniques to identify changes and employing economic theories and methods to identify major drivers and impacts of LCLUC.

2.2 METHODOLOGY

2.2.1 Study Area

The study area is the agricultural region of the Ganges Basin, covering ~600,000 km^2 across seven states in northern India and most of Bangladesh. This area, home to nearly a tenth of the world's population, is South Asia's "breadbasket." Dominant cropping systems are rice and rice-wheat, with rice being prevalent in Bangladesh and the Indian states of Tamil Nadu and Kerala. The region has seen rapid population growth and urbanization, leading to the loss of fertile agricultural land and the conversion of grasslands to agriculture. Numerous river and wetland ecosystems in the basin are threatened by human activities, particularly agriculture. Due to India's support price policy, government policies have influenced agricultural production and cropping patterns, with wheat and oilseed production expanding rapidly since 2000 (Aradhey 2016). Rice production remained relatively stable from 2001 to 2011, except in eastern India, where government programs promoted rice cultivation (Singh 2016). These land use changes significantly impact land use patterns, farm income, and the environment.

2.2.2 Overall Framework of the Research Approach

The research approach integrated remote sensing, GIS, an econometric land use model, and an ecological model to achieve its objectives. The methods for achieving each of the five study objectives are discussed in detail, i.e., land cover/land use change mapping, land use model, ecological impacts, seasonal-spatial optimization model, and result dissemination portal. The integrated modeling framework, which was key to addressing objectives II-IV, includes an econometric land use model for examining determinants of cultivated area, a spatially explicit nutrient delivery ratio (NDR) model (Hamel and Guswa 2015) for assessing the impact of cropping intensity and fertilizer application rate on nutrient runoff, and a seasonal-spatial optimization model for improving environmental performance while maintaining agricultural revenue and food security (Figure 2.1). The optimization problem aimed to minimize total nitrogen runoff across three crop growing seasons by changing the nitrogen application rate and reallocating cultivation between rice and non-rice crops. A geospatial portal was also part of the framework for disseminating the research data and results to stakeholders and the broader LCLUC community.

2.2.2.1 Remote Sensing-Based Assessment of Land Cover/Land Use Change

The research used time-series land use/cover maps to detect three levels of LCLUC over the 15 years from 2000 to 2015. The LCLU maps were produced for 2000, 2005, 2010, and 2015 at a 30-meter spatial resolution. The project adopted the classification schema of the USDA Cropland Data Layer, which includes crop types and

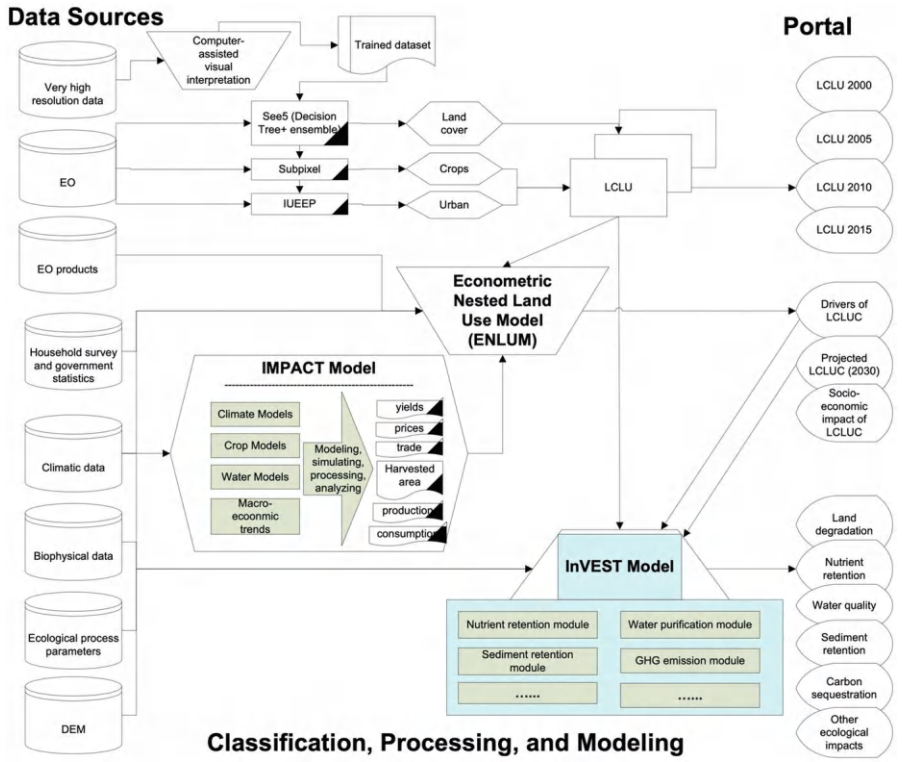

FIGURE 2.1 Workflow of the proposed research.

cropping intensity. The classification algorithm primarily used an ensemble decision tree classifier, with training samples established using very high-resolution multispectral images.

The project addressed several challenges:

- Cloud coverage: Multiple sensors were used to collect clear images during the monsoon season.
- Mixture of pixels: Due to the fragmentation of crop fields in South Asia, classes of mixed pixels were added to ensure accurate crop classification.
- Validation: Ground truth data was limited, so very high-resolution images from Google Earth and other available land cover products were used for validation.
- Impact of aerosol and particulates: The research acknowledged the high levels of aerosol and particulate pollution in many South Asian cities, which could distort Earth Observation and increase the difficulty of adequately classifying urban areas. The study adopted the Improved Urban Extent Extraction Procedure (IUEEP), a specific urban delineation algorithm to address this. This procedure was based on the Normalized Difference Spectral Vector (NDSV), which grouped different normalized difference indices such as the

Normalized Difference Vegetation Index (NDVI), Normalized Difference Water Index (NDWI), and Normalized Difference Built-up Index (NDBI). This approach helped to achieve a reasonably accurate delineation of urban areas in South Asian countries.

2.2.2.2 Land Use Model

Consider a farm that has $\bar{L}$ acres of cropland. Let r denote three cropping seasons: spring, summer, and winter, indexed by 1, 2, and 3, respectively. Let j denote three types of cropland use: rice, non-rice crops, and idle, indexed by 1, 2, and 0, respectively. Let $\pi\left(p_{rj}, L_{rj}\right)$ be the restricted profit function for crop j in season r, where $p_r = \left(p_{r1}, p_{r2}, 0\right)$ is exogenous net prices for rice, non-rice crops, and idle use the farmer faces, and L_{rj} is the amount of land the farmer chooses for land use j in season r. The farmer's objective is to choose the land allocation that maximizes total profit

$$\max_{\{L_{rj}\}} \sum_{r=1}^{3} \sum_{j=0}^{2} \pi\left(p_{rj}, L_{rj}\right), \tag{2.1}$$

subject to

$$\sum_{j=0}^{2} L_{rj} = \bar{L}, \text{For } r = 1,2,3. \tag{2.2}$$

The solution to this problem gives the optimal land allocation $L_{rj}^{*} = L_{rj}\left(p_r, \bar{L}\right)$. Assume that the function $L_{rj}\left(p, \bar{L}\right)$ is homogeneous of degree one in $\bar{L}$. Then

$$L_{rj}^{*} = L_{rj}\left(p_r, \bar{L}\right) = L_{rj}\left(p_r, 1\right)\bar{L}, \quad \forall r, j. \tag{2.3}$$

Equation (2.3) can be written in share form as

$$s_{rj}^{*} \equiv \frac{L_{rj}^{*}}{\bar{L}} = L_{rj}\left(p_r, 1\right), \quad \forall r, j. \tag{2.4}$$

The model assumes that the farmer's profit depends on the net prices of the crops and the amount of land allocated to each crop in each season. The optimal land allocation is determined by a set of share equations, which express the proportion of land allocated to each crop in each season as a function of the net prices.

The model treats idle land as a residual choice, capturing the evolution of cropping intensity in response to changes in seasonal crop net prices and precipitation. It also accounts for inter-seasonal correlation in crop allocation, which is not typically considered in previous models.

The model assumes a logistic form for the share equations, ensuring the predicted shares lie within a zero-one interval. However, due to inter-seasonal correlation, standard logistic regression cannot be used to estimate the share equations. Instead, the model converts the nonlinear share equations into a system of linear equations. Specifically, assume that the share equations take the logistic form:

$$s_{rj}^{*} = \frac{\exp\left(s_{rj}^{0}\alpha_r + x_{rj}\beta_{rj} + \mathbf{z}_r\boldsymbol{\gamma}_{rj}\right)}{\sum_{k=0}^{2}\exp\left(s_{rk}^{0}\alpha_r + x_{rk}\beta_{rk} + \mathbf{z}_r\boldsymbol{\gamma}_{rk}\right)}, \quad \forall r, j, \tag{2.5}$$

where $\exp(\cdot)$ is the exponential function. The term s_{rj}^{0} represents a lagged crop share in the previous period (i.e., in 2013)—an inertia variable that captures the incentive-based variables such as net price, market accessibility, and land use conversion costs, as well as the location-specific characteristics such as land suitability, soil properties, topography, and weather conditions. Including an inertia variable is an empirical strategy to absorb unobserved factors affecting land use choice and is vital to model agricultural land use in Bangladesh. Characterized by highly diversified agroclimatic conditions and soil taxonomy, Bangladesh has 30 agroecological zones. It is practically challenging to observe all variables related to this agroecological diversity. Moreover, the cost associated with land use conversion is difficult to measure, because such cost depends on individual farmers' ability to adopt new practices and their attitudes towards risk. Those factors are generally unobservable. Since s_{rj}^{0} has captured the net price for choice *j* for the previous period, p_{rj} is replaced with x_{rj}, representing the change in net price from the previous period to the current period (i.e., from 2013 to 2017). Analogously, the term $\mathbf{z}_r$ represents a vector of changes in other time-varying variables that may potentially drive land use change and $\mathbf{z}_r$ = (*change in road density*, *change in seasonal precipitation*). Road density measures market accessibility, which is essential for transporting perishable crops such as vegetables to a market. Precipitation change has different implications in different seasons. Higher rainfall may increase the risk of floods and crop failure in the monsoon season but reduce irrigation costs in the dry season. The terms α_r, β_{rj}, and $\boldsymbol{\gamma}_{rj}$ are coefficient parameters on s_{rj}^{0}, x_{rj}, and $\mathbf{z}_r$.

Let the idle use be a residual category ($j = 0$) and define $\boldsymbol{\eta}_{rj} \equiv \boldsymbol{\gamma}_{rj} - \boldsymbol{\gamma}_{r0}$. Equation (2.5) implies that

$$\ln\left(s_{rj}^{*}/s_{r0}^{*}\right) = \left(s_{rj}^{0} - s_{r0}^{0}\right)\alpha_r + x_{rj}\beta_{rj} + \mathbf{z}_r\boldsymbol{\eta}_{rj}, \quad \text{for } r = 1,2,3 \text{ and } j = 1,2. \tag{2.6}$$

By taking the logarithm of *the odds of crop j against idle*, the logistic form is transformed to a set of six linear equations. The seemingly unrelated regression (SUR) method is applied to estimate the systems of equations (2.6) using the cross-sectional district-level data. The SUR method is a generalization of ordinary least squares (OLS) for multi-equation systems and allows the correlation among the errors in different equations to improve the regression estimates (Jackson 2002). Political scientists have applied such an estimation strategy to model election returns in multi-party elections.

The model relies on district-level agricultural statistics for two years, 2013 and 2017, supplemented with other ancillary data. The outputs from the land use model include a system of six equations that establish the relationship between rice and non-rice crop shares and the aforementioned factors for each season.

2.2.2.3 Ecological Impacts of Crop Cultivation and Nitrogen Application

The InVEST's Nutrient Delivery Ratio (NDR) model is a spatially explicit model used to assess the ecological impacts of crop cultivation and nitrogen application (Hamel and Guswa 2015). It calculates a nutrient budget based on nitrogen sources, land cover and land use, and the processes of denitrification or sediment trapping by a given land use type.

The model identifies surface and subsurface flow paths from a digital elevation model and uses the land use types' nutrient load and retention parameters to represent the transport process. The loads are routed along topographically defined flow paths, with a proportion of the load being removed on each cell between the nutrient load and the stream. The nutrient export at the watershed/subwatershed outlet is computed as the sum of the pixel-level contributions.

The model assesses the total nutrient load, nutrients retained by vegetation and topographic features, and nutrients delivered to the water outlet for each growing season. It first estimates the pixel-level nutrient delivery ratios, which are then aggregated to the district level.

The model considers two sources of nutrient loads: fertilizer application of cropland and natural resources such as rainfall. However, since the focus is on the former, nutrients from natural resources are excluded while modeling the delivery ratio. The NDRs are replicated twice, once with nutrient loads from both sources and once with the fertilizer application in the cropland set to 0, so all the nutrient load is from natural resources. This allows for a more accurate assessment of the ecological impacts of crop cultivation and nitrogen application.

2.2.2.4 Seasonal-Spatial Optimization Model

The optimization problem presents an objective of minimizing total annual nitrogen runoff aggregated across districts and seasons, subject to a set of economic and physical constraints concerning total annual output value and cropland availability.

Assume that the central government is concerned about national agricultural runoff pollution and attempts to minimize the total nitrogen runoff while maintaining

the value of total crop production and guaranteeing food security in the country. The government's problem can be written as

$$\min_{\{N_{irj},L_{irj}\}} \sum_{i=1}^{64}\sum_{r=1}^{3}\sum_{j=1}^{2}\theta_{ir}N_{irj}L_{irj} \tag{2.7a}$$

$$\text{s.t.} \sum_{i=1}^{64}\sum_{r=1}^{3}\sum_{j=1}^{2}L_{irj}y_{irj}\left(N_{irj}\right)p_{irj} \geq v^{b} \tag{2.7b}$$

$$\sum_{i=1}^{64}\sum_{r=1}^{3}L_{ir1}y_{ir1}\left(N_{ir1}\right) \geq Y_{1}^{b} \tag{2.7c}$$

$$\sum_{j=1}^{2}L_{irj} \leq \bar{L}_{ir}, \quad i=1,\ldots,64; r=1,2,3 \tag{2.7d}$$

$$\sum_{r=1}^{3}\sum_{j=1}^{2}L_{irj} \leq CI_{i}\bar{L}_{i}, \quad i=1,\ldots,64, \tag{2.7e}$$

where L_{irj} represents the total harvested area of crop j in season r, district i, and N_{irj} represents the associated per acre nitrogen input; L_{irj} and N_{irj} are decision variables that the government jointly controls. The parameter θ_{ir} is a district-specific, season-wise ratio of the nitrogen runoff to the nitrogen input. A linear relationship is assumed between the runoff and the input, and this relationship varies by season and space. Therefore, the term $\theta_{ir}N_{irj}L_{irj}$ in the objective function (2.7a) represents the nitrogen runoff from growing crop j in season r, district i.

The economic constraint in (2.7b) states that the farmers as a whole would not be worse off from the reallocation of crop production and nitrogen application to minimize agricultural runoff pollution. The parameter p_{irj} represents the price of the crop j grown in season r, district i. The parameter v^{b} is the value of total agricultural production in the baseline. It is assumed that crop yield y_{irj} is a function of nitrogen input, denoted as $y_{irj}\left(N_{irj}\right)$, where technology and other inputs are implicitly captured in the function.

The food security constraint in (2.7c) states that the country's total rice production would be maintained at least at the baseline level, denoted as Y_{1}^{b}. As Bangladesh's dominant food crop, rice provides about two-thirds of the total calorie supply and about one-half of the total protein intake of an average person in the country (BRRI). This constraint indicates that national food security is not compromised as a result of the environmental initiative.

The constraints in (2.7d) and (2.7e) are physical constraints, where $\overline{L}_{ir}$ is the area of cropland potential in season r, district i; $\overline{L}_i$ is the area of cropland available in district i; CI_i is the annual cropping intensity in the district i under the baseline. Constraint (2.7d) states that in each season, the total cropping area cannot exceed the land area potentially suitable for crop production. Constraint (2.7e) states that the annual harvested area in each district cannot exceed the baseline annual harvested area at the current cropping intensity.

2.2.2.5 Designing and Developing a Result Dissemination Portal

A standard-compliant geospatial portal was meticulously designed and refined to disseminate research data and results to stakeholders and the broader LCLUC community. The portal is a comprehensive platform that delivers a wealth of information, including the following:

- Historical LCLUC Results: The portal provides land cover/land use (LCLU) results for 2000, 2005, 2010, and 2015, offering a historical perspective on land use changes.
- Drivers of LCLUC: It identifies and presents the key drivers of LCLUC, helping users understand the factors influencing these changes.
- Projected LCLUC: The portal also includes projections for LCLUC up to 2030, providing insights into future trends.
- Socio-Economic Impact of LCLUC: This section assesses and presents the socio-economic impact of LCLUC, highlighting the implications of these changes for society and the economy.
- InVEST Model Outputs: The portal features model outputs from the Integrated Valuation of Ecosystem Services and Tradeoffs (InVEST), including land degradation, nutrient retention, water quality, sediment retention, carbon sequestration, and other ecological impacts.

2.3 RESEARCH AND DEVELOPMENT OUTCOMES

2.3.1 LULC Mapping and Change Monitoring

2.3.1.1 Earth Observation Data Collection and Processing

The project investigated agricultural land use and land cover changes every 5 years from 2000 to 2015. Landsat images were collected for these years, with different Landsat versions used for different years. Supplementary Earth Observation data, including Terra ASTER, MODIS daily surface reflectance data, daily VIIRS NPP, and MODIS NDVI/EVI/LAI 16-day composite data, were collected.

In addition to satellite images, data from Globe Land 30 (GLC30) and the Global Food Security-Support Analysis Data 30 meter (GFSAD30) were collected. GLC30 provides worldwide land cover data in a 30-meter resolution for 2000 and 2010, while GFSAD30 provides cropland extent data across the globe for the nominal year 2015 (2010 for North America) at a 30-meter resolution.

Landsat and MODIS data/products were primarily used in land cover mapping. The high spatial resolution of Landsat images was used to identify the spatial distribution

of farmland. In contrast, the high temporal resolution of MODIS was used to interpret phenology information to identify crop types and cropping intensity.

The Landsat images underwent atmospheric correction on six reflectance bands and were geo-referenced into the UTM-WGS84 map projection. Image-to-image radiometric normalization was conducted between adjacent images, particularly before image mosaicking for the Landsat data. This was implemented by performing a histogram matching between adjacent scenes for the same year.

2.3.1.2 LULC Mapping

This project mapped land use and land cover (LULC) for the study area using Landsat 5 and 8 surface reflectance products. The Normalized Difference Vegetation Index (NDVI) and Normalized Difference Built-up Index (NDBI) were computed for better classification. The Google Earth Engine (GEE) was used to efficiently handle and process large geospatial datasets.

The LULC maps were generated using 66 Landsat scenes covering the study area for 2000, 2005, 2010, and 2015. Reference data included the GlobeLand30 (GLC30) product, MODIS Land Cover Type product (MCD12Q1), ESA CCI Land Cover product, and the Global Land Cover Facility (GLCF): Landsat Tree Cover Continuous Fields.

The GLC30, a global LULC map at 30-meter resolution for 2000 and 2010, was the primary reference (Table 2.1). The MODIS product provides land cover dynamics at 500-meter spatial resolution. The ESA CCI product is a 300-meter resolution land cover covering 1992 to 2015. The GLCF estimates ground covered by woody vegetation more significant than 5 meters in height for 2000, 2005, and 2010. The Hansen Global Forest Change v1.3 (2000–2015) layer was added to cover the year 2015.

2.3.1.2.1 Data Pre-Processing

This project used multi-temporal image sequences to improve land use and land cover (LULC) classification. Instead of a single image, all images that met the criteria were used to extract phenology information. The criteria included a cloud cover of less than 10% and the use of filters on the GEE Landsat 5 Surface Reflectance T1 image collection in a year.

All bands from the selected images were used for classification. Additionally, three normalized indexes – NDVI, NDBI, and MNDWI – were computed and added to each image as single bands. The MNDWI is calculated as

$$\text{MNDWI} = \frac{\text{GREEN} - \text{MIR}}{\text{GREEN} + \text{MIR}} \tag{2.8}$$

To acquire training samples for 2005, pixel values of the GLC30 product were remapped from double digits to single digits. The unchanged regions between 2000 and 2010 were identified and used to generate around 4000 sample points. Points close to the perimeter of the unchanged regions were deleted. This was done by using a raster calculator as

TABLE 2.1
Globeland30 Classification Schema

LULC Type	Value	Remap	Description
Cultivated Land	10	1	Lands used for agriculture, horticulture and gardens, including paddy fields, irrigated and dry farmland, vegetation and fruit gardens, etc.
Forest	20	2	Lands covered with trees, with vegetation cover over 30%, including deciduous and coniferous forests, and sparse woodland with cover 10–30%, etc.
Grassland	30	3	Lands covered by natural grass with cover over 10%, etc.
Shrubland	40	4	Lands covered with shrubs with cover over 30%, including deciduous and evergreen shrubs, and desert steppe with cover over 10%, etc.
Wetland	50	5	Lands covered with wetland plants and water bodies, including inland marsh, lake marsh, river floodplain wetland, forest/shrub wetland, peat bogs, mangrove and salt marsh, etc.
Water Bodies	60	6	Water bodies in the land area, including river, lake, reservoir, fishpond, etc.
Tundra	70	7	Lands covered by lichen, moss, hardy perennial herb and shrubs in the polar regions, including shrub tundra, herbaceous tundra, wet tundra and barren tundra, etc.
Artificial Surfaces	80	8	Lands modified by human activities, including all kinds of habitation, industrial and mining area, transportation facilities, and interior urban green zones and water bodies, etc.
Bareland	90	9	Lands with vegetation cover lower than 10%, including desert, sandy fields, Gobi, bare rocks, saline and alkaline lands, etc.
Permanent Snow and Ice	100	10	Lands covered by permanent snow, glacier and icecap.
Ocean	255	6	Oceans.

$$\text{output} = 10 \times \text{glc2000} + \text{glc2010} \tag{2.9}$$

Where glc2000 and glc2010 represent the LCLU types in 2000 and 2010, respectively.

Buffers were generated around existing sample points and converted to a polygon class feature collection to increase the number of sample points. This collection was used as the training dataset.

2.3.1.2.2 Classification Method

The classification method for land use and land cover (LULC) involved training a Random Forest (RF) classifier on Google Earth Engine (GEE) using a stacked image and training samples. The RF classifier consisted of multiple Decision Tree

TABLE 2.2
Random Forest Classifier Parameters

Parameters	Value	Description
Number of Trees	15	Number of trees to create per class
Variables Per Split	0	Split using square root of the number of variables
Min Leaf Population	2	The minimum size of a terminal node

(DT) classifiers, each trained on different bootstrap data samples. Randomness was introduced in feature selection for each split to reduce tree similarity. Combining the classification results from each DT, the RF classifier achieved better overall performance and robustness against overfitting than a single DT classifier. The parameters for the RF classifier are provided in Table 2.2.

2.3.1.2.3 Post-Classification Process

The post-classification process for land use and land cover (LULC) involved two major steps:

1. *Incremental artificial surface area update*: The performance of the classifier was evaluated using the F1 score, calculated as

$$F1 = \frac{2^{*}Precision \times Recall}{Precision + Recall} \tag{2.10}$$

   The year with the highest $F1$ score for the artificial surface class was identified and used to update the classification results for other years. The rules for updating were as follows:

   - If the previous year is an artificial surface and has the highest score, the following years will be the same surface.
   - If the following year is not an artificial surface and has the highest score, the previous year will be classified as cropland instead of an artificial surface.

2. *Forest cover update based on the GLCF:* The Global Land Cover Facility (GLCF) Landsat Tree Cover Continuous Fields product was used as a reference to update the forest class in the classification. This product provided a tree cover percentage of 30-meter resolution for 2000, 2005, and 2010. For 2015, the Hansen Global Forest Change (2000–2015) product was used. The forest definition provided by the United Nations was adopted, which states that forests are land covers that are at least 0.5 ha and with more than 10% of the area covered by trees that are at least 5 meter high. Therefore, a 10% threshold on the continuous field product was used to derive forest area for 2000, 2005, and 2010. The forest class was updated based on the GLCF and

GLC30 products. For 2000 and 2010, a pixel was updated to forest cover if classified as forest in both GLCF and GLC30 products. For 2005, only the GLCF product was used, while for 2015, the update was based on the forest class in 2000 and the Hansen Global Forest Change (2000–2015) product.

2.3.1.3 Time-Series LCLU Maps

The study uses Landsat image classification to present a time series analysis of land use/land cover (LULC) in a specific area from 2000 to 2015. Four LULC maps were generated at 5-year intervals. The maps identified eight land cover types: cropland, forest, grassland, shrubland, wetland, water, artificial surface, and bare land.

The study area was predominantly covered by croplands, accounting for over 80% of the total land area. Forests, the second most common land cover type, were scattered throughout the area, with a significant portion along the eastern edge bordering the Himalayas. A notable feature was a large wetland area on the Bay of Bengal coast, possessing the world's largest mangrove forest.

While the overall percentage share of land cover types remained relatively consistent from 2000 to 2015, changes in LULC may have occurred at different locations within the study area. The least represented land cover type was bare land, with its share decreasing from 0.06% in 2000 to 0.02% in 2015 (Table 2.3).

2.3.1.4 Validation and Accuracy Assessment

The validation and accuracy assessment of the LULC maps were conducted using 150,000 samples from the unchanged area between 2000 and 2010. The accuracy and kappa scores were calculated using specific formulas. The overall accuracies of the LULC map classified from the remote sensing images for the years 2000, 2005, 2010, and 2015 were 0.957, 0.953, 0.953, and 0.946, respectively, indicating high and consistent accuracy of the selected land cover mapping techniques. The corresponding kappa values were 0.807, 0.796, 0.796, and 0.768 for the same years, showing a high agreement between the LULC types and the ground truth. This demonstrated

TABLE 2.3
Distribution of LULC Types in the Ganges Basin Area

	2000		2005		2010		2015	
	Sq. Km	Percent	Sq. Km	Percent	Sq. Km	Percent	Sq. Km	Percent
Cropland	903182	84.01	905061	84.18	893896	83.14	901291	83.83
Forest	83663	7.78	86686	8.06	88654	8.25	85675	7.97
Grassland	20119	1.87	16990	1.58	21496	2.00	18466	1.72
Shrub land	2761	0.26	426	0.04	2856	0.27	943	0.09
Wetland	7439	0.69	7272	0.68	7523	0.70	7068	0.66
Water	12626	1.17	11876	1.10	11672	1.09	10556	0.98
Artificial Surface	44690	4.16	45908	4.27	48732	4.53	50945	4.74
Bare land	665	0.06	873	0.08	289	0.03	218	0.02
Total	1075145	100	1075092	100	1075118	100	1075162	100

the capability of the techniques used for accurate mapping of land cover types using earth observation.

2.3.2 Agricultural Land Use Change between 2000 and 2015

Between 2000 and 2015, the study area, predominantly farmland, underwent significant land use and land cover (LULC) changes. Impervious surfaces increased from 4.16% to 4.74%, mainly due to farmland and forest conversion. Notably, cropland was transformed into built-up areas, especially around cities.

In the eastern part of the study area, major changes included the conversion of forest to cropland and waterbody to cropland, the latter due to erosion and siltation in Ganges channels. In the southwestern parts, cropland was predominantly converted to grassland.

Around 97% of the 2000 croplands remained unchanged by 2015, but urban expansion led to a net loss of 5668 km² of cropland to impervious surfaces. Some croplands reverted to forest, particularly along river areas.

Major land cover changes occurred in grassland, shrubland, waterbodies, and forests. About 20% of grassland was converted to cropland and 18% to forest. Shrublands saw a 62% conversion to forest and a 390 km² conversion to croplands. A significant gain of 5502 km² of cropland occurred from waterbodies, indicating their filling for crop cultivation (Table 2.4). These changes reflected the impacts of urban expansion, population growth, migration, and international food market dynamics on agricultural land use.

2.3.2.1 Case Study Area

The Delhi metropolitan area, a densely populated region in India, underwent significant LCLUC between 2000 and 2015 (Tang and Di 2019). This period saw rapid urbanization, largely due to migration from other parts of India. The total population surged from 10 million in 1990 to 25 million in 2014. However, the rural population proportion declined from 10.07% in 1991 to 2.50% in 2012. Consequently, the

TABLE 2.4
The LULC Change from 2000 to 2015 for the Study Area in Percentage

2000 \ 2015	Cropland	Forest	Grassland	Shrubland	Wetland	Water Body	Artificial Surface	Bare Land
Cropland	97.31	0.81	0.51	0.01	0.03	0.37	0.95	0.01
Forest	10.30	86.87	1.89	0.46	0.01	0.09	0.38	0.00
Grassland	20.76	18.80	59.50	0.60	0.00	0.07	0.23	0.03
Shrubland	14.11	62.76	8.59	13.16	0.00	0.08	1.23	0.05
Wetland	4.26	0.37	0.09	0.00	90.68	3.46	1.14	0.00
Water body	43.58	0.92	0.11	0.02	0.63	53.33	1.11	0.30
Artificial Surface	6.57	0.02	0.00	0.00	0.00	0.05	93.36	0.00
Bare land	70.04	1.08	1.25	0.19	0.00	16.78	0.19	10.47

region experienced substantial land use changes, particularly the loss of farmland. This case study provides valuable insights into the impacts of urbanization on agricultural LCLUC.

2.3.2.2 Model for Historical Construction and Future Prediction

The Markov-Cellular Automata (CA) model is a systematic framework used for historical construction and future prediction of land use and land cover (LULC). It is driven by four factors: transition probability (f_p), neighboring effect (f_n), suitability driver (f_s), and constrain factor (f_c). The transition probability is derived from a historical Markov model, while the neighboring effect is based on the current cell status. The constraint factor is determined by elements such as water, elevation, and slope, and the suitability driver includes factors like population and road density.

A crucial step in the Markov-CA model is calibration, which assigns appropriate parameters for each input variable. In this process, two LULC maps from 1998 and 2009 were used as empirical data. The model was run at yearly intervals until the calibration years, using the Monte Carlo random selection method to choose the initial data and model code. The parameters with the highest match were selected for the next year's simulation (Shan et al. 2008).

Other factors impacting LULC, such as elevation, distance to roads, road density, and population growth, were defined and included in the transition rules as suitability drivers. Constrain factors like lakes, rivers, and reservoirs were also considered.

The model's accuracy was validated by comparing the predicted LULC map with the empirical map of the same year, using the Root Mean Square Error (RMSE) as the evaluation metric. The RMSE formula is given by:

$$\mathrm{RMSE} = \sqrt{\frac{1}{N}\sum_{i=1}^{N}\left(P_{ei} - P_{pi}\right)^2} \tag{2.11}$$

where P_{ei} is the percentage of each class from the classified map, P_{pi}. is the percentage of each class from the empirical map, and N is the total number of LULC classes.

2.3.2.3 Past and Future Trajectories of Farmland Loss

The Markov-CA model was used to reconstruct historical annual maps and predict future land use and land cover (LULC) changes in Delhi from 1995 to 2030. The model showed that urban areas, driven by factors like population growth and economic development, would continue to expand, primarily at the expense of farmland.

From 1995 to 2005, the urban area increased by 401 km², less than the 455 km² increase from 2005 to 2015, reflecting the rapid urbanization in New Delhi after the 2000s. The model predicted that this trend would continue, with the urban area increasing from 504.13 km² to 2679.54 km², while farmland would decrease from 8778.19 km² to 7242.94 km².

The model's accuracy was validated by comparing the simulated map with the empirical map for the same year. Farmland and urban areas showed high user and producer accuracy.

The results indicate that rapid urbanization is the major reason for farmland loss. Although both urban and farmland areas are changing, their rates of change differ. Farmland shows a relatively stable decrease from 1995 to 2030, while the urban area's increase rate was larger from the 2000s to 2020, consistent with the intensive urbanization in Delhi from the 2000s. The model predicts that this rapid urbanization will continue until 2020 and slow down from 2020 to 2030.

2.3.3 Farming System Change Analysis

The project analyzed farming system changes in Bangladesh, particularly the shift from agricultural land use to aquaculture. The study focused on Singra Upazila, a region experiencing intense land use change from crops to aquaculture. A novel workflow was introduced for detecting fishponds using Sentinel-2 optical images.

The fishery industry in Bangladesh has experienced rapid expansion over the past few decades, becoming a major source of food and economic growth. The fish farming market has grown 25-fold in all aspects of the aquaculture industry over the last three decades. Despite rice being the primary food source, the booming aquaculture industry is diversifying the dietary structure and improving health conditions in Bangladesh. However, this growth puts pressure on the already limited cropland. A significant portion of cropland has been transformed into other land use types, such as fishponds, brickyards, and residential areas. With the advent of Earth Observation (EO) data, particularly the newly published Sentinel-2 MSI 10m resolution images, mapping and monitoring individual fishponds have become feasible.

Fishponds in Bangladesh are usually filled with water all year round, small, and have relatively simple shapes like rectangles. Multi-temporal and multi-spectral remote sensing images were used to detect these features in this study. Sentinel-2 MSI L1C data, popular for land use and land cover (LULC) mapping due to its finer spatial and temporal resolution, was used in this research for fishpond mapping.

Three remotely-sensed Water Indexes (WI), namely the Normalized Difference Water Index (NDWI) (McFeeters 1996), Modified Normalized Difference Water Index (MNDWI) (Xu 2006), and Automated Water Extraction Index (AWEI) (Feyisa et al. 2014), were utilized. These indexes enhance water features on multispectral images by leveraging the low reflectance of water in the near-infrared (NIR) and shortwave-infrared (SWIR) spectra. The AWEI, which uses five bands to compute, is particularly noted for its ability to reduce false positives from shadow pixels.

The challenge of discerning fishponds from other water features was addressed by using a specific feature of fishponds and integrating automatic spectral filtering and spatial filtering using object-based features (OBFs). OBFs, also known as geometrical features or shape metrics, have been used in previous research as ancillary features in object-based image analysis. They have been shown to significantly improve classification accuracy, especially when objects are spectrally similar. The proposed method was implemented on Google Earth Engine (GEE).

2.3.3.1 Study Area and Dataset

The study area was Singra Upazila, a sub-district of Natore district in Northern Bangladesh, with a population density of 607 persons per km². The area, which is primarily agricultural with a focus on rice farming, is undergoing a shift from crop fields to fishponds due to the higher profitability of fish culturing. The data used in this study is the Sentinel-2 MSI Level-1C product, a Top-of-Atmosphere (TOA) reflectance dataset.

2.3.3.2 Methodology

The methodology consists of two main parts: spectral filtering and spatial filtering. Spectral filtering uses multi-temporal images to identify water features that are flooded throughout the year. Spatial filtering calculates object-based features for vectorized water objects identified by spectral filtering and sets thresholds to distinguish fishponds from other water features. The entire workflow is depicted in Figure 2.2. The details of the methodology can be found at Yu et al., 2020.

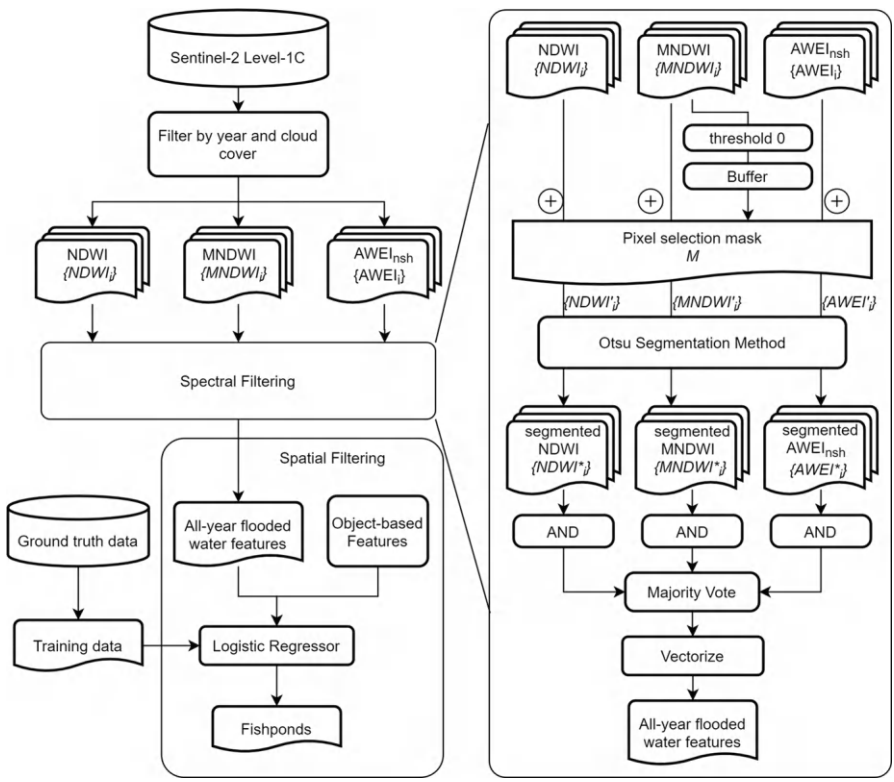

FIGURE 2.2 Flow diagram of the pond change detection method.

2.3.3.3 Result

The fishpond classification results indicated that the Logistic Regression (LR) model outperformed the Decision Tree (DT) model on the test dataset, despite DT's superior performance during training. Specifically, LR correctly classified 663 out of the 841 fishponds, yielding a precision score of 0.788. In contrast, DT identified 789 fishponds and correctly classified 610, resulting in a precision score of 0.773. Compared to DT, LR's precision score was 1.5% higher, its recall rate was over 4% higher, and its overall F1 score was 3.6% higher. Therefore, the LR model is recommended for fishpond classification.

2.3.4 Mapping and Change Analysis of Crop Intensity

Progress was made in detecting crop intensity changes in the study area, with research conducted using harmonic regressions on time series imagery. The forthcoming discussions cover data collection, encountered challenges, employed methodologies, and preliminary results of crop intensity mapping and change analysis.

2.3.4.1 Data

The data for crop intensity mapping was sourced from the Global Food Security Analysis-Support Data at 30m (GFSAD30) project and the Global croplands data portal, yielding 124 ground truth points collected in 2010 in Bangladesh. These points, which include longitude, latitude, crop type, and crop intensity information, were supplemented with statistical data from the Bangladesh Bureau of Statistics' Statistical Yearbook and the Yearbook of Agricultural Statistics. The Moderate Resolution Imaging Spectroradiometer (MODIS) data product was used to analyze the time series of NDVI values in crop fields due to its high temporal resolution, with the 8-day product chosen over the daily product for ease of data processing. Quality assessment bands were used to mask cloud-contaminated pixels.

2.3.4.2 Methodology

2.3.4.2.1 Data Preprocessing

Data preprocessing for crop intensity mapping involved using MODIS Terra/Aqua Surface Reflectance 8-Day L3 Global 250 m products, applying a cloud mask to all images, and calculating NDVI using bands 1 and 2 of the MODIS products; due to high cloud cover in monsoon seasons, Terra and Aqua products were combined to address missing values, with the combination method mathematically illustrated in equation (2.12).

$$\mathrm{V}_{\mathrm{combined}} = \begin{cases} \dfrac{V_{\mathrm{Terra}} + V_{\mathrm{Aqua}}}{2}, & if\ V_{\mathrm{Terra}}, V_{\mathrm{Aqua}} \neq NaN \\ V_{\mathrm{Terra}} \mid V_{\mathrm{Aqua}}, & if\ \{V_{\mathrm{Terra}}, V_{\mathrm{Aqua}}\} = NaN. \\ NaN, & if\ V_{\mathrm{Terra}}, V_{\mathrm{Aqua}} = NaN \end{cases} \tag{2.12}$$

2.3.4.2.2 Harmonic Regression

The Harmonic ANalysis of Time Series (HANTS) method, also known as harmonic regression, was used to detect crop intensity. This method uses Fourier series as base functions, adding up sine and cosine pairs of different frequencies to represent overall trends and local variations. The harmonic regression is more stable than polynomial regressions and is particularly suitable for phenology-related analysis due to its intrinsic periodicity. The harmonic series is mathematically represented as

$$V(t) = a_0 + \sum_{i=1}^{n} \left(a_i \cos(2\pi i t) + b_i \sin(2\pi i t) \right)$$

$$t = \frac{\text{DoY}}{\#\,\text{days}} \tag{2.13}$$

where t is the relative position of the image date in the corresponding year between 0 and 1, and $V(t)$ is the predicted NDVI value for any time of a year. The number of periodic terms n is set to 3, given the highest crop frequency in Bangladesh. The regression is conducted pixel-wise, with each pixel being an array of 46 NDVI values representing the NDVI dynamics at the corresponding pixel location. The Ordinary Least Square (OLS) model was used to estimate parameters, which can be acquired using the normal equation:

$$\theta = \left(X^T X \right)^{-1} \left(X^T y \right) \tag{2.14}$$

where θ is the parameter vector, X is the training sample matrix, and y is the true value vector.

2.3.4.2.3 Crop Frequency Identification

After fitting the harmonic series to the NDVI time series, the crop intensity is determined by counting the number of intersections between a threshold line and the fitted curve. The threshold was set to 0.5 because the NDVI values of healthy crops are usually higher than 0.5. For complete crop cycles, there should be two intersections, one at the curve going up and one going down. However, for incomplete crop cycles, either due to missing values or cropped by the range of a year, there might be an odd number of intersections. Therefore, the crop frequency is determined by rounding up the number of intersections divided by 2; i.e., for even numbers, crop frequency is the number of intersections divided by 2; for odd numbers, crop frequency is the number of intersections plus 1, then divided by 2.

2.3.4.3 Results

The remote sensing derived crop frequency mapping results indicate that the dominant crop frequency in Bangladesh is two seasons, followed by one season, with three seasons being relatively rare. The one-season cropping pattern is typically associated

with seasonal flooding, while the two-season cropping system, comprising one Kharif and one Rabi season, is the most common. Comparisons with the crop intensity map from Banglapedia reveal a rough match, particularly with single-cropped regions. However, the area of triple-cropped regions is smaller than the reference map, possibly due to missing values in the monsoon seasons. A zonal analysis was conducted on the crop frequency map to aggregate crop intensity for each district. The result is shown in Table 2.5.

TABLE 2.5
District and Region-Wise Crop Intensity Summary from our Result and Statistics from Bangladesh Bureau of Statistics (BBS)

Region Name	District Name	Crop Intensity by our Method	Crop Intensity from BBS
Bandarban	Bandarban	1.157534	1.38
Barisal	Barisal	1.72627	1.76
	Bhola	1.543641	
	Jhalokathi	1.680704	
	Pirojpur	1.617375	
Bogra	Bogra	1.980268	2.35
	Joypurhat	1.301246	
Chittagong	Chittagong	1.599386	1.99
	Cox's Bazar	1.702732	
Khagrachhari	Khagrachhari	1.456341	2.12
Rangamati	Rangamati	1.276831	1.44
Comilla	Brahmanbaria	1.560693	1.82
	Chandpur	1.719748	
	Comilla	1.490053	
Dhaka	Dhaka	1.874435	1.72
	Gazipur	1.712432	
	Manikganj	1.345053	
	Munshiganj	1.831956	
	Narayanganj	1.436767	
	Narsingdi	1.765473	
Dinajpur	Dinajpur	1.661731	2.11
	Panchogarh	1.598903	
	Thakurgaon	1.997417	
Faridpur	Faridpur	1.618574	1.92
	Gopalganj	1.458369	
	Madaripur	1.725696	
	Rajbari	1.693322	
	Shariatpur	1.624316	
Jamalpur	Jamalpur	1.772047	2.29
	Sherpur	1.847076	
Jessore	Jessore	1.653473	2.28
	Jhenaidah	1.937731	
	Magura	1.845971	
	Narail	1.637942	

TABLE 2.5 (Continued)
District and Region-Wise Crop Intensity Summary from our Result and Statistics from Bangladesh Bureau of Statistics (BBS)

Region Name	District Name	Crop Intensity by our Method	Crop Intensity from BBS
Khulna	Bagerhat	1.49646	1.34
	Khulna	1.267695	
	Satkhira	1.572612	
Kushtia	Chuadanga	1.855318	2.56
	Kushtia	1.60264	
	Meherpur	1.842816	
Mymensingh	Kishoreganj	1.579946	2.15
	Mymensingh	1.642374	
	Netrokona	1.600508	
Noakhali	Feni	1.823093	2.11
	Lakshmipur	1.681078	
	Noakhali	1.538954	
Pabna	Pabna	1.573781	2.03
	Sirajganj	1.912778	
Patuakhali	Barguna	1.399497	1.49
	Patuakhali	1.346188	
Rajshahi	Chapai Nawabganj	1.529636	1.80
	Naogaon	1.64282	
	Natore	1.461503	
	Rajshahi	1.602412	
Rangpur	Gaibandha	1.613909	2.02
	Kurigram	1.706694	
	Lalmonirhat	1.697256	
	Nilphamari	1.723727	
	Rangpur	1.854516	
Sylhet	Habiganj	1.920637	1.54
	Maulvibazar	1.667063	
	Sunamganj	1.290713	
	Sylhet	1.308794	
Tangail	Tangail	1.848917	1.92
Summary		**1.655**	**1.91**

2.3.5 Scoping Visit and Socioeconomic Data

2.3.5.1 Scoping Visit to Bangladesh and India

A socio-economic survey was conducted during a scoping visit to the study area in November 2017. The team met with key stakeholders, held research seminars, and visited several villages and cities for field visits. Two studies were presented during the seminars. A questionnaire was designed for small group discussions with farmers, focusing on general questions regarding land use and resources, as well as agricultural production. The questions covered topics such as main livelihood

activities, challenges faced, types of land cover/use, government or NGO programs, types of land tenure for cultivated land, major crops, irrigation practices, and changes in agricultural production activities over the last 5–10 years. The survey aimed to gather comprehensive information to understand the socio-economic dynamics of the study area.

2.3.5.2 Socioeconomic Data

Existing socioeconomic data was collected for this study from India and Bangladesh, respectively. The detailed data type and source are listed in Table 2.6.

2.3.6 The Driver and Impact Analysis of Land Use

2.3.6.1 InVEST-NDR model

2.3.6.1.1 Model Description

The InVEST (Sharp et al. 2016) nutrient delivery model (InVEST-NDR) maps nutrient sources from watersheds and their transport to streams, estimates the nutrient retention capacity of land parcels under various land use scenarios, and informs conservation efforts by identifying areas of soil and vegetation that most effectively purify water supply for people and aquatic life.

2.3.6.1.2 Model Calibration and Validation

The calibration of the InVEST model involves ensuring all input data strictly adheres to the model's standard format, processing and preparing various datasets such as the Digital Elevation Model (DEM) and rainfall data of the Climate Hazards Group InfraRed Precipitation with Station data (CHIRPS), calibrating nutrient loading and maximum retention efficiency for each land cover class based on local conditions and using constant landscape-wide values for additional subsurface parameters.

2.3.6.2 Modeling Seasonal Changes in Nutrient Export with InVEST-NDR

The InVEST NDR model was used for the modeling of seasonal changes in nutrient export.

2.3.6.2.1 Data

The InVEST model requires three types of calibrated input data: land cover and land use datasets, geospatial attributes including watershed and sub-watershed, and tabular datasets, which include nutrient loading for each land use class, retention efficiency, and additional subsurface parameters.

2.3.6.2.2 Model Results

The InVEST model results reveal strong seasonal and spatial variations in nitrogen Nutrient Delivery Ratios (NDRs). Nitrogen application intensity is highest in winter, followed by summer and spring. The model shows marked seasonal differences in nutrient pollution in streams, with the highest pollution in winter. High nitrogen

TABLE 2.6
Socioeconomic Data Available

India				
Data Type	**Scale**	**Year**	**Description**	**Source**
Agricultural statistics	District	2000		National statistics bureau and agricultural year book
Agricultural statistics	State	2000/01–2011/12	Production Area Yield	Ministry of Agriculture and Farmers Welfare, Government of India
Agricultural statistics	State	2000/01–2013/14 1986/87–2007/08	Fertilizer Consumption	Indiastat Industrial Databook 2002-03, CIER (Center for Industrial and Economic Research) www.indiastat.com/agriculture/2/consumptionoffertilisers/206871/stats.aspx
Agricultural statistics	District	1980–2007	Production by crop Area by crop Farmgate price by crop Total fertilizer consumption (N,P, Potash)	ICRISAT Note: unbalanced data, contains a bunch of missing obs
India Human Development Survey (IHDS) Most of the survey coverage is over dimensions of human development.	This is a large nationally-representative panel dataset, with data on some 40,000 urban and rural households	2004-5 and 2011-12	Main data files can be downloaded from www.icpsr.umich.edu/icpsrweb/ICPSR/studies/36151?q=india+human+development+survey&searchSource=icpsr-landing. For identification variables linking IHDS-I and IHDS-II you must register on this site and create an account. After this you will be sent an email confirming your subscription to which you will need to respond. Creation of an account will allow you to download	

(*continued*)

TABLE 2.6 (Continued)
Socioeconomic Data Available

India				
Data Type	**Scale**	**Year**	**Description**	**Source**
			the link files and any relevant documentation. Creating an account will also subscribe you to our IHDS emailer that will provide information on data release, conferences and recent publications/findings. Each email will contain a list to unsubscribe if you do not find these emails useful. We appreciate your support in completing basic demographic information for data users since such information is required by our funders and will be needed if we are conduct future rounds of IHDS survey.	
ARIS/REDS	Panel dataset	Rounds in 1969, 1970, 1971, 1982, 1999, and 2006.	The 1969–1971 data are publicly available with no strings attached, while the 1982 data is publicly available but village identifiers masked, so it cannot be merged with the 1969–1971 data. The 1999 and 2006 data are fully secure to prevent deductive disclosure. All datasets can be accessed (with cross-walks to allow for merging), though you would need to first get clearance from IFPRI's IRB and you would only be able to use the data on projects that have IRB approval.	readme by A. Foster: http://adfdell.pstc.brown.edu/arisreds_data/readme.txt http://adfdell.pstc.brown.edu/arisreds_data/
ICRISAT Village Level Surveys (VLS)/Village Dynamics in South Asia (VDSA)	Household (micro) and meso	Generation 1: 1975–1984, 1989. Generation 2: 2001 onwards	These data were incredibly popular among development and agricultural economists, especially in the 1980s and 1990s. The first phase of data collection (the original VLS) ran from 1975 or so to the mid-1980s. It is relatively small in scope (only about 250 households in six districts in Andhra Pradesh and Maharashtra), but I think has data from every year, and has a wide range of questions on farm management, etc. Some of the early studies on how smallholders respond to shocks were conducted using these data. The second phase of data	

			collection (the VDSA) resumed in 2001, and expanded its scope, including more areas and more households. But it is still nowhere near nationally representative (to be fair, ICRISAT's mandate is just the semi-arid tropics, which does not include all of India), and the cross-sectional sample size is pretty small. Their funding from BMGF just ended, so it looks like this program is soon to be disbanded.	
			The meso-level dataset for India and Bangladesh contains data pertaining to the performance, structure and dynamics of agricultural economy at country level and its disaggregation at state/region, district, and sub-district level.	
National Sample Survey (NSS or NSSO)			This is a long, large, repeated nationally-representative cross-section dating back to the 1950s. The surveys do not cover the same material every year, though in most years they cover consumption expenditures. These data are not freely available, and can be rather expensive if you are hoping to combine several cross-sections. And you cannot buy all data for a given year; they sell the data module-by-module.	http://mospi.nic.in/Mospi_New/site/inner.aspx?status=3&menu_id=54

Bangladesh

Data Type	Scale	Year	Description	Source
Agricultural statistics	District (Zilla)	2000, 2010		National statistics bureau and agricultural year book
Bangladesh Integrated Household Survey (BIHS)	Household	2011-2012		
ICRISAT Village Level Surveys (VLS)/Village Dynamics in South Asia (VDSA)	Household (micro) and meso	2009-2012	The meso-level dataset for India and Bangladesh contains data pertaining to the performance, structure and dynamics of agricultural economy at country level and its disaggregation at state/region, district, and sub-district level.	

applications in some districts do not translate into high nitrogen leaching, indicating a potential "win-win" situation of high soil fertility benefits with low environmental impact. The NDRs, defined by nutrient exports divided by nutrient loads, are sensitive to the denominator and influenced by the spatial distribution of land use and land use intensity. The model results highlight the potential for optimizing economic-environmental performance.

2.3.7 Estimating Land Use and Crop Area Allocation Model

2.3.7.1 Two-Level Land Use Model for India

The two-level land use model for India uses pixel-level land use classification data and district-level agricultural statistics data to estimate land use choices. The model structure consists of an upper level that estimates choices among large aggregation categories like cropland, forestland, and urban areas, and a lower level that estimates crop choices within cropland. The model uses a variety of biophysical and socio-economic variables that influence land use choices. The model is estimated in a "bottom-up" sequential fashion, starting from the lower-level model. The model's predictive power is assessed and found to perform well in predicting most land uses, with generally accurate in-sample predictions at both levels.

2.3.7.2 Seasonal Land Use/Crop Area Allocation Model for Bangladesh

A seasonal land use/crop area allocation model was developed to systematically analyze crop choices and cropping frequency in Bangladesh. The model, which uses district-level agricultural statistics and data from the BIHS, allows for the analysis of both intra- and inter-season substitution of different crops. Key explanatory variables include crop prices, production costs, rainfall, population density, and road density. The model transforms the dependent variables into the logarithm of the odds of crop choice and estimates a system of regression equations. The model found that the probabilities of growing both rice and non-rice crops generally increase with their corresponding net price growth, and the odds of choosing summer crops over idle use are positively correlated with road density. The model also revealed that the probability of choosing winter non-rice crops over idle increases with precipitation, but there is no such evidence for winter rice, likely due to the high cost of irrigation and competition for irrigation water use.

2.3.7.3 Migration, Farm Size, Land Ownership, and Shocks in Bangladesh

The seasonal land use/crop area allocation model for Bangladesh reveals that natural shocks drive rural migration, but the number of shocks does not significantly correlate with migration. The effect of landholding on rural migration is nonlinear and non-monotonic, increasing with landholding for most households. International migration is insensitive to natural shocks. When the sample is divided into landless and landholding households, migration in the landless group is uncorrelated with natural shocks, while the effect of natural shocks on migration in the landholding group is statistically significant. A yield reduction of Kharif crops drives rural migration, with the landless group being more sensitive to the reduction than the landholding group.

However, there is no significant correlation between migration and the yield of Rabi crops in both groups.

2.3.8 Integrated Tradeoff Analysis: Balancing Food Security and Environmental Sustainability by Optimizing Crop Allocation

The integrated tradeoff analysis explores how societal outcomes can be improved through optimal crop choices and cultivated areas, focusing on improvements in nitrogen-use efficiency in crop production. The study highlights the importance of a national agricultural land use strategy that balances food security and environmental sustainability. It reveals that there is substantial potential to improve the economic-environmental performance of crop production by considering crop-specific, seasonal, and spatial variations in crop nitrogen use efficiency and nitrogen transport. The analysis helps reveal the economic-environmental tradeoffs and opportunities in agricultural land use planning and can inform policies that target environmentally sustainable food security.

2.3.8.1 Results and Discussion

The integrated tradeoff analysis results reveal that land use for rice and non-rice crops increases with their respective net prices and decreases with cross-net prices. An increase in the net price of rice or non-rice crops significantly affects the share of rice and non-rice crop areas in a district. Land use for summer crops increases with road density, as an expanded road network enhances farmers' access to markets, encouraging them to cultivate summer crops. Increased winter precipitation reduces the share of rice area and increases the share of non-rice crop area, as non-rice crops primarily rely on rainfed farming and are more sensitive to rainfall fluctuations than rice yield.

The optimization analysis results reveal three key findings (Table 2.7). First, there is a significant opportunity for efficiency gain in the economic-environmental performance of crop production through optimizing seasonal allocation of crop cultivation and nitrogen fertilizer use, leading to a substantial decline in total nitrogen runoff. Second, the inefficiencies in the baseline economic-environmental performance stem from both crop choice and nitrogen use, with a larger portion arising from the inefficient use of nitrogen fertilizer. Third, when crop net prices are endogenized within the optimization, the efficiency gain is not as large as when crop areas are optimized, indicating limitations in using price as a policy instrument to incentivize crop reallocations due to the complex relationship between crop prices and cropping areas.

The results also show that there is potential to improve the economic-environmental performance of crop production through optimizing seasonal allocation of crop cultivation and nitrogen fertilizer use. In most districts, the baseline nitrogen use for spring rice and summer and winter non-rice crops is below the optimum level, while the baseline nitrogen use for winter rice is excessive. The seasonal optimization results in decreased cultivated areas of summer rice and spring non-rice crops in most districts. When crop production is allowed to be reallocated across districts, summer rice in most districts and spring rice in some western districts contribute little to improving

TABLE 2.7
Optimization Results under Various Constraints

Decision variable	Baseline	Seasonal opt.			Seasonal-spatial opt.	Integrated opt.
		N	Area	*N* and area	*N* and area	*N* and Δp
	(1)	(2)	(3)	(4)	(5)	(6)
Total output value (billion Tk)	**1410.8**	**1523.9**	**1414.1**	**1416.7**	**1410.8**	**1438.0**
Total rice production (million metric ton)	**35.9**	**35.9**	**35.9**	**35.9**	**35.9**	**36.2**
Total *N* runoff (1,000 metric ton)	**106.8**	**57.2**	**67.5**	**21.3**	**18.2**	**33.5**
Spring rice N runoff	*11.5*	*5.2*	*1.6*	*2.2*	*2.3*	*2.1*
Summer rice N runoff	*34.0*	*22.9*	*19.2*	*2.7*	*1.6*	*11.0*
Winter rice N runoff	*37.0*	*12.7*	*37.5*	*10.6*	*10.4*	*10.5*
Spring non-rice N runoff	*10.2*	*5.2*	*5.6*	*2.4*	*2.4*	*2.7*
Summer non-rice N runoff	*3.4*	*2.2*	*0.2*	*1.8*	*0.2*	*1.9*
Winter non-rice N runoff	*10.7*	*9.0*	*3.3*	*1.6*	*1.3*	*5.3*
Total *N* inputs (1,000 metric ton)	**560.2**	**334.8**	**397.4**	**124.6**	**111.5**	**174.2**
Spring rice N inputs	*55.8*	*30.9*	*9.3*	*13.7*	*13.0*	*10.6*
Summer rice N inputs	*174.1*	*126.2*	*113.4*	*16.3*	*11.5*	*56.2*
Winter rice N inputs	*184.3*	*76.6*	*210.5*	*61.7*	*62.8*	*53.6*
Spring non-rice N inputs	*64.7*	*34.4*	*38.7*	*16.8*	*17.7*	*15.9*
Summer non-rice N inputs	*20.8*	*12.7*	*1.6*	*9.2*	*1.1*	*10.7*
Winter non-rice N inputs	*60.6*	*54.0*	*23.8*	*6.9*	*5.4*	*27.2*
Total cultivated area (million acre)	**43.6**	**43.6**	**38.8**	**31.1**	**27.9**	**43.5**
Spring rice cultivated area	*2.7*	*2.7*	*1.1*	*3.4*	*3.2*	*2.7*
Summer rice cultivated area	*14.0*	*14.0*	*10.7*	*4.1*	*2.9*	*14.0*
Winter rice cultivated area	*12.0*	*12.0*	*14.7*	*15.4*	*15.7*	*13.4*
Spring non-rice cultivated area	*4.0*	*4.0*	*4.0*	*4.2*	*4.4*	*4.0*
Summer non-rice cultivated area	*2.7*	*2.7*	*4.3*	*2.3*	*0.3*	*2.7*
Winter non-rice cultivated area	*8.2*	*8.2*	*4.2*	*1.7*	*1.4*	*6.8*

the economic-environmental performance, leading to a decline in the cultivated areas of these crops. Different from the seasonal-spatial optimization, the baseline nitrogen input of winter non-rice crops is above the integrated optimization level in western and middle-western districts, indicating that it is easier to reallocate the cultivated area of winter crops through price instruments.

2.3.9 Web Portal Development for Information Dissemination

The web portal developed for this project allows stakeholders and the public to visualize and download land use/land cover products derived from satellite images and model-derived geospatial information data (see http://cloud.csiss.gmu.edu/ganges-lulc)

The web portal was designed with a front end developed under the React framework, using Bootstrap, Material UI, and OpenLayers for UI design and geospatial data visualization, and a back end that uses MapServer for rendering and serving raster and vector data through the Web Map Service, with data downloading functionality provided by an Apache HTTP server.

2.3.9.1 User Interface and Functionalities

The portal allows users to visualize, interact with, and download data and products through its user interface (Figure 2.3). The application comprises three main components: the header, the sidebar, and the main map container. The header includes the application name, 'about,' 'publications,' 'documentation' buttons, and logos of participating organizations. The sidebar, organized in a tabbed structure, allows users to switch between the 'LULC' and 'Model' tabs and adjust layer items within each level. Each layer can be individually turned on/off, its transparency adjusted, and downloaded in GeoTIFF format for raster layers and Shapefile format for vector layers. The map container provides web-based visualization of geospatial datasets, with various widgets for navigation and display.

2.4 CONCLUSION

This research investigated changes in LCLU, crop intensity, and cropping systems in the Ganges Basin from 2000 to 2015, driven by urban expansion and agricultural intensification. Using remote sensing-based Earth observation data and advanced

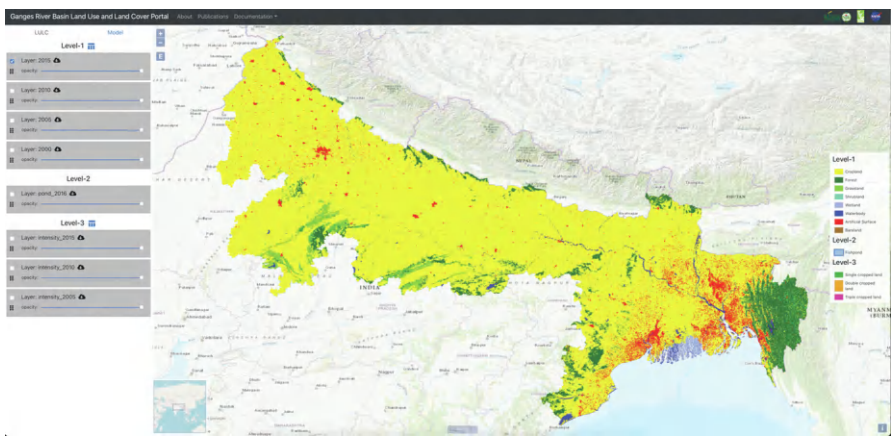

FIGURE 2.3 The Ganges River Basin Land Use and Land Cover Portal.

machine learning algorithms, the study mapped land cover changes from 2000 to 2015 and revealed significant changes in various land cover types. The research also developed an automatic fishpond mapping workflow and detected crop intensity in Bangladesh. An integrated modeling approach was developed to optimize the seasonal and spatial allocation of crop cultivation and nitrogen fertilizer use, demonstrating substantial improvements in the economic-environmental performance of crop production. However, the study also highlighted the limitations of using price as a policy instrument due to the complex relationship between crop prices and cropping areas. The NDR model showed strong seasonal and spatial variations. The study found no significant correlation between rural migration and the number of natural shocks but a significant effect of landholding on migration. A web portal was developed to disseminate the data and products from this project, providing stakeholders and the public with visualization and downloading of the LCLU products derived from satellite images and model-derived geospatial information data.

REFERENCES

Aradhey, A. 2016. *India: Oilseeds and Products Annual*. pp. 1–22. Available at: https://apps.fas.usda.gov/newgainapi/api/report/downloadreportbyfilename?filename=Oilseeds%20and%20Products%20Annual_New%20Delhi_India_4-1-2016.pdf.

Feyisa, G.L., Meilby, H., Fensholt, R. and Proud, S.R. 2014. Automated Water Extraction Index: A new technique for surface water mapping using Landsat imagery. *Remote Sensing of Environment* 140, pp. 23–35. doi: 10.1016/j.rse.2013.08.029.

Goswami, R. 2013. India's population in 2050: Extreme projections demand extreme actions. *East Asia Forum*. Available at: https://eastasiaforum.org/2013/04/05/indias-population-in-2050-extreme-projections-demand-extreme-action/.

Hamel, P. and Guswa, A.J. 2015. Uncertainty analysis of a spatially explicit annual water-balance model: Case study of the Cape Fear basin, North Carolina. *Hydrology and Earth System Sciences* 19(2), pp. 839–853. doi: 10.5194/hess-19-839-2015.

Jackson, J.E. 2002. A seemingly unrelated regression model for analyzing multiparty elections. *Political Analysis* 10(1), pp. 49–65. doi: 10.1093/pan/10.1.49.

McFeeters, S.K. 1996. The use of the Normalized Difference Water Index (NDWI) in the delineation of open water features. *International Journal of Remote Sensing* 17(7), pp. 1425–1432. doi: 10.1080/01431169608948714.

Shan, J., Alkheder, S. and Wang, J. 2008. Genetic algorithms for the calibration of cellular automata urban growth modeling. *Photogrammetric Engineering & Remote Sensing* 74(10), pp. 1267–1277. doi: 10.14358/PERS.74.10.1267.

Sharp, R., Tallis, H.T., Ricketts, T., Guerry, A.D., Wood, S.A., Chaplin-Kramer, R., Nelson, E., Ennaanay, D., Wolny, S., Olwero, N. and Vigerstol, K. 2016. InVEST+ VERSION+ user's guide. *The Natural Capital Project*.

Singh, S.K. 2016. *India: Grain and Feed Annual*. pp. 1–34. Available at: https://apps.fas.usda.gov/newgainapi/api/report/downloadreportbyfilename?filename=Grain%20and%20Feed%20Annual_New%20Delhi_India_2-26-2016.pdf.

Tang, J. and Di, L. 2019. Past and future trajectories of farmland loss due to rapid urbanization using Landsat imagery and the Markov-CA model: A case study of Delhi, India. *Remote Sensing* 11(2), p. 180.

Tsarouchi, G.M., Mijic, A., Moulds, S. and Buytaert, W. 2014. Historical and future land-cover changes in the Upper Ganges basin of India. *International Journal of Remote Sensing* 35(9), pp. 3150–3176. doi: 10.1080/01431161.2014.903352.

Xu, H. 2006. Modification of normalised difference water index (NDWI) to enhance open water features in remotely sensed imagery. *International Journal of Remote Sensing* 27(14), pp. 3025–3033. doi: 10.1080/01431160600589179.

Yu, Z., Di, L., Rahman, M.S. and Tang, J. 2020. Fishpond mapping by spectral and spatial-based filtering on google earth engine: A case study in singra upazila of Bangladesh. *Remote Sensing* 12(17), p. 2692.

3 Spatiotemporal Distribution and Recent Trends in Crop Water Use Across India

Nishan Bhattarai, Afshin Shayeghi, and Meha Jain

3.1 INTRODUCTION

Agriculture plays a significant role in the economic, social, and cultural development of India by serving as a significant contributor to the country's gross domestic product, providing livelihoods for a substantial portion of the population, and ensuring food security. However, agriculture is also the primary cause of groundwater depletion in India, as over 60% of irrigated agriculture depends on groundwater and a growing number of aquifers are being exploited at unsustainable rates. According to the World Bank, approximately 60% of all aquifers in India could be in a critical state within the next 10 years, posing severe challenges to the sustainability of agriculture, long-term food and water security, livelihoods, and economic growth (WorldBank, 2012). Sustainable groundwater management in India requires continuous monitoring of irrigation water use and availability to ensure responsible and efficient utilization of this critical resource.

The spatiotemporal patterns of irrigation water use across India have not been explored much, mainly due to the unavailability of field-scale irrigation water use data. Although groundwater level measurement data are available across thousands of locations in India, they do not capture the spatiotemporal heterogeneity of irrigation water use. Thousands of measurement sites are defunct and not regularly monitored over time (Hora et al., 2019). Remote sensing-based approaches have primarily focused on mapping irrigated areas or water use across small scales. Recent advances in remote sensing-based evapotranspiration (ET) mapping techniques have not been fully utilized to monitor crop water use across India.

ET is a key variable for quantifying agricultural water use and understanding the impacts of climate and ecosystem changes on crops. Reference ET (ET0) measures water demand for a specified crop under given atmospheric conditions. The ratio of ET to PET can reflect crop water demand, as well as the ability of farmers to irrigate crops and the extent to which crops are irrigated. For example, if crops are

 DOI: 10.1201/9781003396260-3

fully irrigated, ET/ET_0 and ET/ PET will be higher (1 if crop and atmospheric water demand is fully met or even higher than 1 for plants with higher water needs). In this chapter, we explore the use of remotely sensed ET/ET_0 to understand the spatiotemporal patterns of irrigation water use across India. The primary objective of this chapter is to identify trends in ET/ET_0 across India and explore whether this trend is associated with warming temperatures and ongoing groundwater depletion. To answer this question, we used a recently developed ET product (Bhattarai et al., 2019) that was validated across India using field- and water-balance-based methods in conjunction with other global datasets.

3.2 STUDY AREA

We studied India because of its substantial impact on global food security, representing approximately 18% of the world's population, recently surpassing China to become the most populated nation in the world (WorldBank, 2023). Most of its rural population comprises smallholder farmers heavily reliant on agriculture for their livelihoods (Fan et al., 2008; Foster and Rosenzweig, 2004). India contributes around 10% of global agricultural production (Alston and Pardey, 2014) and faces significant challenges from climate change (Im et al., 2017) compounded by rapid population growth and excessive groundwater use (Rodell et al., 2009; Asoka et al., 2017). The diverse climatic patterns in India make it a compelling region for investigating crop water use, as these climate variations can impact both the demand and availability of water for crops. For example, the precipitation pattern can be characterized by heavy monsoon rainfall along the western coast, northeastern states, and the Gangetic Plains, while the northwestern regions, Thar Desert, and parts of the Deccan Plateau experience lower rainfall, resulting in arid to semi-arid conditions (Figure 3.1). Similarly, the temperature varies spatially, with very high summer temperatures in the Central, Northwest, and Northern plains, tropical climates in the Southern Peninsula, moderate temperatures on the eastern coast, and cold temperatures in the Himalayas (Mondal et al., 2015).

Understanding the climate patterns, available water resources, and crop water use patterns is crucial for managing water resources and agriculture in India. However, long-term data on irrigation and crop water use in India that could provide spatiotemporal distribution of crop water use and identify regions needing water-saving interventions are nonexistent. Available global products are either coarse resolution or highly unreliable in mapping crop water use across the county (Bhattarai et al., 2019). This study leverages our novel ET product that more accurately captures irrigation use at finer resolutions to understand the spatial patterns of crop water use across India.

3.3 MATERIALS AND METHODS

3.3.1 Data

The primary dataset used to study the spatiotemporal pattern of ET/PET across India includes monthly ET (1 km × 1 km) derived from an ensemble surface energy balance model that estimates ET as the mean of ET estimates from seven thermally driven

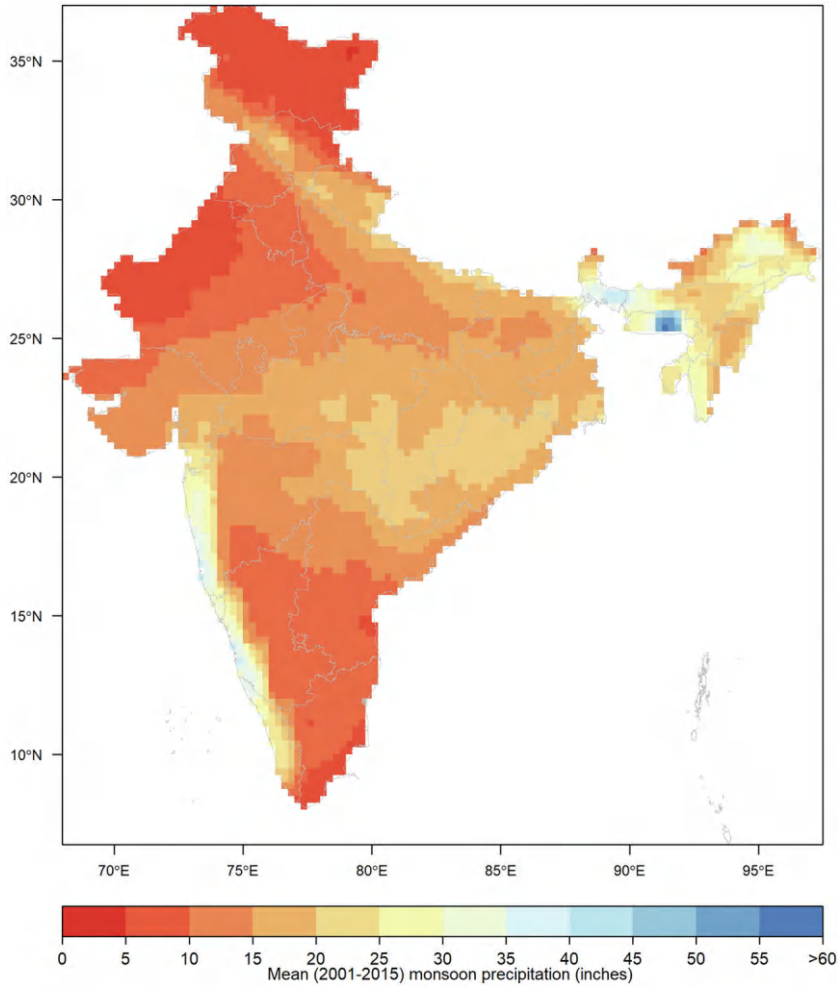

FIGURE 3.1 Mean (2001–2015) monsoon season precipitation across India showing higher precipitation in the east and coastal regions and lower precipitation in the northwest. The polygons in gray indicate the Indian States.

surface energy balance (SEB) models (Bhattarai et al., 2019). These surface energy balance models derive ET as the residual of the SEB by solving the SEB equation using land surface temperature (LST), vegetation indices, and meteorological data. The monthly ET products were developed for India using LST from MOD11A1 products (Wan et al., 2015), vegetation indices from MOD09GA/MOD09A1 (Vermote, 2015), and meteorological inputs from the National Aeronautics and Space Administration (NASA) Modern-Era Retrospective Analysis for Research and Applications, Version 2 (Merra-2) dataset (Gelaro et al., 2017). Additionally, as a robustness check, we also used the global ET and PET product ($0.25° \times 0.25°$) named Global Land Evaporation

Amsterdam Model (GLEAM) that uses a modified Priestley and Taylor (PT) (Priestley and Taylor, 1972) method (Martens et al., 2017; Miralles et al., 2016). GLEAM ET products are derived from assimilating climate data, soil moisture, precipitation, and snow water equivalent (Martens et al., 2017; Miralles et al., 2016). The Moderate Resolution Imaging Spectroradiometer (MODIS) Land Cover product (Friedl et al., 2010) was used to constrain the crop water use trend analysis to ensure that these were examined only across agricultural lands in India. Satellite-based precipitation data (0.25° × 0.25°) were obtained from the Tropical Rainfall Measuring Mission (TRMM; Huffman et al., 2016), and the monthly mean seasonal temperature (0.5° × 0.5°) was obtained from the Climatic Research Unit (CRU; Harris et al., 2014). The groundwater depletion zone map was obtained from the Center Groundwater Board (CGWB) of India (CGWB, 2011).

3.3.2 Approach

3.3.2.1 Derivation of Seasonal ET/PET and Climate Information

We estimated PET using the standardized American Society of Civil Engineering (ASCE)-PM equation (Walter et al., 2005), a modified form of the Penman-Monteith (PM) equation (Monteith, 1981). The meteorological inputs in this model, such as incoming solar radiation, mean daily air temperature (*Ta*, °C), wind speed (u, m s^{-1}), and actual vapor pressure (e_a, kPa), were obtained from the NASA Merra-2 reanalysis product, which was also used in the ensemble ET model (Bhattarai et al., 2019).

$$\mathrm{PETET}_0 = \frac{0.408\Delta\left(R_n - G\right) + \gamma \dfrac{C_n}{Ta + 273} u\left(e_s - e_a\right)}{\Delta + \gamma\left(1 + C_d u_2\right)} \tag{3.1}$$

where R_n and G are net radiation and soil heat flux (MJ m^{-2} day^{-1}), respectively. e_a (kPa) is saturated, Δ is the slope of the saturation vapor pressure-temperature curve, and γ (kPa $°C^{-1}$) is the psychrometric constant. C_n and C_d are coefficients for short grass (Walter et al., 2005). ET_0 was calculated daily and then aggregated to the monthly and seasonal scale to derive monsoon (June–September) and winter (December–March) season PET for the 2001–2015 growing seasons. The monthly ET maps from the Ensemble ET model were summed to derive monsoon and winter season ET for the same period. The ET/ET_0 maps were derived for all monsoon and winter seasons from 2001–2015. Note that because the same meteorological inputs were used in calculating ET and ET_0, the boundary conditions for minimum and maximum ET (i.e., PET) are the same. Hence, the ET/ET_0 represents ratio of water supply to demand (i.e., ET in response to water inputs) under the same climatic conditions. We also derived seasonal ET/ET_0 maps from GLEAM to compare trends in ET/PET ET/ET_0 across India under different spatial scales (1km vs 0.25º) and products. Like ET/ET_0, monthly precipitation and air temperature were aggregated to seasonal scales.

3.3.2.3 Pixel-Scale Trend Analysis

We masked out non-agricultural pixels in India using MODIS Land Cover products (Friedl et al., 2010). We selected pixels classified as croplands in at least 10 annual land cover maps during the 2001–2015 period. We applied the modified Mann–Kendall (MK) test (Kendall, 1976; Mann, 1945; Yue and Wang, 2002) to examine trends in ET/PET across all agricultural lands in India. The Mann–Kendall test is a non-parametric statistical test used to assess trends in time series data. The MS test statistic was utilized to identify positive trends ($Z > 0$) and negative trends ($Z < 0$) in ET/PET for each agricultural pixel, and the significance of these trends was tested at a 0.05 significance level (i.e., considered significant if p-value < 0.05). We also evaluated this trend for GLEAM-based ET/PET, seasonal precipitation, and seasonal mean temperature.

3.4 RESULTS AND DISCUSSION

3.4.1 Spatial Distribution of ET/PET Across India

The seasonal ET/PET across India showed a consistent pattern, with higher values in the north and lower values in the central and western parts of the country (Figure 3.2). As expected, mean seasonal ET/PET values were typically higher across the Indo-Gangetic Plains (IGP), the highly irrigated and major rice (monsoon or kharif season) and wheat (winter or rabi season) producing zones of India. The spatial patterns of ET/ET_0 (or ET/PET) were mainly were consistent across the two datasets (1 km Ensemble ET and 0.25° GLEAM products), except for the monsoon ET/PET in central India, where GLEAM products showed higher values of ET/PET. Both datasets captured the higher winter season ET/PET values in the north, which is consistent with several other global ET products that show higher rates of ET (Bhattarai et al., 2019) and irrigation extent and intensity in this region (Ambika et al., 2016; Meier et al., 2018; Teluguntla et al., 2015).

Winter season ET/PET values in the north consistently exhibited higher levels than those during the monsoon season, suggesting increased irrigation rates during the winter. This pattern aligns with the typical agricultural practices in northern India. In contrast, central and western India displayed the opposite trend, with higher monsoon season ET/PET values. This finding implies drier conditions and reduced irrigation during the winter season in these areas. The distinct patterns in ET/PET values across seasons indicate varying agricultural water management practices in different regions of India. Overall, the seasonal ET/ET_0 maps successfully captured and highlighted these regional irrigation and crop water use patterns, providing insights into the spatial patterns and seasonal dynamics of water use in Indian agriculture.

3.4.2 Trends in ET/PET Across India

While the northwest consistently exhibited higher seasonal ET/PET values compared to other parts of the country, there was no discernible increasing trend from 2001 to 2015 (Figure 3.3). This absence of a trend could be attributed to the already high ET/PET value levels in these regions (ET/PET > 0.8). However, noteworthy variations

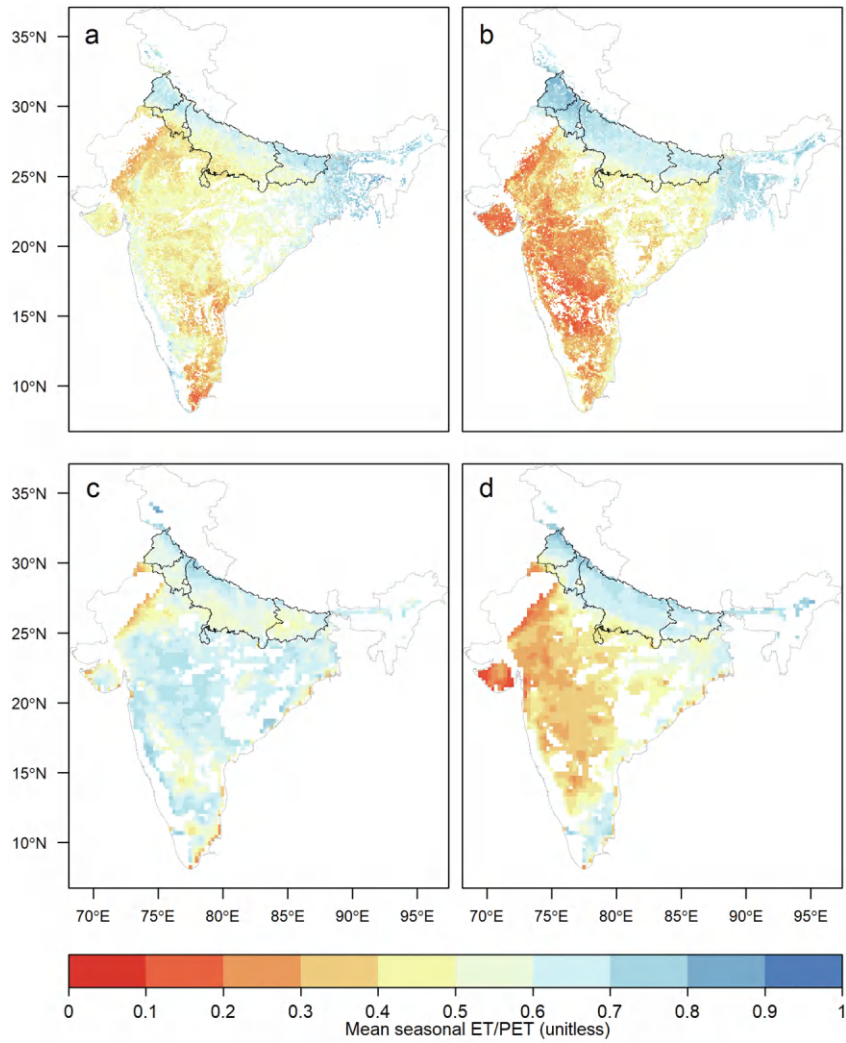

FIGURE 3.2 2001–2015 mean seasonal ET/ET_0 from the ensemble ET products during monsoon (a) and winter (b) seasons. (c) and (d) show the mean seasonal ET/PET from the GLEAM ET products during the monsoon and winter seasons, respectively. The polygons show four states within the IGP (Punjab, Haryana, Uttar Pradesh, and Bihar from left to right).

were observed in certain lower areas of Punjab and Haryana, which are crucial for winter wheat production; these regions displayed increasing trends in ET/ET_0 during the growing season. Particularly significant was the observation of a notable declining trend in monsoon season ET/ET_0 within the eastern Indo-Gangetic Plain (IGP) region, specifically Bihar. This trend suggests a remarkable shift in water dynamics during the monsoon season in this region.

A substantial portion of the country generally exhibited a pronounced and statistically significant increasing trend in ET/ET_0. This trend was particularly prominent in winter, especially in western and central India. Notably, this increasing ET/ET_0 trend was consistent in both datasets during the winter season, suggesting that these regions are experiencing an increase in ET/PET, likely due to increased irrigation.

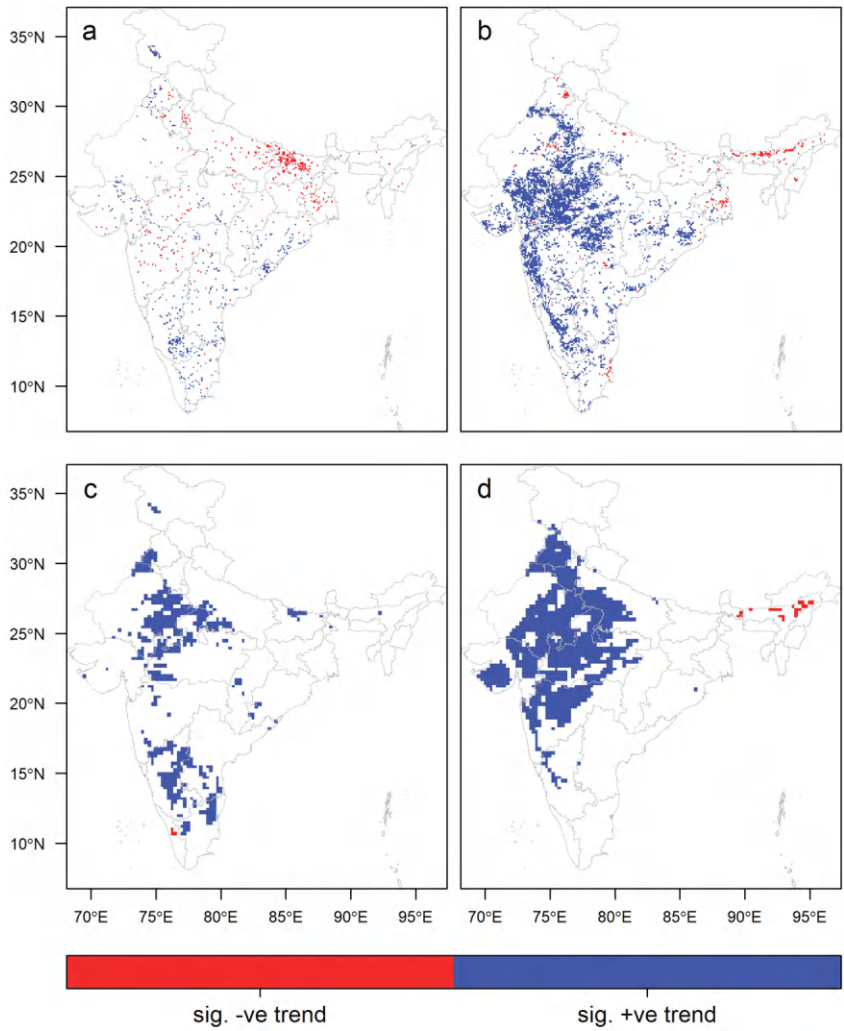

FIGURE 3.3 Trends in ET/ET_0 from the ensemble (a),(b) and GELAM (c),(d) ET products during monsoon [(a) and (c)] and winter [(b) and (d)] seasons. The polygons show four states within the IGP (Punjab, Haryana, Uttar Pradesh, and Bihar from left to right).

3.4.3 ET/PET Trends, Warming Temperatures, and Groundwater Depletion in India

Based on CRU monthly datasets, the IGP and western and southern India have experienced a significant increasing trend in seasonal temperatures, particularly in the winter season (Figure 3.4). The rise in ET/PET during the winter season suggests that agricultural systems across most of these regions can mitigate the adverse effects of warming temperatures through intensified irrigation from groundwater. This finding aligns with recent findings (Zaveri and Lobell, 2019; Bhattarai et al., 2023) and the fact that seasonal precipitation during this period does not exhibit an increasing pattern (figure not shown). Consequently, the increased irrigation, both in terms of extent and intensity, is likely to have contributed to a decline in groundwater tables in India across these regions. The reduction in ET/PET observed in the eastern IGP may indicate increased crop water stress resulting from rising temperatures (Figures 3.3–3.4).

The spatial distribution of the ET/ET_0 trend aligns closely with the critically groundwater-depleted zones in India, as characterized by the CGWB (Figure 3.5). Notably, regions in northwestern and western India are exhibiting an increasing ET/ET_0 trend, which coincides with areas marked as critically depleted or overexploited zones by the CGWB. This alignment strongly implies that a potentially higher water usage rate, particularly during the dry season (winter), is a significant factor contributing to the overexploitation of groundwater in these regions. Notably, while climate change is expected to negatively impact most parts of India by reducing water supply, these specific regions are anticipated to experience an even more pronounced decline in groundwater levels as temperatures warm and farmers increase irrigation to meet the increased demand for water by crops (Bhattarai et al., 2023).

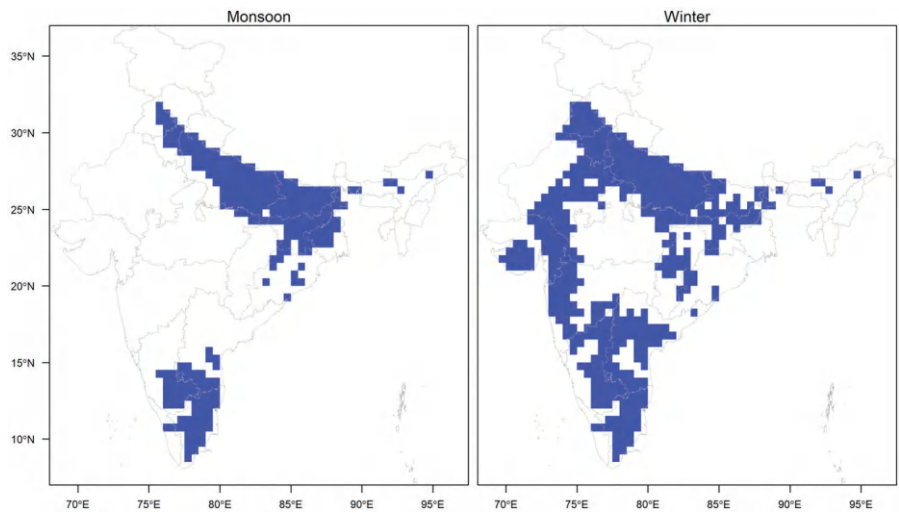

FIGURE 3.4 Increasing trends (blue color) in mean seasonal temperature (1991–2015) during monsoon and winter growing seasons in India.

Notably, regions in the east are displaying a decreasing ET/PET trend that aligns with areas designated as safe groundwater zones (Figure 3.5). Specifically, the eastern IGP exhibits a significant declining trend in monsoon season ET/PET. This can imply an increase in crop stress, changes in cropping patterns, or a reduction in ET due to a decrease in water application. Various climate models indicate an anticipated rise in monsoon precipitation for these regions (Bhattarai et al., 2023), albeit with more intense dry and wet spells (Mukherjee et al., 2018). However, increased pumping rates can constrain the benefits of increased monsoon precipitation (Dangar and Mishra, 2023). Nonetheless, groundwater levels in this region are projected to remain stable in the future (CGWB, 2022). Our findings indicate a consistent pattern where a higher ET/PET trend is typically associated with depleted groundwater zones in India.

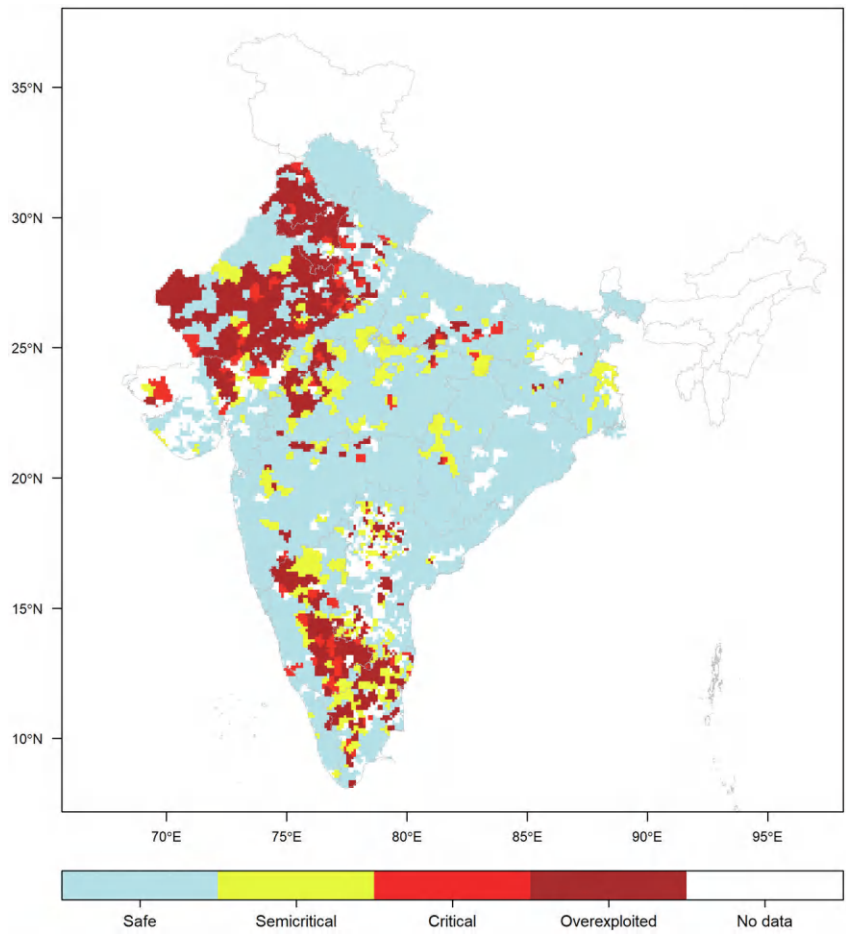

FIGURE 3.5 Characterization of groundwater depletion zones in India (CGWB, 2011).

3.5 CONCLUSION

We investigated the spatiotemporal distribution and trends of monsoon and winter season ET/ET_0 across agricultural lands in India, identifying that ET/ET_0 is generally higher in the IGP, suggesting higher irrigation rates in these areas. Except for certain parts of the western IGP, ET/ET_0 mostly remained stable in the IGP. Specifically, ET/ET_0 is decreasing in the eastern IGP during the monsoon season, where groundwater is anticipated to not be overexploited, according to the CGWB. While seasonal ET/ET_0 is lower in the western non-IGP region, including areas classified as critically depleted zones, a noticeable increasing trend was observed during the 2001–2015 period. Crop production in this region is expected to encounter significant challenges in the future due to increased water demand resulting from climate change. Future studies should establish a linkage between ET/ET_0 trends and observed groundwater levels at the field scale. A key limitation of the study was the inability of the 1 km MODIS pixels to capture water use patterns at the field scale, limiting our analysis to a regional level. Hence, future studies should derive ET at a much finer spatial resolution (<=10 m) to track water use from smallholder farmers. This is imperative because ensuring the responsible and efficient utilization of India's crucial groundwater resources demands continuous monitoring of irrigation water use and availability at a much finer scale than currently available datasets.

REFERENCES

Alston, J. M. & Pardey, P. G. 2014. Agriculture in the global economy. *Journal of Economic Perspectives*, 28(1), pp. 121–146.

Ambika, A. K., Wardlow, B. & Mishra, V. 2016. Remotely sensed high resolution irrigated area mapping in India for 2000 to 2015. *Scientific Data*, 3, p. 160118.

Asoka, A., Gleeson, T., Wada, Y. & Mishra, V. 2017. Relative contribution of monsoon precipitation and pumping to changes in groundwater storage in India. *Nature Geoscience*, 10, p. 109.

Bhattarai, N., Lobell, D. B., Balwinder-Singh, Fishman, R., Kustas, W. P., Pokhrel, Y. & Jain, M. 2023. Warming temperatures exacerbate groundwater depletion rates in India. *Science Advances*, 9(35), p. eadi1401.

Bhattarai, N., Mallick, K., Stuart, J., Vishwakarma, B. D., Niraula, R., Sen, S. & Jain, M. 2019. An automated multi-model evapotranspiration mapping framework using remotely sensed and reanalysis data. *Remote Sensing of Environment*, 229, pp. 69–92.

Central Ground Water Board (CGWB). 2011. *Dynamic Ground Water Resources of India, 2011*. Ministry of Jal Shakti, Department of Water Resources, River Development and Ganga Rejuvenation, Government of India. Retrieved from www.cgwb.gov.in/cgwb pnm/publication-detail/537

Central Ground Water Board (CGWB). 2022. *Dynamic Ground Water Resources of India, 2022*. Ministry of Jal Shakti, Department of Water Resources, River Development and Ganga Rejuvenation, Government of India. Retrieved from www.cgwb.gov.in/old_website/documents/2022-11-11-GWRA%202022.pdf

Dangar, S. & Mishra, V. 2023. Excessive pumping limits the benefits of a strengthening summer monsoon for groundwater recovery in India. *One Earth*, 6(4), pp. 419–427.

Fan, S., Gulati, A. & Thorat, S. 2008. Investment, subsidies, and pro-poor growth in rural India. *Agricultural Economics*, 39(2), pp. 163–170.

Foster, Andrew D. & Rosenzweig, Mark R. 2004. Agricultural productivity growth, rural economic diversity, and economic reforms: India, 1970–2000. *Economic Development and Cultural Change*, 52(3), pp. 509–542.

Friedl, M. A., Sulla-Menashe, D., Tan, B., Schneider, A., Ramankutty, N., Sibley, A. & Huang, X. 2010. MODIS Collection 5 global land cover: Algorithm refinements and characterization of new datasets. *Remote Sensing of Environment*, 114(1), pp. 168–182.

Gelaro, R., McCarty, W., Suárez, M. J., Todling, R., Molod, A., Takacs, L., Randles, C. A., Darmenov, A., Bosilovich, M. G., Reichle, R., Wargan, K., Coy, L., Cullather, R., Draper, C., Akella, S., Buchard, V., Conaty, A., Silva, A. M. d., Gu, W., Kim, G.-K., Koster, R., Lucchesi, R., Merkova, D., Nielsen, J. E., Partyka, G., Pawson, S., Putman, W., Rienecker, M., Schubert, S. D., Sienkiewicz, M. & Zhao, B. 2017. The modern-era retrospective analysis for research and applications, version 2 (MERRA-2). *Journal of Climate*, 30(14), pp. 5419–5454.

Harris, I., Jones, P. D., Osborn, T. J. & Lister, D. H. 2014. Updated high-resolution grids of monthly climatic observations–The CRU TS3.10 Dataset. *International Journal of Climatology*, 34(3), pp. 623–642.

Hora, T., Srinivasan, V. & Basu, N. B. 2019. The groundwater recovery paradox in South India. *Geophysical Research Letters*, 46(16), pp. 9602–9611.

Huffman, G., Bolvin, D., Braithwaite, D., Hsu, K., Joyce, R. & Xie, P. 2016. *Integrated Multi-satellitE Retrievals for GPM (IMERG), Version 4.4*. NASA's Precipitation Processing Center.

Im, E.-S., Pal, J. S. & Eltahir, E. A. B. 2017. Deadly heat waves projected in the densely populated agricultural regions of South Asia. *Science Advances*, 3(8), p.e1603322. pp.1–7.

Kendall, M. 1976. *Rank Auto Correlation Methods*, 4th Ed. Griffin.

Mann, H. B. 1945. Nonparametric tests against trend. *Econometrica: Journal of the Econometric Society*, 13(3), pp. 245–259.

Martens, B., Gonzalez Miralles, D., Lievens, H., van der Schalie, R., de Jeu, R. A., Fernández-Prieto, D., Beck, H. E., Dorigo, W. & Verhoest, N. 2017. GLEAM v3: Satellite-based land evaporation and root-zone soil moisture. *Geoscientific Model Development*, 10(5), pp. 1903–1925.

Meier, J., Zabel, F. & Mauser, W. 2018. A global approach to estimate irrigated areas–A comparison between different data and statistics. *Hydrology and Earth System Sciences*, 22(2), pp. 1119–1133.

Miralles, D. G., Jimenez, C., Jung, M., Michel, D., Ershadi, A., McCabe, M. F., Hirschi, M., Martens, B., Dolman, A. J., Fisher, J. B., Mu, Q., Seneviratne, S. I., Wood, E. F. & Fernandez-Prieto, D. 2016. The WACMOS-ET project–Part 2: Evaluation of global terrestrial evaporation data sets. *Hydrology and Earth System Sciences*, 20(2), pp. 823–842.

Mondal, A., Khare, D. & Kundu, S. 2015. Spatial and temporal analysis of rainfall and temperature trend of India. *Theoretical and Applied Climatology*, 122(1), pp. 143–158.

Monteith, J. L. 1981. Evaporation and surface temperature. *Quarterly Journal of the Royal Meteorological Society*, 107(451), pp. 1–27.

Mukherjee, S., Aadhar, S., Stone, D. & Mishra, V. 2018. Increase in extreme precipitation events under anthropogenic warming in India. *Weather and Climate Extremes*, 20, pp. 45–53.

Priestley, C. & Taylor, R. 1972. On the assessment of surface heat flux and evaporation using large-scale parameters. *Monthly Weather Review*, 100(2), pp. 81–92.

Rodell, M., Velicogna, I. & Famiglietti, J. S. 2009. Satellite-based estimates of groundwater depletion in India. *Nature*, 460, p. 999.

Teluguntla, P. G., Thenkabail, P. S., Xiong, J. N., Gumma, M. K., Giri, C., Milesi, C., Ozdogan, M., Congalton, R., Tilton, J., Sankey, T. T., Massey, R., Phalke, A. & Yadav, K. 2015.

Global Cropland Area Database (GCAD) Derived from Remote Sensing in Support of Food Security in the Twenty-first Century: Current Achievements and Future Possibilities. In: Land Resources Monitoring, Modeling, and Mapping with Remote Sensing (Remote Sensing Handbook). Taylor & Francis, Boca Raton, Florida, pp. 01–45.

Vermote, E. 2015. *MOD09A1MODIS/Terra Surface Reflectance 8-Day L3 Global 500m SIN Grid V006*. https://lpdaac.usgs.gov/products/mod09a1v006/

Walter, I. A., Allen, R. G., Elliott, R., Itenfisu, D., Brown, P., Jensen, M. E., Mecham, B., Howell, T. A., Snyder, R. & Eching, S. 2005. *Task Committee on Standardization of Reference Evapotranspiration*. ASCE.

Wan, Z., Hook, S. & Hulley, G. 2015. *MOD11A2 MODIS/Terra Land Surface Temperature/ Emissivity 8-Day L3 Global 1 km SIN Grid V006*. https://lpdaac.usgs.gov/products/mod11a2v006/

WorldBank. 2012. *India Groundwater: A Valuable but Diminishing Resource*. Available online: www.worldbank.org/en/news/feature/2012/03/06/india-groundwater-critical-diminishing

WorldBank. 2023. *Population Estimates and Projections*. Available online: https://databank.worldbank.org/source/population-estimates-and-projections

Yue, S. & Wang, C. Y. 2002. Applicability of prewhitening to eliminate the influence of serial correlation on the Mann-Kendall test. *Water Resources Research*, 38(6), pp. 4–1–4–7.

Zaveri, E. & B. Lobell, D. 2019. The role of irrigation in changing wheat yields and heat sensitivity in India. *Nature Communications*, 10(1), pp. 4144.

4 Forest Transitions in Dry Tropical Forests of Central India

Insights From Satellite Data and Socioeconomic Surveys

Ruth DeFries, Meghna Agarwala, Sandra Baquie, Pooja Choksi, Yadvendradev Jhala, Sarika Khanwilkar, Pinki Mondal, Harini Nagendra, and Johannes Urpelainen

4.1 INTRODUCTION

Dry tropical forests account for approximately 40% of all tropical forest land area and are extensive across Africa, Latin America, and Eurasia. These forests support livelihoods for millions of people and provide ecosystem services, including carbon storage, watershed protection, non-timber forest products, and habitat for biodiversity. Dry tropical forests are particularly threatened compared to other forest biomes due to high rates of land use conversion, dependence of local populations on forest resources, and climate change. Yet research to understand dry tropical forests' ecological and socio-economic dimensions is sparse compared to humid tropical forests. Additionally, policy and management attention lags behind humid tropical and temperate forests. These dry tropical forests are often overlooked in national policies and development plans (Siyum, 2020).

Although definitions of dry tropical forests vary (see Table 1 in Siyum, 2020), they are loosely defined as "forests in frost-free regions with 500-2000 mm of precipitation annually and a pronounced dry season of 4 to 7 months" (Miles et al., 2006). They play a significant role in the livelihoods and daily needs of forest-dependent rural populations by providing fuelwood, timber for construction, food items, and non-timber forest products for income. Because many of these products support subsistence, informal generation of cash income, and "free" ecosystem services, contributions of dry tropical forests to national incomes and well-being remain underappreciated.

In addition to deforestation from land conversion, degradation of dry tropical forests is prevalent. Degradation results in loss of biomass with trees still present.

DOI: 10.1201/9781003396260-4

It rivals deforestation as a source of carbon emissions (McNicol et al., 2018) and reduces other ecosystem services. Degradation can take many forms and is difficult to define. It can be caused by logging, over-harvesting of forest products, or over-grazing, among other anthropogenic activities. Eurasia's Dry tropical forests are more exposed to these threats than other regions (Miles et al., 2006). Standard methods for remote sensing of degradation have been elusive due to the patchiness, lack of consistent signature in satellite images, and the many processes leading to degradation.

With dense populations in rural areas, forests in India are particularly subject to high anthropogenic pressure. India houses diverse forest types, including dry tropical and subtropical deciduous forests (Reddy et al., 2021). This forest type is extensive in central India, the focus for the studies synthesized in this chapter (see description of the study region). Forests are critical to local communities in this landscape for fuelwood, timber, fodder, and non-timber forest products. This chapter summarizes research carried out under the South Asia Regional Initiative within the NASA Land Use/Cover Change program aimed at applying remote sensing tools to monitor degradation and analyzing socio-economic data to identify anthropogenic influences on these forests.

A key question in this research is whether a forest transition could occur as pressures on the forest reduce as dependence on local communities lessens. In other parts of the world, an initial decline in forest cover at a national level passes an inflection point, and forest cover begins to increase, a process known as the forest transition (Mather, 1992; Meyfroidt and Lambin, 2011; Rudel et al., 2005). Forest transitions have occurred in multiple places due to forest regeneration on abandoned land or tree planting following the depletion of forest resources. In the context of degraded dry tropical forests, conceivably, a transition to reverse degradation for healthier, higher biomass forests ensues with reduced pressure on forest resources. Research to test this hypothesis depends on methodologies to quantify degradation and combine it with socio-economic data on the use of forests.

4.2 STUDY REGION

The landscape for this study region covers the agroecological region designated as the Central Indian Highlands (Gajbhiye and Mandal, 2000) (Figure 4.1). It covers 32 administrative districts spread across Madhya Pradesh, Maharashtra, and Chhattisgarh. The region is within the country's tribal belt, with approximately 22 percent of the population belonging to officially recognized Scheduled Tribes, predominantly Baiga and Gond tribes (Choksi et al., 2021).

The landscape is composed of forests, villages, and small towns. Approximately 37 percent of the villages are within 8 km of forests, and nearly 70 percent of the population belongs to Scheduled Tribes in these forest-fringe villages (Baquie et al., 2020). The people in these villages rely on forests for fuelwood for cooking and heating (though increasingly using alternatives (Khanwilkar et al., 2021)), non-timber forest products for income, and fodder for grazing. For beams, houses are generally made from mud, grass, and local timber. Other livelihood strategies include small-scale, mostly rain-fed agriculture, daily labor, and seasonal migration as labor in urban centers (Choksi et al., 2021).

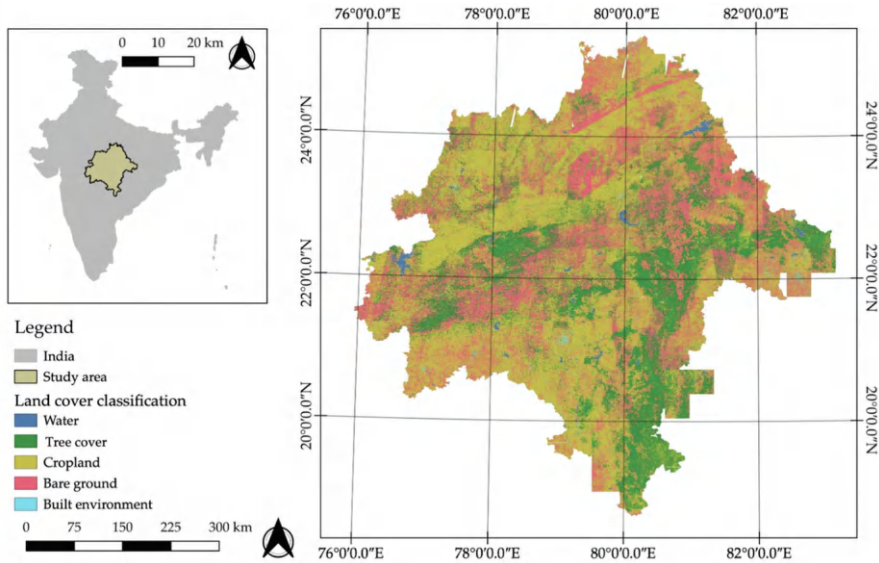

FIGURE 4.1 Location of the central India landscape study region from Khanwilkar et al. (2023).

The region is also a globally important conservation area for tigers (Schoen et al., 2022). It houses a network of Tiger Reserves and other types of protected areas. Landscape connectivity between these protected areas is critical to the genetic health of populations of tigers and other wide-ranging species, with fragmentation occurring from development pressures from road expansion, railroads, mining, and energy infrastructure.

Forests in the region are dry, tropical, and deciduous, with leaf fall occurring in the dry summer months. Dominant trees include Sal (*Shorea robusta*) and *Terminalia* species. Analysis of regenerating tree species indicates that forest grazing and human-caused fire are altering the species composition, with the increased prominence of tree species with traits that confer resistance to trampling and fires (Agarwala et al., 2016). Signs of degradation are prevalent in the forest, with visible signs of narrow trails and lopping.

4.3 DATA

4.3.1 Remote Sensing Data

To quantify the degradation of dry tropical forests in central India, we devised an indicator of forest health using very-high-resolution data (Khanwilkar et al., 2023). The indicator is based on an algorithm to quantify exposed bare ground within forests as a sign of human use. First, we used a Random Forest classifier to derive a thematic land cover map of tree cover and bare ground from 3-meter resolution Planet's PlanetScope data. We used field data and polygons identified from Google Earth

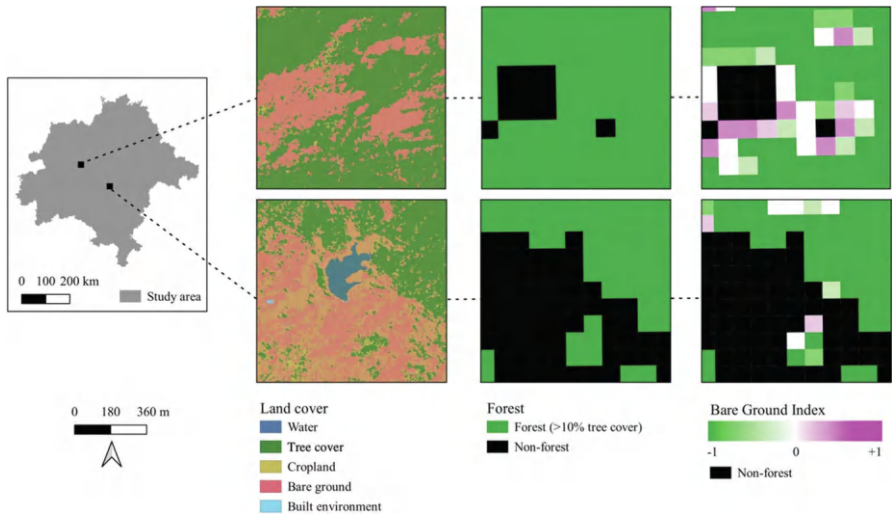

FIGURE 4.2 Two examples of the land cover classification were derived from the Bare Ground Index from Khanwilkar et al. (2023).

imagery as training data. We then aggregated the land cover data to 90-meter resolution to derive a Bare Ground Index (BGI), a normalized index of bare ground relative to tree cover within forested areas (defined as greater than 10% tree cover). The BGI ranges from –1.0 (all forest) to +0.8 (all bare ground). Higher values indicate more degraded forest. Validation with field data indicates that the BGI is a proxy for the intensity of human use.

The BGI was derived from data acquired in the winter to minimize cloud cover (February 28 to March 28, 2018). The time period also coincided with the collection of socio-economic data. The data set is publicly available through the LCLUC data portal, and the code is available as cited in Khanwilkar et al. (2023). The algorithm can be applied to additional years to monitor changes in degradation (Figure 4.2).

4.3.2 Socio-Economic Data

To assess patterns of forest use by forest-fringe communities, we surveyed approximately 5000 households in 500 villages within 8 km of forest from January to April 2018. The villages were randomly selected based on a sampling design accounting for distance to road and distance to town. We surveyed 10 randomly selected households in each village. The survey included basic demographic information, migration patterns within the last 5 years, and the use of forest resources (Baquie et al., 2020).

The surveys revealed that, within the time frame of the surveys, very few households (<0.5%) emigrated permanently from their village with the whole family. Approximately 18 percent of surveyed households had a member who migrated seasonally in the previous 5 years. People were migrating seasonally to many urban destinations in the country for industry jobs and daily labor contracts. The main

reasons for migration were income and better opportunities than those available in the village. Migrants generally send remittances to their families in the villages.

Livestock ownership and adoption of liquefied petroleum gas (LPG, an alternative to fuelwood) were not significantly different between households with and without members who migrated. In addition, the time spent collecting fuelwood, grazing, or collecting non-timber forest products was not significantly different (Baquie et al., 2020).

4.4 IMPLICATION OF RESULTS FOR A FOREST TRANSITION

Combining the satellite-derived Bare Ground Index and socio-economic data from 5000 households in the central Indian landscape offers an opportunity to assess hypotheses about potential forest transitions in this dry tropical forest. A forest transition would improve health, increase biomass, and promote ecosystem services such as carbon sequestration and watershed protection in these forests. Importantly, a sustainable forest transition mandates that local livelihood needs for household cooking, heating, construction, and fodder for livestock are satisfied while reducing pressure on forests.

Based on patterns observed in other parts of the world, one pathway to a forest transition could occur through migration as people leave the landscape or provide additional income that alleviates reliance on forest resources. A second complementary pathway could occur if demands for forest resources are reduced with substitutes for fuelwood, fodder, and construction.

4.4.1 Does Migration Foster a Forest Transition in Central India?

Analysis of the BGI in conjunction with data on migration indicates that landscape migration does not generally promote a transition towards healthier forests, at least over the short term (Baquie et al., 2020). No difference in forest use for cattle grazing or collection of non-timber forest products was observed for households with and without members who migrate seasonally for employment. Pressure on forests is likely to stay constant despite migration. Migration in this landscape is generally seasonal, with only one or a few members migrating to urban areas for a few months.

Contrary to the forest transition pathway from migration associated with land abandonment, we observed a weak but positive relationship between BGI (higher degradation) and the proportion of households with migrants in a village below a threshold of approximately 40 percent of households with migrants. While causality cannot be assumed, this relationship suggests that seasonal migration is necessary as a livelihood strategy where forests are more degraded. In the few villages with greater than 40 percent of households with migrants (10% of surveyed villages), the relationship with BGI is weakly negative, indicating that forest pressure might decline at very high levels of migration. Overall, however, the land abandonment pathway from migration is not likely to be a strong driver of a forest transition in this landscape, at least in the short term.

Seasonal migration in the period of the surveys was primarily associated with investments in mobile phone adoption and housing improvements. Further analysis

of the relationship between climate variability and migration indicated that migration occurred regardless of climate in any particular year for households in the lowest-income districts. These households are dependent on migration for their survival. For households in higher-income districts, first-time migration was more likely in drier years (Choksi et al., 2021). These observations suggest that, despite the standard narrative that the poorest are most sensitive to climate variability, in this landscape, the poorest are heavily reliant on remittances from migration despite climate variability. Higher-income agriculturally-based households are more sensitive to climate variability and are more likely to send a member to migrate in drier years.

4.4.2 Do Increased Living Standards Foster a Forest Transition in Central India?

A second pathway towards a forest transition relies on reducing pressure on forests through reduced dependence on forests. Analysis of the BGI in conjunction with data on forest dependence in 500 villages indicated that improved living standards, specifically LPG as an alternative to fuelwood for cooking and non-forest-based housing materials from concrete instead of timber, were significantly associated with less forest degradation (lower BGI) in 1 km buffers around the villages. The effect was lower with increasing distance from villages, as would be expected (DeFries et al., 2022).

The results suggest that development and improvements in living standards are potential pathways to a forest transition in this landscape, with the dual benefits of reducing forest degradation and alleviating poverty.

4.5 CONCLUSIONS

Dry tropical forests have received less attention from researchers, policymakers, and managers than other forest biomes. Tropical humid forests are widely recognized for their ecosystem services for carbon sequestration and biodiversity and for the need to reduce deforestation that has stubbornly persisted in South America, Southeast Asia, and increasingly in central Africa. Over the last century, temperate forests that were once deforested have regenerated owing to urbanization, land abandonment, and forest restoration.

Many of the world's lowest-income people live in or near degraded, dry tropical forests. The example from dry tropical forests in central India illustrates that pathways to forest transitions differ from those observed in other types of forests. In such a dry tropical forest landscape, where forest dependence and poverty are prevalent, a forest transition from urbanization and land abandonment cannot be assumed, at least on a short time scale. Intentional efforts to improve living standards and reduce dependence on forests through alternatives to forest resources for daily needs potentially foster a transition to healthier forests.

Results also indicate that very high-resolution satellite data can be used to monitor forest degradation in dry tropical forests. However, the methods need to be context-specific for the type of degradation. In the central Indian landscape, heavy forest use

for grazing and collecting forest products generates bare patches within the forest that serve as a proxy for degradation. Application of the algorithm to a time series can monitor future forest health and the potential impacts of interventions to reduce pressure on these forests.

ACKNOWLEDGEMENTS

The SARI LCLUC program provided funds for the studies reported in this chapter. We are also grateful to Chris Galleti. Qamar Qureshi, and Nandini Velho who participated in various aspects of the project.

The Bare Ground Index data is downloadable at https://lcluc.umd.edu/metadatafiles/LCLUC-2017-PI-Defries/.

The views expressed in this paper are the ones of the authors and do not necessarily represent the views of the World Bank Group, its affiliated organizations, its Executive Board, and its management.

REFERENCES

Agarwala, M., DeFries, R., Qureshi, Q. & Jhala, Y. 2016. Factors associated with long-term species composition in dry tropical forests of Central India. *Environmental Research Letters*, 11, 1–10.

Baquie, S., Urpelainen, J., Khanwilkar, S., Galletti, C., Velho, N., Mondal, P., Nagendra, H. & Defries, R. 2020. Migration, assets, and forest degradation in a tropical deciduous forest of South Asia. *Ecological Economics*, 106887.

Choksi, P., Singh, D., Singh, J., Mondal, P., Nagendra, H., Urpelainen, J. & Defries, R. 2021. Sensitivity of seasonal migration to climatic variability in central India. *Environmental Research Letters*, 16(6), 064674.

Defries, R., Agarwala, M., Baquie, S., Choksi, P., Khanwilkar, S., Mondal, P., Nagendra, H. & Uperlainen, J. 2022. Improved household living standards can restore dry tropical forests. *Biotropica*, 54, 1480–1490.

Gajbhiye, K. & Mandal, C. 2000. *Agro-Ecological Zones, Their Soil Resource and Cropping Systems*. National Bureau of Soil Survey and Land Use Planning: Nagpur, India. Available online: www.indiawaterportal.org/sites/indiawaterportal.org/files/01jan00sfm1.pdf

Khanwilkar, S., Galletti, C., Mondal, P., Urpelainen, J., Nagendra, H., Jhala, Y., Qureshi, Q. & Defries, R. 2023. Land cover and forest health indicator datasets for cenrtal India using very-high resolution datellite data. *Scientific Data,* 10, 738. https://doi.org/10.1038/s41597-023-02634-w.

Khanwilkar, S., Gould, C., Defries, R., Habib, B. & Urpelainen, J. 2021. LPG adoption by marginalized, forest-fringe populations in central India. *Energy Research and Social Science*, 75, 1–13.

Mather, A. S. 1992. The forest transition. *Area*, 24, 367–379.

Mcnicol, I. M., Ryan, C. M. & Mitchard, E. T. 2018. Carbon losses from deforestation and widespread degradation offset by extensive growth in African woodlands. *Nature Communications*, 9, 3045.

Meyfroidt, P. & Lambin, E. F. 2011. Global forest transition: Prospects for an end to deforestation. *Annual Review of Environment and Resources*, 36(1), 343–371.

Miles, L., Newton, A. C., Defries, R., Ravilious, C., May, I., Blyth, S., Kapos, V. & Gordon, J. 2006. A global overview of the conservation status of tropical dry forests. *Journal of Biogeography*, 33, 491–505.

Reddy, M., Singh, O., Ahmad, P. I. & Sofi, A. 2021. Criteria and indicators for assessment of forest degradation in dry-tropical forests of India. *Plant Archives*, 21(1), 66–72.

Rudel, T. K., Coomes, O. T., Moran, E. F., Achard, F., Angelsen, A., Xu, J. & Lambin, E. 2005. Forest transitions: Towards a global understanding of land use change. *Global Environmental Change*, 15, 23–31.

Schoen, J., Neelakantan, A., Cushman, S., Dutta, T., Habib, B., Jhala, Y., Mondal, I., Ramakrishnan, U., Reddy, P., Saini, S., Sharma, S., Thatte, P., Yumnan, B. & Defries, R. 2022. Synthesizing connectivity analyses for co-management of a globally important human-dominated tiger (Panthera tigris) conservation landscape. *Conservation Biology*, 36, e13909 (1–15). https://doi.org/10.1111/cobi.13909.

Siyum, Z. G. 2020. Tropical dry forest dynamics in the context of climate change: Syntheses of drivers, gaps, and management perspectives. *Ecological Processes*, 9, 1–16.

5 Remote Measures and Remote Policies

A Critique of Remote Sensing in Indian Forests and Environmental Policy with Suggestions for Moving Forward

Forrest Fleischman, Vijay Ramprasad, and Pooja Choksi

5.1 INTRODUCTION

Remote sensing may be a powerful tool for studying landscapes, yet it is not a neutral instrument (Bennett et al., 2022). Remote sensing empowers people with access to certain kinds of data and skills to analyze that data and values certain elements of landscapes (e.g., those that can be observed from the sky) over other elements that can only be observed on the ground. In this chapter, we examine how remote sensing in India has reinforced ineffective and counterproductive policies in the forest sector and provide suggestions for moving forward. In particular, we argue that remote sensing has reinforced a tendency in Indian policy-making to focus on the area of tree cover as a key metric of success in forestry, to the detriment of other measures of ecosystem function or social benefit. The result has been several highly prominent Indian forestry schemes, such as CAMPA and the new Green Credits Scheme, which emphasize changes in forest cover – i.e., what can be observed from a satellite – while ignoring nearly all social and ecological relationships that make forests essential and valuable. At the same time, we argue that remote sensing, mainly when used with carefully collected data from the ground on social and ecological relationships, can be a powerful tool for rethinking the management of Indian landscapes. The opportunity to use remote sensing to facilitate positive outcomes depends on robust funding for on-the-ground social and ecological research to ensure that what can be measured from the air can be studied in combination with knowledge about people, places, and ecological systems. While our essay primarily aims to engage an audience interested in improving the use of remote sensing in Indian policymaking, it also aims to offer

 DOI: 10.1201/9781003396260-5

broader lessons on the risks of the uncritical application of technology to solving complex social-ecological problems.

Remote sensing became an essential tool for the governance of Indian forests in the 1980s, as the availability first of foreign satellite data (e.g., from LANDSAT) and later India's domestic remote sensing capabilities (e.g., from ISRO) made remote sensing of India's land cover technically and economically feasible. The first "State of India's Forests" report was published in 1987 by the Forest Survey of India, based on LANDSAT data from 1981–1983 (Government of India, Ministry of Environment and Forests, Forest Survey of India 1987), and follow-up reports have been published every 2 years since then. These reports have been highly influential with policymakers and occasionally even used to determine budget allocations (Busch and Mukherjee, 2018; Busch et al., 2020; Chaturvedi 2016). They rely on satellite-based remote sensing of tree cover, initially conducted using visual interpretation of Landsat imagery, but moving by the mid-1990s to the digital interpretation of imagery from ISRO satellites, combined with some ground-truthing (which has rarely been clearly described in State of Forest Reports). Over the years, greater availability of satellite data combined with the increased on-the-ground technical capacity has led Indian forestry agencies towards increased reliance on remote sensing to understand forest conditions on the ground.

As measured by satellite, forest cover is a very poor measure of the diverse values in nature–society relationships in any place in the world, particularly in India. For example, the focus on forest cover has led to an ongoing misunderstanding and degradation of a wide variety of ecosystems that are native to India but do not feature dense tree cover, including grasslands, shrublands, and savannas (Gopalakrishna et al., 2024; Lahiri et al., 2023; Madhusudan and Vanak 2023). These ecosystems provide vital services and protect many of India's most endangered wildlife. The focus on tree cover, as seen from the satellite, has also obscured the values lost and gained as native forests have been converted to plantations (Puyravaud et al., 2010a, 2010b; Davidar et al., 2010) and sizeable old agroforestry trees have been lost (Brandt et al. 2024). Furthermore, a focus on forest cover as a seemingly static stock obscures the ways that Indian ecosystems might be mobilized to support the thriving of people, animals, and plants who depend on forests for their well-being as forests produce ecological dynamics and flows of goods and services that may not be captured effectively by satellites.

The net result of the entrenched reliance on satellite-based forest cover measures is that India's environmental policy framework has been largely ineffective. There are two elements of this ineffectiveness. First, where policies are successful at conserving or increasing tree cover, they often do so in ways that provide limited value to people and nature because those trees that can be grown or conserved most effectively to maximize tree cover are not necessarily the same as those which provide the most significant benefit to people and nature. For example, in the western Himalayas, native pines are the most effortlessly and widely propagated tree, however, native oaks are more beneficial for both people and nature (Das et al. 2021; Shahabuddin et al. 2021), and many Indian ecosystems are most ecologically and economically beneficial when tree cover

is sparse rather than dense (Lahiri et al., 2023; Madhusudan and Vanak 2023; Gopalakrishna et al., 2024). Second, focusing on tree cover has led governments to deprioritize the on-the-ground conservation work that is necessary to understand why people make landscape management decisions and to adopt one-size-fits-all policies that are often ineffective at encouraging conservation and regeneration because they do not correspond to local drivers of land use change.

Remote sensing has been widely adopted in forestry partly because it appears inexpensive relative to other forms of measuring and understanding forests. This is a false appearance. Building a capacity for remote sensing of forests has taken decades of investment in building satellites, purchasing computers, and training technicians. Scientists have long recognized that remote sensing is only valid when accompanied by intensive on-the-ground knowledge of ecosystems, human dynamics, and political institutions (Moran and Ostrom 2005; National Research Council et al. 1998). This combination differs from "ground-truthing," which primarily aims to anchor and verify satellite-based knowledge. It seeks to measure the invisible social and ecological dynamics from space, not merely verify that an algorithm for analyzing remote sensing data is performing correctly. Yet once the infrastructure for remote sensing has been built, it appears expedient to measure forest cover from Earth Observing satellites. In contrast, it is expensive to measure humans' diverse values for diverse kinds of nature. They cannot be measured except by engagement with local communities and intensive site-based measurements using complex combinations of social and ecological measurements. This also requires substantial training and, importantly, political will to engage with communities and face community questions of state accountability and forest rights. Instead, as a straightforward measurement, forest cover has facilitated a type of governance that obscures the complex relationships between people, nature, and well-being in India and simplifies it into one metric.

In presenting this story, we aim to illustrate how alternative uses of remote sensing technology may be harnessed to aid in a broader and deeper understanding of people and nature in South Asia and beyond. Understanding the limitations of the technology and its application in India can unlock new ways of seeing, guiding analysts towards uses of the technology that could aid in broader understanding and/or challenge narrow-minded visions embodied in Indian policies. In addition, the dramatic improvements in earth observing satellites since the 1980s mean that more kinds of values can be incorporated into satellite-based studies of India, which can, in turn, lead to improvements in policy. We begin by outlining the pre-remote sensing history of natural resource management in India, pointing to how the pre-existing policy framework favored a focus on forest cover over other measures of human–environment interactions. We then show how the introduction of remote sensing reinforced this view and how remote sensing continues to support and critique nature conservation in India (Figure 5.1). A key idea in this section is that while remote sensing has numerous potential applications, the simplest ones have tended to be used to develop simple measures of forest cover change that do not reflect the complexity of natural values in India. We conclude with a call to do better research and policy-making, drawing on examples from recent research, with a focus on transparency, a clear understanding of technological limitations, and partnership between remote

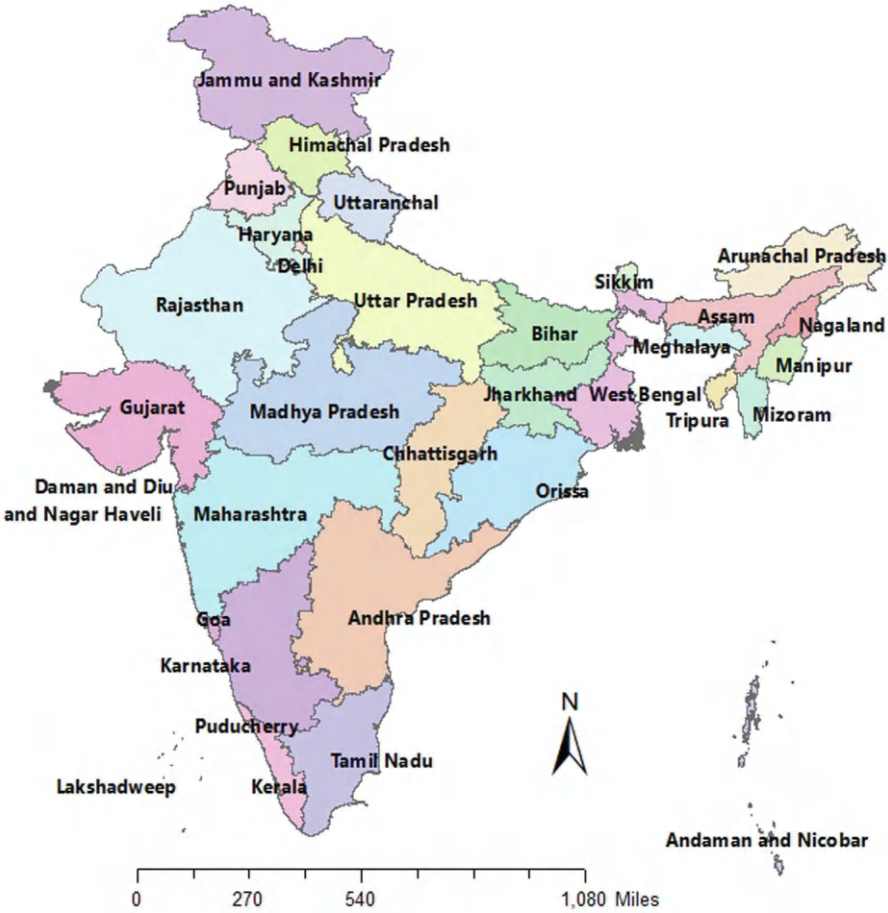

FIGURE 5.1 India with states.

sensing and other research techniques to undo the harms of the past and improve human well-being and nature in India.

5.2 VALUING TREES IN COLONIAL AND POST-COLONIAL INDIA

India's current natural resource policy landscape builds on a legacy set by the colonial era. The British colonial state set up forestry agencies in the middle of the 19th century in an effort to make better use of seemingly unproductive forest resources while also securing timber crucial for the construction of railways needed to shore up colonial power (Gadgil and Guha 1992; Guha 1983; Roy and Fleischman 2022). These agencies prioritized the needs of the colonial state, particularly with regards to prioritizing the provision of timber, initially for railroads and later to serve a variety of other needs of the British, but also were forced to accommodate local demands for access to

forest resources that were integral parts of the livelihoods of rural people (Guha 1989; Rangarajan 1996b; Skaria 1999; Sivaramakrishnan 1999; Rangarajan 1994, 1996a). These accommodations were the source of consistent struggle and contestation, and the formal rights of forest-dependent peoples were greatly limited by colonial policy. Much of India's natural wealth remained outside of the direct control of the state, on a variety of private lands and zamindari estates, and under the control of princely states. Still, these landowners were encouraged to follow policy frameworks derived from British imperial practices (Abdul Thaha 2009). Furthermore, forestry was often seen as secondary to broader goals of encouraging agriculture, providing direct revenue to the colonial state, and providing benefits to farmers and the rural poor (Saberwal 1999; Guha 1983; Gadgil and Guha 1992).

Because of the commercial, industrial, and political nature of the British Empire, the diverse values present in natural systems were viewed through a highly simplified lens. Natural areas with fertile soils and access to water were prioritized for the expansion of agriculture, which could be taxed to the benefit of the state. In contrast, areas with timber were reserved for the production of wood products. Some small areas were set aside as hunting reserves due to the symbolic and recreational value of hunting for the Indian and British ruling classes (Rangarajan 2001). Other areas were viewed as "wastes" – i.e., lands that were not productive for the state. This terminology continues to be used today to refer to lands that are not farmed and do not have dense tree cover despite the now widespread recognition that ecosystems such as wetlands and deserts are indeed very valuable, even on purely economic terms (Baka 2019; Baka 2013, 2014, 2017; Lahiri et al., 2023).

This framework was reinforced with Indian independence. The developmental state that wished to improve the welfare of its citizens focused on industrial and agricultural development with little attention to natural landscapes or the people who depended on them (Gadgil and Guha 1995; Guha 2007). Forest-dependent peoples played a role in the struggle for an independent India (Baker 1984), so they might have expected to receive benefits as newly independent India moved from a state that sought to benefit a distant colonial power to one that aimed to develop and uplift its people. Yet, newly independent India moved in the opposite direction. Not only was the punitive 1927 Forest Act kept in place by the newly independent government (in fact, it is still on the books), but in the early 1950s, India developed a new forest policy (Government of India 1952), which sought to prioritize the use of forests for national needs, primarily understood as industrial production but also soil conservation and water security for high productivity agricultural areas.

The 1952 forest policy not only continued the colonial focus on forests as drivers of industrial activity, it also introduced the first quantitative targets for India's forest land cover: overall, one-third of India's land area was to be forested, including 60% in "mountainous tracts" such as the Himalayas, and 20% in plains areas. These numbers were not based on a systematic analysis of India's current land uses or areas needed to fulfill different goals within the broader frame of economic development and social uplift, nor on the availability of land. Instead, the panel developing the policy based these goals on analyzing the current land area devoted to forests in wealthy countries in Europe and North America (Joshi et al. 2010). This approach appears to have been based on the assumption that these relative areas were somehow contributing to

national wealth (Joshi et al. 2010) instead of being reflections of the areas in those countries most suitable for different ecosystems and land uses or historical accidents as a snapshot of the rapidly changing forest cover of Europe and North America in the 20th century (Joshi et al. 2010; Mather and Needle 1998). No quantitative targets were established for the area of India that might be devoted to other natural ecosystems, such as mangroves, wetlands, deserts, savannas, or grasslands, despite these ecosystems' potential to provide essential ecosystem services.

Between 1952 and 1980, India pursued five important policy initiatives related to the management of nature. First, India nationalized natural areas, including forests, under the control of princely states, zamindars, and other private landowners and placed these under the control of state forest departments (Sarin 2005). This meant not only that there would no longer be private forests and natural areas but also that all of these natural areas, including the deserts of Rajasthan, the alpine areas of the Himalayas, or the remaining terai and shola grasslands, would be managed by agencies that were organized around the industrial production of wood fiber. Second, India developed a new national civil service, the Indian Forest Service, which provided national supervision to state-run forestry agencies. It was based on the Imperial Forest Service, discontinued in 1935 (Forest Research Institute Dehra Dun 1961). The high prestige afforded the Indian Forest Service ensured that local, regional, and national governments had advocates for commercially oriented "scientific" forestry. Still, no similar prestige was given to the conservation of wildlife or the natural systems they depended on, nor to the integration of rural people and forests, nor the management of other kinds of natural systems, such as grasslands, savannas, wetlands, or deserts. Third, in the 1970s, wildlife conservation laws created protected areas and outlawed hunting. These laws were to be enforced by state forest departments in addition to their work as forest managers, and little consideration was given in these laws to people who depended on protected areas or wildlife hunting for their well-being. Fourth, national studies noted an apparent low productivity of Indian forests (National Commission on Agriculture 1976). Although this report was probably mainly in error because it focused on the production of commercial roundwood and ignored the very substantial role forests played in the rural economy, it spurred a strong interest on the part of the state in increasing forest cover and productivity through plantation activity (Roy and Fleischman 2022). Finally, and perhaps most importantly for both policy development and nature, vast areas of India's natural lands were converted to agriculture and other non-forest land uses. Indian states were eager to bring "land to the tiller" and thus quickly regularized such agricultural expansion (Guha and Gadgil 1989; Chhatre 2000; Government of India, Ministry of Environment and Forests, Forest Survey of India 1987).

5.3 THE EMERGENCE OF THE FOREST COVER REGIME IN THE 1980S

In 1972, Indian Prime Minister Indira Gandhi delivered a highly influential speech at the UN Environment Conference in Stockholm, which led her to be recognized globally as a leading environmentalist (Mudaliar and Kashwan 2024). As a politician, Gandhi spearheaded several environmental initiatives, including the wildlife

protection laws of the 1970s referred to above (Mudaliar and Kashwan 2024). Still, her most significant contribution to this essay was the Forest Conservation Act of 1980, which is the first of the three major policy shifts of the 1980s that worked alongside remote sensing to create a tree-cover-focused policy. The Forest Conservation Act responded directly to the widespread loss of forest land to agriculture in the decades since independence by requiring that any diversion of forest land for a "non-forest purpose" be approved by the Central Government. "Non-forest purpose" was defined to mean "the breaking up or clearing of any forest land or portion thereof for (a) the cultivation of tea, coffee, spices, rubber, palms, oil-bearing plants, horticultural crops or medicinal plants; (b) any purpose other than reafforestation."

Notably, the law did not define the term "forest land." The English word "forest" has several meanings, but some specifically refer to tree cover. For example, the Oxford English Dictionary ("Forest, n. Meanings, Etymology and More" 2023) provides three definitions of the use of "forest" as a noun:

1. "An extensive tract of land covered with trees and undergrowth, sometimes intermingled with pasture. Also, the trees collectively of a 'forest'."
2. "Law. A woodland district, usually belonging to the king, set apart for hunting wild beasts and game, etc. (cf. quotes. 1598, 1628), having special laws and officers of its own.
3. "A wild, uncultivated waste, a wilderness."

Notably, the second definition is described as being the legal definition, does not refer to a defined amount of tree cover, and is consistent with the historical legal use of the term in India, which followed the British in using the term forest to refer to reserved natural areas, regardless of the extent of tree cover. Both other definitions include areas without trees as part of "forests" – as in the reference to pastures and wildernesses. India's legally defined forest land area includes extensive tracts of land that lack heavy tree cover due to aridity, altitude, flood regimes, as well as the effects of herbivory and fire (Gopalakrishnan et al., 2024; Roy and Fleischman, 2022; Madhusudan and Vanak 2023; Ratnam et al. 2011). In many other countries, responsibilities for areas such as publicly owned desert and grazing land, wildlife protection areas, and national parks are delegated for better or worse to specialized agencies that are separate from the government's forestry agency. Still, in India, all of these roles are managed by the state forest departments, thus making all or most lands managed for wildlife habitat, publicly available grazing, desert, or other non-agricultural purposes "forest" land despite these lands not having forest land cover. Due to the historical legacy of an emphasis on timber production in Indian forestry, there has been little public or governmental recognition of the fact that many of India's natural areas that contain trees do not naturally have dense tree cover (Joshi et al., 2018; Ratnam et al. 2016).

Eight years later, in 1988, a committee of senior government officials revised India's forest policy. They retained the emphasis on forest cover. However, they revised the purposes for which forests were intended to serve. Under the 1988 forest policy, forests were no longer intended primarily for industrial production – instead, a new priority was given to ecological integrity and the needs of forest-adjacent

communities. This shift was accompanied by the development of a new set of programs to protect and regenerate forests through collaboration with local communities. "Joint Forest Management" appeared, at least at first, to be a revolutionary development (Poffenberger and McGean 1996; Joshi 2000), but over time, was subjected to much criticism for failing to meaningfully engage with local views and priorities (Springate-Baginski and Blaikie 2013).

The final shift in Indian forest policy in the 1980s is the one most relevant to this essay: the emergence of remote sensing as a tool for understanding forests. While neither remote sensing nor forest surveys were new to India in the 1980s, the widespread availability of satellite imagery of forests facilitated the creation of the first of what became the Forest Survey of India's biannual "State of the Forest" reports. It is notable what these reports did and did not include: Although India had a long and distinguished history of developing techniques for forest mensuration based on *in situ* measurements (Stebbing 1922; Barton and Bennett 2008; Barton 2002), the Forest Survey of India did not establish a national network for *in situ* forest measurements. The first State of the Forest report, like all such reports that were to follow, was primarily a report on forest cover as measured by satellite imagery, with a small amount of ground truthing. Forests were ranked by their density, with higher-density forests presumably considered better. Little to no information was provided on aspects of forests such as their biodiversity, contribution to ecosystem services, historical or potential state, or their contribution to the well-being of local people. To this day, there is no regularly occurring survey of India's forests to understand what species of plants and animals they contain, or how local people use them.

5.4 TODAY'S FOREST COVER REGIME AND THE USE OF REMOTE SENSING IN INDIAN POLICY

Although there have been significant changes in forest policy since the 1980s, the trends of the past described here continue to shape the relationship between remote sensing and Indian forests. The Indian government continues to use remote sensing to measure forest cover with little regard for other aspects of forests, and the Forest Survey of India does not provide, nor have governments demanded, data on other aspects of forest, with the notable exceptions of surveys of the populations of endangered charismatic megafauna such as tigers and elephants. The Forest Survey of India uses a set of arbitrary classifications for forest density, which do not reflect the complexity of India's highly varied natural land covers (Madhusudan and Vanak 2023; Gopalakrishna et al. 2024; Ratnam et al. 2016) and differ from the widely varied classifications used to define forest and forest density globally (Savilaakso et al. 2023). The standard classification of forest types used by the Forest Survey of India and other agencies (Champion and Seth 1968) does not incorporate new knowledge about forest types nor savanna and open land cover types (Bahuguna et al. 2016; Madhusudan and Vanak 2023).

While policies, such as the Forest Rights Act, have aimed to improve engagement between forest-dependent peoples, numerous other laws and policies have placed an emphasis on quantitative measurements of forest cover with little concern for other aspects of forests.

The most prominent such policy is Compensatory Afforestation, often referred to as CAMPA. The genesis of Compensatory Afforestation was the Forest Conservation Act of 1980, discussed above. A series of regulatory decisions and court rulings in the 1990s set up a framework under which the central government would approve diversions of forest land for "non-forest purposes" if money was deposited to support reforestation elsewhere (Menon and Kohli 2021; Rosencranz et al., 2007; Thayyil 2009; Upadhyay et al., 2009). These rulings were eventually organized under the aegis of the Compensatory Afforestation Fund Act of 2016, which provided an organized system for receiving funds and investing them in reforestation activities.

The judgments and laws surrounding CAMPA can only be understood if one begins from the false premise that a forest is nothing more than tree cover as seen by a satellite. CAMPA aims to replace diverted forest land, meaning land that *either* has tree cover *or* is legally designated as forest land (and does not necessarily have tree cover for reasons discussed above), and replace them with newly planted trees. The requirement is not to replace equivalent land or a similar ecosystem. Instead, CAMPA envisions planting new trees elsewhere on the landscape, a replacement that can only be understood as equivalent if one assumes (incorrectly) that all forests consist only of trees and that any tree can be substituted for any other tree anywhere. Such a view makes sense only from the abstraction of satellite imagery used to measure tree cover. It makes no sense to examine ecological, economic, or social relationships between people, trees, and the several meanings of the word forest. Stripped of context, the trees envisioned by CAMPA can only be justified through a remote sensing perspective that excludes all other sources of knowledge about nature and human–environment interactions.

Interest in using trees for environmental benefits is not exclusive to India. Since the 1990s, there has been global interest in the potential for ecosystems to mitigate climate change by absorbing carbon, and trees are often seen as the primary tool to accomplish this goal. This has led to the emergence of carbon markets, in which carbon emitters, such as industries, pay those who have the means to sequester carbon to do so. The earliest such large-scale scheme was the Clean Development Mechanism developed under the Kyoto Protocol to the United Nations Framework Convention on Climate Change, which was envisioned as both a technology and financial transfer from wealthy to poor countries. Although most Clean Development Mechanism projects were developed outside of the forest sector, some projects were developed to sequester carbon in forests: evaluations of these projects have mostly been negative (Aggarwal 2021, 2012, 2020).

Nonetheless, there is a growing interest in developing carbon sequestration projects in India. Measuring carbon sequestered in forests is technically complicated and requires accounting not only for above-ground carbon (i.e., stored in the visible parts of trees) but also below-ground carbon, for which dynamics are complicated, poorly understood, and require expensive *in situ* measurements (Oldfield et al. 2022; Pan et al. 2022; Smith et al. 2020). Furthermore, carbon projects require estimation of additionality – i.e., the carbon stored that is additional to what would have occurred without the project. There are substantial questions about whether and how additionality can be measured, as well as evidence that it is not being measured well in

existing carbon projects (Wunder et al. 2024; West et al. 2023; Gill-Wiehl, Kammen, and Haya 2024; Stapp et al. 2023). Nonetheless, the development of various forms of carbon projects, many tied to the voluntary carbon market, has emerged in India. Because existing protocols are lax in terms of many of the measurement issues highlighted in the literature, in practice, many of these carbon projects rely primarily on remotely sensed images of land cover change tied to allometric equations to make carbon estimations. The most promising areas for the voluntary carbon market in India are probably not in the forest sector (DeFries et al. 2022), and many of the most promising locations for more trees in India are on agricultural land as opposed to natural forests (Gopalakrishna et al. 2022); nonetheless, the interest in remote sensing to play into carbon markets remains prominent and is often used as a justification for investing in better remote sensing capabilities that could, for example, improve measurement of trees outside of forests for carbon market benefits. Although improved measurement of tree canopies outside of forests may have various benefits, it will not overcome the fundamental technical constraints on measurements for incorporating forests into carbon markets since it neither addresses below-ground carbon nor enables measurement of additionality.

The flawed perspectives of CAMPA and the carbon market have recently been extended under the aegis of the Government of India's new "Green Credit Scheme" (Sethi 2024). This scheme extends a CAMPA-derived framing of the benefits of tree planting to allow companies to derive credits for supposedly beneficial "green" actions (primarily understood as tree planting) to compensate for various environmentally harmful activities. Most of these environmentally harmful activities do not have harms that can be undone or compensated for in a meaningful sense through tree plantations; moreover, there are a wide variety of reasons why tree planting activities can fail to deliver intended benefits even in circumstances where they might represent appropriate compensatory activities (Holl and Brancalion 2020; Brancalion and Holl 2020; Fleischman, Basant, et al. 2020). Again, such a view can only be justified through the abstraction of the remotely sensed image of a forest, where trees appear to be infinitely substitutable, and, as per the framework laid out in Indian law, trees are seen as synonymous with environmental benefits.

Can we blame remote sensing for these flawed visions? On the one hand, they are partially the result of conditions that long pre-date the existence of remote sensing, such as the regressive laws and focus on lumber productivity that are legacies of the colonial era and the 1952 forest policy's arbitrary delineation of a target for "forest cover." On the other hand, the continuation and extension of these legacies were a choice, and one can clearly see that other countries with similar legacies have made different choices. For example, forestry in Nepal was practiced in a manner quite similar to India from the 1950s until the 1980s but subsequently has seen a dramatic shift towards community-based management, with much less focus on trees for tree's sake (Ojha and Hall 2023; Poudyal et al. 2023). The heavy investment in remote sensing by India and the subsequent large-scale availability of remotely sensed data, which can speak to the presence of trees on the landscape but not to social-ecological relationships, makes trees highly visible in both the Indian public imagination and policymaking. This has reinforced the pre-existing tendency to miss the forest for the trees.

5.5 MOVING FORWARD: HOW REMOTE SENSING CAN BE MORE PRODUCTIVELY APPLIED TOWARDS BETTER FOREST SCIENCE AND POLICY DESIGN

Of course, remote sensing remains a powerful tool for understanding the world. Although remote sensing has reinforced unfortunate policy choices in India, the expense of establishing advanced remote sensing capabilities to study land cover in India has already been made, and it does not need to be abandoned. Instead, remote sensing scientists, including both independent scientists and those working in the forest department and related agencies, can play a leading role in helping Indian society and policy develop a more complex understanding of land cover and land use dynamics that both utilize the capabilities of remote sensing and overcome their limitations. We propose that three broad principles should apply to such efforts:

1. Integrate remote sensing information with knowledge about ecosystems and social systems to develop understanding through collaboration with scientists and practitioners with relevant expertise.
2. Disclose methodological limitations consistently using language that non-scientists can understand.
3. Release data and methods to encourage public discussion and independent error-checking.

To understand how a program utilizing remote sensing-derived knowledge might enhance the management of nature in India, we draw on two examples from our research. We intend these examples to illustrate potential uses, and we know that many other potential uses may exist.

Partly because of its preoccupation with forest cover, Indian forest departments have a long tradition of planting trees. While such plantings have been criticized for leading to the displacement of native land covers with plantation forestry (Puyravaud et al., 2010a, 2010b; Davidar et al. 2010), there has been little evaluation of the impacts of tree plantings. To remedy this, we evaluated the effects of tree planting on forest cover and rural livelihoods in the Kangra District of Himachal Pradesh. Our evaluation began with mapping the boundaries of all plantations we could locate in 60 randomly selected panchayats in the district. Mapping required us to locate local informants who had been closely involved with past plantation activities and walk the boundaries of plantations they remembered (not all of which had obvious visual evidence of plantation – as in the case of past failed plantations). This expensive and time-consuming step illustrates the value of open data: if the Himachal Pradesh forest department had mapped and publicly released the boundaries of plantations as they were planted, our evaluation would have been substantially cheaper, and the cost to the department would have been minimal as in any case, mapping is already undertaken in planning plantations on government land. Unfortunately, attempts to force greater data transparency, such as the requirement to post CAMPA plantations on the E-Greenwatch website, have often met with resistance from field foresters (Comptroller and Auditor General of India 2024). We then located a time series of cloud-free LANDSAT images that covered these plantations dating back to the 1980s. Although tree planting has occurred throughout Indian history (Roy and Fleischman

2022), it accelerated in the 1970s (Government of India, Ministry of Environment and Forests, Forest Survey of India 1987; Ravindranath et al. 2007), and thus the availability of LANDSAT imagery since the 1980s allows for before and after comparisons of land cover for most of the plantations. We conducted extensive ground-truthing for the recent images and compared older images with available higher resolution data sources to estimate the accuracy of the images.

Our comparison of areas before and after planting showed little impact on overall forest cover, but planting did shift tree cover from broadleaf towards needleleaf trees (Coleman et al. 2021). Combining this with household survey data, we found that although needle leaf trees tend to be less helpful to people than broadleaf trees, potential adverse livelihood effects from tree planting were muted because overall forest dependence in the region was low (Coleman et al. 2021; Ramprasad et al., 2020), although effects were more substantial for certain vulnerable social groups (Ramprasad et al., 2020). Win-win outcomes (i.e., where increased forest cover and improved livelihoods co-occurred) were associated with more decisive local collective action and a consolidated local institutional space (Rana et al. 2024). We found that a large percentage of tree planting activity was targeted towards areas where planting did not seem to be necessary and/or tree survival probability was low (Rana et al. 2022), and also that the total potential tree cover for the state of Himachal Pradesh was only about 30% – far below the established target of 60% in mountainous areas (Rana and Varshney 2023).

Overall, these studies relied on remote sensing to establish tree cover but relied on extensive assessment of on-the-ground conditions to understand the implications of that tree cover for people and nature. For example, we used data drawn from a variety of government records and our mapping processes to understand how tree cover related to government programs to plant trees, demonstrating that although there had been changes in tree cover over time, these could not be attributed to planting programs, which had no net effect and were often targeted to the wrong areas. Similarly, we used data from an extensive household survey (Coleman et al., 2021) and community-based mapping (Fleischman et al., 2020) to understand the implications of tree planting for people. Our ongoing research aims to tie changes in tree cover and forest composition to changes in biodiversity, carbon storage, and other ecosystem functions and services while also attempting to understand better how these changes in nature may be related to changes in the social and political changes ongoing in the human communities near the forest areas. Through this integration, we gave remotely sensed images meaning that could be used for more effective policy design. Recent government orders in Himachal influenced by this work have restricted plantations in areas crucial for migration routes for vulnerable pastoral people while also emphasizing the need to more carefully select sites for plantations where they can be most beneficial to people.

Recent studies in Central India also highlight the need for a combination of remotely sensed tree cover products, fine-scale vegetation measurements, and social surveys to make locally relevant natural resource management decisions. Choksi et al. (2023) leveraged remotely sensed tree cover data to create a matched sample of restored and unrestored forest patches using a propensity score. The authors used fine-scale land cover classifications from Planet Lab data for the year restoration took

place (2018) to match the restored and unrestored sites using a propensity score and create a balanced sample. In this case, forest cover data was a starting point for delineating restored patches by removing *Lantana camara* in the understory and those that remain unrestored where no such intervention was made. Once these patches were matched on forest cover and several other geographic and socio-economic characteristics, the authors matched the sites based on overstory characteristics (such as density of trees of a particular size class, species diversity of trees, etc.). This secondary matching process highlights the importance of including fine-scale vegetation measurements and remotely sensed tree cover data to create a balanced set of sampling sites. Several potential unrestored sites were discarded at this stage, as their inclusion would have led to an imbalance of restored and unrestored sites. This study is an example of a robust study design that draws on a combination of remotely sensed forest cover data and fine-scale vegetation measurements to isolate the effects of restoring the understory. Choksi et al. (2023) find that even though these forest patches appear to be no different from each other when the overstory is observed as a forest pixel, differences in the understory have a significant effect on biodiversity, such as insects, illustrating the importance of fine-scale measurement of features that cannot be observed through remote sensing.

Choksi et al. (2023) used household surveys around these same matched forest patches to determine the socio-economic impact of restoring these forest patches. In this case, the overstory characteristics, which most remotely sensed tree and forest cover products measure, were comparable. However, household surveys revealed that restoration through removing *Lantana camara* in the understory significantly changed the impact these forests had on the livelihoods of local human communities. For example, with a clearer understory in the absence of large thickets of *Lantana camara*, respondents reportedly traveled shorter distances to graze their cattle than people living around unrestored sites. Again, this social information about how people used the land and how those uses were valued was unavailable without boots-on-the-ground survey research.

5.6 CONCLUSION

The problem with remotely sensed data in India is that it is too easy to use cheaply available data to reinforce widely held preconceptions about how forests should be managed. In retrospect, it seems unfortunate that some of the vast sums of money used to send satellites into orbit, develop earth-observing sensors, and train scientists in the interpretation of images was not used to develop similarly robust on-the-ground capabilities to monitor biodiversity, the delivery of essential ecosystem services, and the social conditions in rural villages. After all, remote sensing only appears cheap to the users who are not paying for the costs of developing remote sensing infrastructure, and on-the-ground monitoring looks expensive when one ignores the tremendous money wasted on ineffective public programs. Improved management requires knowledge about the conditions and benefits flowing from nature, and remote sensing can only provide a small, albeit significant, portion of the needed information. In the future, more effective management and policies can emerge through better

integrating different types of data to understand and improve the delivery of government programs.

REFERENCES

Abdul Thaha, S. 2009, *Forest Policy and Ecological Change: Hyderabad State in Colonial India*, Foundation Books, New Delhi.

Aggarwal, A. 2012, 'How sustainable are forestry clean development mechanism projects?—A review of the selected projects from India', *Mitigation and Adaptation Strategies for Global Change*, vol. 17, no. 5, pp. 1–19.

Aggarwal, A. 2020, 'Revisiting the land use assumptions in forest carbon projects through a case from India', *Journal of Environmental Management*, vol. 267, no. 8, p. 110673.

Aggarwal, A. 2021, '"Carbon" in forest carbon projects: Evidence from India', *Climate and Development*, vol. 14, no. 2, pp. 1–10.

Bahuguna, V.K., Swaminath, M.H., Tripathi, S., Singh, T.P., Rawat, V.R.S. & Rawat, R.S. 2016, 'Revisiting forest types of India', *International Forestry Review*, vol. 18, no. 2, pp. 135–145.

Baka, J. 2019, 'Do wastelands exist? Perspectives on "productive" land use in India's rural energyscapes', *RCC Perspectives*, vol. 2, pp. 57–64. Available from: www.jstor.org/stable/26631562

Baka, J. 2013, 'The political construction of wasteland: Governmentality, land acquisition and social inequality in South India', *Development and Change*, vol. 44, no. 2, pp. 409–428.

Baka, J. 2014, 'What wastelands? A critique of biofuel policy discourse in South India', *Geoforum: Journal of Physical, Human, and Regional Geosciences*, vol. 54, pp. 315–323.

Baka, J. 2017, 'Making space for energy: Wasteland development, enclosures, and energy dispossessions', *Antipode*, vol. 49, no. 4, pp. 977–996.

Baker, D. 1984, '"A serious time": Forest satyagraha in Madhya Pradesh, 1930', *The Indian Economic and Social History Review*, vol. 21, no. 1, pp. 71–90.

Barton, G.A. 2002, *Empire Forestry and the Origins of Environmentalism*, Cambridge University Press, Cambridge.

Barton, G.A. & Bennett, B.M. 2008, 'Environmental conservation and deforestation in British India 1855–1947: A reinterpretation', *Itinerario*, vol. 32, no. 2, pp. 83–104.

Bennett, M.M., Chen, J.K., Alvarez León, L.F. & Gleason, C.J. 2022, 'The politics of pixels: A review and agenda for critical remote sensing', *Progress in Human Geography*, vol. 46, no. 3, pp. 729–752.

Brancalion, P.H.S. & Holl, K.D. 2020, 'Guidance for successful tree planting initiatives', *Journal of Applied Ecology*, vol. 57, no. 8, pp. 1–7.

Brandt, M., Gominski, D., Reiner, F., Kariryaa, A., Guthula, V.B., Ciais, P., Tong, X. et al. 2024, 'Severe decline in large farmland trees in India over the past decade', *Nature Sustainability*, vol. 7, no. 1, pp. 1–9.

Busch, J., Kapur, A. & Mukherjee, A. 2020, 'Did India's ecological fiscal transfers incentivize state governments to increase their forestry budgets?', *Environmental Research Communications*, vol. 2, no. 3, p. 031006.

Busch, J. & Mukherjee, A. 2018, 'Encouraging state governments to protect and restore forests using ecological fiscal transfers: India's tax revenue distribution reform', *Conservation Letters,* vol. 11, no. 2, pp. 57–64. https://doi.org/10.1111/conl.12416

Champion, H.G. & Seth, S.K. 1968, *A Revised Survey of the Forest Types of India (Spine Title: Forest Types of India)*, Manager of Publications, New Delhi.

Chaturvedi, R. 2016, 'India's forest federalism', *Contemporary Southeast Asia*, vol. 24, no. 1, pp. 1–18.

Chhatre, A. 2000, 'Forest co-management as if history mattered: The case of Western Himalayan forests in India'. Available from: https://eprints.exchange.isb.edu/id/eprint/998/.

Choksi, P., Kotian, M., Biniwale, S. & Mourya, P. 2023, 'Listening for change: Quantifying the impact of ecological restoration on soundscapes in a tropical dry forest', *Restoration,* vol. 4, no. 11, pp. 997–1004. Available from: https://onlinelibrary.wiley.com/doi/abs/10.1111/rec.13864.

Choksi, P., Kotian, M., Burivalova, Z. & DeFries, R. 2023, 'Social and ecological outcomes of tropical dry forest restoration through invasive species removal in Central India', *Ecological Indicators,* vol. 155, no. 11, pp. 1–11. Available from: www.sciencedirect.com/science/article/pii/S1470160X23011962.

Coleman, E., Schultz, B., Ramprasad, V., Fischer, H., Rana, P., Filippi, A.M., Güneralp, B. et al. 2021, 'Limited effects of tree planting on forest canopy cover and rural livelihoods in Northern India', *Nature Sustainability*, vol. 4, no. 11, pp. 997–1004.

Coleman, E., Schultz, B., Ramprasad, V., Fischer, H., Rana, P., Filippi, A. & Güneralp, B. et al. 2021, 'Data for Decades of tree planting in Northern India had little effect on forest canopy cover and rural livelihoods'. Available from: https://doi.org/10.13020/j6sj-jw18.

Comptroller and Auditor General of India, ed. 2024, 'Chapter IV: Detailed compliance audit on state compensatory afforestation fund management and planning authority', in *Report of the Comptroller and Auditor General of India (Compliance Audit) for the Year Ended March 2022: Government of Odisha, Report No. 2 of the Year 2024*, Comptroller and Auditor General of India, New Delhi.

Das, A., Menon, T., Ratnam, J., Thadani, R., Rajashekar, G., Fararoda, R. & Shahabuddin, G. 2021, 'Expansion of pine into mid-elevation Himalayan oak forests: Patterns and drivers in a multiple-use landscape', *Forest Ecology and Management*, vol. 497, October, p. 119491.

Davidar, P., Sahoo, S., Mammen, P.C., Acharya, P., Puyravaud, J.P., Arjunan, M., Garrigues, J.P. & Roessingh, K. 2010, 'Assessing the extent and causes of forest degradation in India: Where do we stand?', *Biological Conservation*, vol. 143, no. 12, pp. 2937–2944.

DeFries, R., Ahuja, R., Friedman, J., Gordon, D.R., Hamburg, S.P., Kerr, S., Mwangi, J., Nouwen, C. & Pandit, N. 2022, 'Land management can contribute to net zero', *Science*, vol. 376, no. 6598, pp. 1163–1165.

Fleischman, F., Basant, S., Chhatre, A., Coleman, E.A., Fischer, H.W., Gupta, D., Güneralp, B. et al. 2020, 'Pitfalls of tree planting show why we need people-centered natural climate solutions', *Bioscience*, vol. 70, no. 11, pp. 947–950.

Forest Research Institute Dehra Dun 1961, *100 Years of Indian Forestry: Issued on the Occasion of the Celebration of Indian Forest Centenary*, 2 vols, Government of India Press, New Delhi.

Gadgil, M. & Guha, R. 1992, *This Fissured Land: An Ecological History of India*, Oxford University Press, New Delhi.

Gadgil, M. & Guha, R. 1995, *Ecology and Equity*, United Nations Research Institute for Social Development, New York.

Gill-Wiehl, A., Kammen, D.M. & Haya, B.K. 2024, 'Pervasive over-crediting from cookstove offset methodologies', *Nature Sustainability*, vol. 7, no. 2, pp. 191–202.

Gopalakrishna, T., Lomax, G., Aguirre-Gutiérrez, J., Bauman, D., Roy, P.S., Joshi, P.K. & Malhi, Y. 2022, 'Existing land uses constrain climate change mitigation potential of forest restoration in India', *Conservation Letters*, vol. 15, e12867. https://doi.org/10.1111/conl.12867

Gopalakrishna, T., Rifai, S., Ratnam, J., Oliveras Menor, I., Stevens, N. & Malhi, Y. 2024, 'The distribution and drivers of tree cover in India', Communications Earth & Environment Vol 5 399. https://doi.org/10.21203/rs.3.rs-3777003/v1

Government of India 1952, '1952 National Forest Policy', Ministry of Food and Agriculture, New Delhi. Available from: http://forest.ap.nic.in/forest%20policy-1952.htm

Government of India, Ministry of Environment and Forests, Forest Survey of India 1987, 'The State of Forest Report 1987'. Available from: https://fsi.nic.in/documents/sfr_1987_hindi.pdf

Guha, R. 1983, 'Forestry in British and post-British India: A historical analysis', *Economic and Political Weekly*, vol. 18, nos. 44–45, pp. 1882–1896, 1940–1947.

Guha, R. 1989, *The Unquiet Woods: Ecological Change and Peasant Resistance in the Himalaya*, Oxford University Press, Oxford.

Guha, R. 2007, *India After Gandhi*, Harper Collins, New York.

Guha, R. & Gadgil, M. 1989, 'State forestry and social conflict in British India', *Past & Present*, vol. 123, no. 1, pp. 141–177.

Holl, K.D. & Brancalion, P.H.S. 2020, 'Tree planting is not a simple solution', *Science*, vol. 368, no. 6491, pp. 580–581.

Joshi, A.K., Pant, P., Kumar, P., Giriraj, A. & Joshi, P.K. 2010, 'National forest policy in India: Critique of targets and implementation', *Small-Scale Forestry*, vol. 10, no. 1, pp. 83–96. https://doi.org/10.1007/s11842-010-9133-z

Joshi, A. 2000, *Roots of Change: Front Line Workers and Forest Policy Reform in West Bengal*, Massachusetts Institute of Technology, Massachusetts, USA. Available from: http://proquest.umi.com/pqdweb?did=727775181&Fmt=7&clientId=12010&RQT=309&VName=PQD

Joshi, A.A., Sankaran, M. & Ratnam, J. 2018, '"Foresting" the grassland: Historical management legacies in forest-grassland mosaics in southern India, and lessons for the conservation of tropical grassy biomes', *Biological Conservation*, vol. 224, pp. 144–152.

Lahiri, S., Roy, A. & Fleischman, F. 2023, 'Grassland conservation and restoration in India: A governance crisis', *Restoration Ecology*, vol. 31, no. 4, p. e13858. Available from: https://onlinelibrary.wiley.com/doi/abs/10.1111/rec.13858

Madhusudan, M.D. & Vanak, A.T. 2023, 'Mapping the distribution and extent of India's semi-arid open natural ecosystems', *Journal of Biogeography*, vol. 50, no. 8, pp. 1377–1387.

Mather, A.S. & Needle, C.L. 1998, 'The forest transition: A theoretical basis', *Area*, vol. 30, no. 2, pp. 117–124.

Menon, M. & Kohli, K. 2021, 'The judicial fix for forest loss: The Godavarman case and the financialization of India's forests', *Journal of South Asian Development*, vol. 16, no. 3, pp. 414–432.

Moran, E.F. & Ostrom, E. 2005, *Seeing the Forest and the Trees: Human-Environment Interactions in Forest Ecosystems*, MIT Press, Cambridge, Mass.

Mudaliar, P. & Kashwan, P. 2024, 'Poverty and pollution', *Environment: Science and Policy for Sustainable Development*, vol. 66, no. 1, pp. 7–18.

National Commission on Agriculture 1976, *Report of the National Commission on Agriculture, Part IX: Forestry*, Ministry of Agriculture and Irrigation, Government of India, New Delhi.

National Research Council, Division of Behavioral and Social Sciences and Education, Board on Environmental Change and Society & Committee on the Human Dimensions of Global Change 1998, *People and Pixels: Linking Remote Sensing and Social Science*, National Academies Press, Washington, DC.

Ojha, H. & Hall, A. 2023, 'Transformation as system innovation: Insights from Nepal's five decades of community forestry development', *Innovation and Development*, vol. 13, no. 1, pp. 109–131.

Oldfield, E.E., Eagle, A.J., Rubin, R.L., Rudek, J., Sanderman, J. & Gordon, D.R. 2022, 'Crediting agricultural soil carbon sequestration', *Science (New York, N.Y.)*, vol. 375, no. 6586, pp. 1222–1225.

Pan, C., Shrestha, A., Innes, J.L., Zhou, G., Li, N., Li, J., He, Y., Sheng, C., Niles, J.-O. & Wang, G. 2022, 'Key challenges and approaches to addressing barriers in forest carbon offset projects', *Journal of Forestry Research*, vol. 33, no. 4, pp. 1109–1122.

Poffenberger, M. & McGean, B. 1996, *Village Voices, Forest Choices: Joint Forest Management in India*, Oxford University Press, New Delhi.

Poudyal, B.H., Khatri, D.B., Paudel, D., Marquardt, K. & Khatri, S. 2023, 'Examining forest transition and collective action in Nepal's community forestry', *Land Use Policy*, vol. 134, November, p. 106872.

Puyravaud, J.-P., Davidar, P. & Laurance, W.F. 2010a, 'Cryptic destruction of India's native forests', *Conservation Letters*, vol. 3, no. 6, pp. 390–394.

Puyravaud, J.-P., Davidar, P. & Laurance, W.F. 2010b, 'Cryptic loss of India's native forests', *Science*, vol. 329, no. 5987, p. 32.

Ramprasad, V., Joglekar, A. & Fleischman, F. 2020, 'Plantations and pastoralists: Afforestation activities make pastoralists in the Indian Himalaya vulnerable', *Ecology and Society*, vol. 25, no. 4. https://doi.org/10.5751/ES-11810-250401

Rana, P., Fischer, H., Coleman, E. & Fleischman, F. 2024, 'Using machine learning to uncover synergies between forest restoration and livelihood support in the Himalayas', *Ecology and Society* vol. 29, no. 1, p. 32. https://doi.org/10.5751/es-14696-290132

Rana, P., Fleischman, F., Ramprasad, V. & Lee, K. 2022, 'Predicting wasteful spending in tree planting programs in Indian Himalaya', World Development vol. 154, 05864. Available from: www.sciencedirect.com/science/article/pii/S0305750X22000547

Rana, P. & Varshney, L.R. 2023, 'Exploring limits to tree planting as a natural climate solution', *Journal of Cleaner Production*, vol. 384, January, p. 135566.

Rangarajan, M. 1994, 'Imperial agendas and India's forests: The early history of Indian forestry, 1800-1878', *The Indian Economic and Social History Review*, vol. 31, no. 2, p. 147.

Rangarajan, M. 1996a, 'Environmental histories of South Asia: A review essay', *Environment and History*, vol. 2, no. 2, pp. 129–143.

Rangarajan, M. 1996b, *Fencing the Forest: Conservation and Ecological Change in India's Central Provinces 1860-1914*, Oxford University Press, New Delhi.

Rangarajan, M. 2001, *India's Wildlife History: An Introduction*, Permanent Black in association with Ranthambhore Foundation, New Delhi.

Ratnam, J., Bond, W.J., Fensham, R.J., Hoffmann, W.A., Archibald, S., Lehmann, C.E.R., Anderson, M.T., Higgins, S.I. & Sankaran, M. 2011, 'When is a 'forest' a savanna, and why does it matter?', *Global Ecology and Biogeography: A Journal of Macroecology*, vol. 20, no. 5, pp. 653–660.

Ratnam, J., Tomlinson, K.W., Rasquinha, D.N. & Sankaran, M. 2016, 'Savannahs of Asia: Antiquity, biogeography, and an uncertain future', *Philosophical Transactions of the Royal Society of London. Series B, Biological Sciences*, vol. 371, no. 1703. https://doi.org/10.1098/rstb.2015.0305

Ravindranath, N.H., Murthy, I.K., Chaturvedi, R.K., Andrasko, K. & Sathaye, J.A. 2007, 'Carbon forestry economic mitigation potential in India, by land classification', *Mitigation and Adaptation Strategies for Global Change*, vol. 12, no. 6, pp. 1027–1050.

Rosencranz, A., Boenig, E. & Dutta, B. 2007, 'The Godavarman case: The Indian Supreme Court's breach of constitutional boundaries in managing India's forests', *Environmental Law Reporter*, vol. 37, pp. 100342–100042.

Roy, A. & Fleischman, F. 2022, 'The evolution of forest restoration in India: The journey from precolonial to India's 75th year of independence', *Land Degradation & Development*. Available from: https://onlinelibrary.wiley.com/doi/abs/10.1002/ldr.4258

Saberwal, V.K. 1999, *Pastoral Politics: Shepherds, Bureaucrats, and Conservation in the Western Himalaya*, Studies in Social Ecology and Environmental History, Oxford University Press, New Delhi; New York.

Sarin, M. 2005, 'Laws, lore and logjams: Critical issues in Indian forest conservation', *IIED Gatekeeper Series*, vol. 116, pp. 1–24. Available from: http://pubs.iied.org/9543IIED.html

Savilaakso, S., Lausberg, N., Waeber, P.O., Hillgén, O., Isotalo, A., Kleinschroth, F., Djenontin, I.N.S., Boul Lefeuvre, N. & Garcia, C.A. 2023, 'Whose perspective counts? A critical look at definitions of terms used for natural and near-natural forests', *One Earth*, pp. 1–14. Available from: https://doi.org/10.1016/j.oneear.2023.10.003

Sethi, P. 2024, '[Commentary] Green credit rules: Death by trees?', *Mongabay India*, 15 July. Available from: https://india.mongabay.com/2024/07/commentary-the-green-credit-rules-death-by-trees/

Shahabuddin, G., Goswami, R., Krishnadas, M. & Menon, T. 2021, 'Decline in forest bird species and guilds due to land use change in the Western Himalaya', *Global Ecology and Conservation*, vol. 25, p. e01447.

Sivaramakrishnan, K. 1999, *Modern Forests: Statemaking and Environmental Change in Colonial Eastern India*, Stanford University Press, Stanford, CA.

Skaria, A. 1999, *Hybrid Histories: Forests, Frontiers and Wildness in Western India*, Oxford University Press, New Delhi.

Smith, P., Soussana, J.F., Angers, D., Schipper, L., Chenu, C., Rasse, D.P., Batjes, N.H. et al. 2020, 'How to measure, report and verify soil carbon change to realize the potential of soil carbon sequestration for atmospheric greenhouse gas removal', *Global Change Biology*, vol. 26, no. 1, pp. 219–241.

Springate-Baginski, O. & Blaikie, P. 2013, *Forests People and Power: The Political Ecology of Reform in South Asia*, Routledge, London, United Kingdom.

Stapp, J., Nolte, C., Potts, M., Baumann, M., Haya, B.K. & Butsic, V. 2023, 'Little evidence of management change in California's forest offset program', *Communications Earth & Environment*, vol. 4, no. 1, pp. 1–10.

Stebbing, E.P. 1922, *The Forests of India Vols. I-III*, Dodley Head, London.

Thayyil, N. 2009, 'Judicial fiats and contemporary enclosures', *Conservation and Society*, vol. 7, no. 4, pp. 268–282.

Upadhyay, S., Chohan, S. & Vaidya, A. 2009, *India's Forests and the Judiciary: The Godavarman Story*, Enviro-Legal Defence Firm and WWF-India, New Delhi.

West, T.A.P., Wunder, S., Sills, E.O., Börner, J., Rifai, S.W., Neidermeier, A.N., Frey, G.P. & Kontoleon, A. 2023, 'Action needed to make carbon offsets from forest conservation work for climate change mitigation', *Science*, vol. 381, no. 6660, pp. 873–877.

Wunder, S., Schulz, D., Montoya-Zumaeta, J.G., Börner, J., Frey, G.P. & Betancur-Corredor, B. 2024, 'Modest forest and welfare gains from initiatives for reduced emissions from deforestation and forest degradation', *Communications Earth & Environment*, vol. 5, no. 1, pp. 1–11.

6 Ecological Evaluation and Assessment of Spatial Variables Influencing the Urban Heat Island Effect in Bangalore, India

Anindita Dasgupta and Uttam Kumar

6.1 INTRODUCTION

The 21st century is a period marked by the rise of urban development, and urban areas, including cities and towns, are the home to most of the global population (UN-Habitat, 2008). As the urban population continues to grow in the coming decades, expanding cities will transform the Earth into a much more urbanized planet. City expansion has posed several challenges to city dwellers and led to the overutilization of natural resources. Cities impact areas within their boundaries and regions outside their borders, influencing the local and regional climate (Marcus and Colding, 2011). For example, the absorption of heat from the sun and re-radiation from the dark surfaces of different objects in an urban environment interact with rising summer temperatures, creating heat waves called urban heat islands (UHI) (Stone, 2012). Urban form, surface properties, vegetation cover, and many other factors influence the urban climate. It differs from the surrounding rural areas, and one causal factor for UHI is ongoing developmental activities in the city. As such, there is an adverse impact on the surroundings, affecting urban people acutely due to environmental degradation. As an increasing urban population demands new settlements, this, in turn, requires the conversion of natural permeable land surfaces to built-up areas. The UHI effect is witnessed more evidently in compact urban structures with high-density populations.

Previous studies, including Aslan and Koc-San (2021), have explored the relationship between UHI and various urban land uses using Landsat-7 ETM+, Landsat-8 OLI, MODIS (Moderate Resolution Imaging Spectroradiometer), and other remotely sensed data. For instance, analysis of parameters like built-up, population, socioeconomic, geo-morphological factors, etc., rendered a better perspective to understand the land surface temperature (LST) pattern and its spatial variation resulting in UHI (Fan and Wang, 2020). The adverse impact of urban environmental

 DOI: 10.1201/9781003396260-6

degradation—often in the name of developmental activities—on its people has been realized at a large scale (Haldar et al., 2021). Therefore, the mitigation strategy for urban climate should include urban green spaces (UGS) that are well known for maintaining the urban environment sustainably. UGS consists of unsealed and permeable soft surfaces, benefitting the city's residents ecologically and socially. Green space affects the quality of the environment, helps in stress relieving, renders feelings of social well-being (Maas et al., 2009), and is also considered a sustainable solution to unplanned developed cities (Gupta et al., 2012). They act like the lungs of the city, and therefore, parks, playgrounds, and recreational spaces should be promoted to uplift the quality of life of residents, reduce the urban heat effects, and promote ecological balance.

The above review revealed that earlier research on UHI mostly focused on data sources, methodology of analysis, driving factors, measures of mitigation, etc. However, it is also equally important to choose appropriate analytical units and seasons for studying UHI. This study uses spatial autocorrelation and a spatial metric model to identify and quantify spatial patterns and variability in UHIs and local environments in the summer season in Bangalore City. Therefore, in this work, we analyze the spatial patterns and effects of various spatial variables such as VIIRS, NDBI (Normalized Difference Built-up Index), DEM (digital elevation model), slope, and percentage of water and vegetation on LST to understand the dynamics between UGS and local temperature. Subsequently, the influence of increasing population on the local and regional climate as a result of urban expansion was examined at the smallest administrative unit/boundary of the city (wards) so as to provide inputs for planning and green space development.

The objectives of this paper are as follows:

(i) To explore the relationship between LST and other spatial indicators.
(ii) To perform an ecological evaluation of Bangalore City at the smallest administrative unit (ward).
(iii) To frame mitigation strategy at the ward level in terms of planning for green space development.

6.2 STUDY AREA

Bangalore is a metropolitan city situated in the state of Karnataka, India, and is popular for its favorable climate, despite changes in local climatic conditions (Nalini, 2021). The cosmopolitan City of Bangalore is also known as the Silicon Valley of India. It is an intellectual and scientific powerhouse with renowned educational institutions, information technology, and biotechnology companies, many governments and private research and development organizations, a large number of pharmaceutical industries, aerospace manufacturing centers, and several micro, small, and medium enterprises. It is an electronic and electrical manufacturing nucleus and currently hosts one of the largest concentrations of start-up companies in the world with huge foreign direct investment and a favorable business growing culture. The presence of a large number of water bodies and vegetation coined it a "city of lakes and gardens", a moniker that has grown less applicable as such features have decreased considerably

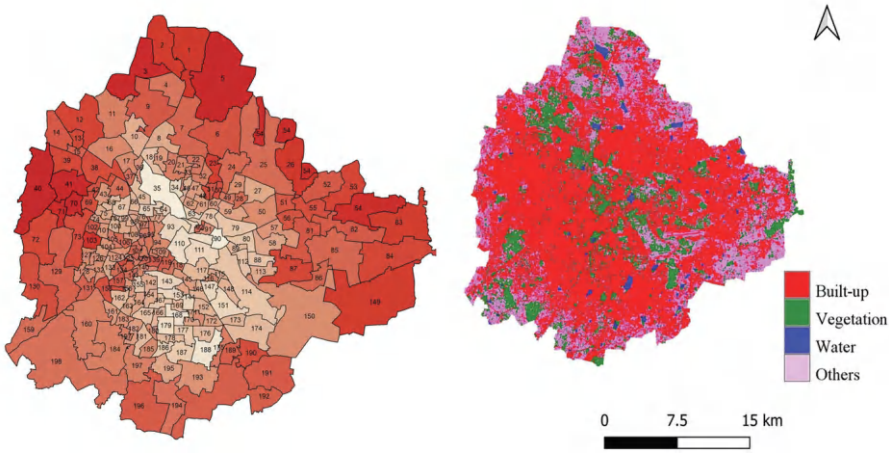

FIGURE 6.1 Ward level map of Bangalore with the LULC map of Bangalore.

and been depleted in the last several decades (Dasgupta and Kumar, 2021). Figure 6.1 shows 198 wards in Bangalore City and the geographical/spatial center or the "City Center" corresponding to the Sampangiriram Nagar and Shantala Nagar wards (i.e., wards no. 100 and 111) that were used as spatial reference points to interpret the results.

6.3 MATERIAL AND METHODS

Landsat-8 OLI/TIRS data, dated April 19, 2021, was used as basic data for calculating LST and determining the UHI effect. VIIRS (The Suomi Visible Infrared and Imaging Radiometer Suite) day and night band (DNB) dataset, which consists of global daily measurements of nocturnal visible and near-infrared (NIR) light was used as one of the spatial variables. These imagery datasets are available with radiance composite at a monthly average of 450 m spatial resolution. Road density was calculated for each ward from the road length obtained from the Open Street Map (OSM). Other derived datasets, which were computed as indices from the Landsat satellite bands, were also used. NDBI uses satellite data to calculate the imperviousness intensity. It focuses on the distribution of impermeable areas, which are defined by a higher shortwave infrared reflectance in comparison to the near-infrared band. Normalized Difference Vegetation Index (NDVI) is a commonly used Vegetation Index (VI) to distinguish vegetation from non-vegetative classes. The spectral interactions between green vegetation and the red and NIR portions of the electromagnetic spectrum determine NDVI. It was added to create a spectral VI that distinguishes green vegetation from the brightness of the adjoining Earth's surface. A land use land cover (LULC) map was obtained using a Random Forest (RF) classifier from where four categories were obtained, namely, built-up, vegetation, water, and bare soil (including open areas and fallow land). Percentages of each of these classes were also derived on a ward level and used as independent variables.

The methodology consisted of three main steps:

(i) Computation of LST from Landsat-8 Thermal band (band 10).
(ii) Performing spatial regression of LST with selected spatial variables.
(iii) Derivation of UTFVI index and ecological evaluation of the city (by dividing the city area into six zones/regions).

6.3.1 LST Estimation

(i) Spectral radiance – LST values were derived using the LANDSAT-8 Data Users Handbook. The digital numbers (DN) of the pixels of the imagery were converted to spectral radiance (L_λ) as per equation (6.1):

$$L_\lambda = M_L Q_{\text{cal}} + A_L \tag{6.1}$$

where, Q_{cal} is the pixel value (DN) and M_L and A_L are the rescaling coefficients obtained from the metadata of respective satellite data.

(ii) Calculation of emissivity – Emissivity was computed using proportional vegetation (P_v), i.e., the vegetation proportion as given by equation (6.2).

$$\varepsilon = 0.004 P_v + 0.986 \tag{6.2}$$

P_v is computed as

$$P_v = \left(\frac{NDVI - NDVI_{\min}}{NDVI_{\max} - NDVI_{\min}} \right) \tag{6.3}$$

where, $NDVI$ gives the distribution of vegetation in the given area. $NDVI_{\min}$ is normally the value of water or bare soil and $NDVI_{\max}$ is the value corresponding to dense vegetation.

(iii) LST computation – Brightness temperature ($T(k)$) was calculated from the obtained L_λ in equation (6.1), where L_λ is the spectral radiance.

$$T(k) = \frac{k_2}{\ln\left(\frac{k_1}{L_\lambda} + 1 \right)} - 273.15 \tag{6.4}$$

The calibration constants k_1 and k_2 were obtained from the metadata of the satellite. Absolute zero (–273.15 K) was added to the above equation to obtain results in °Celsius (°C). LST was computed as shown in equation (6.5):

$$\text{LST} = \frac{T}{1+\left(\lambda \cdot \frac{Ts}{hc}\right)\ln(\varepsilon)} \quad \text{LST} = T(K)/\left[1+(\lambda \times Ts/hc)\times \ln(\varepsilon)\right] \tag{6.5}$$

where, T is the derived brightness temperature, λ = wavelength of emitted radiance, s = Boltzmann constant, and c = velocity of light.

6.3.2 Regression

Regression was used to find the relationship of the dependent variable (LST) with other independent spatial variables using ordinary least squares (OLS) and the spatial error model (SEM).

(i) *Spatial variables:* The percentage of artificial surfaces, such as built-up areas, and natural surfaces, such as vegetation and water bodies, at 30 m spatial resolution was produced by the RF algorithm. Additionally, data from SRTM, slope, altitude, and the area's geomorphology (Zanter, 2019) were taken. The social indicators included VIIRS nighttime light data and road density information. The average of these spatial variables for each ward was computed for the analysis. Figures 6.2 and 6.3 show the spatial variables used in this study.

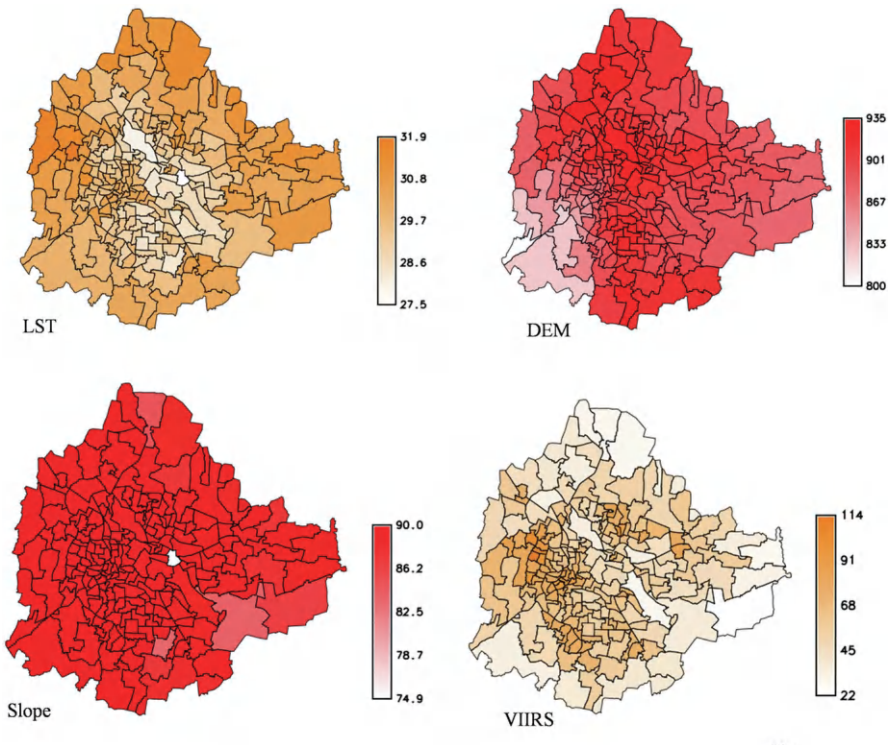

FIGURE 6.2 Spatial variables used against LST in regression.

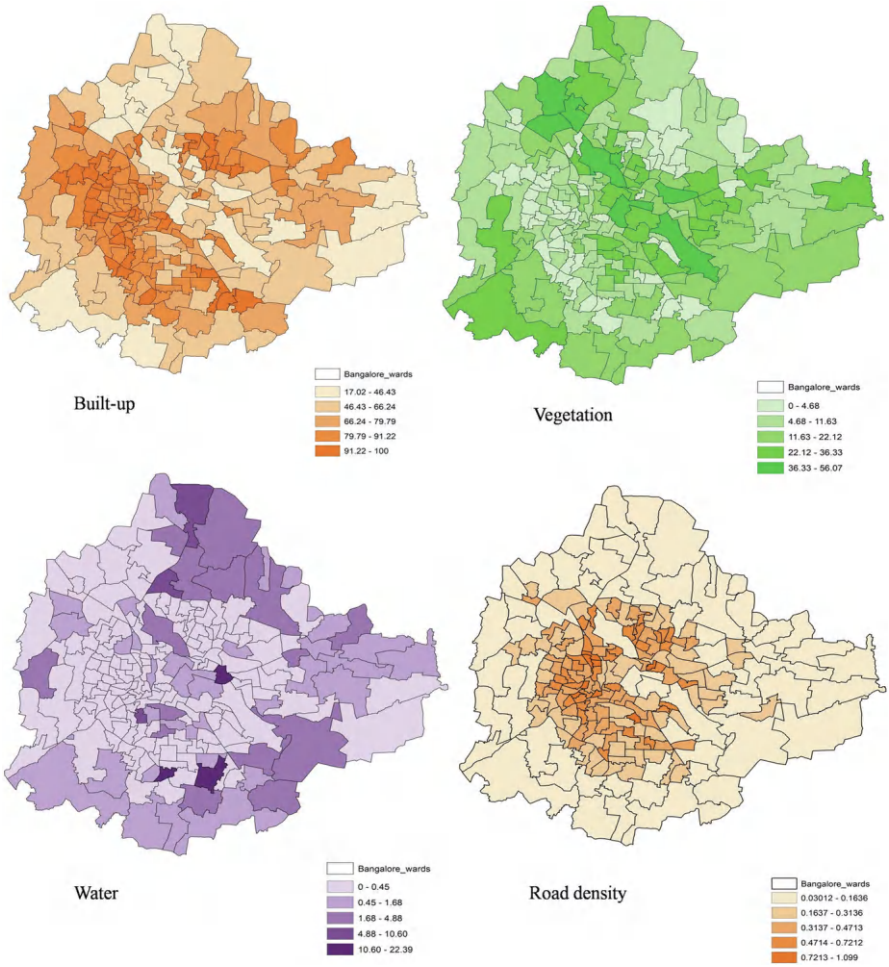

FIGURE 6.3 Spatial variables used against LST in regression.

(ii) Spatial cluster analysis: Spatial cluster analysis detects non-randomness of events in space and time and unusual concentrations. Moran's I is one of the most common indicators of clustering and is used to examine similar or dissimilar attributes of nearby areas, as given by equation (6.6).

$$I = \frac{n}{\sum_{i=1}^{n}\sum_{j=1}^{n} w_{ij}} X \frac{\sum_{i=1}^{n}\sum_{j=1}^{n} w_{ij}\left(x_i - \bar{x}\right)\left(x_j - \bar{x}\right)}{\sum_{i=1}^{n}\left(x_i - \bar{x}\right)^2} \tag{6.6}$$

where n is the total number of observations (points or polygons), i and j represent different locations, x_i and x_j are values of the variable in the i^{th} and

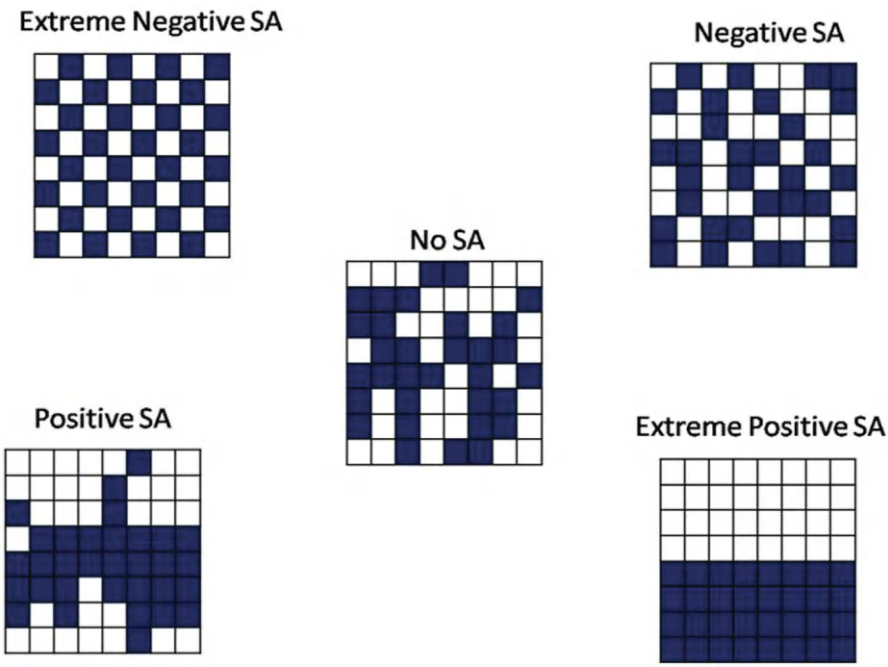

FIGURE 6.4 Demonstration of various cases of spatial autocorrelation (SA).

j^{th} locations, and x is the mean of the variable. w_{ij} is a measure of spatial proximity for pairs i and j. Moran's I value ranges between –1 to 1, where –1 means negative autocorrelation, implying that nearby locations have dissimilar values, and 1 means positive autocorrelation indicating clusters.

A highly clustered spatial pattern is indicated by a high positive local Moran's I score, while a highly dispersed spatial pattern is indicated by a low, negative local Moran's I score (Fan and Wang, 2020).

Figure 6.4 explains spatial autocorrelation. In this work, Moran's I value for LST was 0.63, indicating a positive correlation in terms of spatial distribution.

(iii) Ordinary least squares (OLS), spatial regression model, and spatial error model (SEM)

An OLS regression model is a statistical method based on the assumption that the error terms are independent of each other. If there is spatial interaction (i.e., if spatial autocorrelation exists), spatial regression models (see equation (6.7)) are used to capture these effects.

$$\text{LST} = X\beta + \varepsilon \tag{6.7}$$

where, LST is the dependent variable, X denotes a $N \times k$ vector of independent variables, β denotes a vector of parameters, and ε are normally distributed errors. The spatial error model (SEM) is given as in (6.8):

$$y = X\beta + \lambda W_{\mu} + \mu \tag{6.8}$$

where, λ is the spatial error coefficient, W_{μ} is the spatial weight matrix, β is the regression coefficient, μ is a vector of the error terms and X is the independent variable.

Variance Inflation Factor (VIF) is a measure of collinearity among predictor variables within multiple regression. To avoid multicollinearity in the selected variables, VIF tests were conducted in the R statistical software (Ramachandran and Tsokos, 2020). Only the spatial variables with VIF lower than 5, like VIIRS, NDBI, DEM, slope, percentage of water, and vegetation, were considered in the regression. Considering the effect of spatial autocorrelation, SEM was implemented in GeoDa 1.18 software (Anselin et al., 2022). In this study, SEM showed improvement over the original OLS model. The results of regression models were compared using the coefficient of determination (R^2), Akaike Information Criterion (AIC), Log Likelihood (LogL), and Schwarz Criterion (SC). Higher R^2 and LogL values and lower AIC and SC values decide a better model (Li et al., 2010; Guo et al., 2020).

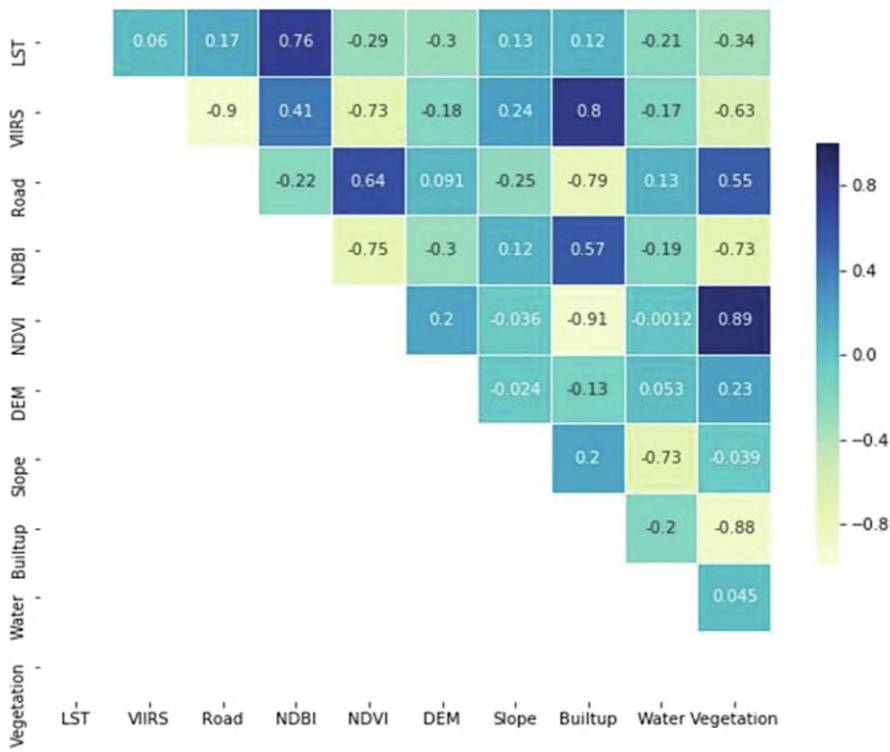

FIGURE 6.5 Correlation between various spatial variables.

Figure 6.5 shows the correlation matrix between various spatial variables. Here the correlation between LST and NDBI was highest, indicating that with an increase in impervious surfaces, the surface temperature also tends to rise.

6.3.3 Urban Thermal Field Variance Index (UTFVI)

UTFVI thermal comfort index (see equation (6.9)) was used to evaluate the UHI impact on the quality of urban life (Sobrino and Irakulis, 2020) in different zones of the city, as shown in Table 6.2. This index evaluates each pixel located within the urban area with respect to the whole urban area (Guha et al., 2018).

$$\text{UTFVI} = \frac{T_S - T_{\text{mean}}}{T_{\text{mean}}} \tag{6.9}$$

where UTFVI = Urban Thermal Field Variance Index, T_S is the LST (°C), and T_{mean} is the mean LST (°C). Ecological evaluation of Bangalore City was done using UTFVI values by dividing it into six zones (Table 6.2). Figure 6.6 gives the outline of the methodology followed in this study.

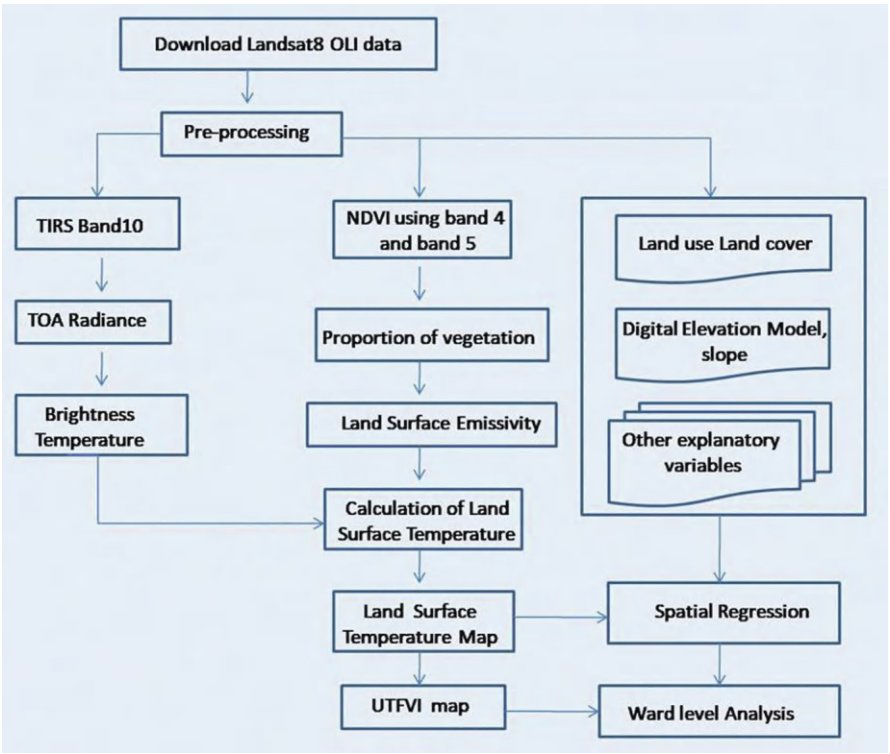

FIGURE 6.6 Flowchart of the overall methodology.

6.4 RESULT AND DISCUSSION

SEM rendered a high R-squared value of 0.89 and a log-likelihood of –20; therefore, it was a suitable model for this study. LST maps were generated from the remotely sensed thermal band as shown in Figure 6.7(a).

The LST map indicated that the wards located on the outskirts of the city, away from the city center, showed higher LST with more impervious surfaces. Figure 6.7(c) shows the frequency of wards lying in different temperature zones. Table 6.1 highlights the descriptive statistics of the spatial variables used in this study.

UTFVI values were generated and divided into six zones by specific ecological evaluation indices (see Figure 6.7(b) and Table 6.2), each of which corresponds to the degree of UHI presence and its impact on eco-environmental quality or thermal comfort in the area (Sobrino and Irakulis, 2020). The wards with high vegetation showed relatively lower temperatures. The presence of green spaces in the city center is the reason for better thermal comfort.

Table 6.2 shows the percentage area coverage of the EEI into six zones. Here, the city was divided into two extremes: (i) the region where the optimum thermal comfort is < 0, and (ii) relatively high-temperature areas or pockets where UTFVI > 0.02.

Approximately half of the study area (36082.8 ha) spatially located towards the city center showed excellent EEI, including Malleshwaram, Tippasandara, Garudachar Playa, Doddanekkundi, Chamrajapet, Hanumanth Nagar, and Gali Anjenaya Temple (wards no. 45, 58, 82, 85,140, 155, 157), while 32.44% of the total area was categorized as a very poor EEI zone. The wards with the highest LST were

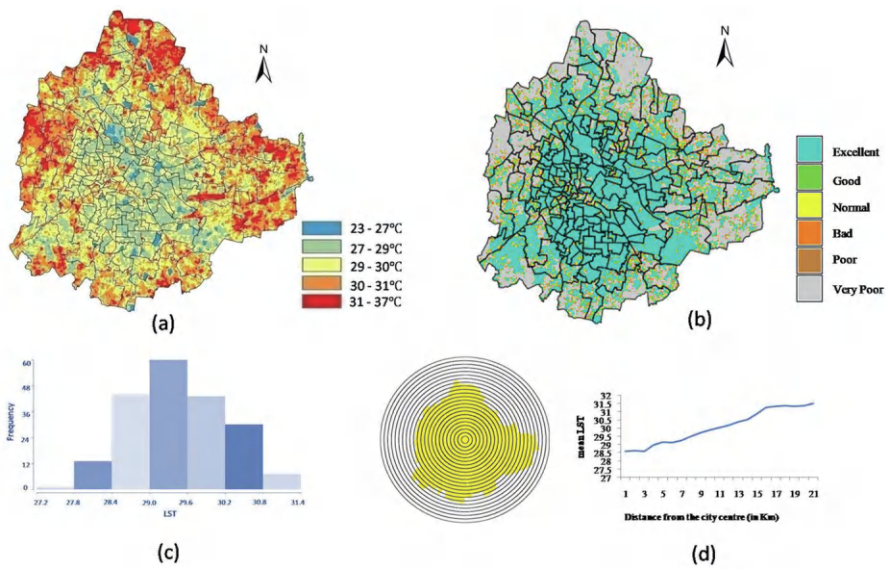

FIGURE 6.7 (a) Land surface temperature (LST) map in ℃. (b) Ward wise EEI distribution in Bangalore. (c) Ward level average LST in ℃ (April 2021). (d) Mean LST in different concentric ring buffers with 1 km radius originating from the city center.

TABLE 6.1
Descriptive Statistics of the Spatial Variables

	Min	Max	Q1	Median	Q3	IQR	Mean	SD
LST	27.23	31.43	28.95	29.43	30.08	1.13	29.49	0.76
NL	22.22	113.53	51.16	63.34	75.72	24.55	63.1	16.37
RD	0.26	1.38	0.39	0.46	0.56	0.17	0.51	0.16
NDBI	-0.08	0.034	-0.03	-0.018	-0.003	0.03	-0.019	0.024
NDVI	0.08	0.24	0.13	0.15	0.17	0.04	0.15	0.03
DEM	799.50	934.85	899.64	901.35	910.19	20.54	897.41	21.04
Slope	74.90	89.99	89.38	89.60	89.76	0.375	89.36	1.30

Note: LST – Land Surface Temperature, NL – Night Light, RD – Road Density, NDBI – Normalized Difference Built-Up Index, NDVI – Normalized Difference Vegetation Index, DEM – Digital Elevation Model.

TABLE 6.2
Ecological Evaluation Index in Bangalore

UTFVI	EEI	Area(in ha)	Percentage
–0.22–0	Excellent	36082.8	50.71
0–0.005	Good	3151.44	4.43
0.005–0.010	Normal	3066.12	4.31
0.010–0.015	Bad	2962.35	4.16
0.015–0.020	Poor	2814.3	3.95
0.020–0.234	Very Poor	23082.39	32.44

also rated as in the very poor category in EEI. Five wards (namely, Rajagopal Nagar, Dodda Bidarakallu, Peenya Industrial Area, Jakkuru, and Atturu, with corresponding ward numbers 70, 40, 41, 5, and 3) exhibited the highest average LST (31.43, 31.36, 31.12, 31.08, and 31.05℃, respectively). The same wards also showed poor EEI with increased levels of thermal discomfort. On the other hand, Aramane Nagara (ward 35) and Halsoor (ward 90) showed the lowest LST.

Multiple concentric ring buffers generated at a radius of 1 km from each other originating from the center of the city were used for the depiction of variations in LST. As we moved from the city center towards the periphery, LST also increased gradually, as depicted in Figure 6.7(d). Increased LST is the consequence of unplanned urbanization in the outskirts, which further exacerbated urban temperature with the rapid rise in the number of impervious surfaces. This fueled a decrease in vegetation cover and open ground and an increase in waste heat emission from industries, vehicles, etc. (Zhang and Gu, 2001).

There is a noteworthy positive influence of green space (urban forests, parks, gardens, etc.) and blue space (wetlands, lakes, rivers, and ponds) on heat islands. UGS is

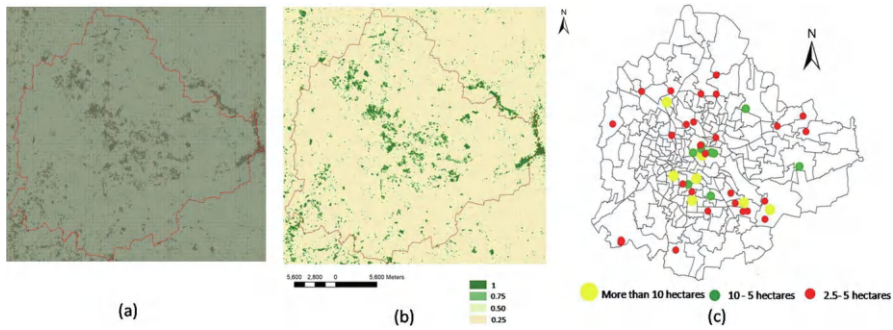

FIGURE 6.8 (a) 100 × 100 m grid overlaid on the study area, (b) Green Index (GI) map of Bangalore (April, 2021) and (c) Bangalore Parks more than 2.5 hectares in size shown at a ward level.

integral for the maintenance of the city's environmental quality and its sustainability. The importance of urban vegetation in improving a city's environmental quality and in several other services to humankind, such as in maintaining water level in aquifers through groundwater recharging, biodiversity enhancement, health and recreation, climate change mitigation, building stronger communities, etc., is well known for its impacts on the surrounding area, and for the social wellbeing of the residents. Urban vegetation is also a way to abate the effects of climate change (Liu and Zhang, 2011). Moreover, the presence of vegetation increases soft, permeable surfaces, which in turn allows rainwater penetration and helps in restoring groundwater levels. Environmental sustainability and social interactions can be maintained by preserving the existing parks and gardens and aspects such as lakes and wetlands. Therefore, the integration of both green and blue spaces lessens the effect of thermal heat islands to create a healthy environment.

Four groups were established for the entire study area: (i) Very high-quality green, (ii) high-quality green, (iii) moderate-quality green, and (iv) low-quality green. The evaluation of urban green areas was conducted using a grid, with each cell containing 75–100% vegetation classified as very high quality, 50–75% as high quality, 25–50% as moderate quality, and 0–25% as low-quality green (Figure 6.8 and Table 6.3). To understand the relationship between urban green space and local temperature in the study area, spatial patterns derived from LST and Green Index (GI) maps were utilized.

This analysis provided input for local/regional green space development planning for urban environmental sustainability. From the results of this analysis, we see a higher concentration of greenery in the central part of the city, while there should be a uniform distribution of green vegetation throughout the city to accommodate the ecological benefits and to avail the ecosystem services by the city's population (Nowak, and Greenfield, 2018). More attention should be given to increasing vegetation near the built-up land to reduce the UHI effect. A major mitigation strategy should be adopted at the planning stage by taking into account building materials, sky view, better roof designs, and other factors.

In future studies, variations in LST in different seasons will explore the relationship between LST and other driving factors. Vegetation affects the urban surface

TABLE 6.3
Percent of Green

Percentage	Value	Qualify classes
0–25	0.25	Low green quality
25–50	0.50	Moderate green quality
50–75	0.75	High green quality
75–100	1	Very high green quality

temperature; therefore, integrating green spaces in urban planning is an essential step toward mitigating UHI (Andersson-Skold et al., 2015; Xiao et al., 2018).

6.5 CONCLUSION

Built-up areas showed a high correlation of 0.76 with LST, and therefore, the warming effect of the built-up area was evident from this study. As agricultural lands are being converted into built-up areas during urbanization, increasing green space should be among the top priorities for mitigating the heat effect. Rajagopal Nagar, Dodda Bidarakallu, Peenya Industrial Area, Jakkuru, and Atturu (corresponding to wards 70, 40, 41, 5, and 3) had the highest average LST with average NDVI of 0.12, 0.15, 0.14, 0.16, and 0.17, respectively. The same wards also showed poor EEI with increased levels of thermal discomfort. In the future, seasonal influence and the effects of other driving factors on surface temperature will be explored. To study the relationship of clustered impervious patches on local LST, spatial metrics will also be utilized.

ACKNOWLEDGEMENTS

We are grateful to the International Institute of Information Technology Bangalore (IIIT Bangalore), India, for the infrastructure support and acknowledge the Mphasis Cognitive Computing Centre of Excellence at IIIT Bangalore for the research grant.

REFERENCES

Andersson-Sköld, Y., Thorsson, S., Rayner, D., Lindberg, F., Janhäll, S., Jonsson, A., Moback, U., Bergman, R. and Granberg, M., 2015. An integrated method for assessing climate-related risks and adaptation alternatives in urban areas. *Climate Risk Management*, *7*, pp. 31–50.

Anselin, L., Li, X. and Koschinsky, J., 2022. GeoDa, from the desktop to an ecosystem for exploring spatial data. *Geographical Analysis*, *54*(3), pp. 439–466.

Aslan, N. and Koc-San, D., 2021. The use of land cover indices for rapid surface urban heat island detection from multi-temporal Landsat imageries. *ISPRS International Journal of Geo-Information*, *10*(6), p. 416.

Dasgupta, A. and Kumar, U., 2021, December. Urban heat Island and its impact on impervious surfaces during two seasons: A case study of Bangalore. In *2021 IEEE International India Geoscience and Remote Sensing Symposium (InGARSS)* Ahmedabad, India, (pp.

250–253). IEEE. doi: 10.1109/InGARSS51564.2021.9792024; https://ieeexplore.ieee.org/document/9792024

Fan, C. and Wang, Z., 2020. Spatiotemporal characterization of land cover impacts on urban warming: A spatial autocorrelation approach. *Remote Sensing*, *12*(10), p. 1631.

Guha, S., Govil, H., Dey, A. and Gill, N., 2018. Analytical study of land surface temperature with NDVI and NDBI using Landsat 8 OLI and TIRS data in Florence and Naples city, Italy. *European Journal of Remote Sensing*, *51*(1), pp. 667–678.

Guo, A., Yang, J., Xiao, X., Xia, J., Jin, C. and Li, X., 2020. Influences of urban spatial form on urban heat island effects at the community level in China. *Sustainable Cities and Society*, *53*, p. 101972.

Gupta, K., Kumar, P., Pathan, S.K. and Sharma, K.P., 2012. Urban Neighborhood Green Index–A measure of green spaces in urban areas. *Landscape and Urban Planning*, *105*(3), pp. 325–335.

Halder, B., Bandyopadhyay, J. and Banik, P., 2021. Monitoring the effect of urban development on urban heat island based on remote sensing and geospatial approach in Kolkata and adjacent areas, India. *Sustainable Cities and Society*, *74*, p. 103186.

Li, S., Zhao, Z., Miaomiao, X. and Wang, Y., 2010. Investigating spatial non-stationary and scale-dependent relationships between urban surface temperature and environmental factors using geographically weighted regression. *Environmental Modelling & Software*, *25*(12), pp. 1789–1800.

Liu, L. and Zhang, Y., 2011. Urban heat island analysis using the Landsat TM data and ASTER data: A case study in Hong Kong. *Remote Sensing*, *3*(7), pp. 1535–1552.

Maas, J., Spreeuwenberg, P., Van Winsum-Westra, M., Verheij, R.A., Vries, S. and Groenewegen, P.P., 2009. Is green space in the living environment associated with people's feelings of social safety?. *Environment and Planning A*, *41*(7), pp. 1763–1777.

Marcus, L. and Colding, J., 2011. Towards a spatial morphology of urban social-ecological systems. Presented at the 18th International Seminar on Urban Form. Retrieved from https://urn.kb.se/resolve?urn=urn:nbn:se:kth:diva-53317.

Nalini, N.S., 2021. Urbanization and changing temperature patterns in the city of Bengaluru. *Environment, Development and Sustainability*, *23*(6), pp. 9090–9109.

Nowak, D.J. and Greenfield, E.J., 2018. Declining urban and community tree cover in the United States. *Urban Forestry & Urban Greening*, *32*, pp. 32–55.

Ramachandran, K.M. and Tsokos, C.P., 2020. *Mathematical statistics with applications in R*. Academic Press.

Sobrino, J.A. and Irakulis, I., 2020. A methodology for comparing the surface urban heat island in selected urban agglomerations around the world from Sentinel-3 SLSTR data. *Remote Sensing*, *12*(12), p. 2052.

Stone Jr, B., 2012. *The city and the coming climate: Climate change in the places we live*. Cambridge University Press.

Un-Habitat, 2008. *State of the World's Cities 2008/9: Harmonious cities*. Earthscan.

Xiao, X.D., Dong, L., Yan, H., Yang, N. and Xiong, Y., 2018. The influence of the spatial characteristics of urban green space on the urban heat island effect in Suzhou Industrial Park. *Sustainable Cities and Society*, *40*, pp. 428–439.

Zanter, K., 2019. *LANDSAT 8 (L8) Data Users Handbook (LSDS-1574 Version 5.0)*. United States Geological Survey: Sioux Falls, SC, USA.

Zhang, Y., Yu, T. and Gu, X., 2001. Land surface temperature retrieval from CBERS-02 IRMSS thermal infrared data and its applications in quantitative analysis of urban heat island effect. *VIRTUAL*, *1*(1), 789–803. https://sid.ir/paper/668910/en

7 Urbanization and Settlement Growth in Forested Areas of South and Southeast Asia

Analysis Using Nighttime Satellite Datasets

Griffin McAvoy, Aditya Eaturu, and Krishna Prasad Vadrevu

7.1 INTRODUCTION

The countries in South and Southeast Asia (S/SEA) are among the most rapidly urbanizing regions in the world, experiencing rapid population growth, economic transformation, and infrastructural expansion (Jones, 2002; Li et al., 2023). The region is home to nearly half of the world's population (www.worldometers.info). As millions of people migrate from rural to urban areas in search of better livelihoods and opportunities, cities across South and Southeast Asia are expanding at an unprecedented pace, with significant implications for the surrounding environment (Sugiyarto, 2014; Fong and Shibuya, 2020).

In South Asia, countries like India, Pakistan, and Bangladesh have experienced substantial urban growth driven by industrialization, the rise of the service economy, and population pressures (Kim and Wood, 2020). Mega-cities such as Delhi, Mumbai, Dhaka, and Karachi have become centers of economic activity, fueled by local and global demands, drawing millions of people. Similarly, Southeast Asia—comprising nations like Indonesia, Thailand, Vietnam, and the Philippines—has seen robust urban expansion fueled by export-driven economies, foreign investments, and infrastructure development. Cities such as Jakarta, Bangkok, Ho Chi Minh City, and Manila are at the forefront of this transformation, becoming regional hubs for trade, technology, and tourism (Wahab et al., 2023; Nguyen, 2024).

Urbanization in both South and Southeast Asia presents opportunities and challenges (Justice et al., 2015; Arfanuzzaman and Dahiya, 2019; Qayyum et al.,

 DOI: 10.1201/9781003396260-7

2021). On the positive side, urbanization has led to economic growth, improved access to education and healthcare, and enhanced connectivity through better infrastructure. However, rapid urbanization also presents significant challenges. Many cities face issues such as overpopulation, inadequate housing, traffic congestion, pollution, and strain on public services. In several South and Southeast Asian countries, informal settlements and slums are typical, as urban development often struggles to keep pace with population growth (Boanada-Fuchs et al., 2024). Environmental degradation, including deforestation, air and water pollution, and rising carbon emissions, is another primary concern (Zafar et al., 2020). Additionally, the urban-rural divide remains distinct, with rural areas often lagging in development (Kanbur and Zhuang, 2013; Barbier, 2023). Understanding urbanization trends in S/SEA is critical for the region's development and management and for global efforts to achieve sustainable and inclusive growth in an era of rapid change.

In particular, forests in South and Southeast Asia are not only hotspots of biodiversity but also crucial for ecosystem services, such as carbon sequestration, water regulation, and cultural significance (Prasad et al., 2001, 2008; Vadrevu et al., 2018). Countries like India and Sri Lanka in South Asia and Indonesia, Malaysia, Myanmar, and Thailand in Southeast Asia boast extensive forest cover that supports local livelihoods and contributes to global ecological balance (Sodhi et al., 2010; Ashton et al., 2014). However, rapid settlement growth and infrastructure development—including road construction, mining, and urban sprawl—have led to large-scale deforestation and fragmentation of these critical habitats (Ma, 2023). The expansion of settlements into forested areas often stems from economic imperatives, such as agricultural intensification, logging, or industrial development, all fueled by increasing population density and regional economic policies. While such growth can generate economic opportunities, it also brings significant challenges (De Jong et al., 2017), including biodiversity loss, changes in local climate patterns, displacement of indigenous communities, and heightened vulnerability to natural disasters like floods and landslides. These challenges are particularly acute in South and Southeast Asia, where many forested regions overlap with high poverty areas, making sustainable development and environmental preservation critical and complex (Shivakoti et al., 2017). The interplay between urbanization and forest loss has thus become a pressing concern, highlighting the need for practical monitoring tools to understand the scale and drivers of these changes.

This study addresses urban sprawl into natural areas, particularly forests. Although urbanization contributes significantly to regional development, it is no longer confined to traditional metropolitan centers or peri-urban areas (Vu et al., 2023). Human settlements and economic activities are increasingly encroaching upon forested regions, driven by the demand for agricultural land, natural resources, and space for industrial and residential development. This trend is reshaping the physical and ecological landscapes of the region, with profound implications for biodiversity, climate resilience, and the well-being of local communities.

Understanding and quantifying the dynamics of urbanization and settlement growth in forested regions is essential for balancing economic and environmental objectives. Nighttime satellite datasets have emerged as a valuable resource for tracking these trends in an area where on-the-ground monitoring is often hindered by logistical and financial constraints (McAvoy and Vadrevu, 2024). By analyzing night

light data, we explore the extent of human encroachment into forested areas across South and Southeast Asia. The results highlight hotspots of forest degradation driven by development, as captured by satellite-derived nighttime lights from 2017 to 2023.

7.2 STUDY AREA

The study's area of interest includes a total of 17 countries in S/SEA (Figure 7.1). The study focused on the forested areas covering these countries (Figure 7.2). Afghanistan in South Asia and Singapore and Timor-Leste in Southeast Asia contain only a very small amount of forest in terms of absolute area and the percentage of the country covered by it. Generally, South Asian countries were less proportionally forested than Southeast Asian ones, though Bhutan (72% forest) is an exception. Indonesia, the second-largest country in the region, contains the largest forest.

7.3 DATASETS

We used two different datasets as input, both accessed through the Google Earth Engine Data Catalog. The first, "MCD12Q1.061 MODIS Land Cover Type Yearly Global 500m," consists of one image per year, where the value of each 500-meter pixel represents the predominant land cover type (https://developers.google.com/earth-engine/datasets/catalog/MODIS_061_MCD12Q1). Each image has multiple bands, each

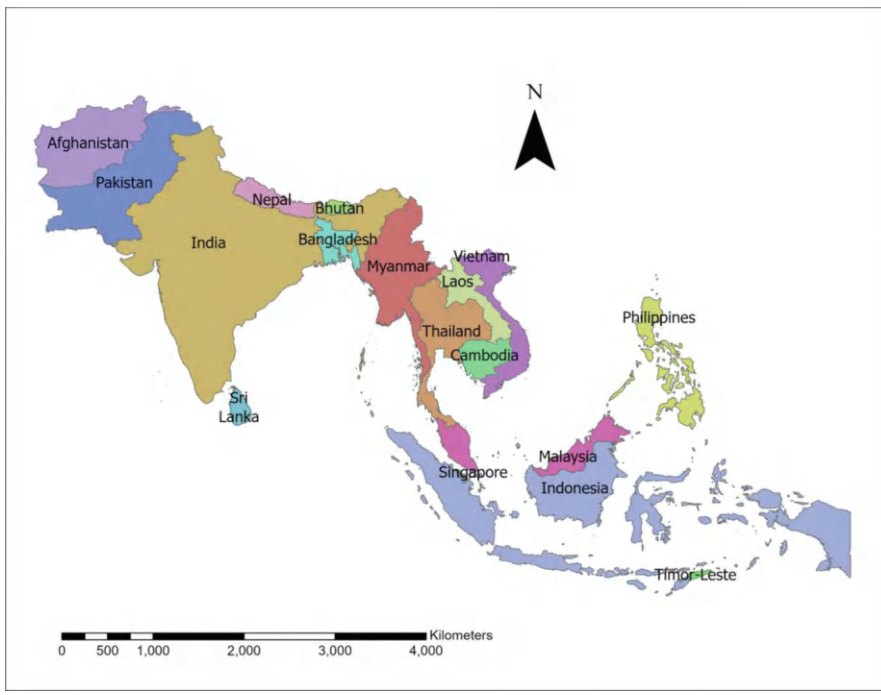

FIGURE 7.1 Study area location map depicting South/Southeast Asian (S/SEA) countries.

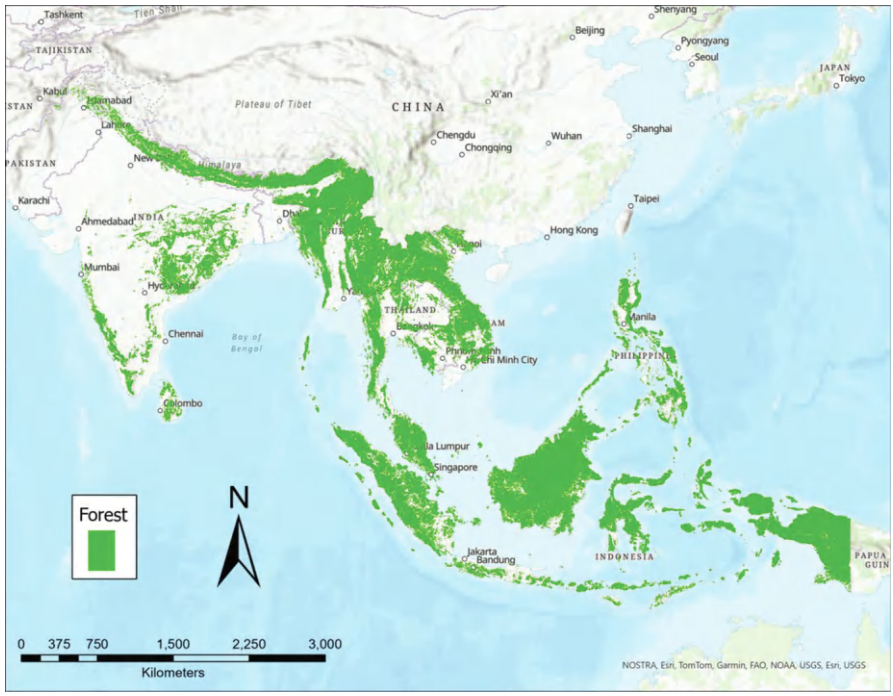

FIGURE 7.2 Forested areas of South and Southeast Asia as retrieved from the MODIS land cover product (500 m). The following classes were merged and denoted as forest in the current study: (1) Evergreen Needleleaf forest; (2). Evergreen Broadleaf forest; (3) Deciduous Needleleaf forest; (4) Deciduous Broadleaf forest; (5) Mixed forest.

corresponding to a different classification scheme. We used the "LC_Type1" band based on the Annual International Geosphere-Biosphere Programme (IGBP) classification for our analysis. The 2017 image was selected as the starting point, as it is the earliest year with reliable data in the nighttime lights dataset. The second dataset used was "VIIRS Stray Light Corrected Nighttime Day/Night Band Composites Version 1," a collection of monthly composited images depicting the brightness of nighttime lights (NTL) worldwide at a resolution of 463.83 meters (https://developers.google.com/earth-engine/datasets/catalog/NOAA_VIIRS_DNB_MONTHLY_V1_VCMSLCFG). The earliest image is from 2015; however, the first two years of data suffer from airglow overcorrection, which produces inaccurately low (and sometimes impossibly negative) values. This issue was corrected in 2017, so only data from 2017 to 2023—the most recent complete year in the dataset was used.

7.4 METHODOLOGY

We used the open-source Google Earth Engine (GEE) for data processing (Figure 7.3). First, the 2017 forest image was reprojected to a 1-km resolution, then processed using the ee.Image.lte(5) method reclassified all pixels classified as forest (land cover

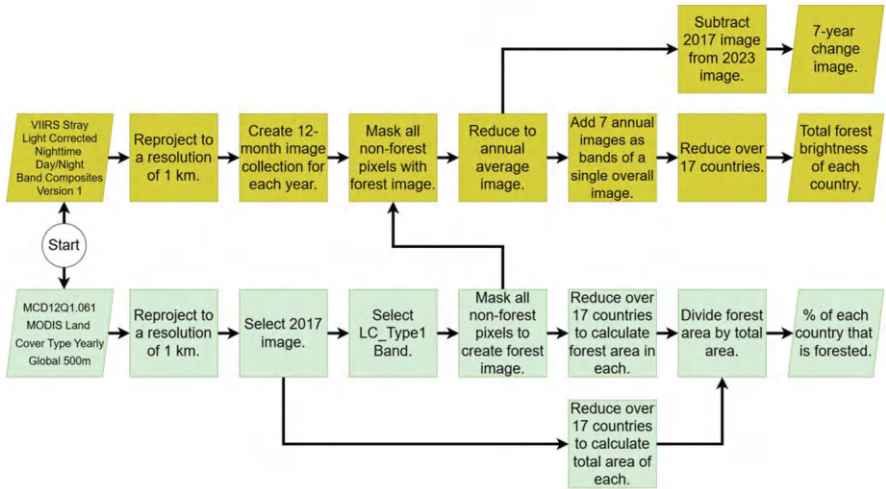

FIGURE 7.3 Flowchart of data processing and analysis methodology.

types 1–5, including any terrain with more than 60% tree cover and a canopy height greater than 2 meters) to 1 and all other pixels to 0. This image was then exported from GEE to be used later in ArcGIS. Simultaneously, the forest image was reduced over the borders of the 17 countries using ee.reducer.sum(). The result was a table listing the number of pixels classified as forests in each country, which was then exported. Next, each monthly NTL image was reprojected to a 1 km resolution and masked using the aforementioned land cover image so that all pixels outside the forest areas would be ignored. The 12 images for each year were then reduced using ee.ImageCollection.mean(), creating seven annual average images, in which each pixel's value represented its mean NTL brightness for that year. These seven annual images were then exported individually. Additionally, they were combined into seven bands of a single image, which was subsequently reduced using ee.Reducer.sum() across the 17 countries of South and Southeast Asia to create a table showing the total brightness of each country's forested areas for each year.

The land cover image and the seven annual average NTL images were further analyzed to assess forest cover changes and visualize the results. First, the 2017 image was subtracted from the 2023 image to produce a different image, where each pixel's value represented its net change in brightness over the 7 years. Next, the land cover image was converted into a collection of two multipart polygons: one encompassing all forested areas and the other encompassing everything else. The latter was promptly deleted, while the former was used to clip the annual average images to include only forest areas.

TABLE 7.1
Brightness of a Specific Pixel in the Dehing Patkai National Park (Marked with an X in Figure 7.8) Over the Years. Notice an Increase in Brightness from 2018 to 2021, Followed by a Decline

Year	Brightness of Marked Pixel (nw/sr/cm^2)
2017	2.227704
2018	1.364792
2019	1.4825
2020	1.535
2021	1.762292
2022	1.436667
2023	1.383958

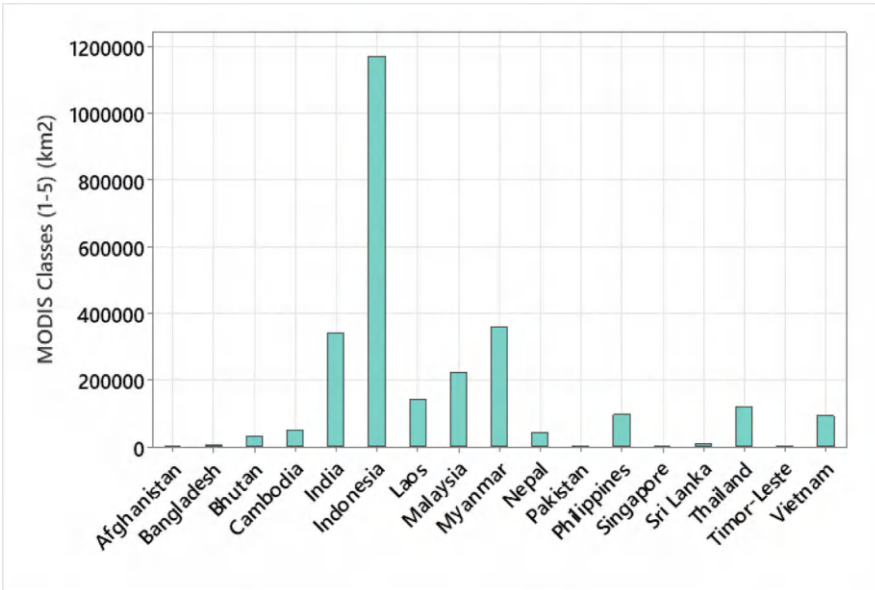

FIGURE 7.4 Total area in forest by merging MODIS land cover classes (1–5). Indonesia, Myanmar, India, and Malaysia had the highest forest cover.

7.5 RESULTS

The results obtained from merging MODIS land cover classes 1–5 for different countries are shown in Figure 7.4. Among the countries analyzed, Indonesia, Myanmar, India, and Malaysia had the highest forest cover.

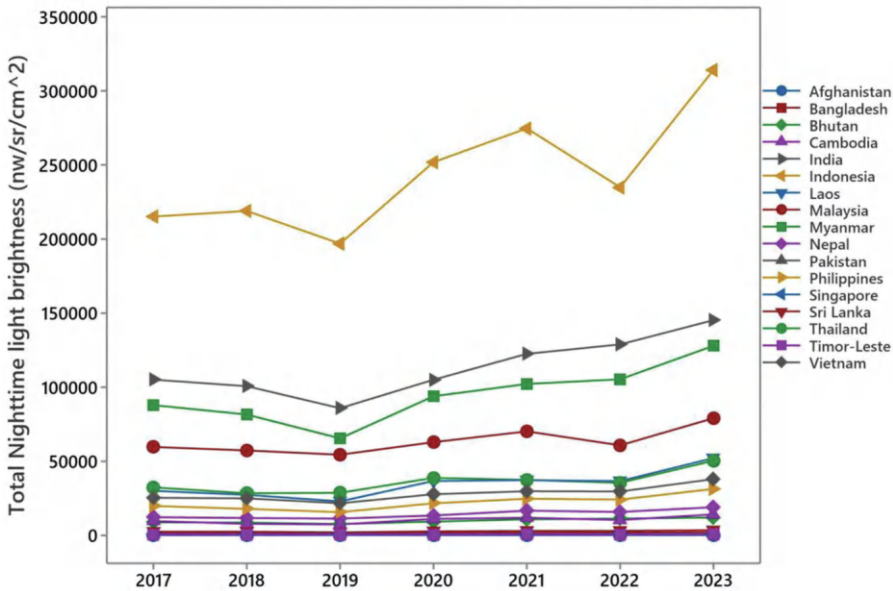

FIGURE 7.5 Change in total nighttime lights brightness of all forested areas in each country, 2017–2023.

A country's change in the total NTL brightness of forested areas suggests urban sprawl or development driven by infrastructure activities. Temporal trends in nighttime lights brightness for different countries are presented in Figure 7.5. Compared to South Asian countries, we observed relatively more significant changes in forested areas in Southeast Asian countries as captured by the NTL. Furthermore, among the countries analyzed, the most significant change in forest areas, as indicated by NTL brightness, was noted in Indonesia, followed by India, Myanmar, Malaysia, and others (Figure 7.6). The change in the total nighttime lights brightness of all forested areas in each country from 2017 to 2023, in increasing order, is given in Figure 7.7, with Laos being the highest, followed by the Philippines, Thailand, Nepal, Bangladesh, and others. As always, the almost-completely urbanized Singapore is an outlier; it is the only country where the total brightness of its forested areas (such as the Central Catchment Nature Reserve depicted in Figure 7.3) decreased over the 7-year study period.

Initially, the change map was difficult to interpret. Almost every pixel in a forested area showed an increase in brightness from 2017 to 2023, but in nearly all of these cases, the increase was minimal, less than 1 nW/sr/cm². To highlight the areas where notable changes had occurred, the layer's symbology was adjusted so that any pixel whose 2023 brightness was within 0.5 nW/sr/cm² of its 2017 brightness appeared as a dark green "background" color. Pixels that increased in brightness by more than 0.5 were displayed in red, while those that decreased by more than that amount were shown in yellow.

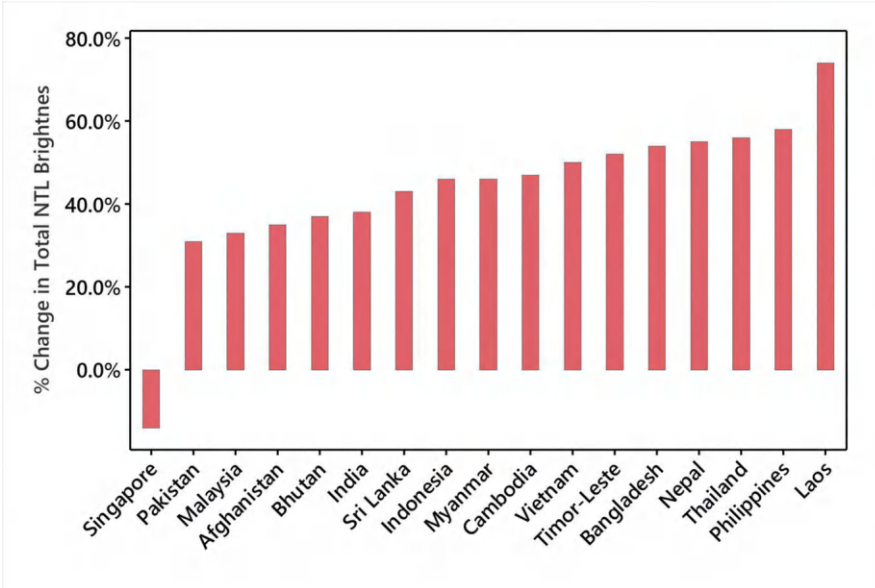

FIGURE 7.6 Change in total nighttime lights brightness of all forested areas in each country from 2017–2023 with increasing order.

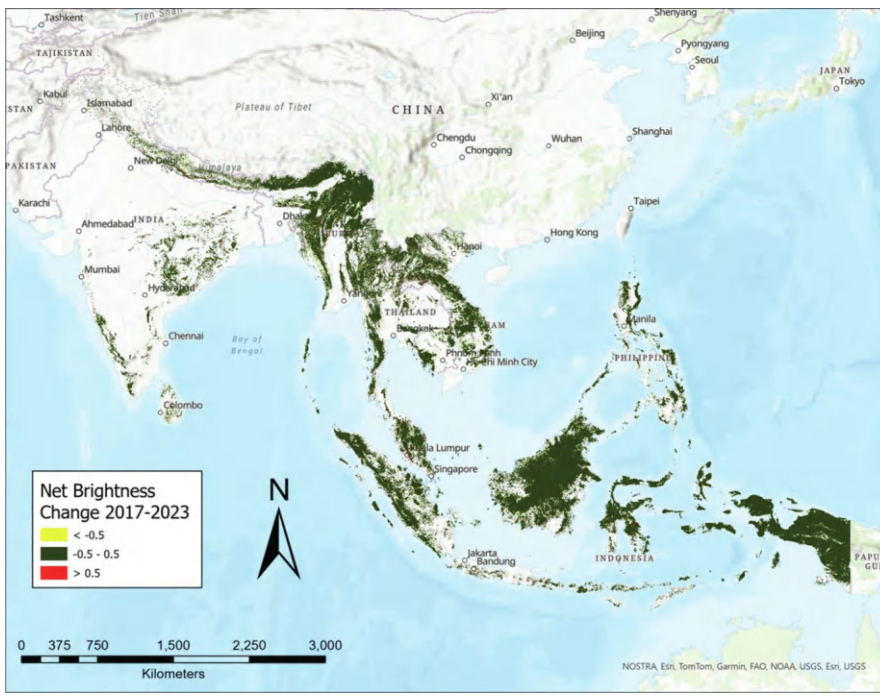

FIGURE 7.7 Change in net nightlight (NTL) brightness in forested areas of South/Southeast Asia.

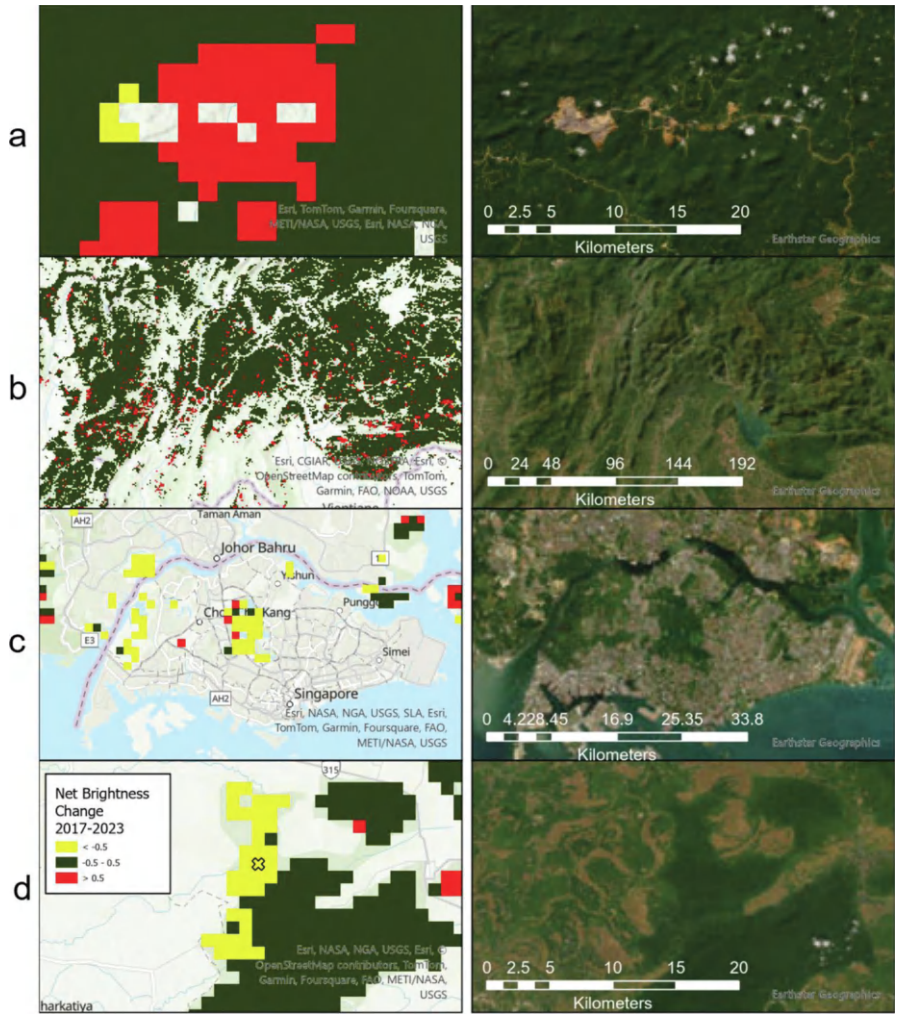

FIGURE 7.8 (a)–(d) Areas of particular interest on the change map (Figure 7.8) compared with satellite imagery of the same locations, taken from the ArcGIS imagery basemap. (a) Asmin Bara Bronang open-pit coal mine in Central Kalimantan, Indonesia; (b) Fragmented forests in Laos experiencing scattered development across the region; (c) The Central Catchment Nature Reserve in Singapore; (d) Dehing Patkai National Park in Assam, India.

In many places, especially in Indonesia, clusters of dozens of red pixels appeared far from any large city or other apparent cause of forest development (Figure 7.8a). Compared to satellite images on Google Earth, these clusters were identifiable as locations of surface mines, where natural forests had been replaced by exposed earth, bright lights, and metal mining equipment. As expected, the development of forested land typically occurs along the edges of expanding cities in forested countries, such

as Kuala Lumpur in Malaysia. However, this effect is not very apparent on the map, as most cities' immediate surroundings consist of cropland or other non-forest land cover types.

In the mountainous inland regions of Southeast Asia (Laos, eastern Myanmar, and northern Thailand), the forests are highly fragmented, with small clusters of increasing brightness scattered throughout. These spots can even be found in Laos's Phou Khao Khouay National Park (visible in the bottom right corner of Figure 7.8b), despite its protected status. Sanjay Gandhi National Park, located on a mountain north of Mumbai, has suffered similarly. Singapore's Central Catchment Nature Reserve (Figure 7.8c) appears to have fared much better, but it is difficult to say for sure; the brightness of Singapore as a whole has decreased over time, possibly due to the large-scale replacement of incandescent lights with LEDs, which are less visible to the VIIRS. If this is the case, the decrease in brightness within the Central Catchment Nature Reserve may be due to the dimming of lights at places like the Singapore Zoo, Night Safari, River Safari, and other public installations. This inference needs validation.

We noted one example of definite forest improvement on this map: Dehing Patkai National Park in India (Figure 7.8d). The NTL brightness of the park has been decreasing since 2021, following a well-documented conservation effort. The Dehing Patkai Landscape comprises over 500 km² of contiguous rainforest, the largest such forest in Assam and the Brahmaputra Valley. Since at least the 1990s, it has been threatened by encroachment from the coal and timber industries, strongly opposed by environmental groups such as Nature's Beckon ("Dehing Patkai National Park," 2024). This opposition achieved some early conservation victories. In 2003, 937 km² of land, including Dehing Patkai and several nearby forests, was designated as an elephant reserve by Project Elephant (Lone et al., 2023). The following year, 111 km² of the forest was designated a wildlife sanctuary due to its high biodiversity (Mohammed, 2020). However, coal mining continued within the elephant reserve despite the expiration of the mining company's lease in 2003. The situation escalated in 2020 when a new mining permit was issued within the wildlife sanctuary. Nature's Beckon organized large-scale protest campaigns both online and in person, and their efforts were successful. In June 2021, more than 200 km² of Dehing Patkai was officially designated as a national park, with all the legal protections that entails (Chakraborty, 2021). As mining ceased and the threatened forest recovered, the NTL brightness of the area would be expected to decrease, which is precisely what was observed.

7.6 DISCUSSION

The analysis of forest cover changes in South and Southeast Asia, based on MODIS land cover classifications and nighttime lights (NTL) data, offers valuable insights into the dynamic landscape of forested areas across the region. Our findings highlight varying patterns of forest change across different countries, with notable differences between South Asia and Southeast Asia and within specific countries, including Indonesia, India, and Malaysia.

From the analysis, it is evident that forested areas in Southeast Asia, particularly in Indonesia, Myanmar, and Malaysia, experienced the most significant changes in NTL brightness, suggesting urban sprawl and development due to infrastructure activities. For instance, the clusters of red pixels observed in Indonesia were identifiable as surface mines, where natural forests had been replaced by exposed earth, mining equipment, and bright lights. This is consistent with the well-documented trends of deforestation driven by resource extraction, particularly mining and logging, which have been prevalent in Southeast Asia.

In contrast, South Asian countries like India and Bangladesh showed relatively smaller changes in forest NTL brightness, though still notable. The overall pattern indicates that Southeast Asian countries may be undergoing more rapid urbanization and development compared to their South Asian counterparts. The greater variability in forested area change within Southeast Asia could be attributed to the complex interplay of rapid industrialization, population growth, and large-scale land use changes driven by agriculture and infrastructure development.

Interestingly, our analysis also revealed areas of forest improvement, such as in Dehing Patkai National Park in India. The decreasing NTL brightness in this region since 2021 might be the result of successful conservation efforts following significant protests against illegal mining activities. Similarly, the Central Catchment Nature Reserve in Singapore showed little to no increase in NTL brightness, suggesting that the area has remained relatively stable. However, this stability is potentially due to changes in lighting infrastructure rather than a true absence of development. The adoption of energy-efficient LED lights, which are less detectable by VIIRS sensors, may account for the observed decrease in brightness across Singapore, including within protected forested areas. Thus, the impact of lighting technologies on nighttime brightness should be considered when interpreting NTL data, especially in urbanized regions.

The use of NTL data for monitoring forest cover change provides a unique perspective on the ongoing transformation of landscapes in regions where traditional monitoring methods may be challenging or resource-intensive (Elvidge et al., 2022). NTL brightness changes offer a proxy for identifying urban expansion, deforestation, and the development of infrastructure. However, the method also has limitations. The subtle brightness changes within forested areas, particularly those under 0.5 nW/sr/cm², suggest that much of the development occurring in these regions is minor or incremental, making it difficult to detect meaningful changes without appropriate thresholds. Furthermore, the use of NTL data must be complemented with other datasets, such as high-resolution satellite imagery, to distinguish between different types of land use and to verify the causes of brightness changes. While surface mining activities can be clearly identified through NTL data, other forms of deforestation or degradation, such as logging or agricultural expansion, may not produce sufficiently high brightness changes to be readily detectable using this method.

7.7 CONCLUSION

This study highlights the complexity of forest dynamics in South and Southeast Asia, revealing both negative and positive trends in forest cover and nighttime lights

brightness. While the increasing NTL brightness in many countries suggests widespread urbanization and deforestation, examples like Dehing Patkai demonstrate that conservation efforts can result in tangible improvements. The use of NTL data offers an effective tool for monitoring large-scale forest changes, though it should be integrated with other methods to improve accuracy and provide a more comprehensive understanding of forest dynamics. As S/SEA continues to face rapid urbanization and development, effective forest management and conservation strategies will be critical in balancing the region's economic growth with the preservation of its vital natural resources.

REFERENCES

Arfanuzzaman, M. and Dahiya, B., 2019. Sustainable urbanization in Southeast Asia and beyond: Challenges of population growth, land use change, and environmental health. *Growth and Change*, 50(2), pp. 725–744.

Ashton, M.S., Goodale, U.M., Bawa, K.S., Ashton, P.S. and Neidel, J.D., 2014. Restoring working forests in human dominated landscapes of tropical South Asia: An introduction. *Forest Ecology and Management*, 329, pp. 335–339.

Barbier, E.B., 2023. Overcoming digital poverty traps in rural Asia. *Review of Development Economics*, 27(3), pp. 1403–1420.

Boanada-Fuchs, A., Kuffer, M. and Samper, J., 2024. A global estimate of the size and location of informal settlements. *Urban Science*, 8(1), p. 18.

Chakraborty, A., 2021, July 3. *Assam forest minister Parimal Suklabaidya inaugurates Dihing Patkai national park*. NorthEast Now. https://nenow.in/north-east-news/assam/assam-forest-minister-parimal-suklabaidya-inaugurates-dihing-patkai-national-park.html

De Jong, W., Liu, J. and Youn, Y.C., 2017. Land and forests in the Anthropocene: Trends and outlooks in Asia. *Forest Policy and Economics*, 79, pp. 17–25.

Dehing Patkai National Park. naparks.com, 2024, May 20. https://naparks.com/dehing-patkai-national-park

Elvidge, C.D., Baugh, K., Ghosh, T., Zhizhin, M., Hsu, F.C., Sparks, T., Bazilian, M., Sutton, P.C., Houngbedji, K. and Goldblatt, R., 2022. Fifty years of nightly global low-light imaging satellite observations. *Frontiers in Remote Sensing*, 3, p. 919937.

Fong, E. and Shibuya, K., 2020. Migration patterns in East and Southeast Asia: Causes and consequences. *Annual Review of Sociology*, 46(1), pp. 511–531.

Jones, G.W., 2002. Southeast Asian urbanization and the growth of mega-urban regions. *Journal of Population Research*, 19(2), pp. 119–136.

Justice, C., Gutman, G. and Vadrevu, K.P., 2015. NASA land cover and land use change (LCLUC): An interdisciplinary research program. *Journal of Environmental Management*, 148, pp. 4–9.

Kanbur, R. and Zhuang, J., 2013. Urbanization and inequality in Asia. *Asian Development Review*, 30(1), pp. 131–147.

Kim, J. and Wood, J., 2020. Service sector development in Asia: An important instrument of growth. *Asian-Pacific Economic Literature*, 34(1), pp. 12–25.

Li, Z., Leong, L.W., Aldoseri, M.M.N., Muda, I., Abu-Rumman, A. and Al Shraah, A., 2023. Examining the role of sustainability and natural resources management in improving environmental quality: Evidence from Asian countries. *Resources Policy*, 80, p. 103136.

Lone, A., Nautiyal, J., Sharma, M., Ghosh, T., Ramesh, K. and Ramesh, C., 2023. *Dihing Patkai Elephant Reserve*. doi: 10.13140/RG.2.2.12697.80481

Ma, J., Li, J., Wu, W. and Liu, J., 2023. Global forest fragmentation change from 2000 to 2020. *Nature Communications*, 14(1), p. 3752.

McAvoy, G. and Vadrevu, K.P., 2024. Nighttime lights and population variations in cities of South/Southeast Asia: Distance-decay effect and implications. *Remote Sensing*, 16(23), p. 4458.

Mohammed, S., 2020, May 21. Battle to protect Dehing Patkai Wildlife Sanctuary, the Amazon of the East. *South Asia Journal*. https://southasiajournal.net/battle-to-protect-dehing-patkai-wildlife-sanctuary-the-amazon-of-the-east

Nguyen, Q.H., 2024. The influence of key economic globalization factors on economic growth and environmental quality: An empirical study in Southeast Asian countries. *Journal of International Trade & Economic Development*, 33(1), pp. 57–75.

Prasad, V.K., Kant, Y. and Badarinath, K.V.S., 2001. CENTURY ecosystem model application for quantifying vegetation dynamics in shifting cultivation areas: A case study from Rampa Forests, Eastern Ghats (India). *Ecological Research*, 16(3), pp. 497–507.

Prasad, V.K., Badarinath, K.V.S. and Eaturu, A., 2008. Effects of precipitation, temperature and topographic parameters on evergreen vegetation greenery in the Western Ghats, India. *International Journal of Climatology: A Journal of the Royal Meteorological Society*, 28(13), pp. 1807–1819.

Qayyum, U., Sabir, S. and Anjum, S., 2021. Urbanization, informal economy, and ecological footprint quality in South Asia. *Environmental Science and Pollution Research*, 28, pp. 67011–67021.

Shivakoti, G., Ullah, R. and Pradhan, U., 2017. Challenges of sustainable natural resources management in dynamic Asia. In *Redefining diversity & dynamics of natural resources management in Asia*, Volume 1 (pp. 3–12). Elsevier.

Sodhi, N.S., Posa, M.R.C., Lee, T.M., Bickford, D., Koh, L.P. and Brook, B.W., 2010. The state and conservation of Southeast Asian biodiversity. *Biodiversity and Conservation*, 19, pp. 317–328.

Sugiyarto, G., 2014. Internal and international migration in Southeast Asia. In *Routledge handbook of Southeast Asian economics. Editor. Ian Coxhead.* (pp. 270–299). Routledge. DOI. https://doi.org/10.4324/9781315742410

Vadrevu, K.P., Ohara, T. and Justice, C. eds., 2018. *Land-atmospheric research applications in South and Southeast Asia*. Springer.

Vu, T.L., Phan, T.T.H., Sadiq, M., Xuyen, N.T.M. and Ngo, T.Q., 2023. Nexus of natural resources, urbanization and economic recovery in Asia: The moderating role of innovation. *Resources Policy*, 81, p. 103328.

Wahab, S., Ahmed, B., Imran, M., Safi, A. and Wahab, Z., 2023. Economic and non-economic drivers of tourism: Bidirectional causality of tourism and environment for South Asian economies. *Environmental Science and Pollution Research*, 30(38), pp. 89740–89755.

Zafar, A., Ullah, S., Majeed, M.T. and Yasmeen, R., 2020. Environmental pollution in Asian economies: Does the industrialisation matter?. *OPEC Energy Review*, 44(3), pp. 227–248.

8 Urbanization's Effects on Heat Dynamics in Bangaluru City Using UTCI and LCZ Classification

Bharath H Aithal, Anita Gautam, and Devireddy Girish Kumar Reddy

8.1 INTRODUCTION

Rapid and irreversible urban growth coupled with climate change has become a prominent worldwide concern in recent decades. This trend is particularly pronounced in India, the most populous country, and poses substantial challenges. Urbanization in India is characterized by the expansion of impermeable surfaces and an increase in population density (Bharath et al., 2018). This demographic shift contributes to the vulnerability resulting from the depletion of natural resources in urban and peri-urban areas (Ramachandra et al., 2012, 2015). According to research published by the UNDRR, India's urban population has almost doubled since 1950, reaching 33% in 2015, and it is anticipated to increase further to 42% by the year 2035. This phenomenon of urban growth, combined with climate change, has been one of the factors causing heat stress. Rising temperatures, increasing faster than the global average, contribute to more frequent and severe heat waves, creating a substantial public health risk. These conditions have a significant impact by contributing to an increase in heat-related mortality. There was a considerable increase in heat-related deaths, with 3014 deaths recorded between 2001 and 2005 (Kumar & Singh, 2021) to 5157 from 2011 to 2015 (Singh et al., 2023). These figures likely understate the actual toll, as many heat-related fatalities go unreported. Various factors such as climate change, urbanization, and population change all contribute to the incidence of heat stress and its health consequences in India.

8.1.1 Land Cover and Local Climate Zone Classification

Urbanization changes city landscapes, land cover, and the dynamics of the city environment. Land use (LU) changes due to urbanization present innumerable challenges

DOI: 10.1201/9781003396260-8

for urban management. These changes must facilitate sustainable urban design and enhance the overall quality of urban life (Pradhesta et al., 2019). Remote sensing technologies can assist in tracking these changes by providing precise and continuous data (Justice et al., 2015). These technologies allow us to observe the effects of urbanization on land cover patterns (Chandan et al., 2019). Among these advances, the LCZ classification system provides a more advanced approach to examining urban-related climatic studies on a local scale (Kotharkar & Bagade, 2018). Initially, Stewart & Oke (2012) established a climate-related classification of homogenous urban structure, thermal behavior, and land cover. It is found that urban areas are distinguished by a range of land cover types and building forms, which can substantially impact energy balance and microclimate (Xu et al., 2017). Based on this understanding, the LCZ mapping is classified into 10 built-type areas. These range from Class 1 to Class 10, which represent built-up areas, namely compact high-rise, compact mid-rise, compact low-rise, open high-rise, open mid-rise, open low-rise, lightweight low-rise, large low-rise, sparsely built, and light industry, respectively. Furthermore, LCZ mapping also includes seven land cover type areas from Class A to Class G, which consist of dense trees, scattered trees, bush/scrub, low-plant, bare rock/paved, bare soil/sand, and water, respectively (Stewart & Oke, 2012). This classification system offers a comprehensive framework for analyzing the thermal behavior of urban areas by integrating buildings and natural land cover types. In Bechtel et al. (2015), this system was presented by a supervised classification method using remote sensing satellite data at level 0 with satisfactory accuracy, successfully implemented through the World Urban Database and Access Portal Tools (WUDAPT). Researchers worldwide have used the LCZ classification approach for urban mapping, incorporating local expert knowledge. Xu et al. (2017) used Landsat and ASTER data within the WUDAPT framework, obtaining kappa values of 0.65 to 0.85. To map land cover zones, Pradhesta et al. (2019) used a Random Forest classifier to examine land surface temperature (LST) differences. Similarly, Saxena and Agrawal (2023) utilized the WUDAPT classification to investigate the link between LST and LCZs in four Indian cities. These investigations highlight the importance of satellite-based LCZ classification as a practical approach for investigating urban geometry and its climate interactions at the city scale.

8.1.2 Thermal Comfort and Urban Thermal Climate Index (UTCI)

Rapid urbanization has resulted in more than 50% of the world's population currently residing in urban areas, leading to substantial transformations in their daily lives (Wu et al., 2022). Previous studies suggest that the impact of global warming (Grimm et al., 2008), rapid urban expansion, and the urban heat island phenomena (Chen & Ng, 2012) is causing a decline in urban climates, influencing the perception of heat, and increasing the susceptibility to heat-related health issues. Thus, it is vital to comprehend the thermal comfort state within the city to assess individuals' perspectives of the urban thermal environment (Wu et al., 2022). Thermal comfort is a subjective experience impacted by air temperature, wind speed, radiant heat, and humidity. It is a condition of mind in which people experience contentment with their thermal environment. When the human body is in an optimal thermal

environment, it develops a balance between heat production and heat loss. However, when the environment is too hot or too cold, the body must work to maintain its internal temperature. In a hot environment, the body increases sweat production to cool down, while the body shivers and constricts blood vessels to conserve heat in a cold environment (Fiala et al., 2012). It is possible to attain and assess the urban thermal comfort of a given population through a calibrated thermal comfort index assessment, which should be selected according to the local climate (Potcher et al., 2018; Silva & Hirashima, 2021). Recent studies include several thermal indices, and some initiatives provide for adjusting their ranges to account for regional populations. The assessment scale of these indices can be calibrated to forecast the thermal comfort category and identify realistic periods of thermal perception (Hirashima et al., 2018; Silva & Hirashima, 2021).

For assessing the thermal environment in urban areas, four important indices are used: Physicological Equivalent Temperature (PET), Perceived Temperature (PT), UTCI, and Standard Effective Temperature (SET). Among these indices, the UTCI is especially useful for urban areas and incorporates a novel approach that addresses urbanization factors (Staiger et al., 2019; Silva & Hirashima, 2021). The UTCI is a physiological index that quantifies how air temperature, humidity, wind speed, and mean radiant temperature on human thermal comfort. It is a more comprehensive measure than traditional temperature-based indices such as the Heat Index or the Wet Bulb Globe Temperature (WBGT), as it considers the effects of multiple environmental factors (Bröde et al., 2012). Previous research, including Kumar & Sharma (2020) and Setiawati et al. (2021), highlights its relevance in studying urban thermal dynamics and land use change and shows that urbanization increases UTCI hazard levels.

Due to high population densities that increase the risk of heat stress, cities are significantly influenced by the urban heat island effect (UHI) and frequently record higher temperatures than rural locations. According to Aithal et al. (2019) urban variables that contribute to higher UHI and its effects on local climatic regimes, for instance, can raise temperatures by as much as 12°C (20°F), which has a detrimental impact on human health by obstructing natural cooling and increasing the risk of heatstroke. Additionally, the UTCI, which is critical to evaluating urban heat stress, indicates that urban design components such as high-rise structures could worsen this effect by creating a 'canyon effect' that absorbs more heat, potentially raising temperatures by an extra 2°C (3.6°F) (Singh et al., 2023). Hence, this study aims to assess urban heat stress and its relation to urban geometry in Bangalore, a tropical city, and address the urgent need for spatial heat stress mapping. The objectives include assessing the urban spatiotemporal change through local climate zones, preparing UTCI maps, and analyzing the correlation between LCZ classifications and UTCI levels to understand urban heat dynamics better.

8.2 STUDY AREA

Bangalore, commonly referred to as Bengaluru, is the state of Karnataka. It has a tropical savanna climate with distinct wet and dry seasons and is also located on the Deccan Plateau at 921 meters (3,020 feet) above sea level. This study area,

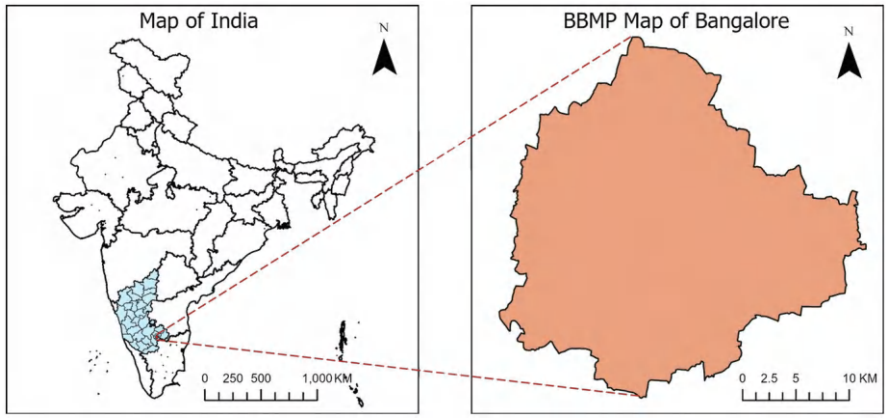

FIGURE 8.1 Study area map of the Greater Bangalore region.

which includes the Greater Bengaluru region, is delineated by the Bruhat Bengaluru Mahanagara Palika (BBMP) borders, chosen due to its notable infrastructural improvements and fast urbanization in recent decades. In this, the hottest month is typically April, with an average high temperature of 34.1°C (93.4°F), while January is the coolest month, with an average low temperature of 15.1°C (59.2°F). The highest temperature ever recorded in Bengaluru is 39.2°C (103°F), recorded on April 24, 2016, and the lowest ever recorded is 7.8°C (46°F) in January 1884, as per the Indian Metrological Department (IMD). Geographically, Bengaluru spans from 12°39'00"N to 13°13'00"N latitude and 77°22'00"E to 77°52'00"E longitude (Figure 8.1). The total area of the Greater Bangalore region, as per the BBMP boundary, is around 741 km^2. Known as the "Silicon Valley of India", it is one of the fastest-growing cities, with a population of over 12.3 million in 2021. Urbanization, migration, and economic expansion are the main drivers of the region's rapid expansion (Bharath et al., 2018). However, the city also faces challenges due to unplanned growth. Its primary challenge is its highly populated urban layout, which results from spontaneous and unforeseen urbanization and mixes limited natural areas with constructed surroundings. The city lacks three-dimensional built data and high-resolution temperature data despite many studies on the effects of UHI.

8.3 DATA AND METHODS

8.3.1 DATA

The meteorological data such as air temperature (T_a), relative humidity (R_h), and wind speed (W_s) are availed from the ground stations located in the area of interest managed by the Indian Meteorological Department (IMD) and the Karnataka State Pollution Control Board (KSPCB). To synchronize with the time of Landsat passage over the area of interest, the average hourly meteorological data between 9 am and 12 pm is calculated. This averaged dataset is subsequently utilized in our study.

8.3.2 Satellite Data

The study primarily utilizes temporal satellite data from Landsat 5, Landsat 8, and Landsat 9 from the USGS Earth Explorer public repository. For April and May of 2009 and 2011, all Thematic Mapper (TM) bands from Landsat 5 were obtained. Data were collected for Landsat 8 in April 2021 and 2022 using the Thermal Infrared Sensor (TIRS) bands and Operational Land Imager (OLI) bands (except Panchromatic and Cirrus). For April 2023, data were acquired from repositories of Landsat 9. This data was resampled to 100 m for analysis, with a spatial resolution of 30 m. Furthermore, Google Earth was utilized to train samples to classify local climate zones (LCZs).

8.3.3 Approach

8.3.3.1 Local Climate Zone Classification

The LCZ classification for 2011 and 2023 was conducted using high-resolution historical imagery from Google Earth and Landsat data by following the established WUDAPT approach from 2009 and 2023. The approach began with the creation of a composite of chosen Landsat data. Training samples for various LCZ classes were manually created with Google Earth images from both years. Using the supervised classification technique, these samples and composite band data were then utilized to construct the LCZ maps. This study includes all standard LCZ classes, as Bangalore encompasses a diverse land use and cover range. The class distribution of LCZs within the city is depicted in Figure 8.2. Throughout the study period, training samples for each of the 17 LCZ classes were constructed with the utmost by manually identifying them with experts. The Random Forest algorithm, renowned for its high accuracy (Pradhest et al., 2019), was selected for the classification. The created training samples acted as input, and the algorithm is configured with 128 trees and a depth of 30 trees, thereby facilitating the categorization and mapping of local climate zones within the study area. The images were resampled to a resolution of 100 m as specified by WUDAPT. Classification accuracy has been validated using the confusion matrix method by creating random points in the area of interest and matching them with the ground data.

8.3.3.2 Universal Thermal Climate Index

The Universal Thermal Climate Index is the function of four climatic variables: air temperature (T_a), mean radiant temperature (T_{mrt}), relative humidity (R_h), and wind speed (W_S). The equation of UTCI defined by (eq. 8.1) (Błazejczyk et al., 2013) is as follows:

$$\mathrm{UTCI} = T_a + \mathrm{offset}\left(T_a, T_{mrt}, R_h, W_S\right) \tag{8.1}$$

UTCI can be estimated using ground-based data at a local site scale or a larger regional scale. However, this is ineffective in studying the city scale variations due to complex structures and the requirement of high-resolution data. Hence a method

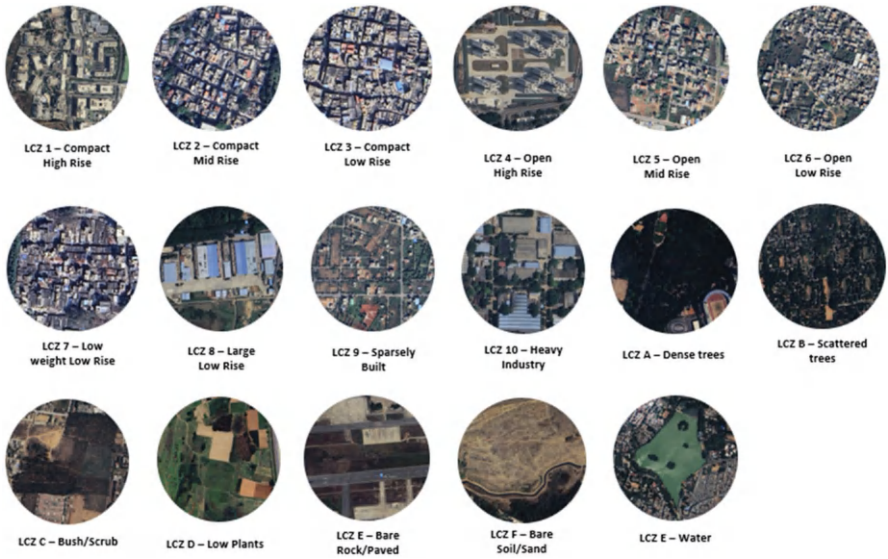

FIGURE 8.2 Sample LCZ classes in Bangalore.

based on remotely sensed data can be of greater help for such studies (Wang et al., 2020). Variables such as air temperature, mean radiant temperature, and relative humidity can be derived from the satellite data at the required spatial resolution, whereas wind speed shall be derived from ground-based measurements. For this study, the average data of all the selected dates from 2009 to 2011 are considered data for 2009, and the average data of all the selected dates from 2021 to 2023 are considered data for 2023. The entire study is performed using the raster data of 100 m resolution, and a resampling technique is used wherever required to match the resolution with 100 m.

8.3.3.2.1 Air Temperature (T_a) and Relative Humidity (R_h)

Air temperature and relative humidity are the two most important variables in estimating the UTCI index. Ground observations rather than satellite data can accurately measure these climatic variables. However, as the requirement is spatial data with good resolution, here we have used the average hourly data from ground stations (refer to Section 8.3.1) and established a function of T_a (eq. 8.2) and R_h (eq. 8.3) with satellite-based variables (refer to Section 8.3.2) such as LST, Surface Albedo, Digital Elevation Model (DEM), Normalized Difference Vegetation Index (NDVI), and other variables using multiple linear regression (MLR) models. The following is the function of T_a and R_h with the selected independent variables and constants.

$$T_a = Albedo * a_1 + DEM * a_2 + NDVI * a_3 + LST * a_4 + DDL * a_5 + X_1 * a_6 + X_2 * a_7 + C_1 \quad (8.2)$$

$$R_h = Albedo * b_1 + DEM * b_2 + NDVI * b_3 + LST * b_4 + DDL * b_5 + X_1 * b_6 + X_2 * b_7 + C_2 \ \# \quad (8.3)$$

Here, $a_1, a_2, a_3, a_4, a_5, a_6, a_7, b_1, b_2, b_3, b_4, b_5, b_6, b_7$ are the coefficients and C_1, C_2 are the intercepts.

- Surface Albedo (Albedo) is spatially calculated following the method proposed by (Ramachandra et al., 2021) using the Landsat band data of selected dates.
- A Digital Elevation Model (DEM) for Bangalore city is acquired from the ASTER satellite and clipped to the required area of interest.
- Normalized Difference Vegetation Index (NDVI) is calculated using the (eq. 8.4).

$$\text{NDVI} = \frac{\text{NIR} - \text{Red}}{\text{NIR} + \text{Red}} \quad (8.4)$$

LST is calculated using the thermal band 6 of Landsat 5 and 10 of Landsat 9. The procedure is given by Avdan & Jovanovska (2016) is followed to retrieve LST from Landsat 8 and 9 whereas the LST was retrieved from Landsat 5 following the method proposed by Govind & Ramesh (2020).

- Duration Day Length (DDL) is an independent variable calculated based on (eq. 8.5).

$$\text{DDL} = \frac{24}{\text{À}} * \arccos\left(\tan\frac{\varphi}{180}\pi\right) * \tan\left(\frac{23.45\pi}{180}\sin(\delta)\right) \quad (8.5)$$

  where φ is local latitude and δ is the declination angle which is equal to $\frac{2\pi(284 + DY)}{365}$; DY = Day of the Year (Al-Anbari et al., 2019).

- X_1 and X_2 are the variables (Liu et al., 2021b) based on the day of the year and LST where $X_1 = (\text{DY} - 200)^2$, $X_2 = X_1 * \text{LST}$ (Liu et al., 2021).

The coefficients are calculated by the MLR model and the equations of T_a, R_h achieved a root mean square error (RMSE) of 0.52 (°C) and 3.76 (%), respectively. Then the raster images of spatially distributed T_a and R_h at 100 m are generated using the raster calculator function in ArcGIS Pro.

8.3.3.2.2 Mean Radiant Temperature (T_{mrt})

The mean radiant temperature is the quantification of the exchange of radiant heat between a human and their surrounding environment based on long and short-wave radiation. The human thermal comfort largely depends on T_{mrt}. This can be quantified

using satellite data based on the Man Environment Heat Exchange (MENEX) model, using the following (eq. 8.6) (Wang et al., 2020).

$$T_{mrt}\left(^{\circ}\mathrm{C}\right)=\left(\frac{S_w+L_w}{\varepsilon_p*\sigma}\right)^{0.25}-273.15 \tag{8.6}$$

where S_w is shortwave radiation, L_w is long-wave radiation, ε_p is human body emissivity, which is taken as 0.97 and σ is Stefan Boltzmann constant.

The shortwave radiation S_w is estimated using the SolAlt model proposed by Blazejczyk (2001).

$$S_w=1.4*\left(-100.428+73.981*\ln\left(h\right)\right)*\left(1-a_c\right)*IRC \tag{8.7}$$

where h is sun altitude in degrees (taken from the metadata of Landsat bands), a_c is skin albedo (set as 0.5 for Indian regions), IRC is the reduction coefficient of heat transfer through clothing. The (eq. 8.7) is used in the case of $h > 4°$ and cloud cover less than 20%.

The longwave radiation L_w is based on two factors, l_a, which is atmospheric emitted radiation and l_g is the ground emitted radiation and it can be written as the following eq. 8.8 (Wang et al., 2020).

$$L_w=0.5*\varepsilon_p*\left(l_a+l_g\right) \tag{8.8}$$

where $l_a=\varepsilon_{sky}*\sigma*T_a^4$ and $l_g=\varepsilon_g*\sigma*LST^4$; here ε_g is surface emissivity calculated based on the proportion of vegetation and ε_{sky} is the emissivity of the sky, calculated as follows

$\varepsilon_{sky}=\varepsilon_a*\left(0.82-0.25*10^{-0.094*vp}\right)$ where ε_a is atmosphere emissivity set at 0.97 and vp is vapour pressure, which is estimated using R_h and LST as per Chakraborty et al. (2015).

8.3.3.2.3 Wind Speed (W_s)

As the wind speed is impossible to estimate from the remotely sensed data, the spatial wind speed at 100 m resolution is estimated using the Kriging interpolation method with the available ground station data.

8.3.3.2.4 Calculation of Spatial UTCI

Once the above-mentioned variables are derived in the form of 100 m resolution raster files, the UTCI look-up table method (Bröde et al., 2012) is used with the help of the pythermal package in python (Tartarini & Schiavon, 2020) to calculate

the spatial UTCI. The UTCI raster images are prepared for both the 2009–2011 and 2021–2023 periods. These are divided into five categories of UTCI classes as per stress levels (Blazejczyk et al., 2014).

8.4 RESULTS AND DISCUSSION

8.4.1 Local Climate Zone Classification

LCZ maps for the years 2011 and 2023 were produced for the area within the BBMP boundaries, as shown in Figure 8.3. In the maps, red tones depict the compactly built classes ranging from high-rise to low-rise buildings, and orange tones represent the open-built classes from high-rise to low-rise. Vegetation is marked in green shades, and water bodies are shown in blue. Figure 8.4 presents the area and changes in area for each LCZ class across both years.

In 2011, the area of LCZ 9, sparsely built typology, was 106 sqkm, and it was the biggest LCZ in terms of area, followed by LCZ 5, open mid-rise, with 76.5 sqkm area and LCZ 6, open low-rise, with 75 sqkm. These three LCZs contribute 37.5% of the total area. These are the classes that can be found along the outer periphery of the city while the city is expanding. The city's inner core mainly consists of compact build typologies that are the LCZ classes 1, 2, 3, and LCZ A, dense trees, which are part of the natural classes. The area of LCZ G, water bodies, is 14.15 sqkm and is distributed over the entire region, mainly consisting of the lakes that are present. Also, LCZ F, bare soil, covers 37.6 sqkm and is located in the region's peripheral part. Figure 8.4 for 2023 shows that the largest LCZ is the compact mid-rise, covering an area of 120 km^2. The area classified as sparsely built has decreased by nearly 50% from 2011, down to 57.4 km^2, primarily due to increased settlements on the city outskirts. There has been a significant expansion in the compact high-rise category, increasing from 9.7 km^2 in 2011 to 31.6 km^2 in 2023, a growth of over 200%. Additionally, there is a 50% reduction in heavy industry areas as industrial facilities have moved beyond city limits. A 150% increase in paved areas reflects more roads and impervious surfaces.

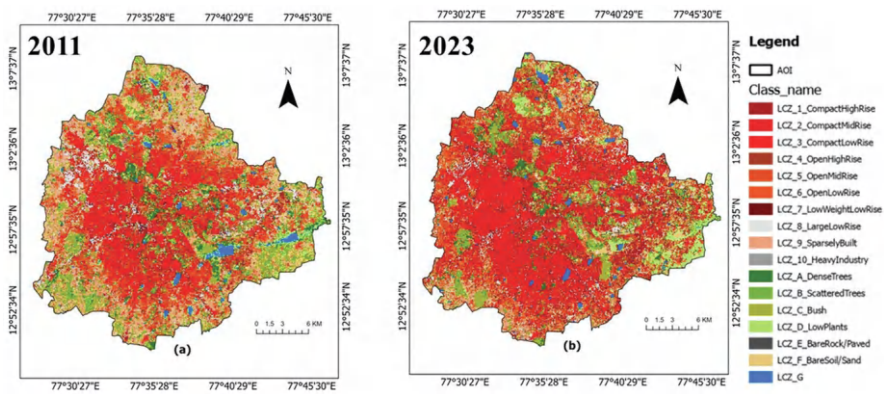

FIGURE 8.3 LCZ map of Bangalore (a) 2011, (b) 2023.

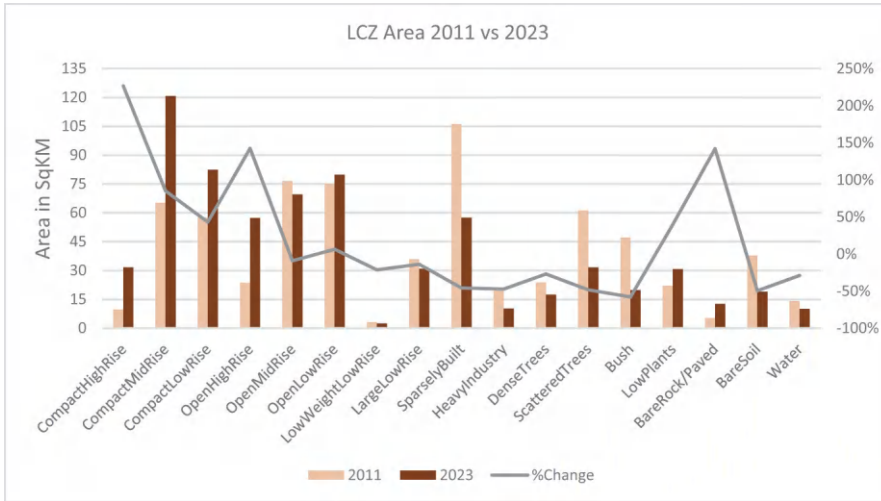

FIGURE 8.4 Graph showing change in area of LCZ classes.

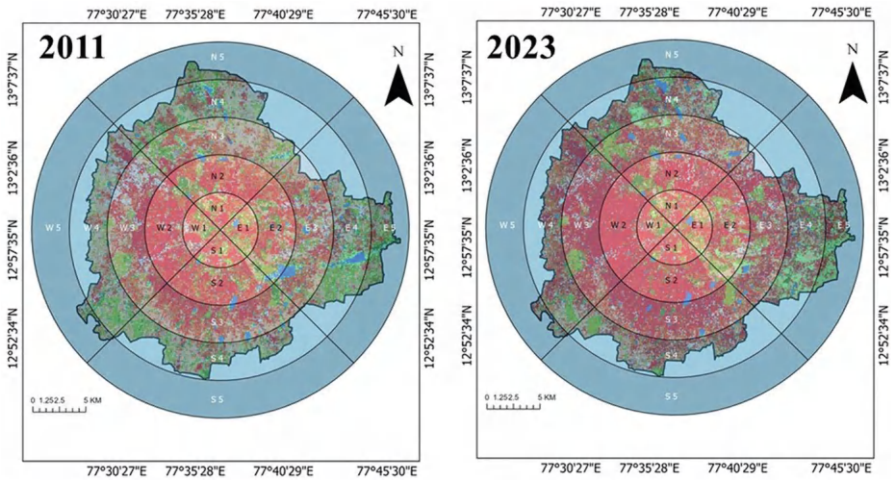

FIGURE 8.5 LCZ maps with sectoral ring divisions.

The sectoral ring approach is used to analyze LCZ growth over the period. From the geometric center of the city, the concentric circles are marked with a 4 km incremental radius, and then these circles are divided into four sectors in four directions: North, East, South, and West. This gives a total of 20 sectors which are named N1, N2, N3, N4, N5, E1, E2, and so on, as shown in Figure 8.5. This process has been done on both the LCZ maps from 2011 and 2023. Then, the statistics of LCZ classes in each sector are calculated for both years. The percentage share of each LCZ among the different sectors in both 2011 and 2023 is presented in Table 8.1.

The sectoral ring analysis shows that in sector W2, the compact mid-rise class accounts for up to 50% of its total area in 2023, up from 38% in 2011. Similarly, sector S2 has the majority of its area in the form of the compact mid-rise class with 41%, previously at 26% in 2011. The increase in compact mid-rise can be attributed to the conversion of open mid-rise to the compact class over the decade (refer to Table 8.1). The inner core of the city, ring 1 (N1, E1, S1, W1), does not see any significant change in the LCZ classes apart from a slight increase in the high-rise development from open and natural classes. In ring 3, there has been a notable increase in compactly built classes and a decrease in open-built classes with compact mid-rise predominating, illustrating the urban sprawl. Similarly, ring 4 experienced a rise in built classes over the decade, transitioning from sparsely built to more open and compact classes. Specifically, the sparsely built class reduced from 16% to 3% in ring 3 and 24% to 15% in ring 4. Across all rings, there was a decline in vegetation classes, with the inner rings showing more reduction than the peripheral rings. All these findings show the growth of impervious classes in every direction. The central core majorly experienced a transformation from open to compactly built classes, while the outer rings shifted from sparsely built and bare soil to more compact and open classes. For detailed data on the changes in individual classes within each section from 2011 to 2023, refer to Table 8.1.

8.4.2 Universal Thermal Climate Index

The UTCI maps of 2009 and 2023 are produced for the area of interest as detailed in section 8.3.3.2, with results in Figure 8.6. In 2009, UTCI values ranged from 26°C to 31°C, whereas in 2023, there was a slight increase from 27°C to 32°C. The spatial change of UTCI over the region can be seen in Figure 8.6, illustrating a rise in UTCI over many parts of the city.

Figure 8.7 displays the UTCI change map over the past decade, showing an increase of up to 3.5°C in certain parts of the city, while most areas experienced a rise of 1°C to 1.5°C. The mean UTCI index was also calculated across different LCZ classes for relational analysis.

Figure 8.8 illustrates the graph in the sectorial area of LCZs and the variation of the mean UTCI of each LCZ class. It is observed that there is a more significant increase in mean UTCI for built classes than the natural classes with around 2°C. This can be attributed to the increase of area in the decade for built classes and the reduction of natural courses. The sizeable low-rise and sparsely built classes show the highest mean UTCI for both years. This is due to the exposure to the direct sun, higher LST, and less green cover in these classes. The compactly built classes show a lesser mean UTCI of about 1°C than the considerable low rise due to the protection by the green cover and the mild climate of Bangalore city.

8.5 CONCLUSION

In the past few decades, urban areas such as Bangalore have experienced significant urbanization and a notable surge in migration. Despite the high density of growth

TABLE 8.1
Statistics of LCZ Classes Based on Sectoral Ring Approach

Sectoral Ring Approach LCZ 2011 vs 2023 (% percentage of the class in the sector)										
	Open High Rise		Open Mid Rise		Open Low Rise		Sparsely Built		Compact High Rise	
	2011	2023	2011	2023	2011	2023	2011	2023	2011	2023
N1	3.07	6.14	20.93	14.48	14.87	17.86	4.09	10.70	15.11	10.86
E1	4.44	5.63	13.49	15.24	6.03	5.00	3.73	9.13	18.10	8.25
S1	4.26	8.20	21.86	30.87	15.19	14.23	6.99	8.04	12.78	4.26
W1	4.39	9.09	20.89	20.97	8.77	17.38	5.18	10.45	13.16	2.87
Total 1	4.04	7.27	19.29	20.39	11.22	13.62	5.00	9.58	14.79	6.56
N2	1.08	5.40	17.25	17.30	15.32	24.58	4.81	6.96	21.06	9.52
E2	2.54	5.45	12.10	13.19	7.12	10.88	5.69	7.73	16.34	10.96
S2	5.71	7.67	26.33	41.17	7.80	11.41	6.37	8.97	22.25	2.89
W2	3.58	5.89	38.56	49.67	18.14	23.36	3.53	5.89	12.70	1.30
Total 3	3.23	6.10	23.56	30.33	12.10	17.56	5.10	7.39	18.09	6.17
N3	0.44	3.15	2.74	8.56	4.15	7.70	2.16	7.43	8.35	15.23
E2	1.03	9.74	3.45	7.01	8.45	15.94	7.90	13.17	12.42	11.59
S2	1.29	5.69	9.70	28.84	12.64	13.96	5.35	9.25	16.82	9.35
W2	0.48	3.62	9.69	31.64	15.36	17.21	1.42	4.99	11.57	6.47
Total 3	0.81	5.55	6.39	19.01	10.15	13.70	4.21	8.71	12.29	10.66
N4	0.69	2.06	1.90	5.36	3.40	5.32	1.75	8.46	7.17	11.94
E4	0.85	4.90	1.40	2.37	2.95	6.33	2.87	13.40	4.01	12.20
S4	0.51	2.25	0.97	6.39	3.47	7.49	1.79	7.31	4.86	10.54
W4	0.12	1.69	1.10	12.65	5.70	7.78	0.41	7.18	5.34	17.80
Total 4	0.54	2.73	1.35	6.69	3.88	6.73	1.70	9.09	5.34	13.12
N5	0.26	1.58	0.13	0.53	0.92	1.84	1.19	8.56	2.37	11.99
E5	0.00	2.75	0.31	1.46	1.09	4.94	0.42	7.12	2.75	11.85
W5	0.00	0.85	0.85	0.64	1.06	6.17	0.85	1.28	0.43	7.02
Total 5	0.09	1.73	0.43	0.87	1.03	4.32	0.82	5.65	1.85	10.29

within the confines of the BBMP, notable changes have occurred in land utilization, building classifications, and infrastructure. Nevertheless, this expansion has presented environmental obstacles that impact the thermal well-being of inhabitants, heightening their susceptibility to heat waves. This research investigates the correlation between past alterations in land use and the level of comfort in terms of temperature utilizing the LCZ classification and the UTCI index. Specifically, it focuses on the urban geometry of cities and also addresses the challenges possessed by the complexity of urban forms. LCZ classification relied on free available 30 m resolution Landsat data. While higher resolution data and expert local knowledge could

Compact Mid Rise		Compact Low Rise		Dense Trees		Scattered Trees		Bush		Bare Soil		Water		Others	
2011	2023	2011	2023	2011	2023	2011	2023	2011	2023	2011	2023	2011	2023	2011	2023
8.42	8.42	3.93	4.88	7.47	5.43	7.55	7.87	1.020.94		2.122.36		0.31	0.24	11.09	9.83
9.21	11.75	4.60	9.05	10.08	6.43	13.17	13.49	3.101.67		1.431.59		2.86	3.17	9.76	9.60
5.71	8.68	1.93	3.54	7.23	3.70	7.96	6.19	2.731.29		0.320.40		0.08	0.40	12.94	10.21
5.02	5.10	1.67	2.63	11.24	8.69	4.23	6.86	2.310.88		0.000.64		0.08	0.16	23.05	14.27
7.09	8.49	3.04	5.02	9.01	6.06	8.23	8.60	2.291.19		0.971.25		0.83	0.99	14.21	10.98
12.67	8.31	5.85	3.23	5.87	4.55	5.21	5.05	1.301.69		1.061.67		1.77	1.61	6.75	10.13
8.18	8.55	7.04	6.72	7.97	2.38	8.71	11.36	6.063.39		1.092.99		3.76	0.48	13.40	15.91
5.84	8.02	2.04	2.18	5.26	3.48	4.65	3.80	2.041.51		1.250.85		2.57	2.68	7.88	5.36
4.85	4.03	1.25	0.58	1.88	1.17	2.55	1.22	0.480.13		0.370.29		0.21	0.32	11.91	6.15
7.89	7.23	4.04	3.18	5.25	2.89	5.28	5.36	2.471.68		0.941.45		2.08	1.27	9.98	9.39
15.76	16.69	22.28	10.35	2.84	2.17	10.43	6.31	7.933.83		9.544.04		1.87	2.61	11.51	11.94
14.96	9.87	14.12	5.64	2.00	1.24	7.72	4.43	5.471.46		4.423.27		4.47	1.44	13.59	15.20
13.31	10.90	16.97	4.79	2.88	1.13	4.39	1.39	3.633.29		2.161.33		2.44	2.33	8.42	7.72
12.81	9.67	12.71	4.52	1.13	2.68	6.44	3.22	6.233.03		1.451.15		0.65	0.18	20.07	11.65
14.21	11.78	16.52	6.33	2.21	1.80	7.24	3.84	5.812.90		4.392.44		2.36	1.64	13.40	11.63
11.90	17.36	23.03	13.98	2.26	3.12	11.09	5.18	9.482.67		12.965.22		2.02	3.85	12.35	15.47
9.67	10.10	16.21	10.64	2.99	3.01	15.38	2.73	12.893.86		10.667.00		4.31	1.30	15.82	22.16
10.72	17.10	28.42	21.04	2.56	1.41	14.70	4.40	13.927.18		7.823.23		1.24	0.84	9.02	10.81
11.26	19.00	30.66	13.67	1.51	1.70	10.48	4.36	11.522.93		7.711.65		1.17	0.64	13.01	8.95
10.89	15.89	24.58	14.83	2.33	2.31	12.91	4.17	11.954.16		9.794.28		2.19	1.66	12.55	14.35
9.75	12.78	24.24	22.00	0.40	2.11	15.55	9.88	13.182.50		21.345.14		0.13	1.19	10.54	19.89
10.40	9.88	13.93	8.42	5.93	3.07	17.26	1.14	10.974.42		16.224.89		1.30	0.26	19.44	39.81
2.55	14.47	26.81	26.81	0.64	0.85	13.83	6.60	20.434.04		10.009.36		1.70	2.77	20.85	19.15
7.57	12.37	21.66	19.08	2.30	2.01	15.54	5.87	14.863.65		15.856.46		1.04	1.40	16.94	26.29

enhance accuracy, preliminary results show significant LCZ shifts from 2011 to 2023, with central areas remaining unchanged but adjacent areas becoming more dense. The outskirts have transformed considerably, converting natural areas into built-up regions with more impervious surfaces. The UTCI calculation involves multiple steps, but this study demonstrates that it can be accomplished using open-source satellite and ground data. The major challenge in generating the UTCI map is the availability of spatio-temporal meteorological data. However, this can be tackled with specific models, like Menex for mean radiant temperature, based on the satellite data. The accuracy of UTCI calculations is influenced by the availability and resolution of the data utilized in the process. The findings reveal a noticeable upward trend

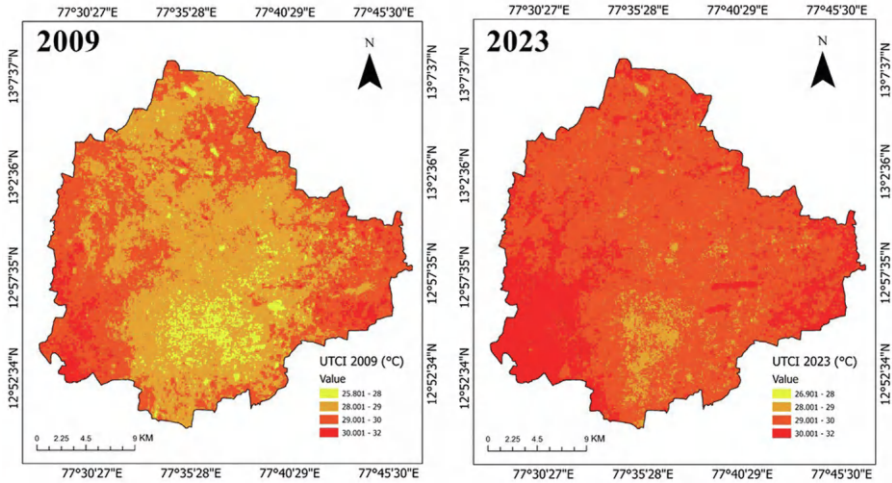

FIGURE 8.6 The spatial change of UTCI over the region.

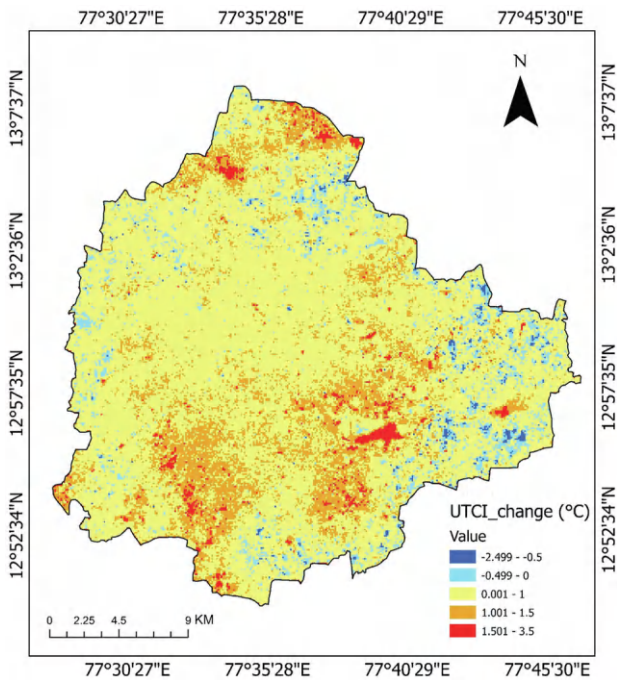

FIGURE 8.7 Map showing UTCI change from 2009 to 2023.

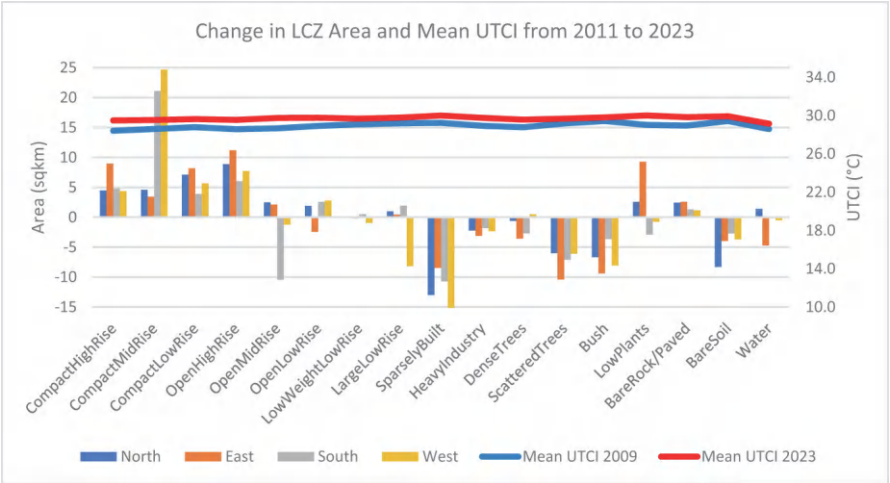

FIGURE 8.8 Graph showing variation of mean UTCI.

in UTCI, particularly in the peripheral regions of the city characterized by built-up areas. This trend is closely linked to urbanization patterns in these areas. The expansion of impervious surfaces and decreased natural features such as vegetation and water bodies contribute to this phenomenon. The findings of this study will aid in formulating planning strategies, such as recommendations for the Floor Space Index (FSI), placement and maintenance of vegetation and water bodies, and policy-making for urban planners and local bodies. Additionally, this will assist in disaster planning, including for events like heat waves, by facilitating prompt assessment of vulnerability and risk, thereby contributing to resilient cities.

ACKNOWLEDGEMENTS

We thank the Indian Institute of Technology Kharagpur and Ranbir and Chitra Gupta School of Infrastructure Design and Management for financial and Infrastructure support. We also thank the NASA LULCC team for giving us an opportunity in this publication.

REFERENCES

Aithal, B.H. and Chandan M.C., 2019. Assessing land surface temperature and land use change through spatio-temporal analysis: a case study of select major cities of India. *Arabian Journal of Geosciences*, *12*, pp. 1–16. https://doi.org/10.1007/s12517-019-4547-1.

Al-Anbari, R.H., Jasim, O.Z. and Mohammed, Z.T., 2019. Estimation high resolution air temperature based on landsat8 images and climate datasets. *IOP Conference Series: Materials Science and Engineering*, *518*(2), pp. 1–9. https://doi.org/10.1088/1757-899X/518/2/022033.

Avdan, U. and Jovanovska, G., 2016. Algorithm for automated mapping of land surface temperature using LANDSAT 8 satellite data. *Journal of Sensors*, *2016*, pp. 1–8. https://doi.org/10.1155/2016/1480307.

Bechtel, B., Alexander, P.J., Böhner, J., Ching, J., Conrad, O., Feddema, J., Mills, G., See, L. and Stewart, I., 2015. Mapping local climate zones for a worldwide database of the form and function of cities. *ISPRS International Journal of Geo-Information*, *4*(1), pp. 199–219. https://doi.org/10.3390/ijgi4010199.

Bharath, H.A., Chandan, M.C., Vinay, S. and Ramachandra, T.V., 2018. Modelling urban dynamics in rapidly urbanising Indian cities. *Egyptian Journal of Remote Sensing and Space Science*, *21*(3), pp. 201–210. https://doi.org/10.1016/j.ejrs.2017.08.002.

Blazejczyk, K., 2001, December. Assessment of recreational potential of bioclimate based on the human heat balance. In *First International Workshop on Climate Tourism and Recreation, Int J Biometeorology* (pp. 133–152). International Society of Biometeorology. Wisconsin, USA.

Błażejczyk, K., Jendritzky, G., Bröde, P., Fiala, D., Havenith, G., Epstein, Y., Psikuta, A. and Kampmann, B., 2013. An introduction to the universal thermal climate index (UTCI). *Geographia Polonica*, *86*(1), pp. 5–10. https://doi.org/10.7163/GPol.2013.1.

Błażejczyk, K., Kuchcik, M., Błażejczyk, A., Milewski, P. and Szmyd, J., 2014. Assessment of urban thermal stress by UTCI–experimental and modelling studies: an example from Poland. *DIE ERDE–Journal of the Geographical Society of Berlin*, *145*(1–2), pp. 16–33. https://doi.org/10.12854/erde-145-3.

Bröde, P., Fiala, D., Błażejczyk, K., Holmér, I., Jendritzky, G., Kampmann, B., Tinz, B. and Havenith, G., 2012. Deriving the operational procedure for the Universal Thermal Climate Index (UTCI). *International Journal of Biometeorology*, *56*, pp. 481–494. https://doi.org/10.1007/s00484-011-0454-1.

Chakraborty, S.D., Kant, Y. and Mitra, D., 2015. Assessment of land surface temperature and heat fluxes over Delhi using remote sensing data. *Journal of Environmental Management*, *148*, pp. 143–152. https://doi.org/10.1016/j.jenvman.2013.11.034.

Chandan, M.C., Nimish, G. and Bharath, H.A., 2019. Analysing spatial patterns and trend of future urban expansion using SLEUTH. *Spatial Information Research*, *28*, pp. 11–23. https://doi.org/10.1007/s41324-019-00262-4.

Chen, L. and Ng, E., 2012. Outdoor thermal comfort and outdoor activities: A review of research in the past decade. *Cities*, *29*(2), pp. 118–125.

Fiala, D., Havenith, G., Bröde, P., Kampmann, B. and Jendritzky, G., 2012. UTCI-Fiala multi-node model of human heat transfer and temperature regulation. *International Journal of Biometeorology*, *56*, pp. 429–441. https://doi.org/ 10.1007/s00484-011-0424-7.

Govind, N.R. and Ramesh, H., 2020. Exploring the relationship between LST and land cover of Bengaluru by concentric ring approach. *Environmental Monitoring and Assessment*, *192*, pp. 1–25. https://doi.org/10.1007/s10661-020-08601-x.

Grimm, N.B., Faeth, S.H., Golubiewski, N.E., Redman, C.L., Wu, J., Bai, X. and Briggs, J.M., 2008. Global change and the ecology of cities. *Science*, *319*(5864), pp. 756–760. https://doi.org/10.1126/science.1150195.

Justice, C., Gutman, G. and Vadrevu, K.P., 2015. NASA land cover and land use change (LCLUC): an interdisciplinary research program. *Journal of Environmental Management*, *148*, pp. 4–9.

Kotharkar, R. and Bagade, A., 2018. Local Climate Zone classification for Indian cities: a case study of Nagpur. *Urban Climate*, *24*, pp. 369–392. https://doi.org/10.1016/j.uclim.2017.03.003.

Kumar, A. and Singh, D.P., 2021. Heat stroke-related deaths in India: an analysis of natural causes of deaths, associated with the regional heatwave. *Journal of Thermal Biology*, *95*, p. 102792. https://doi.org/10.1016/j.jtherbio.2020.102792.

Kumar, P. and Sharma, A., 2020. Study on importance, procedure, and scope of outdoor thermal comfort–a review. *Sustainable Cities and Society*, *61*, p. 102297. https://doi.org/10.1016/j.scs.2020.102297.

Liu, Y., Ortega-Farías, S., Tian, F., Wang, S. and Li, S., 2021. Estimation of surface and near-surface air temperatures in arid northwest china using landsat satellite images. *Frontiers in Environmental Science*, *9*, p. 791336. https://doi.org/10.3389/fenvs.2021.791336.

Potchter, O., Cohen, P., Lin, T.P. and Matzarakis, A., 2018. Outdoor human thermal perception in various climates: a comprehensive review of approaches, methods and quantification. *Science of the Total Environment*, *631*, pp. 390–406. https://doi.org/10.1016/j.scitotenv.2018.02.276.

Pradhesta, Y.F., Nurjani, E. and Arijuddin, B.I., 2019, July. Local Climate Zone classification for climate-based urban planning using Landsat 8 Imagery (A case study in Yogyakarta Urban Area). In *IOP Conference Series: Earth and Environmental Science* (Vol. 303, No. 1, p. 012022). IOP Publishing. https://doi.org/10.1088/1755-1315/303/1/012022.

Ramachandra, T.V. and Bharath, H.A., 2012. Spatio-temporal pattern of landscape dynamics in Shimoga, tier II city, Karnataka state, India. *International Journal of Emerging Technology and Advanced Engineering*, *2*(9), pp. 563–576. https://doi.org/10.46338/ijetae0912_11.

Ramachandra, T.V., Bharath, H.A. and Sowmyashree, M.V., 2015. Monitoring urbanization and its implications in a mega city from space: spatiotemporal patterns and its indicators. *Journal of Environmental Management*, *148*, pp. 67–81. https://doi.org/10.1016/j.jenvman.2014.02.015.

Ramachandran, J., Lalitha, R., Sivasubramanian, K. and Vallal, S., 2021. Spatio-temporal assessment of surface Albedo using Landsat 8 images in Lalgudi block of Trichy District, Tamil Nadu. *Journal of Agricultural Physics*, *21*(2), pp. 341–349. www.agrophysics.in.

Saxena, S. and Agrawal, S., 2023. Seasonal variations in land surface temperature based on local climatic zone in the major metropolitan cities of India. *Spatial Information Research*, *31*(6), pp. 609–623.

Silva, T.J.V. and Hirashima, S.Q.S., 2021. Predicting urban thermal comfort from calibrated UTCI assessment scale–a case study in Belo Horizonte city, southeastern Brazil. *Urban Climate*, *36*, p. 100652. https://doi.org/10.1016/j.uclim.2020.100652.

Singh, S., Priyadarshni, P. and Pandey, P., 2023. Impact of urban heat Island: a local-level urban climate phenomenon on urban ecology and human health. In Mustak, S.K., Singh, D., and Srivastava, P.K. (eds.), *Advanced Remote Sensing for Urban and Landscape Ecology* (pp. 113–128). Springer Nature Singapore. https://doi.org/10.1007/978-981-99-3006-7_5.

Setiawati, M.D., Jarzebski, M.P., Gomez-Garcia, M. and Fukushi, K., 2021. Accelerating urban heating under land-cover and climate change scenarios in Indonesia: application of the universal thermal climate index. *Frontiers in Built Environment*, *7*, p. 622382. https://doi.org/fbuil.2021.622382.

Staiger, H., Laschewski, G. and Matzarakis, A., 2019. Selection of appropriate thermal indices for applications in human biometeorological studies. *Atmosphere*, *10*(1), p. 18. https://doi.org/10.3390/atmos10010018.

Stewart, I.D. and Oke, T.R., 2012. Local climate zones for urban temperature studies. *Bulletin of the American Meteorological Society*, *93*(12), pp. 1879–1900. https://doi.org/10.1175/BAMS-D-11-00019.1.

Tartarini, F. and Schiavon, S., 2020. pythermalcomfort: a Python package for thermal comfort research. *SoftwareX*, *12*, p. 100578. https://doi.org/10.1016/j.softx.2020.100578.

Wang, C., Zhan, W., Liu, Z., Li, J., Li, L., Fu, P., Huang, F., Lai, J., Chen, J., Hong, F. and Jiang, S., 2020. Satellite-based mapping of the Universal Thermal Climate Index over the Yangtze River Delta urban agglomeration. *Journal of Cleaner Production*, *277*, p. 123830. https://doi.org/10.1016/j.jclepro.2020.123830.

Wu, J., Liu, C. and Wang, H., 2022. Analysis of Spatio-temporal patterns and related factors of thermal comfort in subtropical coastal cities based on local climate zones. *Building and Environment*, *207*, p. 108568. https://doi.org/10.1016/j.buildenv.2021.108568.

Xu, P., Gao, F., He, J., Ren, X. and Xi, W., 2017. Modelling and optimization of land use/land cover change in a developing urban catchment. *Water Science and Technology*, *75*(11), pp. 2527–2537. https://doi.org/10.2166/wst.2017.121.

9 Assessment of Indian Flying Fox (*Pteropus medius*) Roosting Sites in Northern Kerala using Landsat-derived NDVI

Amal Joseph, M V Anusree, M R Midhunlal, P Neethu, V V Saritha, C C Stefina, T Christina Grace, M K Smija, G Sreenivasa, Rathinakumar A, P K Prasadan, Takuya Iwamura, and Joseph J Erinjery

9.1 INTRODUCTION

Land use change due to anthropogenic activities has led to the drastic decline of populations of several species of animals (Newbold *et al.*, 2015; Di Minin *et al.*, 2016; Sales *et al.*, 2020), including habitat generalists and commensal species (Erinjery *et al.*, 2017). On the other hand, it has been observed that some native generalists could become hyperabundant and cause problems for both humans and nature (Moore *et al.*, 2023). However, since most of the habitat generalist species occur in large numbers and can adapt to multiple habitats, they are generally understudied and usually considered "least concern" species, receiving less conservation attention (Erinjery *et al.*, 2017). Habitat loss due to land use change can lead to more human–animal contact, increasing zoonotic spillover incidences across the globe (White and Razgour, 2020; Goldstein *et al.*, 2022). Such spillover events have been found especially between mammals such as bats, primates, rodents, ungulates, etc., and humans, and it is critical to assess the changes/loss in habitats due to land use change. It is important to assess whether these species are declining or becoming abundant, and assessing the habitats of such habitat generalist species from a conservation and health perspective is critical (Erinjery, Kavana and Singh, 2014; Moore *et al.*, 2023).

Bats provide several ecosystem services, including pollination and dispersal of seeds and control of pests in agricultural landscapes (Shilton *et al.*, 1999; Kessler *et al.*, 2018), serving critical ecosystem functions such as regeneration of forest and

DOI: 10.1201/9781003396260-9

economic trees. However, their natural foraging and roosting habitats are severely degraded significantly for plant-dependent bats belonging to Family Pteropodidae (Old World Fruit Bats), forcing them to shift their habitats closer to human habitations such as gardens, plantations, and urban areas (Kessler *et al.*, 2018; Tsang, 2020). Remotely sensed satellite images confirmed that the populations of Black Flying Fox (*Pteropus alecto*) in Australia move closer to urban areas after the loss of winter foraging habitat (Baranowski and Bharti, 2023). A study based on historical land use change patterns in Bangladesh has shown that Indian Flying Fox (*P. medius)* bats can shift their habitats closer to human habitations due to loss of habitats, and such bat colonies closer to human habitations may have a lesser number of individuals in the colony than colonies in the wilderness (McKee *et al.*, 2021). Shifting of bat colonies nearer to human habitations has led to zoonotic spillovers of Hendra virus in Australia and of Nipah virus in South/Southeast Asia (Plowright *et al.*, 2014).

The Indian Flying Fox, belonging to the family Pteropodidae, is widely distributed in south Asia, and is observed to use multiple habitats, significantly closer to human habitations (McKee *et al.*, 2021). They are often seen roosting as colonies in large numbers (usually hundreds to thousands of individuals/roost). They are generally found roosting in tall trees with large diameters at breast height (Devi and Kumar, 2024). They are listed as "least concern," and their populations are found to be decreasing across their distribution range (IUCN, 2021). The major threats are the destruction of their habitats, both roosting and foraging, electrocution, hunting, and other anthropogenic activities linked to urbanization (Pandian and Suresh, 2021). They have been linked to causing Nipah in Bangladesh, eastern India, south India, Malaysia, and Singapore (CDC, 2024), and the presence of Henipaviruses in the bats has been reported from many regions in south India (Sudeep *et al.*, 2021). Raman *et al*. (2023) have identified 52 roosting sites of Indian Flying Fox in the Western Ghats, and Madala *et al*. (2022) have studied roosting tree characteristics from 11 roosting sites from Northern Kerala. Although the species is medically important, little is known about the species populations and ecology, mainly from northern Kerala.

Satellite remote sensing provides an excellent opportunity to continuously assess and monitor the habitats of various species of animals. Remotely sensed NDVI can be used to monitor regular vegetation changes (Van Leeuwen *et al.*, 2006; Kinyanjui, 2011), and since flying foxes mainly prefer vegetation, in particular tall trees, for their roosting and foraging NDVI change can be used to detect changes in their roosting and foraging habitats. In the present study, we mainly focus on the roosting habitats of Indian Flying Foxes in four districts of northern Kerala, i.e., Kozhikode, Kannur, Wayanad, and Kasaragod, and assess the utility of Landsat-derived NDVI in monitoring the roosting site loss of the Indian Flying Fox. Nipah has been previously reported from one of the districts (Kozhikode) selected for the present study in 2018 (17 deaths), 2021 (1 death), and 2023 (2 deaths) with a case fatality rate of 89.4% in 2018 (CDC, 2024). Populations of Indian Flying Foxes with the prevalence of Henipaviruses were also detected from the locality (Sudeep *et al.*, 2021). Also, a high rate of development is seen within these regions, probably leading to the destruction of bat habitats (Shimod *et al.*, 2022).

Here, we would like to report our analyses on the roosting habitat use of Indian Flying Foxes. In particular, we focus on the degrees of habitat degradation for roosting sites for the known populations across four Northern Kerala, India districts. Further, we test whether remotely sensed satellite images NDVI can be used to detect roosting site loss in the known locations of roosting site loss of these species. Since remotely sensed satellite images are frequently captured for earth observation, our study can offer insights for effectively monitoring known bat populations in these districts and other regions worldwide.

9.2 MATERIALS AND METHODS

9.2.1 Study Area

The current study was carried out in four northern districts of Kerala (11°7' -12°47' N, 74°51' -76°26' E), namely Kasaragod, Kannur, Wayanad, and Kozhikode. These districts are part of one of the significant bat hotspots in India, the Western Ghats, which comprise 63 species (Raman and Hughes, 2021). The landscape included evergreen and moist-deciduous forests, rubber monocultures, agroforestry plantations, orchards, and human settlements (Deshpande and Kelkar, 2015).

Kasargod, Kerala's northernmost district, lies between the Western Ghats to the east and the Arabian Sea to the west, having a tropical to subtropical climate with an annual average rainfall of 3350 mm. Covering an area of 2966 sq. km, Kannur district has humid weather with an intense hot season from March to May and an annual rainfall of 3438 mm. Moving southward, Kozhikode district stretches approximately 80 km along the southwest coast, featuring an annual rainfall of 2540 mm (https://spb.kerala.gov.in/). Considering the landscape and climate, Kannur, Kozhikode, and Kasaragod are similar, with all three districts having coastal regions, midlands, high-altitude Western Ghats region, and typical tropical weather with monsoons. Wayanad District, nestled within the Western Ghats, spans altitudes ranging from 700 meters to 2100 meters above sea level, characterized by an annual rainfall of around 2921 mm and an average annual temperature of 22.3°C (Madhu, Namboodiri, and Vijay, 2021).

9.2.2 Roosting Site Locations and Sites of Loss

We used different survey sampling methods to obtain the locations of roosting sites and sites of loss. Sampling was conducted from December 2021 to September 2022, and data was collected using Volunteered Geographic Information (VGI) sources, field-based surveys, and community-based wildlife surveys. Additionally, data on previous locations of bats were collected from already published reports to check the loss of roosting sites (Saritha, 2015).

Preliminary information about roosting site locations was collected through VGI sources (Cui *et al.*, 2021), particularly utilizing social media platforms like WhatsApp. A write-up was prepared and circulated to inquire about potential roosting site locations near users' houses or any other premises. This resulted in active participation from users ($N = 62$) in the form of replies regarding the roosting site locations.

The roosting site locations were also collected from a comprehensive review of previously published reports, scholarly articles, newspapers, and other media sources. Furthermore, roosting site locations were gathered by traveling through major and minor roads in these districts, covering almost all places, and inquiring with local people, drivers, shopkeepers, etc.

Following that, we conducted field surveys at these potential locations to verify the presence of roosting sites of Indian Flying Foxes. We collected data on the characteristics of the roosting sites. A total of 3060 km was traveled in all these districts during our survey, with the length of the traversed roads in the respective districts as follows: Kasargod – 635 km, Kannur – 604 km, Kozhikode – 1170 km, and Wayanad – 650 km. During our surveys, we obtained geospatial coordinates of the roosting sites, approximate number of roosting fruit bats, habitat type, species and number of roosting trees, roosting tree characteristics (height, canopy width, and diameter at breast height), and any nearby disturbance to the roosting site. Additionally, during our field visits to previously documented roosting sites, we documented the loss of roosting sites from our present visit.

Finally, a community-based wildlife survey (Lunney and Matthews, 2001) was conducted with residents in the neighborhood living close to the roosting locations/previous roosting locations. This involved using an open-ended questionnaire with a central emphasis on gathering information about bat species, location of roosting sites (geospatial coordinates), age of roosting sites, disturbances to the sites, any loss of roosting sites (whether seasonal or permanent), the emergence of new roosting sites, and attitudes of people towards bats, with individual respondents ($N = 233$). The age of respondents ranged from 15 to 60 years. The entire survey was conducted following the Code of Ethics of the International Society of Ethnobiology (2006), obtaining participants' free, prior, and informed consent before conducting interviews. From the survey, we mainly used the information on the loss of roosting sites for the present study. Further, for the analysis of loss of roosting sites, we categorized the roosting sites into four categories: (1) roosting site loss due to highway development/drying of trees, (2) roosting site loss due to habitat loss (loss of habitats around roosting site, mainly due to urbanization and other developmental activities), (3) roosting site shifts due to other unknown reasons, (4) the present roosting site locations of Indian Flying Fox.

9.2.3 Satellite Data Used and Approach

The primary objective of our study was to test the efficacy of NDVI changes derived from Landsat for monitoring and assessing roosting site loss of Indian Flying Foxes. As mentioned in the previous section, from the field, we observed the loss of several roosting sites of Indian Flying Foxes, and we categorized them into four categories. Based on the locations of four categories, we extracted the NDVI values from the exact locations of roosts. Further, we created a buffer of 1 km around the roosting site locations to analyze the changes in NDVI occurring around a roosting site. The NDVI changes were calculated from the derived NDVI between 2014 and 2023 (as the previously published report of roosting site location was from 2015; Saritha, 2015).

9.2.4 NDVI Derivation from Landsat Satellite Data

We downloaded the Landsat 8 (for 2014) and 9 (for 2023) satellite images (surface reflectance product) from the USGS Earth Explorer website (https://earthexplorer.usgs.gov/) for calculating NDVI. We ensured that the images downloaded were cloud-free and were less than one month apart (the images downloaded were from November and December months for consistency of NDVI values). Further, we mosaicked the images of the region using ArcGIS version 10.2 and made image composites with band 5 (0.845–0.885 μm), band 4 (0.630–0.680 μm), band 3 (0.525–0.600 μm), and band 2 (0.450–0.515 μm). The equation for calculating NDVI for Landsat 8 and 9 is

$$\text{NDVI} = (\text{Band 5} - \text{Band 4}) / (\text{Band 5} + \text{Band 4}) \quad (9.1),$$

where band 5 is the near-infrared band and band 4 is the red band.

We calculated the NDVI of respective years using this equation in ArcGIS version 10.2.

9.2.5 Human Footprint Analyses at Roosting Sites

We examined whether human footprint (a proxy for anthropogenic activities (Venter *et al.*, 2016)) can explain the reason for roosting site loss. The loss of roosting sites is expected to be more likely in locations where human pressure is higher, which reflects the fact that anthropogenic activities are leading to the loss of roosting sites of bats. Therefore, we extract the value of the 'human footprint' in locations where current flying fox roosting sites are present and historically used as roosting sites but then abandoned. The human footprint data provides the cumulative human pressure at 1 km resolution, which provides the aggregated values of the eight human activities, including built-up environments, population density, electric power infrastructure, crop lands, pasture lands, roads, railways, and navigable waterways with the data value between 0–50 (Venter *et al.*, 2016). The human footprint data was downloaded from the SEDAC website (https://sedac.ciesin.columbia.edu/data/set/wildareas-v3-2009-human-footprint), and the values of human footprint data were extracted for each location of the study region.

9.2.6 Data Analysis

We performed non-parametric statistics to compare the NDVI values between different categories of roost site loss, as sample sizes were low for some categories. Wilcoxon's signed rank test was performed to find the differences in the NDVI values between 2014 and 2023 for each location. Kruskal–Wallis H test was performed to compare the human footprint between different categories and districts. For the vegetation change analysis, we created a distribution based on the NDVI values of the current locations in 2023 and a distribution of NDVI values below those values. After creating the distribution, we reclassified them into two classes for 2014 and 2023 and calculated the change in ArcGIS 10.2. The tests performed are given in parentheses after each test in the result section. The significance value was kept at 0.05.

9.3 RESULTS

9.3.1 Roosting Sites in Each District

We recorded 118 roosting sites (71 479 individuals; 606 individuals/roosting site) of *Pteropus medius* bats in four districts of Northern Kerala (Figure 9.1). Kozhikode district had higher roosting sites (53), followed by Kannur (24), Kasaragod (23), and

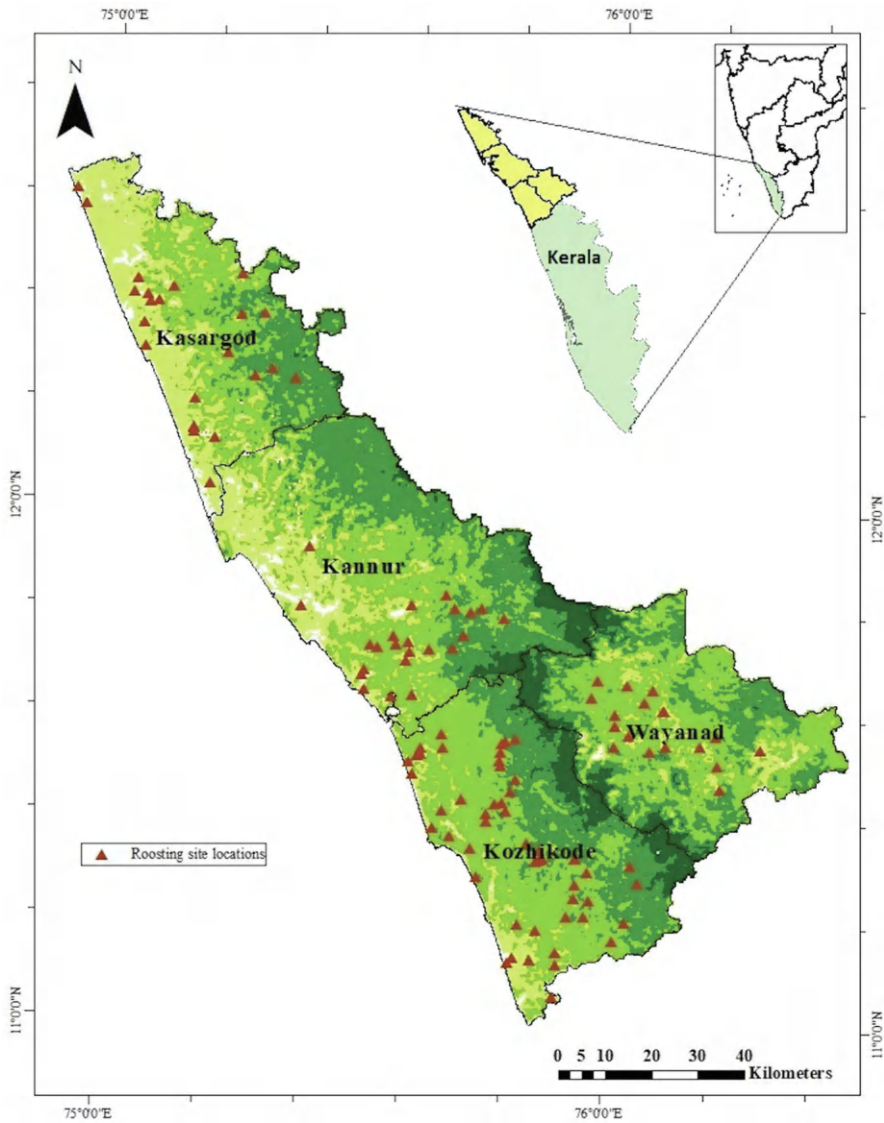

FIGURE 9.1 Locations of bat roosts in four districts of Northern Kerala. Inset: Map of south India with location of Kerala (green) and four districts (yellow) of our present study.

Wayanad (18). Within these districts, the most abundant bats were in Kozhikode (36 217 individuals), followed by Kannur (17,138 individuals), Kasargod (9,340 individuals), and Wayanad (8,784 individuals).

9.3.2 Roosting Site Decline

We observed a loss of 54 roosting sites across these districts. In 88.8% (48 sites), the bats permanently shifted their roosting sites, mainly due to habitat loss, highway development/tree cutting/drying of trees, and the colony shift due to unknown reasons. In the remaining 11.1% (six sites) sites, bats temporarily shifted their roosting sites, such as seasonal shifts during the rainy season (Table 9.1).

In Wayanad district, there was no loss of roosting sites. However, in Kozhikode district, habitat loss (73.7%) was identified as the primary cause for the decline in roosting sites, with 14 sites lost. In comparison, 26.3% of the decline was attributed to colony shifts for unknown reasons, resulting in five lost sites. In Kannur, 62.5% of the declines were temporary due to colony shifts during monsoons, resulting in five lost sites, while 37.50% were due to habitat loss, leading to three lost sites. In Kasargod district, roosting site declines due to colony shifts for unknown reasons accounted for 44.4% (12 lost sites), followed by road widening/cutting of trees (37.0%; 10 lost sites), habitat loss (7.40%, two lost sites), drying of trees (7.40%; two lost sites), and seasonal shifts (3.70%; one lost site).

9.3.3 NDVI Change and Roosting Site Decline

We could detect NDVI changes at the lost roosting sites due to highway development/drying of trees (median = 0.08, Figures 9.2, 9.3). Most sites with highway development showed significant declines in NDVI (Wilcoxon's signed rank test: $Z = -2.6$, $p = 0.01$). The locations with habitat loss (0.03; $Z = -3.4$, $p<0.001$, Figure 9.5) and the present locations (0.02, $Z = -6.5$, $p<0.001$) of bat roosts also showed a decline in NDVI values. In the sites of habitat loss, some sites showed higher NDVI loss than others. The locations with other reasons did not show a decline in NDVI values

TABLE 9.1
Potential Causes for the Loss of Roosting Sites in Four Districts: Kasargod, Kannur, Kozhikode, and Wayanad

	District (Number of Lost Sites)				
Reason for Roosting Site Decline	**Kannur**	**Kasargod**	**Kozhikode**	**Wayanad**	**Total**
(a) Permanent shift					
Highway development/Drying of trees	0	12	0	0	12
Habitat loss	3	2	14	0	19
Colony shifts due to Unknown reason	0	12	5	0	17
(b) Temporary shift					
Seasonal shift	5	1	0	0	6

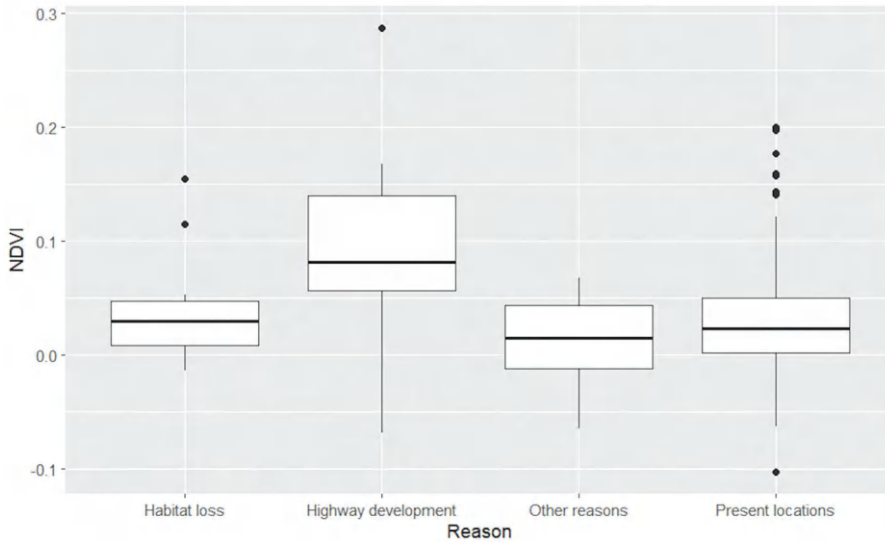

FIGURE 9.2 The boxplot showing the change of NDVI values (exact locations) of different categories at locations of roosting site loss and the present locations.

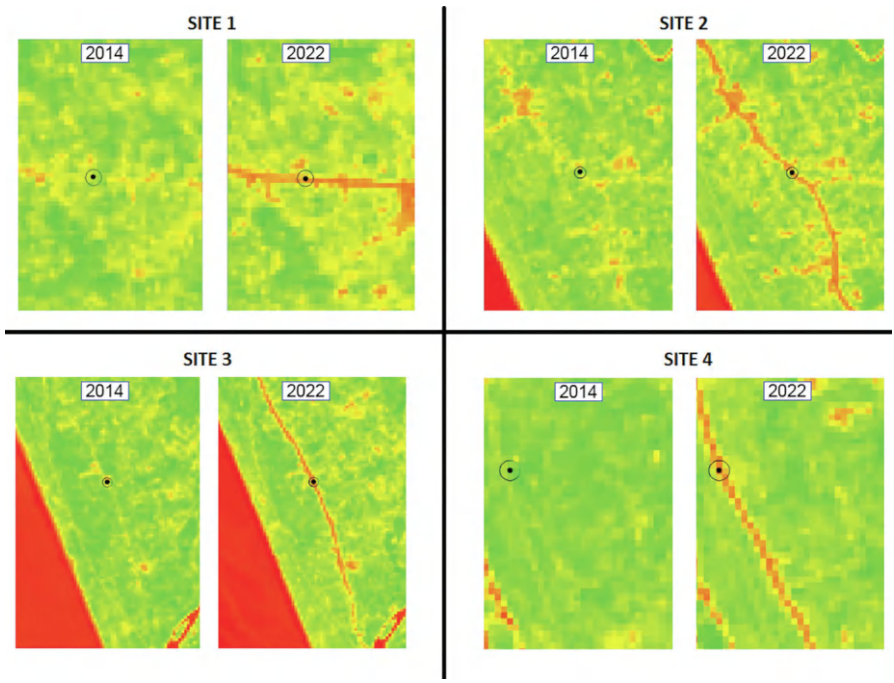

FIGURE 9.3 The NDVI images derived from Landsat showing the changes in NDVI between 2014 and 2022 at the example sites of roosting site loss due to highway development/drying of trees.

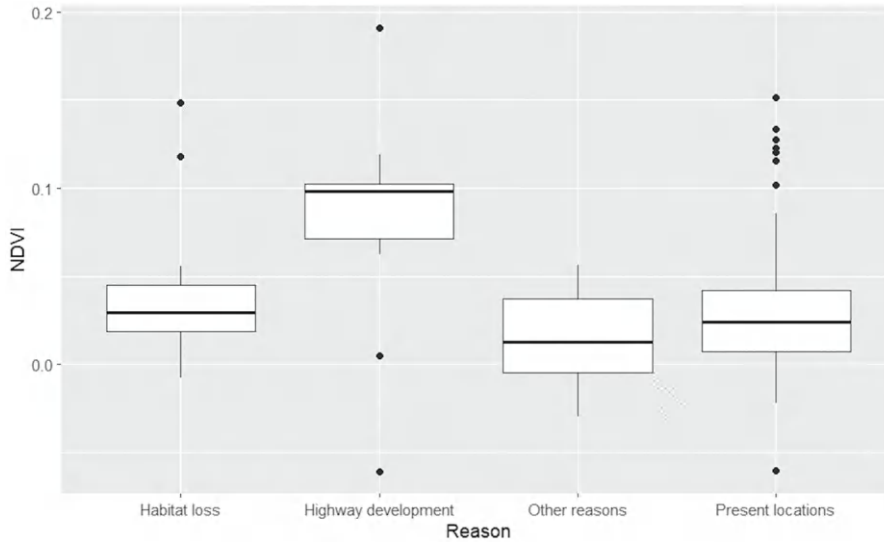

FIGURE 9.4 The boxplot showing the change of NDVI values (buffer regions around the location) of different categories at locations of roosting site loss and the present locations.

(0.01, $Z = -1.4$, $p = 0.17$). The NDVI values of the buffer regions also showed similar trends, with the highest NDVI change at lost sites due to highway development/tree cutting (0.10), habitat loss (0.03), other reasons (0.01), and present locations (0.02; Figures 9.4, 9.5). Overall, potentially suitable habitats for roosting sites (vegetation based on NDVI/also probably foraging sites) declined by 183 km^2 in the study region between 2014 and 2022 (Figure 9.6).

9.3.4 Human Footprint and Roosting Site Decline

We found that there are differences in human footprint values at sites of roosting decline due to highway development/drying of trees, habitat loss, roosting site loss due to other reasons, and current roosting sites (Figure 9.7; Kruskal–Wallis $H = 8.1$, $P = 0.045$). More human footprint values were present in the sites of roosting site decline due to highway development/drying of trees and habitat loss than in other locations. Among the current roosting site locations, Kozhikode (median = 18), Kasaragod (17), and Kannur (16.5) had more human pressure than Wayanad district (9; Figure 9.8). In Kozhikode district, several high outlier values indicated high human pressure in those sites.

9.3.5 Land Use Preference for Selecting Roosting Sites

Within the selected four districts, Indian Flying Foxes were observed to prefer sacred groves, roadsides, private and government properties, temple premises, mosques, school properties, sacred trees, riversides, and mangroves as their primary roosting sites (Table 9.2). It was observed that fruit bats were notably more prevalent in sacred groves (20,208 bats), constituting approximately 30.2% of the total population.

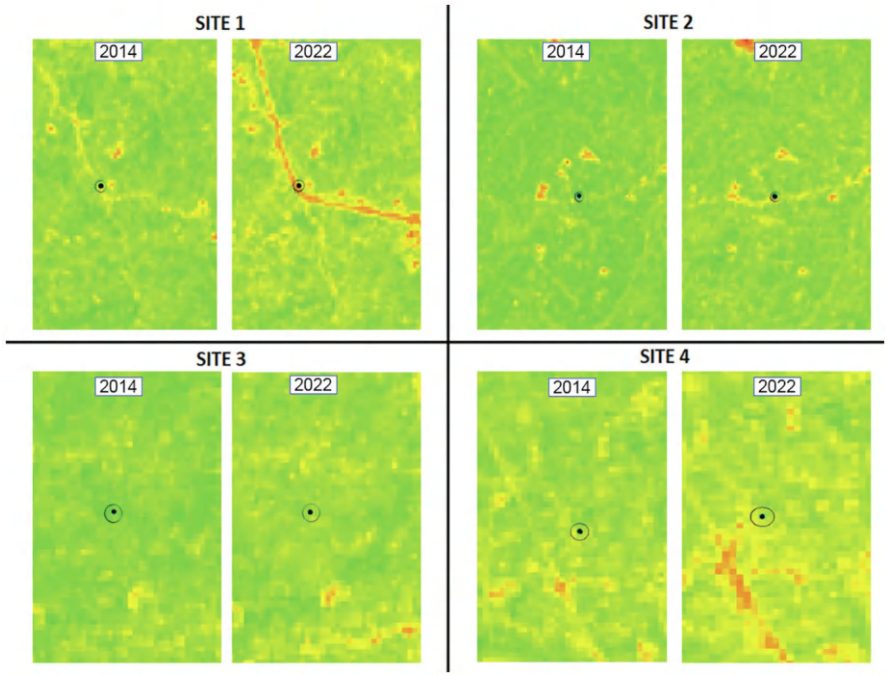

FIGURE 9.5 The NDVI images derived from Landsat showing the changes in NDVI between 2014 and 2022 at the example sites of roosting site loss due to habitat loss.

This was followed by private property, where 18,976 bats were recorded (28.4%). Mangroves housed 13,600 bats (20.3%), while the lowest count was observed on school property, with only 190 bats, amounting to 0.3%.

When comparing the four districts, bats primarily opt for sacred groves in Kasargod and Kozhikode, whereas in Kannur and Wayanad, they prefer private property over other sites. Across all four districts, their preference for government properties was less. Bats that inhabit school premises are exclusively located in the Kannur district, while those inhabiting riverside areas are observed solely in the Kozhikode district. Similarly, bats roosting in sacred trees are only found in the Kasargod district.

9.3.6 Tree Preference for Roosting

Indian Flying Foxes were observed roosting in 32 distinct tree species, with *Holigarna grahamii* (11.1%), *Terminalia bellirica* (10.86%), and *Caryota urens* (10.8%) standing out as the most highly preferred trees across all districts (Table 9.3). Within the districts, *Terminalia bellirica* (32.4%) was notably preferred by bats in Wayanad, *Ficus religiosa* and *Holigarna grahamii* (each 12.3%) emerged as the highly preferred tree species in Kasargod, *Caryota urens* (10.8%) stood out prominently in Kozhikode, and Kannur. *Artocarpus heterophyllus, Ficus religiosa,* and *Caryota urens* (each 9.3%) were identified as the most preferred tree species.

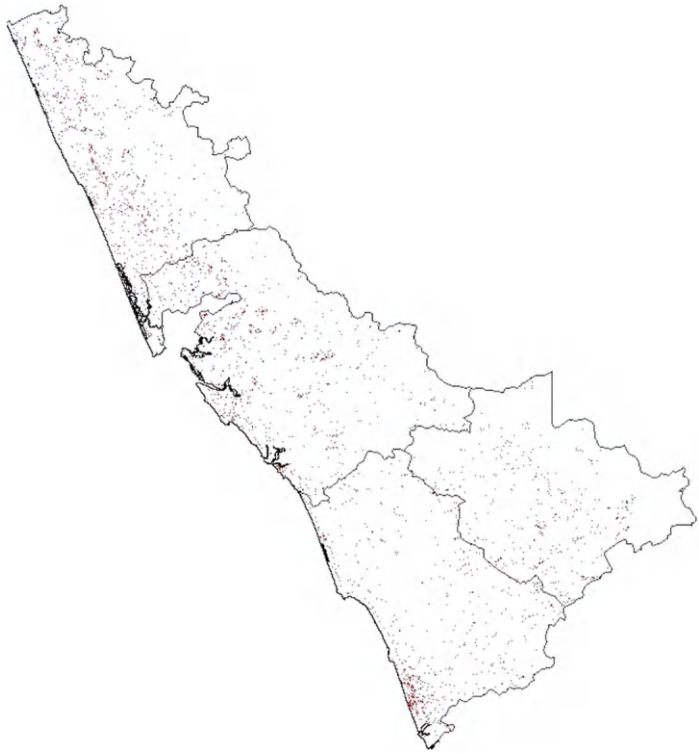

FIGURE 9.6 The NDVI change (purple color) showing the decline of vegetation in the four districts of northern Kerala between 2014 and 2022.

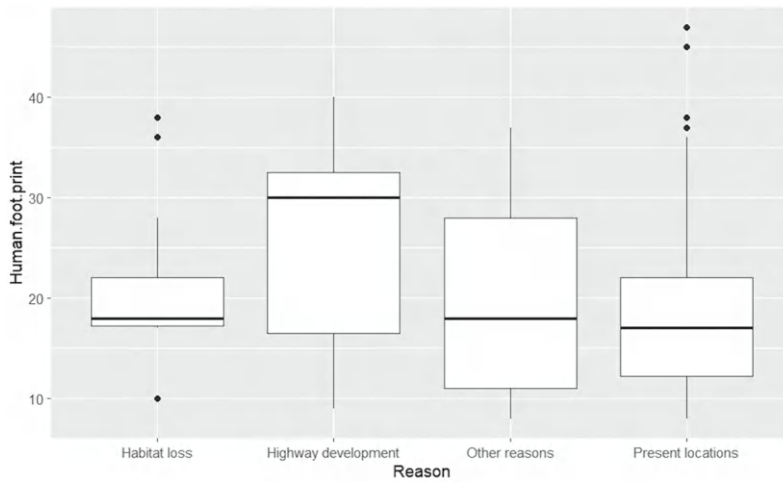

FIGURE 9.7 The boxplot showing the distribution of human footprint values (exact locations) at different categories of roosting site loss and the present locations.

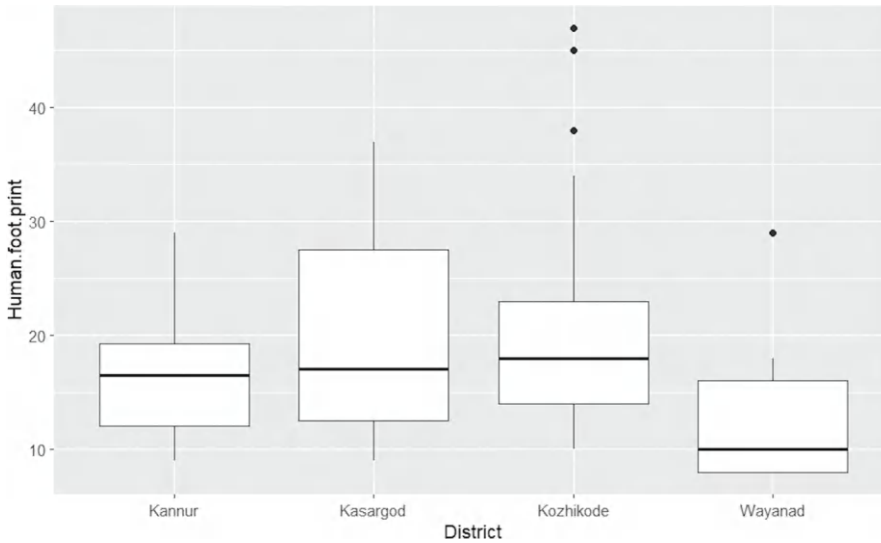

FIGURE 9.8 The boxplot showing the distribution of human footprint values (exact locations) at present locations of roosting sites at different districts of Northern Kerala.

TABLE 9.2
Different Habitats Preferred by *Pteropus medius* Bats for Roosting

		Abundance (in Numbers)				
Habitat	**No. of Sites**	**Kasargod (23 sites)**	**Kannur (24 sites)**	**Wayanad (18 sites)**	**Kozhikode (53 sites)**	**Mean**
Sacred Grove	34	5975 (10 sites)	621 (3 sites)	0	13612 (21 sites)	594.4
Road Side	11	675 (4 sites)	700 (1 site)	0	3740 (6 sites)	465.0
Private Property	42	1330 (5 sites)	4444 (12 sites)	6382 (14 sites)	6820 (11 sites)	451.8
Government Property	3	0	133 (1 site)	1117 (1 site)	500 (1 site)	583.3
Temple Premise	5	0	450 (2 site)	0	1125 (3 sites)	315.0
Mosque	4	0	600 (1 site)	1285 (3 sites)	0	471.3
School Property	2	0	190 (2 sites)	0	0	95.0
Sacred tree	4	1360 (4 sites)	0	0	0	340.0
Riverside	10	0	0	0	6820 (10 site)	682.0
Mangrove	3	0	10000 (2 sites)	0	3600 (1 sites)	4533.3

TABLE 9.3
Tree Species Preferred by Indian Flying Fox Bats for Roosting

	Tree Species Preferred by Indian Flying Fox (in %)				
Tree Species	**Kasargod**	**Kannur**	**Wayanad**	**Kozhikode**	**Total**
Holigarna grahamii	12.3	2.3	21.6	8	11.1
Terminalia bellirica	7	0	32.4	4	10.9
Caryota urens	7	9.3	8.1	18.6	10.8
Mangifera indica	10.5	7	8.1	12	9.4
Ficus religiosa	12.3	9.3	0	8	7.4
Strychnos nux-vomica	8.8	7	0	5.3	5.3
Delonix regia	1.8	7	10.8	0	4.9
Artocarpus heterophyllus	3.5	9.3	0	6.7	4.9
Alstonia scholaris	3.5	9.3	0	5.3	4.5
Tectona grandis	5.2	4.7	0	6.7	4.1
Adenanthera pavonina	7	4.7	0	2.7	3.6
Artocarpus hirsutus	0	0	10.8	1.3	3
Swietenia mahagoni	0	7	0	2.7	2.4
Abrus precatorius	1.8	4.7	0	1.3	1.9
Hevea brasiliensis	0	2.3	2.7	2.7	1.9
Mangrove *sps.*	0	4.7	0	1.3	1.5
Ficus benghalensis	3.5	2.3	0	0	1.4
Cocos nucifera	1.8	2.3	0	1.3	1.4
Bambusa sps.	0	0	5.4	0	1.4
Pongamia pinnata	3.5	0	0	1.3	1.2
Tamarindus indica	3.5	0	0	1.3	1.2
Terminalia paniculata	1.8	2.3	0	0	1.0
Schleichera oleosa	1.8	0	0	1.3	0.8
Others	3.5	4.6	0	8	4.0

9.4 DISCUSSION

It is critical to continuously monitor and assess the habitats of Indian Flying Foxes as their habitats are declining, and their numbers are decreasing throughout their distribution range. The current study found that Landsat-derived NDVI can continuously monitor bat roosting sites. We also observed that roosting and possibly foraging habitats of Indian Flying Foxes have declined in our study region due to human-induced land use change.

9.4.1 NDVI Change and Bat Roosting Site Loss

From this study, we observed that NDVI change can be a good indicator of the roosting site loss of Indian Flying Foxes in south India. Once the roosting sites are identified through surveys like ours, we can continuously monitor the habitats of Indian Flying Fox using remotely sensed NDVI. Our study found considerable differences in NDVI values at all highway development/tree loss sites. In the case of habitat loss, at some

locations, we found considerable differences in the values of NDVI, and in some places, we could only find a slight decline in values. In the case of current habitats, we also found a decline in values, indicating that the current roosting habitats of the Indian Flying Fox may be declining and reducing in quality. However, we did not find any change in NDVI values due to site shift due to other reasons. We deduce that the site shift of the bats at these locations might not be due to habitat loss or degradation but might be for foraging purposes. Since most of the foraging trees of the Indian Flying Fox may have similar values of NDVI to that of the roosting trees, it is possible that the foraging habitats of these species would be declining as well. Remote sensing has been previously used to observe the winter foraging habitats of *Pteropus* species in Australia (Baranowski and Bharti, 2023), and here we show that remote sensing can be an excellent alternative for observing roosting habitats of *Pteropus* species as well. Also, Vleut *et al.* (2015) have shown that canopy openness and tree height can influence *Pteropus* abundance in Mexico. The occurrence of bats belonging to another genus is also associated with a specific range of NDVI values (*Perimyotis subflavus*: Meierhofer *et al*., 2019, 2022), and using NDVI could be favorable for disease spillover modeling (Escobar *et al.*, 2015). Such satellite remote sensing monitoring and prevention strategies can save money invested towards biodiversity conservation and healthcare systems (Baranowski and Bharti, 2023). However, not all *Pteropus* species (*P. lylei*) abundances show a correlation with NDVI, and a correlation between bats and NDVI needs to be first established before such monitoring exercises (Chaiyes *et al.*, 2020).

9.4.2 Conservation of Indian Flying Fox in South India

Most of the habitats of Indian Flying Foxes we found were closer to urban habitats/human settlements, which was also confirmed using human footprint data. McKee *et al.* (2021) observed that Indian Flying Foxes shifted their roosting sites from forests and other rural landscapes to urban areas and human settlements due to the historical land use change over the past decades. From our study, the most important habitats for flying foxes were sacred groves, roadsides, mangrove habitats, and private properties, indicating that these could be preferred roosting site habitats of Indian Flying Foxes in Northern Kerala. Sacred groves are important sites of biodiversity conservation (Decher, 1997; Mgumia and Oba, 2003; Bhagwat *et al.*, 2005), and in Kerala, sacred groves have been found to host roosting sites of different bat species (Aiswaryalakshmi *et al.*, 2023). Erinjery *et al.* (2017) have shown that roadsides with continuous vegetation and canopy connectivity can provide suitable habitats for many habitat generalist species. The mangrove habitats that we found the bats to inhabit were undisturbed continuous mangrove forests. Also, the private properties inhabited by bats had huge land areas with many trees (not just a house, but home gardens; JJE pers. Obs.). Similarly, riversides with many trees are considered significant habitats of bats across the region (Pandian and Suresh, 2021). Over the past few decades, all these habitats have been declining due to urbanization, and it is vital to protect, conserve, and manage these habitats with the help of local communities.

It has been observed that even in urban habitats, flying foxes prefer trees with considerable height and canopy width for their roosting (Madala *et al.*, 2022). Our study

also shows that flying foxes prefer specific tree species over others, possibly due to the trees' height and canopy width. Protecting these, especially native trees, is critical for conserving flying foxes. Further, it was noted recently that exotic species of trees are planted in home gardens, especially rambutan, sapota, lychee, avocado, mangosteen, etc., which could attract bats to the home gardens and induce physiological stress (Neethu, 2022). Future studies should also concentrate on the foraging habitats of Indian flying foxes in the region.

Further, we observed that land use changes over the past decades, significantly road widening and habitat loss, have led to the decline of permanent bat roosting sites in the study districts. Previously, although these areas were closer to human settlements, they had a good amount of vegetation, which has now declined due to urbanization (JJE pers. obs). The presence of Indian Flying Foxes closer to human habitations will increase the contact/negative interactions between Indian Flying Foxes and humans. It could pose a conservation challenge to these species.

9.4.3 Zoonotic Spillover

Proximity to bat feeding sites and roosting sites, high human population density, low precipitation/temperature, forest fragmentation, poor housing, and seasonal patterns are a significant reason for the spillover of zoonotic diseases such as Nipah in south Asia (Durrance-Bagale *et al.*, 2021). After the outbreak of Nipah, especially in Kozhikode district, we have found that people are afraid of bats, and many do not feed on fruits fed by bats (Neethu, 2022). Also, people feel bats provide more ecological disservices than services (Neethu, 2022). This change in attitude of people has led to more human–bat conflict in the region. This has led to detrimental activities such as cutting down the trees where bats roost, chasing them away by bursting crackers, etc. (Neethu, 2022). Such detrimental activities can only bring flying foxes and humans closer. Human footprint and population density have been positively associated with Nipah Zoonotic spillover in South/South East Asia (Walsh, 2015; Epstein *et al.*, 2020). We found the human footprint in Kozhikode, Kasaragod, and Kannur to be high in the areas where the present bat roosting locations are located. Hence, mitigation and prevention measures for zoonotic spillover need to be strong in these districts. Also, studies suggest that extreme stress due to the loss of habitats and urbanization in flying foxes could lead to increased viral shedding, leading to more cases of zoonotic diseases such as Nipah (Plowright *et al.*, 2017; Epstein *et al.*, 2020). Bats also could have other parasites, bacteria, and viruses, which could potentially spill over to humans (Dovih *et al.*, 2019; Khan *et al.*, 2022; Devnath *et al.*, 2023), including coronaviruses (Ruiz-Aravena *et al.*, 2021), and this could lead to several new emerging diseases (Wang and Anderson, 2019).

9.5 CONCLUSION

We observed that, due to land use change and zoonotic spillover potential, the populations of Indian Flying Foxes could be in peril. Protecting and restoring sacred groves, sacred trees, mangrove habitats, riverside habitats, and roadside

trees are crucial for conserving Indian Flying Foxes in South India. Awareness should be provided to people on how to protect the bat roosting sites in their private properties and other land uses, as well as how to minimize contact with bats. Bat gardens can also be a good alternative for the conservation of bats (Callas *et al.*, 2024). Netting fruit trees and preventing bats from entering the gardens is a good solution for reducing human–bat contact (Russo and Fenton, 2024). On the other hand, altered diet, behavior, and roosting site shifts can increase zoonotic spillover from these bats and are critical to protecting the remnant habitats. Central, state, and local governments should take steps to manage both the populations and zoonotic spillover of diseases from these bats in these districts from an ecological and social science perspective and a health perspective. More research should aim to understand this species' roosting and foraging ecology in these districts and other districts of the Kerala state and other states in India. Landsat-derived NDVI can aid in such activities as protecting bat habitats and preventing global zoonotic spillover.

ACKNOWLEDGEMENTS

Joseph J Erinjery acknowledges the Science and Engineering Research Board, Government of India, startup research grant (SRG/2021/001098). We thank Dr RSM Shamsudeen, Department of Zoology, Kannur University, for all his support. We also thank the Kerala Government and all survey participants for their support.

REFERENCES

Aiswaryalakshmi, A.R., Sunil, A.M., Bharath, M.R., Raja, F., Sahal, H., Sabu, T. and Nameer, P.O., 2023. A biodiversity assessment report of Poredam Temple Sacred Grove, Chadayamangalam, Kollam, India. *Ecology, Environment and Conservation*, *29*, pp. 240–48. https://doi.org/10.53550/eec.2023.v29i06s.035.

Baranowski, K. and Bharti, N., 2023. Habitat loss for black flying foxes and implications for Hendra virus. *Landscape Ecology*, *38*(6), pp. 1605–1618. https://doi.org/10.1007/s10980-023-01642-w.

Bhagwat, S.A., Kushalappa, C.G., Williams, P.H. and Brown, N.D., 2005. A landscape approach to biodiversity conservation of sacred groves in the Western Ghats of India. *Conservation Biology*, *19*(6), pp. 1853–1862. https://doi.org/10.1111/J.1523-1739.2005.00248.X.

Callas, M., Lumsden, L.F., Rendall, A.R. and Yokochi, K., 2024. More trees and fewer roads: The importance of local and landscape features for insectivorous bats in open urban green spaces. *Wildlife Research*, *51*(4), pp. 1–4. https://doi.org/10.1071/WR23079.

CDC, 2024. *What is Nipah Virus?*, CDC. Available at: www.cdc.gov/vhf/nipah/about/index.html#:~:text=Nipah.

Chaiyes, A., Escobar, L.E., Willcox, E.V., Duengkae, P., Suksavate, W., Watcharaanantapong, P. and Hemachudha, T., 2020. An assessment of the niche centroid hypothesis: Pteropus lylei (Chiroptera). *Ecosphere*, *11*(5), pp. 1–13 https://doi.org/10.1002/ECS2.3134.

Cui, N., Malleson, N., Houlden, V. and Comber, A., 2021. Using VGI and social media data to understand urban green space: A narrative literature review. *ISPRS International Journal of Geo-Information*, *10*(7), p. 425. https://doi.org/10.3390/IJGI10070425.

Decher, J., 1997. Conservation, small mammals, and the future of sacred groves in West Africa, *Biodiversity and Conservation*, *6*(7), pp. 1007–1026. https://doi.org/10.1023/A:1018991329431.

Deshpande, K. and Kelkar, N., 2015. How do fruit bat seed shadows benefit Agroforestry? Insights from local perceptions in Kerala, India. *Biotropica*, *47*(6), pp. 654–659. https://doi.org/10.1111/BTP.12275.

Devi, R. and Kumar, P., 2024. Distribution status and roost characteristics of Indian Flying Fox Pteropus medius Temminck, 1825 (Mammalia: Chiroptera: Pteropodidae) in Kurukshetra district, Haryana, India. *Journal of Threatened Taxa*, *16*(2), pp. 24694–24706.

Devnath, P., Karah, N., Graham, J.P., Rose, E.S. and Asaduzzaman, M., 2023. Evidence of antimicrobial resistance in bats and its planetary health impact for surveillance of zoonotic spillover events: A scoping review. *International Journal of Environmental Research and Public Health*, *20*(1), p. 243. https://doi.org/10.3390/IJERPH20010243/S1.

Di Minin, E., Slotow, R., Hunter, L.T., Montesino Pouzols, F., Toivonen, T., Verburg, P.H. and Moilanen, A., 2016. Global priorities for national carnivore conservation under land use change. *Scientific Reports*, *6*(1), pp. 1–9. https://doi.org/10.1038/srep23814.

Dovih, P., Laing, E.D., Chen, Y., Low, D.H., Ansil, B.R., Yang, X. and Mendenhall, I.H., 2019. Filovirus-reactive antibodies in humans and bats in Northeast India imply zoonotic spillover. *PLoS Neglected Tropical Diseases*, *13*(10), p. e0007733. https://doi.org/10.1371/JOURNAL.PNTD.0007733.

Durrance-Bagale, A., Rudge, J.W., Singh, N.B., Belmain, S.R. and Howard, N., 2021. Drivers of zoonotic disease risk in the Indian subcontinent: A scoping review. *One Health*, *13*, p. 100310. https://doi.org/10.1016/J.ONEHLT.2021.100310.

Epstein, J.H., Anthony, S.J., Islam, A., Kilpatrick, A.M., Ali Khan, S., Balkey, M.D. and Daszak, P., 2020. Nipah virus dynamics in bats and implications for spillover to humans. *Proceedings of the National Academy of Sciences of the United States of America*, *117*(46), pp. 29190–29201. https://doi.org/10.1073/PNAS.2000429117.

Erinjery, J.J., Kumar, S., Kumara, H.N., Mohan, K., Dhananjaya, T., Sundararaj, P. and Singh, M., 2017. Losing its ground: A case study of fast declining populations of a "least-concern" species, the bonnet macaque (Macaca radiata). *PLoS ONE*, *12*(8), p. e0182140 https://doi.org/10.1371/journal.pone.0182140.

Erinjery, J.J., Kavana, T.S. and Singh, M., 2014. Food resources, distribution and seasonal variations in ranging in lion-tailed macaques, *Macaca silenus* in the Western Ghats, India. *Primates*, *56*(1), pp. 45–54. https://doi.org/10.1007/s10329-014-0447-x.

Escobar, L.E., Peterson, A.T., Papeş, M., Favi, M., Yung, V., Restif, O. and Medina-Vogel, G., 2015. Ecological approaches in veterinary epidemiology: Mapping the risk of bat-borne rabies using vegetation indices and night-time light satellite imagery. *Veterinary Research*, *46*(1), pp. 1–10. https://doi.org/10.1186/s13567-015-0235-7.

Goldstein, J.E., Budiman, I., Canny, A. and Dwipartidrisa, D., 2022. Pandemics and the human-wildlife interface in Asia: Land use change as a driver of zoonotic viral outbreaks. *Environmental Research Letters*, *17*(6), p. 063009. https://doi.org/10.1088/1748-9326/AC74D4.

IUCN., 2021. *The IUCN Red List of Threatened Species. Version* 2021-3. IUCN. Available at: www.iucnredlist.org.

Kessler, M.K., Becker, D.J., Peel, A.J., Justice, N.V., Lunn, T., Crowley, D.E. and Plowright, R.K., 2018. Changing resource landscapes and spillover of henipaviruses. *Annals of the New York Academy of Sciences*, *1429*(1), pp. 79–99. https://doi.org/10.1111/nyas.13910.

Khan, S.A., Imtiaz, M.A., Islam, M.M., Tanzin, A.Z., Islam, A. and Hassan, M.M., 2022. Major bat-borne zoonotic viral epidemics in Asia and Africa: A systematic review and meta-analysis. *Veterinary Medicine and Science*, *8*(4), pp. 1787–1801. https://doi.org/10.1002/VMS3.835.

Kinyanjui, M.J., 2011. NDVI-based vegetation monitoring in Mau forest complex, Kenya. *African Journal of Ecology*, *49*(2), pp. 165–174. https://doi.org/10.1111/J.1365-2028.2010.01251.X.

Lunney, D. and Matthews, A., 2001. The contribution of the community to defining the distribution of a vulnerable species, the spotted-tailed quoll, *Dasyurus maculatus*. *Wildlife Research*, *28*(5), pp. 537–545. https://doi.org/10.1071/WR00018.

Madala, M.F., Guna, C., Pradeepan, A. and Chalil, A.K., 2022. Roost tree characteristics of *Pteropus medius* (Chiroptera: Pteropodidae) in the midland laterite hillocks of northern Kerala, India'. *Journal of Asia-Pacific Biodiversity*, *15*(4), pp. 465–472. https://doi.org/10.1016/j.japb.2022.04.011.

Madhu, V., Namboodiri, G.A. and Vijay, G., 2021. An analytical study of rainfall characteristics over Wayanad District of Kerala. *Turkish Journal of Computer and Mathematics Education (TURCOMAT)*, *12*(13), pp. 1971–1979. https://doi.org/10.17762/TURCOMAT.V12I13.8869.

McKee, C.D., Islam, A., Luby, S.P., Salje, H., Hudson, P.J., Plowright, R.K. and Gurley, E.S., 2021. The ecology of nipah virus in bangladesh: A nexus of land-use change and opportunistic feeding behavior in bats. *Viruses*, *13*(2), p. 169. https://doi.org/10.3390/v13020169.

Meierhofer, M.B., Leivers, S.J., Fern, R.R., Wolf, L.K., Young Jr, J.H., Pierce, B.L. and Morrison, M.L., 2019. Structural and environmental predictors of presence and abundance of tri-colored bats in Texas culverts. *Journal of Mammalogy*, *100*(4), pp. 1274–1281. https://doi.org/10.1093/JMAMMAL/GYZ099.

Meierhofer, M.B., Leivers, S.J., Pierce, B.L., Powers, G.W., Evans, J.W. and Morrison, M.L., 2022. Structural and environmental predictors of tricolored bat presence and abundance in Texas caves. *Journal of Mammalogy*, *103*(2), pp. 407–414. https://doi.org/10.1093/JMAMMAL/GYAB143.

Mgumia, F.H. and Oba, G., 2003. Potential role of sacred groves in biodiversity conservation in Tanzania. *Environmental Conservation*, *30*(3), pp. 259–265. https://doi.org/10.1017/S0376892903000250.

Moore, J.H., Gibson, L., Amir, Z., Chanthorn, W., Ahmad, A.H., Jansen, P.A. and Luskin, M. S., 2023. The rise of hyperabundant native generalists threatens both humans and nature, *Biological Reviews*, *98*(5), pp. 1829–1844. https://doi.org/10.1111/BRV.12985.

Neethu, P., 2022. Did nipah change the attitude of people? A study on distribution and abundance of indian flying fox (pteropus medius) in calicut district, kerala. MSc Dissertation, Kannur University.

Newbold, T., Hudson, L.N., Hill, S.L., Contu, S., Lysenko, I., Senior, R. A. and Purvis, A., 2015. Global effects of land use on local terrestrial biodiversity. *Nature, 520*(7545), pp. 45–50. https://doi.org/10.1038/nature14324.

Pandian, M. and Suresh, S., 2021. Roosting habits and habitats of the Indian Flying Fox *Pteropus medius* Temminck, 1825 in the northern districts of Tamil Nadu, India. *Journal of Threatened Taxa*, *13*(12), pp. 19675–19688.

Plowright, R.K., Eby, P., Hudson, P.J., Smith, I.L., Westcott, D., Bryden, W.L. and McCallum, H., 2014. Ecological dynamics of emerging bat virus spillover. *Proceedings of the Royal Society B: Biological Sciences*, *282*(1798), pp. 1–9. https://doi.org/10.1098/RSPB.2014.2124.

Plowright, R.K., Parrish, C.R., McCallum, H., Hudson, P.J., Ko, A.I., Graham, A.L. and Lloyd-Smith, J.O., 2017. Pathways to zoonotic spillover. *Nature Reviews Microbiology*, *15*(8), pp. 502–510. https://doi.org/10.1038/nrmicro.2017.45.

Raman, S., Shameer, T.T., Pooja, U. and Hughes, A.C., 2023. Identifying priority areas for bat conservation in the Western Ghats mountain range, peninsular India. *Journal of Mammalogy*, *104*(1), pp. 49–61. https://doi.org/10.1093/jmammal/gyac060.

Raman, S. and Hughes, A.C., 2021. Echobank for the bats of Western Ghats biodiversity hotspot, India. *Acta Chiropterologica*, *22*(2), pp. 349–364. https://doi.org/10.3161/1508 1109ACC2020.22.2.010.

Ruiz-Aravena, M., McKee, C., Gamble, A., Lunn, T., Morris, A., Snedden, C.E. and Plowright, R.K., 2021. Ecology, evolution and spillover of coronaviruses from bats. *Nature Reviews Microbiology*, *20*(5), pp. 299–314. https://doi.org/10.1038/s41579-021-00652-2.

Russo, D. and Fenton, B., 2024. *A Natural History of Bat Foraging Evolution, Physiology, Ecology, Behavior, and Conservation*. Academic Press.

Sales, L.P., Galetti, M. and Pires, M.M., 2020. Climate and land-use change will lead to a faunal "savannization" on tropical rainforests. *Global Change Biology*, *26*(12), pp. 7036–7044. https://doi.org/10.1111/GCB.15374.

Saritha, V.V., 2015. Distribution and ecological studies on different roost of Indian Flying Fox Pteropus giganteus in Kasaragod district, Kerala. MSc Dissertation, Kannur University. pp. 1–38.

Shilton, L.A., Altringham, J.D., Compton, S.G. and Whittaker, R.J., 1999. Old World fruit bats can be long–distance seed dispersers through extended retention of viable seeds in the gut. *Proceedings of the Royal Society of London. Series B: Biological Sciences*, *266*(1416), pp. 219–223. https://doi.org/10.1098/RSPB.1999.0625.

Shimod, K.P., Vineethkumar, V., Prasad, T.K., and Jayapal, G., 2022. Effect of urbanization on heavy metal contamination: A study on major townships of Kannur District in Kerala, India. *Bulletin of the National Research Centre, 46*(1), pp. 1–14. https://doi.org/10.1186/S42269-021-00691-Y.

Sudeep, A.B., Yadav, P.D., Gokhale, M.D., Balasubramanian, R., Gupta, N., Shete, A. and Mourya, D.T., 2021. Detection of Nipah virus in Pteropus medius in 2019 outbreak from Ernakulam district, Kerala, India. *BMC Infectious Diseases*, *21*(1), pp. 1–7. https://doi.org/10.1186/s12879-021-05865-7.

Tsang, S.M., 2020. *Pteropus giganteus (Errata Version Published in 2021). The IUCN Red List of Threatened Species 2020: e.T18725A194134899*. IUCN.

Van Leeuwen, W.J., Orr, B.J., Marsh, S.E. and Herrmann, S.M., 2006. Multi-sensor NDVI data continuity: Uncertainties and implications for vegetation monitoring applications. *Remote Sensing of Environment*, *100*(1), pp. 67–81. https://doi.org/10.1016/J.RSE.2005.10.002.

Venter, O., Sanderson, E.W., Magrach, A., Allan, J.R., Beher, J., Jones, K.R. and Watson, J. E., 2016. Sixteen years of change in the global terrestrial human footprint and implications for biodiversity conservation. *Nature Communications*, *7*(1), pp. 1–11. https://doi.org/10.1038/ncomms12558.

Vleut, I., Galindo-González, J., de Boer, W.F., Levy-Tacher, S.I. and Vazquez, L.B., 2015. Niche differentiation and its relationship with food abundance and vegetation complexity in four frugivorous bat species in Southern Mexico. *Biotropica*, *47*(5), pp. 606–615. https://doi.org/10.1111/BTP.12238.

Walsh, M.G., 2015. Mapping the risk of Nipah virus spillover into human populations in South and Southeast Asia. *Transactions of The Royal Society of Tropical Medicine and Hygiene*, *109*(9), pp. 563–571. https://doi.org/10.1093/TRSTMH/TRV055.

Wang, L.F. and Anderson, D.E., 2019. Viruses in bats and potential spillover to animals and humans. *Current Opinion in Virology*, *34*, pp. 79–89. https://doi.org/10.1016/J.COVIRO.2018.12.007.

White, R.J. and Razgour, O., 2020. Emerging zoonotic diseases originating in mammals: A systematic review of effects of anthropogenic land-use change. *Mammal Review*, *50*(4), pp. 336–352. https://doi.org/10.1111/MAM.12201.

10 Analysis of Relationship Between Cloud Fraction (CF) and Aerosol Optical Depth (AOD) for Heterogeneous Rainfall Regimes Over Peninsular India

Tharani Kotrike, Venkata Reddy Keesara, Sangwoo Kim, and Venkataramana Sridhar

10.1 INTRODUCTION

Aerosols have direct and indirect effects on climate patterns and climate variability (Ramanathan et al., 2001, Chen et al., 2014, 2018; Sridhar et al., 2013). The direct effect of aerosols is interacting with incoming solar radiation, which in turn can impact the surface energy and water budgets (Sridhar and Wedin, 2009; Sridhar et al., 2009; Sridhar, 2013; Sridhar and Anderson, 2017; Valayamkunnath et al., 2018; Kant et al., 2019). The indirect effect of aerosols is on the optical and macro-physical properties of clouds (Sheng et al., 2019; Misumi et al., 2022). Also, aerosols can influence cloud lifetime by increasing the cloud condensation nuclei (CCN) and ice nuclei (Twomey 1977; Koren et al., 2010; Kusensica et al., 2012; Liu et al., 2020). The amount of water vapor gets distributed over many cloud droplets in the presence of large CCN concentrations. This results in smaller sizes of cloud, higher albedo (Twomey 1977), and less precipitation (Rosenfeld et al., 2008), which in turn impacts the partitioning of net radiation into latent, sensible, and ground heat fluxes (Jaksa et al., 2013) and variability in rainfall (Setti et al., 2020a, 2020b).

The impact of AOD on cloud lifetime and precipitation has been extensively studied in recent years (Balakrishnaiah et al., 2012; Liu et al., 2020). Furthermore, the type of aerosols had a strong influence on the forcing phenomenon. For example, carbonaceous aerosols resulted in positive forcing, whereas sulfate aerosols resulted

DOI: 10.1201/9781003396260-10

in negative forcing at the top of the atmosphere (Grandey et al., 2013). The previous analysis of the relationship between AOD and CF was based on humidity and stability conditions in low and polluted regions (Remer et al., 2002; Koren et al., 2005). MODIS provides the aerosol index, calculated as the product of the angstrom exponent and the AOD. Previous research on the effect of aerosols used the aerosol index as the primary parameter. However, some researchers have stated that the aerosol index was unreliable over land (Kourtidis et al., 2015; Liu et al., 2020). Existing conditions in a region, such as biomass burning and anthropogenic emissions, may alter the relationship substantially.

Therefore, it is recognized that the impact of AOD on CF can offer new insights into various atmospheric stability states (*K*-index). The amount and vertical extent of low-level moisture in the atmosphere, along with the vertical temperature lapse rate, are the two factors that determine thunderstorm potential, which is measured by the *K*-index.

The study is intended to understand better the effects of AOD on CF for the light, moderate, and heavy rain regimes for different atmospheric stability states across Peninsular India. The study is carried out on the data from the south-west monsoon season for 15 years from 2005–2019. The satellite products are initially aggregated to a single resolution for better analysis. The AOD is divided into 11 bins based on pixel values ranging from 0 to 1.5. Higher values of AOD are not considered in the analysis to avoid ambiguity in mixed pixels. The correlation analysis is then performed using R statistical software for 11 AOD bins with the accumulated data. Finally, spatial variations in AOD and CF are evaluated over Peninsular India.

The objective of this study is to observe the changes in AOD and CF for the rainfall regimes in Southern India. Currently, the stability of the atmosphere and the behavior of related variables are only partially understood based on correlation studies. Also, previous studies rarely discuss the research on AOD and CF in Southern India. This study aims to develop a novel approach to obtaining a statistical relationship between the AOD and CF for different stability states of the atmosphere.

10.2 STUDY AREA

The present study area encompasses several states, namely Maharashtra in Western India, Orissa in Eastern India, Chhattisgarh in Central India, as well as Goa, Andhra Pradesh, Telangana, Karnataka, Tamil Nadu, and Kerala in Southern India. Figure 10.1 depicts the geographical scope of the research area. The region in Figure 10.1 was chosen as the study area because there has been little research on the statistical correlation of AOD and CF in this region. Furthermore, the monsoon patterns in Southern India have changed significantly in recent years (Mishra et al., 2019).

The primary source of income in this region is agriculture. The southwest monsoon is the primary source of rainfall on which productivity is dependent in most of the study area. Every year, the southwest monsoon begins in June and lasts until September. As a result, the AOD, CF, and rainfall products for the southwest monsoon season, i.e., JJAS, are considered (June–July–August–September).

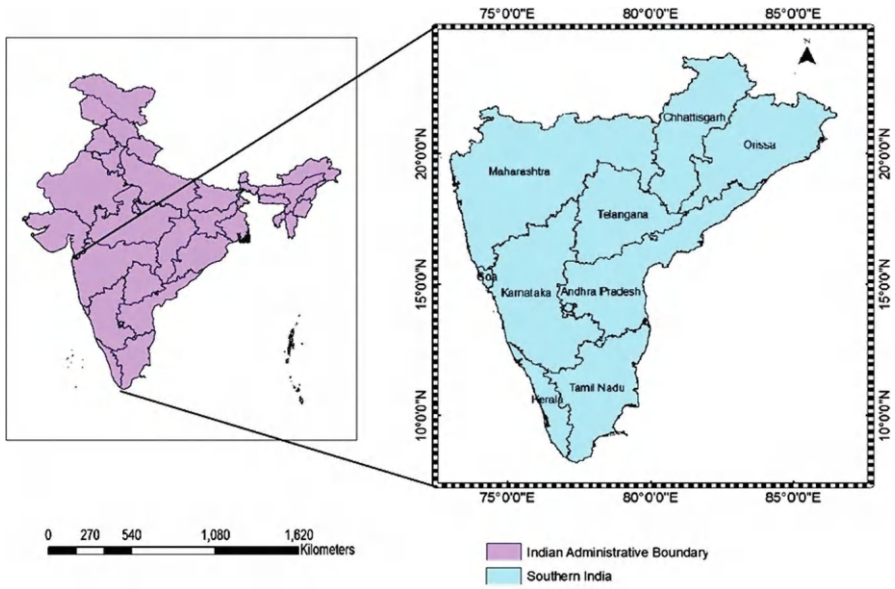

FIGURE 10.1 Location map of study area covering nine states in India.

10.3 DATA AND METHODS

10.3.1 Satellite Data Used

The datasets used for the current study are obtained from the MODIS onboard Terra and Aqua Satellites. MODIS products have become widely used for a variety of analyses due to their broad spectral coverage and high spatial resolution (Liu et al., 2020). The observation period constituted the monsoon season from 2005 to 2019. The data is averaged for cumulative 5-, 10-, and 15-year periods. All three products were obtained from the NASA website. Details of the data products used in the present study are given as follows:

MOD04_L2 denotes the aerosol product the dark target/deep blue algorithm generates. The parameter used is the Optical Depth of Land and Ocean, and the spatial resolution is 10 km × 10 km. MODIS aerosol retrievals are based on a look up table (LUT) procedure in which satellite-measured radiances are matched to pre-calculated values in the LUT and the values of the aerosol properties used to create the calculated radiances are retrieved (Kumar et al., 2013; Vijaykumar et al., 2018). The estimated satellite radiances at 470 and 670 nm wavelengths are used to calculate AOD at 550 nm using the Angstrom exponential law. The satellite product is validated against ground truth data, and the results are satisfactory (Gopal et al., 2016; Kotrike et al., 2021). The AOD data ranged from 0 to 1.5, and data above 1.5 were not included in the analysis to prevent cloud particles and aerosols from being misclassified (Liu et al., 2020).

MOD06_L2: It refers to cloud data. The macro-physical cloud parameters used in the study are Cloud Top Pressure (CTP), Cloud Top Temperature (CTT), and CF (CF). All three parameters are measured at 5 km × 5 km spatial resolution. CTP and

CTT are measured using infrared and CO_2 absorption bands, respectively, whereas CF is collected using visible bands (Platnick et al., 2015; Kumar et al., 2020).

MOD07_L2: It denotes the atmospheric profile data. The *K*-index is the parameter used. It is a measure of thunderstorm potential based on vertical temperature lapse rate, lower atmosphere moisture content, and the vertical extent of the moist layer. The temperature difference between 850 hPa and 500 hPa is used to parameterize the vertical temperature lapse rate. The dew point at 850 hPa indicates the moisture content of the lower atmosphere. The vertical extent of the moist layer is represented by the difference between the 700 hPa temperature and 700 hPa dew point. This is called the 700 hPa temperature-dew point depression. The index is derived arithmetically. MODIS provides *K*-index daily data when at least nine fields of view (FOV) are clear. The mathematical equation governing *K*-index is given in equation (10.1) (Borbas et al., 2015).

$$K = (T_{850} - T_{500}) + T_{d_{850}} - \left(T_{700} - T_{d_{700}}\right) \tag{10.1}$$

where T_{850} is the temperature at 850 hPa, T_{700} is the temperature at 700 hPa, T_{500} is the temperature at 500 hPa, $T_{d_{850}}$ is the dew point temperature at 850 hPa, and $T_{d_{700}}$ is the dew point temperature at 700 hPa.

The multi-satellite precipitation product comes from the Integrated Multi-satellite Retrievals for Global Precipitation Mission (IMERG). This dataset is the GPM Level 3 IMERG Final Daily 10 × 10 km (GPM_3IMERGDF) derived from the half-hourly GPM_3IMERGHH. The derived result represents the final estimate of daily accumulated precipitation. PrecipitationCal, also known as complete calibrated precipitation, is the parameter used in this study. It displays the daily accumulated precipitation in millimeters. Table 10.1 displays the datasets. Note: Data source for 1–5: https://ladsweb.modaps.eosdis.nasa.gov/ 6: (https://disc.gsfc.nasa.gov/).

TABLE 10.1
Details About the Satellite Data, Parameters, and Spatial Resolution Used in this Study

S.No	Data	Parameter	Spatial Resolution
1	Moderate Resolution Imaging Spectrometer (MODIS) Terra MOD04_L2	Optical Depth Land and Ocean	10 km × 10 km
2	Moderate Resolution Imaging Spectrometer (MODIS) Terra MOD06_L2	Cloud Fraction	5 km × 5 km
3	Moderate Resolution Imaging Spectrometer (MODIS) Terra MOD06_L2	Cloud Top Pressure	5 km × 5 km
4	Moderate Resolution Imaging Spectrometer (MODIS) Terra MOD06_L2	Cloud Top Temperature	5 km × 5 km
5	Moderate Resolution Imaging Spectrometer (MODIS) Terra MOD07_L2	*K*-Index	5 km × 5 km
6	GPM IMERG Final Precipitation L3 (GPM_3IMERGDF)	Precipitation	10 km × 10 km

10.3.2 Approach

Figure 10.2 depicts the methodology used in the current study. Cloud formation begins with the activation of cloud condensation nuclei (CCN). Aerosols are essential in the formation of CCN. The present study used AOD as the primary parameter to characterize aerosols.

Cloud parameters are used to identify low-warm clouds. Low, warm clouds were defined as pixels with CTP greater than 680 hPa and CTT greater than 0°C. MODIS products are available in a variety of spatial resolutions (Wang et al., 2015). Using R statistical software, all cloud parameters and atmospheric stability data were resampled to a resolution of 10 km × 10 km. The files were cropped to the required size for the study.

The atmospheric stability states are classified into four categories based on the values: isolated thunderstorms ($20<K<25$), widely scattered thunderstorms ($20<K<25$), scattered thunderstorms ($30<K<35$), and numerous thunderstorms ($K>35$). Rainfall is classified into three types based on intensity: light, moderate, and heavy (Soni et al., 2020). Equal value plots represent the changes in CF for each bin of AOD. The Pearson correlation method performs the spatial correlation between cumulative AOD and CF for different *K*-index classes. The R code is scripted to identify the parametrical data corresponding to pixels of each rainfall regime and to average the corresponding cloud parameters for 11 AOD bins. AOD bins range from 0 to 1 with an increment of 0.1.

Also, the significance of the correlation was evaluated using the *p*-value. If the *p*-value is less than 0.05, the correlation is said to be significant at a 95% confidence

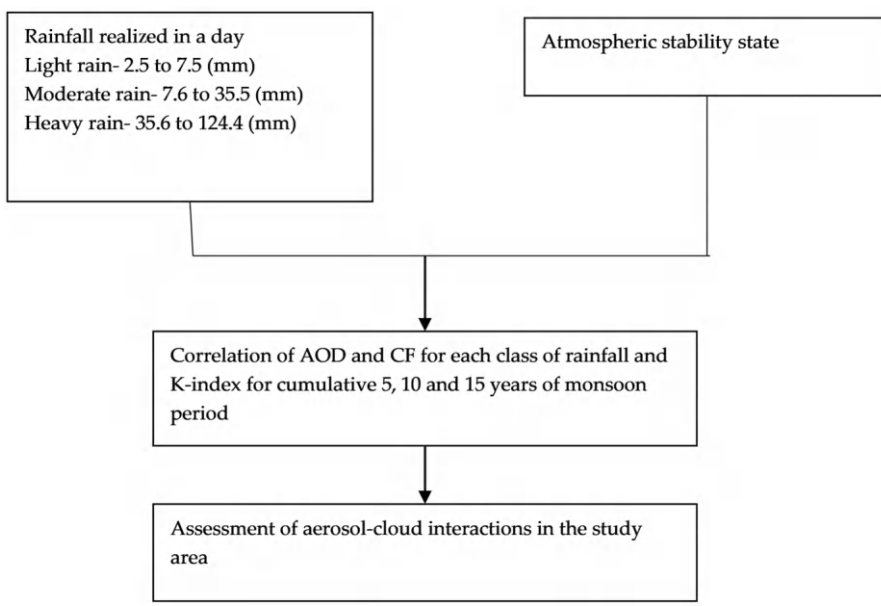

FIGURE 10.2 Flow chart showing the methodology adopted for study.

level. The analysis is performed for three cumulative datasets, namely 5, 10, and 15 years of data. The cumulative 5 years indicate the dataset from 2015 to 2019, the 10 years indicate the dataset from 2010 to 2019, and the 15 years indicate the dataset from 2005 to 2019. To comprehend the behavior of AOD and CF for various atmospheric stability states as the number of samples increases, the cumulative periods for the analysis are taken into account.

Theoretically, higher AOD refers to a hazy atmosphere, and lower AOD refers to a clear atmosphere. The spatial distribution of AOD for the three cumulative datasets in light, moderate, and heavy rain conditions is investigated by categorizing the study area into three classes based on the pixel values: 0–0.5 (low polluted), 0.5–1 (moderately polluted), and greater than 1 (highly polluted) (David et al., 2018). This classification is followed so that the current study can interpret the results explicitly.

The temperature change is related to the state of atmospheric stability. As temperature is a primary climate parameter, the study area was divided into five climate zones concerning Koppen's world climate classification. Accordingly, the study area is divided into five climate zones of the study area are classes namely monsoon climate (Am), tropical savanna climate (Aw), warm semi-arid climate (BSh), humid subtropical climate (Cwa), subtropical oceanic highland climate (Cwb). The tropical monsoon climate (Am) region has a mean temperature greater than 180°C every month of the year. In this region, the driest month has an average precipitation of less than 60 mm but more than the precipitation obtained as per the equation (10.2). The tropical monsoon climate regions have fewer temperature variations.

$$\text{Precipitation} = 100 - \frac{Total\ Annual\ Precipitation\left(mm\right)}{25} \tag{10.2}$$

Because tropical savannas are located within tropical latitudes, their climates are generally warm. The average monthly temperature rises above 18°C throughout the year. Temperatures in the wet season range from 25 to 30°C. The year's dry season sees temperatures in between 20 and 25°C. Daytime temperatures are higher than nighttime temperatures. The driest month of the tropical savanna climate (Aw) region experiences an average precipitation of less than 60 mm and less than the precipitation obtained as per equation (10.2). The warm semi-arid climate (BSh) sees hot to extremely hot summers and warm to cool winters. The mean annual temperature in this region is 18°C. The humid subtropical climate (Cwa) region witnesses an average precipitation of 80–165 cm. The region has a mean temperature in between 0°C to –3°C in the coldest month and more significant than 22°C in the warmest month. The sub-tropical oceanic highland climate (Cwb) region tends to have dry winters and wet summers (Kottek et al., 2006; Adam et al., 2021; Anil et al., 2021).

Given the diverse climatic conditions across Southern India, it is essential to analyze land use changes and precipitation during the monsoon period based on these climatic conditions. This study analyzed the impact of land use changes on precipitation in Southern India during the monsoon period from 2005 to 2019. Landsat-based GLAD (Global Land Analysis and Discovery) data was used to analyze land use

changes. Land use maps are provided every 5 years (2005–2020) and have a spatial resolution of 30 m.

10.4 RESULTS AND DISCUSSION

10.4.1 Comprehensive Effect of AOD on CF

The CF changes for different AOD ranges are analyzed by means of equal-value plots. The AOD data is divided into 30 bins. The data ranges from 0 to 1.5, and each bin is incremented by 0.05. The average of AOD and CF data corresponding to each bin is calculated. A min-max scale normalizes the data. The expression used for the normalization of the data is as follows:

$$X_n = \frac{\left(X_i - X_{\min}\right)}{\left(X_{\max} - X_{\min}\right)}, i = 1,2,3.....30 \tag{10.3}$$

Where X_n is the normalized data, X_i is the existing data, $X_{\min}$ is the minimum value, and $X_{\max}$ is the maximum value. The AOD and CF are normalized by using equation (10.3). The scatterplot of normalized data with reference line is then plotted to obtain the equal value plot between AOD and CF. The reference line is the 1:1 line obtained by joining the corresponding minimum and maximum of AOD and CF. Although the equal value plots are prepared for each cumulative dataset of three rainfall regimes, the plots with points closer to the reference line are shown in the manuscript.

The analysis using equal value plots for different rainfall regimes, which possess points closer to the reference line, suggested that the cumulative 10-year dataset for each of the three rainfall regimes performs better. The scaled values of CF are significantly concentrated in the range of 0.4–0.6 for the light rain regime, whereas the scaled values of AOD are widely distributed in the range of 0–1. When the CF value is more than 0.5, and the AOD falls between 0.6 and 0.8, the plot seems to move closer to the reference line.

The scaled values of CF are in the range of 0.2–0.4 for a moderate rain regime, which means that the vertical development of clouds does not influence the intensity of moderate rain. The plot shows that the points with AOD and CF in the range of 0.2–0.4 are much closer to the reference line, and the CF appears to be staggered with an increase in AOD. Low AOD might result in low CF, and an increase in AOD does not influence the formation of clouds for a moderate rain regime. The AOD and CF are in the 0.2–0.6 range for the cluster of points that is closer to the reference line for the heavy rainfall regime. After the AOD crosses 0.6, the CF does not exhibit any pattern. During moderate and heavy rainfall, evaluating the formation of clouds at different AOD ranges more significant than 0.6 is challenging.

10.4.2 Observed Relationship Between AOD and CF Based on Atmospheric Stability

Theoretically, the likelihood of heavy rain increases with the *K*-index value. However, lower *K* values may also lead to precipitation. Since the *K*-index incorporates the

TABLE 10.2
Number of Samples Used for Analysis

Intensity of Rainfall	Light			Moderate			Heavy		
K-index	5 year	10 year	15 year	5 year	10 year	15 year	5 year	10 year	15 year
20<*K*<25	39	827	1598	4	675	1452	70	173	339
25<*K*<30	57	1564	3148	–	1356	2904	145	411	755
30<*K*<35	71	2083	4420	–	1962	4457	219	794	1303
K>35	257	4151	7663	35	4006	7685	628	1645	2507

dewpoint depression (i.e., the difference between the temperature and dewpoint temperature) at 700 mb, the chance of occurrence of rain is also likely with low *K* values. But strong thunderstorms and even a lot of rain can still happen when there is moisture below 700 mb due to unstable air and a lifting mechanism. Scattered diurnal convection can produce a brief but powerful downpour in an area with high *K* values.

Table 10.2 gives the number of samples for each intensity of rainfall and cumulative period that satisfied the low-warm cloud condition. The spread of CF over the range of AOD for different classes of *K* is analyzed by means of a heat map representation. The AOD is divided into 11 bins starting from 0 to 1.5. Heat maps, not shown here, are prepared for each cumulative period of study and suggest a strong correlation.

A CF in the range of 0.3–0.7 has been observed in the isolated thunderstorm state (20°C < *K* <25°C) in the light rain regime for the cumulative 15-year dataset. For 0 < AOD < 0.7, it is found to consistently increase. For AOD > 0.7, the rise in CF does not exhibit a specific pattern. The CF is found to decline when AOD is less than 0.6 and increases further in a widely scattered thunderstorm state (25°C < *K* <30°C). The fall in CF has followed the same pattern in scattered thunderstorm states (30°C < *K* <35°C). For 0.6 < AOD < 0.9, CF did not follow a particular pattern, but later, for AOD >0.9, CF was found to increase consistently. The CF is almost the same for 0 <AOD <0.9 in numerous thunderstorm states (*K* > 35°C). For AOD > 0.9, the CF is found to increase rapidly. The potential of aerosols to act as cloud condensation nuclei and form new clouds or form additional smaller droplets in the existing clouds may cause the initial decrease in CF for all four atmospheric stability states. These smaller droplets could delay the cloud's lifetime, prevent collision-coalescence, and even deepen the cloud due to stronger updrafts produced by the condensation process (Koren et al., 2005; Small et al., 2011).

From the analysis of the observed relationship between AOD-CF for moderate rain regime for the cumulative 15-year dataset, for pixels with 0.1 < AOD <0.2, the CF is found to increase and later decrease for 0.2 < AOD <0.9. A sharp rise in CF is observed for 1 < AOD <1.5 for isolated thunderstorm state (20°C < *K* <25°C). The CF is almost the same for 0 < AOD <1 in a widely scattered thunderstorm state (25°C < *K* <30°C) and then rises abruptly. For 0 < AOD < 0.4, the CF is almost the same in

a scattered thunderstorm state (30°C < K <35°C). A rise in CF is observed for 0.4 < AOD <0.7 and a fall for pixels with 0.7< AOD<1. For numerous thunderstorm states (K > 35°C), the relationship between AOD-CF is almost the same for 0 < AOD <0.7 and then found to decrease consistently. The increase in CF for AOD>1 might be due to contamination of AOD pixel data with clouds. The data analysis shows that the 0.7 < AOD <0.9 has invigorated the formation of fresh clouds, resulting in the fall of CF.

The observed relationship between AOD-CF for heavy rain regime for a cumulative 15-year dataset implied that the CF has its peak for 0.6 < AOD <0.7 and is found to decrease abruptly for AOD > 0.7 in isolated thunderstorm state (20°C < K <25°C). In a widely scattered thunderstorm state (25°C < K <30°C), CF appears to be the same for 0 < AOD <0.9 and is found to rise for AOD > 0.9. The CF is found to have its peak for 0.4 < AOD <0.7 but does not follow a specific pattern in scattered thunderstorm states (30°C < K <35°C). Corresponding to numerous thunderstorm states (K >35°C), the CF is found to increase for two bins of AOD and decrease in the consecutive bin of AOD. Overall, the CF is in the range of 0.4–0.6 for 0 < AOD <0.9 for all the atmospheric stability states. It can be said that aerosols help in the formation of clouds, but further studies are required to know whether the clouds are supported by updrafts such that they result in precipitation.

Table 10.3 shows the correlation between AOD and CF at different K-indices for cumulative datasets. There is a positive significant correlation between AOD and CF regardless of atmospheric stability (Varpe et al., 2022; Zhang et al., 2022). This indicates that aerosol influences the cloud development process, which may result in precipitation. Table 10.3 shows that the correlation between AOD and CF has become stronger as the number of samples increased, regardless of atmospheric stability. There is a noticeable increase in cloud cover during the light rain regime, as evidenced by the strongest and most significant correlation between AOD and CF in isolated thunderstorm states. The correlation is almost the same but not statistically significant for scattered thunderstorm states and numerous thunderstorm states in light rain regimes. This describes how clouds form vertically and whether they produce precipitation (Constantino et al., 2013; Liu et al., 2020).

TABLE 10.3
Correlation Coefficients between AOD and CF for Various Atmospheric Stability States

	Light rain			Moderate rain			Heavy rain		
K-index	**5 years**	**10 years**	**15 years**	**5 years**	**10 years**	**15 years**	**5 years**	**10 years**	**15 years**
20<K<25	–0.35	**0.669**	**0.653**	0.878	0.200	**0.703**	–0.422	–0.383	–0.464
25<K<30	**0.628**	0.386	0.351	–	0.540	0.476	**0.764**	**0.596**	**0.662**
30<K<35	0.131	0.287	0.509	–	0.080	**0.633**	0.28	0.306	0.283
K>35	0.401	0.208	0.499	–0.250	**–0.711**	–0.555	0.385	0.083	–0.061

Note: Bold values indicate statistically correlated values at 5% level of significance.

In the moderate rain regime, AOD and CF have a negative correlation when $K>35$ for all cumulative datasets. For cumulative 15-year data, the correlation was strongest and most significant for isolated thunderstorm states and widely scattered thunderstorm states. This indicates that the atmospheric stability conditions influenced cloud formation. For isolated thunderstorm states, the correlation between AOD and CF for heavy rain regimes is found to be negative. Widely scattered thunderstorm states (250°C< K < 300°C) were correlated with maximum and significant values for all three cumulative datasets in the heavy rain regime. As the duration lengthens, the correlation becomes less significant for both widespread and isolated thunderstorm states in the heavy rain regime. In both the light and moderate rain regimes within the isolated thunderstorm state, the thorough analysis shows a strong correlation between AOD and CF. Likewise, a significant correlation is observed between AOD and CF in the heavy rainfall regime within the widely scattered thunderstorm state (250°C < K < 300°C).

10.4.3 Spatial Distribution of AOD and CF

The distribution of AOD and CF in the study area's light rain regime suggested that most of the study area is classified as low polluted. A tropical savanna climate covers nearly 173 lakh ha of low-polluted land, while a warm semi-arid climate covers 107 lakh ha. The cumulative 10-year and 15-year data show a similar pattern. The distribution of AOD increased with the number of samples collected in low-polluted areas. In contrast, AOD distribution has decreased in moderately polluted areas. According to the Koppen climate classification, the AOD distribution corresponding to the low polluted region has nearly quadrupled in the humid subtropical region. However, in the moderately polluted region, AOD has decreased by 50% over a 15-year period.

Nearly 182 lakh ha of the region in tropical savanna climate had moderate CF based on 5-year data. Conversely, the CF has a moderate to high distribution in most tropical savanna regions, followed by warm semi-arid regions. For a cumulative 10-year analysis, nearly 427 lakh ha of the study area is classified as a tropical savanna climate region, followed by 220 lakh ha classified as a warm semi-arid climate region. Most of the humid subtropical and tropical savanna region has lower AOD. Nonetheless, some areas in the monsoon region have seen low and high distributions of AOD and CF, respectively. Overall, it can be concluded that as the number of samples increased, most of the study area exhibited AOD in the range of 0–0.5. Similarly, the CF was in the 0.8–0.9 range.

From the spatial distribution of AOD and CF in the moderate rain regime, it was clear that in 5 years, most of the tropical savanna region of 158 lakh ha experienced low pollution, followed by humid and subtropical oceanic highland climates. The cumulative 10-year and 15-year time periods were treated in the same manner. For all three cumulative time periods, moderate pollution was observed in tropical savanna climate and humid subtropical climate regions. It was also clear that the area with low pollution for cumulative 10-year and 15-year data has increased, while the area with moderate pollution has decreased significantly. The main reason for changes in AOD distribution can be attributed to mitigation and adaptation measures implemented by

the Indian government, as mentioned in the IPCC climate change reports from 2001 and 2014. (Metz et al., 2001; Edenhofer et al., 2015; Kotrike et al., 2021) The moderate CF was nearly the same for all climate regions with 10-year and 15-year data.

The tropical savanna climate has the lowest AOD distribution across all three cumulative datasets, followed by the subtropical oceanic highland climate. For all five climate regions corresponding to heavy rain, the area with a moderate AOD distribution was the smallest. In the spatial distribution, the higher range of CF was limited. The majority of the population in the study area had moderate CF and low AOD. For all three cumulative datasets, the distribution of CF was most noticeable in the tropical savanna region, followed by the humid subtropical climate region.

Table 10.4 depicts the area under each climate region corresponding to light rain for cumulative data analysis. For low AOD distribution, the tropical savanna climate experienced an 11% and 13% increase in distribution for cumulative 10- and 15-year data, respectively. On the other hand, the tropical savanna climate has decreased by 47% and 75% distribution for cumulative 10-year and 15-year data, respectively, for the moderate distribution of AOD. For both cumulative periods, the increase in moderate CF is on the higher end of the order of 35% for warm, semi-arid climates. In contrast, the higher CF range has seen a decline of the order of 13% and 19% for cumulative 10- and 15-year data, respectively.

The areal distribution of AOD and CF in the study area for moderate rain is shown in Table 10.5. For cumulative 10-year and 15-year data, the tropical savanna climate has seen an increase in lower AOD of about 50% and 70%, respectively. Moderate AOD has decreased by 35% and 39% for the same climate region, respectively. Lower AOD has increased by 26% and 42% for cumulative 10-year and 15-year datasets in the humid subtropical climate region. The moderate AOD is expected to decrease by 40% and by 55%, respectively. The cumulative 10-year and 15-year datasets revealed a 35 percent increase in moderate CF in the tropical savanna climate region. The higher end of CF, on the other hand, has declined by approximately 8%. On the other hand, the humid subtropical climate region has seen a 1% and a 20% decrease in the cumulative 10-year and 15-year datasets, respectively.

Table 10.6 shows the areal distribution of AOD and CF in the study area's heavy rain regime. For the cumulative 10-year and 15-year datasets, the tropical savanna climate has seen three and five times lower AOD, respectively. For the cumulative 10-year and 15-year datasets, the humid subtropical climate has increased twice and nearly three times. A similar observation was made for the moderate distribution of AOD. Lower CF in the tropical savanna climate region increased by 72% over 10 years. Lower CF have increased by 56% and 89% in the humid subtropical climate region. When compared to a cumulative 5-year dataset, moderate CF increased nearly threefold in all climate regions.

10.4.4 Analysis of Monsoon Precipitation Trends Based on Land Use Change

As of 2020, the land use composition in Southern India consists of 40.3% cropland, 23.9% forest, 23.9% grassland, 6.2% urban areas, 2.5% water, and 2.2% pasture. Cropland, which occupies the largest portion of land use, has steadily increased from

TABLE 10.4
Areal Distribution of AOD and CF for Each Climatic Region Under Light Rain in 100,000 ha

Climatic region	AOD						CF								
	Low			Moderate			Low			Moderate			High		
	5 year	10 year	15 year	5 year	10 year	15 year	5 year	10 year	15 year	5 year	10-year	15-year	5-year	10-year	15-year
Aw	5.023	11.302	11.302	1.159	0.290	0.290	0.000	0.000	0.000	1.159	0.193	0.193	11.205	11.592	11.592
Am	173.006	356.252	406.966	103.070	93.313	73.028	38.736	4.443	19.416	181.604	427.734	449.469	79.017	20.479	13.524
BSh	107.610	193.388	219.566	76.216	48.878	20.672	28.593	21.058	37.190	120.844	220.049	200.730	71.289	2.222	2.995
Cwa	15.745	54.867	60.180	21.348	12.075	6.762	15.069	5.892	3.961	22.121	61.146	63.078	0.097	-	-
Cwb	1.256	–	–	–	–	–	0.869	–	–	0.386	-	-	-	-	-

TABLE 10.5
Areal Distribution of AOD and CF for Each Climatic Region Under Moderate Rain in 100,000 ha

Climatic region	AOD						CF								
	Low			Moderate			Low			Moderate			High		
	5 year	10 year	15 year	5 year	10 year	15 year	5 year	10 year	15 year	5 year	10 year	15-year	5-year	10-year	15-year
Aw	39.315	185.274	165.858	105.871	336.256	19.609	32.747	31.298	44.918	89.739	178.609	133.788	157.068	10.626	8.018
Am	0.966	35.065	36.707	0.097	1.835	1.352	0.000	0.000	0.000	0.483	4.443	4.540	28.786	34.292	34.582
BSh	14.393	5.892	4.347	24.149	3.961	0.097	7.341	3.381	4.057	29.076	6.375	0.386	34.389	0.097	0.000
Cwa	34.389	60.760	56.799	26.468	6.472	5.892	53.225	38.156	30.525	12.364	30.428	33.519	8.984	0.193	0.193
Cwb	17.871	43.566	56.799	0.290	0.000	5.892	5.796	5.120	10.529	13.620	33.036	30.718	18.160	5.409	2.318

TABLE 10.6
Areal Distribution of AOD and CF for Each Climatic Region Under Heavy Rain in 100,000 ha

Climatic region	AOD						CF								
	Low			Moderate			Low			Moderate			High		
	5 year	10 year	15 year	5 year	10 year	15 year	5 year	10 year	15 year	5 year	10-year	15-year	5-year	10-year	15-year
Aw	41.827	123.838	200.826	23.570	47.719	36.128	29.269	50.327	81.239	33.519	117.173	152.334	2.898	4.250	3.381
Am	2.029	10.626	11.688	–	0.483	0.290	–	–	–	0.193	2.125	2.608	1.835	8.984	9.370
BSh	4.057	23.473	44.628	10.433	18.740	14.393	9.660	21.831	33.713	4.637	19.996	25.212	0.193	0.386	0.097
Cwa	15.456	29.076	40.474	6.569	8.018	7.631	17.291	27.144	32.747	4.830	10.143	15.552	-	-	-
Cwb	17.194	30.332	34.679	–	–	–	8.211	7.824	10.626	8.790	21.155	23.473	0.193	1.352	0.580

35.7% in 2000 to 40.3% in 2020. Similarly, urban areas have grown from 3.3% in 2000 to 6.2% in 2020. In contrast, grassland has decreased from 30.3% in 2000 to 23.9% in 2020, primarily due to the increase in cropland and urban development. The analysis also showed that the rainfall trends in the study area during the monsoon period have exhibited a slight decreasing trend since 2005.

Figure 10.3 shows the changes in land use and precipitation across the five climate zones of the study area. The primary land use type in the monsoon (Am) region is forest. Although more than 1000 mm of rainfall was recorded in 2010, the high percentage of forest cover remained stable, indicating minimal changes in land use despite fluctuations in rainfall. This suggests that forests may play a buffering role in land-atmosphere feedback against rainfall variability (Sridhar and Valaymkunnath, 2018). In the tropical savanna (Aw) region, more than 30% of the land is cropland, which has been steadily increasing since 2005. The annual rainfall during the monsoon period ranges from 880 mm to 1090 mm, with the highest rainfall recorded in 2010. The abundant rainfall in 2010 likely contributed to the increase in cropland. The warm semi-arid (Bsh) region, which experiences relatively low rainfall during the monsoon period, also has over 50% of its land as cropland. Similar to the Aw region, cropland is increasing while grassland is decreasing. This indicates that agricultural land management in semi-arid areas is adapting to changes in rainfall. In the humid subtropical (Cwa) region, higher rainfall was recorded in 2020 than in 2010. The majority of land use comprises cropland (32–36%), forest (31%), and grassland (25–31%). There is a trend of increasing cropland and decreasing grassland. In the subtropical oceanic highland (Cwb) region, cropland and forest are the primary land use types, with grassland also occupying a significant portion. Following high

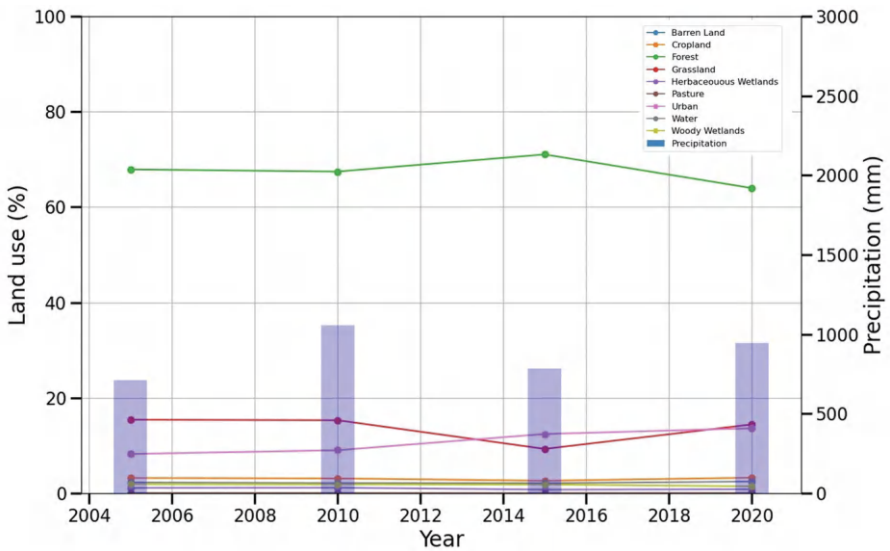

FIGURE 10.3 Land use and precipitation change of study area with an example of monsoon (Am) climate.

rainfall in 2010, the percentage of grassland gradually decreased, while urban areas increased. Across all five regions, urban areas have steadily increased over the past 15 years.

The land cover and land use analysis reveals that the monsoon (Am) region, predominantly composed of mountainous areas, exhibited the highest CF across all rainfall regimes. This suggests that the forest areas in this region contribute to higher rainfall amounts compared to other regions. The subtropical oceanic highland (Cwb) region also showed high CF in the moderate and heavy rain regimes, indicating that the significant cropland and forest areas in the Cwb region lead to higher rainfall. The decreasing trend in rainfall in the study area could be associated with increased urban development. The decrease in grassland and the increase in urban areas can reduce evapotranspiration, leading to reduced rainfall. While Southern India, with its primarily consisting of cropland, grassland, and forest, appears to be less affected by land use changes, unregulated conversion of cropland and urban development reduces grassland areas, making it challenging to respond to sudden rainfall changes during the monsoon period. Therefore, strategic measures are needed to address these issues.

10.5 CONCLUSION

The effect of atmospheric stability and AOD on the macrophysical properties of warm clouds in southern India was studied from 2005 to 2019. The effect of AOD on precipitation was also studied for cumulative 5-year, 10-year, and 15-year data.

The results of the cumulative data show a positive relationship between AOD and CF. The correlation is lower for cumulative 10-year data and higher for cumulative 15-year data. Although there is a positive relationship for all atmospheric stability states, a significant correlation is observed in cumulative 10-year and 15-year data for isolated thunderstorm states. The widely scattered thunderstorm state showed a significant correlation over 5 years. This could be due to emissive aerosols. Emissive aerosols do not absorb solar radiation, amplified by their presence in clouds. This effect slows cloud droplet evaporation and increases cloud coverage in the study area.

The spatial distribution of AOD and CF in light, moderate, and heavy rain regimes is also plotted for cumulative 5-year, 10-year, and 15-year data for various Koppen-classified climatic regions. The distribution of AOD in the study area is found to be low to moderate. In addition, for cumulative 10-year and 15-year data, there is an increase in the overall distribution of lower AOD in light rain areas of about 12% and 16%, respectively. In contrast, the moderate distribution of AOD decreased by 28% and 60% for the cumulative datasets. Similarly, in the moderate rain regime, there was an increase of 32% and 47% in lower AOD and a decrease of 36% and 42% in moderate AOD.

For cumulative 10-year and 15-year data, the overall CF corresponding to light rain regimes in the moderate range increased by 9% and 16%, respectively, while the higher range decreased by 2% and 14%. As a result, moderate CF in the moderate region increased by 17 percent, while higher CF decreased by 8 percent and increased by 4 percent. The distribution of AOD and CF in light rain is most visible in the tropical savanna region, followed by the warm semi-arid climate region, whereas in moderate rain, the tropical savanna climate region and

the humid subtropical climate region were most visible. The lower AOD found a threefold increase in value when compared to the cumulative 5-year dataset in the heavy rain regime. The moderate AOD in heavy rain has increased by 84% and 44% for cumulative 10-year and 15-year datasets, respectively. Under heavy rain, there was also a noticeable increase in low and moderate CF for the entire study area. The rise in AOD and CF could be attributed to emissions from industries that produce a lot of sulfates and nitrate aerosols. The consideration of atmospheric stability for establishing a relationship between AOD and CF is achieved for different rainfall regimes of peninsular India. Also, the current study contributes to a better understanding of cloud behavior for various AOD loadings in each climate region. The moderate and heavy loading of AOD has a significant impact on cloud fraction and, thus, indirectly on precipitation of the study area. The research can be expanded to understand the type of aerosol that influences cloud formation and precipitation in a specific climatic region.

The analysis of land use changes and precipitation trends in Southern India from 2005 to 2020 has provided significant insights into the region's climatic dynamics. As observed, cropland and urban areas have consistently increased, while grassland areas have decreased. This shift in land use is primarily driven by agricultural expansion and urban development. The monsoon (Am) region, predominantly covered by forests, has shown minimal land use changes despite fluctuations in precipitation. This indicates that forests play a crucial role in buffering against precipitation variability. In contrast, regions like the tropical savanna (Aw) and warm semi-arid (Bsh) have seen substantial increases in cropland at the expense of grassland, reflecting adaptive agricultural management practices in response to precipitation patterns. The observed decrease in precipitation since 2005 can be partially attributed to the increase in urban areas, which reduces evapotranspiration and rainfall. This trend underscores the need for strategic land use planning and management to mitigate the adverse effects of urbanization on regional precipitation patterns.

ACKNOWLEDGEMENTS

The corresponding author's (V. Sridhar) effort was funded in part by the Virginia Agricultural Experiment Station (Blacksburg) and through the Hatch Program of the National Institute of Food and Agriculture at the United States Department of Agriculture (Washington, DC) and in part as a Fulbright-Nehru senior scholar funded by the United States India Educational Foundation.

REFERENCES

Adam, M.G., Tran, P.T. and Balasubramanian, R. (2021) Air quality changes in cities during the COVID-19 lockdown: A critical review. *Atmospheric Research*, 264, p. 105823.

Anil, S., Manikanta, V. and Pallakury, A.R. (2021) Unravelling the influence of subjectivity on ranking of CMIP6 based climate models: A case study. *International Journal of Climatology*, 41(13), pp. 5998–6016.

Balakrishnaiah, G., Reddy, B.S.K., Gopal, K.R., Reddy, R.R., Reddy, L.S.S., Swamulu, C., Ahammed, Y.N., Narasimhulu, K., KrishnaMoorthy, K. and Babu, S.S. (2012)

Spatio-temporal variations in aerosol optical and cloud parameters over Southern India retrieved from MODIS satellite data. *Atmospheric Environment*, 47, pp. 435–445.

Borbas, E.E., Seemann, S.W., Kern, A.N.I.K.O., Moy, L.E.S.L.I.E., Li, J., Gumley, L.I.A.M. and Menzel, W.P. (2011) MODIS atmospheric profile retrieval algorithm theoretical basis document [online]. Available at: http://modis-atmos.gsfc.nasa.gov/MOD07_L2/atbd.html [Accessed 10 August 2015].

Chen, Y.C., Christensen, M.W., Stephens, G.L. and Seinfeld, J.H. (2014) Satellite-based estimate of global aerosol–cloud radiative forcing by marine warm clouds. *Nature Geoscience*, 7(9), pp. 643–646.

Chen, S., Jiang, N., Huang, J., Xu, X., Zhang, H., Zang, Z., Huang, K., Xu, X., Wei, Y., Guan, X. and Zhang, X. (2018) Quantifying contributions of natural and anthropogenic dust emission from different climatic regions. *Atmospheric Environment*, 191, pp. 94–104.

Constantino, L. and Bréon, F.M. (2013) Aerosol indirect effect on warm clouds over South-East Atlantic, from co-located MODIS and CALIPSO observations. *Atmospheric Chemistry and Physics*, 13(1), pp. 69–88.

David, L.M., Ravishankara, A.R., Kodros, J.K., Venkataraman, C., Sadavarte, P., Pierce, J.R., Chaliyakunnel, S. and Millet, D.B. (2018) Aerosol optical depth over India. *Journal of Geophysical Research: Atmospheres*, 123(7), pp. 3688–3703.

Edenhofer, O. ed. (2015) *Climate change (2014) Mitigation of climate change*. Cambridge University Press.

Gopal, K.R., Reddy, K.R.O., Balakrishnaiah, G., Arafath, S.M., Reddy, N.S.K., Rao, T.C., Reddy, T.L. and Reddy, R.R. (2016) Regional trends of aerosol optical depth and their impact on cloud properties over Southern India using MODIS data. *Journal of Atmospheric and Solar-Terrestrial Physics*, 146, pp. 38–48.

Grandey, B.S., Stier, P. and Wagner, T.M. (2013) Investigating relationships between aerosol optical depth and CF using satellite, aerosol reanalysis and general circulation model data. *Atmospheric Chemistry and Physics*, 13(6), pp. 3177–3184.

Jaksa, W.T., Sridhar, V., Huntington, J.L. and Khanal, M. (2013) Evaluation of the complementary relationship using Noah Land Surface Model and North American Regional Reanalysis (NARR) data to estimate evapotranspiration in semiarid ecosystems. *Journal of Hydrometeorology*, 14(1), pp. 345–359.

Kant, S., Panda, J. and Gautam, R. (2019) A seasonal analysis of aerosol-cloud-radiation interaction over Indian region during 2000–2017. *Atmospheric Environment*, 201, pp. 212–222.

Koren, I., Kaufman, Y.J., Rosenfeld, D., Remer, L.A. and Rudich, Y. (2005) Aerosol invigoration and restructuring of Atlantic convective clouds. *Geophysical Research Letters*, 32(14), pp. 1–4.

Koren, I., Remer, L.A., Altaratz, O., Martins, J.V. and Davidi, A. (2010) Aerosol-induced changes of convective cloud anvils produce strong climate warming. *Atmospheric Chemistry and Physics*, 10(10), pp. 5001–5010.

Kotrike, T., Pratap, D. and Keesara, V.R. (2021) Validation and trend analysis of satellite-based AOD data over Southern India. *Aerosol Science and Engineering*, 5(1), pp. 32–43.

Kottek, M., Grieser, J., Beck, C., Rudolf, B. and Rubel, F. (2006) World map of the Köppen-Geiger climate classification updated. *Meteorologische Zeitschrift*, 15(3), pp. 259–263.

Kourtidis, K., Stathopoulos, S., Georgoulias, A.K., Alexandri, G. and Rapsomanikis, S. (2015) A study of the impact of synoptic weather conditions and water vapor on aerosol–cloud relationships over major urban clusters of China. *Atmospheric Chemistry and Physics*, 15(19), pp. 10955–10964.

Kumar, A. (2013) Variability of aerosol optical depth and cloud parameters over North Eastern regions of India retrieved from MODIS satellite data. *Journal of Atmospheric and Solar-Terrestrial Physics*, 100, pp. 34–49.

Kumar, A. (2020) Spatio-temporal variations in satellite based aerosol optical depths & aerosol index over Indian subcontinent: Impact of urbanization and climate change. *Urban Climate*, 32, p. 100598.

Kucienska, B., Raga, G.B. and Romero-Centeno, R. (2012) High lightning activity in maritime clouds near Mexico. *Atmospheric Chemistry and Physics*, 12(17), pp. 8055–8072.

Liu, Q., Cheng, N., He, Q., Chen, Y., Liu, T., Liu, X., Zhang, H., Li, J. and Zhan, Q. (2020) Meteorological conditions and their effects on the relationship between aerosol optical depth and macro-physical properties of warm clouds over Shanghai based on MODIS. *Atmospheric Pollution Research*, 11(9), pp. 1637–1644.

Metz, B., Davidson, O., Swart, R. and Pan, J. eds. (2001) *Climate change 2001: Mitigation: Contribution of Working Group III to the third assessment report of the Intergovernmental Panel on Climate Change*. Cambridge University Press.

Mishra, A.K. (2019) Quantifying the impact of global warming on precipitation patterns in India. *Meteorological Applications*, 26(1), pp. 153–160.

Misumi, R., Uji, Y., Miura, K., Mori, T., Tobo, Y. and Iwamoto, Y. (2022) Classification of aerosol-cloud interaction regimes over Tokyo. *Atmospheric Research*, 272, p. 106150.

Platnick, S., King, M.D., Meyer, K.G., Wind, G., Amarasinghe, N., Marchant, B., Arnold, G.T., Zhang, Z., Hubanks, P.A., Ridgway, B. and Riedi, J. (2015) MODIS cloud optical properties: User guide for the Collection 6 Level-2 MOD06/MYD06 product and associated Level-3 Datasets. *Version*, 1, p. 145.

Ramanathan, V., Crutzen, P.J., Kiehl, J.T. and Rosenfeld, D. (2001) Aerosols, climate, and the hydrological cycle. *Science*, 294(5549), pp. 2119–2124.

Remer, L.A., Kaufman, Y.J., Levin, Z. and Ghan, S. (2002) Model assessment of the ability of MODIS to measure top-of-atmosphere direct radiative forcing from smoke aerosols. *Journal of the Atmospheric Sciences*, 59(3), pp. 657–667.

Rosenfeld, D., Lohmann, U., Raga, G.B., O'Dowd, C.D., Kulmala, M., Fuzzi, S., Reissell, A. and Andreae, M.O. (2008) Flood or drought: How do aerosols affect precipitation?. *Science*, 321(5894), pp. 1309–1313.

Setti, S., Maheswaran, R., Radha, D., Sridhar, V., Barik, K.K. and Narasimham, M.L. (2020b) Attribution of hydrologic changes in a tropical river basin to climate and land use change: A case study from India. *ASCE Journal of Hydrologic Engineering*, 25(8), doi: 10.1061/(ASCE)HE.1943-5584.0001937.

Setti, S., Maheswaran, R., Sridhar, V., Barik, K.K., Merz, B. and Agarwal, A. (2020a). Intercomparison of gauge-based gridded data, reanalysis and satellite precipitation product with an emphasis on hydrological modelling. *Atmosphere*, 11, p. 1252, doi: 10.3390/atmos11111252.

Sheng, Z., Che, H., Chen, Q., Liu, D., Wang, Z., Zhao, H., Gui, K., Zheng, Y., Sun, T., Li, X. and Liu, C. (2019) Aerosol vertical distribution and optical properties of different pollution events in Beijing in autumn 2017. *Atmospheric Research*, 215, pp. 193–207.

Small, J.D., Jiang, J.H., Su, H. and Zhai, C. (2011) Relationship between aerosol and cloud fraction over Australia. *Geophysical Research Letters*, 38(23), pp. 1–7.

Soni, A.R. and Chandel, M.K. (2020) Impact of rainfall on travel time and fuel usage for Greater Mumbai city. *Transportation Research Procedia*, 48, pp. 2096–2107.

Sridhar, V. (2013) Tracking the influence of irrigation on land surface fluxes and boundary layer climatology. *Journal of Contemporary Water Research & Education*, 152, pp. 79–93, doi: 10.1111/j.1936-704X.2013.03170.x.

Sridhar, V. and Anderson, K.A. (2017) Human-induced modifications to boundary layer fluxes and their water management implications in a changing climate. *Agricultural and Forest Meteorology*, 234, pp. 66–79, doi: 10.1016/j.agrformet.2016.12.009.

Sridhar, V., Jin, X. and Jaksa, W.T. (2013) Explaining the hydroclimatic variability and change in the Salmon River basin. *Climate Dynamics*, 40, pp. 1921–1937, doi: 10.1007/s00382-012-1467-0.

Sridhar, V. and Valayamkunnath, P. (2018) Land-atmosphere interactions in South Asia: A regional earth systems perspective: Chapter 30. In K.P. Vadrevu et al., eds. *Land-atmospheric research applications in South and Southeast Asia* (pp. 699–712). Springer Remote Sensing/Photogrammetry, doi: 10.1007/978-3-319-67474-2_30.

Sridhar, V. and Wedin, D.A. (2009) Hydrological behavior of Grasslands of the Sandhills: Water and energy balance assessment from measurements, treatments and modeling. *Ecohydrology*, 2, pp. 195–212, doi: 10.1002/eco.61.

Twomey, S. (1977) The influence of pollution on the shortwave albedo of clouds. *Journal of Atmospheric Sciences*, 34, pp. 1149–1152.

Valayamkunnath, P., Sridhar, V., Zhao, W. and Allen, R.G. (2018) Intercomparison of surface energy fluxes, soil moisture, and evapotranspiration from eddy covariance, large-aperture scintillometer, and modeling across three ecosystems in a semiarid climate. *Agricultural and Forest Meteorology*, 248, pp. 22–47.

Varpe, S.R., Mahajan, C.M. and Kolhe, A.R. (2022) Aerosol–cloud interaction over South-Central India and adjoining coastal areas. *Aerosol Science and Engineering*, 6, pp. 45–60.

Vijayakumar, K., Devara, P.C.S., Giles, D.M., Holben, B.N., Rao, S.V.B. and Jayasankar, C.K. (2018) Validation of satellite and model aerosol optical depth and precipitable water vapour observations with AERONET data over Pune, India. *International Journal of Remote Sensing*, 39(21), pp. 7643–7663.

Wang, F., Guo, J., Zhang, J., Huang, J., Min, M., Chen, T., Liu, H., Deng, M. and Li, X. (2015) Multi-sensor quantification of aerosol-induced variability in warm clouds over eastern China. *Atmospheric Environment*, 113, pp. 1–9.

Zhang, X., Cai, C., Hu, X.M., Gao, L., Xu, X., Hu, J. and Chen, H. (2022) Aerosols consistently suppress the convective boundary layer development. *Atmospheric Research*, 269, p. 106032.

11 The Role of Land Cover/Land Use in Malaria Transmission in Myanmar

Amanda Hoffman-Hall

11.1 INTRODUCTION

As the scientific community's ability to map and monitor land cover and land use change (LCLUC) has advanced, so too has our ability to understand the complex interactions between LCLUC and the environment including weather and climate, hydrology, carbon and nutrient cycling, habitat loss and fragmentation, biodiversity, and other Earth systems (Bergen et al., 2020; de Beurs & Henebry, 2004; Chen et al., 2014; Justice et al., 2015; Nakalembe et al., 2022; Rappaport et al., 2018; Shevade et al., 2017; Thieme et al., 2020; Zalles et al., 2021, among others). Land cover and land use have been recognized as prominent factors impacting human health worldwide for decades (McFarlane et al., 2013; Myers, 2012; Orlov et al., 2023), and they are known to play a dominant role in outbreaks of various vector-borne and zoonotic diseases (Morand & Lajaunie, 2021). In malaria risk assessments, LCLUC significantly impacts vector habitat suitability and host availability (Debebe et al., 2018; Munga et al., 2009). For example, ecological disturbances such as forest loss have been shown to alter existing host–vector–parasite relationships (Rice et al., 2018; Sutherst, 2004), including the creation of new habitats for parasites and their vectors (Patz et al., 2008). Land use patterns have also been used to describe how humans are exposed to pathogenic vectors (Hoffman-Hall et al., 2023; Vanwambeke et al., 2007). For example, human modification of natural landscapes can bring humans directly into areas of high vector prevalence, dramatically increasing the risk of disease transmission, both immediately and delayed, when seasonal migrant workers return to populated areas (Tilaye et al., 2022). However, land use is often not prominently featured in disease ecology (Vanwambeke et al., 2019) and is generally considered an external factor influencing malaria transmission (Fornace et al., 2021). This omission could be partially explained by the exceptional complexity of human–environment interaction and the lack of knowledge about the spatially- and culturally-explicit interactions between people and their surrounding landscape. While extensive spatially representative socio-demographic surveys of land use are prohibitively time-consuming and expensive, maps derived from satellite earth observations can serve as

DOI: 10.1201/9781003396260-11

clear indicators for human activities on the landscape, increasing the ability to assess exposure successfully (Hoffman-Hall et al., 2020; Wimberly et al., 2021).

The relationship between LCLUC and malaria is particularly complex and, at times, appears to have contradictory impacts on the occurrence of malaria. Early research observed a reduction of the malaria vector *Anopheles nili* alongside deforestation in Africa (Guerra et al., 2006). However, during a rapid land use change in Rondônia, Brazil, de Castro et al. (2006) explored the complicated phenomenon of "frontier malaria," determining that malaria risk varies significantly with LCLUC across spatiotemporal scales. During an initial frontier expansion phase of rapid deforestation, the resulting ecosystem transformations increased larval habitats of *Anopheles darlingi*, one of the significant mosquito species responsible for malaria in the Amazonian region. Rapid deforestation has been continually demonstrated to lead to favorable conditions for other malaria vectors, such as *Anopheles gambiae, Anopheles funestus,* and others (Burkett-Cadena & Vittor, 2018).

As the vector populations surge, mosquito–human interactions spike, dramatically increasing malaria incidence. Such patterns have been observed globally in frontier regions experiencing large-scale land-use transformations, including East Africa (Himeidan & Kweka, 2012; Lindblade et al., 2000; Rice et al., 2018), Amazonia (Basurko et al., 2013; de Castro et al., 2006; MacDonald & Mordecai, 2019), and Southeast Asia (Grigg et al., 2017; Tangena et al., 2016; Yasuoka & Levins, 2007). However, as time progresses and land use advances toward establishing agriculture and urban development, malaria transmission is substantially reduced (de Castro et al., 2006; Laporta et al., 2021; Valle & Clark, 2013). Reduction is not elimination, however, and new infection risk remains, primarily driven by land use behavioral factors. As the World Health Organization aims to eradicate malaria globally, understanding the relationship between LCLUC and malaria remains a high priority.

The country of Myanmar (Figure 11.1) connects South and Southeast Asia. The country is currently experiencing land use transformations similar to those regions described previously. Between 2002 and 2014, Myanmar's intact forests declined at a rate of 0.94% annually, totaling more than 2 million ha of forest loss due to the combined pressures of severe logging, conversion to agriculture and plantations, and general degradation due to human encroachment (Bhagwat et al., 2017). However, a history of diplomatic isolation has resulted in little research concerning how this rapid development and land conversion may impact malaria in the country.

In 2012, Myanmar improved its international relations, leading to fruitful collaborations between international research teams and the Myanmar National Malaria Control Programme. During this time, Myanmar's government achieved incredible malaria reduction success, reducing malaria cases by a staggering 95% from 2012 to 2020 (WHO, 2021). However, as of 2023, Myanmar bears the highest malaria burden in the Greater Mekong Subregion, experiencing a nearly sixfold increase in the malaria mortality rate from 2021 to 2022, likely related to the political upheaval that occurred in 2021 (WHO, 2023). Much of the work described in this paper was completed before this most recent political turmoil. While the observed malaria increase in 2022 is disheartening, the work presented here on investigating the role of LCLUC in malaria transmission represents tools and insights that can be

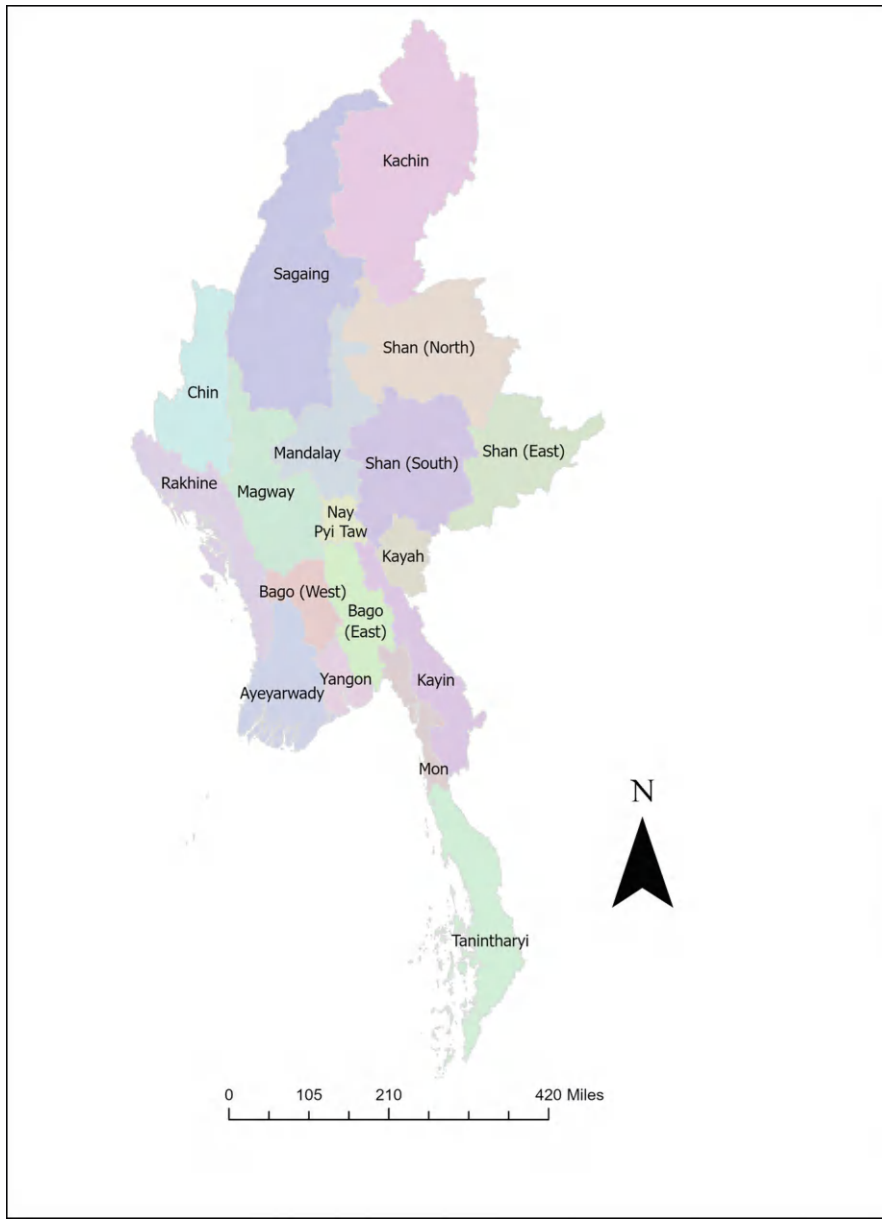

FIGURE 11.1 Myanmar.

applied to malaria intervention in-country to regain some of the lost ground in the fight against malaria in Myanmar.

11.2 RECENT ADVANCES IN LCLUC MAPPING IN MYANMAR

Remote sensing technologies have dramatically advanced data availability in Myanmar, increasing the ability to determine the relationship between LCLUC and malaria. Myanmar is considerably data-poor, coinciding with a long history of political and economic isolation (Hoffman-Hall et al., 2019). However, this isolation has resulted in some of the most expansive swaths of intact forests across the globe. Following the desire to determine the level of intact forests in-country, early LCLUC mapping attempts focused on forests. The earliest systematic assessment of forest cover was conducted by Leimgruber et al. (2005), and further forest change was investigated by Bhagwat et al. (2017). Both studies identified increasing deforestation hotspots, particularly as diplomatic isolation began to end and political and economic reforms led to increases in large-scale resource extraction, timber production, and commercial plantations, placing more significant pressures on remaining forests (Rao et al., 2013).

Data on other land cover types, particularly human settlements, remained sparse. Myanmar has attempted four recent censuses (1973, 1983, 2014, 2023), each plagued by political instability, civil wars, and boycotts (RFA Burmese, 2023). However, satellite earth observations have allowed significant success in mapping population distribution across other countries – previously unattainable without conducting a resource-intensive census – especially for urban areas. Nevertheless, considerable gaps still exist for rural and remote populations globally, which experience a disproportionate share of adverse health outcomes (Suwonkerd et al., 2013) and can serve as the main drivers of infectious disease transmission, such as malaria, into previously disease-free regions (Martens & Hall, 2000). The United Nations estimates that 70% of Myanmar's population lives in rural areas ("Country profile," 2016), with the most remote areas of Myanmar, typically the mountainous border regions, home to minority ethnic groups such as the Shan, Rohingya, and Chin, where vague land tenure policies result in dynamic settlements, which are constantly moving to locate work. Accurately and consistently mapping the population is critically important but nearly impossible via census under current conditions.

Developing a cost-effective approach to mapping and monitoring the population distribution and engagement with the land, with a previously un-emphasized focus on rural areas, was critical in identifying people at risk of malaria. Hoffman-Hall et al. (2019) used satellite remote sensing to address this data gap in a cost-effective and repeatable way. Previous global coarse-resolution mapping attempts (Bartholomé & Belward, 2005; Elvidge et al., 2001), combined satellite and auxiliary data sets (Dobson et al., 2000; Doxsey-Whitfield et al., 2015; Frye et al., 2018; Gaughan et al., 2013), and moderate-resolution human settlement grids (Pesaresi et al., 2015) are helpful in studies conducted at sub-continental to global scales, especially in urban areas, but, it was determined that their output resolutions limit their ability to map small, isolated rural settlements with fine spatial precision. Similarly, very high

resolution (VHR) satellite data was limited due to a lack of a VHR dataset with a high repeat frequency and free public availability, limiting the usability of VHR in resource-poor Myanmar. Hoffman-Hall et al. (2019) argued that moderate spatial resolution remote sensing data (10–90 m) could offer a compromise between the fine spatial resolution of VHR data and the frequent temporal resolution of coarse spatial resolution data.

However, at the moderate resolution, settlements will present a mixed spectral signal of roof material, trees, bare ground, and other minor signals. For this reason, Landsat and other moderate-resolution datasets had previously been considered insufficient to map small human settlements (particularly those < 30 m across in size, smaller than the dimensions of a Landsat pixel). Indeed, mapping structural properties (such as metal roofs vs. thatched roofs) remains challenging due to these spectral constraints. Hoffman-Hall et al. (2019) took advantage of long-standing archaeological methods, where ancient human settlements are most often discovered in areas with modern-day favorable settlement conditions, such as areas of shallow slopes close to fresh water. Applying this framework to contemporary settlements, spectral signatures were combined with contextual human behavior information to bolster the limited spectral separability of the fine-scale built environment signal within 30 m pixels for a remote region in Myanmar, Ann Township, which houses a highly mobile population of isolated rural communities. Auxiliary geospatial data that describes relationships common to human settlements were incorporated, for example, distance to roads, distance to water sources, elevation, and distance to recent active fire as mapped by either the Moderate Resolution Imaging Spectroradiometer (MODIS) (Giglio et al., 2016) or Visible Infrared Imaging Radiometer Suite (VIIRS) active fire products (Schroeder et al., 2014). Active fire detection via satellite was identified as a highly valuable data source due to the widespread slash-and-burn land clearing and management practices (*taungya*) (FAO, 2020). Although Myanmar has considerable wildfire occurrence, nearly all fires are ignited by people (Lay, 2022) and, therefore, serve as a strong indicator of human presence in the landscape since fire is otherwise not natural in deciduous tropical forests (Murphy & Lugo, 1986). This fusing of moderate-resolution satellite earth observations with auxiliary geospatial datasets successfully located settlements across Ann Township, significantly increasing the number of rural settlements over previous census results.

Building on the successful mapping of Ann Township settlements, the methodology was refined and expanded to identify settlements across the country. Chen et al. (2021) developed a land cover classification map for all of Myanmar, explicitly supporting malaria research and interventions. Therefore, the classification scheme prioritized land cover classes related to human exposure to malaria vectors and classes associated with the habitat suitability of the malaria vector. Through the implementation of a hierarchical classification scheme alongside the locally significant village algorithm, a land cover classification was produced that offered a more spatially comprehensive representation of classes related to human presence than other similar datasets, such as the SERVIR Mekong land cover dataset (Saah et al., 2020), Global Human Settlement Layer (Corbane et al., 2019), and Global Human Built-up and Settlement Extent (Wang, 2017).

11.3 CONNECTING LCLUC TO MALARIA

Several human behaviors and activities have been linked to increased exposure to vector-borne diseases across the globe. In French Guiana, mining has been associated with leptospirosis, logging with cutaneous leishmaniasis, and slash-and-burn agriculture with hantavirus pulmonary syndrome (de Thoisy et al., 2021). In Belgium, forest and farm workers have an increased risk of nephropathia epidemica and Lyme borreliosis (Barrios et al., 2012). For malaria in the Greater Mekong Subregion specifically, forest work and staying in the forest overnight have been shown to increase the risk of malaria in Vietnam (Erhart et al., 2005), while short- and long-term forest workers were a high-risk group in Lao PDR (Kounnavong et al., 2017). Similarly, rubber farmers and tappers in Thailand have increased exposure to malaria vectors (Bhumiratana et al., 2013). Narrowing further to Myanmar, forest-related activities, including agriculture, wood, and bamboo cutting, have been associated with an increased risk of malaria (Soe et al., 2017; Zaw et al., 2017). However, collecting this type of occupational and activity data is generally cost-prohibitive. Therefore, capturing potential occupation- or livelihood-related malaria exposure is desirable through satellite-based LCLUC mapping. LCLUC maps can be used as a proxy for human activity on the landscape, allowing for incorporating livelihood exposure metrics into malaria models.

Recent work in Myanmar (Chen et al., 2021; Hoffman-Hall et al., 2023; Hoffman-Hall et al., 2020; Li et al., 2023; Shevade et al., 2021) has sought to contextualize moderate-resolution remotely sensed land cover data using survey data that questions how people live, work, and travel through their landscape, to define criteria for easy-to-implement remote sensing methodologies that can increase the efficiency of targeted malaria elimination strategies. Participants were surveyed on the frequency, duration, and timing of six land use activities: (1) attending to crops/farming; (2) working at plantations; (3) working at mining areas; (4) traveling to refugee camps; (5) conducting household chores that involve trips to the water; and (6) conducting household chores that involve trips to the forest (e.g., hunting, firewood and construction material collection, fruit gathering). Participants were also asked how far they traveled to work and what times of day they conducted this travel. Each participant provided their primary occupation, indicating if that occupation was primarily indoor or outdoor and if it was seasonal. Lastly, all participants provided a blood sample to reveal the presence of malaria parasites in their blood.

To determine which land covers are most significantly linked with malaria, a 2 km radius surrounding the participants' village center was selected to be the spatial unit analyzed, consistent with the flight range of *Anopheles dirus*, the principal malaria vector in Myanmar (Oo, 2003). For residents of Ann Township, Myanmar, the odds of malaria infection increased by 1.96 per 1 square kilometer increase in natural forest cover near their village of residence (OR: 1.96, 95% CI: 1.60–2.41) (Hoffman-Hall et al., 2020). Conversely, villagers living near croplands experienced decreased malaria risk unless they were directly engaged in farm work. However, it was surmised that the "protective" effect of croplands is due to the minimizing of the "riskier" LC, natural forest, and not necessarily an indication that croplands are "safe" (Hoffman-Hall et al., 2020).

Following the increased risk of malaria for participants living near an area of high natural forest land cover, the land use factors that contributed most significantly to increased malaria risk were those that put people in direct contact with forests, including conducting forest chores, having an outdoor job, and having a primary occupation in the logging and plantation industry (Hoffman-Hall et al., 2023). Beyond participating in forest work, forest workers also encountered the highest malaria exposures in their daily travel patterns (Li et al., 2023). However, participants engaged in a wide diversity of land use activities outside of their primary occupation, with many participants who did not claim forest-related occupations interacting with the forest environment in other ways, such as through chores (Shevade et al., 2021). For the non-working population, day-to-day chores constituted their primary landscape interaction, with survey respondents identifying as students and dependents also engaged in land use activities through water – and forest-related household chores in addition to farming and plantation work. In regions with high levels of individual land use behavior diversity, remote sensing is a powerful tool for identifying areas where people may come into contact with land cover types not immediately apparent from their primary occupation title.

These results naturally point to a potential link between deforestation and malaria. Similar to the high deforestation rates between 2002–2014 (Bhagwat et al., 2017), the study region experienced significant forest cover loss as mapped by the Global Forest Change dataset (Hansen et al., 2013) from 2014–2018. Notably, one village lost 3.86 sq km of forest out of the 12.56 sq km village analysis area during this period (Hoffman-Hall et al., 2023). However, no significant association between the amount of local deforested land and malaria was found, except for a substantial decrease in the risk of malaria for villagers living in an area with high amounts of deforestation within the year of blood sample data collection (2018).

These results could be explained by the differential vector abundances in the future land use of a deforested area. For example, the land cover results indicate that forested landscapes allow for higher malaria exposure than croplands; therefore, if the deforested site is later converted to croplands, it could lower the risk of malaria for that area. However, a high amount of forest conversion in Myanmar is clearing natural forests for conversion to plantation. A study from along the China-Myanmar border found that the pupation rate of *Anopheles minimus* increased from 3.8% in natural forest (tropical rainforest) to 12.5% in banana plantations to a substantially higher 52.5% in deforested areas (X. Wang et al., 2016). To our knowledge, no such study exists for the natural bamboo and mixed deciduous forests of Ann Township, nor the rubber and teak plantations that dominate. However, it is highly likely that these factors greatly influence vector abundance. A study that quantifies vector species abundance along the continuum of forest, to clear, to cropland, or plantation would be a welcome addition to the literature. The large number and diversity of Anopheles species (>20) known to transmit malaria in Southeast Asia (Van Dung et al., 2023) make it extremely difficult to develop a detailed understanding of the impact of LCLUC on malaria-transmitting vectors and their populations. However, this understanding is critical for the malaria elimination agenda as new evidence emerges of changes in mosquito biting behavior and, subsequently, the effectiveness

of existing protective interventions. Satellite remote sensing lends itself well to procuring the necessary land cover time series analysis to assess this relationship.

11.4 CONCLUSIONS

Advances in LCLUC mapping via satellite remote sensing have significantly contributed to understanding malaria transmission in Myanmar. Amidst the recent political turmoil in Myanmar, employing remote sensing in land cover mapping has become even more critical for malaria elimination. The unrest has disrupted healthcare systems and hindered on-the-ground efforts to combat malaria and obtain data. As described here, remote sensing technologies have been pivotal in identifying and monitoring land cover and land use factors contributing to the spread of malaria. By utilizing remote sensing, health practitioners and researchers can gather essential data for accurate risk assessments, allowing for targeted interventions and resource allocation even in areas that may be difficult to access due to political instability. This technological approach becomes imperative for supporting the ongoing efforts to eliminate malaria, ensuring that public health initiatives can adapt to and address the challenges presented by the complex socio-political landscape in Myanmar.

REFERENCES

Barrios, J. M., Verstraeten, W. W., Maes, P., Clement, J., Aerts, J.-M., & Coppin, P. (2012). Trends in the spatial spread of nephropathia epidemica and Lyme borreliosis incidence in Belgium. In *Proceedings of the GIS Research UK* (pp. 25–32). University of Edinburgh. United Kingdom.

Bartholomé, E., & Belward, A. S. (2005). GLC2000: A new approach to global land cover mapping from Earth observation data. *International Journal of Remote Sensing*, *26*(9), 1959–1977. https://doi.org/10.1080/01431160412331291297

Basurko, C., Demattei, C., Han-Sze, R., Grenier, C., Joubert, M., Nacher, M., & Carme, B. (2013). Deforestation, agriculture and farm jobs: A good recipe for Plasmodium vivax in French Guiana. *Malaria Journal*, *12*(1), 90. https://doi.org/10.1186/1475-2875-12-90

Bergen, K. M., Loboda, T., Newell, J. P., Kharuk, V., Hitztaler, S., Sun, G., et al. (2020). Long-term trends in anthropogenic land use in Siberia and the Russian Far East: A case study synthesis from Landsat. *Environmental Research Letters*, *15*(10), 105007.

Bhagwat, T., Hess, A., Horning, N., Khaing, T., Thein, Z. M., Aung, K. M., et al. (2017). Losing a jewel—Rapid declines in Myanmar's intact forests from 2002-2014. *PLOS ONE*, *12*(5), e0176364.

Bhumiratana, A., Intarapuk, A., Sorosjinda-Nunthawarasilp, P., Maneekan, P., & Koyadun, S. (2013). Border malaria associated with multidrug resistance on Thailand-Myanmar and Thailand-Cambodia borders: Transmission dynamic, vulnerability, and surveillance. *BioMed Research International*, *2013*, 1–13.

Burkett-Cadena, N. D., & Vittor, A. Y. (2018). Deforestation and vector-borne disease: Forest conversion favors important mosquito vectors of human pathogens. *Basic and Applied Ecology*, *26*, 101–110. https://doi.org/10.1016/j.baae.2017.09.012

Chen, D., Loboda, T., Channan, S., & Hoffman-Hall, A. (2014). Long-term record of sampled disturbances in Northern Eurasian Boreal forest from pre-2000 Landsat data. *Remote Sensing*, *6*(7), 6020–6038. https://doi.org/10.3390/rs6076020

Chen, D., Shevade, V., Baer, A., He, J., Hoffman-Hall, A., Ying, Q., et al. (2021). A disease control-oriented land cover land use map for Myanmar. Data, *6*(6). https://doi.org/10.3390/data6060063

Corbane, C., Pesaresi, M., Kemper, T., Politis, P., Florczyk, A. J., Syrris, V., et al. (2019). Automated global delineation of human settlements from 40 years of Landsat satellite data archives. *Big Earth Data*, *3*(2), 140–169.

Country Profile. (2016, June 9). Retrieved February 29, 2024, from https://myanmar.unfpa.org/en/country-profile-0

de Castro, M. C., Monte-Mór, R. L., Sawyer, D. O., & Singer, B. H. (2006). Malaria risk on the Amazon frontier. *Proceedings of the National Academy of Sciences*, *103*(7), 2452–2457. https://doi.org/10.1073/pnas.0510576103

Debebe, Y., Hill, S. R., Tekie, H., Ignell, R., & Hopkins, R. J. (2018). Shady business: Understanding the spatial ecology of exophilic Anopheles mosquitoes. *Malaria Journal*, *17*(1), 351. https://doi.org/10.1186/s12936-018-2499-7

de Beurs, K. M., & Henebry, G. M. (2004). Land surface phenology, climatic variation, and institutional change: Analyzing agricultural land cover change in Kazakhstan. *Remote Sensing of Environment*, *89*(4), 497–509. https://doi.org/10.1016/j.rse.2003.11.006

Dobson, J. E., Bright, E. A., Coleman, P. R., Durfee, R. C., & Worley, B. A. (2000). LandScan: A global population database for estimating populations at risk. *Photogrammetric Engineering and Remote Sensing*, *66*(7), 849–857.

Doxsey-Whitfield, E., MacManus, K., Adamo, S. B., Pistolesi, L., Squires, J., Borkovska, O., & Baptista, S. R. (2015). Taking advantage of the improved availability of census data: A first look at the gridded population of the world, version 4. *Papers in Applied Geography*, *1*(3), 226–234.

Elvidge, C. D., Imhoff, M. L., Baugh, K. E., Hobson, V. R., Nelson, I., Safran, J., et al. (2001). Night-time lights of the world: 1994-1995. *ISPRS Journal of Photogrammetry and Remote Sensing*, *56*, 81–99. https://doi.org/10.1016/S0924-2716(01)00040-5

Erhart, A., Thang, N. D., Van Ky, P., Tinh, T. T., Van Overmeir, C., Speybroeck, N., et al. (2005). Epidemiology of forest malaria in central Vietnam: A large scale cross-sectional survey. *Malaria Journal*, *4*(1), 1–11.

FAO. (2020). Integrated National Strategic Action Plan on Fire Management in Myanmar–TCP/MYA/3608. Retrieved February 21, 2024, from www.fao.org/3/ca8777en/CA8777EN.pdf

Fornace, K. M., Diaz, A. V., Lines, J., & Drakeley, C. J. (2021). Achieving global malaria eradication in changing landscapes. *Malaria Journal*, *20*(1), 69. https://doi.org/10.1186/s12936-021-03599-0

Frye, C., Wright, D. J., Nordstrand, E., Terborgh, C., & Foust, J. (2018). Using classified and unclassified land cover data to estimate the footprint of human settlement. *Data Science Journal*, *17*, 1–12.

Gaughan, A. E., Stevens, F. R., Linard, C., Jia, P., & Tatem, A. J. (2013). High resolution population distribution maps for Southeast Asia in 2010 and 2015. *PLOS ONE*, *8*(2), e55882. https://doi.org/10.1371/journal.pone.0055882

Giglio, L., Schroeder, W., & Justice, C. O. (2016). The collection 6 MODIS active fire detection algorithm and fire products. *Remote Sensing of Environment*, *178*, 31–41. https://doi.org/10.1016/j.rse.2016.02.054

Grigg, M. J., Cox, J., William, T., Jelip, J., Fornace, K. M., Brock, P. M., et al. (2017). Individual-level factors associated with the risk of acquiring human Plasmodium knowlesi malaria in Malaysia: A case-control study. *The Lancet Planetary Health*, *1*(3), e97–e104. https://doi.org/10.1016/S2542-5196(17)30031-1

Guerra, C. A., Snow, R. W., & Hay, S. I. (2006). Mapping the global extent of malaria in 2005. *Trends in Parasitology*, *22*(8), 353–358.

Hansen, M. C., Potapov, P. V., Moore, R., Hancher, M., Turubanova, S. A., Tyukavina, A., et al. (2013). High-resolution global maps of 21st-century forest cover change. *Science*, *342*(6160), 850–853. https://doi.org/10.1126/science.1244693

Himeidan, Y. E., & Kweka, E. J. (2012). Malaria in East African highlands during the past 30 years: Impact of environmental changes. *Frontiers in Physiology*, *3*, 315. https://doi.org/10.3389/fphys.2012.00315

Hoffman-Hall, A., Loboda, T. V., Hall, J. V., Carroll, M. L., & Chen, D. (2019). Mapping remote rural settlements at 30 m spatial resolution using geospatial data-fusion. *Remote Sensing of Environment*, *233*, 111386. https://doi.org/10.1016/j.rse.2019.111386

Hoffman-Hall, A., Puett, R., Silva, J. A., Chen, D., Baer, A., Han, K. T., et al. (2020). Malaria exposure in Ann Township, Myanmar, as a function of Land Cover and Land Use: Combining satellite earth observations and field surveys. *GeoHealth*, *4*(12), e2020GH000299. https://doi.org/10.1029/2020GH000299

Hoffman-Hall, A., Puett, R., Silva, J. A., Chen, D., Bredder, A., Shevade, V., et al. (2023). Comparison of deforestation and forest land use factors for malaria elimination in Myanmar. *IJID Regions*, *8*, 75–83. https://doi.org/10.1016/j.ijregi.2023.06.006

Justice, C., Gutman, G., & Vadrevu, K. P. (2015). NASA Land Cover and Land Use Change (LCLUC): An interdisciplinary research program. *Journal of Environmental Management*, *148*, 4–9. https://doi.org/10.1016/j.jenvman.2014.12.004

Kounnavong, S., Gopinath, D., Hongvanthong, B., Khamkong, C., & Sichanthongthip, O. (2017). Malaria elimination in Lao PDR: The challenges associated with population mobility. *Infectious Diseases of Poverty*, *6*(1), 81.

Laporta, G. Z., Ilacqua, R. C., Bergo, E. S., Chaves, L. S. M., Rodovalho, S. R., Moresco, G. G., et al. (2021). Malaria transmission in landscapes with varying deforestation levels and timelines in the Amazon: A longitudinal spatiotemporal study. *Scientific Reports*, *11*(1), 6477. https://doi.org/10.1038/s41598-021-85890-3

Lay, L. (2022). About 95% of Forest Fires in Myanmar Caused by Human Error. Retrieved February 29, 2024, from https://myanmar.gov.mm/news-media/news/latest-news/-/asset_publisher/idasset354/content/about-95%2525-of-forest-fires-in-myanmar-caused-by-human-error

Leimgruber, P., Kelly, D. S., Steininger, M. K., Brunner, J., Müller, T., & Songer, M. (2005). Forest cover change patterns in Myanmar (Burma) 1990–2000. *Environmental Conservation*, *32*(4), 356–364. https://doi.org/10.1017/S0376892905002493

Li, Y., Stewart, K., Han, K. T., Han, Z. Y., Aung, P. P., Thein, Z. W., et al. (2023). Understanding spatiotemporal human mobility patterns for malaria control using a multiagent mobility simulation model. *Clinical Infectious Diseases*, *76*(3), e867–e874.

Lindblade, K. A., Walker, E. D., Onapa, A. W., Katungu, J., & Wilson, M. L. (2000). Land use change alters malaria transmission parameters by modifying temperature in a highland area of Uganda. *Tropical Medicine & International Health*, *5*(4), 263–274. https://doi.org/10.1046/j.1365-3156.2000.00551.x

MacDonald, A. J., & Mordecai, E. A. (2019). Amazon deforestation drives malaria transmission, and malaria burden reduces forest clearing. *Proceedings of the National Academy of Sciences*, *116*(44), 22212–22218.

Martens, P., & Hall, L. (2000). Malaria on the move: Human population movement and malaria transmission. *Emerging Infectious Diseases*, *6*(2), 103–109. https://doi.org/10.3201/eid0602.000202

McFarlane, R. A., Sleigh, A. C., & McMichael, A. J. (2013). Land-use change and emerging infectious disease on an Island Continent. *International Journal of Environmental Research and Public Health*, *10*(7), 2699–2719. https://doi.org/10.3390/ijerph10072699

Morand, S., & Lajaunie, C. (2021). Outbreaks of Vector-Borne and zoonotic diseases are associated with changes in forest cover and oil palm Expansion at global scale. *Frontiers in Veterinary Science*, *8*, 661063. https://doi.org/10.3389/fvets.2021.661063

Munga, S., Yakob, L., Mushinzimana, E., Zhou, G., Ouna, T., & Minakawa, N. (2009). Land use and land cover changes and spatiotemporal dynamics of anopheline larval habitats during a four-year period in a highland community of Africa. *Amercian Journal of Tropical Medicine and Hygiene*, *81*, 1–15. https://doi.org/10.4269/ajtmh.2009.09-0156

Murphy, P. G., & Lugo, A. E. (1986). Ecology of tropical dry forest. *Annual Review of Ecology and Systematics*, *17*(1), 67–88.

Myers, S. S. (2012). Land use change and human health. In J. C. Ingram, F. DeClerck, & C. Rumbaitis del Rio (Eds.), *Integrating ecology and poverty reduction: Ecological dimensions* (pp. 167–186). Springer. https://doi.org/10.1007/978-1-4419-0633-5_11

Nakalembe, C., Zubkova, M., Hall, J. V., Argueta, F., & Giglio, L. (2022). Impacts of large-scale refugee resettlement on LCLUC: Bidi Bidi refugee settlement, Uganda case study. *Environmental Research Letters*, *17*(6), 064019. https://doi.org/10.1088/1748-9326/ac6e48

Oo, T. T. (2003). Doctor of science dissertation. In *The biology and vector competence of the Anopheline mosquitoes in Myanmar with special consideration of Anopheles dirus*. Ph.D dissertation, University of Heidelberg. https://archiv.ub.uni-heidelberg.de/volltextserver/3305/1/Thesis.pdf

Orlov, A., Aunan, K., Mistry, M. N., Lejeune, Q., Pongratz, J., Thiery, W., et al. (2023). Neglected implications of land-use and land-cover changes on the climate-health nexus. *Environmental Research Letters*, *18*(6), 061005. https://doi.org/10.1088/1748-9326/acd799

Patz, J. A., Olson, S. H., Uejio, C. K., & Gibbs, H. K. (2008). Disease emergence from global climate and land use change. *Medical Clinics of North Amercia*, *92*. https://doi.org/10.1016/j.mcna.2008.07.007

Pesaresi, M., Ehrilch, D., Florczyk, A. J., Freire, S., Julea, A., Kemper, T., et al. (2015). *GHS built-up grid, derived from Landsat, multitemporal (1975, 1990, 2000, 2014)*. European Commission, Joint Research Centre, JRC Data Catalogue.

Rao, M., Saw Htun, Platt, S. G., Tizard, R., Poole, C., Than Myint, & Watson, J. E. M. (2013). Biodiversity conservation in a changing climate: A review of threats and implications for conservation planning in Myanmar. *AMBIO*, *42*(7), 789–804. https://doi.org/10.1007/s13280-013-0423-5

Rappaport, D. I., Morton, D. C., Longo, M., Keller, M., Dubayah, R., & dos-Santos, M. N. (2018). Quantifying long-term changes in carbon stocks and forest structure from Amazon forest degradation. *Environmental Research Letters*, *13*(6), 065013. https://doi.org/10.1088/1748-9326/aac331

RFA Burmese. (2023). Junta Claims Near-Complete Census in Myanmar, But Experts Say That's Impossible. Retrieved February 21, 2024, from www.rfa.org/english/news/myanmar/census-06282023093501.html

Rice, B. L., Golden, C. D., Randriamady, H. J., Arisco, N. J., & Hartl, D. L. (2018). Integrating approaches to study land use change and hotspots of malaria transmission in rural Madagascar: An observational study. *The Lancet Planetary Health*, *2*, S19. https://doi.org/10.1016/S2542-5196(18)30104-9

Saah, D., Tenneson, K., Poortinga, A., Nguyen, Q., Chishtie, F., Aung, K. S., et al. (2020). Primitives as building blocks for constructing land cover maps. *International Journal of Applied Earth Observation and Geoinformation*, *85*, 101979. https://doi.org/10.1016/j.jag.2019.101979

Schroeder, W., Oliva, P., Giglio, L., & Csiszar, I. A. (2014). The New VIIRS 375 m active fire detection data product: Algorithm description and initial assessment. *Remote Sensing of Environment*, *143*, 85–96.

Shevade, V., Hoffman-Hall, A., & Loboda, T. (2021). Using land use engagement surveys to improve understanding of malaria exposure in Ann Township, Myanmar, 2021, GH45C-0826. *Presented at the AGU Fall Meeting Abstracts*. https://ui.adsabs.harvard.edu/abs/2021AGUFMGH45C0826S/abstract

Shevade, V. S., Potapov, P. V., Harris, N. L., & Loboda, T. V. (2017). Expansion of industrial plantations continues to threaten Malayan Tiger Habitat. *Remote Sensing*, *9*(7), 747. https://doi.org/10.3390/rs9070747

Soe, H. Z., Thi, A., & Aye, N. N. (2017). Socioeconomic and behavioural determinants of malaria among the migrants in gold mining, rubber and oil palm plantation areas in Myanmar. *Infectious Diseases of Poverty*, *6*(1), 142. https://doi.org/10.1186/s40249-017-0355-6

Sutherst, R. W. (2004). Global change and human vulnerability to vector-borne diseases. *Clinical Microbiology Review*, *17*, 136–173. https://doi.org/10.1128/CMR.17.1.136-173.2004

Suwonkerd, W., Ritthison, W., Ngo, C., Tainchum, K., Bangs, M., & Chareonviriyaphap, T. (2013). Vector biology and malaria transmission in Southeast Asia. In S. Manguin (Ed.), *Anopheles mosquitoes—New insights into malaria vectors* (pp. 273–325). InTech, London, United Kingdom.

Tangena, J.-A. A., Thammavong, P., Wilson, A. L., Brey, P. T., & Lindsay, S. W. (2016). Risk and control of mosquito-Borne diseases in Southeast Asian rubber plantations. *Trends in Parasitology*, *32*(5), 402–415. https://doi.org/10.1016/j.pt.2016.01.009

Thieme, A., Yadav, S., Oddo, P. C., Fitz, J. M., McCartney, S., King, L., et al. (2020). Using NASA Earth observations and Google Earth Engine to map winter cover crop conservation performance in the Chesapeake Bay watershed. *Remote Sensing of Environment*, *248*, 111943. https://doi.org/10.1016/j.rse.2020.111943

de Thoisy, B., Duron, O., Epelboin, L., Musset, L., Quénel, P., Roche, B., et al. (2021). Ecology, evolution, and epidemiology of zoonotic and vector-borne infectious diseases in French Guiana: Transdisciplinarity does matter to tackle new emerging threats. *Infection, Genetics and Evolution*, *93*, 104916. https://doi.org/10.1016/j.meegid.2021.104916

Tilaye, T., Tessema, B., & Alemu, K. (2022). High asymptomatic malaria among seasonal migrant workers departing to home from malaria endemic areas in northwest Ethiopia. *Malaria Journal*, *21*, 184. https://doi.org/10.1186/s12936-022-04211-9

Valle, D., & Clark, J. (2013). Conservation efforts may increase malaria burden in the Brazilian Amazon. *PLoS One*, *8*(3), e57519.

Van Dung, N., Thieu, N. Q., Canh, H. D., Le Duy, B., Hung, V. V., Ngoc, N. T. H., et al. (2023). Anopheles diversity, biting behaviour and transmission potential in forest and farm environments of Gia Lai province, Vietnam. *Malaria Journal*, *22*(1), 204. https://doi.org/10.1186/s12936-023-04631-1

Vanwambeke, S. O., Lambin, E. F., Eichhorn, M. P., Flasse, S. P., Harbach, R. E., Oskam, L., et al. (2007). Impact of land-use change on dengue and malaria in northern Thailand. *EcoHealth*, *4*(1), 37–51.

Vanwambeke, S. O., Linard, C., & Gilbert, M. (2019). Emerging challenges of infectious diseases as a feature of land systems. *Current Opinion in Environmental Sustainability*, *38*, 31–36. https://doi.org/10.1016/j.cosust.2019.05.005

Wang, P. (2017). *Human Built-up and Settlement Extent (HBASE) dataset From Landsat*. NASA Socioeconomic Data and Applications Center (SEDAC). https://doi.org/10.7927/H4DN434S

Wang, X., Zhou, G., Zhong, D., Wang, X., Wang, Y., Yang, Z., et al. (2016). Life-table studies revealed significant effects of deforestation on the development and survivorship of

Anopheles minimus larvae. *Parasites & Vectors*, *9*(1), 323. https://doi.org/10.1186/s13071-016-1611-5

WHO. (2021). *World malaria report 2021*. www.who.int/teams/global-malaria-programme/reports/world-malaria-report-2021

WHO. (2023). *World malaria report 2023*. www.who.int/teams/global-malaria-programme/reports/world-malaria-report-2023

Wimberly, M. C., de Beurs, K. M., Loboda, T. V., & Pan, W. K. (2021). Satellite observations and malaria: New opportunities for research and applications. *Trends in Parasitology*, *37*(6), 525–537. https://doi.org/10.1016/j.pt.2021.03.003

Yasuoka, J., & Levins, R. (2007). Impact of deforestation and agricultural development on anopheline ecology and malaria epidemiology. *The American Journal of Tropical Medicine and Hygiene*, *76*(3), 450–460.

Zalles, V., Hansen, M. C., Potapov, P. V., Parker, D., Stehman, S. V., Pickens, A. H., et al. (2021). Rapid expansion of human impact on natural land in South America since 1985. *Science Advances*, *7*(14), eabg1620.

Zaw, M. T., Thant, M., Hlaing, T. M., Aung, N. Z., Thu, M., Phumchuea, K., et al. (2017). Asymptomatic and sub-microscopic malaria infection in Kayah State, eastern Myanmar. *Malaria Journal*, *16*(1), 138. https://doi.org/10.1186/s12936-017-1789-9

12 Ongoing Issues in Land Cover and Land Use Change in Thailand and Priority Actions for Policy

Manoj Potapohn, Ditchaphong Phoomikiattisak, and Phadungpon Supinit

12.1 INTRODUCTION

The capacity of the Thai government to manage natural and environmental resources has dramatically improved with the advent of remote sensing technology. Thai citizens, who regularly watch television, are becoming increasingly familiar with using GIS maps to display forest fire hotspots and the scope of flooding. In meeting rooms, GIS maps are relied upon to show areas where paddy rice is grown during the dry season despite opposition from irrigation officials. Risk mitigation measures, such as crop insurance, are being developed based on the growth levels of crops before damage occurs. Additionally, fishing boats in the open ocean are monitored to ensure compliance with European Union regulations. The authors are convinced that remote sensing technology can improve the lives of ordinary people—provided that better information is placed in the hands of agencies that are mandated to take action upon receiving new, validated information from the ground.

Geo-Informatics and Space Technology Development Agency (GISTDA), Thailand's space agency, is at the forefront of remote sensing technology, human resources, and access to GIS resources in the country. As part of the plan stemming from the launch of the THEOS-2 satellite, which was placed into orbit in October 2023, GISTDA developed a tool to enable stakeholder engagement in regulatory policy formulation, thus promoting legitimacy and compliance. The tool called the Actionable Intelligence Policy (AIP) Platform, was designed to support area-based development, with two pilot sites selected. One site is in the northern Thai province of Nan, where upland agriculture is under pressure to be converted back to forest. Still, there is also a need to generate enough livelihoods to win over current occupants of formerly encroached forest land. The other site focuses on deepening the development of the manufacturing industry in the Eastern Economic Corridor (EEC) to develop new industries and escape the middle-income trap.

DOI: 10.1201/9781003396260-12

The unique lessons learned from the introduction of AIP Nan and AIP EEC are crucial for the country to better utilize remote sensing to its full potential. One of the biggest lessons learned is that when information generated from space is combined with ground-level data, it can better inform public decision-making. Ground-level data, generated for in-house use, can be administrative data that is increasingly available as agencies digitize their operations. However, the process of data sharing, mainly through the synchronization of ground-level data with data from space, is delicate. GISTDA's experiment with AIP has succeeded in the EEC and is still a work in progress in Nan. When it was successful, it was almost an accident, as the agency that adopted the AIP EEC tool was not initially tasked with synchronizing industrial development in the EEC. Instead, it was the water resource agency that had a closely related coordination function and a strong incentive to use GISTDA's AIP EEC tool to improve how it carried out its mandate.

The purpose of this study is to share the story that emerged from interviews with developers and stakeholders, as well as field research for data validation. The story highlights Thailand's recent experience in applying remote sensing technology through developing and adopting its Actionable Intelligence Policy (AIP). Section 12.2 begins by discussing what has become familiar to Thailand's television viewers—the use of remote sensing technology for monitoring forest fires. It raises the question of whether and to what extent these fires are accompanied by forest clearing. The study was not successful in answering this question directly because the forest clearing data is highly sensitive, so maize was used as a proxy to illustrate the challenges in data availability. A remedy for this issue is recommended. Section 12.3 introduces the technology behind AIP, while Section 12.4 discusses the ecosystem that enables the effective use of data from space. It also outlines priority actions for policy audiences to maximize the benefits of remote sensing technology. Section 12.5 concludes the study with a summary and final thoughts.

12.2 WHAT DO FIRE STATISTICS TELL US, IF ANYTHING, ABOUT FOREST COVER LOSS?

Data on fire statistics for Thailand from 2001 to 2023, courtesy of Dr. Krishna Vadrevu from NASA's Marshall Space Flight Center in Huntsville, Alabama, USA, was obtained from the MODIS MCD54A1 (version 6.1) dataset, with a resolution of 500 m (Figures 12.1(a)–(b), 12.2(a)–(d)). The total burnt area over the 23 years is shown on the left-hand side panel, with a slight declining trend. The data is further broken down into three different land cover types: cropland (green), grassland (brown), and forest fires (red).

In Figure 12.2, panels (a), (b), and (c) show the 23-year trends for land scars caused by forest fires, cropland fires, and grassland fires, respectively. The burnt areas due to grassland and cropland fires are showing declining trends, while the trend for forest fires is slightly increasing. The pie chart in panel (d) indicates that, on average, burnt areas under forest fires account for 35% of the total, while cropland and grassland fires account for 59% and 6%, respectively.

Time series data on forest cover loss for 2001–2023 was obtained from Thailand's Royal Forestry Department. A correlation test was performed between the fire

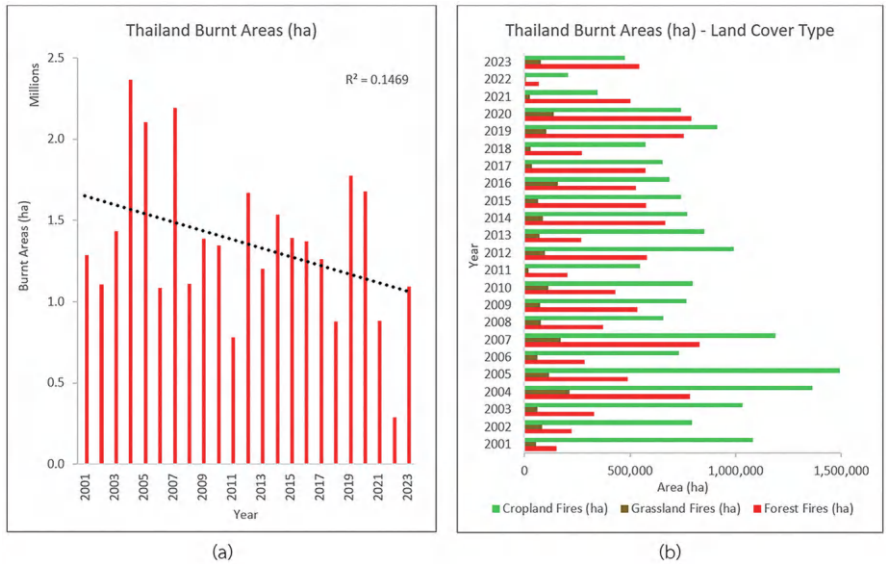

FIGURE 12.1 (a) Total burnt areas in Thailand (ha) and (b) burnt areas in Thailand by land cover types.

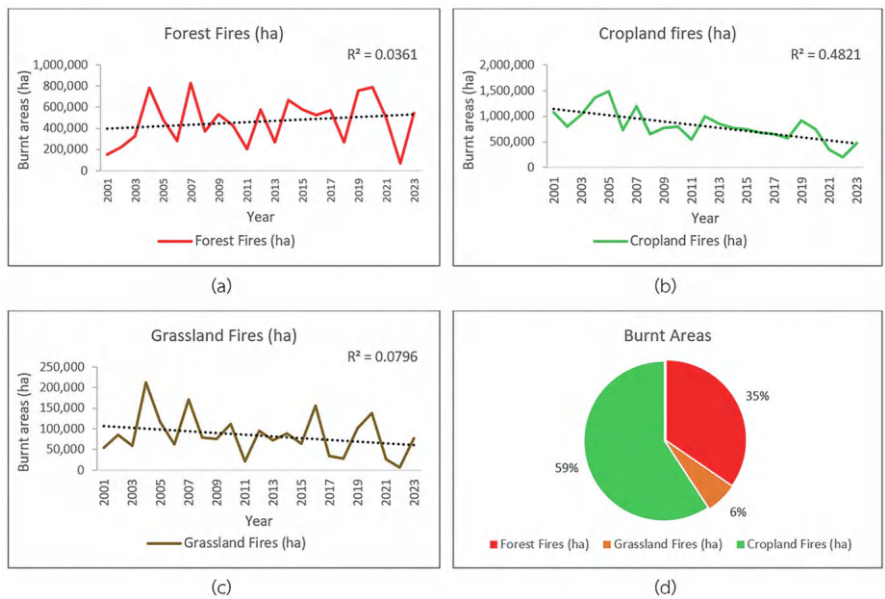

FIGURE 12.2 (a), (b), (c) 23-year trend of land scar for each land cover types and (d) burnt area percentage.

TABLE 12.1
Maize Cultivation Area (Rai)

Provinces\Year	2002	2007	2012	2017	2022
Chiang Mai	36,080	180,103	175,273	184,166	286,816
Lamphun	47,654	80,684	97,728	83,439	78,627
Lampang	21,849	169,358	189,462	232,444	276,475
Phrae	56,900	318,666	250,604	286,537	221,384
Nan	182,414	798,567	786,581	637,231	608,923
Phayao	133,974	318,054	347,567	271,571	220,410
Chiang Rai	117,899	457,247	565,471	387,449	336,014
Mae Hong Son	24,509	67,338	89,778	71,477	101,770
Total	621,279	2,390,017	2,502,464	2,154,314	2,430,419

Source: Greenpeace and GISTNORTH.

statistics and the forest cover loss data. Still, the result suggested that the correlation is statistically insignificant, meaning no significant relationship between the two datasets was detected. Therefore, the forest cover loss data is not shown here.

A closer examination at the provincial scale revealed that forest cover loss is concentrated in northern Thailand, particularly in the headwaters of the Chao Phraya River, which feeds into the central plain. Forest cover loss is a significant issue in land cover and land use change in Thailand, often driven by unsustainable agricultural practices, mainly maize and corn cultivation. Addressing this challenge requires well-informed and targeted policies. However, even when such information is available, agencies are sometimes subject to self-censorship.

One exception is the data in Table 12.1, which suggests the cropped area for maize. Researchers at CMU's GISTNORTH conducted this analysis for Greenpeace, showing that the maize-growing area in eight provinces of upper northern Thailand increased from 621,279 rai (with 6.25 rai equaling one hectare) in 2002 to 2,430,419 rai in 2022, a growth over 20 years. Nan has the largest maize-growing area, though the trend is declining.

The rise in maize cultivation is likely due to a reduction in other forest cover types. It is unlikely that virgin forests will be converted into maize-growing areas; instead, shifting cultivation fields and secondary forests will be replaced, according to Agrawal and Lumpkin (2024). However, Nan is one of the areas in northern Thailand that has experienced communist insurgency against the government since the late 1960s. By the mid-1970s, the military adopted a new tactic to win over sympathizers, investing in constructing a road network and allowing the local population to access land, which was subsequently turned into farmland. This fits with the pattern of land use conversion linked to improved market access, supported by Von Thünen's model, and the experience of road networks and ranchland replacing forest cover in Brazil.

12.3 TECHNOLOGY FOR INTERVENTION: GISTDA'S ACTIONABLE INTELLIGENCE POLICY (AIP) PLATFORM

GISTDA (Geo-Informatics and Space Technology Development Agency) is a public organization owned by the Thai government and tasked with developing and applying geoinformatics, space technologies, and geographic information systems (GIS). This section introduces the Actionable Intelligence Policy (AIP) Platform as both a policy tool and an outcome-based approach to policy development. The AIP platform is built on an integrated data system that combines remotely sensed data from space with ground-level data. This solution leverages the information and communication technology (ICT) infrastructure available in Thailand, along with the country's new satellite, THEOS-2, which has been in orbit since 2023.

12.3.1 What is AIP?

The Actionable Intelligence Policy (AIP) platform, developed by GISTDA in 2018, enhances policymaking in Thailand by providing concrete, evidence-based insights using Earth Observation (EO) data. The concept behind AIP is rooted in "Actionable Intelligence" (Fantuzzo and Culhane, 2015), which emphasizes how integrated data systems can drive more effective and efficient decision-making, particularly within government sectors.

As shown in Figure 12.3, the AIP Ecosystem begins with integrating multi-source data, primarily EO data from satellite imagery. This raw data is processed into various geospatial products, such as land use and land cover (LULC) maps, Digital Elevation Models (DEM), flood maps, and urban maps. These products are crucial for policymakers to monitor, analyze, and make data-driven decisions. AIP serves two key functions: (1) identifying problems in specific areas using measurable and quantitative insights known as 'indicators,' and (2) simulating the effects of different policy interventions on these indicators. By doing so, AIP enables the design of policies that align with local, national, and future priorities, allowing policymakers to foresee both positive and negative outcomes before implementation.

The AIP development process can be broken down into the following steps:

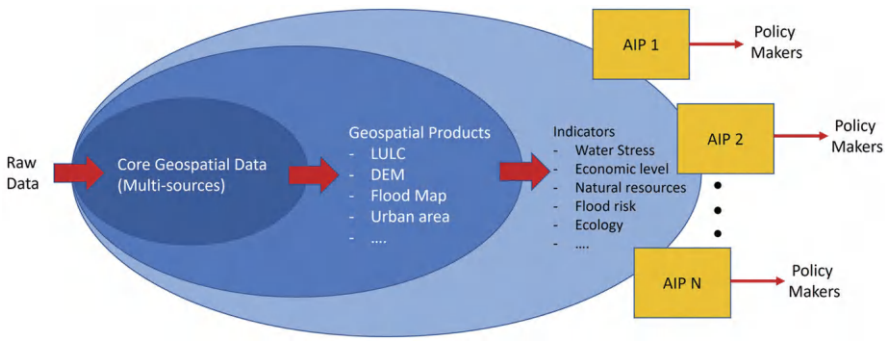

FIGURE 12.3 AIP ecosystem.

(a) Problem Statement

The initial step involves defining an apparent problem to be addressed and the geographic scope, typically at the provincial level. The problem statement should align with local or national policies, and a comprehensive list of stakeholders should be identified. These stakeholders may include those interested in the results, users of the AIP, and those affected by or contributing to the policy (e.g., through data provision). Early engagement with stakeholders is essential to ensure their requirements are met.

(b) Indicators Design

The second step involves identifying indicators that represent the magnitude and location of the problem. These indicators are often linked to established measures such as the Sustainable Development Goals (SDGs) and The Human Development Index (HDI). Some indicators may consist of sub-indicators that support a more significant measure. The designed indicators should be reviewed and confirmed by stakeholders.

(c) Identify Data Sources

Once the indicators are identified, the next task is determining which data sources are needed to develop them. For AIP, EO data products are prioritized. These products have been created by GISTDA to serve specific missions and are categorized into six dimensions as follows:

- **Mapping** – such as satellite-based maps and other basic products like Digital Elevation Models (DEM) and land use and land cover (LULC).
- **Agriculture** – such as crop classification, crop health monitoring, and yield predictions.
- **Water Management** – such as surface water monitoring.
- **Urban** – such as urban maps, building footprints, urban green areas, and 3D building models.
- **Disasters** – such as flood monitoring, historical floods, fire hotspots, PM2.5, and other aerosol data.
- **Natural Resources** – such as forest areas, mangrove areas, and carbon credit maps.

However, EO data alone may be insufficient to cover some issues. External data sources, such as surveys and public records, may also be necessary, with stakeholder input helping to identify relevant data.

(d) Indicators Development

After gathering the necessary data, the next step is to develop the indicators. Some indicators, like population density, can be derived directly from the data, while others may require more complex scientific methodologies, as will be described below for AIP-NAN and AIP-EEC.

(e) Dashboard Development

The final step is creating a visualization dashboard to present integrated geomatics information and other data results. This dashboard gives decision-makers a comprehensive view of the indicators, helping them simulate action plans, assess potential outcomes, and make informed policy decisions before implementation.

12.3.2 AIP to Support Policymaking

Policymaking is a complex process often involving multiple stakeholders, diverse interests, and various contextual factors. AIP addresses these complexities by providing objective, data-driven insights that guide decision-making throughout the policy cycle. Drawing from the five stages of the policy cycle (Howlett and Ramesh, 1995), AIP supports each stage as follows:

- **Agenda Setting**: The policy agenda overview is the primary input for developing the AIP. Additionally, the AIP can strengthen agenda setting by providing relevant indicators that emphasize the issue's importance.
- **Policy Formulation**: Policymakers can develop multiple policy options based on the observed indicators and other supporting data.
- **Decision Making**: AIP provides scenario-based simulations for each policy option. Policymakers can see the potential impacts, both positive and negative, before launching the policy, which allows them to select the most appropriate option for implementation.
- **Policy Implementation**: AIP provides an evidence-based rationale to align stakeholders at all levels and ensure coherent implementation.
- **Policy Evaluation**: After implementing the policy, AIP monitors actual outcomes and compares them with the simulations, suggesting adjustments if necessary.

To demonstrate the feasibility of using geospatial data to support policy decision-making, GISTDA has developed proof-of-concept AIP platforms in two key areas: Nan province and the Eastern Economic Corridor (EEC) of Thailand. These platforms, AIP-NAN and AIP-EEC, exemplify how the AIP ecosystem can be applied to real-world policy challenges, following the policy cycle and contributing to evidence-based governance.

12.3.3 AIP-NAN: A Bottom-Up Approach

AIP-NAN addresses specific regional development challenges in Nan province by leveraging EO data to support local policymaking and sustainable development. Deforestation has become a chronic issue in Nan province, driven by a lack of arable land, limited agricultural knowledge and practices, poverty, and agricultural expansion, particularly maize cultivation. Standard deforestation practices, including logging and slash-and-burn techniques, transform forested areas into maize plantations. A previous study by Agarwal and Lambin (2024) highlighted this issue of forest loss from swidden cultivation. Additionally, the intensive use of chemicals in maize cultivation leads to land degradation, water pollution, and soil contamination. Local communities grow maize primarily for animal feed, creating a "vicious cycle" of low incomes and ecological damage, including deforestation, increased CO_2 emissions, water pollution, and soil erosion. Therefore, the primary challenges in Nan province include reforestation, environmental restoration, and increasing local community income. Improving regional income strategies must consider land limitations, and poverty alleviation remains a key policy objective.

While forest management policies are crucial, they remain under-researched. The absence of precise mechanisms to manage conflicts over forest land between local communities and authorities in Nan province has led to strong resistance from local people against relocation and continued use of forest areas. The Thai government aims to end deforestation and reclaim forest land from local communities. One initiative, the Nan Sandbox, is a public–private partnership to end deforestation in the province. It promotes a land policy model known as "72-18-10," in which 72% of the area is preserved forest, 18% is designated for reforestation with economic crops grown under tree cover, and 10% is fully permitted for crop cultivation. Understanding forest change patterns is crucial for policymakers in developing effective land use plans for Nan province.

AIP-NAN supports local policymakers in balancing forest ecosystem management with the economic needs of the local population. The indicators used in AIP-NAN are categorized into two main aspects: Natural Resources and Economics. The indicators and sub-indicators were developed through interview workshops with local stakeholders, including community leaders, local government agencies, and representatives from educational institutions. This step is a critical component of AIP development, as the indicators reflect the current status of Nan province. Selecting the appropriate indicators ensures that the AIP aligns with the priorities and concerns of local stakeholders, accurately representing their interests.

The Natural Resources indicators include four main sub-indicators: Good Soil, Good Forest, Good Water, and Disaster Security. Each sub-indicator is derived from different EO data sources and other secondary data, as described below.

- **Good Soil**: This indicator consists of two sub-indicators. The first is soil erosion, which reflects the erosion occurring in agricultural areas, calculated using the Universal Soil Loss Equation (USLE) (Wischmeier and Smith, 1978). It considers rainfall, soil texture (e.g., the relative content of silt, clay, loam, and sand), crop management, soil conservation practices, and topography (e.g., slope length and steepness). The second sub-indicator is land suitability, calculated from rainfall, temperature, soil properties, and topography.
- **Good Forest**: This indicator includes three sub-indicators: forest area, the ratio of agricultural land to reserved forest, and cohesion of the forest. The cohesion of the forest reflects the overall health of the forest by assessing its fragmentation within the landscape, which indicates habitat connectivity (Laurance et al., 2011).
- **Good Water**: This indicator primarily focuses on the availability of water resources within the area, emphasizing surface water, which can be directly measured using EO data.
- **Disaster Security**: This indicator assesses flood and drought risks, derived from historical flood and drought records.

The **economic indicator primarily measures land productivity for each parcel**. It is calculated by considering the suitability score of the grown crop (obtained from the Land Development Department), crop yield (derived from literature review and Thai statistical records), and crop price (from the Office of Agricultural Economics).

Land Productivity = Suitability × Crop Yield × Price

Once these indicators are calculated, they are visualized on the AIP dashboard, allowing policymakers to understand the overall characteristics of Nan province at the sub-district (Tambon) level. Figure 12.4(a) shows the Natural Resources Indicator at the sub-district level, highlighting that the central area of Nan province, predominantly residential, has lower scores for natural resources. However, some reserved forest areas also show low natural resource scores, indicating deforestation issues. Figure 12.4(c) displays the Economic Indicator for Nan province, derived from land productivity data. A comparison reveals that areas with higher economic scores generally have lower natural resource scores, reflecting the common practice of using land for agriculture without regard for the ecosystem. However, some areas with high economic scores also have medium to high natural resource scores, indicating effective practices of cultivating 'forest-friendly' crops that sustain forest ecosystems while generating adequate income for local communities.

Once AIP identifies the current status of Nan province through various indicators, the next step is to develop strategies to solve existing problems – specifically,

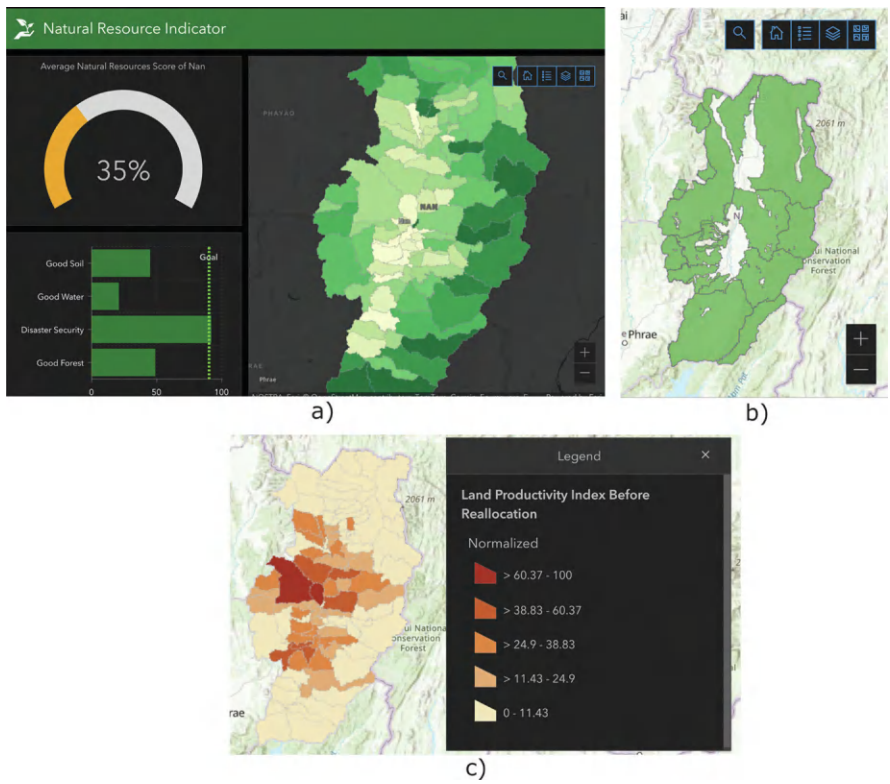

FIGURE 12.4 (a) Natural resources indicator in Nan province, (b) reserved forest in Nan province, (c) economic indicator in Nan province, represented by the Land Productivity Index.

improving the forest ecosystem without negatively impacting the local economy. One extreme solution would be to reclaim all forest areas from local communities to comply with the 72-18-10 policy. However, this would severely impact the local economy. After recalculating the economic and natural resource indicators following the reclamation of forest areas, land productivity in Nan province would decrease by 54%, while natural resources would improve by 24.5%. This is not an optimal solution. A more practical approach involves a 'bottom-up' strategy: if converting some agricultural land back to forest is necessary, what is the best alternative? One possible solution is to reduce agricultural land while transitioning to higher-value crops, considering the land's suitability and the local population's skills.

The previously mentioned land suitability analysis was used to identify alternative crops for replacing maize. Key attributes of each land parcel, including rainfall, temperature, soil properties, and topography, were calculated and matched with crop profiles provided by the Land Development Department. As illustrated in Figure 12.5, the AIP dashboard provides recommendations for crops suitable for specific areas, enabling policymakers to promote environmentally sustainable and familiar options to local farmers. By selecting a crop parcel (e.g., an orange area representing corn), the AIP system displays alternative crop options along with their suitability scores. For instance, Figure 12.5 indicates that vegetables, with a suitability score of 0.71, are the best alternative to replace the selected corn parcel. While additional factors such as the landowner's skills, market demand, and economic viability must also be considered, the AIP serves as an initial guideline. This empowers local policymakers to collaborate with communities to facilitate a transition from corn and maize to more forest-friendly crops.

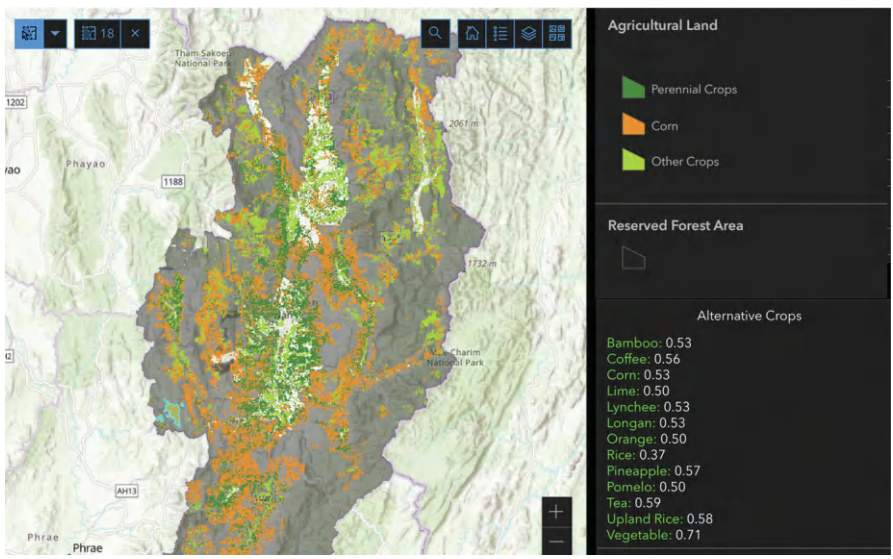

FIGURE 12.5 Alternative crops recommended by AIP for the selected land parcel. The higher number of scores, the more suitable of the crops.

By integrating earth observation data with local survey data, AIP-NAN provides a comprehensive overview of the region. This unified dashboard allows all stakeholders to access essential information in one place. Residents can see how their agricultural activities affect forest areas, while policymakers can identify regions suitable for 'forest-friendly' crops. Although the dashboard alone cannot drive policy implementation, it is a critical starting point, enabling policymakers to make informed decisions based on scientific evidence.

12.3.4 AIP-EEC: A Top-down Approach

The Eastern Economic Corridor (EEC) encompasses three provinces in Thailand: Chachoengsao, Chonburi, and Rayong. It is set to become a vital hub for trade, investment, tourism, and regional transportation, serving as a modern gateway to Asia. The AIP-EEC initiative aims to foster economic growth in this region by utilizing Earth Observation (EO) data to monitor and optimize various aspects of development. With the introduction of the Thailand 4.0 policy, the government is focusing on developing new growth hubs, starting with the EEC, to support and accelerate economic expansion. Water management in the EEC has been recognized as a critical factor due to its essential role in daily life, economic progress, and environmental sustainability.

The AIP-EEC platform enables the comparative analysis of conditions before and after the implementation of the EEC initiatives, incorporating insights from surveys of the public and various stakeholders in the region.

A study by the Office of the National Water Resources (ONWR) predicts that water demand in the EEC will increase by nearly 30% by 2037 compared to 2017, potentially leading to water shortages (OECD, 2022). To address this issue, ONWR has developed a comprehensive plan that includes several large-scale projects, such as constructing reservoirs, initiating water diversion programs, and implementing other measures to mitigate the anticipated water scarcity. However, these projects have faced objections due to concerns about their potential environmental impacts and skepticism about their overall effectiveness and value.

To reconcile these differing perspectives, AIP-EEC provides scientific evidence to visualize future water scarcity. By integrating hydrological and geospatial data, AIP-EEC can accurately identify areas at risk of water shortages in the future. Like AIP-NAN, AIP-EEC uses specific indicators derived from EO and other data to characterize and identify regional challenges. For the EEC, the Water Stress Index (WSI) has been developed as a primary indicator of water scarcity in the area and given as

$$WSI(\%) = \frac{Demand}{Supply} \times 100$$

Earth observation data, such as land use and land cover (LULC), is critical for calculating water demand and supply. LULC data helps identify supply sources, such as water bodies, and various demand sources, including agricultural (based on agricultural land use), domestic (from urban land use), and industrial (from industrial

TABLE 12.2
Core Data for Water Demand and Water Supply Calculations

Indicators	Sub-indicators	Data
Water Demand	Agriculture water demand	LULC, Crop coefficient (Kc), Rainfall, Temperature
	Industrial water demand	LULC, water requirement for each industrial type
	Domestic water demand	LULC, population data, water consumption per capita
Water Supply	Natural flow	LULC, Topography, Soil types, Rainfall, Temperature
	Reservoirs	Reservoir data, Waterway infrastructure, Water transfer pump data

land use). Table 12.2 outline the core data required for WSI calculations. In addition to EO data, secondary data from relevant organizations such as the Royal Irrigation Department (RID) is also necessary.

Various established scientific models are used to calculate water demand and supply, such as the Soil and Water Assessment Tool (SWAT) for water supply calculations and the Blaney–Criddle method (Blaney and Criddle, 1950) for agricultural water demand calculations. These models allow for estimating the current Water Stress Index (WSI). However, the challenge for the EEC lies in forecasting future water stress amid the development of multiple mega-projects and a growing population.

Future data are essential to estimating future WSI. The Eastern Economic Corridor Office of Thailand (EECO) has provided projections for future land use and land cover (LULC). However, some assumptions are required, such as maintaining the types of crops currently grown. Additionally, future population estimates have been studied and provided by the EECO. Figure 12.6 illustrates the projected WSI in 2037 at the sub-basin level, with critical areas marked in red.

Recognizing the severity of future water scarcity in the EEC, proactive mitigation plans must be initiated. The ONWR, Thailand's national policymaker for water management, has proposed several projects, including reservoir upgrades, new water diversion systems, and the construction of additional reservoirs and water sources. These initiatives aim to enhance water storage capacity during the rainy season, when excess water often leads to flooding, and to ensure sufficient water availability during the dry season. The AIP-EEC platform supports this effort by simulating "what-if" scenarios, allowing policymakers to evaluate these proposed projects' potential impacts and effectiveness. The data on future projects are sourced from ONWR. Figure 12.7 demonstrates the improvement in water scarcity, represented by the WSI in the EEC area in 2037, following the implementation of Action Plan 1 (comprising 13 projects) and Action Plan 2 (comprising 29 projects). This simulation enables policymakers and stakeholders to visualize the benefits of these projects and determine whether they are sufficient or if further measures are needed. Thus,

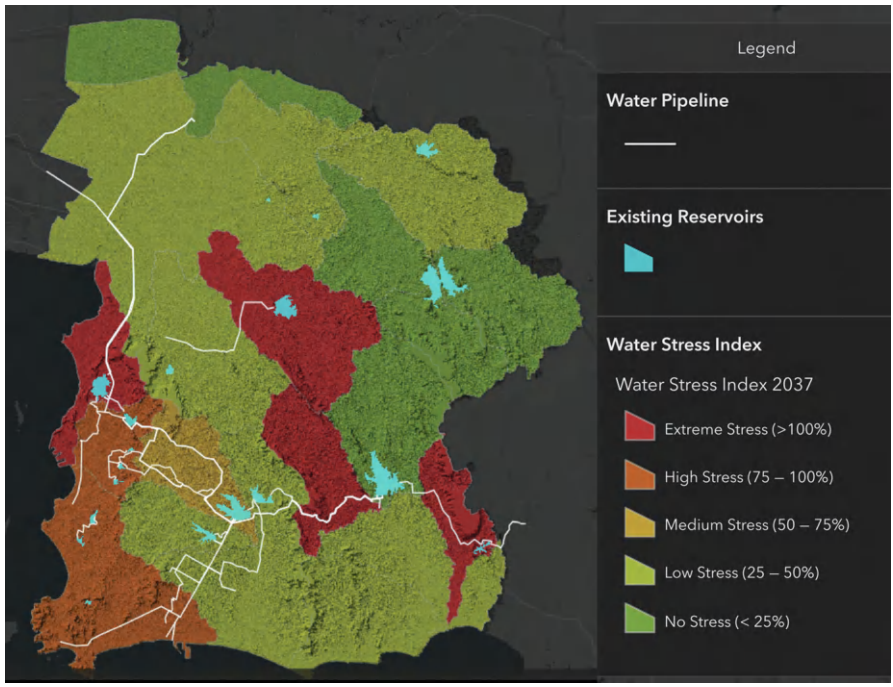

FIGURE 12.6 Water scarcity levels in the EEC area in 2037.

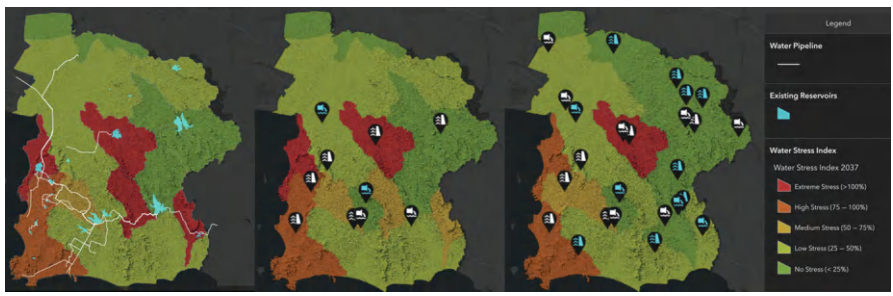

FIGURE 12.7 Water Stress Index of the EEC area in 2037, from left to right: without any intervention, with Action Plan 1 (13 projects), and with Action Plan 2 (29 projects).

AIP-EEC provides a holistic view, facilitating a comprehensive understanding of the area's water management challenges and enabling more effective problem-solving. EO data plays a crucial role by offering scientific evidence of the area's characteristics.

However, AIP-EEC also faces certain limitations. First, the level of engagement with local stakeholders is relatively lower compared to AIP-NAN. This is a critical aspect, as implementing some projects must account for their broader impacts on

local communities beyond the immediate benefits of water management. Second, the platform does not fully represent the potential impacts on regions adjacent to the EEC. For instance, provinces like Chanthaburi, which border the EEC, could be affected by initiatives that redirect water resources to support the EEC area, potentially leading to unintended consequences in those regions.

In contrast to AIP-NAN, AIP-EEC utilizes a 'top-down' approach for policy implementation. As the primary authority responsible for water management policy in Thailand, ONWR can use AIP-EEC as a powerful tool to support evidence-based policymaking and develop practical strategies to address potential water shortages in the future.

12.3.5 Lessons Learned

After several years of implementing the AIP platform, two critical factors have been identified that determine its success.

The first factor is the importance of a clear problem statement. Defining the specific issue that AIP aims to address is crucial. For instance, the Eastern Economic Corridor (EEC) region faces multiple challenges, including economic growth, megaproject implementation, education, social issues, environmental concerns, and water management. Initially, the strategy was to simultaneously tackle as many of these problems as possible. However, after a few years of designing the AIP, it became apparent that this approach was too complex to implement effectively. Consequently, the focus was narrowed to a single problem: water management, which was identified as a core resource underpinning all development in the EEC.

The second critical factor is securing buy-in from key stakeholders, who are the primary users of AIP. In the development of AIP-EEC, strong support was received from key stakeholders, such as ONWR and the Royal Irrigation Department (RID). This support enabled the translation of insights from AIP into concrete policy actions. In contrast, in Nan province, key stakeholders were not fully engaged because it remained unclear who should lead the reforestation efforts and reallocating land policy. While AIP-NAN was presented to local authorities, such as the governor, local forest department, and community leaders, many limitations persisted because these stakeholders lacked the authority to implement the recommendations effectively. Therefore, it is vital to carefully identify AIP's appropriate users—those with the power and authority to act as policymakers.

When these conditions are met, AIP can be expanded to support policymakers in other areas or on different issues. For example, ONWR now intends to extend AIP-EEC to support water management policies in other regions.

In conclusion, the AIP platform is an essential tool for developing and managing area-based policies. By integrating Earth Observation (EO) data and scientific modeling, AIP provides clear and accurate insights through relevant indicators. These insights help bridge the gap between the perspectives of various stakeholders, enabling evidence-based decision-making and ensuring sustainable and balanced development.

12.4 INSTITUTIONS: MANAGEMENT IMPACTS THROUGH ADOPTION OF AIP AT NAN AND EEC

12.4.1 Reflection from Developers' Focus Group Discussion

The initial development phase of AIP, associated with the advent of THEOS-2, has already been completed. According to a recent focus group discussion with AIP developers, the current status is as follows. First, out of the two versions of AIP developed, only one has been practically implemented at the EEC. This is because GISTDA continuously updates remotely sensed data. However, the Eastern Economic Corridor Office of Thailand (EECO), which is responsible for industrializing the three coastal provinces with the best infrastructure, has not been the adopter. Instead, the EECO prioritizes attracting foreign direct investment and mega infrastructure projects. The Office of National Water Resources (ONWR) stepped in as a partner of GISTDA, using remotely sensed data from space technology alongside ground-level data from the agencies linked with ONWR to pursue water management goals.

In contrast, land management in the upland part of Nan has not seen the same outcome. GISTDA had expected the formation of an organization similar to the EECO to coordinate policy actions for reforestation, but this did not materialize. Instead, a policy process for managing forest land was conducted under the "Nan Sandbox," which involved private philanthropy from Mr. Bantoon Lamsam, the former CEO of Kasikorn Thai Bank. However, government agencies felt marginalized, and the private sector did not receive broad popular support. As a result, the experiment did not progress far.

Without a single organization with a strong administrative mandate to coordinate field actions, the feedback system—linking ground-level data to remotely sensed data and, importantly, analyzing the data—was not established. Consequently, unlike in the EEC, GISTDA's data is not continuously updated in the Nan case.

Second, the data interface between GISTDA and AIP users is currently operating at around 50% capacity. In Nan province, specific land holdings cannot be obtained through remote sensing and require ground surveys. For instance, the boundary of a plot of land can only be established by recognizing the adjacent claimant's plot. Additionally, ground surveys is required to show how a specific plot of land is used, its history of land clearing, and how long it has been in the possession of the current owner. These surveys were funded through private donations, and this information is not integrated into the AIP system. As a result, it is impossible to determine whether a specific plot of land has received authorization based on how long the current claimant has held possession.

It is tempting to explain the data system's fragmentation by the absence of a data-sharing protocol. However, data hoarding may also result from an agent seeking a strategic advantage in land management negotiations.

Third, in a world with growing interest in open government and open data ecosystems, GISTDA developers do not consider themselves threatened by competition, especially from agencies involved in data integration. Moreover, in servicing clients, GISTDA characterizes its relationship as akin to a tailor creating customized

AIP solutions based on the client's needs. However, a client must have a clearly defined problem and the mandate to obtain links to data from other organizations, especially for non-remote sensing data. They also need strong scientific knowledge based on socio-economic impacts to facilitate ground-level surveys and data collection.

Currently, the crop types included in land use calculations are limited to conventional crops such as upland rice, vegetables, and some fruits. These crops provide smaller profits than maize, the preferred replacement. Higher margins can be obtained from growing crops for herbal medicine or ecotourism. However, estimating land suitability for these crops is more complicated. The omission of these crops may contribute to the failure to find a win-win solution, suggesting significant room for improvement in the further development of AIP Nan.

12.4.2 Discussion

A research team from Chiang Mai University (CMU) conducted field research to validate the predictions made by AIP Nan. They identified two shortcomings. First, the government's policy to close land frontiers is in flux. Nan has adopted the 78-12-10 policy for allocating upland land into three categories: conservation, restricted use, and free use, with the latter category eventually granting land titles. This policy is considered a steady state. In Nan, the target is set, and a specific form of land governance is being explored using AIP Nan, under an experiment called the "Sandbox." This experiment was intended to be free from existing legal obligations but has not progressed. On other sides, Chiang Mai relies on a different model, which is more lenient and allows current occupants—viewed by the government as encroachers—to continue staying and negotiating for eventual land title recognition. This approach keeps both the forest occupants and government officials engaged, with third-party investors in carbon credit-related businesses potentially being involved. These investors represent distant stakeholders who benefit from carbon sequestration services provided by the trees to be planted. The author believes that Nan's approach is relatively extreme, making acceptance by current occupants unlikely.

Second, spontaneous land use changes have been ongoing, as revealed during the field trip. Ecotourism offers alternative livelihoods, and land previously used for maize cultivation has been converted back into forest. However, the trend toward a decline in land under maize cultivation remains unclear due to conflicting data from two agencies. The Nan provincial agricultural office suggests that the area under maize this year is about 357,014 rai, while GISTDA projects the area to be around 502,000 rai.

As discussed above, such data discrepancies were weeded out 10 years ago when each province was tasked with bottom-up estimations of gross provincial products (GPP). Staff from the northern branch of the Bank of Thailand and the National Economic and Social Development Board (NESDB) worked with the provincial treasury department to synchronize and analyze data. Unfortunately, when the GPP of all provinces was combined, it did not add up to the country's gross domestic product (GDP), leading to the abandonment of the bottom-up approach. The authors argue

that the bottom-up approach should be revived because AIP Nan cannot function effectively without reliable information at the ground level.

12.4.3 Priority Action for Policy

During the research, an economist on the team had the opportunity to consult with a lawyer from the Office of the Council of State, the major organization responsible for introducing new laws. The immediate topic of discussion was the regulatory impact assessment law introduced in 2019. Philosophically, the intention is to make laws outcome-oriented, which aligns with AIP's goals. The conversation led to an observation that almost all government decision-making in Thailand occurs in Bangkok. The centralization of administrative decision-making has roots in the reform of the local system of government. In the "Thesaphiban" era, Thailand began sending governors from Bangkok to replace the former system, in which provinces had a certain degree of self-rule. The reorganization of local administration aimed to consolidate control in Bangkok during the threat of Western colonization. For over 120 years, the centralization of decision-making has remained unchanged, only being waived in exceptional cases, such as the development of the EEC. A reader may wonder why the ONWR is a viable alternative to link up with GISTDA. This is due to water law and the functioning of the water agency, which follows the principle of centralization in times of crisis and decentralization in normal times. The 2011 Great Flood changed public attitudes, leading to the development of water law in 2018. Subsequent developments in water administration, organized by the river basin, and the promotion of stakeholder engagement have led to the agency's partnership with GISTDA in the Eastern Economic Corridor.

ONWR's water law was reviewed under the regulatory impact assessment law in June 2024. The results revealed that ministerial regulations addressing water quality and headwater area protection, which were supposed to be introduced, have been delayed. It is hoped that headwater protection can eventually be carried out under the water law since the agency is technically the most capable of tracking and measuring the hydrological consequences of forest cover loss and restoration. However, the multidimensional benefits of forest land make building a broad-based platform for stakeholder engagement difficult. As a result, the efforts championed by the pioneers of AIP still have a long way to go.

12.5 SUMMARY AND CONCLUSION

This study provides an overview of land cover and land use change issues in Thailand, including fire scar statistics and introducing the Actionable Intelligence Policy (AIP) platform as a policy support tool. It also examines the experiences of agencies utilizing AIP and highlights gaps that require further development. The chapter emphasizes the need for continued advancements by GISTDA, coupled with strong government support, to fully realize AIP's potential. The authors posit that AIP is a valuable tool for advancing policymaking in Thailand by leveraging remote sensing technologies.

By identifying potential challenges, especially those caused by land cover and land use changes, and simulating various policy interventions, AIP facilitates engagement with diverse stakeholders, promotes mutual benefits, and helps policymakers select optimal courses of action. However, AIP alone cannot guarantee successful policy implementation. The challenge lies in choosing a balanced and community-friendly approach, as past experiences, such as the "72-18-10" policy in Nan, have shown that rigid enforcement measures are unlikely to succeed. Collaboration between policymakers, technology providers, and local stakeholders is key to delivering sustainable policies that address the challenges of land cover and land use change in Thailand.

REFERENCES

Agarwal, S. and Lambin, E.F. (2024). Interventions to control forest loss in a swidden cultivation landscape in Nan Province, Thailand. *Regional Environmental Change* 24, 127. https://doi.org/10.1007/s10113-024-02286-5

Blaney, H.F. and Criddle, W.D. (1950). *Determining water requirement in irrigated areas from climatological and irrigation data*, Soil Conservation Service Technical Publication No. 96. Washington DC: US Department of Agriculture, 48 p.

Fantuzzo, J. and Culhane, D.P. (Eds.) (2015). *Actionable Intelligence: Using Integrated Data Systems to Achieve a More Effective, Efficient, and Ethical Government*. Palgrave Macmillan, United Kingdom (235 pages).

Howlett, M. and Ramesh, M. (1995). *Studying Public Policy: Policy Cycles and Policy Subsystems*. 2nd Edition. Toronto: Oxford University Press.

Laurance, W.F., Camargo, J.L.C., Luizão, R.C.C., Laurance, S.G., Pimm, S.L., Bruna, E.M., Stouffer, P.C., Bruce Williamson, G., Benítez-Malvido, J., Vasconcelos, H.L., Van Houtan, K.S., Zartman, C.E., Boyle, S.A., Didham, R.K., Andrade, A. and Lovejoy, T.E. (2011). The fate of Amazonian forest fragments: A 32-year investigation. *Biological Conservation* 144(1), 56–67. https://doi.org/10.1016/j.biocon.2010.09.021

OECD. (2022). *Managing and Financing Water for Growth in Thailand: Highlights of a National Dialogue on Water*, OECD Studies on Water. Paris: OECD Publishing. https://doi.org/10.1787/839a4f70-en

Wischmeier, W.H. and Smith, D.D. (1978). *Predicting Rainfall Erosion Losses: A Guide to Conservation Planning*. Health & Environmental Research Online (HERO). US EPA. USDA, Purdue Agricultural Experiment Station, USA. https://hero.epa.gov/hero/index.cfm/reference/ details/reference_id/624965

13 Understanding Observed Agricultural Landscape Change in Đồng Tháp Province, Vietnam

Local Perceptions and Drivers of Land Use and Land Cover Change around Tràm Chim National Park

Jarrod Brown, Stanley Toops, Peou Touch, Jessica McCarty, Maryam Zamanialaei, Peter Potapov, Svetlana Turubanova, Bui Thi Minh Ha, Justin Fain, and Greg Treiman

13.1 INTRODUCTION

How do we understand the landscapes that we see?

This is a bold question but the overarching goal of this work. This project sought to understand both the physical and human landscape of a community in Đồng Tháp Province, Vietnam, that is adjacent to Tràm Chim National Park. The project sought to describe agricultural land use change, identify the drivers of that change, and understand the community members' perceptions of that change by employing remote sensing, social science, and humanities methodologies. At the beginning of this work, we hypothesized that the built environment and current landscape would reflect human histories and human values. Therefore, in order to understand observed land cover/land use (LCLU) changes in the satellite record, it was necessary also to understand those histories and those values.

DOI: 10.1201/9781003396260-13

Of importance is the recognition that the study area is a historically contentious and post-conflict environment that has undergone radical transformation. This part of the Mekong Delta has not been rice paddy since immemorial, as it was previously covered by a vast Plain of Reeds wetland ecosystem. For example, in 1879, major hydrological projects aimed at developing colonial plantation agriculture by colonial powers in France and Japan occupying forced and navigable waterways broke ground and were completed (Biggs, 2012). After persistent conflict and war in the mid-twentieth century, market liberalization reforms launched in 1986 led to the intensification of agriculture (Chu, 2019). Đồng Tháp Province is an environment highly vulnerable to the impacts of climate change and upriver hydroelectric dam projects (Shaw, 2006; Kondolf et al., 2014). Our study area further represents a unique cultural-political subset within Vietnam, as the province is majority Hòa Hảo Buddhist, a form of Buddhism that emerged in the early twentieth century and was frequently in conflict with state actors. These actors included the French colonists and both Saigon- and Hanoi-based Vietnamese states, and these conflicts continue up to the present ("Hoa Hao follower arrested again in Vietnam," 2023).

13.1.1 Study Aims

Remote sensing and GIS technologies specifically identify the extent and rate of LCLU changes; however, they do not explain the underlying causes of these dynamics on the landscape (Kindu et al., 2013). This study aimed to compare the expectation of changes claimed by local communities through semi-structured interviews completed in person in 2018 and 2019 and monitor those changes using the moderate resolution 30 m classifications for 2015 to 2019 for the communities surrounding Tràm Chim National Park in Đồng Tháp, southern Vietnam. Further, it aims to identify local-scale drivers of LCLUC through discourse analysis using local interviews, public-facing press, and government publications.

13.1.1.1 Research Questions

Our overarching research questions in this work were as follows:

1. Do perceptions of land use change observed and explained by the local populations accord with actual land use change as observed by remote sensing?
2. How do people explain the drivers of landscape change?
3. What are the drivers of landscape change?

13.1.1.2 Research Site

This study focuses on areas around Tràm Chim National Park in Tam Nông District. Specifically, it includes Phú Thọ commune and Tràm Chim Commune-level Town in Đồng Tháp Province, Southern Vietnam (Figure 13.1(a),(b)). Phú Thọ has a population of approximately 10,000 people and an area of 63.76 km² (*Niên Giám Thống Kê* 2022, 2023), while the district it occupies, Tam Nông, has a population of 100,144 people and 474 km² of area (including 33,810 ha of agricultural land and 7,518 ha

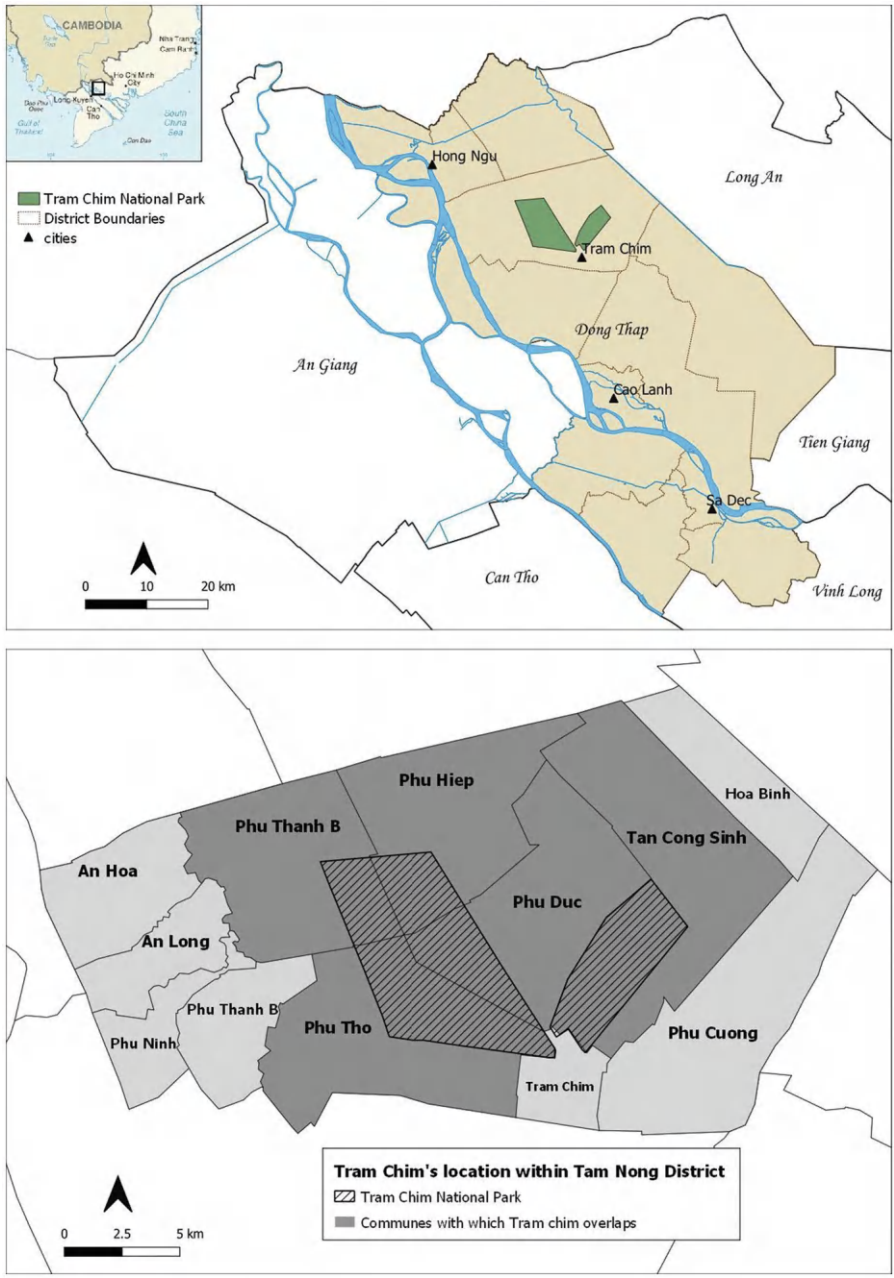

FIGURE 13.1 (a) District map of Đồng Tháp, Vietnam. (b) Inset map of Phú Thọ and Tràm Chim Communes.

of forest). Tràm Chim Town has an area of 12.28 km²; the population in 2019 was 10,761 people (*Niên Giám Thống Kê* 2022, 2023).

Tràm Chim National Park covers approximately 7,313 hectares and is roughly located at 10.4249°N and 105.3012°E. Tràm Chim is one of the last remnants of the Plain of Reeds wetland ecosystem, which previously covered some 700,000 ha of the Mekong Delta in southwestern Vietnam. The site is one of the few places in the region where the Brownbeard Rice (*Oryza rufipogon*) communities survive (https://rsis.ramsar.org/ris/2000). The Tràm Chim National Park is a Ramsar-designated wetland and a popular domestic tourism spot (https://rsis.ramsar.org/ris/2000). It is a habitat for the culturally essential flagship species Sarus Crane (*Grus antigone*) and hosts around 20,000 water birds.

13.1.2 Social Science and Humanities Approaches to Remote Sensing

Satellite imagery and remote sensing give a clear view of LCLUC. It does not, however, explain observed changes; as noted by Wood and Skole (1998), discussing their own on deforestation in the Amazon, "a fundamental limitation" of remote sensing is "the inability to explain the reasons for the observed outcomes in land-cover change" (71). Some changes observed will result from natural phenomena, but many changes will result from human activity. Built environments reflect the values of the inhabitants of those environments, or at least the individuals with the capacity, through political, economic, or other types of power, to act upon it (Lewis & Kuttler, 1978; Pratt, 2009; Spalding, 2017). Understanding the drivers of LCLUC means grappling with the complexities of the social world and the intersection of worldviews, systems of values, land tenure regimes, economics, and, as our research discovered, local history, particularly economic history (Rindfuss & Stern, 1998).

The relationship of the social sciences to remote sensing has been well explored over the previous two decades (Liverman et al., 1998; Crews and Walsh, 2009; Joyce et al., 2022). In addition to social science approaches, this project utilized approaches more at home in the humanities, such as documentary historical research and engagement with religious and cultural texts related to environmental and agricultural values. It sought to articulate LCLUC in the epistemic, ontological, and ethical setting of the inhabitants of the landscape and the historical and socio-economic setting, contextualizing the changes observed within the cultural, social, and political realities of the inhabitants occupying that space. This work builds on current scholarship linking remote sensing to digital humanities (Trevisani and Omodeo, 2021).

13.1.2.1 Critical Remote Sensing

This research was informed by the practices of critical remote sensing, particularly to foreground the social science and humanities approaches to attempt to capture better the entire story given from local knowledge and experiences and not solely rely on "neutral" satellite imagery (Bennett et al., 2024). Critical geography and critical remote sensing/GIS are undertakings that are aware of the operations of powers in both the landscapes and people they observe, in the structures that make observations and research possible, and in the researchers' embeddedness in historical processes

and structures of power (Pickles, 1995). Additionally, it is the use of these technologies to address injustices in society (Wilson, 2015). Bennett et al. (2022) identify two additional practices of critical remote sensing: "engaging local, Indigenous, and other knowledge typically perceived as situated, and, in so doing, acknowledging remote sensing's own subjectivities" and "seeking to empower marginalized actors with remote sensing data and skills [sic]" (732).

The project engaged deeply in autochthonous knowledge systems primarily through the engagement with the Hòa Hảo community through ethnographic methods both in-country and among American diaspora communities, careful study of the sect's religious canon, and conferring with religious and community leaders, allowing us to frame issues and questions with greater ontological resonance (Hinton, 2005; Nygren, 1999). Co-investigator and lead author Brown has been visiting the area for over a decade and has long-standing social, familial, and research connections in the community. Researchers relied on local public discourses throughout to inform understanding of the area. Datasets and findings were made available to in-country collaborators, and annual reports were provided to in-country partners. In-country collaborators were offered training using QGIS, although this was declined. It remains an open question how this research will be consumed and used by the communities in which it was conducted. It has, however, opened up new perspectives and approaches, pointed in new directions for more critically aligned remote sensing projects, and better equipped the researchers to work in the region. Ultimately, we hope this work was improved by and can contribute to the growing field of critical remote sensing.

13.1.3 The Đồng Tháp Agricultural Landscape

The Mekong Delta has restructured agriculture towards climate-change adaptation and market demand by establishing specialized farming areas for its key agricultural products, growing other crops on ineffective rice fields, or rotating rice with other crops on the same field (*Vietnam Plus*, 2019). Paddy prices in the Mekong Delta have fallen sharply, and what has happened with the tra fish (*Pangasius court*) is no better, with prices dropping steadily. In 2018, farmers in Đồng Tháp began to use more than 3,000 ha of low-yield rice fields for growing fruits and other crops, mainly growing corn, sesame, soybean, sweet potato, lotus, mango, longan, orange, and dragon fruit. Farmers growing fruits and other crops have seen their incomes double or even triple, according to local authorities (*Niên Giám Thống Kê* 2022, 2023). Those growing corn have average yields of 8–12 tonnes per hectare per crop and each time earn 7–10 million VND (300–430 USD) higher than rice. Provincial authorities have encouraged farmers to use infertile paddies to grow corn and establish concentrated areas for the crop in Hồng Ngự, Thanh Bình, Tam Nông, Lấp Vò, and Lai Vung districts (*Vietnam Economic News*, 2018). Đồng Tháp province, which was the country's first locality to implement restructuring agriculture 5 years ago, has chosen rice, flowers and ornamental plants, mango, tra fish, and ducks as key products for restructuring (*Viêt Nam News*, 2019).

The impacts of climate change on Đồng Tháp are increasingly evident. Storms, floods, irregular tornados, thunderstorms, and lightning create serious risks (Ministry of Natural Resources and Environment, 2016). Many localities in Đồng Tháp face a riverbank erosion situation that is very dangerous; there is an estimated annual loss of 30 to 50 hectares of land due to erosion along the river (Tri et al., 2023). Agriculture faces trouble because cultivated areas tend to be acidified, especially in Đồng Tháp Mười. Biodiversity is also severely affected in wetland ecosystems in Tràm Chim National Park (Duong et al., 2015). Under climate change scenarios, the water level in Đồng Tháp province will increase by 20 cm and 48 cm by 2050 and 2100, respectively (Ministry of Natural Resources and Environment, 2016), flooding current farmlands. The water level rise will cause deep flooding in some areas, such as Tan Hong, Hồng Ngự, Hồng Ngự township, and a part of Tam Nông district. Areas affected by river erosion will be Sa Đéc city, Hồng Ngự township, Thanh Bình and Hồng Ngự districts. Areas affected by drought will be Tràm Chim National Park, Tháp Mười, and Tam Nông districts. Climate change will also increase pollution, decline the quality and quantity of the aquatic ecosystem, and change the purpose of use of water resources (Ministry of Natural Resources and Environment, 2016).

13.2 DATA AND METHODS

13.2.1 Analytical Framework

This study identified LCLU changes that occurred with remote sensing between 2015 and 2019. This was combined with perceived changes that local people reported by conducting interviews. In addition, other governmental and media sources reporting LCLUC change and explanations of drivers of these changes were presented (Figure 13.2).

13.2.2 Interviews

In 2019, human subjects' institutional review at two U.S. institutions of higher learning (Berea College and Miami University) and governmental review within Vietnam resulted in 11 approved questions for semi-structured interviews, including verbal survey questions asked of each participant. Questions were translated into Vietnamese. The questions centered around the approximate amount of land worked, the crops and fruit grown, animals and fish raised, land use changes, and changes in roads, buildings, and construction practices (Table 13.1). Ten participants were interviewed in 2019; subsequent follow-up interviews were not possible due to Covid-19 border closures. Participants ranged in age from early twenties to seventies, and all indicated they lived in the immediate area. Most of the conversations were in-depth, ranging from 10 to 30 minutes. Both convenience and snowball sampling approaches were used to identify participants (Bernard, 2002). Interviewees were approached outside by going inside nearby establishments to ask about the owners of nearby land and through introductions by other participants. We also observed the families in their homes and, in some cases, on their land. Co-author Touch administered the

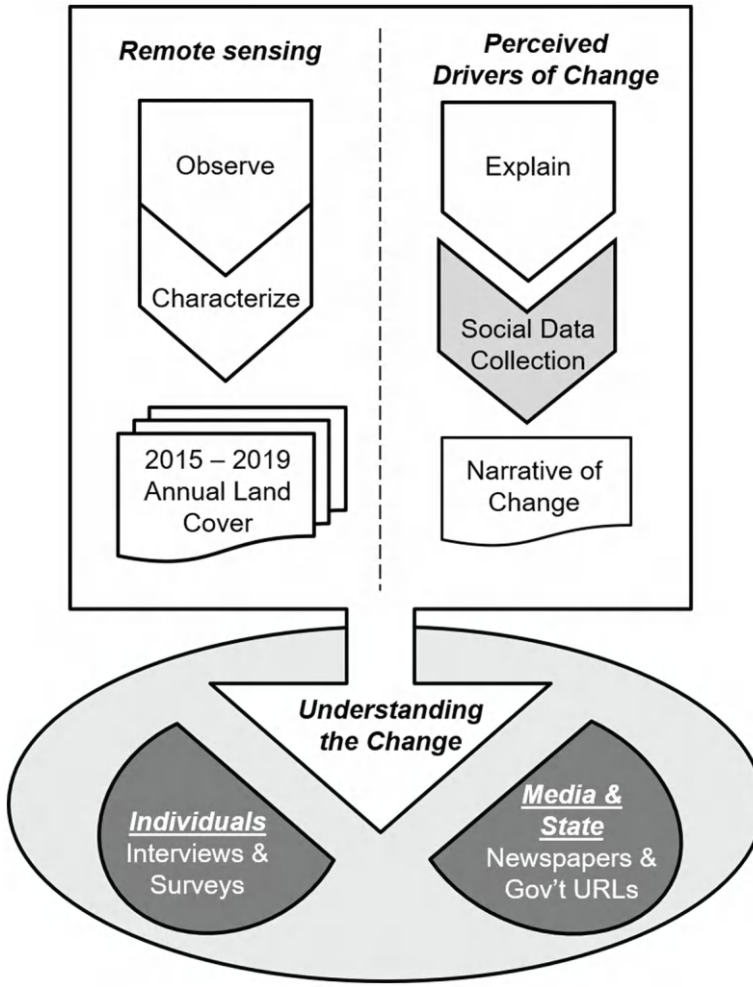

FIGURE 13.2 Analytical framework used in this analysis.

questionnaire in Vietnamese, with follow-up questions by Co-authors Brown and Toops in a combination of English, Vietnamese, and Mandarin. Written notes were taken of interviews, and the locations were logged using a smartphone GPS application. Outside images, if applicable, were taken using location-enabled mobile phones to record landscapes and to document any changes being identified. These interviews were supplemented by informal conversations the previous year (2018) as we surveyed the research site and prepared for formal governmental review. The identity of the interviewees was not recorded, per the recommendations of the human subjects' board; in this work, results are reported generically by "family" or by approximate but not exact location to protect privacy.

TABLE 13.1
Questionnaire Used for Semi-Structured Interviews; Note that the Same Questions Were Asked of Each Participant

1. What crops and/or fruit trees are produced? Has this changed from past years?
2. How much land do you farm? Has this changed from past years?
3. What animals are raised? Has this changed from past years?
4. How many animals have you raised? Has this changed from past years?
5. What forest plants are produced? Has this changed from past years?
6. How much forest (size) or windbreaks do you keep? Has this changed from past years?
7. What aquatic products (fish) are produced? Has this changed from past years?
8. How much fish are produced? Has this changed in past years?
9. What changes in land-use or land-cover have you seen in the past years?
10. What road improvements have you seen in the past years?
11. How many new buildings have you seen in the past years? How many renovated buildings have you see in the past years? Have you seen any new construction (for example medical, temples, mining, sluice gates/dikes/ponds) in the past years? In general, what are the sizes of these new constructions?

13.2.2 Discourse Analysis

Initially, social media data collection was attempted using Twitter, Instagram, and Facebook social media networking platforms. However, there was a lack of geo-tagged postings for the research area. Therefore, we identified other accessible domains of public discourse regarding land use change. These were the province-level local government's Vietnamese language website, *Cổng Thông tin Điện Tử Tỉnh Đồng Tháp* (dongthap.gov.vn), and its district-level sub-domain, *Trang Thông tin Huyện Tam Nông* (tamnong.dongthap.gov.vn). Posts were retrieved from January 1, 2016, to July 1, 2021. A subset of 53 pages mentioning "Phú Thọ" was used for analysis. Data was also collected from the Vietnamese-language provincial online newspaper, *Báo Đồng Tháp Online* (baodongthap.vn), based in Cao Lãnh, Đồng Tháp province. A subset of pages was identified using mentions of "Phú Thọ" from January 1, 2016, to July 1, 2021. 212 were returned. All pages were public-facing, and translation was conducted by co-authors Touch and Brown.

Retrieved web pages were human-reviewed, sorted for relevance, and hand-coded for impressionistic analysis (Schutt, 2015). This approach differs from work that 'scrapes' text and qualitative data from the Internet and web-based databases (Parvez et al., 2018), since all data was subjected to human analysis and review. Documents were then auto-coded using Atlas.ti, a computer-assisted qualitative data analysis software, for keywords generated from interviews and *a priori* keywords related to land use (Friese et al., 2018; Guest et al., 2012). A list of 41 Vietnamese terms associated with land use and land use change was used. Auto-coding was to ensure relevant

TABLE 13.2
Output Land Cover Classes with Accompanying definitions

Pixel Value	Class	Description
1	Build-up	Landsat pixel includes build-up area or paved road
2	Permanent water	Permanent water (Landsat pixel covered with water >=75% of the year)
3	Tree cover	Tree canopy cover >=50% of a pixel. The class includes forests, tree plantations, and orchards.
4	Cropland	Annually/seasonally rotating crops (rice, corn, sweet potato, other). May include non-crop grasslands and intensively managed pastures
5	Intermittent water	Non-crop treeless area covered with water >=25% of the year. This class includes aquaculture, wetlands, and mangroves.
6	Other	Mixed land cover pixels (rural mosaic), unused lands, transitional land cover, specific agriculture types (some vegetables, dragon fruit plantations, mixed orchard/crops and orchards with very small and sparse trees), natural wetlands/grass, fresh logging sites, dry shrubs/rocks on slopes, and other.

information was not overlooked during hand-coding. All auto-coding was manually confirmed. Word frequency analysis was also generated for each subset using Atlas.ti (Paulus & Lester, 2016). Word-frequency analysis identified emergent themes, most notably the Covid-19 pandemic. The high frequency of one of the *a priori* terms ("cá lóc," "snakehead fish") led us to investigate the creation of an *appellation d'origine contrôlée* for Phú Thọ dried snakehead fish (primarily *Channidae channa*). This subject was significant and is discussed in the findings.

13.2.3 Remote Sensing Approaches

Given extensive knowledge of the region from a decade of working in the region, in addition to the 2018 and 2019 field collects and interviews indicating LCLUC occurring at relatively rapid time steps, this analysis relied on the moderate resolution University of Maryland's Global Land Analysis & Discovery's (GLAD) 30 m Landsat Analysis Ready Data (ARD) collected from 1997 to 2019 at 16-day intervals (Potapov et al., 2020). Previous work with very high-resolution commercial data and high-resolution synthetic aperture radar data had been successful in mapping changes in rice paddy field boundaries across several years (Thomas et al., 2020) but not in determining more complex LCLUC changes across multiple land use types known to occur in Đồng Tháp intra- and inter-annually. The GLAD 30 m Landsat Analysis ARD product also features an observation quality flag layer

(QF) to perform study region-specific analysis (Potapov et al., 2020). The QF pixel value indicates the presence of clouds/cloud shadows and land or water detection for clear-sky observations (Table 13.3). For this research, there was a need to creatively adapt the standard GLAD Landsat ARD products to detect known local land uses and LCLUC, namely fine spatial scale changes in water permanence, built-up trees, and croplands—beyond just rice.

13.2.3.1 Annual Water Permanence: Mapping Paddy and Fishponds

The annual water permanence is defined as the ratio of water detections to all clear-sky observations within a year. Due to an inconsistent number of cloud-free observations between years, water permanence has a high variation between years. To create a consistent time-series, an annual water permanence (%) was converted into water permanence type. Various values are assigned to distinct criteria depending on the water percentage in different land types. Land with a water percentage equal to or less than 25% is given a value of 0. Areas featuring intermittent water, with a water percentage greater than 25% but less than 75%, are assigned a value of 1. A value of 2 is reserved for land characterized by permanent water, where the water percentage equals or exceeds 75%. Then, two consecutive 7-year median filters were applied to the water permanence type time series to reduce high-frequency noise. The output layers represent the annual water permanence type, whereby the intermittent water may indicate paddy rice and certain types of aquaculture.

13.2.3.2 Annual Built-Up Area: Expanding Housing and Transportation

The built-up area class includes buildings and transportation infrastructure. This class was mapped using Landsat annual phenological metrics (see Potapov et al., 2020 for details). Training sites were manually allocated. The output time series consists of annual class detection layers. The built-up class is spectrally similar to other non-vegetated surfaces (sand bars, construction sites, fallow fields, or exposed ground). To reduce the presence of false detections, we implemented the temporal filtering of the annual built-up class time series. We applied consecutively a 5-year median and a 7-year median filter to class time series to reduce high-frequency noise. Instances of the built-up area loss were then removed. If the built-up area loss was detected during the time series, but the area was classified as built-up in 2000 and 2019, the built-up class was assigned to all years; otherwise, we removed built-up detections from the time series. The output layers represent the annual built-up area presence.

13.2.3.3 Annual Tree Cover

Tree cover is defined as the presence of trees within a 30 m Landsat data pixel. A pixel was included in this class if it has >=50% of tree canopy cover. The tree cover class was detected visually, and the exact threshold may vary depending on tree cover type and other conditions. The class was mapped using Landsat annual phenological metrics (Potapov et al., 2020). Training sites were manually allocated. The output time series consists of class detection layers. To reduce high-frequency noise in the

time series, we applied two consecutive 5-year median filters. The output layers represent the annual tree cover area extent.

13.2.3.4 Annual Crop Extent: Permanent Row Crops and Not Just Paddy Rice

Crop class is defined as row crops, with the annual and seasonal rotation including paddy rice, sweet potato, corn, and vegetables—crop types noted during the 2019 field collection in Đồng Tháp. This class does not include shrub/tree or dragon fruit plantations, which have been extensively mapped by Jia et al. (2022). The Landsat pixels with crops occupying most of the pixel area are assigned to this class. Landsat annual phenological metrics were used, with the metric set for crop mapping specifically designed to map permanent agriculture. For each year, the data is collected from the current and three preceding years and aggregated using vegetation indices ranking. This way, we create a metric set that highlights the crop presence even if crops are intermittent by fallows. Training sites were manually allocated within the entire Southeast Asia. The output time series consists of class detection layers. To reduce high-frequency noise in the time series, we again applied two consecutive 5-year median filters. The output layers represent the annual crop extent.

13.2.3.5 Annual Land Cover

SERVIR-Mekong Regional Land Cover Monitoring System data mask is used to limit land cover mapping (https://servir.adpc.net/tools/regional-land-cover-monitoring-system). The mask represents the land boundary (GADM V2.0) with a 10 km buffer to preserve shoreline and small islands. Land cover class was defined for each year using the hierarchy of the thematic layers. The following algorithm was used to define the land cover class:

```
if (data mask==1) {
        if      (built-up==1)     {LC = 1;}
        else if (water==2)        {LC = 2;}
        else if (tree==1)         {LC = 3;}
        else if (crops==1)        {LC = 4;}
        else if (water==1)        {LC = 5;}
        else                      {LC = 6;}
}
else {LC = 0;}
```

The output land cover classes are reported in Table 13.2.

13.3 RESULTS AND DISCUSSION

13.3.1 Remote Sensing-Based LCLUC

Remote sensing often involves the analysis of large-scale data collected from satellite or aerial sources, and applying statistical approaches to ground-level data may not yield accurate or meaningful results. A confusion matrix is a tool commonly used to

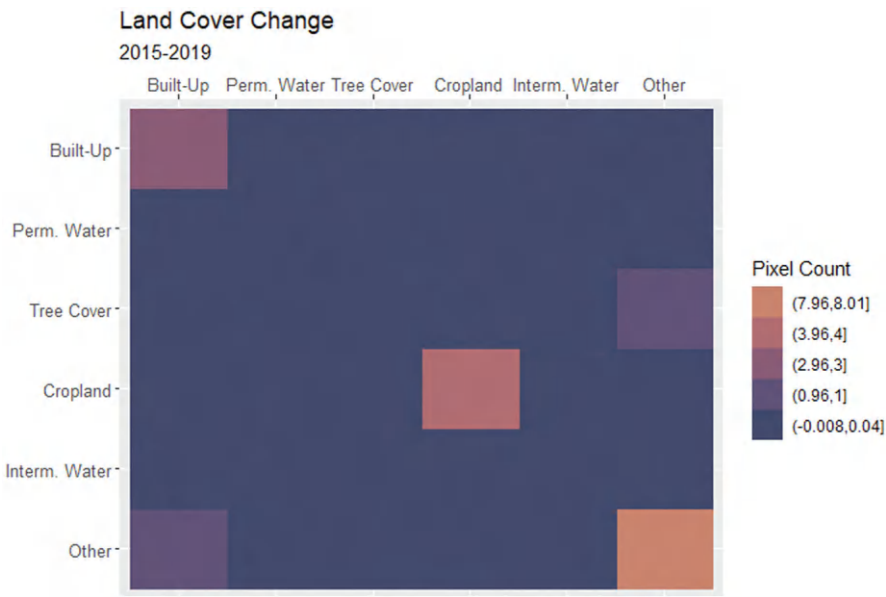

FIGURE 13.3 Quilt plot showing the confusion matrix of land cover class changes between 2015 and 2019.

evaluate the performance of a classification algorithm; here we visualize this (lack of) directional change via a quilt plot. In the context of remote sensing, it would typically be used to assess the accuracy of land cover classifications. The data presented in Figure 13.3, depicting the confusion matrix, offers insights into the outcomes of land cover classification between the years 2015 and 2019. The analysis indicates that there were no significant LCLUC shifts across the main LCLUC types of permanent water, built-up, crops, trees, and mixed-use, as observed at the 30 m resolution in the GLAD Landsat ARD classifications created for this specific study region and study period. With this finding, we turned to official governmental statistics and local perceptions of change, in addition to field-observed collects of the landscape.

13.3.2 Agricultural LCLUC from the Đồng Tháp Statistical Yearbook

Tam Nông District experienced a change in agricultural land use as recorded in the Đồng Tháp Statistical Yearbook from 2005–2019. In 2019, there was 70,959 ha of paddy, a decrease from 2015 with 72,416 ha of paddy and in 2010 with 60,193 ha of paddy (Ha, 2020). However, in 2019, paddy yield was 66.02 quintals/ha (the highest in the province), up from 58.58 quintals/ha in 2015 and 58.77 quintals/ha in 2010. This indicates less area in paddy rice, but higher yields. Vegetables and flowers experienced an ebb and flow, with 728 ha in 2019, which was less than the 1,230 ha in 2015 but greater than the 590 ha of vegetables and flowers in 2010. Fruit trees, mainly mango and coconut with some orange and longan, showed an increase in area in 2019, with 117 ha, compared to 88 ha of fruit trees in 2015 and 97 ha in 2010. Corn

(maize) had decreased some in 2019, with 88 ha, compared to the high of 113 ha in 2015. In 2010, only 7 ha of corn (maize) was grown. Sesame production decreased by over 100 ha in 2019 to only 6 ha of sesame, compared to 108 ha of sesame in 2015. In 2019, there was 988 ha aquaculture, an increase from 2015, with 881 ha aquaculture, but a slight decrease from 2010, with 1,046 ha aquaculture. As of 2019, Tam Nông District was planted mostly with rice with some aquaculture, vegetables, and flowers, as well as fruit trees.

What is surprising is the decrease in aquaculture area from 2010 to 2015, although from 2015 to 2019, 107 ha of aquaculture was added. However, the gross output of aquaculture per ha in Tam Nông increased from 391 million VND in 2005 to 456 million VND in 2010 to 1,348 million VND in 2015 (*Thông tin, báo cáo thống kê năm 2015*, 2015). Production increased from 42,857 tons in 2015 to 76,057 tons in 2019 (Ha, 2020, 385). So, despite the falling area of aquaculture between 2010 and 2015, the gross value of the product nearly tripled. While productivity in tonnes was not available between 2005 and 2010, tonnage nearly doubled from 2015 to 2019. This suggests a shift from 2005 onward to higher-value products and more productive ponds, possibly from a combination of more intensive aquaculture and improved fishery management. In 2013, a fish drying plant was opened focused on snakehead fish, and production then at 60 ha was expected to increase to 200 ha over the coming years—although that number could include existing ponds being transitioned to snakehead fish production given that snakehead is a higher-value product despite market fluctuations ("Chế Biến Khô Cá Lóc Bằng Hệ Thống Sấy," 2013; Sinh et al., 2014).

13.3.3 Individual Perceptions of Change and Drivers of Change

The field interviews and collected field data reveal significant shifts in LCLUC across the study period years, as reported by nine farming families interviewed in 2018 and 2019 in the vicinity of Tràm Chim National Park. The predominant vegetation includes *Melaleuca cajuputi,* a member of the myrtle family. The continuity of these features over the past 5 years suggests a commitment to environmental preservation. However, the changes in the Phú Thọ Commune in 2019 present a more dynamic picture. Family 1, for example, transitioned from solely growing sticky rice to engaging in aquaculture activities. Family 2 diversified their agricultural activities, transitioning from cultivating melons on dikes to managing a variety of crops such as lotus, coconuts on dikes, and freshwater shrimps and catfish. Such land-use transformations highlight the adaptability and diversification strategies employed by local farmers and represent LCLUC from predominantly rice paddy to more complex hyperspatial resolution changes.

From the 2019 interviews of ten participants, respondents had between 0.5 and 4.0 *cong* of land (or approximately 0.05 hectares to 0.4 hectares). Crops included sticky rice, rice, lotus, melon, vegetables, bamboo, and medicinal herbs. Animals included chicken and geese, with fish being mainly shrimp and catfish. Jackfruit and coconut were commonly grown. Some respondents built new fishponds circa 2014 on formerly rice and lotus lands. One respondent built a fishpond circa 2000. Many tables of drying fish were observed on the roadside, with another party grinding up spoiled

fish from the market into fish food. Another had a fishpond that went bad and is now stagnant.

The data from 2018 also provides insights into land use changes. Phú Thọ Commune, for instance, witnessed alterations in crops, with a shift from rice and water lotus to a focus on sticky rice (or glutinous rice) cultivation. Similarly, Tràm Chim Town underwent noticeable changes, with some properties appearing abandoned or overgrown, signaling potential migration trends. Economic pressures were mentioned in the Hòa Hảo Temple area, underscoring the complex interplay between tradition and economic necessities, leading to changes in the way of life.

People are aware of visible changes in their surroundings, but individuals' reports of change were often not reliable predictors of change observed from the remote sensing method or the reported official agricultural statistics. During interviews, individuals could indicate changes had occurred. For example, individuals were aware of visible changes, such as the installation of a new bridge and canal dredging that was observed by our team, and were able to recollect road paving work. However, recollections of transitioning an aquaculture pond from one product to another were not reported.

People primarily attributed land change on privately held land to individuals' economic decisions. Fluctuations in the rice market, in the price of fish, or other agricultural products were often given as reasons for their own or observed changes to the landscape. Infrastructure changes, like a new bridge, road, or canal dredging, were assigned to the state. During interviews, individuals were unaware of how such changes were being financed or why—and never mentioned the private sector or development partners' role in the changes or specific policies. Therefore, individuals interviewed were unable to identify drivers of change outside of agricultural price fluctuations and state activity.

13.3.4 Linking the Local-Scale Remote Sensing Observed Change to Perceived Drivers

Tables 13.3–13.5 show the perceived and mapped changes for each study location in 2019 and 2018, with GLAD Landsat ARD product mapping LCLUC in both 2015 and 2019. In Location 1 for 2019, the interview highlighted a continuation of built-up activities, which aligns with the remote sensing data showing sustained built-up. Location 2 witnessed an increase in shrimp and catfish production, along with coconut, lotus, and vegetable cultivation; the remote sensing data suggests some similarity in land cover patterns between 2015 and 2019, encompassing mixed land cover pixels and specific agriculture types. Similarly, Location 3's perception of lotus and chicken cultivation aligns with the remote sensing data depicting mixed land cover pixels with specific agriculture types. Location 4 reported a cessation of fish farming, leading to land use shifting towards built-up activities, consistent with the remote sensing data. Location 5 exhibited a change from rice, lotus, jackfruit, and bamboo cultivation to shrub leaves for drinks. The remote sensing data indicated a transition from tree cover in 2015 to mixed land cover pixels in 2019, emphasizing alterations in vegetation types. Location 6 reported rice, turmeric, and herb cultivation, consistent with the remote sensing data showing built-up and mixed land cover pixels in

TABLE 13.3
Perceived and Mapped Change for Each 2019 Study Location (road 1–7)

Location	Perceived LCLUC from Interview	Remote Sensing LCLUC
Location 1	Sticky rice and small fish pond between buildings	2015: Build-up 2019: Build-up
Location 2	Increasing shrimp and catfish production, with coconut, lotus, and vegetables	2015: Mixed land cover pixels (rural mosaic), specific agriculture types (some vegetables, dragon fruit plantations, mixed orchard/crops and orchards with very small and sparse trees), natural wetlands/grass, fresh logging sites, dry shrubs/rocks on slopes, and others. 2019: Mixed land cover pixels (some vegetables, dragon fruit plantations, mixed orchard/crops and orchards with very small and sparse trees), natural wetlands/grass, fresh logging sites, dry shrubs/rocks on slopes, and others.
Location 3	Lotus and chicken Coconut, veg	2015: Mixed land cover pixels specific agriculture types (some vegetables, mixed orchard/crops and orchards with very small and sparse trees) 2019: Mixed land cover pixels specific agriculture types (some vegetables, mixed orchard/crops and orchards with very small and sparse trees)
Location 4	Fish died, not using pond	2015: Build-up 2019: Build-up
Location 5	rice, lotus, jackfruit, bamboo Shrub leaves for drinks	2015: Tree Cover 2019: Mixed land cover pixels (Orchards and Crops)
Location 6	Rice, turmeric, herbs	2015: Build up and Mixed land cover pixels (rural mosaic) 2019: Build up and Mixed land cover pixels (rural mosaic)
Location 7	Rice to big fish pond (catfish)	2015: Mixed land cover pixels (rural mosaic), Wetlands 2019: Mixed land cover pixels (rural mosaic), Wetlands

TABLE 13.4
Perceived and Mapped Change for Each Study Location 2019 (canal 8–10)

Location	Interview	LCLUC Change
Location 8	Rice, lotus to fish ponds	2015:Cropland 2019:Cropland
Location 9	Rice to fish ponds	2015:Cropland 2019:Cropland
Location 10	Rice to fish ponds	2015:Cropland 2019:Cropland

TABLE 13.5
Perceived and Mapped Change for Each 2018 Study Location

Location	Perceived LCLUC from Interview	Remote Sensing LCLUC
Location 1	- Water Lotus (Seeds and Roots) - Chicken, Ducks and Cows - Fish pond adjacent	2015: Cropland 2019: Cropland
Location 2	- Sticky rice (tripled-crop per year)	2015: Mixed land cover pixels (rural mosaic), specific agriculture types (some vegetables, dragon fruit plantations, mixed orchard/crops and orchards with very small and sparse trees), natural wetlands/grass, fresh logging sites, dry shrubs/rocks on slopes, and others. 2019: Mixed land cover pixels (some vegetables, dragon fruit plantations, mixed orchard/crops and orchards with very small and sparse trees), natural wetlands/grass, fresh logging sites, dry shrubs/rocks on slopes, and others.
Location 3	- Regular Rice and Sticky Rice - Several properties look abandoned/overgrown - people have moved away to Saigon - road improved in the last few years - Things have not changed much in last ten years	2015: Mixed land cover pixels (rural mosaic), specific agriculture types (some vegetables, dragon fruit plantations, mixed orchard/crops and orchards with very small and sparse trees), natural wetlands/grass, fresh logging sites, dry shrubs/rocks on slopes, and others. 2019: Mixed land cover pixels (some vegetables, dragon fruit plantations, mixed orchard/crops and orchards with very small and sparse trees), natural wetlands/grass, fresh logging sites, dry shrubs/rocks on slopes, and others.
Location 4	- Rice - Contains small fish enclosures	2015: Mixed land cover pixels (rural mosaic) and Intermittent Water 2019: Mixed land cover pixels (rural mosaic) and Intermittent Water
Location 5	- Hoa Hao Temple established 1961, built 1962, 2007 remodel - Way of life is changing due to economic pressures. - fishing is not allowed inside even if land cannot be cultivated - Acknowledges special place rice farming has in Hoa Hao but now too many people and not enough land to be farmers	2015: Build-up 2019: Build-up

(*continued*)

TABLE 13.5 (Continued)
Perceived and Mapped Change for Each 2018 Study Location

Location	Perceived LCLUC from Interview	Remote Sensing LCLUC
Location 6	- Rice fields adjacent - Some sticky rice	2015: Mixed land cover pixels specific agriculture types 2019: Mixed land cover pixels specific agriculture types
Location 7	- Big and small fish ponds - Sugar cane field growing adjacent to pond - Coconut palms - Mango trees	2015: Mixed land cover pixels (rural mosaic), specific agriculture types (some vegetables, dragon fruit plantations, mixed orchard/crops and orchards with very small and sparse trees), natural wetlands/grass, fresh logging sites, dry shrubs/rocks on slopes, and others. 2019: Mixed land cover pixels (some vegetables, dragon fruit plantations, mixed orchard/crops and orchards with very small and sparse trees), natural wetlands/grass, fresh logging sites, dry shrubs/rocks on slopes, and others.

a rural mosaic pattern. Location 7 experienced a shift from rice cultivation to a large fishpond (catfish), with the remote sensing data showcasing mixed land cover pixels and wetlands.

Table 13.4 also depicts changes in locations adjacent to canals (Locations 8–10). These areas transitioned from rice and lotus to fishponds, as indicated by the interview and remote sensing data classifying them as cropland in 2015 and 2019.

Additionally, Table 13.5 details the perceived and mapped changes in 2018 for various study locations. For instance, Location 1 reported water lotus, chicken, ducks, cows, and an adjacent fishpond, corresponding with the remote sensing data showing cropland in both 2015 and 2019. Similarly, Location 2's perception of sticky rice aligns with the remote sensing data depicting mixed land cover pixels and specific agriculture types. Location 3 indicated regular rice and sticky rice cultivation, acknowledging abandoned properties and economic pressures leading to changes in the way of life. The remote sensing data supports these findings by showcasing mixed land cover pixels in both 2015 and 2019.

13.3.5 Narrative of Change From Media and Public-Facing Government Document Analysis

The provincial-level Vietnamese language website (dongthap.gov.vn) posts for the time period of January 1, 2016–July 1, 2021, and the district-level website (tamnong.dongthap.gov.vn) posts for the time period of January 1, 2016–July 1, 2021, were

used to analyze state discourse. These government portals generally discussed three drivers of change: agricultural economics and agricultural policy; development and development policy, and environmental policies, particularly water and water management. Development and development policy was discussed specifically in the context of The National Target Program for New Rural Development (NTP-NRD) and the World Bank Mekong Delta Integrated Climate Resilience and Sustainable Livelihoods Project (MD-ICRSL/WB9, or simply WB9), which both focus on sustainable and climate resistant development.

NTP-NRD supported "initiatives towards climate-resilient agriculture or environment-friendly agriculture and/or livelihoods [and] adapt rural infrastructure quality specifications to address climate variability issues" (*New Rural Development and Sustainable Poverty Reduction Support Program*, 2017). Infrastructure developments (bridge construction, road repairs, canal dredging) were largely associated with policies like NTP-NRD. The WB9 Project, which will run until 30 June 2024, seeks to "improve climate resilience of land and water management practices in selected provinces of the Mekong Delta in Vietnam" and is reportedly being used in the district to fund sustainable development focusing on converting low-efficiency paddy fields into more productive crops, including orchards, soybeans, and aquaculture; repairing fishery infrastructure; and the piloting of dual cropping of rice and fish products (*Mekong Delta Integrated Climate Resilience and Sustainable Livelihoods Project*, 2023; *Project Report*, 2020). Therefore, while the provincial- and district-level government portals did not offer a narrative of land use change per se, they were instrumental in identifying policies impacting land use and land use change.

The *Báo Đồng Tháp Online* was analyzed, with pages mentioning "Phú Thọ" [138], seeking drivers or descriptions of land use change. The news source largely attributed the change to government policies aimed at economic and infrastructure development and policy as the driver of change and closely aligned with state pronouncements. The major issue [setting aside Covid-19] associated with Phú Thọ was the development over 2020–2021 of an *appellation d'origine contrôlée* certification for dried snakehead fish (*Channa striata*) and various mechanisms, like a ""Phú Nông Hội Quán" (PNHQ), an assembly hall for snakefish farmers, to create/expand the local market for "Phú Thọ Dried Snakehead Fish." Using the *Báo Đồng Tháp Online*, we were able to construct a micro-history of Phú Thọ that helped contextualize the emphasis on aquaculture development in Phú Thọ and particularly snakehead fish production.

13.3.5.1 The Development of the Dried Snakehead Fish Industry in Phú Thọ

In 1961, Nguyen Van Dinh immigrated with his family from An Giang, near Châu Đốc, to Phú Thọ to escape wartime conditions there. They raised some rice and some vegetables, fished, and collected snails, investing their earnings in reclaiming "swampland" for agriculture (Trung, 2012). They endured extreme hardships due to wartime conditions and disruptions. "By 1990, too many people were fishing … Fisheries were exhausted," reported Nguyen. "In April 1992, I began to collect fish fry

in the wild to bring home and raise in the ponds around my house" (Trung, 2012). His efforts were very successful: After 8 months, he harvested 20,000 snakeheads from a 700 m^2 pond. This harvest earned Dinh the equivalent of $8,300–$8,600 adjusted for inflation (the average per capita income was $137) (World Bank World Development Indicators, n.d.). Encouraged, Nguyen began experimenting with fish breeding and different fish foods, reinvesting part of his income into further ponds. By 2004, he was raising 200 tonnes of snakehead each year (Trung, 2012). Dinh's success inspired neighbors, and in 2006, he was awarded a "Model Farmer" award. His fish farm was used as a showcase farm, with individuals brought to his farm in order to learn more about the techniques he had pioneered (Trung, 2012).

In 2013, the Tu Quy Joint Stock Company opened a commercial fish drying and packing facility devoted, at the time of its opening, exclusively to processing snakehead fish ("Chế Biến Khô Cá Lóc Bằng Hệ Thống Sấy," 2013). At that time, according to Mr. Do Cong Binh, director of the company, the company had invested 300 million VND to build a factory and install a drying system; the facility could process up to 500 kg of fresh fish (140 kg of dried fish) per day, and by December 2014 had invested a total of over 4 billion VND (about $164,700 USD), partially funded by the state ("Chế Biến Khô Cá Lóc Bằng Hệ Thống Sấy," 2013; Nhật, 2014).

It was reported in 2013 that 60 ha in the district of Tam Nông were devoted to snakehead fish production, with plans to expand the farming area to 200 hectares ("Chế Biến Khô Cá Lóc Bằng Hệ Thống Sấy," 2013). That may have included transitioning existing ponds from other species to snakehead production. By 2015, 30 households and some 300 individuals were involved in dried snakehead production. By 2017, there were 40 households involved in production. While outside our analysis timeline, by 2022, it was reported that 200 households were involved in snakehead fish production, a fivefold increase in just 5 years (Chí, 2022).

In 2017, a "Snakehead Farmers Assembly Hall" was constructed to encourage training and development for farmers (Khánh, 2017). By that time, there were a total of 15 processing facilities for drying snakehead fish (Dương, 2017). By January 2021, that number had at least doubled, with the Tu Quy Joint Stock Company alone operating more than 30 establishments for processing and selling dried aquaculture goods (Mẫn, 2021). The industry's growth was tied in part to the well-developed infrastructure of roads and waterways that connected the commune to outside markets and the strong brand recognition (Mẫn, 2021). In 2019, "Phú Thọ Dried Snakehead Fish" ("Khô Cá Lóc Phú Thọ") received an appellation of origin from the Vietnamese government, designating it an official geographical origin product, and in 2021, the Department of Agriculture and Rural Development developed a certification process for regulating and managing products with the designation (Mỹ, 2021).

Hence, the analysis of public-facing news sources allowed for the construction of a local economic history that greatly informs understanding of the combination of local conditions that have fueled the expansion of aquaculture, first snakehead fish production, and subsequently other products such as *Pangasius bocourti* or species of freshwater crustaceans. A single entrepreneurial farmer in 1992 helped establish a local industry of snakehead fish production; his success served as a model for subsequent farmers. As development funds became available, this pre-existing industry, with its regional recognition, was invested in by both the state, using in part development

funds from the World Bank, and private companies to encourage and capitalize on its growth. From this narrative, one can expect to see shifts from other forms of agriculture to aquaculture and the continuing growth of infrastructure, like processing and packing plants and the accompanying power and transportation infrastructure, required to support the industry's continued growth and development. Given these investments and the supporting infrastructure emphasizing aquaculture and snakehead fish production, it can be expected that additional lands will be transitioned to aquaculture around Phú Thọ.

13.4 CONCLUSION

The study employs established remote sensing techniques (Potapov et al., 2020) to understand between-year LCLU changes of the Đồng Tháp agricultural landscape. Our work acknowledges the limitations of applying statistical methods to ground-level data, as it may not yield precise or meaningful results or understanding across a landscape. Thus, the combination of social science and humanities approaches with remote sensing provided a more complete picture of the changes themselves and the drivers of the LCLUC. The analysis concludes that, according to remote sensing data, no significant changes in classification outcomes were observed between 2015 to 2019 for the larger region, but when looking at site-specific examples, the 30 m Landsat-based analysis did concur with what was reported by individual farmers. This work benefitted from the rich archive of analysis-ready 16-day Landsat imagery. Future work would benefit from mapping high temporal LCLUC occurring at seasonal time steps in this complex agricultural system via fusion products like the Harmonized Landsat and Sentinel-2 (HLS) product to shorten the 16-day temporal resolution to nearly weekly. Further, weekly to monthly tasks of very high resolution (< 10 m) commercial satellite imagery, like Planet or MAXAR Digital Globe, may reveal the complex LCLUC noted by the local populations at spatial resolutions necessary to map different crop types, expand aquaculture in real-time, and potentially expand snakehead fish processing into built-up areas. Finally, it should be noted that much of this work (~2015–2019) represents pre-Covid market and landscape change conditions, meaning that observed changes happening now may not align with drivers identified in this study.

Additionally, while we found interviews with individuals could identify local changes, these were often not significant enough to be detectable by the moderate remote sensing methods used here. Individuals identified the prices of agricultural products and economics as the reasons for private land change and assigned infrastructure projects to state actors. They were unable to articulate local, regional, or national policies impacting these observed changes. Discourse analysis of a local news source and local government publications identified policies and initiatives, in part funded by development partners and including private–public partnerships, impacting both local economic and infrastructure changes. Furthermore, discourse analysis enabled the production of an economic micro-history of the district that, in part, explained statistical information regarding the increase of district-level aquaculture's value and productivity. This easily replicable approach can be deployed in other geographies to help identify drivers of LULC. While significant increases in

aquaculture acreage were not observed in Phú Thọ commune, it is likely that existing ponds have transitioned to snakehead fish production—especially given the investment by private and state actors noted in the sources used for the discourse analysis, snakehead fish production will continue as a major industry in Phú Thọ. This research went beyond mapping the landscape into understanding the individuals inhabiting it, equipping the authors to conduct future and culturally sensitive research in the Mekong Delta of Vietnam and to expand the application of critical remote sensing to better characterize drivers of LCLUC at local to regional scales.

ACKNOWLEDGEMENTS

We would like to dedicate this work to our dear colleague, Dr. Stanley Toops, who passed during this project – may his love of Geography live on in his students, colleagues, and his scholarship. This research was supported by a National Aeronautics and Space Administration LULUC SARI grant (80NSSC18K0335; PI McCarty) and a Florence Tan Moeson Fellowship from the Library of Congress.

REFERENCES

Báo Đồng Tháp Online, 2013. Chế biến khô cá lóc bằng hệ thống sấy. 6 October. Available at: www.baodongthap.vn/kinh-te/che-bien-kho-ca-loc-bang-he-thong-say-31352.aspx (Accessed: 16 November 2023).

Bennett, M.M., Chen, J.K., Alvarez León, L.F., Gleason, C.J., 2022. The politics of pixels: A review and agenda for critical remote sensing. *Progress in Human Geography* 46, 729–752. https://doi.org/10.1177/03091325221074691

Bennett, M.M., Gleason, C.J., Tellman, B., Alvarez Leon, L.F., Friedrich, H.K., Ovienmhada, U., Mathews, A.J., 2024. Bringing satellites down to Earth: Six steps to more ethical remote sensing. *Global Environmental Change Advances* 2, 100003 https://doi.org/10.1016/j.gecadv.2023.100003

Bernard, H.R., 2002. *Research Methods in Anthropology: Qualitative and Quantitative Methods*. 3rd edition. AltaMira Press.

Biggs, D.A., 2012. *Quagmire: Nation-Building and Nature in the Mekong Delta*. University of Washington Press.

Chí, C., 2022. Công bố Làng nghề khô cá lóc xã Phú Thọ. *Báo Đồng Tháp Online*, 8 January. Available at: www.baodongthap.vn/kinh-te/cong-bo-lang-nghe-kho-ca-loc-xa-phu-tho-107179.aspx (Accessed: 16 November 2023).

Chu, V.L., 2019. Doi Moi in Vietnamese agriculture. In William S. Turley and Mark Selden (eds), *Reinventing Vietnamese Socialism: Doi Moi in Comparative Perspective*. Taylor & Francis, pp. 151–163.

Development Projects: Mekong Delta Integrated Climate Resilience and Sustainable Livelihoods Project P153544, 2023. *World Bank*. Available at: https://projects.worldbank.org/en/projects-operations/project-detail/P153544 (Accessed: 16 November 2023).

Crews, K.A., Walsh, S.J., 2009. Remote sensing links to the social sciences. In *Handbook of Remote Sensing,* Warner, T.A., Nellis, M.D., Foody, G.M. (eds), Sage Publications, pp. 437–445.

Dương, Ú., 2017. Huyện Tam Nông chuẩn bị ra mắt "Phú nông hội quán." *Báo Đồng Tháp Online*, 3 May. Available at: www.baodongthap.vn/kinh-te/huyen-tam-nong-chuan-bi-ra-mat-phu-nong-hoi-quan--68470.aspx (Accessed: 16 November 2023).

Duong, T., Bouttavong, P., Latuso, K., Phuong, L., Tumpeesuwan, S., 2015. The water management at Tram Chim National Park, Vietnam. *Asian Journal of Agriculture and Biology* 2014, 86–95.

Friese, S., Soratto, J., Pires, D., 2018. Carrying out a computer-aided thematic content analysis with ATLAS.ti. *MMG Working Paper* 18(2). Available at: www.mmg.mpg.de/62130/wp-18-02 (Accessed: 24 September 2021).

Guest, G., MacQueen, K.M., Namey, E.E., 2012. *Applied Thematic Analysis*. Sage Publications.

Ha, T., 2020. *Niên Giám Thống Kê 2020*. Tổng cục Thống kê (General Statistics Office of Vietnam).

Hinton, A.L., 2005. *Why Did They Kill?: Cambodia in the Shadow of Genocide* (Vol. 11). University of California Press.

Jia, S., Nghiem, S.V., Kim, S.H., Krauser, L., Gaughan, A.E., Stevens, F.R., Kafatos, M., Ngo, K.D., 2022. Extreme development of Dragon Fruit agriculture with nighttime lighting in Southern Vietnam. In *Remote Sensing of Agriculture and Land Cover/Land Use Changes in South and Southeast Asian Countries*, Vadrevu, K.P., Le Toan, T., Ray, S.S., Justice, C. (eds), Springer. https://doi.org/10.1007/978-3-030-92365-5_32

Joyce, K.E., Nakalembe, C.L., Gómez, C., Suresh, G., Fickas, K., Halabisky, M., Kalamandeen, M., Crowley, M.A., 2022. Discovering inclusivity in remote sensing: Leaving no one behind. *Frontiers in Remote Sensing* 3. https://doi.org/10.3389/frsen.2022.869291

Khánh, P., 2017. Ra mắt Phú Nông Hội quán. *Báo Đồng Tháp Online*, 3 December. Available at: www.baodongthap.vn/kinh-te/ra-mat-phu-nong-hoi-quan-68621.aspx (Accessed: 16 November 2023).

Kindu, M., Schneider, T., Teketay, D., Knoke, T., 2013. Land use/land cover change analysis using object-based classification approach in Munessa-Shashemene landscape of the Ethiopian Highlands. *Remote Sensing* 5, 2411–2435. https://doi.org/10.3390/rs5052411

Kondolf, G.M., Rubin, Z.K., Minear, J.T., 2014. Dams on the Mekong: Cumulative sediment starvation. *Water Resources Research* 50, 5158–5169. https://doi.org/10.1002/2013WR014651

Lewis, W.C., Kuttler, W.E., 1978. Land-use controls and the political process. *The Annals of Regional Science*, 12(1), 24–35. https://doi.org/10.1007/BF01287492

Liverman, D., Moran, E.F., Rindfuss, R.R., Stern, P.C. (eds), 1998. *People and Pixels: Linking Remote Sensing and Social Science*. National Academies Press. https://doi.org/10.17226/5963

Mẫn, N., 2021. Khô Phú Thọ được nhiều khách hàng ưa chuộng. *Báo Đồng Tháp Online*, 1 September. Available at: www.baodongthap.vn/kinh-te/kho-phu-tho-duoc-nhieu-khach-hang-ua-chuong-95355.aspx (Accessed: 16 November 2023).

Ministry of Natural Resources and Environment, 2016. *Responding to Climate Change, Đồng Tháp Needs More Assistance*. Ministry of Natural Resources and Environment. Available at: https://monre.gov.vn/English/Pages/Responding-to-climate-change-Dong-Thap-needs-more-assistance.aspx

Mỹ, L., 2021. Làng nghề làm cá khô lớn nhất Đồng Tháp. *Báo Đồng Tháp Online*, 21 December. Available at: www.baodongthap.vn/kinh-te/lang-nghe-lam-ca-kho-lon-nhat-dong-thap-102705.aspx (Accessed: 16 November 2023).

Nhật, K., 2014. Nâng tầm thương hiệu khô cá Tứ Quý. *Báo Đồng Tháp Online*, 19 December. Available at: www.baodongthap.vn/kinh-te/nang-tam-thuong-hieu-kho-ca-tu-quy-45419.aspx (Accessed: 16 November 2023).

Niên Giám Thống Kê 2022, 2023. Vietnam: Tổng cục Thống kê (General Statistics Office of Vietnam).

Nygren, A., 1999. Local knowledge in the environment–development discourse: From dichotomies to situated knowledges. *Critique of Anthropology*, 19(3), 267–288. https://doi.org/10.1177/0308275X9901900304

Paulus, T.M., Lester, J.N., 2016. ATLAS.ti for conversation and discourse analysis studies. *International Journal of Social Research Methodology*, 19(4), 405–428. https://doi.org/10.1080/13645579.2015.1021949

Pervez, S., ur Rehman, S., Alandjani, G., 2018. Role of internet of things (iot) in higher education. *Proceedings of ADVED*, 792–800. www.ocerints.org/adved18_e-publication/papers/216.pdf

Pickles, J. (ed.), 1995. *Ground Truth: The Social Implications of Geographic Information Systems*. Guilford Press.

Potapov, P., Hansen, M.C., Kommareddy, I., Kommareddy, A., Turubanova, S., Pickens, A., Adusei, B., Tyukavina, A., Ying, Q., 2020. Landsat analysis ready data for global land cover and land cover change mapping. *Remote Sensing* 12, 426. https://doi.org/10.3390/rs12030426

Pratt, A.C., 2009. Social and economic drivers of land use change in the British space economy. *Land Use Policy*, 26, S109–S114. https://doi.org/10.1016/j.landusepol.2009.09.006

Project report, 2020. *Mekong delta integrated climate resilience and sustainable livelihoods (MD- ICRSL/WB9). Cổng thông tin điện tử Bộ NN và PTNT*. Available at: www.mard.gov.vn/en/Pages/environmental-and-social-impact-assessment-report.aspx (Accessed: 30 November 2023).

Rindfuss, R.R., Stern, P.C., 1998. Linking remote sensing and social science: The need and the challenges. In Liverman, D., Moran, E.F., Rindfuss, R.R. and Stern, P.C. (eds), *People and Pixels: Linking Remote Sensing and Social Science*. National Academies Press, pp. 1–27. Available at: https://doi.org/10.17226/5963

Schutt, R.K., 2015. *Investigating the Social World: The Process and Practice of Research*. SAGE.

Shaw, R., 2006. *Community-Based Climate Change Adaptation in Vietnam: Inter-Linkages of Environment, Disaster, and Human Security*. TERI Press.

Sinh, L.X., Navy, H., Pomeroy, R.S., 2014. Value chain of Snakehead fish in the Lower Mekong Basin of Cambodia and Vietnam. *Aquaculture Economics & Management* 18, 76–96. https://doi.org/10.1080/13657305.2014.855956

Spalding, A.K., 2017. Exploring the evolution of land tenure and land use change in Panama: Linking land policy with development outcomes. *Land Use Policy*, 61, 543–552. https://doi.org/10.1016/j.landusepol.2016.11.023

Thomas, N., Neigh, C.S., Carroll, M.L., McCarty, J.L., Bunting, P., 2020. Fusion approach for remotely-sensed mapping of agriculture (FARMA): A scalable open source method for land cover monitoring using data fusion. *Remote Sensing*, *12*(20), 3459.

Thông tin, báo cáo thống kê năm 2015, 2015. Tổng cục Thống kê (General Statistics Office of Vietnam), Vietnam.

Trevisani, S., Omodeo, P.D., 2021. Earth scientists and sustainable development: Geocomputing, new technologies, and the humanities. *Land* 10, 294. https://doi.org/10.3390/land10030294

Tri, V.P.D., Trung, P.K., Trong, T.M., Parsons, D.R., Darby, S.E., 2023. Assessing social vulnerability to riverbank erosion across the Vietnamese Mekong Delta. *International Journal of River Basin Management* 21, 501–512. https://doi.org/10.1080/15715124.2021.2021926

Trung, T.T., 2012. Fish farmer hailed as legend in his lifetime. *Viet Nam News*, 21 November. http://vietnamnews.vn/sunday/features/233045/fish-farmer-hailed-as-legend-in-his-lifetime.html.

Two years after prison release, Hoa Hao follower arrested again in Vietnam (2023). Radio Free Asia, 8 April. www.rfa.org/english/news/vietnam/hoa-hao-second-arrest-08042023150030.html (Accessed: 15 December 2023).

Vietnam Economic News, 2018. Đồng Tháp Rice Farmers Switch to Other Crops, Incomes Rise, 2018. *Vietnam Economic News*, 22 November. Available at: http://ven.vn/dong-thap-rice-farmers-switch-to-other-crops-incomes-rise-36327.html

Vietnam–National Targeted Programs for New Rural Development and Sustainable Poverty Reduction Support Program (NTPSP) Program-for-Results Project, 2017. *World Bank*. Available at: https://documents.worldbank.org/en/publication/documents-reports/documentdetail/975721498874530249/Vietnam-National-Targeted-Programs-for-New-Rural-Development-and-Sustainable-Poverty-Reduction-Support-Program-NTPSP-Program-for-Results-Project (Accessed: 16 November 2023).

Vietnam Plus, 2019. Mekong Delta Agriculture Adapts to Climate Change, 2019. https://en.vietnamplus.vn/mekong-delta-agriculture-adapts-to-climate-change/160993.vnp

Wilson, M.W., 2015. On the criticality of mapping practices: Geodesign as critical GIS? *Landscape and Urban Planning*, 142, 226–234. https://doi.org/10.1016/j.landurbplan.2013.12.017

Wood, C.H., Skole, D., 1998. Linking satellite, census, and survey data to study deforestation in the Brazilian Amazon. In *People and Pixels: Linking Remote Sensing and Social Science*. National Academies Press, pp. 70–93. https://doi.org/10.17226/5963

World Development Indicators | DataBank (n.d.). Available at: https://databank.worldbank.org/source/world-development-indicators (Accessed: 20 October 2021).

14 Enhancing Agricultural Forecasting

Remote Sensing and Climate Data Integration for Crop Yield Predictions in the Chi Basin, Thailand

Siwa Kaewplang, Akkarapon Chaiyana, Rattana Hormwichian, Anongrit Kangrang, Ratchawatch Hanchoowong, Neti Srihanu, Haris Prasanchum, Werapong Koedsin, and Alfredo Huete

14.1 INTRODUCTION

Thailand is a leading global rice exporter, with a value estimated at approximately $7.4 billion in 2018, making rice a cornerstone of its economy. The country boasts a production output of around 20.3 million metric tons, solidifying its status as the world's largest milled rice producer. Key production areas encompass the central, northeastern, and northern regions, with the central region leading in terms of output.

The rice sector contributes significantly to Thailand's GDP, accounting for about 3.3%, and employs approximately 10 million people, representing roughly 20% of the nation's workforce. For many smallholder farmers, rice farming is a crucial income source, often constituting up to 60% of their earnings. Pursuing higher rice yields remains imperative in the face of global population growth. However, achieving this goal is fraught with challenges, including environmental conditions and changes in land use that impact productivity. Climate change and alterations in land use pose significant threats, affecting crop yields through extreme weather events and changes in resource availability (Change, 2014). Natural disasters such as droughts and floods intensify these challenges, further disrupting rice production and livelihoods.

Moreover, Thailand, characterized by its tropical climate, frequently grapples with droughts, resulting in prolonged dry spells and water scarcity. A report indicated that in 2021, approximately 3.8 million hectares of land in Thailand were affected by prolonged drought conditions, with forecasts suggesting an annual escalation in severity. Measuring crop yield in vast agricultural areas presented challenges

 DOI: 10.1201/9781003396260-14

due to time, budget, and surveyor limitations. A recent data-driven remote sensing approach offered an efficient means of assessing crop conditions and predicting yield remotely (Ju et al., 2021; Johnson et al., 2021; Faisal et al., 2020; Faisal et al., 2019). Utilizing various sensors and platforms, such as satellites, enables data collection on land usage, vegetation, and weather patterns (Justice et al., 2015). Numerous studies leveraged remote sensing data to forecast agricultural production (Vadrevu et al., 2019; 2022). Weather variables, including land surface temperature (LST), enhanced vegetation index (EVI), and normalized difference vegetation index (NDVI), alongside machine learning (ML), improved yield predictions (Ju et al., 2021). For example, ML techniques like eXtreme Gradient Boosting (XGBoost) integrated remote sensing and weather data to enhance cereal yield forecasts, reducing prediction errors (Tan et al., 2021). Additionally, derived indices from remotely sensed data, such as the vegetation health index and temperature condition index, combined with machine learning, outperform traditional methods in predicting crop production (Joshi et al., 2023).

Accurate prediction of crop yields was crucial for sustainable food security and agriculture, aiding farmers in decision-making and enabling policymakers to mitigate potential food shortages. Traditional regression methods were surpassed by ML and deep learning, offering precise statistical forecasts. Recent studies evaluated ML algorithms like SVR, RF, and XGBoost for local crop production prediction. Notably, SVR, RF, and GPR emerged as top performers, exhibiting an R-squared (R^2) value > 0.75. While ML approaches generally excelled in crop yield prediction, evidence suggested that multivariate ordinary least squares may yield lower error rates for soybean yield prediction compared to RF and LSTM (Schwalbert et al., 2020). Hyper-validation of ML models, facilitated by grid search cross-validation, could be complex. Additionally, some studies attempted regional agricultural yield forecasting using remote sensing data alone, disregarding meteorological factors crucial for accurate predictions (Memon et al., 2019). The RMSE based on remote sensing varied considerably, indicating uncertainty in solely relying on this data (Pang et al., 2022). The combination of remote sensing and climatic data remained unexplored, particularly in tropical regions. Thus, this study aimed to provide input datasets and model methods to minimize crop production forecast errors.

This study significantly advanced crop yield prediction by integrating climatic and remote sensing data, providing a comprehensive understanding of the climatic drivers influencing production and enhancing precision through novel remote sensing indicators. By innovatively utilizing crop phenological phases, the study identified factors influencing yield, thus enhancing our understanding, and informing agricultural and policy strategies. Moreover, the study's findings offered a foundational system to support informed decision-making for farmers and government entities based on the identified factors influencing yield. This report presented results to assess the predictive capability of MLR models and machine learning algorithms (RF, XGBoost, and SVR) using various satellite-derived indices and climate variables. Variable selection preceded model training, and different combinations of predictors were tested. Model performance was evaluated using metrics like R^2 and RMSE, and the most effective model was applied to predict crop yields at the provincial scale.

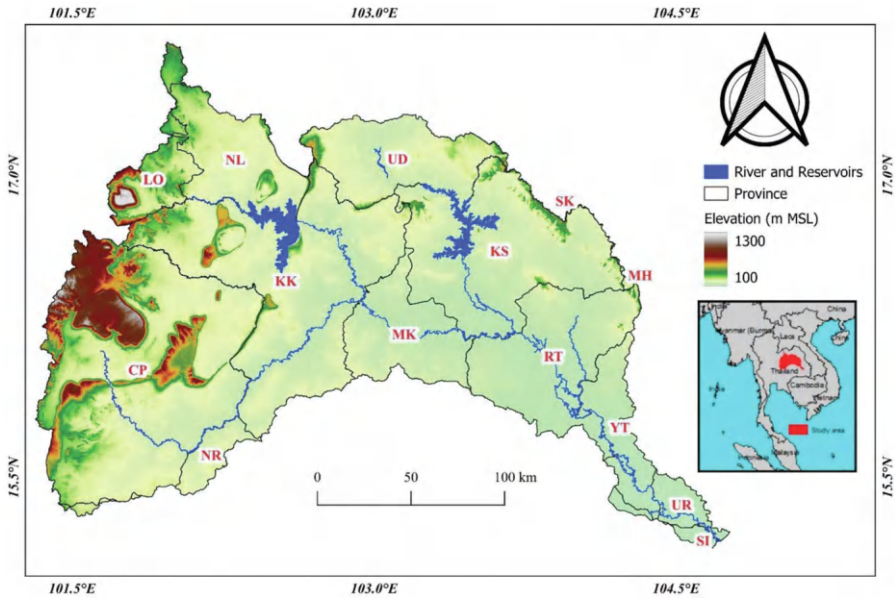

FIGURE 14.1 Study area.

14.2 STUDY AREA

The Chi basin, located in central Thailand between 15°13′ and 17°40′ N latitude and 101°14′ and 104°46′ E longitude. It encompasses an elevation range of 104 to 1060 meters above sea level (Figure 14.1), spanning approximately 4.91 million hectares. Approximately 3.22 million hectares are designated as cropland. The prevailing climate is characterized by humid, tropical conditions, with temperatures averaging between 27 to 32°C. The region experiences two distinct monsoon seasons: the Southwest Monsoon prevailing from May to October and the Northeast Monsoon from November to April. The rainy season typically extends from May to October, with an average annual precipitation of 1380 mm. Crop cultivation predominantly occurs from June to November, culminating in harvest during December (Boonwichai et al., 2018).

14.3 DATA AND METHODS

14.3.1 Crop Yield Data and Their Phenology

This study analyzed historical crop yields at the provincial level from 2011 to 2019 using data sourced from the Office of Agricultural Economics for 14 provinces (www.oae.go.th/, accessed on July 25, 2022), as detailed in Table 14.1. Field observations were conducted across 24 areas covering Thailand, with each sample represented by a square box. Rice milling was employed to estimate production, converting it into units (ton/ha). Additionally, annual crop production was calculated by dividing total

TABLE 14.1
The Rice Milling Data for 14 Study Areas in the Chi Basin, Measured in Tons per Hectare (ton/ha)

No.	Province	Acronym	2011	2012	2013	2014	2015	2016	2017	2018	2019
1	NAKHON RATCHASIMA	NS	2.59	2.25	2.31	2.24	2.26	2.22	2.26	2.22	2.27
2	SI SA KET	SK	2.51	2.30	2.45	2.28	2.26	2.27	2.29	2.28	2.17
3	UBON RATCHATHANI	UR	2.16	2.15	2.15	2.06	2.06	2.09	2.18	2.27	2.25
4	YASOTHON	YT	2.54	2.27	2.28	2.31	2.21	2.23	2.22	2.27	2.25
5	CHAIYAPHUM	CP	2.46	2.36	2.39	2.21	2.19	2.25	2.32	2.29	2.32
6	NONG BUA LAMPHU	NL	2.41	2.33	1.97	2.01	1.98	2.11	2.16	2.07	2.08
7	KHON KAEN	KK	2.16	2.09	2.11	2.12	2.11	2.15	2.14	2.02	1.98
8	UDON THANI	UD	2.47	2.32	2.24	2.32	2.34	2.37	2.40	2.28	2.23
9	LOEI	LO	2.41	2.42	2.46	2.34	2.31	2.43	2.46	2.33	2.11
10	MAHA SARAKHAM	MK	2.37	2.32	2.33	2.30	2.28	2.30	2.23	2.18	2.25
11	ROI ET	RT	2.37	2.32	2.33	2.34	2.38	2.39	2.37	2.21	2.15
12	KALASIN	KS	2.32	2.26	2.26	2.29	2.30	2.32	2.30	2.31	2.33
13	MUKDAHAN	MH	2.40	2.24	2.26	2.40	2.40	2.40	2.38	2.47	2.19
14	PHETCHABUN	PB	3.54	3.54	3.61	4.37	4.36	3.46	4.33	3.53	4.40

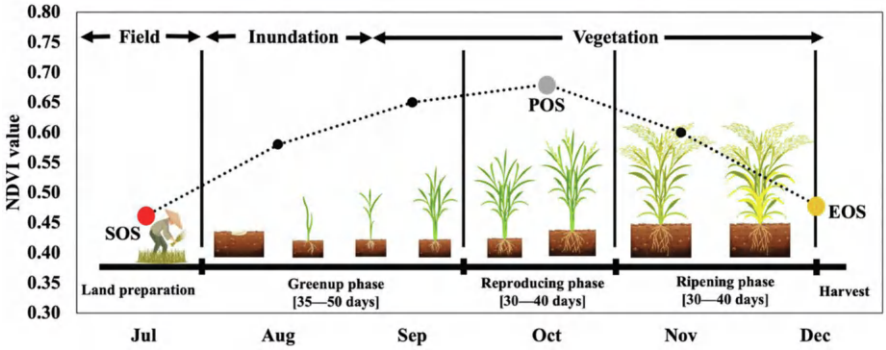

FIGURE 14.2 Mean temporal NDVI profile of crops across growth stages in the Chi basin region from 2011 to 2019. SOS, POS, and EOS represent the start, peak, and end of the season, respectively. (Chaiyana et al., 2024.)

production by harvested area, resulting in annual crop yields ranging from 1.97 to 4.4 tons/ha, varying by region.

According to the crop calendar period (Sujariya et al., 2020), crops in this region were typically transplanted between June and July, flowered from late October to November, and harvested around December. In Thailand, rice underwent several stages of growth, including nursery, vegetative, reproductive, and maturity stages, lasting approximately 5–6 months (Ramadhani et al., 2021), subject to environmental conditions and crop variety (Figure 14.2) (Chaiyana et al., 2024). Throughout these stages, changes in rice growth affected its reflectance at different wavelengths. Previous studies indicated that indices like NDVI effectively monitored rice growth (Guo et al., 2021, Son et al., 2014). Initially, NDVI was low during the early vegetative stage due to limited vegetation cover but increased as chlorophyll content and foliage developed (Peñuelas and Filella, 1998). However, as the plant matured, NDVI decreased due to biomass reduction, chlorophyll decline, and grain filling increase (Mosleh et al., 2015).

14.3.2 Remote Sensing and Climate Data Integration

The research leveraged remote sensing (RS) data sourced from the MODIS sensor to delineate crop areas within the Chi basin, Thailand, drawing upon land use data provided by the Land Development Department (LDD) of Thailand for the year 2020. Vegetation indices, notably EVI, NDVI, and LST daytime and nighttime products, were instrumental in the monitoring process. Moreover, the study factored in variables such as drought and climate, utilizing indices like TCI, VCI, and VHI (Zeng et al., 2022, Hashemzadeh Ghalhari et al., 2022, Alahacoon et al., 2021) derived from NDVI and temperature metrics (Xie and Fan, 2021, Bento et al., 2020). All remote sensing datasets were aggregated into monthly mean data points. Concurrently, essential climatic variables encompassed monthly mean rainfall, T_{min}, T_{mean}, and T_{max} spanning from June to November. For ease of reference, Table 14.2 provides a concise summary of the variables integral to the study.

TABLE 14.2
The Predictors to be Applied for Modeling and Predicting Crop Production

Data Type	Product	Variable	Spatial Resolution	Temporal Resolution	Acquisition Date	Data Source
Yield recorded		Crop yield	Provincial level	Annual	2011–2019	**www.oae.go.th/** , (accessed on July 20, 2022).
RS data	MOD13Q1	NDVI	250 m	16-day interval	2011–2022	**https://lpdaac.usgs.gov/products/mod13q1v006/**, (accessed on July 20, 2022).
		EVI			2011–2022	
	MOD11A2	LST daytime	1 km	8-day interval	2011–2022	**https://lpdaac.usgs.gov/products/mod11a1v006/**, (accessed on July 20, 2022).
		LST nighttime			2011–2022	
Climatic data	ERA5	Rainfall	27.83 km	Monthly	2011–2022	www.ecmwf.int/en/forecasts/dataset/ecmwf-reanalysis-v5, (accessed onJuly 20, 2022).
		T_{mean}			2011–2022	
		T_{min}			2011–2022	
		T_{max}			2011–2022	

All RS and climatic data were averaged into the crop growth season from June to November.

14.3.3 Feature Selection: Correlation Analysis (CA) and Variance Inflation Factor

Various techniques could be employed to mitigate overfitting, such as eliminating one of the correlated variables, merging correlated ones, and utilizing principal component analysis (PCA). However, in the context of predicting crop yield based on limited indicators, removing, or merging correlated variables might not align with the procedure. Alternatively, PCA offered a method to consolidate multiple correlated variables into a single predictor (Uddin et al., 2021). Nevertheless, a constraint of this study was the number of variables involved, necessitating the adoption of an appropriate approach. On another note, multiple linear regression commonly encountered multicollinearity issues, where certain variables exhibited high correlations. To address this, correlation analysis (CA) was utilized for variable selection, helping to identify and potentially remove highly correlated variables (Guechi et al., 2021; Boori et al., 2021; Guha and Govil, 2020). Additionally, the variance inflation factor (VIF) served as a tool in multiple regression analysis to gauge multicollinearity among independent variables. Excessive multicollinearity could yield unstable and unreliable regression coefficients (Hamzehpour et al., 2019, Kang et al., 2018). Previous research has proposed integrating the VIF as an indicator to mitigate multicollinearity (VIF < 5–10) (Browning et al., 2018, Alsharif and Pradhan, 2014). In this study, a VIF score threshold of 5 was applied, indicating moderate to considerable correlation. Both CA and VIF were employed as statistical methods to analyze influential factors in crop yield prediction, with significance determined by a *p*-value < 0.05 and VIF < 5 (Maya and Bhargavi, 2019) (refer to Figure 14.3). The selected variables from this stage would serve as predictor variables for subsequent analysis.

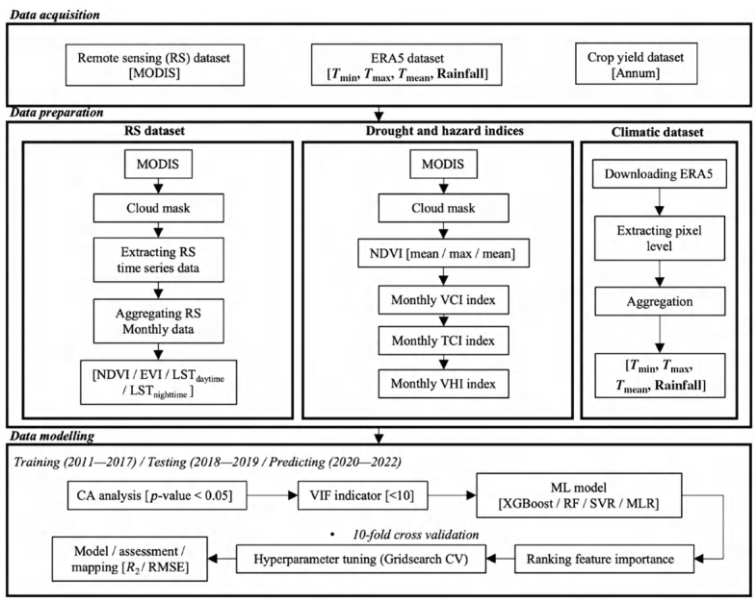

FIGURE 14.3 Research framework for predicting crop production. (Chaiyana et al., 2024.)

14.3.4 Crop Yield Prediction Models

Regression models, including multiple linear regression (MLR), random forest (RF) regression, XGBoost regression, and SVR, were applied to investigate the relationship between independent variables and a dependent variable. These models estimated the effect of independent variables, assuming a specified functional form such as linear or nonlinear. Model parameters were estimated using statistical techniques, and goodness of fit was assessed using metrics like R^2 and RMSE. The crop yield dataset, comprising 126 samples, was divided into training (98 samples, 2011–2017) and testing (28 samples, 2018–2019) datasets. Hyperparameters for each ML model were optimized using grid search cross-validation (GridSearchCV) from the sci-kit-learn library in Python (Yu and Zhu, 2020). GridSearchCV evaluated different hyperparameter combinations to find the optimal set according to a chosen metric (Dong et al., 2020). RMSE and R^2 were used to evaluate model performance, implemented in Python using the scikit-learn library. The predictive model was used to forecast crop yield at the provincial scale, aiding farmers, and policymakers in decision-making. Additionally, analyzing future trends was crucial for informed agricultural practices and resource allocation.

14.4 RESULTS AND DISCUSSION

14.4.1 Variable Selection

This study employed CA and VIF to eliminate redundant variables, preserving essential ones to enhance model accuracy and prevent overfitting. Results revealed six significant variables from RS data—TCI, NDVI, $LST_{nighttime}$, VCI, VHI, and EVI, all with *p*-values under 0.05 (Table 14.3). Climatic data retained only T_{mean} after VIF

TABLE 14.3
The Statistical Metrics of Correlation Analysis (CA) and the Variance Inflation Factor (VIF)

Data Type	Variable	*p*-Value	VIF
RS data	TCI	0.001 **	1.31
	NDVI	0.023 *	1.22
	$LST_{nighttime}$	0.001 **	2.17
	VCI	0.001 **	15.49
	VHI	0.001 **	65.2
	EVI	0.035 *	20.67
	$LST_{daytime}$	0.37	11.19
Climate data	Tmean	0.001 **	2.05
	Rainfall	0.213	1.76
	T_{max}	0.24	13.44
	T_{min}	0.051	5

Note: * and ** refer to the confidence interval for *p*-values < 0.05 and 0.01, respectively.

TABLE 14.4
Training and Testing of Each Model and Data Type for Predicting Crop Yield Production

	R-Square (Training: 2011–2017)			
Category	**MLR**	**RF**	**XGBoost**	**SVR**
RS data	0.42	0.74	0.89	0.64
Climatic data	0.55	0.94	0.93	0.88
Combination	0.63	0.92	0.95	0.81
	RMSE (Testing: 2018–2019) (ton/ha)			
RS data	0.36	0.42	0.45	0.4
Climatic data	0.3	0.23	0.21	0.18
Combination	0.26	0.19	0.18	0.29

assessment, resulting in four remaining variables (Table 14.3). Thus, for training and testing the model, variables with VIF values below 5—TCI, NDVI, $LST_{nighttime}$ for RS data, and T_{mean} for climatic data—were selected, ranging from 1.31 to 2.17 (Table 14.3).

14.4.2 Regression Model Predictions for Province-Level Crop Yield Prediction in the Chi Basin

This study utilized 126 samples to analyze provincial-scale crop yield production, split into two periods: 2011–2017 (98 samples) and 2018–2019 (28 samples). Three categories of data, including remote sensing (RS), climatic, and a fusion of both, were subjected to four regression models (MLR and machine learning techniques) (Table 14.3). The MLR model using RS data exhibited the lowest R^2 value of 0.42 in the training dataset, whereas the XGBoost model using fusion data demonstrated the highest R^2 value of 0.95 (Table 14.4), aligning with previous findings (Bouras et al., 2021). Regarding validation (RMSE), the XGBoost model with combined data showed the lowest RMSE of 0.18 ton/ha, followed by the support vector regression (SVR) model using climatic data with an RMSE ranging from 0.18 to 0.3 ton/ha, within acceptable error thresholds for European agro-statistics (Genovese et al., 2006). Overall, the XGBoost model emerged as the most dependable for predicting crop yield production, boasting the highest R^2 and lowest RMSE (Table 14.4).

14.4.3 Temporal Trend of Crop Production Measurement and Changes of Crop Production Validation

To further elaborate on the findings presented in Figure 14.4, it is vital to assess both observed and predicted crop yield data using four distinct approaches: three non-parametric (RF, XGBoost, SVR) and one parametric (MLR). These methods forecasted crop yield one month before harvest. Despite fluctuations in variables

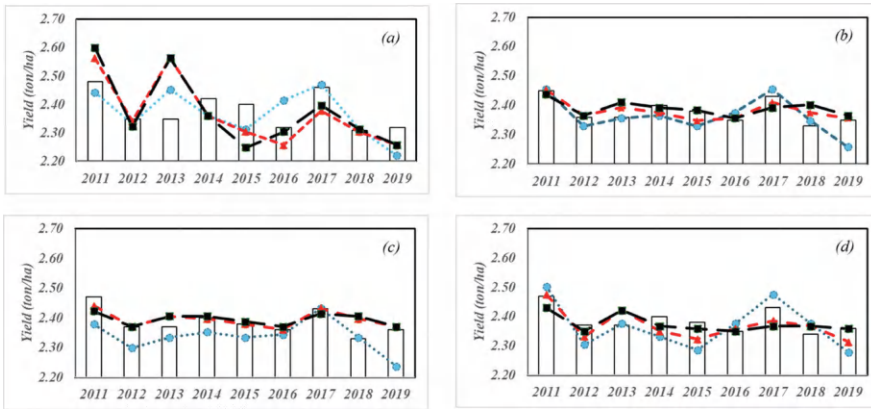

FIGURE 14.4 Comparison of annual average crop yield prediction (ton/ha) and average historical data for (a) the MLR model, (b) the RF model, (c) the XGBoost model, and (d) the SVR model; the bar chart represents the average historical crop yield production; the red, blue, and black dot lines represent the combination, RS, and climatic data, respectively.

and models, peak yields in 2011 and 2017 led to reduced yields in 2018. Evaluation during validation periods (2018 and 2019) revealed MLR's strong performance across most predictors, with minimal differences in yields. Conversely, XGBoost and RF showed negligible discrepancies between observed and predicted data in 2019. Overall, non-parametric and parametric approaches effectively forecasted crop yield, with MLR and XGBoost standing out. Notably, while MLR performed well with testing data, its training statistical results suggested caution. MLR assumes linear correlations, whereas XGBoost, a non-parametric technique, employs boosting with decision trees for predictions, offering flexibility for non-linear relationships but with higher complexity and resource requirements. Consequently, XGBoost was chosen for provincial-scale yield prediction due to its adaptability and accuracy with diverse data.

14.4.4 Crop Yield Prediction Between 2018 and 2022

XGBoost, a selected machine learning algorithm, forecasts crop yield production, as previously mentioned. Employing the XGBoost model, the crop yield ratio (tons/ha) across 14 provinces from 2018 to 2022 (Table 14.5) was determined. In 2018 and 2019, PB province exhibited the highest crop yield ratio at 3.77 tons/ha, contrasting with NL province, which recorded the lowest at 2.23 tons/ha. By 2020, PB province maintained the highest ratio at 3.60 tons/ha, marking a decrease of 4.5% and 2.9% from 2018 and 2019, respectively. Notably, CP and KK provinces boasted the most extensive areas suitable for crop production, with 0.699 million hectares and 0.683 million hectares, respectively. By 2022, PB province's crop yield ratio decreased by 11.9% compared to 2021 and 2018. These results highlight the effectiveness of the XGBoost model in provincial-level crop outcome prediction and stress

TABLE 14.5
Changes of the Crop Yield Validation Relative to the Historical Values of Each Model

			Variable			Change		
			Combination	RS	Climate			
Model	Year	Mean Actual Yield (ton/ha)	Mean Predicted Yield (ton/ha)	Mean Predicted Yield (ton/ha)	Mean Predicted Yield (ton/ha)	ΔCombination	ΔRS	ΔClimate
Linear	2018	2.34	2.37	2.35	2.34	0.03	0.01	0.01
	2019	2.36	2.45	2.51	2.45	0.10	0.15	0.09
RF	2018	2.34	2.28	2.32	2.26	–0.05	–0.01	–0.07
	2019	2.36	2.35	2.45	2.35	0.00	0.10	–0.01
XGBoost	2018	2.34	2.28	2.36	2.27	–0.06	0.02	–0.07
	2019	2.36	2.35	2.50	2.35	–0.01	0.14	–0.01
SVR	2018	2.34	2.31	2.30	2.31	–0.02	–0.04	–0.02
	2019	2.36	2.41	2.45	2.36	0.05	0.10	0.00

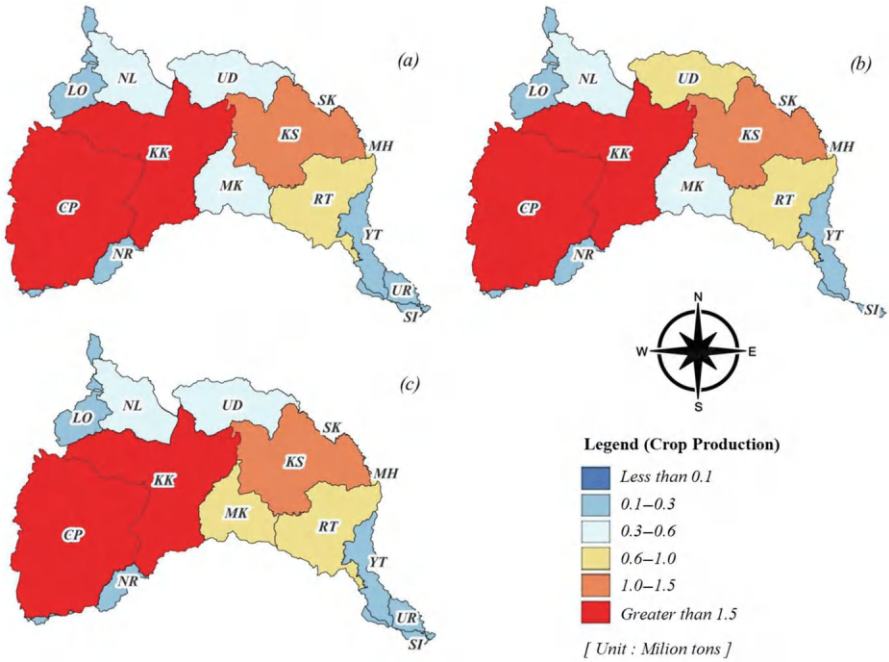

FIGURE 14.5 Total predicted crop yield production at the provincial scale for (a) 2020, (b) 2021, and (c) 2022.

the importance of considering both yield and production area in forecasts. Conversely, crop yield prediction in CP province ranged from 1.61 to 1.74 million tons annually between 2018 and 2022, while KK province, the second-largest region, produced yields ranging from 1.55 to 1.62 million tons per year. Predicted crop yield production in the Chi basin region ranged from 7.33 to 7.88 million tons annually from 2018 to 2022. The total predicted crop yield production maps for 2020–2022 at the provincial scale are depicted in Figure 14.5, providing insights into the country's economic performance and the standard of living for Thailand's citizens.

14.4.5 Discussion on Accuracy and Implications

Monitoring, mapping, and predicting crop production across vast regions aid farmers and policymakers in making sustainable management decisions, crucially benefiting the Chi basin region, a key crop producer in Thailand. This is particularly critical now, given the frequent impact of natural hazards on tropical monsoon areas and the looming challenge of climate change in global agriculture. Since crop yield significantly affects global food security, timely and accurate monitoring of threats to production is imperative. Early and precise estimation of crop production facilitates effective trade and food management strategies. While various methods exist for estimating crop yield (Sakamoto et al., 2014; Doraiswamy et al., 2005), predictive

models leveraging remote sensing data and machine learning techniques have emerged (Mkhabela et al., 2011). Nonetheless, the accuracy of these approaches can vary. For instance, a study by Mkhabela et al. (2011) utilizing NDVI to forecast crop production in the Canadian Prairies yielded R^2 values between 0.8 and 0.9. Similarly, research by Dong et al. (2020), employing MODIS EVI and LAI data to predict rice crop production in Vietnam's Mekong Delta, demonstrated maximum correlation coefficients of 0.70 and 0.74 during crop growth stages, respectively.

Agricultural production is closely related to environmental factors such as climate data (rainfall, temperature, humidity, solar radiation) (Lin, 2007; Nguyen and Drakou, 2021). Integrating climatic and remote sensing data for crop yield prediction (Ju et al., 2021; Medina et al., 2021), aligns with this study's conclusions. Evaluating various methods and predictors for provincial-scale crop yield prediction in Thailand's Chi basin before harvest, this research discovered that combining satellite imaging with climatic data enhances accuracy. Notably, employing $LST_{nighttime}$, NDVI, TCI, and T_{mean} data with the XGBoost algorithm yielded an R^2 value of up to 0.95 and improved RMSE to 0.18 ton/ha. Similarly, previous research by Bouras et al. (2021) found that integrating remote sensing-based drought, climate, and weather indicators with XGBoost enhanced cereal yield forecasting accuracy. Although XGBoost's temporal crop yield predictions closely matched actual data, deviations occurred in 2018 due to natural hazards, resulting in a difference of 0.05 tons/ha.

Recent research by Kheir et al. (2024) reported the fusion of remote sensing, soil, and weather datasets for estimating smallholder crop yields in Egypt, with the result showing that the NDVI, EVI, GCVI, GNDVI, and WDRVI indices gained the highest R^2 of 0.70. Future research entails exploring the potential of remote sensing to estimate smallholder crop yields at the individual plot level by fusing data from satellite and UAV imagery (Cheng et al., 2024; Sangjan et al., 2024), which can be combined with climate data in the area.

In 2018, floods ravaged 66 provinces and 420 districts, devastating agricultural regions, particularly lowland rice areas. Our study forecasts a gradual decline in rainfed rice production, contrary to previous projections, with an estimated annual reduction of 0.078 million tons from 2020 to 2022 (Table 14.6). Drought effects, with an expected 5% mean absolute percentage error (MAPE) (Raksapatcharawong et al., 2020), are linked to El Niño southern oscillation (Anderson et al., 2017), further complicating yield forecasts in Thailand. Despite fluctuating crop yield predictions, climate change threatens to exacerbate agricultural challenges, potentially raising temperatures by 1.4 to 5.8°C by 2100 (Change, 2014), intensifying crop water requirements, and impacting production (Astuti et al., 2022). However, our study offers reliable crop yield predictions useful for policymaking at both national and provincial levels. The methodology presented herein could serve as a template for crop yield forecasting in similar contexts, aiding economic management, given rice's pivotal role in Thailand's economy as a primary staple and key export.

Thailand's rice crop yield significantly influences regional trade and industry performance, contributing notably to the GDP. This is driven by modern agricultural practices like hybrid seeds and precision agriculture, alongside enhanced irrigation and fertilization methods. Despite robust infrastructure support, including roads,

TABLE 14.6
Estimation of Crop Yield Prediction Over Crop Area in the Chi Basin Between 2018 and 2022

		Crop Yield Ratio (ton/ha)					Total Crop Yield (Mton)				
		Validation Period		Predicting Period			Validation Period		Predicting Period		
Area	Crop Yield Area (ha)	2018	2019	2020	2021	2022	2018	2019	2020	2021	2022
NS	81,076	2.29	2.26	2.9	2.31	2.36	0.19	0.18	0.23	0.19	0.19
SK	16,562	2.29	2.29	2.36	2.26	2.45	0.04	0.04	0.04	0.04	0.04
UR	44,155	2.27	2.27	2.36	2.26	2.42	0.1	0.1	0.1	0.1	0.11
YT	125,803	2.29	2.26	2.36	2.38	2.36	0.29	0.28	0.3	0.3	0.3
CP	699,264	2.3	2.26	2.72	2.27	2.49	1.61	1.58	1.9	1.59	1.74
NL	216,043	2.23	2.23	2.27	2.66	2.2	0.48	0.48	0.49	0.57	0.48
KK	683,868	2.28	2.26	2.34	2.36	2.36	1.56	1.55	1.6	1.61	1.62
UD	256,024	2.29	2.26	2.3	2.36	2.32	0.59	0.58	0.59	0.6	0.59
LO	61,150	2.31	2.24	2.7	2.6	2.6	0.14	0.14	0.16	0.16	0.16
MK	247,999	2.28	2.28	2.32	2.32	2.45	0.56	0.56	0.58	0.57	0.61
RT	366,514	2.29	2.28	2.36	2.38	2.45	0.84	0.83	0.86	0.87	0.9
KS	418,757	2.29	2.28	2.32	2.36	2.26	0.96	0.95	0.97	0.99	0.95
MH	1254	2.32	2.26	2.36	2.66	2.33	0.01	0.01	0.01	0.01	0.01
PB	11,195	3.77	3.66	3.6	3.77	3.32	0.04	0.04	0.04	0.04	0.04
Sum							7.40	7.34	7.89	7.65	7.73

ports, and storage facilities, crop yield remains susceptible to factors like droughts and market fluctuations. Additionally, shifts in market demand may prompt farmers to adjust their crop choices. Reduced yields could escalate chemical usage, posing environmental risks. Thus, proactive measures for early yield prediction and sustainable development policies are crucial to mitigate adverse impacts.

14.5 CONCLUSION

Predicting crop yields is vital for farmers to enhance management techniques and increase production before harvest. Here, we present methods to forecast crop production using remote sensing (RS) and climate data, focusing on Thailand's Chi basin from 2011 to 2019. By analyzing various RS and meteorological variables, we identified key factors using correlation analysis and variance inflation factor. Four regression models (MLR, RF, XGBoost, and SVR) were trained, with XGBoost exhibiting superior performance, achieving a minimum root-mean-square error of 0.18 ton/ha. Applying the XGBoost model to predict total crop production for 2020–2022 in the Chi basin yielded estimates of approximately 7.88, 7.64, and 7.72 million tons. Our study demonstrates the effectiveness of using satellite-based drought indicators, vegetation indices, and meteorological data in conjunction with machine learning algorithms for timely yield predictions. These findings can aid decision-making during the growing season and inform agricultural planning at provincial levels in Thailand and neighboring countries. However, addressing land use changes is crucial for refining prediction models and reducing errors in future studies.

ACKNOWLEDGEMENTS

We would like to express our sincere gratitude to Mahasarakham University for providing financial support for this research. Their funding has been instrumental in the successful completion of our study.

REFERENCES

Alahacoon, N., Edirisinghe, M. & Ranagalage, M. 2021. Satellite-based meteorological and agricultural drought monitoring for agricultural sustainability in Sri Lanka. *Sustainability*, 13, 3427.

Alsharif, A. A. & Pradhan, B. 2014. Urban sprawl analysis of Tripoli Metropolitan city (Libya) using remote sensing data and multivariate logistic regression model. *Journal of the Indian Society of Remote Sensing*, 42, 149–163.

Anderson, W., Seager, R., Baethgen, W. & Cane, M. 2017. Crop production variability in North and South America forced by life-cycles of the El Niño Southern Oscillation. *Agricultural and Forest Meteorology*, 239, 151–165.

Astuti, I. S., Wiwoho, B. S., Purwanto, P., Wagistina, S., Deffinika, I., Sucahyo, H. R., Herlambang, G. A. & Alfarizi, I. A. G. 2022. An application of improved MODIS-based potential evapotranspiration estimates in a humid tropic brantas watershed—implications for agricultural water management. *ISPRS International Journal of Geo-Information*, 11, 182.

Bento, V. A., Gouveia, C. M., Dacamara, C. C., Libonati, R. & Trigo, I. F. 2020. The roles of NDVI and land surface temperature when using the vegetation health index over dry regions. *Global and Planetary Change*, 190, 103198.

Boonwichai, S., Shrestha, S., Babel, M. S., Weesakul, S. & Datta, A. 2018. Climate change impacts on irrigation water requirement, crop water productivity and rice yield in the Songkhram River Basin, Thailand. *Journal of Cleaner Production*, 198, 1157–1164.

Boori, M. S., Choudhary, K., Paringer, R. & Kupriyanov, A. 2021. Spatiotemporal ecological vulnerability analysis with statistical correlation based on satellite remote sensing in Samara, Russia. *Journal of Environmental Management*, 285, 112138.

Bouras, E. H., Jarlan, L., Er-Raki, S., Balaghi, R., Amazirh, A., Richard, B. & Khabba, S. 2021. Cereal yield forecasting with satellite drought-based indices, weather data and regional climate indices using machine learning in Morocco. *Remote Sensing*, 13, 3101.

Browning, M. H., Kuo, M., Sachdeva, S., Lee, K. & Westphal, L. 2018. Greenness and school-wide test scores are not always positively associated–A replication of "linking student performance in Massachusetts elementary schools with the 'greenness' of school surroundings using remote sensing". *Landscape and Urban Planning*, 178, 69–72.

Chaiyana, A., Hanchoowong, R., Srihanu, N., Prasanchum, H., Kangrang, A., Hormwichian, R., Kaewplang, S., Koedsin, W. & Huete, A. 2024. Leveraging remotely sensed and climatic data for improved crop yield prediction in the Chi Basin, Thailand. *Sustainability*, 16, 2260.

Change, C. 2014. *Synthesis report. Contribution of working groups I, II and III to the fifth assessment report of the Intergovernmental Panel on Climate Change. Core Writing Team, RK Pachauri and LA Meyer*. IPCC, Geneva, Switzerland.

Cheng, Z., Gu, X., Zhou, Z., Zhang, Y., Yin, H., Li, W. & Du, Y. 2024. Enhancing in-season yield forecast accuracy for film-mulched wheat: A hybrid approach coupling crop model and UAV remote-sensing data by ensemble learning technique. *European Journal of Agronomy*, 156, 127174.

Dong, W., Huang, Y., Lehane, B. & Ma, G. 2020. XGBoost algorithm-based prediction of concrete electrical resistivity for structural health monitoring. *Automation in Construction*, 114, 103155.

Doraiswamy, P. C., Sinclair, T. R., Hollinger, S., Akhmedov, B., Stern, A. & Prueger, J. 2005. Application of MODIS derived parameters for regional crop yield assessment. *Remote Sensing of Environment*, 97, 192–202.

Faisal, B. R., Rahman, H., Sharifee, N. H., Sultana, N., Islam, M. I. & Ahammad, T. 2019. Remotely sensed boro rice production forecasting using MODIS-NDVI: A Bangladesh perspective. *AgriEngineering*, 1, 356–375.

Faisal, B. R., Rahman, H., Sharifee, N. H., Sultana, N., Islam, M. I., Habib, S. A. & Ahammad, T. 2020. Integrated application of remote sensing and GIS in crop information system—A case study on Aman rice production forecasting using MODIS-NDVI in Bangladesh. *AgriEngineering*, 2, 264–279.

Genovese, C. R., Roeder, K. & Wasserman, L. 2006. False discovery control with p-value weighting. *Biometrika*, 93, 509–524.

Guechi, I., Gherraz, H. & Alkama, D. 2021. Correlation analysis between biophysical indices and Land Surface Temperature using remote sensing and GIS in Guelma city (Algeria). *Bulletin de la Société Royale des Sciences de Liège*, 90, 158–180.

Guha, S. & Govil, H. 2020. Land surface temperature and normalized difference vegetation index relationship: A seasonal study on a tropical city. *SN Applied Sciences*, 2, 1661.

Guo, Y., Fu, Y., Hao, F., Zhang, X., Wu, W., Jin, X., Bryant, C. R. & Senthilnath, J. 2021. Integrated phenology and climate in rice yields prediction using machine learning methods. *Ecological Indicators*, 120, 106935.

Hamzehpour, N., Shafizadeh-Moghadam, H. & Valavi, R. 2019. Exploring the driving forces and digital mapping of soil organic carbon using remote sensing and soil texture. *Catena*, 182, 104141.

Hashemzadeh Ghalhari, M., Vafakhah, M. & Damavandi, A. A. 2022. Agricultural drought assessment using vegetation indices derived from MODIS time series in Tehran Province. *Arabian Journal of Geosciences*, 15, 412.

Johnson, D. M., Rosales, A., Mueller, R., Reynolds, C., Frantz, R., Anyamba, A., Pak, E. & Tucker, C. 2021. USA crop yield estimation with MODIS NDVI: Are remotely sensed models better than simple trend analyses? *Remote Sensing*, 13, 4227.

Joshi, A., Pradhan, B., Chakraborty, S. & Behera, M. D. 2023. Winter wheat yield prediction in the conterminous United States using solar-induced chlorophyll fluorescence data and XGBoost and random forest algorithm. *Ecological Informatics*, 77, 102194.

Ju, S., Lim, H., Ma, J. W., Kim, S., Lee, K., Zhao, S. & Heo, J. 2021. Optimal county-level crop yield prediction using MODIS-based variables and weather data: A comparative study on machine learning models. *Agricultural and Forest Meteorology*, 307, 108530.

Justice, C., Gutman, G. & Vadrevu, K. P. 2015. NASA land cover and land use change (LCLUC): An interdisciplinary research program. *Journal of Environmental Management*, 148, 4–9.

Kang, J., Jin, R., Li, X., Zhang, Y. & Zhu, Z. 2018. Spatial upscaling of sparse soil moisture observations based on ridge regression. *Remote Sensing*, 10, 192.

Kheir, A., Nangia, V., Elnashar, A., Devakota, M., Omar, M., Feike, T. & Govind, A. 2024. Developing automated machine learning approach for fast and robust crop yield prediction using a fusion of remote sensing, soil, and weather dataset. *Environmental Research Communications*, 6, 041005.

Lin, B. B. 2007. Agroforestry management as an adaptive strategy against potential microclimate extremes in coffee agriculture. *Agricultural and Forest Meteorology*, 144, 85–94.

Maya Gopal, P. & Bhargavi, R. 2019. Selection of important features for optimizing crop yield prediction. *International Journal of Agricultural and Environmental Information Systems (IJAEIS)*, 10, 54–71.

Medina, H., Tian, D. & Abebe, A. 2021. On optimizing a MODIS-based framework for in-season corn yield forecast. *International Journal of Applied Earth Observation and Geoinformation*, 95, 102258.

Memon, N., Patel, S. B. & Patel, D. P. 2019. Comparative analysis of artificial neural network and XGBoost algorithm for PolSAR image classification. *International Conference on Pattern Recognition and Machine Intelligence*, Springer, pp. 452–460.

Mkhabela, M., Bullock, P., Raj, S., Wang, S. & Yang, Y. 2011. Crop yield forecasting on the Canadian Prairies using MODIS NDVI data. *Agricultural and Forest Meteorology*, 151, 385–393.

Mosleh, M. K., Hassan, Q. K. & Chowdhury, E. H. 2015. Application of remote sensors in mapping rice area and forecasting its production: A review. *Sensors*, 15, 769–791.

Nguyen, N. & Drakou, E. G. 2021. Farmers intention to adopt sustainable agriculture hinges on climate awareness: The case of Vietnamese coffee. *Journal of Cleaner Production*, 303, 126828.

Pang, A., Chang, M. W. & Chen, Y. 2022. Evaluation of random forests (RF) for regional and local-scale wheat yield prediction in Southeast Australia. *Sensors*, 22, 717.

Peñuelas, J. & Filella, I. 1998. Visible and near-infrared reflectance techniques for diagnosing plant physiological status. *Trends in Plant Science*, 3, 151–156.

Raksapatcharawong, M., Veerakachen, W., Homma, K., Maki, M. & Oki, K. 2020. Satellite-based drought impact assessment on rice yield in Thailand with SIMRIW− RS. *Remote Sensing*, 12, 2099.

Ramadhani, F., Pullanagari, R., Kereszturi, G. & Procter, J. 2021. Mapping a cloud-free rice growth stages using the integration of Proba-V and Sentinel-1 and its temporal correlation with sub-district statistics. *Remote Sensing*, 13, 1498.

Sakamoto, T., Gitelson, A. A. & Arkebauer, T. J. 2014. Near real-time prediction of US corn yields based on time-series MODIS data. *Remote Sensing of Environment*, 147, 219–231.

Sangjan, W., Carter, A. H., Pumphrey, M. O., Hagemeyer, K., Jitkov, V. & Sankaran, S. 2024. Effect of high-resolution satellite and UAV imagery plot pixel resolution in wheat crop yield prediction. *International Journal of Remote Sensing*, 45(5), 1678–1698.

Schwalbert, R. A., Amado, T., Corassa, G., Pott, L. P., Prasad, P. V. & Ciampitti, I. A. 2020. Satellite-based soybean yield forecast: Integrating machine learning and weather data for improving crop yield prediction in southern Brazil. *Agricultural and Forest Meteorology*, 284, 107886.

Son, N., Chen, C., Chen, C., Minh, V. & Trung, N. 2014. A comparative analysis of multitemporal MODIS EVI and NDVI data for large-scale rice yield estimation. *Agricultural and Forest Meteorology*, 197, 52–64.

Sujariya, S., Jongrungklang, N., Jongdee, B., Inthavong, T., Budhaboon, C. & Fukai, S. 2020. Rainfall variability and its effects on growing period and grain yield for rainfed lowland rice under transplanting system in Northeast Thailand. *Plant Production Science*, 23, 48–59.

Tan, W., Wei, C., Lu, Y. & Xue, D. 2021. Reconstruction of all-weather daytime and nighttime MODIS aqua-terra land surface temperature products using an XGBoost approach. *Remote Sensing*, 13, 4723.

Uddin, M. P., Mamun, M. A. & Hossain, M. A. 2021. PCA-based feature reduction for hyperspectral remote sensing image classification. *IETE Technical Review*, 38, 377–396.

Vadrevu, K.P., Le Toan, T., Ray, S.S. & Justice, C.O. eds. 2022. *Remote Sensing of Agriculture and Land Cover/Land Use Changes in South and Southeast Asian countries*. Springer.

Vadrevu, K.P., Dadhwal, V.K., Gutman, G. & Justice, C. 2019. Remote sensing of agriculture–South/Southeast Asia research initiative special issue. *International Journal of Remote Sensing*, 40(21), 8071–8075.

Xie, F. & Fan, H. 2021. Deriving drought indices from MODIS vegetation indices (NDVI/EVI) and Land Surface Temperature (LST): Is data reconstruction necessary? *International Journal of Applied Earth Observation and Geoinformation*, 101, 102352.

Yu, T. & Zhu, H. 2020. Hyper-parameter optimization: A review of algorithms and applications. arXiv preprint arXiv:2003.05689.

Zeng, J., Zhang, R., Qu, Y., Bento, V. A., Zhou, T., Lin, Y., Wu, X., Qi, J., Shui, W. & Wang, Q. 2022. Improving the drought monitoring capability of VHI at the global scale via ensemble indices for various vegetation types from 2001 to 2018. *Weather and Climate Extremes*, 35, 100412.

15 Biomass Burning Emission Inventory and Modeling in the Northern Part of the Association of Southeast Asian Nations (nASEAN)

Justin Sentian, Teo Yu Rou, Franky Herman, and Chin Jia Hui

15.1 INTRODUCTION

Burning biomass, which involves the open or partially open combustion of organic materials from plants and animals, has historically played a crucial role in meeting energy needs, managing agricultural lands, and preserving cultural traditions in various societies (Cole, 2001). However, its importance has come under increased scrutiny from both the general public and scientific communities due to its substantial contributions to air pollution and its association with climate change (Wang et al., 2018). Biomass burning has been identified as a significant source of global climate indicators, with human activities responsible for 90% of the planet's fires, resulting in the release of carbon dioxide (CO_2) and other pollutants (Trewin et al., 2021; Yadav & Devi, 2018). This process of burning releases a complex mixture of pollutants, including carbon monoxide (CO), volatile organic compounds (VOCs), and fine particulate matter ($PM_{2.5}$), posing health risks to respiratory systems (Le et al., 2014; Biswas et al., 2015; Alabar et al., 2018; Yin et al., 2019).

From a climate perspective, biomass burning impacts the Earth's radiative balance, releasing CO_2 and gases that contribute to global warming while emitting aerosols that have cooling effects (Jacobson, 2000; Levy, 2004; Yadav & Devi, 2018). Over time, the warming effect from CO_2 surpasses the cooling effect, resulting in an overall net global warming impact. The practice of biomass burning in the northern ASEAN (nASEAN) region, encompassing countries such as Thailand, Myanmar, Laos, Cambodia, Vietnam, and the Philippines, is significant and driven by agricultural activities like slash-and-burn for land clearance (Yin et al., 2019a). The tropical

 DOI: 10.1201/9781003396260-15

climate of this region, characterized by distinct wet and dry seasons, creates favorable conditions for biomass burning, particularly during dry periods (Huang et al., 2013; Yin et al., 2019b).

The effects of biomass burning in the nASEAN region are wide-ranging, impacting air quality, atmospheric chemistry, climate, economy, and public health (Harris et al., 2016; Chen et al., 2017). Emissions from this process introduce active trace gases and greenhouse gases, exacerbating global warming (Akagi et al., 2011). Particulate matter (PM) generated by biomass burning poses health risks and contributes to haze events, influencing air quality indices and respiratory health (Lee et al., 2018; Ho et al., 2014). Moreover, the transboundary air pollution from biomass burning affects neighboring countries, notably China and Taiwan, as pollutants are transported over long distances via prevailing wind patterns and atmospheric circulation, carrying particulate matter, gases, and other emissions across borders (Huang et al., 2013).

Having emission inventories is crucial for comprehending the impacts of biomass burning on the Earth system, offering valuable data on pollutants released into the atmosphere (Mangino, 1997; Gupta et al., 2001; Prasad et al., 2002; Vadrevu et al., 2018; Bond & Scott, 2022). This study seeks to provide estimates of the true scale of greenhouse gases, particulate matter, and other emissions released into the atmosphere, illuminating the region's role in global climate change and air pollution. It aims to contribute to a more precise understanding of the environmental and health consequences of biomass burning. As concerns about climate change and air quality mount, having comprehensive emissions' data from this source enables more effective policy-making and the development of targeted strategies to combat climate change, reduce air pollution, and protect local ecosystems.

15.2 STUDY AREA

The Northern Association of Southeast Asian Nations (nASEAN) holds significant importance within Southeast Asia, encompassing a vast land area of approximately 2,238,768 km^2 (Chaisse & Hsieh, 2023). nASEAN comprises six countries: Myanmar, Thailand, Cambodia, Laos, Vietnam, and the Philippines. The inclusion of the Philippines in this investigation is justified by its climatic similarities with mainland Southeast Asia (MSEA), resulting in a comparable burning season (Miettinen et al., 2014). The physical geography of nASEAN showcases a wide variety of terrains, including forests, mountains, valleys, rivers, deltas, and coastlines, with a predominant mountainous feature. Emerging from the Tibetan plateau, the Himalayan foothills lend nASEAN a distinctive geography distinct from other continental Asian regions (Frederick & Leinbach, 2018). Situated between India to the east and China to the west, nASEAN is bordered by the Pacific Ocean on the east and the Indian Ocean on the west. Falling mainly within the tropical zone, it experiences a tropical climate characterized by two seasons influenced by monsoon winds (Keane, 2017). Similarly, the Philippines lies entirely within the tropical zone. The Philippines, an archipelago encompassing the entire northeastern section of nASEAN, is a complex group of over 7,000 islands formed through geological shifts and tectonic movements (Boquet, 2017). These islands are commonly divided into three main groups: Luzon in the north, Visayas in the center, and Mindanao in the south (Matsumoto et al., 2020).

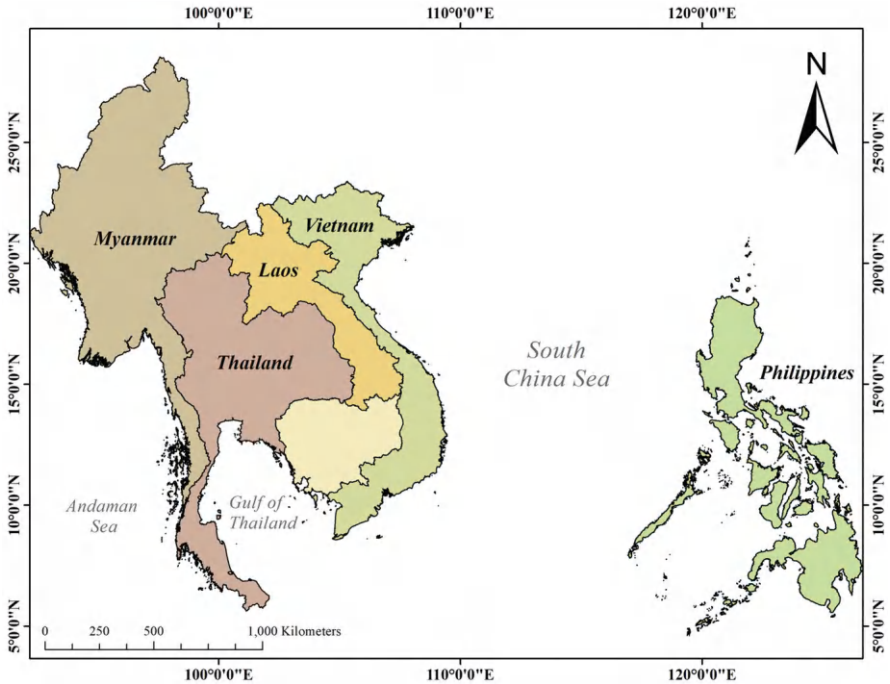

FIGURE 15.1 Map of northern Association of Southeast Asian Nations (nASEAN).

The climate of nASEAN is influenced by the shift between the southwest (SW) monsoon prevailing from May to September, marked by summer downpours and intense storms brought about by moisture-laden clouds carried by winds originating from the Indian Ocean, often culminating in typhoons during the late summer season. As the southwest monsoon transitions to the northeast (NE) monsoon from November to April, the area encounters milder and drier winters, characterized by dry conditions and calm winds. The period of transition between these monsoons, typically occurring from March to April, ushers in warmer temperatures (Keane, 2017; Matsumoto et al., 2020).

Regarding vegetation, Southeast Asian flora is generally divided into tropical rainforests or tropical evergreen rainforests, further categorized into wet evergreen forests, semi-evergreen forests, freshwater swamp forests, and evergreen montane forests. However, under this classification, there are forests with distinctive attributes, and the climate of nASEAN sustains a diverse array of tropical evergreen and deciduous forests housing various tree species (Rundel, 1999).

15.3 DATA AND METHODS

The methodology for evaluating biomass burning emissions in the nASEAN region primarily relies on combining remote sensing and geographical information system (GIS) techniques to generate maps and collect necessary data regarding burned

biomass mass and land cover types. Each country analyzes the data in subsequent sections. The pollutants under scrutiny in this study include key contributors to air pollution from biomass burning, such as CO_2, CO, CH_4, NO_x, PM (Particulate Matter), NMVOC (Non-Methane Volatile Organic Compounds), SO_2, NH_3, and carbonaceous aerosols.

To obtain information on land cover and burned areas, the study utilizes the Moderate Resolution Imaging Spectroradiometer (MODIS), favored for continental-scale research as it provides images twice daily (Lu & Weng, 2007). Significantly, MODIS applies surface reflectance correction to land, which is crucial for ensuring the accuracy of the data (Mccullough et al., 2013). The emissions' inventory development involves various essential processes, such as processing activity data and parameters, determining emission factors (EF), deciding on spatial and temporal distribution, and specifying details related to $PM_{2.5}$ and NMVOCs. This study focuses on open biomass burning from human-made and natural sources, excluding domestic burning activities. Furthermore, the research compares emission inventories from 2013 and 2021 to identify temporal variations and trends in biomass burning emissions. This comparative analysis enhances the understanding of how biomass burning dynamics have changed in the nASEAN region over time.

15.3.1 Land Cover

The data collection process for land cover is guided by the methodology outlined by Sulla-Menashe and Friedl (2018). This study employs the IGBP land classification because it offers superior remote-sensing data quality compared to other global land cover databases (Thenkabail, 2018). The MCD12Q1, a MODIS product that integrates Aqua and Terra supervised classification data, provides high-quality global land data (Friedl & Sulla-Menashe, 2019). The MCD12Q1 legacy classification of IGBP includes 17 types of land cover. However, due to the variation in land cover types across different regions, reclassification of land cover is necessary. This adaptation from the original 17 classes ensures the accuracy of describing the land cover to prevent misclassification. The reclassified IGBP land classes for the suitability of the nASEAN region are detailed in the table provided below.

Determining the annual rate changes for each land use and land cover (LULC) class is conducted using the formula established by Puyravaud (2003) and Batar et al. (2017):

$$r = \left(\frac{1}{t2 - t1}\right) \times ln\left(\frac{A2}{A1}\right) \times 100 - \tag{15.1}$$

Where,

r = annual change for each specific LULC class (%)
t = number of years spanning
$A1$ = area of land class at the beginning
$A2$ = area of land class at the end

This formula, denoted as 'r,' calculates the annual variation for each LULC class. It considers the respective areas of the class at the beginning ($A1$) and end ($A2$) of the assessment period spanning. 't' years. This formula plays a pivotal role in analyzing the annual changes in various land use and land cover classes, providing valuable insights into the evolving dynamics that influence the environmental landscape of the study area.

15.3.1.1 Statement of Land Cover Accuracy

The validation of the MODIS Collection 6 Land Cover product, explicitly focusing on the International Geosphere-Biosphere Programme (IGBP) layer within MCD12Q1, has reached stage 2, with a validation process yielding a global accuracy estimate of around 73.6%. It is important to note that there is currently no universally comprehensive dataset based on independent probability samples available for validation. Therefore, this accuracy estimate is supported through a quantitative analytical approach that involves cross-validating a training site database. This validation status highlights the reliability of the data included in this product despite the lack of a universally standardized validation dataset. It emphasizes the usability of this data for use in various environmental research and studies, positioning it as a valuable asset for scientific investigations and analyses (NASA MODIS Land, 2021).

15.3.2 Biomass Burning Emission Inventory

The mapping of burned areas for the emission inventory relied on MCD64A1 as the primary data source, offering data in 500×500 m^2 grids for 2013 and 2021 (Yin et al., 2019a, b). The estimation of biomass burning emissions (E_i) was conducted using equation (15.2):

$$E_i = \Sigma \frac{\mathrm{A}_j \mathrm{x}\, EF_{i,j}}{1000} \tag{15.2}$$

Where,

E: annual typical pollutant emission (Mg/year)
i: type of pollutant
j: biomass burning source
A: annual amount of dry biomass burned (Mg/year)
EF: Emission factor (g/kg)

For the annual amount of biomass burned (A), equation (15.3) was used:

$$A = \left[\sum (BA_{x,j} \times FL_{x,j} \times CF_j)\right] \times 10^{-6} \tag{15.3}$$

Where,

j: land cover type
x: location
$BA_{x,j}$: burned area (m^2/year) of land cover type j at x $FL_{x,j}$: fuel loading of land cover type j at x (g/m^2)
CF_j: combustion factor of land cover type j

The values for fuel loading (FL) in each land class are as follows: forests: 7184.80 g/m^2; shrublands: 2196.16 g/m^2; savannas: 133.87 g/m^2 (Michel, 2005); wetlands: 1100 g/m^2; croplands: 60 g/m^2 (Song et al., 2009). The combustion factor (CF), also known as burning efficiency, represents the ratio of available fuel exposed to the fire to the portion that actually burns. The CF values obtained for each land cover category are as follows: forests 0.25, shrublands 0.40, savannas 0.95 (Michel, 2005), wetlands 0.30, and croplands 0.6 (Song et al., 2009). The emission factor signifies the quantity of pollutants released per kilogram of biomass burned (Akagi et al., 2011). EF is typically expressed in g/kg, calculated by dividing the mass of pollutants by the mass of biomass burned. The EF values used in this study, as outlined in Table 15.1, are sourced from various literature references.

15.3.2.1 Burned Area Identification and Measurement

The land cover type and amount of biomass burned are essential factors in determining the pollutants released in biomass burning emissions. This study utilized a burn scar methodology to estimate total emissions, with the burned area in the nASEAN region being a key factor in this calculation. Burned areas were identified and measured using data from the MCD64A1 Collection 6, which incorporates

TABLE 15.1
Emission factors (EF) (g/kg) from different biomass sources

	CO_2	CO	CH_4	NO_x	NH_3	SO_2	PM_{10}	$PM_{2.5}$	EC	OC	NMVOC
Evergreen Forests	1643[a]	92[a]	5.1[a]	2.6[a]	0.76[a]	0.45[a]	12.8[c]	10.2[c]	0.5[a]	4.7[a]	24[a]
Deciduous Forests	1630[a]	102[a]	5[a]	1.3[a]	1.5[a]	1[b]	12.8[c]	12.3[c]	0.6[a]	9.2[a]	11[a]
Mixed Forests	1630[a]	102[a]	5[a]	1.3[a]	1.5[a]	1[b]	12.8[c]	12.3[c]	0.6[a]	9.2[a]	14[a]
Shrublands	1716[a]	68[a]	2.6[a]	3.9[a]	1.2[a]	0.68[a]	8.5[c]	7.9[c]	0.5[d]	6.6[d]	4.8[a]
Savannas	1692[a]	59[a]	1.5[a]	2.8[a]	0.5[a]	0.68[a]	9.9[c]	6.3[c]	0.4[a]	2.6[a]	9.3[a]
Wetlands	1765.5[c]	94[c]	1.5[c]	2.1[c]	0.6[c]	0.8[c]	12.5[c]	11.2[c]	0.52[c]	6.3[c]	6.8[c]
Croplands	1353.5[c]	76.1[c]	2.8[c]	2.9[c]	1.4[c]	0.4[c]	6.3[c]	5[c]	0.63[c]	2[c]	9.8[c]
Others	-	-	-	-	-	-	-	-	-	-	-

Sources: [a](Akagi *et al*., 2011); [b](Andreae & Merlet, 2001); [c](Song *et al*., 2009); [d](McMeeking, 2008)

daily surface reflectance and active fire input data for detection. The enhanced MCD64A1(C6) algorithm has reduced errors from data gaps and is more effective in detecting small fires, as demonstrated by Giglio et al. (2016, 2018).

15.4 RESULTS AND DISCUSSIONS

15.4.1 Land Cover of nASEAN

The land cover data for the nASEAN region in 2013 and 2021 was obtained from the MODIS Land Cover Satellite, MCD12Q1, and classified according to IGBP legends. Subsequently, they were reclassified from the 17 land classes in the IGBP classification to eight classes, as shown in Figures 15.2 and 15.3.

Significant shifts in land cover have been observed in the nASEAN countries, which include Cambodia, Laos, Myanmar, Thailand, Vietnam, and the Philippines, from 2013 to 2021. In 2013, evergreen forests covered 29.96% of the region, followed by croplands (23.17%), shrublands (18.31%), and savannas (18.03%). By 2021, evergreen forests remained the dominant land cover, occupying 28.44% of the area, while croplands maintained their share at 23.17%. Similarly, shrublands (18.31%) and savannas (18.03%) retained their significance. Evergreen forests, noted for their perpetual green canopy, play a crucial role in biodiversity preservation, carbon sequestration, and environmental services provisioning. The persistence of evergreen forests underscores their ecological importance (Brockerhoff et al., 2017). In the nASEAN context, croplands hold pivotal importance due to the region's heavy dependence on

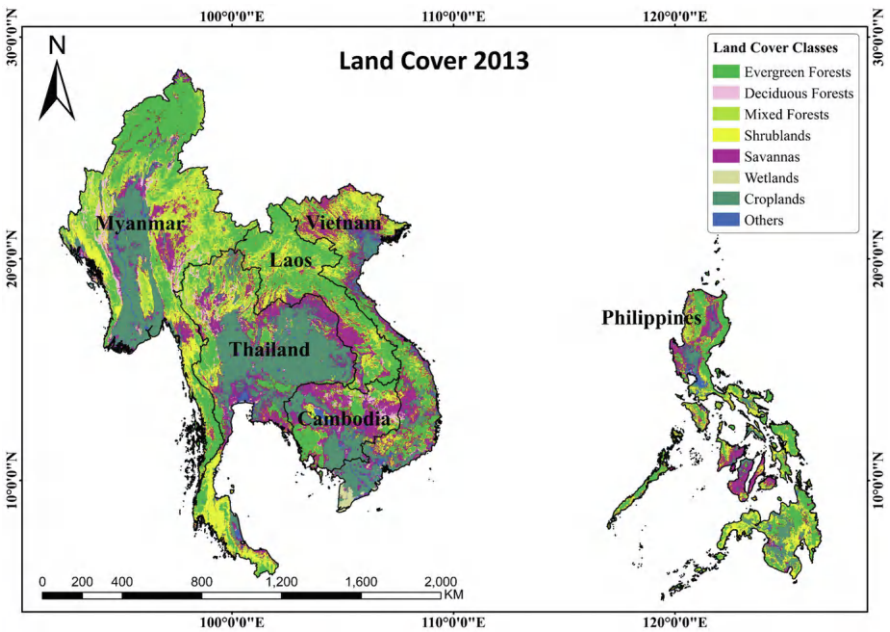

FIGURE 15.2 Land cover of nASEAN in 2013 derived from MODIS MCD12Q1 data.

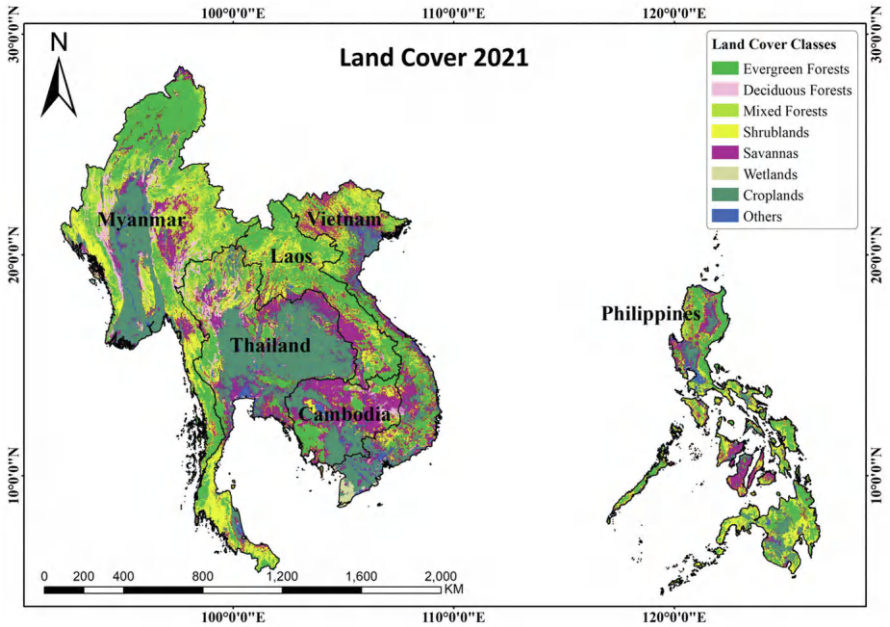

FIGURE 15.3 Land cover of nASEAN in 2021 derived from MODIS MCD12Q1 data.

agriculture as a key driver of economic growth. The substantial expansion of the agricultural sector from the 20th century to 2010 corresponds to the increasing food demand fueled by population growth (Booth, 2018). Southeast Asia plays a vital role in global agriculture, ensuring food security and nutritional sufficiency on a worldwide scale (Takeshima & Joshi, 2019).

Savannas, prominently present in Cambodia, Vietnam, the Philippines, and Thailand, exhibit a range of compositions ranging from grasslands with sparse trees to open canopy forests with grassy undergrowth. These ecosystems often arise from forest degradation attributed to human-induced mismanagement practices (Puri, 1989; George & Seth, 2005). Human interventions such as logging, forest fires, and shifting cultivation have resulted in the transformation of forests into savannas (Miettinen et al., 2014). Savannas utilizing C4 photosynthetic pathways function as transitional zones that fill the voids created by tree mortality driven by factors like fire and drought. Nonetheless, the expansion of C4 savannas can intensify conditions of drought and fire, leading to the development of adverse feedback loops (Beerling & Osborne, 2006). Land cover in the nASEAN region has undergone changes from 2013 to 2021. In 2013, evergreen forests made up 29.96% of nASEAN, with croplands (23.17%), shrublands (18.31%), and savannas (18.03%) in close succession. By 2021, evergreen forests remained dominant, covering 28.44% of the area, while croplands held steady at 23.17%. Shrublands (18.31%) and savannas (18.03%) also remained significant during this period.

Evergreen forests maintain their green foliage throughout the year, unlike deciduous forests that undergo leaf color changes or lose their leaves (Dreiss & Volin,

2014). The prevalence of evergreen forests underscores their significance in preserving biodiversity, storing carbon, and offering environmental benefits (Brockerhoff et al., 2017). Croplands play a vital role in the nASEAN region, given that agricultural activities are a primary driver of economic advancement in Southeast Asia. The substantial expansion of the agricultural sector, particularly between the 1900s and 2010, correlates with the heightened food demand resulting from population growth (Booth, 2018). Southeast Asia plays a crucial role in global agriculture, providing essential food sources and nutritional sustenance (Takeshima & Joshi, 2019).

In Cambodia, Vietnam, the Philippines, and Thailand, savannas are a prominent component of land cover. Savannas can encompass various landscapes, ranging from grasslands with scattered trees to dense open canopy forests with grassy undergrowth (Sankaran et al., 2005; Hirota et al., 2011; Staver et al., 2011; Lehmann et al., 2014). These ecosystems are typically the result of forest degradation due to human mismanagement practices (Puri, 1989; George & Seth, 2005), with human activities such as logging, forest fires, and shifting cultivation playing a role in the conversion of forests into savannas (Miettinen et al., 2014). Savannas utilizing C4 photosynthetic pathways serve as transitional areas that fill the voids left by tree mortality following events like fire and drought. However, the expansion of C4 savannas can exacerbate drought and fire conditions, leading to the creation of negative feedback loops (Beerling & Osborne, 2006).

Agricultural cultivation plays a vital role in the nASEAN region, given the area's heavy dependence on agriculture for sustenance and economic progress. Agriculture serves as the primary engine of economic advancement in Southeast Asia, with marked growth witnessed in the agricultural sector from the early 1900s to 2010, aligning with the rising food demand due to population expansion (Booth, 2018). Southeast Asia is a significant contributor to global agriculture, serving as a critical source of food and nutritional provisions (Takeshima & Joshi, 2019). The fertile soils and favorable climate conditions in the nASEAN region support agricultural productivity, leading to the expansion of cropland areas to meet the increasing need for food and agricultural goods (Lim et al., 2023). In 2013, Thailand's croplands covered 41% of the land, making it the most extensive land cover category, followed by Cambodia at 27% and Myanmar at 20%, the second most significant land cover type in these nations. Vietnam had 21% of croplands, placing it third in terms of coverage. By 2021, the extent of cropland areas had expanded to 42% in Thailand, 29% in Cambodia, 21% in Myanmar, and 21% in Vietnam.

Thailand holds a pivotal position in agriculture, particularly in the production of rice, standing as one of the leading global exporters in this sector (Titapiwatanakun, 2012; Wongchai & Ngamsomsuke, 2015). Similarly, Vietnam, Myanmar, and Cambodia, among other nASEAN countries, are noteworthy players in rice production and exportation (Workman, 2019). Data from the USDA (2023) indicates that from 2019 to 2022, Vietnam (5th), Thailand (6th), the Philippines (7th), Myanmar (8th), and Cambodia (12th) ranked among the top 15 rice-producing nations worldwide. In the Philippines, the diverse geography and unique land formations give rise to three distinct agroecological zones (AEZ) designated as the wet zone, moist zone, and dry zone (Dikitanan et al., 2017). The majority of cultivated areas are dedicated to rice, coconut, and maize cultivation, with rice serving as the primary staple crop

(Mamiit et al., 2021). The Philippines holds a prominent position in global coconut production and is a leading exporter of mangoes, ranking this fruit as the fourth most exported, alongside bananas, coconuts, and pineapples. This highlights the country's thriving agricultural sector and export industry (Dikitanan et al., 2017).

The assessment of changes in land use and land cover (LULC) is of paramount importance in analyzing environmental shifts on a global, regional, and local scale. This has become a foundational element of sustainability research, providing crucial insights into ecosystem dynamics and the effects of human activities on the environment (Seyam et al., 2023). By comparing changes in LULC over time, we can better understand the interactions between human behaviors and the environment, enabling evidence-based decision-making to ensure the responsible and sustainable management of natural resources for both current and future generations. As illustrated in Figure 15.4, there was a significant decrease in the area of evergreen and mixed forests by 32,551.27 km^2 and 21,018.35 km^2, respectively, along with a corresponding reduction in savannas by 11,475.93 km^2. In contrast, there was an expansion in the area of deciduous forests and croplands, with increases of 21,811.52 km^2 and 22,106.97 km^2, respectively.

Forest compositions are heavily influenced by climatic elements such as temperature and precipitation (Yang et al., 2005; Bagaria et al., 2021). As temperatures rise and rainfall patterns shift in Southeast Asia, forecasts suggest a drier Indo-Burma region and a wetter Sundaland (Zhuang, 2009; Namkhan et al., 2022), leading to the transition of evergreen forests into deciduous forests within the span of 8 years. Ongoing temperature and precipitation variations could further convert deciduous forests into savanna woodlands, presenting notable consequences, particularly in Thailand and Vietnam (Zhuang, 2009). Nevertheless, the increase in deciduous forest cover fails to offset the decline in evergreen and mixed forest areas, which might be attributed to the unregulated exploitation of forest resources and the conversion of forests into commercially driven landscapes (Ansori, 2021).

The rapid expansion of urban areas and infrastructure development, influenced by economic integration policies, has significantly impacted land use, resulting in the decline of vegetated regions and an increase in the classification of 'others' in land use categories (Hurni et al., 2017). Government initiatives aimed at transforming the livelihood practices and strategies of small-scale farmers have spurred heightened agricultural activities over the past two decades, leading to conflicts between agriculture and the natural environment (Fox & Castella, 2013; Tanentzap et al., 2015; Hurni et al., 2017). These conflicts, particularly notable from 1990 to 2020, have resulted in substantial deforestation as forests are converted into croplands, underscoring significant agricultural expansion within the nASEAN region (Zhai et al., 2022).

15.4.2 Total Emission in nASEAN

15.4.2.1 Burned Area of nASEAN

The biomass burning data for the nASEAN region in 2013 and 2021 is obtained from MODIS data, specifically MCD12Q1 version 6 for land cover classifications and MCD64A1 for burned area delineations. MCD64A1 provides valuable information

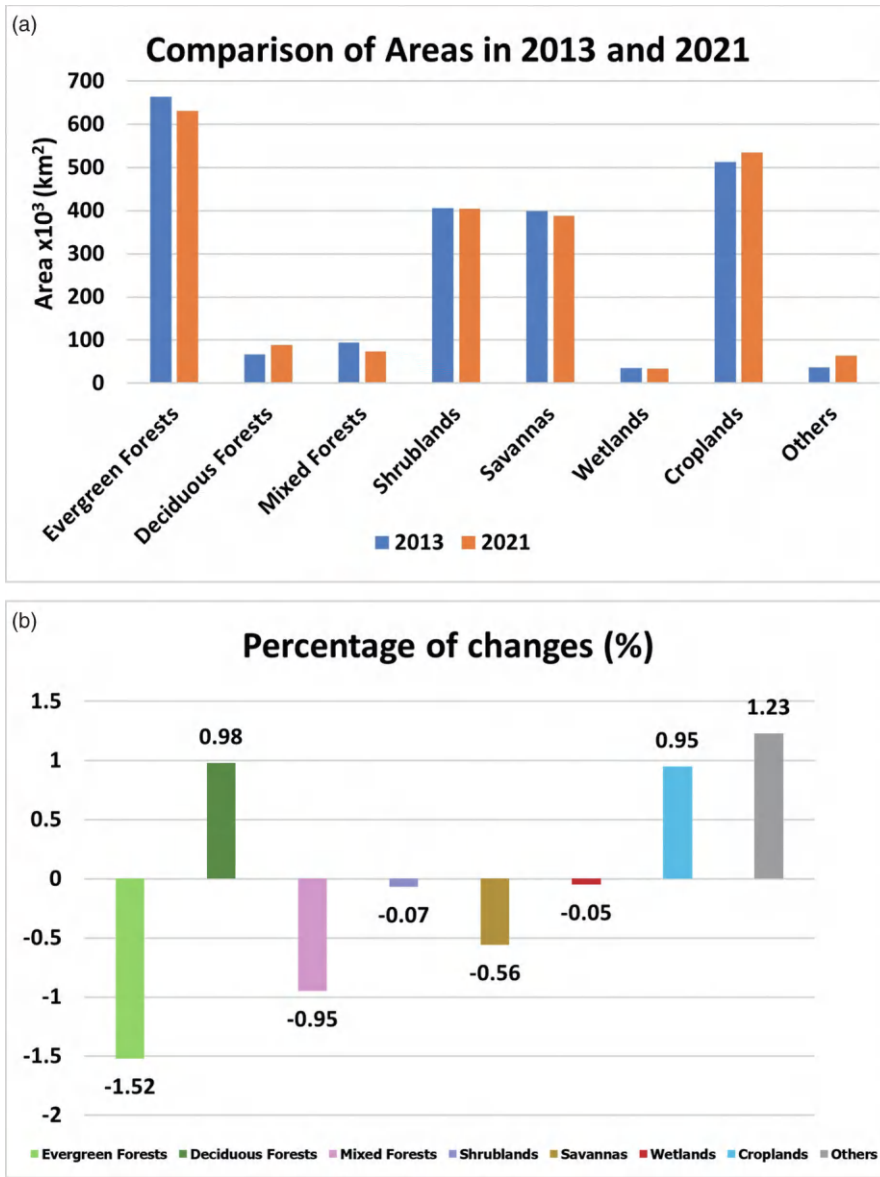

FIGURE 15.4 Comparisons of area and percentage change of each land cover of nASEAN in 2013 and 2021.

on the location, timing, and intensity of active fires, serving as a pivotal resource for comprehending fire behavior, trends, and their impacts on ecosystems and landscapes. This dataset is extensively employed in fire management, ecological studies, and environmental surveillance. The determination of burned areas in nASEAN, categorized

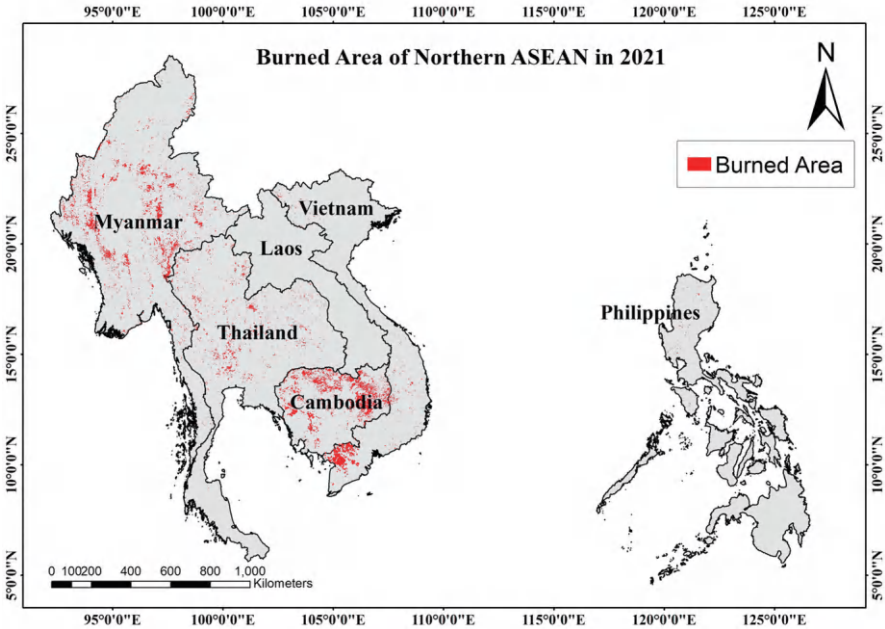

FIGURE 15.5 Burned area and land cover types of nASEAN in 2013.

according to respective land cover types, involves estimations and computations within the ArcGIS software. This process is essential for evaluating the annual dry biomass burned, as depicted in Figures 15.5 and 15.6 are critical for estimating the emissions of various pollutants generated annually from each land cover type. The calculation of the annual dry biomass burned entails multiplying the burned area by the combustion efficiency and fuel loading specific to each land cover classification.

The scale of the burned area does not always correspond to a higher quantity of biomass burned, as the mass of dry biomass burned is influenced by both fuel loading and combustion efficiency. Fuel loading refers to the amount of available fuel present during biomass burning, or the density of biomass situated above the ground surface, while combustion efficiency represents the proportion of burned fuel, specifically the biomass above the ground surface (Shi & Yamaguchi, 2014; Zhou et al., 2017). Despite exhibiting a high combustion factor, savannas display a lower burned mass due to their reduced fuel loading. In contrast, evergreen forests, characterized by a low combustion factor, harbor higher fuel loading, resulting in a greater amount of dry mass burned. The combustion triangle—comprising oxygen, heat, and fuel—significantly influences the quantity of dry mass burned (Asian Development Bank, 2001). Forests, notably dense evergreen forests, contain abundant oxygen, which impacts the combustion process. Various fire types lead to differing levels of fuel consumption, including burning on the surface and below ground (Hungerford et al., 1990). Additionally, meteorological conditions such as humidity, temperature, and precipitation can affect the intensity of burning (Toh et al., 2013). Upon

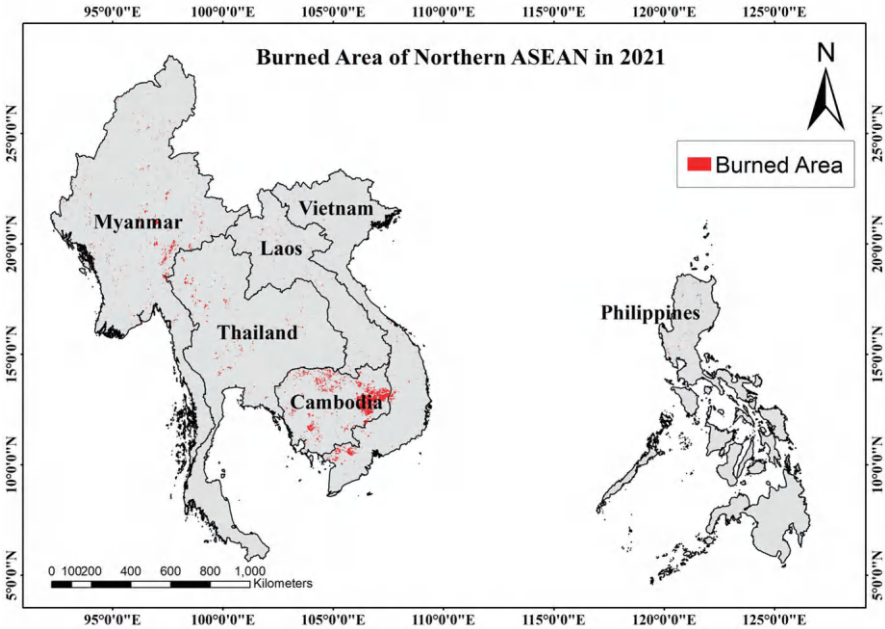

FIGURE 15.6 Burned area and land cover types of nASEAN in 2021.

visual examination of the fires in 2013 and 2021, as depicted in the figure, it is evident that extensive fire activity occurred across the ASEAN region in 2013, with fewer incidents in Myanmar and Laos, while heightened burning was observed in Cambodia by 2021. In 2013, significant portions of evergreen, deciduous, and mixed forests were affected by fires in terms of burned areas and associated biomass burned, indicating the susceptibility of these forest types to fire events. Savannas also played a significant role in the total biomass burned, emphasizing their vulnerability to wildfires. However, there was a decrease in burning activities for nearly half of the total burned area when comparing data between 2013 and 2021. A noticeable shift in the distribution of burned areas and biomass burned among different land cover types is evident from 2013 to 2021. There is a substantial increase in burned areas and biomass burned in deciduous forests, along with a notable decrease in burned areas and biomass in evergreen forests. This shift could have implications for carbon sequestration and greenhouse gas emissions (Li et al., 2020). Deciduous trees primarily store carbon in their woody biomass, whereas evergreen forests allocate only 70% of their net ecosystem production (NEP) to woody components, releasing the remainder into the soil and other carbon reservoirs (Holtmann et al., 2021). Storing carbon in woody biomass makes deciduous forests more effective at carbon sequestration due to superior carbon capture efficiency and longer residence time in biomass compared to evergreen forests. However, the burning of deciduous forests results in greater carbon emissions into the atmosphere than from evergreen forests, contributing to increased greenhouse gas emissions (Baccini et al., 2019).

15.4.2.2 Sources of Biomass Burning Emission

The Biomass Burning Emission Inventory data outlined in Tables 15.2 and 15.3 for ASEAN countries in 2013 and 2021 offer valuable insights into the release of various air pollutants. Deciduous forests emerge as the primary contributors in both years, with evergreen forests, mixed forests, and shrublands following closely. The noticeable variation in emissions originating from evergreen forests compared to deciduous forests in 2021 may be attributed to climate change-induced alterations in land classifications, resulting in a higher proportion of CO_2 and CO emissions from deciduous forests. CO_2 stands out as the most prevalent pollutant emitted across all land cover types, followed by CO, which is generated when carbon in biomass reacts with oxygen to produce CO_2 during complete combustion. Additionally, a corresponding amount of sequestered CO_2 from biomass is released through photosynthesis, while incomplete combustion of organic matter yields CO.

Deciduous forests were the main source of emitted pollutants in both 2013 and 2021, while evergreen forests were responsible for NO_x and NMVOC emissions in 2013. However, by 2021, emissions of NO_x and NMVOC had decreased slightly due to a reduction in the proportion of evergreen forests and a decrease in burned area. Evergreen forests release higher levels of NO_x and NMVOC due to their high photosynthesis and metabolic rates. On the other hand, deciduous forests, which have higher moisture content, can lead to incomplete combustion and increased VOC emissions. Various factors, such as temperature differentials, tree heat tolerance, and atmospheric conditions, can influence emissions from both types of forests. Additionally, shrublands also contribute significantly to NO_x emissions due to high emission factors.

The smoke produced by burning biomass contains a wide range of compounds that can have harmful effects on human health, causing chronic or acute respiratory problems and, in severe cases, even death, especially affecting vulnerable populations. Human activities such as clearing land for agriculture and urban expansion are major contributors to forest fires. In Southeast Asia, peatlands are often burned for agricultural purposes, leading to the conversion of organic-rich peatlands into farmland or for urban development. In countries within the nASEAN region where extensive agricultural practices are common, swidden agriculture is practiced, resulting in a decrease in forested areas. Additionally, the different topographies in the region cause variations in the composition of biomass, influencing the emission patterns of pollutants and the intensity of fires.

Upon examining the relationship between changes in land cover area and emitted pollutants, interesting patterns are revealed. Evergreen forests show a positive correlation with various pollutants like CO_2, CO, CH_4, NO_x, NH_3, SO_2, PM_{10}, $PM_{2.5}$, EC, OC, and NMVOC, indicating reduced emissions in line with decreased forest area, while deciduous forests exhibit a negative correlation, suggesting a lesser impact on emissions. Mixed forests, savannas, wetlands, and croplands demonstrate positive correlations, whereas other land cover types show negative correlations with most pollutants, indicating that emissions increase with expanded land coverage. These findings provide valuable insights for policymakers and conservationists regarding the environmental effects of changes in land cover on biomass burning emissions in the nASEAN region.

TABLE 15.2
Area of each land cover class in nASEAN in 2013

	Division (km^2)							
Classes	**Cambodia**	**Laos**	**Myanmar**	**Thailand**	**Vietnam**	**Philippines**	**Total**	**Percentage (%)**
Evergreen Forests	40210.43	134018.2	216887.8	89597.63	84322.61	98471.21	663507.88	29.96
Deciduous Forests	10172.06	2134.975	36322.48	16870.39	1537.804	166.8399	67204.5489	3.03
Mixed Forests	4067.442	2254.927	81523.15	5030.51	1719.602	22.14944	94617.78044	4.27
Shrublands	13910.71	53555.32	111467.8	85321.06	65639.13	75628.52	405522.54	18.31
Savannas	58249.85	32581.24	71402.3	92552.7	86881.59	57495.04	399162.72	18.03
Wetlands	1944.835	463.6999	7338.367	5533.619	11907.48	7860.748	35048.7489	1.58
Croplands	48472.17	3808.264	136328.3	210100.6	67299.48	47142.91	513151.724	23.17
Others	4254.13	1036.421	6782.042	8542.49	8432.894	7081.203	36129.18	1.63
Total	181281.63	229853.05	668052.24	513549	327740.59	293868.62	2214345.12224	100

TABLE 15.3
Area of each land cover class in nASEAN in 2021

	Division (km^2)							
Classes	**Cambodia**	**Laos**	**Myanmar**	**Thailand**	**Vietnam**	**Philippines**	**Total**	**Percentage (%)**
Evergreen Forests	31704.72	122468.9	214089.1	86850.17	86654.18	89189.54	630956.61	28.44
Deciduous Forests	7912.65	2466.03	49445.5	27437.29	1622.665	131.9311	89016.0661	4.01
Mixed Forests	1045.503	1151.691	67206.48	2324.445	1866.635	4.680483	73599.43448	3.32
Shrublands	13682.22	58421.79	110625.9	80888.99	62699.75	78426.77	404745.42	18.24
Savannas	67635.33	38054.96	68875.66	81359.09	81275.13	50486.62	387686.79	17.47
Wetlands	1970.484	397.8411	7443.724	5469.73	11981.16	6672.029	33934.9681	1.53
Croplands	52452.13	5957.963	141766.9	217314.3	69372.08	48395.32	535258.693	24.12
Others	4954.877	962.4244	9821.409	12403.28	12910.24	22501.42	63553.6504	2.86
Total	181357.914	229881.5995	669274.673	514047 .295	328381.84	295808.3106	2218751.632	100

In terms of biomass burning emissions by country, Myanmar had the highest burned area in 2013, followed by Cambodia, Thailand, Vietnam, Laos, and the Philippines. However, when considering the burned area as a percentage of the total land area, Cambodia had the highest percentage in both years. By 2021, Cambodia saw an increase in the percentage of burned area compared to 2013, while other countries experienced a decrease in burning activities. Cambodia remained the leader in burned areas in 2021, followed by Myanmar, Vietnam, Thailand, Laos, and the Philippines. Particularly noteworthy is that Cambodia had the largest percentage increase in burned area compared to the total land area.

When examining the annual typical emissions of nASEAN countries, emission patterns varied among the nations between 2013 and 2021. In 2013, Myanmar had the highest emissions, but by 2021, Cambodia had become the leading emitter, with noticeable reductions observed in Myanmar and Laos. Vietnam and Thailand also saw decreased emissions, while the Philippines consistently maintained lower emission levels in both years. Overall, emissions for each pollutant decreased in 2021 compared to 2013, which can be attributed to the implementation of enhanced policies and regulations such as the ASEAN Transboundary Haze Pollution (ATHP), Asia-Pacific Forestry Commission (APFC) of FAO, Sustainable Use of Peatland and Haze Mitigation in ASEAN (SUPA), ASEAN Peatland Management Strategy (APMS), Asian Forest Cooperation Organization (AFoCo) fire management and training initiatives, among others, as highlighted in studies by Muhammad (2021), AFoCo (2022), and Charusombat (2023). Alternatively, the decrease in emissions may also be linked to global lockdown measures during the COVID-19 pandemic, which restricted daily activities, including burning practices, leading to a reduction in human-induced emissions, as noted in research by Kanniah et al. (2020).

Forests play a crucial role in driving biomass burning emissions in Cambodia, particularly with deciduous forests experiencing a concerning increase in burning activities from 2013 to 2021. Additionally, shrublands and savannas also make significant contributions to these emissions. It is important to note that agriculture plays a vital role in Cambodia's economy, as emphasized by the Food and Agriculture Organization (FAO, 1999), contributing to 35% of the country's GDP, with crop production contributing 54% to the agricultural sector's GDP. Cambodia is a major rice exporter and also cultivates other crops such as corn, beans, and fruits. However, during the early 2010s, the expansion of the rubber industry led to extensive deforestation in Cambodia, followed by a decline that prompted a shift to alternative plantations, as discussed in studies by Mermoz et al. (2021). In the dry season, characterized by intense wildfires in Cambodia, farmers burn crop residues and grasses for land preparation, as highlighted in research by Sim et al. (2023). Being the least densely populated country in ASEAN, with a majority of the population living in rural areas and limited access to electricity, wood, and charcoal remain the primary sources of energy for households and industries, as noted by NIS (2009) and Yadav and Devi (2018). Wood is extensively used for domestic cooking, with approximately 98% of the population relying on it, as indicated by Top et al. (2004). This heavy dependence on wood is correlated with research findings linking deforestation to an increase in fire incidents. Fire activities are particularly concentrated in regions like Battambang and Pailin in the northwest, as well as Kartie and Kampong Thom in the east of

Cambodia, according to research by Sim et al. (2023). Despite designating 40% of its land area as protected zones across 69 sites, Cambodia has faced significant forest disturbances, which have escalated to around 55% from 2018 to 2020, highlighting the challenges in implementing effective forest conservation policies, as discussed in studies by Mermoz et al. (2021).

In Laos, evergreen forests, shrublands, and savannas have been identified as the main sources of biomass burning emissions. Forests play a crucial role in the economy of Laos, with wood fuel and non-wood forest products serving as important sources of income. However, unchecked logging practices and shifting cultivation have significantly contributed to extensive deforestation in the country over the past few decades, as discussed by Yadav and Devi (2018). An analysis of the percentage of forest area loss in Laos has revealed a notable deforestation trend linked to the expansion of plantation crops, including rubber in the northern region and various crops such as pulp trees, sugarcane, coffee, and rubber in the southern part of the country. There is also a focus on commodities in northwestern Laos. Particularly, the most substantial deforestation was observed in northern Laos between 2018 and 2021, as indicated in studies by Mermoz et al. (2021). Laos reportedly has the lowest number of protected areas, with only 31 designated sites covering a small portion of the total land area, amounting to 18.7%, highlighting deficiencies in policies and regulatory frameworks, as highlighted in research by Mermoz et al. (2021).

Myanmar stands out for having the highest area of land burned among the six countries in nASEAN, which can be attributed to its extensive geographical size. Emissions in Myanmar primarily stem from forests, followed by shrublands, savannas, and croplands, although there has been a decrease in contributions observed from 2013 to 2021. Myanmar is predominantly an agrarian society, with 70% of the population involved in agriculture, where biomass serves as a crucial source of energy, making up 64% of their energy mix, according to Yadav and Devi (2018). Logging activities and the collection of fuelwood hold significant importance in the country. Despite Myanmar having nearly half of its land covered by forests, it ranked among the top ten in terms of deforestation rates from 2010 to 2015. Illegal logging continues to be a prevalent issue, despite existing laws against forest exploitation, as highlighted by Kyaw et al. (2016) and Miettinen et al. (2014). Analysis has shown that deciduous and mixed forests are significant sources of emissions due to timber production, with evergreen forests having the largest area coverage. Mixed and deciduous forests are important sources for timber harvesting, as they contain robust and durable wood species, as discussed by Kyaw et al. (2016). Additionally, crop cultivation plays a vital role in Myanmar's economy, with the country being well-known for its production of rice, sugarcane, and dry beans, as mentioned by Moore (2020).

In Thailand, biomass burning emissions are primarily linked to the burning of garbage, crops, and forests, as indicated by Yadav and Devi (2018). Croplands represent the largest burned area in Thailand, largely due to the extensive coverage of croplands throughout the country. This is followed by forests, which account for a significant burned area, and then by savannas, shrublands, and wetlands. Despite shrublands having a smaller burned area compared to forests, savannas, and croplands, they contribute significantly to emissions due to their elevated fire load (FL) and emission factor (EF). Like Myanmar, Thailand is known as an agricultural nation with diverse

forest reserves, as discussed in research by Ohara et al. (2007) and Streets et al. (2003). Approximately two-thirds of the land is utilized for agricultural activities, with 25% covered with forests, according to Yadav and Devi (2018). The remainder is designated for non-agricultural purposes, with over 50% dedicated to paddy fields, 25% for other crops, and 14% for fruit tree plantations.

Vietnam, on the other hand, demonstrates the second lowest biomass-burning emissions compared to other countries in the region. Forests, particularly evergreen and deciduous forests, are highlighted as the main sources of biomass burning emissions in Vietnam. The burned areas are predominantly concentrated in the southern region of Vietnam, notably around the Mekong River Delta. Vietnam holds a significant position as one of the world's top rice exporters, ranking third in 2013, as reported by Maierbrugger (2015). The Mekong River Delta, known for its agricultural profitability, has attracted migrants seeking new land for cultivation, especially smallholders, as highlighted by Smith (2014). In 2015, the Mekong River Delta contributed to 57% of Vietnam's annual rice production, and in 2011, it accounted for 41% of the country's annual GDP, as mentioned by Smith (2014).

The Philippines demonstrated the lowest levels of biomass burning emissions among ASEAN countries in both 2013 and 2021, despite having a larger land area compared to Cambodia and Laos. Savannas and croplands are notable areas where biomass is burned, with emissions primarily originating from evergreen forests and shrublands. Like many Southeast Asian nations, the Philippines allocates a significant portion of its land for croplands to support agriculture, which plays a key role in the country's economy and food production, as discussed by Madayag and Estanislao (2021). The diverse topography of the Philippines, with its tall mountains, hilly upland regions, flat plains, fertile volcanic soils, seasonal monsoons, abundant rainfall, and high temperatures, offers favorable conditions for cultivating a variety of crops across its diverse islands, according to the World Bank (2016).

The traditional land-use practice of shifting cultivation, locally known as "kaingin," is widespread in the Philippines, aligning with agricultural traditions and the subsistence farming practices of indigenous communities, as highlighted by Mukul et al. (2016). This practice contributes to the burning of savannas and croplands, as well as the initial stages of deforestation in the agricultural sector. Agricultural expansion and illegal logging were significant issues in the early 1990s, but the agricultural sector has gradually declined since 2018 (Madayag & Estanislao, 2021). Deforestation in the Philippines has been linked to activities such as mining and urbanization, resulting in changes in land use for recreational areas, road construction, and dam projects.

The Greater Mekong Subregion (GMS) has been identified as a significant hotspot for forest loss, with Vietnam undergoing the most drastic change in primary forest cover, as noted by Mermoz et al. (2021). By the year 2020, only 0.5% of Vietnam's total forest area remained as primary forests. Countries in the GMS region are confronted with substantial deforestation resulting from activities like forest conversion and development, such as dam construction, with current laws, policies, and regulations proving insufficient in addressing illegal logging practices. When comparing the biomass burning and emissions of nASEAN countries from 2013 to 2021, notable improvements are seen in all nations except for Cambodia. The COVID-19 pandemic likely played a role in these positive trends, as many countries enforced

strict measures to limit movement and travel, potentially reducing human-induced pressures on natural ecosystems. Given that a majority of fires in Asia stem from human activities, the temporary decline in fire incidents in 2020, in comparison to 2019, can be attributed to COVID-related travel restrictions. It is important to note that agricultural fires, mainly used for clearing agricultural residues post-harvest, are prevalent in both South Asia and Southeast Asia. The lockdown measures imposed due to COVID-19 had impacts on the agricultural sector, affecting the availability of labor for various activities such as planting, harvesting, transportation, marketing, and processing. Additionally, the forest-related tourism industry and visits to natural areas may have slowed down due to COVID-19 travel restrictions in multiple countries, potentially leading to a decrease in accidental fires, according to Vadrevu et al. (2022). Furthermore, the La Niña event in 2021, which brought about a global cooling effect, likely contributed to the downward trend observed in emissions during that time period.

15.5 CONCLUSION

The profound effects of climate change present a significant global challenge that is reshaping environmental, social, and economic landscapes. Climate-related hazards, ranging from extreme heat to coastal flooding, are becoming more frequent, highlighting the urgent need to address the root causes of these changes. The build-up of greenhouse gases, mainly from human activities, is the primary driver behind climate change, resulting in increasing global temperatures and a wide array of environmental repercussions. Amidst the intricate array of climate-related challenges, biomass burning is a prevalent practice with broad environmental and health implications. Despite the critical need to limit temperature increases globally, biomass burning continues to be a widespread practice in developing regions, making a significant contribution to emissions. In Southeast Asia, where biomass burning is common, countries face significant challenges concerning air quality and health. The development of biomass-burning emission inventories and robust emissions modeling is crucial in gaining insight and addressing the extensive impacts of this practice.

This study utilized remote sensing and GIS techniques to evaluate biomass burning emissions in the nASEAN region by analyzing crucial data on burned biomass mass and land cover types. The research examines the different pollutants produced by biomass burning, such as CO_2, CO, CH_4, NO_x, PM, NMVOC, SO_2, NH_3, and carbonaceous aerosols. The initial phase involved generating a comprehensive land cover map using GIS tools and MODIS data, ensuring accuracy through surface reflectance correction. The process of developing an emissions inventory included processing activity data, determining emission factors, and outlining the spatial and temporal distribution, focusing specifically on open biomass burning while excluding domestic burning from the study scope. Additionally, this study offers valuable insights by contrasting emission inventories from 2013 to 2021 with a spatial resolution of 500 m × 500 m, highlighting temporal fluctuations and patterns in biomass burning emissions within the dynamic nASEAN region.

The analysis of land cover patterns in the nASEAN region during the years 2013 and 2021 reveals significant trends. Evergreen forests, croplands, shrublands, and savannas dominate both in 2013 and 2021, with a notable decrease in evergreen (1.52%) and mixed (0.95%) forests and an increase in deciduous forests (0.98%) and croplands (0.95%) in 2021 compared to 2013. This shift indicates intricate interactions involving climatic conditions, changes in land use, and human activities. The prevalence of croplands underscores the region's dependence on agriculture, especially in countries like Thailand, where it represents the largest land cover class at 42%. The decline in evergreen forests raises concerns regarding biodiversity conservation and the provision of environmental services. The change in biome patterns points to the potential impacts of shifting temperatures and rainfall patterns, highlighting the importance of implementing sustainable land management strategies. Furthermore, urbanization and infrastructure development contribute to the reduction in vegetated areas, underscoring the delicate balance between economic progress and environmental preservation in the nASEAN region.

Conversely, the examination of biomass burning across nASEAN nations uncovers the intricate connections among environmental, socio-economic, and policy elements. The changes in burned areas, biomass consumption, and emissions between 2013 and 2021 illustrate the dynamic nature of these phenomena. While certain countries have shown progress, Cambodia stands out for the escalation in burning activities, rising from 14% to 15.98% of the country's total area. The complex interplay between land cover categories, economic practices, and emissions underscores the importance of tailored policy interventions. Analyzing the impact on carbon sequestration, greenhouse gas emissions, and public health highlights the pressing need for comprehensive strategies to tackle biomass burning. The observed discrepancies among countries underscore the significance of accounting for regional nuances when devising effective mitigation strategies. In addressing these challenges, ongoing initiatives like the ASEAN Transboundary Haze Pollution initiative and others are crucial, yet a collaborative and region-specific approach is imperative to navigate the complexities of biomass burning within the continually evolving landscape of nASEAN.

This study significantly advances our comprehension of the environmental and health ramifications arising from biomass burning, providing invaluable data for global concerns regarding climate change and air quality. The enhanced emission inventory focused on the nASEAN region informs evidence-based policies for managing climate and air quality and enables nASEAN governments to craft targeted strategies. The cross-border aspect of the issue underscores the necessity for regional collaboration, potentially fostering cooperative climate and air quality agreements. Additionally, this research is a vital repository for evaluating future climate trends in the nASEAN region. The refined modeling and analysis of emitted pollutants and biomass-burning activities contribute to more efficient policy development, ultimately enhancing regional air quality. Overall, the outcomes of this study underscore the significance of ongoing monitoring and strategic interventions to address the intricate dynamics of land cover alterations and their repercussions for environmental sustainability and human well-being.

However, the utilization of GIS and remote sensing techniques presents certain constraints. The accuracy of GIS analyses heavily relies on the quality of input data as well as the software used for data generation. Inaccuracies or outdated information in land cover or other GIS layers could propagate into the emission inventory, impacting overall reliability. Given the spatial constraints inherent in MODIS data, with a resolution of 500 m × 500 m, fine-scale variations in biomass burning may not be captured, particularly in diverse landscapes. The monthly temporal resolution of the data may overlook short-term fluctuations, potentially affecting data accuracy. Moreover, satellite data is contingent on clear atmospheric conditions, and issues like cloud cover could introduce uncertainties or data gaps, influencing the precision of the emissions inventory. The reliance on remote sensing and GIS techniques may lack extensive ground validation, introducing uncertainties regarding the actual alignment between satellite data and ground-truth classifications.

On the other hand, equations derived from the literature review may involve assumptions or simplifications, potentially introducing uncertainties, as the conditions under which these equations were formulated differ from the study area. Equations from the literature may be generalized and not tailored to the specific conditions of the nASEAN region. Local factors' variability, such as vegetation types and burning practices, could impact the applicability and accuracy of these equations.

REFERENCES

AFoCo. (2022). *Forest Fire Management in the Tropics*. Asian Forest Cooperation Organization. Available at: https://afocosec.org/wp-content/uploads/2022/04/KN2022-007-Forest-Fire-Management-in-the-Tropics-220621_compressed.pdf [Accessed: 18 August 2024].

Akagi, S.K., Yokelson, R.J., Wiedinmyer, C., Alvarado, M.J., Reid, J.S., Karl, T., Crounse, J.D. and Wennberg, P.O. (2011). 'Emission factors for open and domestic biomass burning for use in atmospheric models'. *Atmospheric Chemistry and Physics*, 11(9), pp. 4039–4072. https://doi.org/10.5194/acp-11-4039-2011

Albar, I., Jaya, I.N.S., Saharjo, B.H., Kuncahyo, B. and Vadrevu, K.P. (2018). Spatio-temporal analysis of land and forest fires in Indonesia using MODIS active fire dataset. In *Land-atmospheric Research Applications in South and Southeast Asia*, pp. 105–127. Springer, Cham, Switzerland.

Ansori, S. (2021). 'The politics of forest fires in Southeast Asia'. *Contemporary Southeast Asia*, 43(1), pp. 179–202. https://doi.org/10.1355/cs43-1p

Asian Development Bank. (2001). www.adb.org/sites/default/files/institutional-document/31330/ar2001.pdf

Baccini, A., Walker, W., Carvalho, L., Farina, M. and Houghton, R.A. (2019). Response to comment on 'Tropical forests are a net carbon source based on aboveground measurements of gain and loss'. *Science*, 363(6423). https://doi.org/10.1126/science.aat1205

Bagaria, P., Thapa, A., Sharma, L.K., Joshi, B.D., Singh, H., Sharma, C.M., Sarma, J., Thakur, M. and Chandra, K. (2021). 'Distribution modelling and climate change risk assessment strategy for rare Himalayan Galliformes species using archetypal data abundant cohorts for adaptation planning'. *Climate Risk Management*, 31, p. 100264. https://doi.org/10.1016/j.crm.2020.100264

Batar, A., Watanabe, T. and Kumar, A. (2017). 'Assessment of land-use/land-cover change and forest fragmentation in the Garhwal Himalayan region of India'. *Environments*, 4(2), p. 34. https://doi.org/10.3390/environments4020034

Beerling, D.J. and Osborne, C.P. (2006). 'The origin of the savanna biome', *Global Change Biology*, 12(11), pp. 2023–2031. https://doi.org/10.1111/j.1365-2486.2006.01239.x

Biswas, S., Lasko, K.D. and Vadrevu, K.P. (2015a). 'Fire disturbance in tropical forests of Myanmar—Analysis using MODIS satellite datasets'. *IEEE Journal of Selected Topics in Applied Earth Observations and Remote Sensing*, 8(5), pp. 2273–2281.

Bond, T.C. and Scott, C.E. (2022) 'Aerosol and precursor gas emissions'. *Aerosol and Climate*, pp. 299–342. https://doi.org/10.1016/b978-0-12-819766-0.00006-7

Booth, A. (2018). 'Southeast Asian agricultural growth: 1930–2010'. In P. J. Roberts & P. A. G. van der Heide (Eds.), *Agricultural Development in the World Periphery*, pp. 235–255. Routledge, London. https://doi.org/10.1007/978-3-319-66020-2_9

Boquet, Y. (2017). '7107 Islands'. In D. J. B. Silliman (Ed.), *The Philippine Archipelago*, pp. 11–36. Springer, Heidelberg, Germany. https://doi.org/10.1007/978-3-319-51926-5_2

Brockerhoff, E.G., Barbaro, L., Castagneyrol, B., Forrester, D.I., Gardiner, B., González-Olabarria, J.R., Lyver, P.O.B., Meurisse, N., Oxbrough, A., Taki, H., Thompson, I.D., van der Plas, F. and Jactel, H. (2017). 'Forest biodiversity, ecosystem functioning and the provision of ecosystem services'. *Biodiversity and Conservation*, 26(13), pp. 3005–3035. https://doi.org/10.1007/s10531-017-1453-2

Chaisse, J. and Hsieh, P.L. (2023). 'Rethinking Asia-Pacific regionalism and new economic agreements'. *Asia Pacific Law Review*, 31(2), pp. 451–468.

Charusombat, P. (2023). 'ASEAN cooperation on transboundary haze pollution: The perspective of institutional incremental change'. *Journal of Environmental Information Science*, 2. https://doi.org/10.11492/ceispapersen.2022.2_1

Chen, J., Li, C., Ristovski, Z., Milic, A., Gu, Y., Islam, M.S., Wang, S., Hao, J., Zhang, H., He, C., Guo, H., Fu, H., Miljevic, B., Morawska, L., Thai, P., Lam, Y.F., Pereira, G., Ding, A., Huang, X. and Dumka, U.C. (2017). 'A review of biomass burning: Emissions and impacts on air quality, health and climate in China'. *Science of the Total Environment*, 579, pp. 1000–1034. https://doi.org/10.1016/j.scitotenv.2016.11.025

Cole, J. (2001). 'Biomass burning'. *NASA Earth Observatory*, 19 March. Available at: https://earthobservatory.nasa.gov/features/BiomassBurning [Accessed: 16 June 2024].

Dikitanan, R., Grosjean, G., Nowak, A. and Leyte, J. (2017). *Climate-Resilient Agriculture in the Philippines*. CSA Country Profiles for Asia Series. International Center for Tropical Agriculture (CIAT); Department of Agriculture – Adaptation and Mitigation Initiatives in Agriculture, Government of the Philippines, 24 pp.

Dreiss, L.M. and Volin, J.C. (2014). 'Forests: Temperate evergreen and deciduous'. In *Encyclopedia of Natural Resources*, Ed. Y. Wang, 1st ed., Vol. 1, pp. 214–223. CRC Press.

FAO. (1999). Cambodia Agricultural Strategies and Policy Framework for Sustainable Food Security and Poverty Alleviation. Rep. No. RAPP/01/99. Cambodian Ministry of Agriculture, Forestry and Fisheries/ FAO: Phnom Penh, Cambodia/ Rome, Italy.

Fox, J. and Castella, J.C. (2013). 'Expansion of rubber (*Hevea brasiliensis*) in mainland Southeast Asia: What are the prospects for smallholders?'. *Journal of Peasant Studies*, 40(1), pp. 155–170. https://doi.org/10.1080/03066150.2012.750605

Frederick, W.H. and Leinbach, T.R. (2018). Southeast Asia. Retrieved from www.britannica.com/place/Southeast-Asia

Friedl, M. and Sulla-Menashe, D. (2019). *MCD12Q1 v006, MODIS/Terra+Aqua Land Cover Type Yearly L3 Global 500m SIN Grid*. NASA EOSDIS Land Processes DAAC. https://doi.org/10.5067/MODIS/MCD12Q1.006 [Accessed: 16 June 2024]

George, H. and Seth, S.K. (2005). *A Revised Survey of the Forest Types of India*. Natraj Publishers, p. 404.

Giglio, L., Boschetti, L., Roy, D.P., Humber, M.L. and Justice, C.O. (2018). 'The Collection 6 MODIS burned area mapping algorithm and product'. *Remote Sensing of Environment*, 217, pp. 72–85. https://doi.org/10.1016/j.rse.2018.08.005

Giglio, L., Boschetti, L., Roy, D., Hoffmann, A. and Humber, M. (2016). *Collection 6 MODIS Burned Area Product User's Guide Version 1.0*. Available at: https://modis-land.gsfc.nasa.gov/pdf/MODIS_C6_BA_User_Guide_1.0.pdf [Accessed: 25 June 2024].

Gupta, P.K., Prasad, V.K., Sharma, C., Sarkar, A.K., Kant, Y., Badarinath, K.V.S. and Mitra, A.P. (2001). 'CH4 emissions from biomass burning of shifting cultivation areas of tropical deciduous forests–experimental results from ground-based measurements'. *Chemosphere-Global Change Science*, 3(2), pp. 133–143.

Harris, R.M.B., Remenyi, T.A., Williamson, G.J., Bindoff, N.L. and Bowman, D.M.J.S. (2016). 'Climate-vegetation-fire interactions and feedbacks: Trivial detail or major barrier to projecting the future of the Earth system?'. *Wiley Interdisciplinary Reviews: Climate Change*, 7(6), pp. 910–931. https://doi.org/10.1002/wcc.428

Hirota, M., Holmgren, M., Van Nes, E.H. and Scheffer, M. (2011). 'Global resilience of tropical forest and savanna to critical transitions'. *Science*, 334(6053), pp. 232–235. https://doi.org/10.1126/science.1210657

Ho, R.C., Zhang, M.W., Ho, C.S., Pan, F., Lu, Y. and Sharma, V.K. (2014). 'Impact of 2013 South Asian haze crisis: Study of physical and psychological symptoms and perceived dangerousness of pollution level'. *BMC Psychiatry*, 14, p. 81. https://doi.org/10.1186/1471-244X-14-81

Holtmann, A., Huth, A., Pohl, F., Rebmann, C. and Fischer, R. (2021). 'Carbon sequestration in mixed deciduous forests: The influence of tree size and species composition derived from model experiments'. *Forests*, 12(6), p. 726. https://doi.org/10.3390/f12060726

Huang, K., Fu, J.S., Hsu, N.C., Gao, Y., Dong, X., Tsay, S.-C. and Lam, Y.F. (2013). 'Impact assessment of biomass burning on air quality in Southeast and East Asia during BASE-ASIA'. *Atmospheric Environment*, 78, pp. 291–302. https://doi.org/10.1016/j.atmosenv.2012.03.048

Hungerford, R.D., Harrington, M.G., Frandsen, W.H., Ryan, K.C. and Niehoff, G.J. (1991, August). Influence of fire on factors that affect site productivity. In Proceedings of the symposium on management and productivity of western-montane forest soils (pp. 32–50). USDA Forest Service, Intermountain Research Station, Ogden, UT, USA.

Hurni, K., Schneider, A., Heinimann, A., Nong, D. and Fox, J. (2017). 'Mapping the expansion of boom crops in mainland Southeast Asia using dense time stacks of Landsat data'. *Remote Sensing*, 9(4), p. 320. https://doi.org/10.3390/rs9040320

Jacobson, M.C., Hansson, H.-C., Noone, K.J. and Charlson, R.J. (2000) 'Organic atmospheric aerosols: Review and state of the science'. *Reviews of Geophysics*, 38(2), pp. 267–294. https://doi.org/10.1029/1998rg000045

Kanniah, K.D., Kamarul Zaman, N.A.F., Kaskaoutis, D.G. and Latif, M.T. (2020) 'COVID-19's impact on the atmospheric environment in the Southeast Asia region'. *Science of the Total Environment*, 736, p. 139658. https://doi.org/10.1016/j.scitotenv.2020.139658

Keane, A.H. (2017). *Eastern Geography, a Geography of the Malay Peninsula, Indo-China, the Eastern Archipelago, the Philippines and New Guinea*. Hansebook, p. 208.

Kyaw, S.W.T., Di Stefano, J. and Volkova, L. (2016). 'Forest management influences aboveground carbon and tree species diversity in Myanmar's mixed deciduous forests'. *Forests*, 7(12), p. 217. https://doi.org/10.3390/f7100217

Le, T.H., Nguyen, T.N.T., Lasko, K., Ilavajhala, S., Vadrevu, K.P. and Justice, C. (2014). 'Vegetation fires and air pollution in Vietnam'. *Environmental Pollution*, 195, pp. 267–275.

Lee, H.-H., Iraqui, O., Gu, Y., Yim, S.H.-L., Chulakadabba, A., Tonks, A.Y.-M., Yang, Z. and Wang, C. (2018). 'Impacts of air pollutants from fire and non-fire emissions on the regional air quality in Southeast Asia'. *Atmospheric Chemistry and Physics*, 18(9), pp. 6141–6156. https://doi.org/10.5194/acp-18-6141-2018

Lehmann, C.E.R., Anderson, T.M., Sankaran, M., Higgins, S.I., Archibald, S., Hoffmann, W.A., Hanan, N.P., Williams, R.J., Fensham, R.J., Felfili, J., Hutley, L.B., Ratnam, J., San Jose, J., Montes, R., Franklin, D., Russell-Smith, J., Ryan, C.M., Durigan, G., Hiernaux, P. and Haidar, R. (2014). 'Savanna vegetation-fire-climate relationships differ among continents'. *Science*, 343(6170), pp. 548–552. https://doi.org/10.1126/science.1247355

Levy, D. (2004). *Burnt Biomass Causes Short-term Global Cooling, Long-term Warming*. Stanford University. Available at: https://news.stanford.edu/news/2004/august4/biomass-84.html [Accessed: 14 June 2024].

Li, M., Cui, Y., Fu, Y., Li, N., Tang, X., Liu, X. and Run, Y. (2020). 'Simulating the potential sequestration of three major greenhouse gases in China's natural ecosystems'. *Forests*, 11(2), p. 128. https://doi.org/10.3390/f11020128

Lim, J.A., Yaacob, J.S., Mohd, A., Eyahmalay, J.E., El, A. and Mohd (2023). 'Mitigating the repercussions of climate change on diseases affecting important crop commodities in Southeast Asia for food security and environmental sustainability—a review'. *Frontiers in Sustainable Food Systems*, 6. https://doi.org/10.3389/fsufs.2022.1030540

Lu, D. and Weng, Q. (2007). 'A survey of image classification methods and techniques for improving classification performance'. *International Journal of Remote Sensing*, 28(5), pp. 823–870. https://doi.org/10.1080/01431160600746456

Madayag, W. and Estanislao, H. (2021). *A Sector Study on Philippine Agriculture—Is It Growing or Dying?* University of the Philippines. Available at: www.researchgate.net/publication/353295428_Sector_Study_on_Philippine_Agriculture [Accessed: 12 May 2024].

Maierbrugger, A. (2015). 'Myanmar, Cambodia seek investors for rice business'. *Gulf Times*, 13 February. Available at: https://m.gulf-times.com/story/426906/Myanmar-Cambodia-seek-investors-for-rice-business [Accessed: 08 June 2024].

Mamiit, R.J., Yanagida, J. and Miura, T. (2021). 'Productivity hot spots and cold spots: Setting geographic priorities for achieving food production targets'. *Frontiers in Sustainable Food Systems*, 5. https://doi.org/10.3389/fsufs.2021.727484

Mangino, J. (1997). *Introduction to the Emission Inventory Improvement Program, Volume I*. Eastern Research Group Inc. Available at: www.epa.gov/sites/production/files/2015-08/documents/i01.pdf [Accessed: 14 July 2024].

Matsumoto, J., Olaguera, L.M.P., Nguyen-Le, D., Kubota, H. and Villafuerte, M.Q. (2020). 'Climatological seasonal changes of wind and rainfall in the Philippines'. *International Journal of Climatology*, 40(11), pp. 4843–4857. https://doi.org/10.1002/joc.6492

Mccullough, I.M., Loftin, C.S. and Sader, S.A. (2013). 'A manual for remote sensing of Maine lake clarity'. *Maine Agricultural and Forest Experiment Station Technical Bulletin* 207. Available at: www.researchgate.net/publication/304124818_TB207_A_Manual_for_Remote_Sensing _of_Maine_Lake_Clarity [Accessed: 27 April 2024].

Mermoz, S., Bouvet, A., Koleck, T., Ballère, M. and Le Toan, T. (2021). 'Continuous detection of forest loss in Vietnam, Laos, and Cambodia using Sentinel-1 data'. *Remote Sensing*, 13(23), p. 4877. https://doi.org/10.3390/rs13234877

Michel, C. (2005). 'Biomass burning emission inventory from burnt area data given by the SPOT-VEGETATION system in the frame of TRACE-P and ACE-Asia campaigns'. *Journal of Geophysical Research*, 110(D9). https://doi.org/10.1029/2004jd005461

Miettinen, J., Stibig, H.-J. and Achard, F. (2014). 'Remote sensing of forest degradation in Southeast Asia—Aiming for a regional view through 5–30 m satellite data'. *Global Ecology and Conservation*, 2. https://doi.org/10.1016/j.gecco.2014.07.007

Moore, M. (2020). 'Agriculture in Myanmar'. *Statista*. Available at: www.statista.com/topics/5805/agriculture-in-myanmar/#:~:text=Myanmar 24–36 [Accessed: 23 May 2024].

Muhammad, F. (2021). 'Environmental agreement under the non-interference principle: The case of ASEAN agreement on transboundary haze pollution'. *International Environmental Agreements: Politics, Law and Economics*, 22. https://doi.org/10.1007/s10784-021-09545-4

Mukul, S.A., Herbohn, J. and Firn, J. (2016). 'Tropical secondary forests regenerating after shifting cultivation in the Philippines uplands are important carbon sinks'. *Scientific Reports*, 6(1). Available at: https://doi.org/10.1038/srep22483 [Accessed: 27 May 2024].

Namkhan, M., Sukumal, N. and Savini, T. (2022). 'Impact of climate change on Southeast Asian natural habitats, with focus on protected areas'. *Global Ecology and Conservation*, 39, e02293. https://doi.org/10.1016/j.gecco.2022.e02293

NASA MODIS Land. (2021). *MODIS Land Team Home Page*. Available at: https://modis-land.gsfc.nasa.gov/ValStatus.php?ProductID=MCD12 [Accessed:11 March 2024].

NIS. (2009). *General Population Census of Cambodia 2008, Analysis of the Census Result Report 12-Population Projection of Cambodia. Ministry of Planning, Phnom Penh, Cambodia*. Available at: https://camnut.weebly.com/uploads/2/0/3/8/20389289/2009_census_2008.pdf [Accessed 16 April 2024].

Ohara, T., Akimoto, H., Kurokawa, J., Horii, N., Yamaji, K., Yan, X. and Hayasaka, T. (2007). 'An Asian emission inventory of anthropogenic emission sources for the period 1980–2020'. *Atmospheric Chemistry and Physics*, 7(16), pp. 4419–4444. https://doi.org/10.5194/acp-7-4419-2007

Prasad, V.K., Kant, Y., Gupta, P.K., Elvidge, C. and Badarinath, K.V.S. (2002). 'Biomass burning and related trace gas emissions from tropical dry deciduous forests of India: A study using DMSP-OLS data and ground-based measurements'. *International Journal of Remote Sensing*, 23(14), pp. 2837–2851.

Puri, G.S., Gupta, R.K. and Meher-Homji, V.M. (1989). *Forest Ecology: Plant Form, Diversity, Communities and Succession*. 2nd ed. South Asia Books.

Puyravaud, J.-P. (2003). 'Standardizing the calculation of the annual rate of deforestation'. *Forest Ecology and Management*, 177(1–3), pp. 593–596. https://doi.org/10.1016/s0378-1127(02)00335-3

Rundel, P. (1999). *Forest Habitats and Flora in Laos PDR, Cambodia and Vietnam*. Available at: www.researchgate.net/publication/259623025_Forest_Habitat_and_Flora_in_Laos_PDR_Cambodia_and_Vietnam [Accessed 17 June 2024].

Sankaran, M., Hanan, N.P. and Scholes, R.J. (2005) 'Determinants of woody cover in African savannas'. *Nature*, 438, pp. 846–849. https://doi.org/10.1038/nature04070

Seyam, M.M.H., Haque, M.R. and Rahman, M.M. (2023). 'Identifying the land use land cover (LULC) changes using remote sensing and GIS approach: A case study at Bhaluka in Mymensingh, Bangladesh'. *Case Studies in Chemical and Environmental Engineering*, 7, p. 100293. https://doi.org/10.1016/j.cscee.2022.100293

Shi, Y. and Yamaguchi, Y. (2014). 'A high-resolution and multi-year emissions inventory for biomass burning in Southeast Asia during 2001–2010'. *Atmospheric Environment*, 98, pp. 8–16. https://doi.org/10.1016/j.atmosenv.2014.08.050

Sim, M.-S., Wee, S.Y. and Park, E. (2023). 'Deforestation as the prominent driver of the intensifying wildfire in Cambodia, revealed through geospatial analysis'. *Remote Sensing*, 15(13), pp. 3388–3388. https://doi.org/10.3390/rs15133388

Smith, W. (2014). *Agriculture in the Central Mekong Delta: Opportunities for Donor Business Engagement*. Available at: www.odi.org/sites/odi.org.uk/files/ odiassets/publications-opinion-files/9060.pdf [Accessed: 14 May 2024].

Song, Y., Liu, B., Miao, W., Chang, D. and Zhang, Y. (2009). 'Spatiotemporal variation in non-agricultural open fire emissions in China from 2000 to 2007'. *Global Biogeochemical Cycles*, 23(2). https://doi.org/10.1029/2008gb003344

Staver, A.C., Archibald, S. and Levin, S.A. (2011). 'The global extent and determinants of savanna and forest as alternative biome states'. *Science*, 334(6053), pp. 230–232. https://doi.org/10.1126/science.1210465

Streets, D.G., Bond, T.C., Carmichael, G.R., Fernandes, S.D., Fu, Q., He, D., Klimont, Z., Nelson, S.M., Tsai, N.Y., Wang, M.Q. and Woo, J.H. (2003). 'An inventory of gaseous and primary aerosol emissions in Asia in the year 2000'. *Journal of Geophysical Research: Atmospheres*, 108(D21).

Sulla-Menashe, D. and Friedl, M. (2018). *User Guide to Collection 6 MODIS Land Cover (MCD12Q1 and MCD12C1) Product*. United States Geological Survey. Available at: https://lpdaac.usgs.gov/documents/101/MCD12_User_Guide_V6.pdf [Accessed: 22 March 2024].

Takeshima, H. and Joshi, P.K. (2019). *Overview of the Agricultural Modernization in Southeast Asia*. IFPRI Discussion Paper 1819. Available at: https://doi.org/10.2499/p15738coll2.133195 [Accessed 11 May 2024].

Tanentzap, A.J., Lamb, A., Walker, S. and Farmer, A. (2015). 'Resolving conflicts between agriculture and the natural environment'. *PLOS Biology*, 13(9), p. e1002242. https://doi.org/10.1371/journal.pbio.1002242

Thenkabail, P.S. (2018). *Remote Sensing Handbook* – Three Volume Set. CRC Press, p. 2304. https://doi.org/10.1201/b19355

Titapiwatanakun, B. (2012). 'The rice situation in Thailand'. *TACR*. Available at: www.adb.org/sites/default/files/project-document/73082/43430-012-reg-tacr-03.pdf [Accessed 27 April 2024].

Toh, Y.Y., Lim, S.F. and von Glasow, R. (2013). 'The influence of meteorological factors and biomass burning on surface ozone concentrations at Tanah Rata, Malaysia'. *Atmospheric Environment*, 70, pp. 435–446. https://doi.org/10.1016/j.atmosenv.2013.01.018

Top, N., Mizoue, N., Ito, S. and Kai, S. (2004). 'Spatial analysis of woodfuel supply and demand in Kampong Thom Province, Cambodia'. *Forest Ecology and Management*, 194(1–3), pp. 369–378. https://doi.org/10.1016/j.foreco.2004.02.028

Trewin, B., Cazenave, A., Howell, S., Huss, M., Isensee, K., Palmer, M.D., Tarasova, O. and Vermeulen, A. (2021). 'Headline indicators for global climate monitoring'. *Bulletin of the American Meteorological Society*, 102(1), pp. E20–E37. https://doi.org/10.1175/BAMS-D-19-0196.1

Vadrevu, K., Eaturu, A., Casadaban, E., Lasko, K., Schroeder, W., Biswas, S., Giglio, L. and Justice, C. (2022). 'Spatial variations in vegetation fires and emissions in South and Southeast Asia during COVID-19 and pre-pandemic'. *Scientific Reports*, 12(1). Available at: https://doi.org/10.1038/s41598-022-22834-5 [Accessed:11 May 2024].

Vadrevu, K.P., Ohara, T. and Justice, C. eds. (2018). *Land-atmospheric Research Applications in South and Southeast Asia*. Springer.

Wang, J., Yue, Y., Wang, Y., Ichoku, C., Ellison, L. and Zeng, J. (2018). 'Mitigating satellite-based fire sampling limitations in deriving biomass burning emission rates: Application to WRF-Chem model over the Northern sub-Saharan African region'. *Journal of Geophysical Research: Atmospheres*, 123(1), pp. 507–528. https://doi.org/10.1002/2017jd026840

Wongchai, A. and Ngamsomsuke, K. (2015). *Efficiency Measurement on Rice Production in Thailand*. Available at: www.researchgate.net/publication/280573041_Efficiency_Measurement_on_Rice_Production_in_Thailand [Accessed: 23 Jun 2024]

Workman, D. (2019). *Rice Exports by Country*. World's Top Exports. Available at: www.worldstopexports.com/rice-exports-country/ [Accessed: 26 May 2024].

World Bank (2016). *An Overview of Agricultural Pollution in the Philippines: The Crops Sector 2016*. Available at: https://documents1.worldbank.org/curated/en/975561516769366821/pdf/122928-WP-P153343-PUBLIC-Philippines-Crops.pdf [Accessed 22 April 2024].

Yadav, I. and Devi, N. (2018). Biomass burning, regional air quality, and climate change. In: *Earth Systems and Environmental Sciences*. Available at: https://doi.org/10.1016/B978-0-12-409548-9.11022-X [Accessed 07 June 2024].

Yang, Y., Watanabe, M., Li, F., Zhang, J., Zhang, W. and Zhai, J. (2005). 'Factors affecting forest growth and possible effects of climate change in the Taihang Mountains, northern China'. *Forestry: An International Journal of Forest Research*, 79(1), pp. 135–147. https://doi.org/10.1093/forestry/cpi062

Yin, L., Du, P., Zhang, M., Liu, M., Xu, T. and Song, Y. (2019a). 'Estimation of emissions from biomass burning in China (2003–2017) based on MODIS fire radiative energy data'. *Biogeosciences*, 16(7), pp. 1629–1640. https://doi.org/10.5194/bg-16-1629-2019

Yin, S., Wang, X., Zhang, X., Guo, M., Miura, M. and Xiao, Y. (2019b). 'Influence of biomass burning on local air pollution in mainland Southeast Asia from 2001 to 2016'. *Environmental Pollution*, 254, p. 112949. https://doi.org/10.1016/j.envpol.2019.07.117

Zhai, J., Xiao, C., Feng, Z. and Liu, Y. (2022). 'Spatio-temporal patterns of land-use changes and conflicts between cropland and forest in the Mekong River Basin during 1990–2020'. *Land*, 11(6), p. 927. https://doi.org/10.3390/land11060927

Zhou, Y., Xing, X., Lang, J., Chen, D., Cheng, S., Wei, L., Wei, X. and Liu, C. (2017). 'A comprehensive biomass burning emission inventory with high spatial and temporal resolution in China'. *Atmospheric Chemistry and Physics*, 17(4), pp. 2839–2864. https://doi.org/10.5194/acp-17-2839-2017

Zhuang, J. (2009). *The Economics of Climate Change in Southeast Asia: A Regional Review Plan of Talk*. Available at: www.icem.com.au/documents/climatechange/mdcc_report/6_juzhong_zhuang_en.pdf [Accessed: 21 May 2024].

16 Estimates of Emissions from Open Biomass Burning in South-Southeast Asia

Utilizing Fengyun-3D Fire Spot Monitoring Data

Yusheng Shi, Yajun Wang, and Yang Liu

16.1 INTRODUCTION

In recent years, fires caused by nature or humans have become the focus of public attention, such as bushfires in Australia (Celermajer et al., 2021) and wildfires in Canada (Metsaranta et al., 2023). Increasingly frequent fires directly cause severe air pollution, which has a huge impact on climate change, human health, etc., and has an increasing impact on developing countries, especially those in South and Southeast Asia (SSEA) (Reddington et al., 2021; Singh et al., 2021; Irfan, 2024). Extensive Open Biomass Burning (OBB) occurs year-round, leading to widespread exposure to trace gases (CO, NO_X, NMVOC, SO_2, and NH_3), particulate matter ($PM_{2.5}$) levels surpassing World Health Organization (WHO) guidelines (Linh Thao et al., 2022). These burning activities release substantial carbon emissions, negatively affecting not only global climate dynamics but also the health of local inhabitants. Forest clearing, accidental fires, firewood burning, agricultural residue burning, peatland burning, and straw burning are among the significant fire types worldwide (Xu et al., 2022). Moreover, particulate matter and organic carbon emitted from biomass burning adversely affect human health (Yin, 2020). It is an urgent mission to construct an OBB inventory to quantify the local biomass burning's contribution to regional and global carbon emissions, offering a foundation for devising emission reduction policies and strategies.

Previous studies have explored numerous methods for estimating biomass burning emissions (Shi et al., 2021; Pereira et al., 2022; Liu and Popescu, 2022). Globally, several OBB emission datasets have been developed, including the Global Fire Emissions Database (GFED), Global Fire Assimilation System (GFAS), and Fire Emissions and Energy Research (FEER). However, these methods heavily rely

 DOI: 10.1201/9781003396260-16

on fire detection precision, particularly for small fires. Additionally, the activity data used to calculate emissions carries significant uncertainties, resulting in limitations and unreliability (van Wees et al., 2022). All these methods rely on MODIS active fire products. Equipped with the MEIRSI-2 instrument, the Fengyun-3D (FY-3D) satellite offers spatial resolutions of 250 and 1000 m at the nadir (Yin et al., 2020), when compared to MODIS, which significantly enhances its capacity to detect and analyze various phenomena, including fires, aerosols, and changes in land and ocean surfaces (Zheng et al., 2021). Furthermore, the Global Fire Monitoring (GFR) product with FY-3D employs optimized automatic identification algorithms for fire spots (Chen et al., 2022), improving fire point detection accuracy. It resulted in an impressive overall accuracy rate of 79.43% and an exclusion omission error accuracy of 88.50%, surpassing the capabilities of MODIS satellite products (Xian et al., 2021; Chen et al., 2022). Therefore, employing the FY-3D GFR product and allocation approaches for small fires is expected to yield reliable estimates of OBB emissions.

In this study, we endeavor to create a high-resolution daily inventory of OBB emissions in SSEA, based on the burned area method, and to scrutinize various fire events and their emission patterns. To estimate OBB emissions from forest, savanna/shrubland, grassland, and other areas, we use the updated FY-3D GFR product. This product incorporates continuous spatiotemporal dynamics of aboveground biomass (AGB), spatiotemporally varying combustion efficiency, and specific emissions factors for different land types. Our comprehensive, high-resolution OBB emissions inventory serves as a valuable resource for applications in air quality modeling, atmospheric transport simulation, and biogeochemical cycle studies. It provides a robust framework for in-depth understanding and analysis of the environmental impact of OBB in SSEA.

16.2 STUDY AREA

South and Southeast Asia (SSEA) is a region with a complex and diverse geographical environment, consisting of many islands and peninsulas. In the past 30 years, due to the continuous growth of population and limited land resources, the fallow period of traditional slash and burn agriculture has been shortened, resulting in the destruction and degradation of large forests, endangering biodiversity and climate change (Yin et al., 2019). With the earth getting hotter, dry soil and vegetation conditions will put more areas at risk of both human and natural wildfires (Kim et al., 2015).

On average, about 20 million fires occur globally each year (Li et al., 2020a,b), with a total burning area of 350 million hectares (Giglio et al., 2013; Chuvieco et al., 2016; Fu et al., 2023). SSEA is one of the regions with the most severe fire activity in the world (Li et al., 2020), contributing nearly 30% of global fires along with Brazil and the Democratic Republic of Congo. This has a significant impact on local development (Celermajer et al., 2021), human health (Anita et al., 2024), and regional and even global air quality and climate (Yin et al., 2019). OBB emissions brought a large amount of $PM_{2.5}$, which could cause significant harm to human health (Shi et al., 2015). Exposure to $PM_{2.5}$ in 2015 resulted in 4.2 million deaths worldwide,

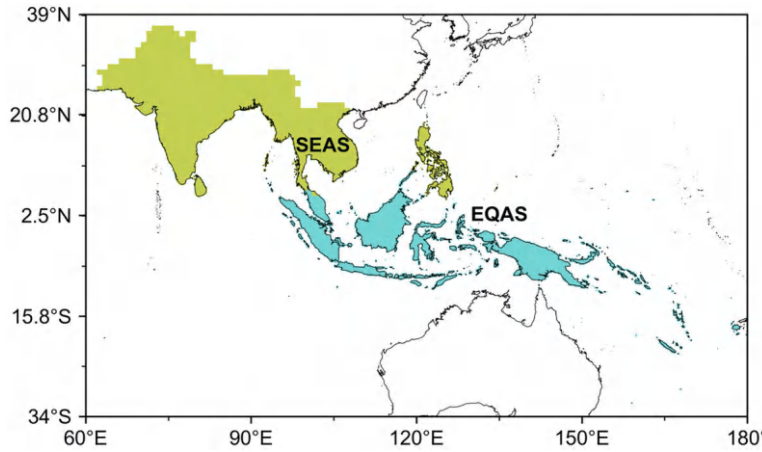

FIGURE 16.1 Geographic zone results for South-Southeast Asia and its abbreviations. SEAS: Southeast Asia; EQAS: Equatorial Asia.

with approximately 59% of deaths occurring in South Asia (1.36 million) and East Asia (1.14 million) (Cohen et al., 2017), where daily $PM_{2.5}$ emissions far exceed WHO safety standards. Moreover, the drought caused by climate change also leads to the death of a large number of vegetation, causing a rapid increase in flammable and combustible materials and further increasing the frequency and severity of fires. Nowadays, there are very few fire-resistant forests in Indonesia's peatlands, which means that fires in Indonesia may become more frequent and dangerous in the future (Adam et al., 2021). Therefore, in the context of sustained global warming and frequent forest fires, it is crucial to construct a high-resolution OBB combustion emission inventory in SSEA.

In order to facilitate the calculation and subsequent analysis in SSEA, we have divided the study area into two distinct regions: Southeast Asia (SEAS) and Equatorial Asia (EQAS) (Figure 16.1). The SEAS includes Pakistan, India, Bangladesh, Myanmar, Cambodia, Laos, Thailand, and Vietnam, and the EQAS includes Indonesia, Malaysia, the Philippines, etc.

16.3 DATA AND METHODS

16.3.1 Approach

The SSEA emissions inventory from Open Biomass Burning (OBB) (1 km daily) was estimated using the burned area method based on the framework defined by Wiedinmyer et al. (2006) and Shi et al. (2015). We utilized burned area data derived from active fire data obtained from the FY-3D satellite, available biomass data from satellite and ground measurements, CF adjusted by tree cover and NDVI, and emission factors based on land cover, then multiplied these data using the following formula to estimate the OBB emissions from SSEA.

$$Emissions = \sum_{i=1}^{n} B \times F \times CF \times EF \tag{16.1}$$

where i represents the type of land cover; B is the burned area (km^2); F signifies the available biomass fuel (kg m^{-2}); CF conveys the combustion factor, defined as the ratio of actual burned fuel to the available amount; and EF is the emission factor, indicating the amount of species per kg dry matter burned (g kg^{-1}).

16.3.1.1 FY-3D Global Fire Spot Monitoring Data Based Burned Area (*B*)

We used the FY-3D GFR product to determine the location and timing of the fire events. The Fengyun-3 series of satellites are China's second-generation polar-orbiting meteorological satellites. The FY-3D satellite is the fourth satellite in the Fengyun-3 series of satellites. It was launched on November 15, 2017, with an orbit altitude of 836 kilometers (Li et al., 2017). FY-3D completes 14 global Earth surface orbital observations twice in one day. The MERSI-2 instrument carried has been highly enhanced on the basis of the MERSI-1 carried by the FY-3C, equipping it with high-precision space-borne and lunar calibration capabilities. Compared to MODIS, MERSI-2 offers superior spatial resolution across the visible (0.4–0.7 μm) and near-infrared spectral bands (0.7–1.0 μm), thus rendering it particularly well-suited for precise meteorological and environmental applications (Abbasi et al., 2020). The GFR product integrated with the MERSI-2 instrument shows superior judgment accuracy in terms of fire detection results (Dong et al., 2022). The location and timing of the fire events used in the OBB from SSEA were defined using the FY-3D GFR product (Chen et al., 2022). It is available to get these processed fire event detection data from the Fengyun Satellite Remote Sensing Data Service Network of the China National Satellite Meteorological Center. These data cover daily fire location, time, and confidence level of fire detection at a confidence level greater than 20%, with a 1-km spatial resolution (Liu and Shi, 2023). Additionally, the same fire may be counted multiple times in a single day, resulting in a repetition of data. To tackle this issue, we conducted global identification and removed multiple detections of the same fire pixels daily. Specifically, we removed single daily fire detections within a 1 km^2 radius of another fire detection. Thus, only one fire per 1 km^2 of a hotspot can be counted per day, and it will be reset the next day (Liu and Shi, 2023).

16.3.1.2 Fuel (*F*)

In previous studies about emission inventories built upon wildfire areas, F is generally defined by different fire types in different zones (Wiedinmyer et al., 2011). There is a certain discontinuity in the data generated by this method, which may lead to large deviations at the boundaries of different regions. It is unreasonable, and it cannot reflect the spatial distribution pattern of F. Ground observation data shows obvious merit in accuracy and reliability, but they are incapable of comprehensive global coverage, restricted by the sparse distribution of observation stations. In comparison, satellite data not only reaches global coverage but also provides rich earth parameters to achieve biomass estimation. Nonetheless, its accuracy and usability are

affected by some factors, such as temporal and spatial resolution and cloud cover. Therefore, it is an effective way to combine ground observations with satellite data. This fusion approach integrates high-precision ground observation data with widely available satellite data, yielding reliable and precise global biomass products. Using this method, the limitations of relying solely on a single data source can be overcome, thus enhancing the accuracy and reliability of biomass estimation.

In this study, we used multi-source satellite data, including the Normalized Vegetation Index (NDVI), Tree Cover (TC), and Aboveground Biomass (AGB), to assess terrestrial biomass. The NDVI data were obtained using the MODIS Combined 16-Day NDVI fusion product available on the Google Earth Engine (GEE) platform. TC data were derived from the MOD44B product generated based on MODIS onboard the Terra satellite, which provides a continuous global vegetation field at 250 m resolution for each year from 2000 to the present. The AGB data during 2020–2022 is based on Global Aboveground and Belowground Biomass Carbon Density Maps for the Year 2010 (Spawn and Sullivan, 2020). They are remotely sensed maps of woody, grassland, cropland, and tundra biomass at a 300 m spatial resolution, and annual TC and NDVI data to calculate F as,

$$F = \left(\frac{NDVI_{\text{now}}}{NDVI_{2010}} + \frac{TC_{\text{now}}}{TC_{2010}} \right) * AGB \tag{16.2}$$

where $NDVI_{\text{now}}$ is the mean value of the month before a single fire event, $NDVI_{2010}$ is the average value of *NDVI* in 2020, TC_{now} is the tree coverage in the year of the fire, TC_{2010} is the tree coverage in 2010, and *AGB* is the Above Ground Biomass data in 2010.

16.3.1.3 Combustion Factor (CF)

The CF is primarily defined as the percentage of fuel consumed in a single fire event, which is always affected by fuel type and local humidity conditions. CF is often treated as a constant, which may inevitably cause biases in emission estimations and bring some uncertainties. Some studies have used TC to measure CF and elucidate its spatial and temporal changes (Bray et al., 2018; Lasslop et al., 2020), but these research studies mainly focus on areas covered by herbaceous vegetation, where TC is usually in the range of 40% to 60%. They also assumed that the CF is in line with other land types, consistently, such as farmland, forest, and grassland.

A major influence on fire discharge in the framework is the condition of the subsurface at the location of the fire event. Different types of subsurface have different biological qualities and correlates. In GEIOBB, we used IGBP categorized data from MODIS LCT (Friedl and Sulla-Menashe, 2022). To match LCT types with subsequent assignments on biomass and related factors better, we reclassified the original 17 classifications into seven categories (Table 16.1), including grassland and savanna (V1), woody savanna or shrub (V2), tropical forest (V3), temperate forest (V4), boreal forest (V5), temperate evergreen forest (V6), and crop (V7). Therefore, when estimating OBB in SSEA, the CF for all fires in each grid cell was determined as a function of TC,

TABLE 16.1
Reclassification method

IGBP LCT Description	LCT Value	Method and Value
Evergreen Needleleaf Forest	1	If latitude>50, then V5; else V6
Evergreen Broadleaf Forest	2	If latitude>-23.5 and <23.5, then V3; else V4
Deciduous Needleleaf Forest	3	If latitude >50, then V5; else V4
Deciduous Broadleaf Forest	4	V4
Mixed Forest	5	If latitude >50, then V5; if latitude>-23.5 and <23.5, then V3; else V4
Closed Shrubland	6	V2
Open Shrubland	7	V2
Woody Savanna	8	V2
Savanna	9	V1
Grassland	10	V1
Permanent Wetland	11	V1
Cropland	12	V7
Urban and Built-up Land	13	If tree cover < 40, then V1; if tree cover >40 and <60, then V2; if tree cover >60 then assign to Mixed Forests.
Cropland/Natural Vegetation Mosaic	14	V1
Permanent Snow and Ice	15	-
Barren	16	V1
Water Bodies	17	-

Where V1 is grassland and savanna, V2 is woody savanna or shrub, V3 is tropical forest, V4 is temperate forest, V5 is boreal forest, V6 is temperate evergreen forest, and V7 is crop.

fire types, and NDVI (Ito and Penner, 2004). Then, the CF calculations are divided into four categories based on the reclassification results. Briefly, we combined the reclassification outcomes of V3, V4, V5, and V6 into a forest type category, designated V1 as grasslands type, V2 as woodlands type, and V7 as crop.

For woodland, the CF was highly correlated with *TC*

$$CF_{\text{woodland}} = EXP(-0.013 \times TC) \tag{16.3}$$

For grassland, the change of NDVI is often associated with fire occurrence, especially during dry seasons or in areas prone to wildfires. In general, a decrease in vegetation NDVI may indicate deteriorating vegetation health, which increases fire risk because dry or dead vegetation is more likely to burn. Therefore, we introduced the vegetation condition index (*VCI*), a factor that measures vegetation drought conditions, to

ascertain the fuel moisture conditions. We utilized the *VCI* as a metric to determine fuel moisture levels as a means to evaluate the contemporaneous state of vegetation (Shi et al., 2019). The *VCI* was calculated using the *NDVI* with a 16-day time interval at a spatial resolution of 1 km from 2020 to 2022.

$$VCI = \frac{NDVI_{now} - NDVI_{min}}{NDVI_{max} - NDVI_{min}} \tag{16.4}$$

$$CF_{grassland} = \frac{1}{100} \times \left(-213 \times VCI + 138\right) \tag{16.5}$$

where $NDVI_{now}$ is the average value of the month before a single fire event, $NDVI_{max}$ is the maximum value of *NDVI* in the same period in the previous 3 years of the fire events, and $NDVI_{min}$ is the minimum value of *NDVI* in the same period in the previous 3 years of the fire events.

For forest, we employed moisture category factors (*MCF*) to gauge forest moisture level, and based on the *MCF* values (very dry: 0.33, dry: 0.5, moderate: 1, moist: 2, wet: 4, very wet: 5) provided by Anderson et al. (2004). Then, we used *VCI* as a standard for judging humidity and dryness and found that it approximately conforms to the power function distribution characteristics in *VCI*. Subsequently, function fitting was performed ($R^2 = 0.94$), allowing us to further determine the CF based on MCF as,

$$MCF = 0.1759 \times e^{3.5181 \times VCI} \tag{16.6}$$

$$CF_{forest} = \left(1 - e^{-1}\right)^{MCF} \tag{16.7}$$

For crops, we set the CF to 0.98, the upper limit proposed by Wiedinmyer et al. (2006), because most fires on croplands are artificially active fires, resulting in a combustion process tailored for non-woody fuels.

16.3.1.4 Emission Factor (EF)

EF is used to convert dry matter burned into emissions of trace gases and aerosols, representing the number of pollutants discharged per unit of fuel burned. In this study, EF values were assigned based on the seven reclassified categories (Akagi et al., 2011), including grassland and savanna, woody savanna or shrub, tropical forest, temperate forest, boreal forest, temperate evergreen forest, and crop. We employed the reclassification of the LCT product to assign each fire pixel land type and its EF. Due to significant variations among measured values, we computed the average emission factor within each reclassification type for areas with multiple measurements. Subsequently, we updated the EF values of Carbon Content (C) for the seven land types. The EF values of C of grassland and savanna, woody savanna or shrub, tropical forest, temperate forest, boreal forest, temperate evergreen forest, and crop are 488.31

(g/kg), 489.41 (g/kg), 491.77 (g/kg), 468.31 (g/kg), 478.88 (g/kg), 493.18(g/kg), and 437.18 (g/kg), respectively.

16.3.2 Validation Data

In our study, we used the following widely used OBB emission datasets to validate our experimental results.

GFED4.1s combines satellite information on fire activity and vegetation productivity to estimate gridded monthly burned area and fire emissions. It provides monthly burned area, monthly emissions, and fractional contributions of different fire types at a global scale, as well as scalars that can be used to calculate emissions at higher temporal resolutions. The current version is 4, with a spatial resolution of 0.25 degrees, and has been available since 1997.

GFAS1.2, provided by Copernicus, assimilates fire radiative power (FRP) observations from the NASA Terra MODIS and Aqua MODIS to produce daily estimates of emissions from wildfires and biomass burning. On the grid of longitude and latitude, it has a resolution of 0.1°, with data available from 2003 to the present.

FEER1.0 is a site dedicated to the research of fire energetics and emissions. It provides the MODIS Fire Radiative Power Product and FEER Emission Coefficients and Inventory, with the main motivation of better understanding the strengths and effects of fires on the environment and climate. It has been available every day since 2003 and has a spatial resolution of 0.1°.

16.4 RESULTS AND DISCUSSION

16.4.1 Spatial Map of OBB Emission Estimates

The spatial distribution of annual OBB emissions from 2020 to 2022 and average OBB emissions in SSEA were presented (Figure 16.2). On the whole, OBB emissions exhibited distinct spatial patterns and strong changes throughout the study area. The annual and average OBB emissions from Indochina, including Myanmar, Thailand, Laos, Cambodia, and Vietnam, were higher than other regions from 2020 to 2022. Specifically, the OBB emission level in the entire Laos was the highest, greater than 400 (g C/m^2/year), and some areas even reached 1,000 (g C/m^2/year). The western parts of Myanmar and Thailand and the northern part of Cambodia followed closely, with OBB emission values greater than 200 (g C/m^2/year). Additionally, other areas with high OBB emissions were mainly in central Indonesia, western Malaysia, eastern Papua New Guinea, northern Philippines, eastern and northwest India, and Nepal.

The average OBB emission in SSEA from 2020 to 2022 was 210.49 Tg. Additionally, the annual OBB emissions from 2020 to 2022 were 234.27, 267.54, and 129.68 Tg, respectively. From a geographical perspective, the OBB emissions in SEAS totaled 217.46 (2020), 255.15 (2021), and 119.27 (2022) Tg, each accounting for more than 90% of the total emissions. And there was a clear increasing tendency in SEAS from its west to east. The emissions in EQAS only accounted for less than

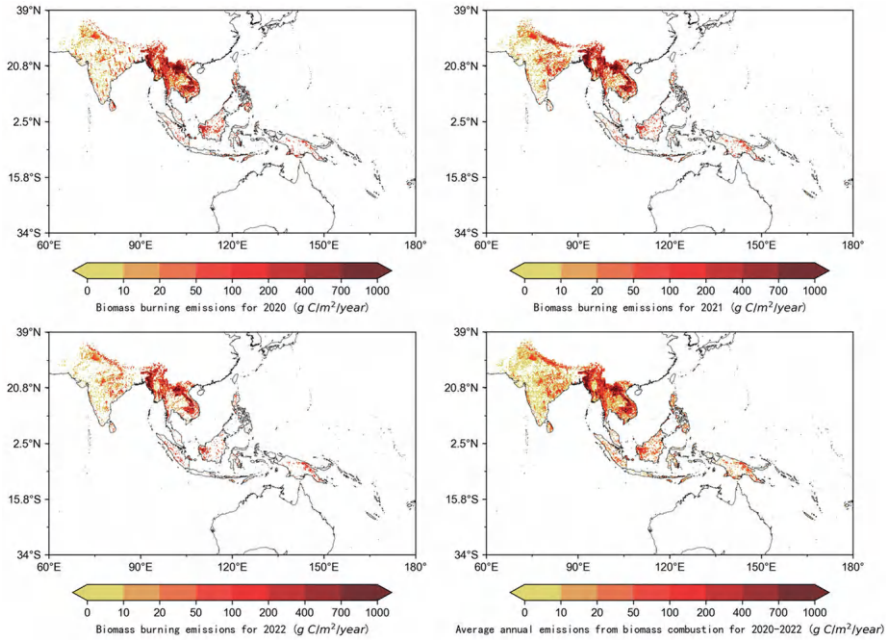

FIGURE 16.2 Spatial distributions of annual and average OBB emissions in SSEA from 2020 to 2022.

10% of the total emissions, and the high-concentration areas were relatively evenly distributed in all directions.

The distribution of average OBB carbon emissions caused by different fire types from 2020 to 2022 in SSEA was displayed (Figure 16.3). It was obvious that OBB carbon emissions resulting from crops were mainly in India and southern Thailand; while emissions caused by forests were mainly in Myanmar, Laos, the Philippines, central Indonesia, and Papua New Guinea. The emissions from grassland were mainly in Cambodia and the Indian Peninsula, while the emissions caused by wood were mainly in Nepal, Myanmar, northern Thailand, and Indonesia. The variation could be associated with the ecological and climatic conditions unique to each region (Santana et al., 2016; Sahu et al., 2021).

Then, we quantified the SSEA total OBB carbon emissions from different regions and fire types from 2020 to 2022 (Table 16.2). SEAS was found to be the primary source of annual average SSEA OBB carbon emissions from 2020 to 2022 (589.05 Tg, 93.71%). Additionally, the contributions of each fire type to the SSEA OBB carbon emissions were also quantified. In SEAS, woody savanna/shrub was the largest contributor (296.16 Tg, 50.28%), followed by forest (205.16 Tg, 34.83%). This result was consistent with EQAS, for carbon emissions from woody savanna/shrub reached 21.23 Tg (53.77%) and that from forest leveled 13.72 Tg (34.76%). Therefore, it was obvious that OBB emissions from woody savannas/shrubs and forests are the main source of SSEA.

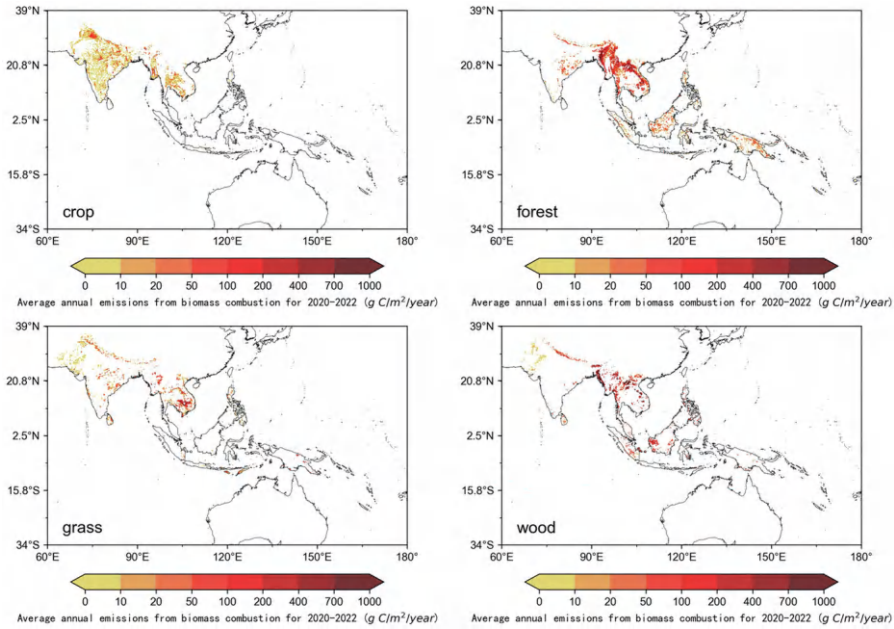

FIGURE 16.3 The distribution of mean OBB carbon emissions by fire type from 2020 to 2022 in SSEA.

TABLE 16.2
Total carbon emissions from SSEA OBB in different regions during 2020–2022 (Unit: Tg)

Different Region	Woody Savanna/Shrub	Forest	Savanna grassland	Crop	Total
SEAS	296.16	205.16	60.77	26.96	589.05
EQAS	21.23	13.72	4.32	0.21	39.48
SSEA	317.38	218.88	65.09	27.17	628.53

16.4.2 Temporal Variations in OBB Carbon Emissions

Figure 16.4 illustrates the monthly carbon emissions at regional levels. Overall, OBB carbon emissions in SSEA experienced notable shifts, with considerable monthly variations from 2020 to 2022. Peak emissions were observed in March 2021 (131.79 Tg).

OBB carbon emissions in SSEA were 234.27 Tg in 2020, rising slightly to 267.54 Tg in 2021, but showing a significant decline to 129.68 Tg in 2022. Monthly emissions for the two regions showed significant differences. EQAS's OBB monthly carbon emissions exhibited two annual peaks, occurring in March and August, respectively, and the first peak was lower than the second one, primarily due to the

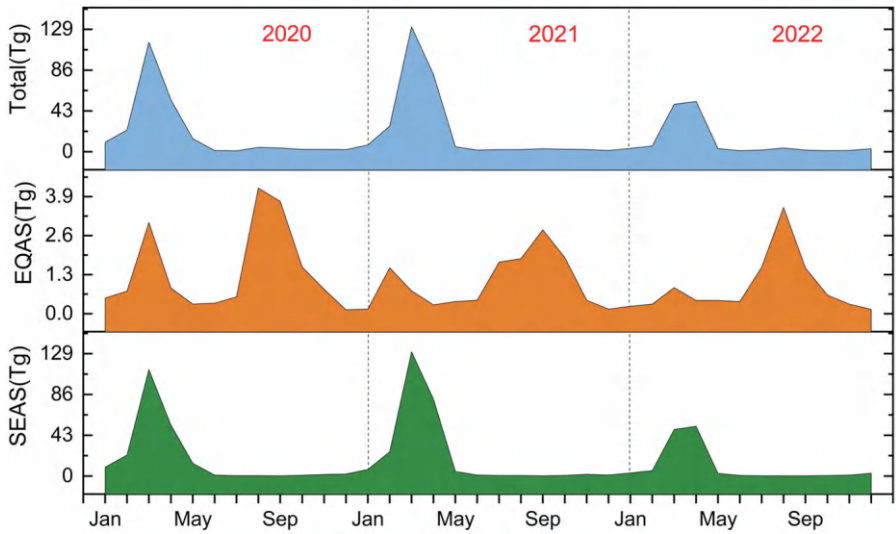

FIGURE 16.4 SSEA OBB carbon emissions in different regions during 2020–2022.

El Niño-Southern Oscillation and associated droughts (Kim et al., 2015; Hu et al., 2021). The maximum emissions demonstrated a pattern of initially decreasing and then increasing, dropping from 4.18 Tg in 2020 to 2.80 Tg in 2021, before rising to 3.53 Tg in 2022. While in SEAS, monthly carbon emissions displayed noticeable cyclicality during these 3 years, with the peak consistently appearing in March, primarily due to changes in forestry practices (Shi et al., 2014). Throughout the entire study duration, the peak values exhibited an initial rise followed by a decline, escalating from 112.45 Tg in 2020 to 131.03 Tg in 2021, then rapidly dropping to 52.50 Tg in 2022. In the broader study area, OBB carbon emissions predominantly originated from the SEAS region, with EQAS contributing only a minor fraction (<10%). Consequently, the monthly carbon emission curve for the entire study area closely mirrored that of the SEAS region, with peak emissions reaching 131.79 Tg in March 2021 and the minimum value occurring in July 2020 (0.91 Tg).

The differences in spatiotemporal fluctuations of OBB emissions not only reflected the diversity of ecosystems and climate conditions in different geographical locations (Fagre et al., 2003), but also reflected the impact of human activities and natural fire regimes to some extent (Jones et al., 2022). For example, Southeast Asia had vast tropical forests, which often resulted in high levels of OBB emissions due to the prevalence of natural and anthropogenic fire activities (Wiggins et al., 2020; Williams et al., 2019). As per the Global Natural Disaster Assessment Report, 2021 witnessed record-high temperatures, increasing the chance of droughts. Specific meteorological conditions such as high temperatures and low humidity foster heightened biomass flammability, leading to a peak in carbon emissions (Russell-Smith et al., 2021). But in 2022, natural disaster levels were generally low, with a reduced frequency of extreme temperature events, consequently resulting in a sharp decrease in carbon emissions. The reduction in carbon emissions from SEAS OBB may be related to the

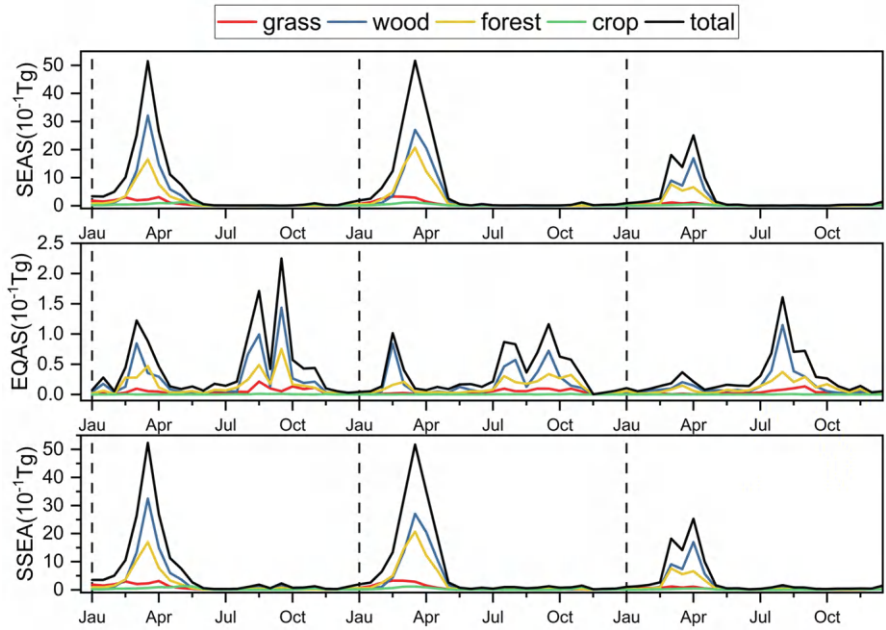

FIGURE 16.5 OBB emissions for different fire types in different regions (averaged over a 15-day window) from 2020 to 2022.

assistance provided by the Food and Agriculture Organization (FAO) in implementing comprehensive forest fire management methods in some countries, such as Cambodia and Myanmar.

More importantly, we quantified the carbon emissions caused by different fire types daily in SSEA from 2020 to 2022 (Figure 16.5). This analysis revealed the main sources of carbon emissions from SSEA fires on a daily scale and obtained the main fire types burning in different regions. Emission patterns in different areas of the region varied both temporally and spatially. SEAS was the main emission area in the study area, and its emission pattern was closely related to the SSEA emission trend, especially the emission peak in March. Over the three years, OBB conditions in the SEAS had been relatively stable, with a daily peak of 5.17 Tg. But August to October was dominated by EQAS burning activities, which may be due to the combination of dry weather, strong winds, and specific meteorological conditions (Li et al., 2023). Together, these factors increased the flammability of biomass, making combustion more likely.

In general, distinct regional disparities existed in the monthly distribution of active fires in EQAS and SEAS. Influenced by El Niño, active fires in the Indian Peninsula and Indochina concentrated during the dry season from February to April, while those in the Malay Archipelago peaked from August to October (Li et al., 2020). During the El Niño cycle, particularly from August to October, the likelihood of triggering active fires in tropical Asia increased significantly, resulting in Southeast Asia experiencing

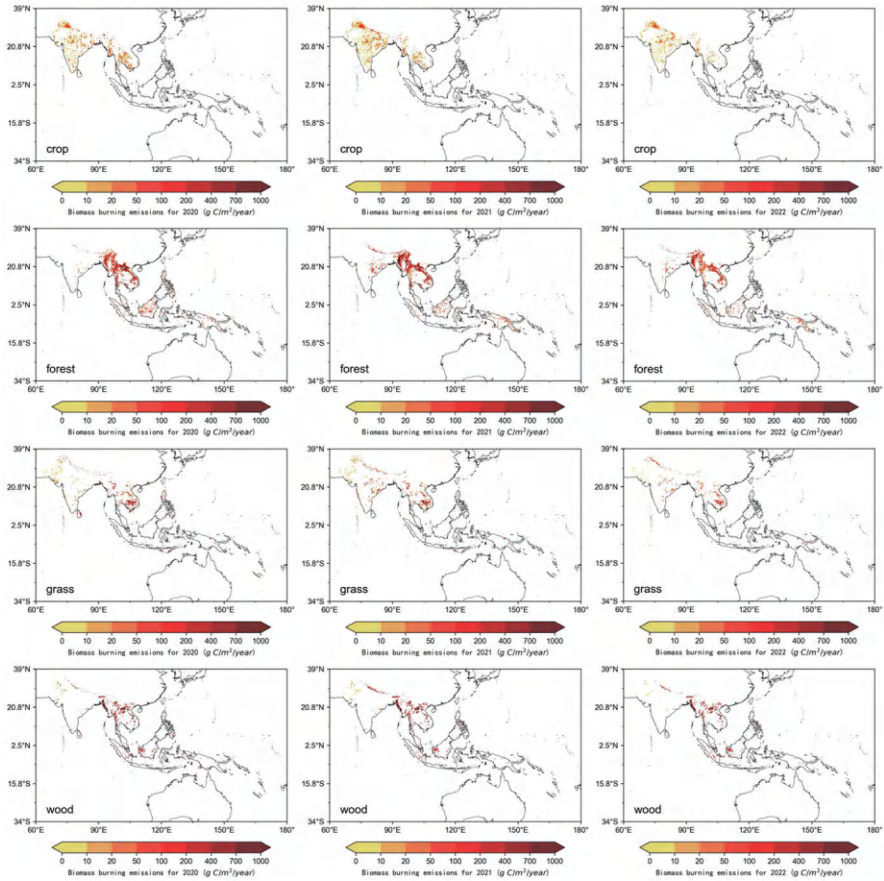

FIGURE 16.6 The distribution of OBB carbon emissions by fire type from 2020 to 2022.

its peak fires (Wang and Ma, 2024). This variability is reflected in our daily and monthly carbon emissions.

Figure 16.6 shows the distribution of OBB carbon emissions by fire type from 2020 to 2022. Emissions in the SEAS region could be divided into two parts: one was the emissions from crops in the Indian Peninsula, and the other was the emissions from forests and wood in the Indochina Peninsula. The Indian peninsula was one of the major food-producing areas in the world, and agriculture in countries such as India, Bangladesh, and Pakistan was mainly based on food planting. Most of the agriculture here relied on traditional farming and planting methods and lacked modern agricultural technology and equipment. To quickly clear fields for planting the next crop, local people more often choose field burning methods to save time and costs, thus causing a large amount of carbon emissions (Dutta et al., 2022). Peatlands are unique and rare ecosystems that store one-third of the world's soil carbon despite covering only 3–4% of the Earth's land surface. Indonesia had the largest share of tropical peatland area (47%) (Page et al., 2011), and previous

studies have demonstrated that Indonesia's carbon emissions were dominated by peatland degradation (Miettinen et al., 2017; Lu et al., 2022). From a spatial perspective, the high emission areas of OBB carbon were consistent with the distribution of peatlands; high emissions here were related to the destruction of peatlands. Therefore, emissions from forest and wood accounted for a large proportion of SSEA. However, in EQAS, forest constituted the vast majority, followed by woody savanna/shrub. There was the third-largest tropical rainforest in the world, with high forest coverage and rich biodiversity. Studies indicated that forest fires and human activities, such as deforestation and land use changes, were the main drivers of increased carbon emissions from OBB in this place (Chandra and Bhardwaj, 2015; Sannigrahi et al., 2020). In conclusion, when considering the different regions, the primary sources of pollutants from OBB varied. Fire events in woody savannas/shrubs and forests were the primary sources in SEAS and EQAS, whereas crop-related fire events mainly occurred in SEAS.

16.4.3 Cross-Verification in Different Databases

In order to compare our results with published data such as GFED, GFAS, and FEER, and considering the different resolutions of the datasets, we resampled them all to 0.5°×0.5°. Figure 16.7 shows the comparison of our results with these datasets of OBB carbon emissions in SSEA from 2020–2022. Spatially, our results were highly consistent with the distribution of these datasets. In SEAS, OBB high emission areas

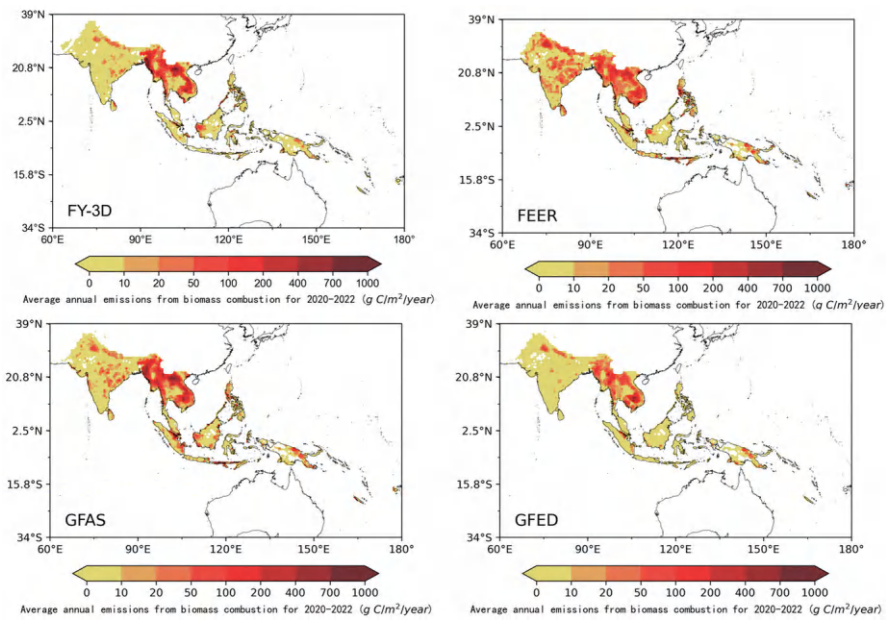

FIGURE 16.7 Comparison between this study and other emission inventories during 2020–2022 average emissions at 0.5° resolution.

TABLE 16.3
OBB emissions in the SSEA region from 2020 to 2022 based on the results obtained from FY-3 and used datasets (Unit: Tg)

	FY-3		GFED		GFAS		FEER	
	SEAS	EQAS	SEAS	EQAS	SEAS	EQAS	SEAS	EQAS
2020	217.46	16.81	115.83	13.51	96.14	24.59	208.80	56.43
2021	255.15	12.39	107.98	11.86	99.98	28.53	233.73	53.21
2022	119.27	10.41	56.32	9.84	52.49	21.94	143.00	54.00
Total	591.88	39.61	280.14	35.22	248.61	75.06	585.53	163.54

were in Myanmar, Thailand, and Vietnam (>100 g C/m^2/year); in EQAS, high emission areas were in central Indonesia and eastern Papua New Guinea. Then in terms of numerical values, it could be seen from Table 16.3 that the numerical values obtained by our method were consistent with the existing datasets to a certain extent. In SEAS, our result (591.88 Tg) was highly consistent with the value of FEER (585.53 Tg), but much greater than GFED's 280.14 Tg and GFAS's 248.61 Tg. In EQAS, GFED's 35.22 Tg was more consistent with our 39.61 Tg. The GFAS (75.06 Tg) was nearly twice ours, and the FEER (163.54 Tg) was three times more than ours. Our research results showed that the correlation coefficient with FEER in SSEA is 0.99 ($p < 0.01$). There was a strong positive correlation and consistency in the data trends between our data and the three inventories in SEAS.

Previous studies have investigated numerous methods for estimating biomass burning emissions (Ito and Penner, 2004; Wiedinmyer et al., 2006). The burned area method demonstrated good accuracy in quantifying larger fire events. For instance, Shi et al. (2021) estimated OBB emissions in tropical continents from 2001 to 2017 using widely used inventory data, such as the GFED (Jiang et al., 2012; van Wees et al., 2022). However, this method heavily relied on fire detection precision, particularly for small fires. The methods based on the fire radiative power could effectively enhance the assessment of small fire events, thereby addressing this issue to some extent. Similar approaches have been employed in FEER and GFAS (Di Giuseppe et al., 2017). However, this approach had a drawback in that it tends to overestimate emissions during localized fire events. From this point of view, our results are relatively reasonable. On the one hand, we can better identify small fires in SEAS, and on the other hand, we avoid overestimates of EQAS emissions (Pan et al., 2020).

Our findings aligned closely with existing emission inventories such as GFAS, GFED, and FEER, albeit with some disparities attributable to methodological variations and resolution disparities. But our result, boasting a high spatial resolution of 1 km × 1 km, offered a finer-grained analysis compared to the coarser resolutions (0.1° × 0.1°, 0.25° × 0.25°, and 0.1° × 0.1°) employed by others.

Furthermore, all these used datasets relied on MODIS active fire products. Our reliance on FY-3D GFR data enhanced accuracy and enabled the detection of smaller fires, offering a distinct advantage over MODIS satellite data used by GFED.

Discrepancies arose from differences in satellite data and parameter definitions adopted during inventory compilation. Notably, we augmented our estimates with locally measured emission factors and refined correlation coefficients, enhancing the reliability and precision of our emissions assessments. This meticulous approach significantly bolstered the accuracy of local emission estimates, setting our inventory apart in terms of reliability and robustness (Spawn et al., 2020).

Furthermore, emission estimates during GFAS, GFED, and FEER were generated using data from the Terra and Aqua satellites, which captured data at 10:30 and 13:30 LT, respectively. Therefore, GFED's burned area algorithm is not effective in detecting small, short-lived agricultural fires that occur briefly between satellite passes due to their intermittency (Giglio et al., 2010). However, using FY-3D, which captures data at 14:00, is very effective in capturing such events.

16.5 CONCLUSION

We have developed a daily high-resolution (1 km × 1 km grid) emission inventory focusing on OBB in SSEA. Our inventory used the updated satellite-based burned area product (FY-3D GFR), observational and satellite-based AGB, and vegetation index-based spatiotemporally variable combustion efficiency data to estimate OBB carbon emissions in SSEA.

We segmented the study area into two regions: SEAS and EQAS, and found that SEAS contributed significantly more to OBB emissions than EQAS. The peak emissions occurred in March across all years, with 2020 registering the highest at 115.50 Tg. Notable high-emission zones were northern India, Myanmar, Thailand, Laos, central Indonesia, and eastern Papua New Guinea. We further differentiated emissions by fire types, with woody savanna/shrub fires contributing the most (50.5%), followed closely by forest fires (34.82%). And seasonal trends in emissions were evident, with SEAS exhibiting a single peak in March, while EQAS displayed two peaks in March and August. Carbon emissions fluctuated over time due to local policies and climate conditions, underscoring the impact of both human intervention and natural factors. By comparing with other emission inventories, we found that our approach has the stronger detection capability, particularly in identifying smaller fires undetectable by MODIS satellite data.

Our comprehensive emission inventory and spatiotemporal analysis provide crucial insights for carbon emission policies, climate assessments, and environmental health considerations. Effective management of tropical forests and savanna/shrub fires holds promise for substantial OBB emission reduction. Additionally, our data support regional biogeochemical modeling and atmospheric chemistry studies, showcasing the potential of integrating bottom-up and top-down approaches for future research enhancements.

ACKNOWLEDGEMENTS

This research was supported by National Key R&D Program of China (2023YFB3907404), and National Natural Science Foundation of China (42071398).

REFERENCES

Abbasi, B., Qin, Z., Du, W., Fan, J., Zhao, C., Hang, Q., Zhao, S. and Li, S., 2020. An algorithm to retrieve total precipitable water vapor in the atmosphere from FengYun 3D Medium Resolution Spectral Imager 2 (FY-3D MERSI-2) data. *Remote Sensing*, *12*(21), p. 3469.

Adam, M.G., Tran, P.T.M., Bolan, N. and Balasubramanian, R., 2021. Biomass burning-derived airborne particulate matter in Southeast Asia: A critical review. *Journal of Hazardous Materials*, *407*, p. 124760.

Akagi, S.K., Yokelson, R.J., Wiedinmyer, C., Alvarado, M.J., Reid, J.S., Karl, T., Crounse, J.D. and Wennberg, P.O., 2011. Emission factors for open and domestic biomass burning for use in atmospheric models. *Atmospheric Chemistry and Physics*, *11*(9), pp. 4039–4072.

Anderson, G. K.,Sandberg, D. V. and Norheim, R.A., 2004. *Fire Emission Production Simulator (FEPS) User's Guide*. USDA Forest Service.

Anita, W.M., Uttajug, A., Seposo, X.T., Sudo, K., Nakata, M., Takemura, T., Takano, H., Fujiwara, T. and Ueda, K., 2024. Interplay of climate change and air pollution—Projection of the under-5 mortality attributable to ambient particulate matter ($PM_{2.5}$) in South Asia. *Environmental Research*, *248*, p. 118292.

Bray, C.D., Battye, W., Aneja, V.P., Tong, D.Q., Lee, P. and Tang, Y., 2018. Ammonia emissions from biomass burning in the continental United States. *Atmospheric Environment*, *187*, pp. 50–61.

Celermajer, D., Lyster, R., Wardle, G.M., Walmsley, R. and Couzens, E., 2021. The Australian bushfire disaster: How to avoid repeating this catastrophe for biodiversity. *WIREs Climate Change*, *13*(6), p. 101418.

Chandra, K.K. and Bhardwaj, A.K., 2015. Incidence of forest fire in India and its effect on terrestrial ecosystem dynamics, nutrient and microbial status of soil. *International Journal of Agriculture and Forestry*, *5*(2), pp. 69–78.

Chen, J., Yao, Q., Chen, Z., Li, M., Hao, Z., Liu, C., Zheng, W., Xu, M., Chen, X., Yang, J., Lv, Q. and Gao, B., 2022. The Fengyun-3D (FY-3D) global active fire product: Principle, methodology and validation. *Earth System Science Data*, *14*(8), pp. 3489–3508.

Chuvieco, E., Yue, C., Heil, A., Mouillot, F., AlonsoCanas, I., Padilla, M., Pereira, J.M., Oom, D. and Tansey, K., 2016. A new global burned area product for climate assessment of fire impacts. *Global Ecology and Biogeography*, *25*(5), pp. 619–629.

Cohen, A.J., Brauer, M., Burnett, R., Anderson, H.R., Frostad, J., Estep, K., Balakrishnan, K., Brunekreef, B., Dandona, L., Dandona, R., Feigin, V., Freedman, G., Hubbell, B., Jobling, A., Kan, H., Knibbs, L., Liu, Y., Martin, R., Morawska, L., Pope, C.A., Shin, H., Straif, K., Shaddick, G., Thomas, M., Van Dingenen, R., Van Donkelaar, A., Vos, T., Murray,

Di Giuseppe, F., Rémy, S., Pappenberger, F. and Wetterhall, F., 2017. Using the Fire Weather Index(FWI) to improve the estimation of fire emissions from fire radiative power (FRP) observations. *Atmospheric Chemistry and Physics*, *18*, pp. 5359–5370.

Dong, Z., Yu, J., An, S., Zhang, J., Li, J. and Xu, D., 2022. Forest fire detection of FY-3D using genetic algorithm and brightness temperature change. *Forests*, *13*(6), p. 963.

Dutta, A., Patra, A., Hazra, K.K., Nath, C.P., Kumar, N. and Rakshit, A., 2022. A state of the art review in crop residue burning in India: Previous knowledge, present circumstances and future strategies. *Environmental Challenges*, *8*, p. 100581.

Fagre, D.B., Peterson, D.L. and Hessl, A.E., 2003. Taking the pulse of mountains: Ecosystem responses to climatic variability. *Climatic Change*, *59*(1/2), pp. 263–282.

Friedl, M. and Sulla-Menashe, D., 2022. *MODIS/Terra+Aqua Land Cover Type Yearly L3 Global 500m SN Grid Vo61*. Available at: https://doi.org/10.5067/MODIS/MCD12Q1.061

Fu, Y., Hu, J., Song, W., Cheng, Y. and Li, R., 2023. Satellite observed response of fire dynamics to vegetation water content and weather conditions in Southeast Asia. *ISPRS Journal of Photogrammetry and Remote Sensing*, *202*, pp. 230–245.

Giglio, L., Randerson, J.T. and Van Der Werf, G.R., 2013. Analysis of daily, monthly, and annual burned area using the fourth-generation global fire emissions database (GFED4). *Journal of Geophysical Research: Biogeosciences*, *118*(1), pp. 317–328.

Giglio, L., Randerson, J.T., Van Der Werf, G.R., Kasibhatla, P.S., Collatz, G.J., Morton, D.C. and DeFries, R.S., 2010. Assessing variability and long-term trends in burned area by merging multiple satellite fire products. *Biogeosciences*, *7*(3), pp. 1171–1186.

Hu, Y., Zhao, F., Chen, F. and Shu, L., 2021. Impacts of global warming and large-scale climate fluctuation on forest fires and forest carbon emissions. *Terrestrial Ecosystem and Conservation*, *1*(1), pp. 75–81.

Irfan, H., 2024. Air pollution and cardiovascular health in South Asia: A comprehensive review. *Current Problems in Cardiology*, *49*(2), p. 102199.

Ito, A. and Penner, J.E., 2004. Global estimates of biomass burning emissions based on satellite imagery for the year 2000. *Journal of Geophysical Research: Atmospheres*, *109*(D14).

Jiang, X., Wiedinmyer, C. and Carlton, A.G., 2012. Aerosols from fires: An examination of the effects on ozone photochemistry in the Western United States. *Environmental Science & Technology*, *46*(21), pp. 11878–11886.

Jones, M.W., Abatzoglou, J.T., Veraverbeke, S., Andela, N., Lasslop, G., Forkel, M., Smith, A.J.P., Burton, C., Betts, R.A., Van Der Werf, G.R., Sitch, S., Canadell, J.G., Santín, C., Kolden, C., Doerr, S.H. and Le Quéré, C., 2022. Global and regional trends and drivers of fire under climate change. *Reviews of Geophysics*, *60*(3), pe2020RG000726.

Kim, P.S., Jacob, D.J., Mickley, L.J., Koplitz, S.N., Marlier, M.E., DeFries, R.S., Myers, S.S., Chew, B.N. and Mao, Y.H., 2015. Sensitivity of population smoke exposure to fire locations in Equatorial Asia. *Atmospheric Environment*, *102*, pp. 11–17.

Lasslop, G., Hantson, S., Harrison, S.P., Bachelet, D., Burton, C., Forkel, M., Forrest, M.,

Li, F., Melton, J.R., Yue, C., Archibald, S., Scheiter, S., Arneth, A., Hickler, T. and Sitch, S., 2020a. Global ecosystems and fire: Multi-model assessment of fire-induced tree-cover and carbon storage reduction. *Global Change Biology*, *26*(9), pp. 5027–5041.

Li, F., Zhu, Q., Riley, W.J., Zhao, L., Xu, L., Yuan, K., Chen, M., Wu, H., Gui, Z., Gong, J. and Randerson, J.T., 2023. AttentionFire_v1.0: Interpretable machine learning fire model for burned-area predictions over tropics. *Geoscientific Model Development*, *16*(3), pp. 869–884.

Li, W., Li, M., Shi, C., Fang, R., Zhao, Q., Meng, X., Yang, G. and Bai, W., 2017. GPS and BeiDou differential code bias estimation using Fengyun-3C satellite onboard GNSS observations. *Remote Sensing*, *9*(12), p. 1239.

Li, W., Xiao, C., Feng, Z., Li, P. and Qi, Y., 2020b. Occurrence types and impact analysis of active fires in the major countries of Southeast Asia during the 2015 strong El Nino. *Journal of Natural Resources*, *35*(10), pp. 2539–2552.

Linh Thao, N.N., Pimonsree, S., Prueksakorn, K., Bich Thao, P.T. and Vongruang, P., 2022. Public health and economic impact assessment of PM2.5 from open biomass burning over countries in mainland Southeast Asia during the smog episode. *Atmospheric Pollution Research*, *13*(6), p. 101418.

Liu, M. and Popescu, S., 2022. Estimation of biomass burning emissions by integrating ICESat-2, Landsat 8, and Sentinel-1 data. *Remote Sensing of Environment*, *280*, p. 113172.

Liu, Y. and Shi, Y., 2023. Estimates of global forest fire carbon emissions using FY-3 active fires product. *Atmosphere*, *14*(10), p. 1575.

Lu, X., Zhang, X., Li, F. and Cochrane, M.A., 2022. Improved estimation of fire particulate emissions using a combination of VIIRS and AHI data for Indonesia during 2015–2020. *Remote Sensing of Environment*, *281*, p. 113238.

Metsaranta, J.M., Hudson, B., Smyth, C., Fellows, M. and Kurz, W.A., 2023. Future fire risk and the greenhouse gas mitigation potential of forest rehabilitation in British Columbia, Canada. *Forest Ecology and Management*, *529*, p. 120729.

Miettinen, J., Shi, C. and Liew, S.C., 2017. Fire distribution in peninsular Malaysia, Sumatra and Borneo in 2015 with special emphasis on peatland fires. *Environmental Management*, *60*(4), pp. 747–757.

Page, S.E., Rieley, J.O. and Banks, C.J., 2011. Global and regional importance of the tropical peatland carbon pool. *Global Change Biology*, *17*(2), pp. 798–818.

Pan, X., Ichoku, C., Chin, M., Bian, H., Darmenov, A., Colarco, P., Ellison, L., Kucsera, T., Da Silva, A., Wang, J., Oda, T. and Cui, G., 2020. Six global biomass burning emission datasets: Intercomparison and application in one global aerosol model. *Atmospheric Chemistry and Physics*, *20*(2), pp. 969–994.

Pereira, G., Longo, K.M., Freitas, S.R., Mataveli, G., Oliveira, V.J., Santos, P.R., Rodrigues, L.F. and Cardozo, F.S., 2022. Improving the south America wildfires smoke estimates: Integration of polar-orbiting and geostationary satellite fire products in the Brazilian biomass burning emission model (3BEM). *Atmospheric Environment*, *273*, p. 118954.

Reddington, C.L., Conibear, L., Robinson, S., Knote, C., Arnold, S.R. and Spracklen, D.V., 2021. Air Pollution from forest and vegetation fires in Southeast Asia disproportionately impacts the poor. *GeoHealth*, *5*(9), p. e2021GH000418.

Russell-Smith, J., Yates, C., Vernooij, R., Eames, T., Van Der Werf, G., Ribeiro, N., Edwards, A., Beatty, R., Lekoko, O., Mafoko, J., Monagle, C. and Johnston, S., 2021. Opportunities and challenges for savanna burning emissions abatement in southern Africa. *Journal of Environmental Management*, *288*, p. 112414.

Sahu, S.K., Mangaraj, P., Beig, G., Samal, A., Chinmay Pradhan, Dash, S. and Tyagi, B., 2021. Quantifying the high resolution seasonal emission of air pollutants from crop residue burning in India. *Environmental Pollution*, *286*, p. 117165.

Sannigrahi, S., Pilla, F., Basu, B., Basu, A.S., Sarkar, K., Chakraborti, S., Joshi, P.K., Zhang, Q., Wang, Y., Bhatt, S., Bhatt, A., Jha, S., Keesstra, S. and Roy, P.S., 2020. Examining the effects of forest fire on terrestrial carbon emission and ecosystem production in India using remote sensing approaches. *Science of The Total Environment*, *725*, p. 138331.

Santana, V.M., Alday, J.G., Lee, H., Allen, K.A. and Marrs, R.H., 2016. Modelling carbon emissions in *Calluna vulgaris*—Dominated ecosystems when prescribed burning and wildfires interact. *PLOS One*, *11*(11), p. e0167137.

Shi, Y., Gong, S., Zang, S., Zhao, Y., Wang, W., Lv, Z., Matsunaga, T., Yamaguchi, Y. and Bai, Y., 2021. High-resolution and multi-year estimation of emissions from open biomass burning in Northeast China during 2001–2017. *Journal of Cleaner Production*, *310*, p. 127496.

Shi, Y., Matsunaga, T. and Yamaguchi, Y., 2015. High-resolution mapping of biomass burning emissions in three tropical regions. *Environmental Science & Technology*, *49*(18), pp. 10806–10814.

Shi, Y., Sasai, T. and Yamaguchi, Y., 2014. Spatio-temporal evaluation of carbon emissions from biomass burning in Southeast Asia during the period 2001–2010. *Ecological Modelling*, *272*, pp. 98–115.

Shi, Y., Zhao, A., Matsunaga, T., Yamaguchi, Y., Zang, S., Li, Z., Yu, T. and Gu, X., 2019. High-resolution inventory of mercury emissions from biomass burning in tropical continents during 2001–2017. *Science of The Total Environment*, *653*, pp. 638–648.

Singh, P., Roy, A., Bhasin, D., Kapoor, M., Ravi, S. and Dey, S., 2021. Crop fires and cardiovascular health – A study from North India. *SSM – Population Health*, *14*, p. 100757.

Spawn, S.A., Sullivan, C.C., Lark, T.J. and Gibbs, H.K., 2020. Harmonized global maps of above and belowground biomass carbon density in the year 2010. *Scientific Data*, *7*(1), p. 112.

Wang, L. and Ma, S., 2024. Extreme winter-spring drought in Southwest China in 2023: response to the phase transition from La Niña to El Niño. *Environmental Research Letters*, *19*(8), p. 084042.

van Wees, D., van Der Werf, G.R., Randerson, J.T., Rogers, B.M., Chen, Y., Veraverbeke, S., Giglio, L. and Morton, D.C., 2022. Global biomass burning fuel consumption and emissions at 500 m spatial resolution based on the Global Fire Emissions Database (GFED). *Geoscientific Model Development*, *15*(22), pp. 8411–8437.

Wiedinmyer, C., Akagi, S.K., Yokelson, R.J., Emmons, L.K., Al-Saadi, J.A., Orlando, J.J. and Soja, A.J., 2011. The Fire INventory from NCAR (FINN): A high resolution global model to estimate the emissions from open burning. *Geoscientific Model Development*, *4*(3), pp. 625–641.

Wiedinmyer, C., Quayle, B., Geron, C., Belote, A., McKenzie, D., Zhang, X., O'Neill, S. and Wynne, K.K., 2006. Estimating emissions from fires in North America for air quality modeling. *Atmospheric Environment*, *40*(19), pp. 3419–3432.

Wiggins, E.B., Soja, A.J., Gargulinski, E., Halliday, H.S., Pierce, R.B., Schmidt, C.C., Nowak, J.B., DiGangi, J.P., Diskin, G.S., Katich, J.M., Perring, A.E., Schwarz, J.P., Anderson, B.E., Chen, G., Crosbie, E.C., Jordan, C., Robinson, C.E., Sanchez, K.J., Shingler, T.J., Shook, M., Thornhill, K.L., Winstead, E.L., Ziemba, L.D. and Moore, R.H., 2020. High temporal resolution satellite observations of fire radiative power reveal link between fire behavior and aerosol and gas emissions. *Geophysical Research Letters*, *47*(23), p. e2020GL090707.

Williams, A.P., Abatzoglou, J.T., Gershunov, A., Guzman-Morales, J., Bishop, D.A., Balch, J.K. and Lettenmaier, D.P., 2019. Observed impacts of anthropogenic climate change on wildfire in California. *Earth's Future*, *7*(8), pp. 892–910.

Xian, D., Zhang, P., Gao, L., Sun, R., Zhang, H. and Jia, X., 2021. Fengyun meteorological satellite products for earth system science applications. *Advances in Atmospheric Sciences*, *38*(8), pp. 1267–1284.

Xiang, M., Xiao, C., Feng, Z. and Ma, Q., 2023. Global distribution, trends and types of active fire occurrences. *Science of The Total Environment*, *902*, p. 166456.

Xu, Y., Huang, Z., Ou, J., Jia, G., Wu, L., Liu, H., Lu, M., Fan, M., Wei, J., Chen, L. and

Yin, S., 2020. Biomass burning spatiotemporal variations over South and Southeast Asia. *Environment International*, *145*, p. 106153.

Yin, S., Wang, X., Zhang, X., Guo, M., Miura, M. and Xiao, Y., 2019. Influence of biomass burning on local air pollution in mainland Southeast Asia from 2001 to 2016. *Environmental Pollution*, *254*, p. 112949.

Zheng, B., Ciais, P., Chevallier, F., Chuvieco, E., Chen, Y. and Yang, H., 2021. Increasing forest fire emissions despite the decline in global burned area. *Science Advances*, *7*(39), p. eabh2646.

Index

D

E

F

L

P

R

S

W